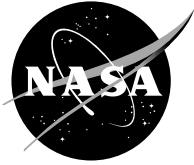


NASA/CR—2004-213132



HSCT Sector Combustor Evaluations for Demonstration Engine

Stuart Greenfield, Paul Heberling, John Kastl, John Matulaitis, and Cynthia Huff
General Electric Aircraft Engines, Cincinnati, Ohio

October 2004

The NASA STI Program Office . . . in Profile

Since its founding, NASA has been dedicated to the advancement of aeronautics and space science. The NASA Scientific and Technical Information (STI) Program Office plays a key part in helping NASA maintain this important role.

The NASA STI Program Office is operated by Langley Research Center, the Lead Center for NASA's scientific and technical information. The NASA STI Program Office provides access to the NASA STI Database, the largest collection of aeronautical and space science STI in the world. The Program Office is also NASA's institutional mechanism for disseminating the results of its research and development activities. These results are published by NASA in the NASA STI Report Series, which includes the following report types:

- **TECHNICAL PUBLICATION.** Reports of completed research or a major significant phase of research that present the results of NASA programs and include extensive data or theoretical analysis. Includes compilations of significant scientific and technical data and information deemed to be of continuing reference value. NASA's counterpart of peer-reviewed formal professional papers but has less stringent limitations on manuscript length and extent of graphic presentations.
- **TECHNICAL MEMORANDUM.** Scientific and technical findings that are preliminary or of specialized interest, e.g., quick release reports, working papers, and bibliographies that contain minimal annotation. Does not contain extensive analysis.
- **CONTRACTOR REPORT.** Scientific and technical findings by NASA-sponsored contractors and grantees.

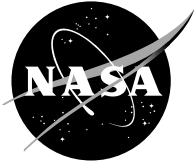
- **CONFERENCE PUBLICATION.** Collected papers from scientific and technical conferences, symposia, seminars, or other meetings sponsored or cosponsored by NASA.
- **SPECIAL PUBLICATION.** Scientific, technical, or historical information from NASA programs, projects, and missions, often concerned with subjects having substantial public interest.
- **TECHNICAL TRANSLATION.** English-language translations of foreign scientific and technical material pertinent to NASA's mission.

Specialized services that complement the STI Program Office's diverse offerings include creating custom thesauri, building customized databases, organizing and publishing research results . . . even providing videos.

For more information about the NASA STI Program Office, see the following:

- Access the NASA STI Program Home Page at <http://www.sti.nasa.gov>
- E-mail your question via the Internet to help@sti.nasa.gov
- Fax your question to the NASA Access Help Desk at 301-621-0134
- Telephone the NASA Access Help Desk at 301-621-0390
- Write to:
NASA Access Help Desk
NASA Center for Aerospace Information
7121 Standard Drive
Hanover, MD 21076

NASA/CR—2004-213132



HSCT Sector Combustor Evaluations for Demonstration Engine

Stuart Greenfield, Paul Heberling, John Kastl, John Matulaitis, and Cynthia Huff
General Electric Aircraft Engines, Cincinnati, Ohio

Prepared under Contract NAS3-26617

National Aeronautics and
Space Administration

Glenn Research Center

October 2004

Document History

This research was originally published internally as HSR063 in June 1998.

Trade names or manufacturers' names are used in this report for identification only. This usage does not constitute an official endorsement, either expressed or implied, by the National Aeronautics and Space Administration.

Note that at the time of research, the NASA Lewis Research Center was undergoing a name change to the NASA John H. Glenn Research Center at Lewis Field. Both names may appear in this report.

Available from

NASA Center for Aerospace Information
7121 Standard Drive
Hanover, MD 21076

National Technical Information Service
5285 Port Royal Road
Springfield, VA 22100

Available electronically at <http://gltrs.grc.nasa.gov>

Table of Contents

	<u>Page</u>
Summary	1
Introduction	3
1.0 Analyses of the Combustor System and Subcomponents	5
1.1 CFD Modeling	7
1.1.1 Cyclone Swirler Pilot CFD Modeling	7
1.1.2 IMFH Tube CFD Modeling	16
1.1.3 Combustor System CFD Modeling	29
1.2 Spreadsheet Models of Combustor Systems	55
1.2.1 General Description of Combustor System Models	55
1.2.2 IMFH Fuel Jet Penetration Study	57
2.0 Premixer Laser Diagnostic Studies	61
2.1 Pennsylvania State University Combustor Diagnostics Program	61
2.2 GE Corporate R&D Diagnostics Studies	70
2.2.1 PDPA Measurements in an Unfired Cyclone Swirler	71
2.2.2 Mie Scattering Tests	81
2.2.3 Fired Tests	83
3.0 Subcomponent Evaluations	89
3.1 Integrated Mixer Flame Holder (IMFH) Evaluations	90
3.2 Curved Tube IMFH Evaluations	104
3.3 Swirl-IMFH Evaluations	117
3.3.1 Swirl-IMFH (Standard Tube Dimensions) Evaluations	117
3.3.2 Mini Swirl-IMFH Evaluations	125
3.3.3 Venturi Swirl-IMFH Evaluations	130
3.4 Cyclone Swirler Evaluations	139
3.5 Swirl-Jet Premixer Evaluations	147
3.6 Summary of Subcomponent Evaluations	159
4.0 Sector Combustor Design and Evaluation	161
4.1 Sector Test 1 - Pressure Test of Baseline Sector Combustor	165
4.2 Sector Test 2 - Atmospheric Pressure Test of Baseline Sector	168
4.3 Sector Test 3 - Pressure Test of Baseline Sector Combustor	173
4.4 Sector Test 4 - Lamilloy Liner Sector Combustor Test	183
4.5 Sector Test 5 - Pilot Aft and Heat Transfer Sector Combustor	189
4.6 NASA 3-Cup Sector Design and Fabrication	190
4.7 Summary of Sector Combustor Evaluations	194
5.0 Variable Geometry Lean-Burn Fuel-Air Mixer	197
5.1 Fuel Staging Compared to Air-scheduling	198
5.2 Variable Geometry Premixer Design	199
5.3 Conceptual Design of Combustor System	200
6.0 Demonstration Engine Combustor Preliminary Design	203
6.1 Design Requirements	203
6.2 Previous HSCT LPP/LDI Combustor System Designs	206
6.3 Stepped Dome with Internal Fuel Manifolds	206
6.4 Stepped Dome with Removable Main Injectors	208
6.5 Multistage Radial Axial System Design (Original MRA)	208
6.6 MRA Version II	211
6.7 Summary of Preliminary Combustor Designs	215

Table of Contents (Continued)

	<u>Page</u>
7.0 Summary and Conclusions	217
References	219
Appendix A - First 5-Cup Sector Combustor Test Data	221
Appendix B - Second 5-Cup Sector Combustor Test Data (Atmospheric)	229
Appendix C - Third 5-Cup Sector Combustor Test Data	241
Appendix D - Fourth 5-Cup Sector Combustor Test Data (Lamilloy liner)	269
Appendix E - Pennsylvania State University Final Report	283

Summary

In LET Task 10, critical development issues of the HSCT lean-burn low emissions combustor were addressed with a range of engineering tools. Laser diagnostics and CFD analysis were applied to develop a clearer understanding of the fuel-air premixing process and premixed combustion. Subcomponent tests evaluated the emissions and operability performance of the fuel-air premixers. Sector combustor tests evaluated the performance of the integrated combustor system. A 3-cup sector was designed and procured for laser diagnostics studies at NASA-Lewis. The results of these efforts supported the earlier selection of the Cyclone Swirler as the pilot stage premixer and the IMFH (Integrated Mixer Flame Holder) tube as the main stage premixer of the LPP combustor.

In the combustor system preliminary design subtask, initial efforts to transform the sector combustor design into a practical subscale engine combustor met with significant challenges. Concerns about the durability of a stepped combustor dome and the need for a removable fuel injection system resulted in the invention and refinement of the MRA (Multistage Radial Axial) combustor system in 1994. The MRA combustor was selected for the HSR Phase II LPP subscale combustor testing in the CPC Program.

Introduction

A key issue in the development of the next generation High Speed Civil Transport (HSCT) is environmental acceptability. Of particular concern is the impact of combustion-generated NO_x emissions on the stratospheric ozone layer. The most straightforward method for reducing NO_x emissions is using a Lean Premixed, Prevaporized (LPP) combustor. An LPP combustor generates a uniform premixture of fuel and air and burns it within a controlled, narrow range of flame temperatures. The flame temperature is selected to not only minimize NO_x emissions, but to minimize CO and unburned hydrocarbon emissions. The LPP concept was chosen for development for the HSCT by GE Aircraft Engines because the approach has been proven in stationary gas turbine applications using gaseous fuels. GE's LM6000 and LM2500 DLE (Dry Low Emissions) combustors are very successful premixed combustors used in stationary applications. The DLE combustors have in common with the HSCT application engine cycles with very severe combustor inlet conditions, mission requirements for operation at full power for long periods, economic requirements for long combustor lifetimes, and environmental requirements for low emissions. The low emissions requirements for the HSCT and DLE combustors lead to additional similarities: both use multiple fuel stages with large numbers of fuel injection sites to maintain the fuel-air ratio in the optimum range and backside convection for liner cooling to minimize CO quenching. The reliability of the LM6000 and LM2500 DLE combustors with convectively-cooled liners have been proven in thousands of hours of service.

LET Task 10 builds upon the accomplishments in Task 5 of NASA Contract NAS3-25951 (Aero-Propulsion Technology or APT) in the development of a HSCT low emissions combustor. Those accomplishments include: 1) initial lean low emissions combustor system conceptual designs, 2) fuel-air mixer design, procurement and tests, and 3) the rectangular stepped-dome sector combustor design and procurement. At the completion of APT Task 5, the lean low emissions combustor was only loosely defined and several major design challenges remained. The lean combustor tentatively utilized a Cyclone Swirler as the pilot (first) fuel stage and IMFH tubes for the main stages. The Cyclone Swirler is a radial swirler in which the fuel is partially

premixed. The IMFH is a straight tube in which fuel is injected and premixed. The flame is stabilized at the exit of the IMFH tube. These fuel-air premixers were combined into combustor systems using a series of steps in the dome to isolate the fired from the unfired stages. This was done to minimize the quenching of CO. Preliminary designs for the subscale and full scale combustors which specified the number of Cyclone Swirlers, IMFH tubes, fuel stages, steps in the dome had been defined, but the details were very tentative. At the completion of APT Task 5 there was almost no definition of the fuel injector system. Based upon the single-cup tests of the IMFH, there was also a major concern about the combustion efficiency of the IMFH at subsonic cruise conditions.

The objective of Task 10 of NASA Contract NAS3-26617 (Large Engine Technology or LET) was to complete the HSR Phase I combustor development of the LPP combustor. The principal objectives of LET Task 10 were four tests of the stepped-dome sector combustor with the goal of making initial assessments of the performance of the LPP combustor as an integrated system. Supporting efforts in LET Task 10 were the continuation of the subcomponent testing begun in APT Task 5, further analysis of the subcomponents and the combustor systems using CFD, and the continued application of laser diagnostics to study the fuel-air premixing process.

Certain lean combustor development issues were addressed in separate LET Tasks. Thermal design issues of the lean combustor, including the liners and the fuel system were addressed in LET Task 42. The MRA (Multistage Radial Axial) combustor system proposed in LET Task 10 as an alternate to the baseline stepped-dome system was designed and procured in LET Task 43. Those efforts are documented in their respective task final reports.

Task 10 culminates in preliminary definition of LPP combustor system designs, discussed in Section 6 of this report. These LPP combustor designs are the starting point for further development and testing in HSR Phase II. In the second quarter of 1998, either a lean combustor design (being developed by GE) or an RQL (Rich burn, Quick quench, Lean burn) combustor design (being developed by P&W) will be downselected for further development in the HSR Program.

Section 1

Analyses of the Combustor System and Subcomponents

Several types of analyses were performed in support of the LPP combustor development. The two most effective analyses were the CFD modeling and the spreadsheet combustor system models. The CFD models of the premixers and the integrated combustion system were used to investigate the two-phase flow in the premixers, analyze the flow fields in the combustor, and study the interactions of the premixers in the combustion system. Predictions in the trends of the various performance metrics (mainly emissions and exit profiles) with changes in design were used to identify design improvements. The spreadsheet models of the combustor systems were used to understand how the combustor's fuel stages would operate over the range of power codes, altitudes, and Mach numbers within the aircraft's flight envelope. Once the number of fuel stages is determined at a cycle point, models and data correlations were used to predict the performance of the combustor and its subcomponents at that cycle point. The spreadsheet models also were used to generate the input data for the CFD models.

Early in LET Task 10, the Mach 2.4 FLADE GE21/FLA1 C1 engine cycle was the standard cycle for the combustor studies. Table 1.1 lists the combustor conditions at key engine cycle points of the FLADE C1 engine cycle. Later in Task 10, the A5B mixed flow turbofan engine cycle became the standard cycle for the design of both the LPP and RQL combustors. Table 1.2 lists the combustor conditions for key points of the A5B MFTF engine cycle. The significant change between the two cycles was that the T_4 increased by 200 R. This results in a similar increase in the temperature in the combustion zone, making it more difficult to meet the supersonic cruise NOx emissions goal.

Point	Ground Idle	Begin Takeoff	Min Subsonic Cruise	Max Subsonic Cruise	Max Supersonic Cruise	End Supersonic Cruise
Power Code	22	50	31.11	31.71	-	41.59
Altitude (ft)	0	0	34000	37000	55000	65000
Mach Number	0	0	0.95	0.95	2.4	2.4
W3 (lb/sec)	109.1	421.8	160.8	142.3	238.8	147.2
W36 (lb/sec)	89.3	348.2	132.1	116.8	196.7	120.9
WF36 (lb/hr)	3896	35036	10344	9078	19248	11982
P3 (psia)	56.2	305.6	105.4	92.7	181.1	111.6
P4 (psia)	51.9	285.7	98.2	86.4	167.9	103.5
T3 (degrees R)	815	1350	1159	1141	1662	1662
T4 (degrees R)	1593	3018	2526	2502	3226	3247
FAR4	0.0121	0.0280	0.0218	0.0216	0.0272	0.0275

Point	Ground Idle	Begin Takeoff	Begin Subsonic Cruise	End Subsonic Cruise	Begin Supersonic Cruise	End Supersonic Cruise
Power Code	21	50	35.54	35.51	48.27	47.42
Altitude (ft)	0	0	32500	34300	62900	68100
Mach Number	0	0	0.9	0.9	2.4	2.4
W3 (lb/sec)	72.7	424.8	148.1	137.1	172.8	131.9
W36 (lb/sec)	60.2	356.8	123.7	114.4	144.5	110.1
WF36 (lb/hr)	2517	38011	8242	7521	161.4	12321
P3 (psia)	35.2	306.8	89.4	82.2	131.9	100.5
P4 (psia)	33.0	289.6	83.9	77.1	123.8	94.3
T3 (degrees R)	702	1385	1065	1048	1690	1686
T4 (degrees R)	1523	3130	2265	2237	3441	3441
FAR4	0.0116	0.0296	0.0185	0.0183	0.0310	0.0311

1.1 CFD Modeling

CFD combustor models were developed using CONCERT, which is GE's proprietary CFD code. The CONCERT models used in Task 10 were all 3-dimensional. CONCERT 3D is a steady-state, viscous, turbulent flow code that was developed primarily for use in modeling combustors. The grid system used by CONCERT 3D is a structured, body-fitted, curvilinear mesh.

The CFD models of the Cyclone Swirler pilot and IMFH main stage premixers were used to study the fuel-air mixing process. Since these models were only used to study the interior of the premixers, no combustion was modeled and no emissions could be projected. The results of these models were used to project the performance of the various design permutations to screen concepts and to identify design changes to improve performance. CFD models of the integrated combustor system were used to better understand how the burning fuel-air mixture interacts with air from the unfired stages and the cooling flows. The system models were developed in parallel with the preparations for the sector combustor tests documented in Section 4. The predictions of the CFD models were later compared with sector combustor data, primarily exit plane emissions and temperature profile measurements. An anchored CFD sector combustor model resulted. The anchored CFD models were used for design studies (some of which were not performed in Task 10). The MRA CFD model was derived from the anchored Stepped-Dome sector combustor CFD model and used to expedite the process of improving the MRA combustor's performance.

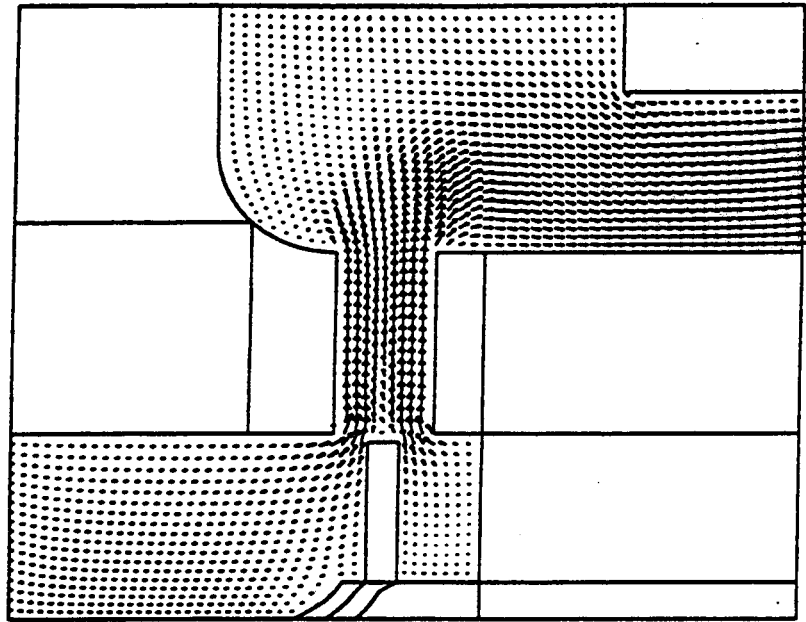
1.1.1 Cyclone Swirler Pilot CFD Modeling

Two CFD models of Configuration 3 of the Cyclone Swirler pilot were generated. Configuration 3 of the Cyclone Swirler pilot is discussed in Section 3.4. A cross-section of Configuration 3 is shown there. Configuration 3 is a slightly scaled-down version (in terms of size and effective flow area) of the Configuration 2 design tested in APT Task 5.⁽¹⁻¹⁾ Both simulations were performed at the HSCT mid-supersonic cruise mission point in the Mach 2.4 FLADE GE21/FLA1 C1 engine cycle, the first engine cycle selected as a standard at GEAE for the HSCT low emissions combustor development. The combustor conditions were: $T_3 = 1213^\circ\text{F}$ (1673 R) $P_3 =$

146 psia, $\Delta P = 7.2\%$, and fuel-air ratio = 0.03444. The air flow rate was 0.521 lb/sec. The fuel flow rate was 62.48 lb/hr. The fuel was assumed to be injected with a Sauter mean diameter (SMD) of 50 μm . This assumption is based upon the results of the GE CR&D measurements, which are discussed in Section 2. The CFD model used a Rosin-Rammler drop size distribution function with droplets ranging in size from 6.9 to 131.1 μm . Figure 1.1 shows the vector flow field resulting from the first Cyclone Swirler CFD model. Figure 1.2 shows the predicted fuel droplet trajectories in the radial-circumferential plane. The Cyclone Swirler's high radial acceleration assists the vaporization and mixing of droplets because the density difference combined with the radial acceleration maintains high relative velocities between the liquid droplets and the air. In this model, it was assumed that droplets vaporized instantaneously when they reached a boundary.

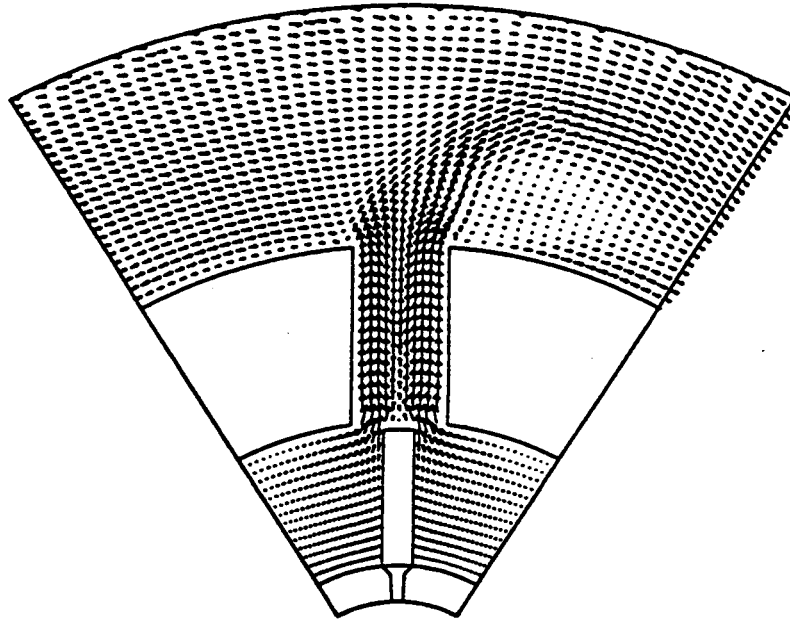
The second CFD model of the Cyclone Swirler pilot was identical to the first, except that instantaneous evaporation of fuel at the wall was not assumed. Instead, the droplets were constrained to bounce off the wall with a coefficient of restitution of unity (angle of incidence equals angle of reflection). The velocity vector field for the evaporating case and reflecting case vector are identical. The vector flow fields are shown in the radial-circumferential plane in Figure 1.4 and in the radial-axial plane in Figure 1.5. Figures 1.6 and 1.7 are contour plots comparing the fuel vapor concentrations for the two vaporization models in the two planes.

Vaporization on the wall, as assumed in the first model, is not desirable because once the fuel evaporates, there is no significant difference in the densities of the fuel and the air. The relative motion between the fuel and the air, due to the high radial acceleration, ceases. This causes the rich streaks exiting the Cyclone Swirler as is shown in Figure 1.3. Re-atomized fuel in the flow field will mix more uniformly with the air because the droplets within the cyclone are in a very high acceleration field. The CFD results using the bouncing droplet model, which closely simulates re-atomized fuel, shows a less pronounced rich streak exiting the premixer. Figure 1.8 shows the difference in the droplet trajectories with the two vaporization models.



→ 783.158

Side View



→ 754.568

End View (ALF)

Figure 1.1 - CONCERT 3D results for plain-jet airblast atomizer of Configuration 3 of the Cyclone Swirler pilot. Velocity vector fields are shown in the radial-axial plane and the radial-circumferential plane.

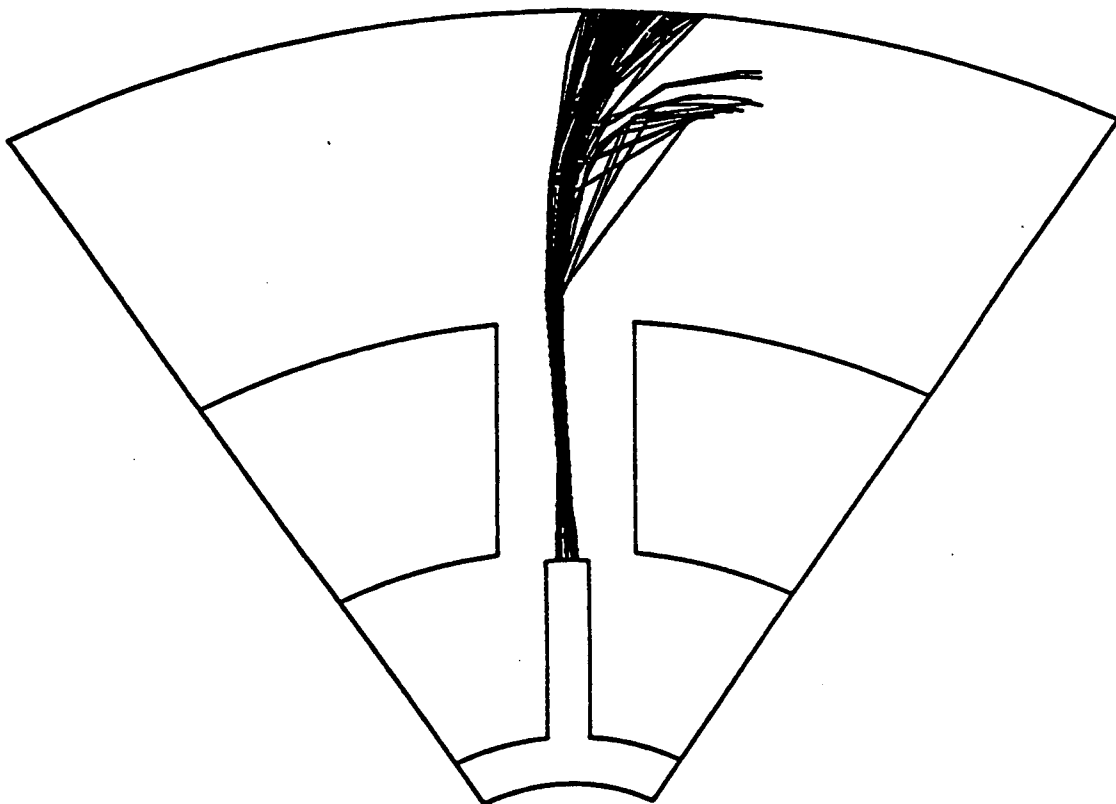
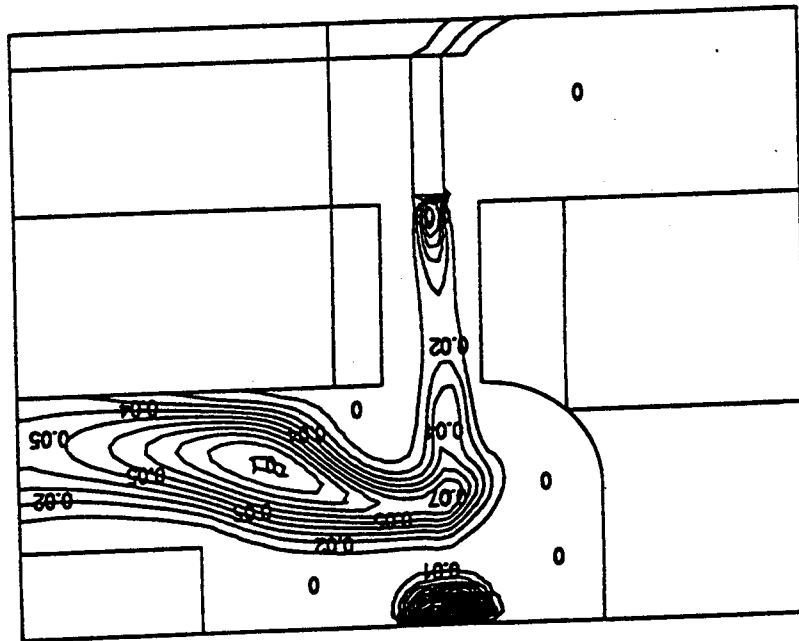
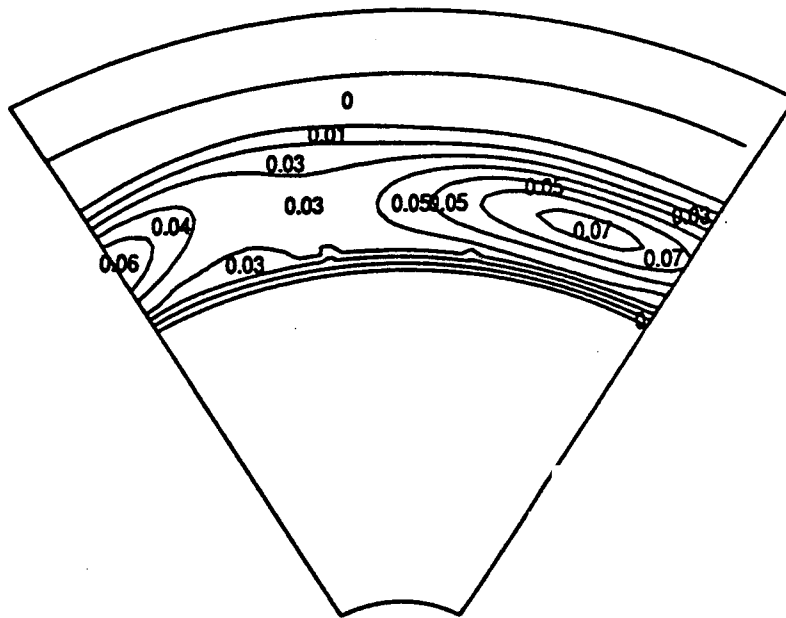


Figure 1.2 - CONCERT 3D results for plain-jet airblast atomizer of Configuration 3 of the Cyclone Swirler pilot. Droplet trajectories are shown in the radial-circumferential plane.



Side View



End View (ALF)

Figure 1.3 - CONCERT 3D results for Configuration 3 of the Cyclone Swirler pilot. Contours of constant vaporized fuel mass fraction are shown in the radial-axial plane and the radial-circumferential plane. The axial position of this radial-circumferential plane is at the upstream end of the annular throat.

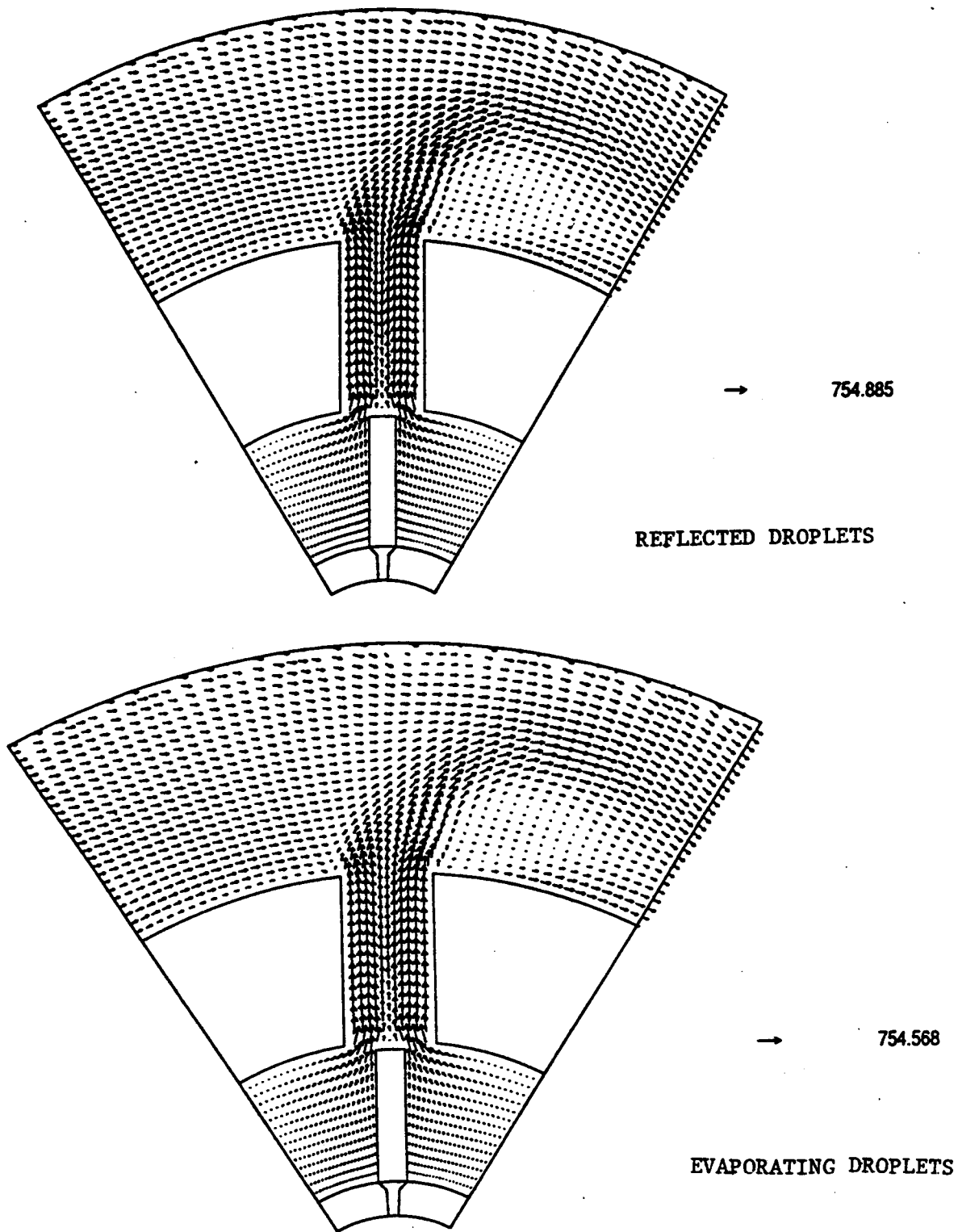


Figure 1.4 - CONCERT 3D results for plain-jet airblast atomizer of Configuration 3 of the Cyclone Swirler pilot. Velocity vector fields are shown in the radial-circumferential plane comparing the results for the reflected droplet model and the evaporating droplet model. The results are nearly identical.

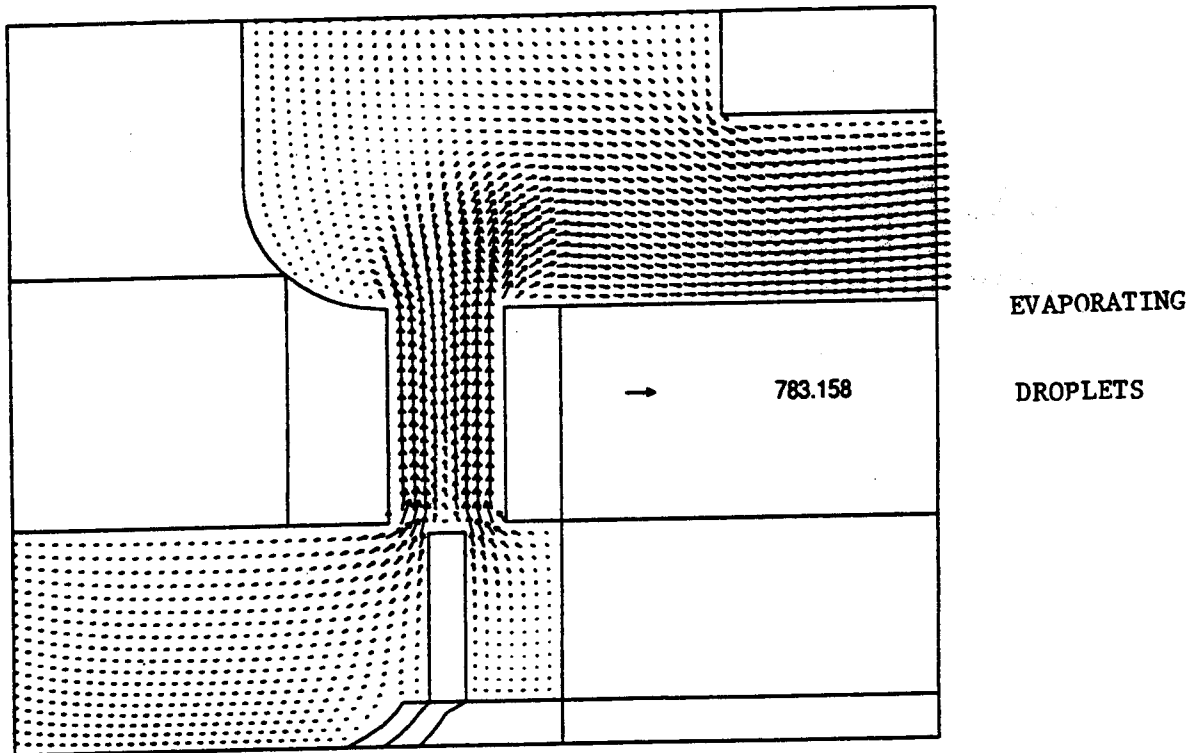
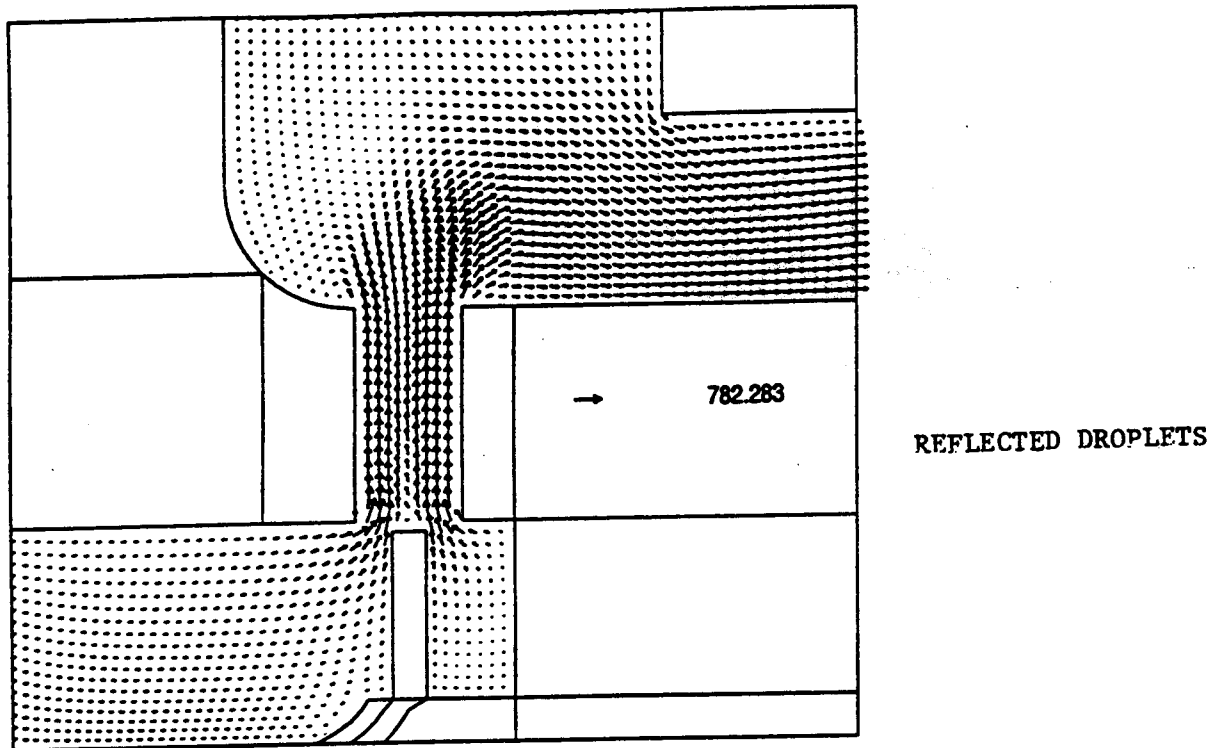


Figure 1.5 - CONCERT 3D results for plain-jet airblast atomizer of Configuration 3 of the Cyclone Swirler pilot. Velocity vector fields are shown in the radial-axial plane comparing the results for the reflected droplet model and the evaporating droplet model. The results are nearly identical.

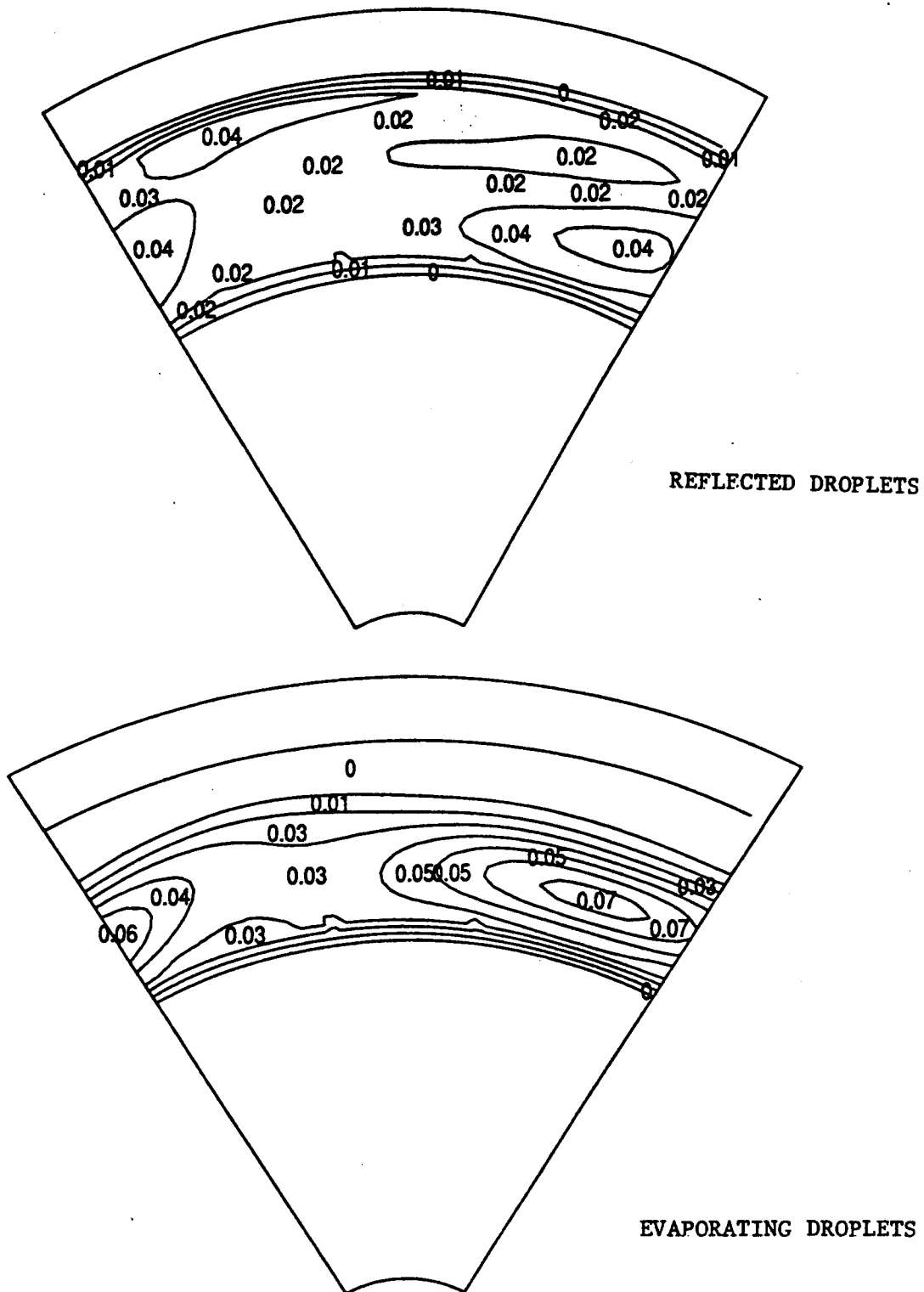
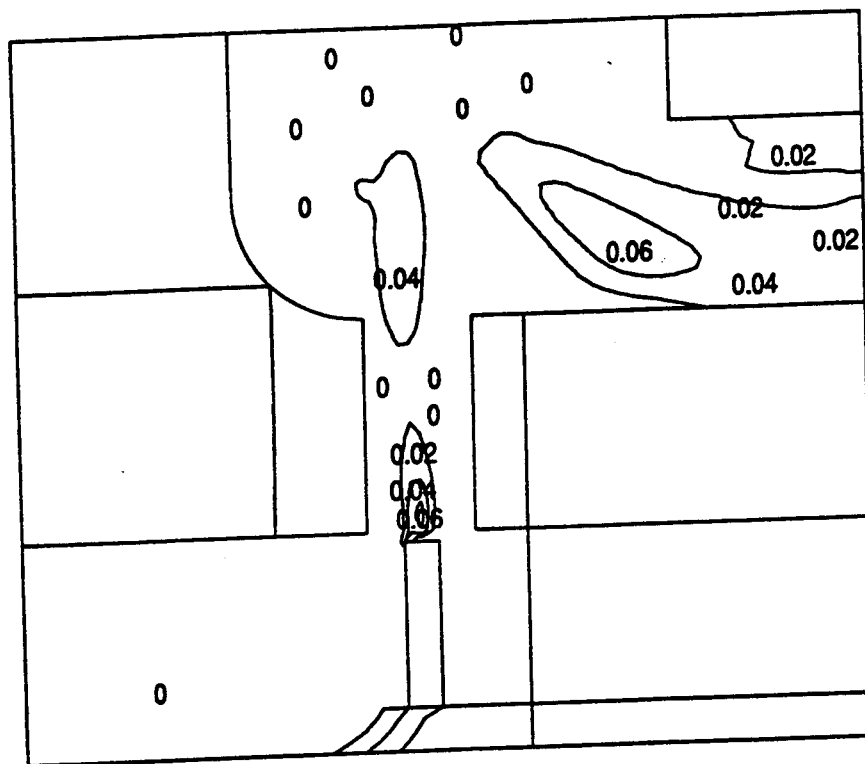
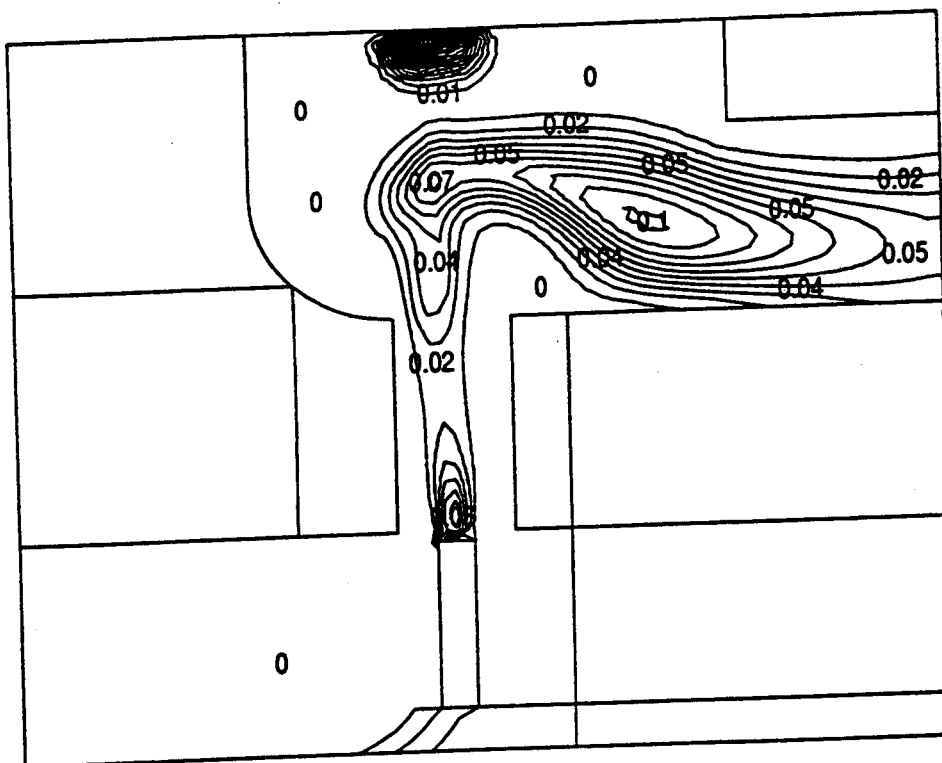


Figure 1.6 - CONCERT 3D results for plain-jet airblast atomizer of Configuration 3 of the Cyclone Swirler pilot. Contours of constant vaporized fuel mass fraction are shown in the radial-circumferential plane comparing the results for the reflected droplet model and the evaporating droplet model.

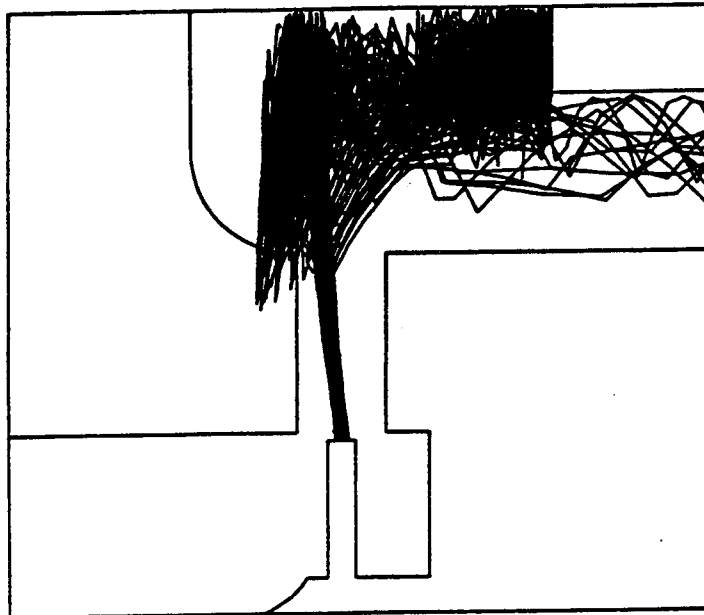


REFLECTED DROPLETS

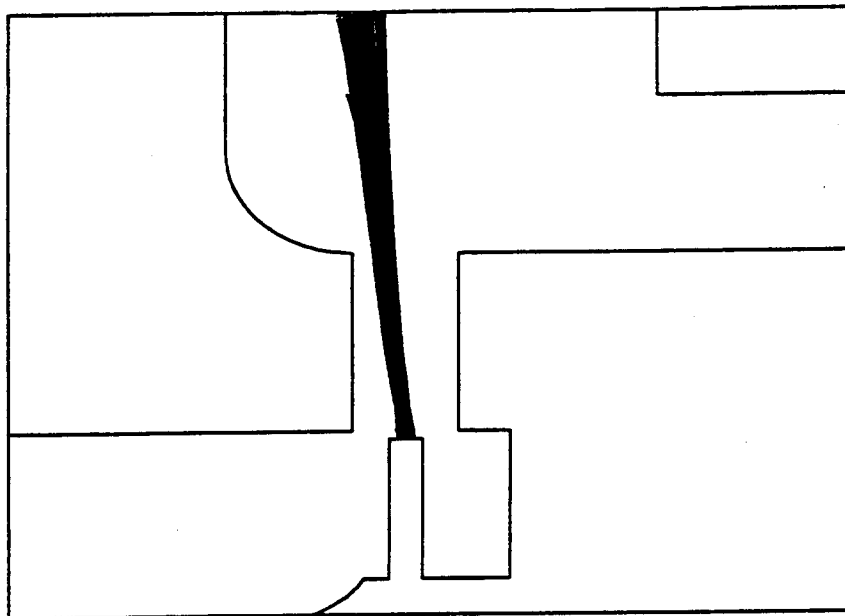


EVAPORATING DROPLETS

Figure 1.7 - CONCERT 3D results for plain jet air-blast atomizer of Configuration 3 of the Cyclone Swirler pilot. Contours of constant vaporized fuel mass fraction are shown in the radial-axial plane comparing the results for the reflected droplet model and the evaporating droplet model.



REFLECTED DROPLETS



EVAPORATING DROPLETS

Figure 1.8 - CONCERT 3D results for plain jet air-blast atomizer of Configuration 3 of the Cyclone Swirler pilot. Fuel droplet trajectory plots are shown in the radial-axial plane comparing the results for the reflected droplet model and the evaporating droplet model.

In a Cyclone Swirler, the major portion of the fuel that impinges on the swirler vanes is expected to be re-atomized and entrained back into the flow field by air passing between the swirler vanes. This re-atomization process is more closely modeled by bouncing droplets of the second model than it is by the evaporating droplets of the first model. However, some of the fuel may be evaporated by contacting the hot surface. Thus, the results of the two CFD models may actually bracket the actual mixing in the Cyclone Swirler.

With the reflecting droplet model, with slower fuel evaporation, only a few of the larger droplets exit the Cyclone Swirler before being vaporized. The conclusion is that the Cyclone Swirler pilot, the primary purpose of which is to insure good combustor stability and low emissions under low engine power conditions, appears to be able to totally vaporize the fuel at supersonic cruise conditions. Although the fuel may be totally vaporized, it is not uniformly premixed. NO_x emissions are dependent on the degree of mixing of the vaporized fuel and the air. However, this unfired subcomponent CFD model could not be used to make NO_x emissions predictions.

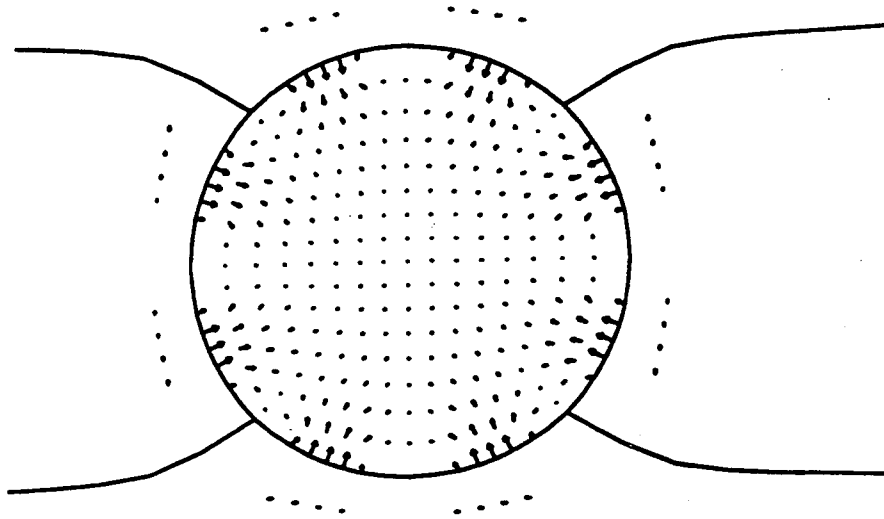
1.1.2 IMFH Tube CFD Modeling

The conditions at which the IMFH tube was modeled were based on the A5B Mixed Flow Turbofan cycle mid-supersonic cruise point. For the IMFH CFD model, the mid-supersonic cruise cycle point was de-rated to the conditions actually run in the high pressure single-cup test of IMFH Configuration 5B (configuration used in the stepped-dome rectangular sector combustor). The conditions that were modeled were $P_3 = 11.47$ atmospheres and $T_3 = 1100^\circ\text{F}$ (1560 R). The fuel flow rate was 19.17 lb/hr and the total air flow rate was 0.161 lb/sec., 11.5% of which went through the cooling circuit. The tube is 5.5 inches long with the fuel injected 1 inch from the inlet through a fuel injector tube with a 0.02 inch inner diameter. The fuel injector tube extends to the centerline of the IMFH tube and is slanted 15 degrees downstream from the radius. At the exit of the IMFH tube there are eight spent cooling air dump holes. Case 1 of the CFD model has eight dome spent cooling air dump holes centered 0.23 inch from the exit of the pre-mixer tube of the actual hardware.

Case 2 uses four larger diameter spent cooling air dump holes in order to maintain the same total air flow and jet velocity as the first case. The flow fields in the radial-circumferential plane at the axial position of the spent cooling holes are compared for Cases 1 and 2 in Figure 1.9. The four-hole case results in better penetration of the dome cooling dump air. The baseline fuel injector tube used for Cases 1 and 2 is a wall injector with 50% immersion. Figure 1.10 provides a close-up view of the sidewall injector tube location. Again, this injector configuration is the one used in Configuration 5A and 5B of the single-cup IMFH and the stepped-dome sector combustor. In the CFD model, fuel is injected as a single 20 μm SMD stream at the tip of an obstacle representing the fuel injector. The droplet trajectories in the radial-axial plane are compared for Cases 1 and 2 in Figure 1.10. The vaporized fuel fraction in the radial-axial plane are compared in Figure 1.11 and the radial-circumferential plane in Figure 1.12. There is no significant differences in droplet trajectories and fuel vapor mass fractions are only slightly different. The 4-hole configuration is slightly more successful in moving fuel away from the tube wall.

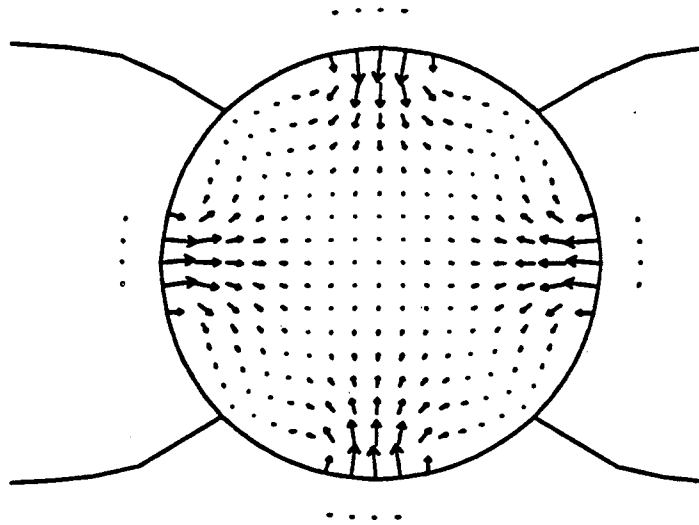
Two additional cases of the IMFH single tube mixer model were run investigating non-uniform spent cooling hole spacing. Case 3 uses four spent cooling air dump holes like Case 2. However, the holes are rearranged such that hole 1 is nearly in line with the fuel injector, hole 2 is 180° opposite hole 1, and holes 3 and 4 are 45° on each side of holes 2. Case 4 uses the same hole pattern as Case 3, but it reduces the immersion of the fuel injector from 50% to 20%.

Comparison of Case 2 in Figures 1.9 through 1.12 with Case 3 in Figures 1.13 through 1.16 leads to several conclusions. Penetration of the spent cooling air jets for Cases 2 and 3 is nearly the same. Since Case 3 dumps more dome cooling air opposite the fuel injector than Case 2, the droplet trajectories are pushed away from the mixer tube wall at this location. The fuel vapor mass fraction profiles at the exit of the mixer tube are similar for Cases 2 and 3 and the peak fuel streak is in nearly the same location for both cases. Since fuel mass fraction profiles at the exit of the mixer tube, as well as the droplet trajectories, are only slightly different between Cases 1, 2 and 3; very little difference in NO_x emissions, stability, or combustion efficiency would be expected.



→ 218.446

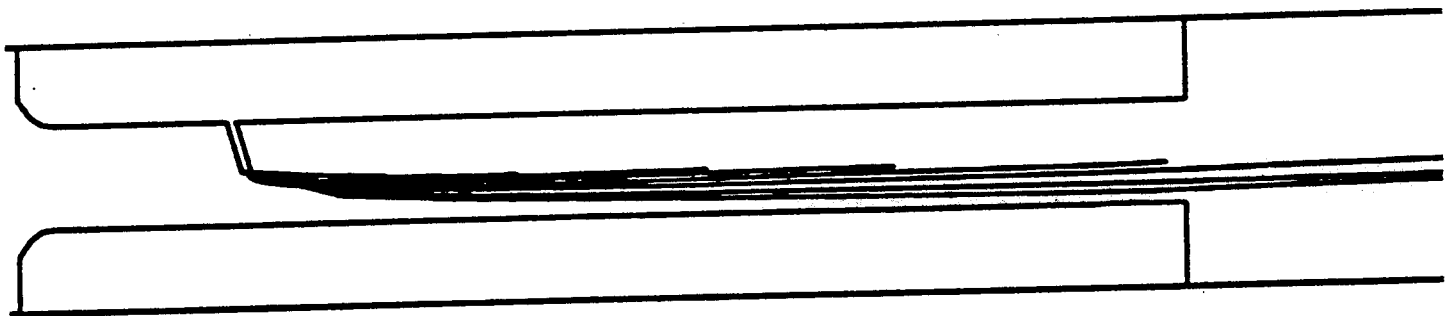
Configuration 1 - 8 Dome Cooling Dump Holes.
(End View)



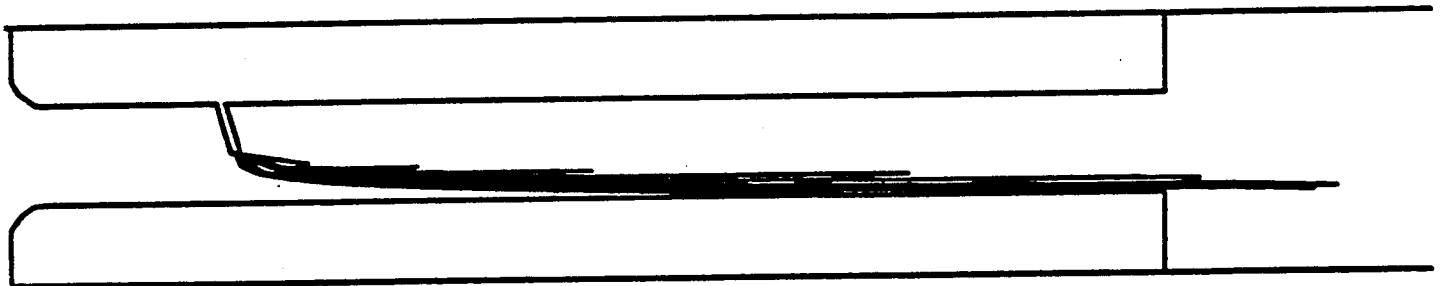
→ 233.047

Configuration 2 - 4 Dome Cooling Dump Holes.
(End View)

Figure 1.9 - CONCERT 3D results for IMFH tube. Velocity vector plots are shown in the radial-circumferential plane passing through the spent dome cooling air injection holes. 8 cooling air holes are compared to 4 cooling air holes.

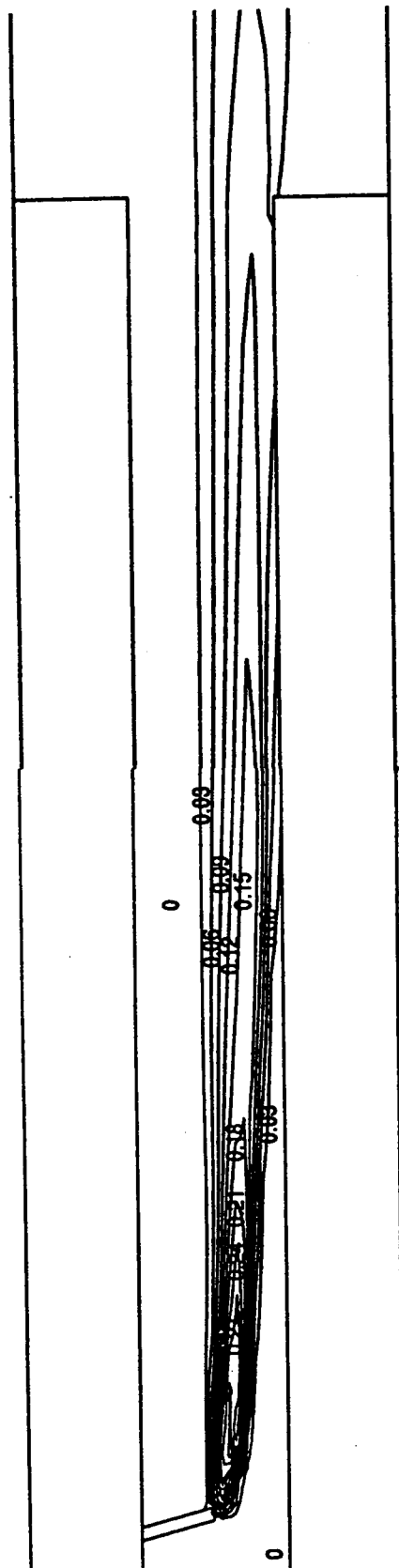


Configuration 1 - 8 Dome Cooling Dump Holes.
(Side View)

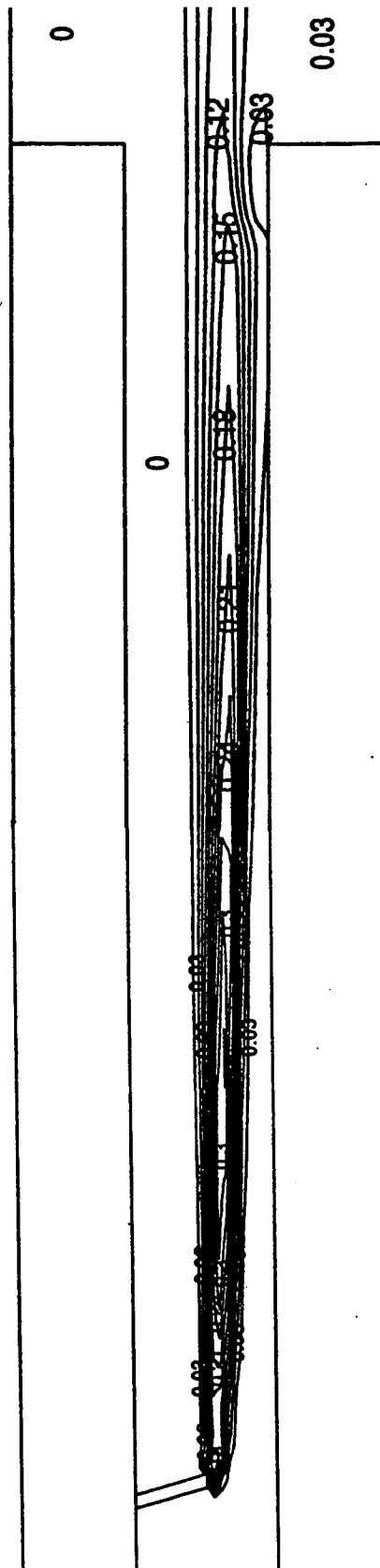


Configuration 2 - 4 Dome Cooling Dump Holes.
(Side View)

Figure 1.10 - CONCERT 3D results for IMFH tube. Fuel droplet trajectory plots are shown in the radial-axial plane passing through the fuel injector tube. The effect of 8 cooling air holes on the droplet trajectories are compared to 4 cooling air holes.

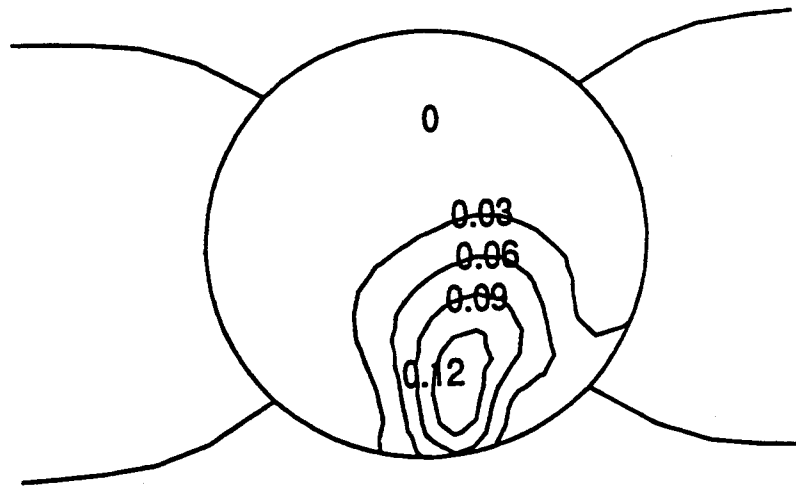


Configuration 1 - 8 Dome Cooling Dump Holes.
(Side View)



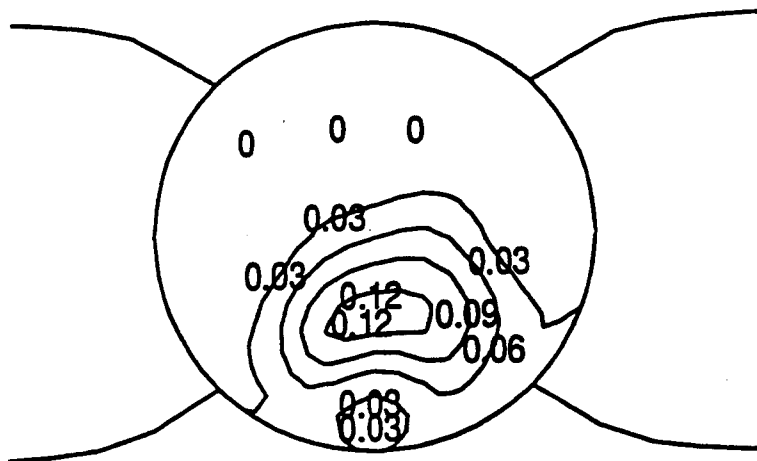
Configuration 2 - 4 Dome Cooling Dump Holes.
(Side View)

Figure 1.11 - CONCERT 3D results for IMFH tube. Plots of contours of constant vaporized fuel mass fraction are shown in the radial-axial plane passing through the fuel injector tube. The effect of 8 cooling air holes on the droplet trajectories are compared to 4 cooling air holes.



PDF-MEAN

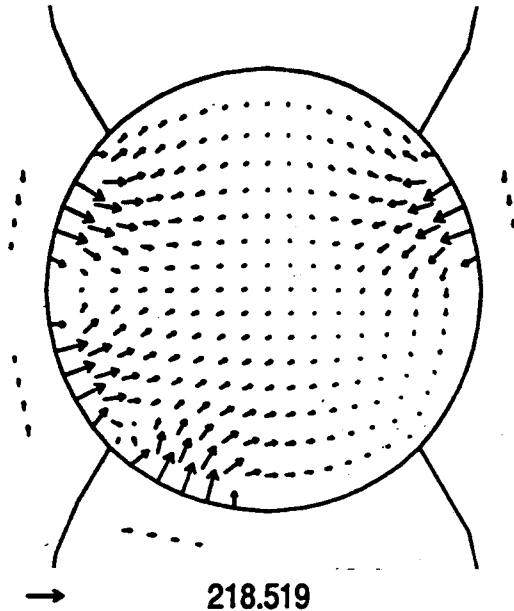
Configuration 1 - 8 Dome Cooling Dump Holes.
(End View)



PDF-MEAN

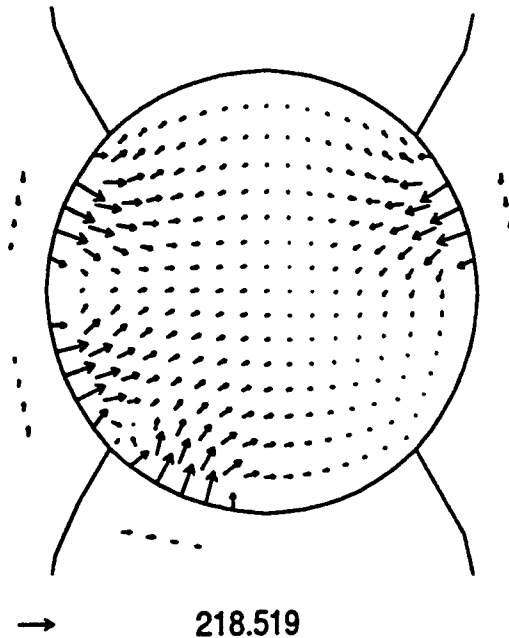
Configuration 2 - 4 Dome Cooling Dump Holes.
(End View)

Figure 1.12 - CONCERT 3D results for IMFH tube. Plots of contours of constant vaporized fuel mass fraction are shown in the radial-circumferential plane at the axial position of the of the spent dome cooling air injection holes. The effect of 8 cooling air holes on the droplet trajectories are compared to 4 cooling air holes.



218.519

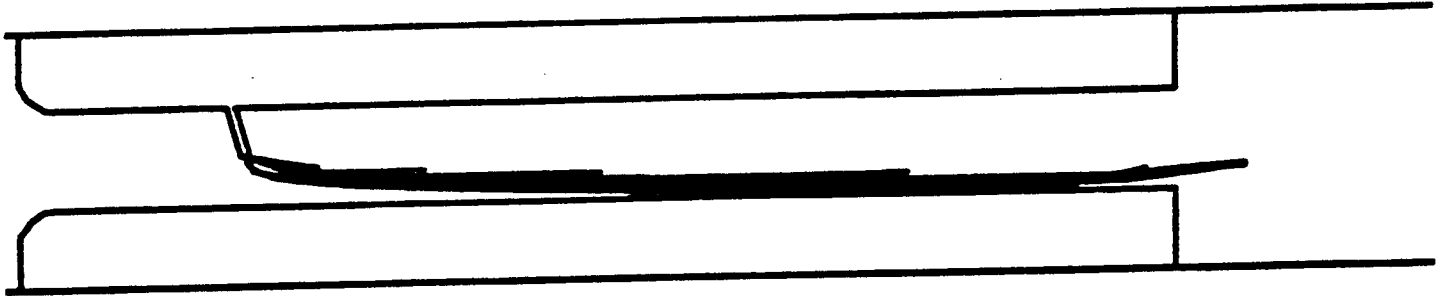
Configuration 3 - 4 Dome Cooling Dump Holes,
 Unequally Spaced, 50% Hypo Fuel Tube Immersion.
 (End View)



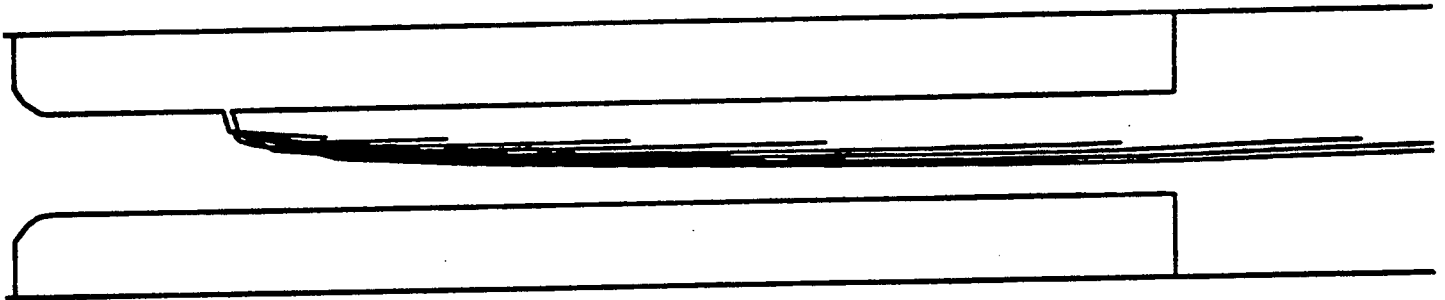
218.519

Configuration 4 - 4 Dome Cooling Dump Holes,
 Unequally Spaced, 20% Hypo Fuel Tube Immersion.
 (End View)

Figure 1.13 - CONCERT 3D results for IMFH tube. Plots of velocity vectors are shown in the radial-circumferential plane in the plane of 4 spent cooling air holes unequally spaced around the tube wall. Results are shown for 50% immersions of the fuel injector tube and 20% immersion. There is no difference for this particular result.

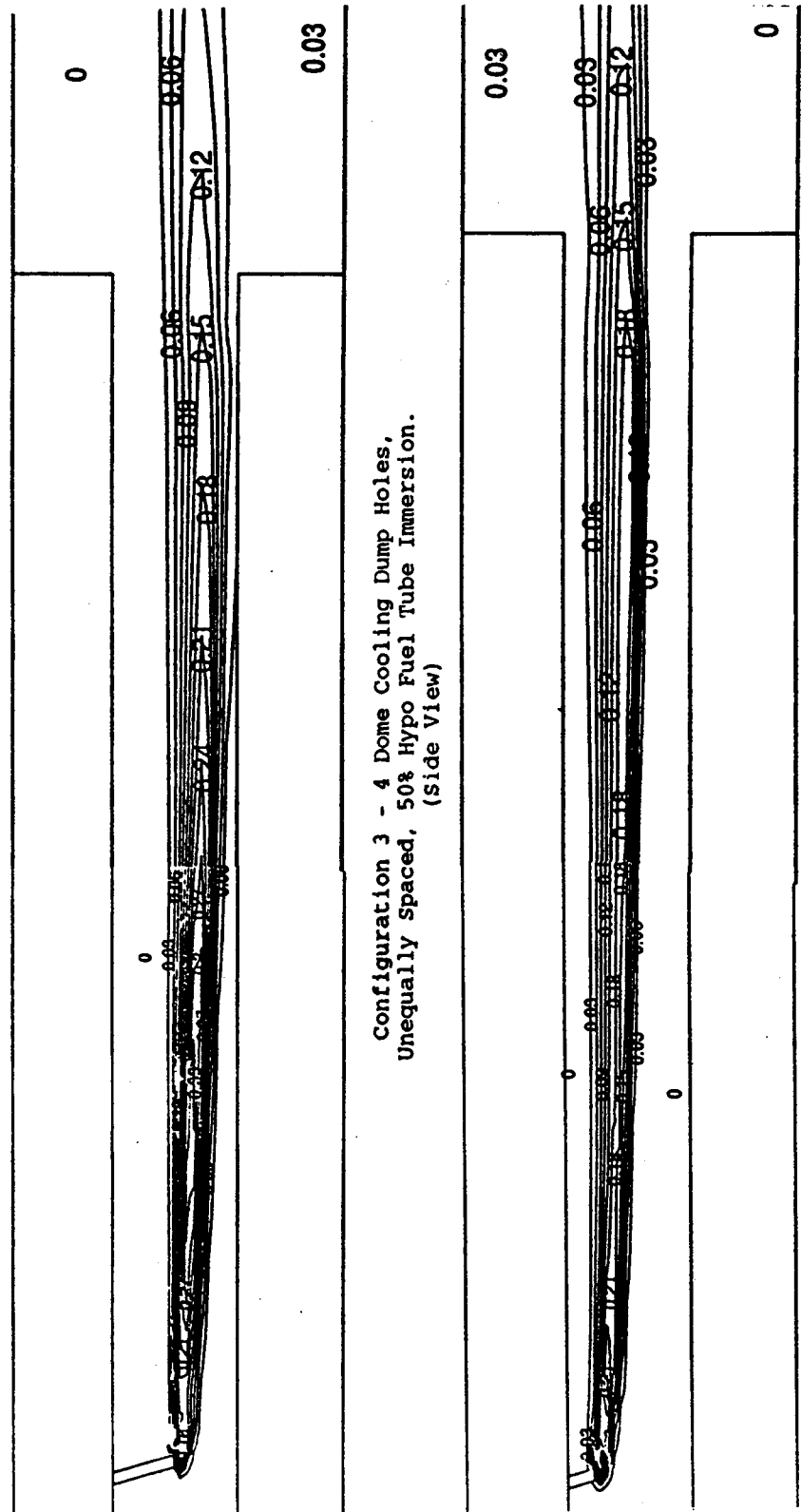


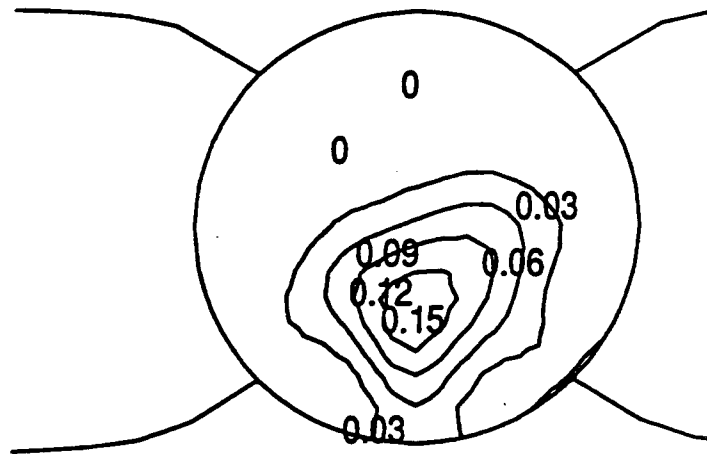
Configuration 3 - 4 Dome Cooling Dump Holes,
Unequally Spaced, 50% Hypo Fuel Tube Immersion.
(Side View)



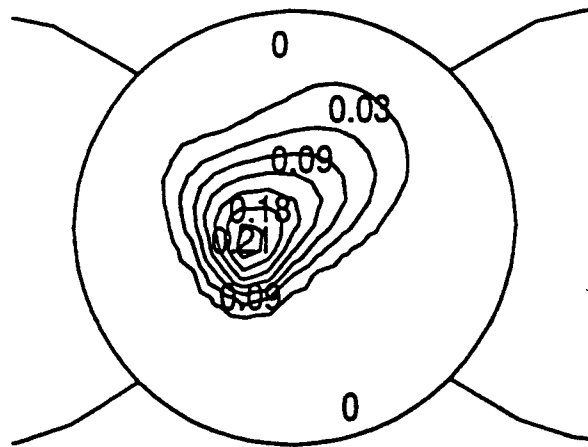
Configuration 4 - 4 Dome Cooling Dump Holes,
Unequally Spaced, 20% Hypo Fuel Tube Immersion.
(Side View)

Figure 1.14 - CONCERT 3D results for IMFH tube. Plots of fuel droplet trajectories are shown in the radial-axial plane through the fuel injector tube. The 4 spent cooling air holes are unequally spaced around the tube wall. Results are shown for 50% immersions of the fuel injector tube and 20% immersion.





PDF-MEAN
 Configuration 3 - 4 Dome Cooling Dump Holes,
 Unequally Spaced, 50% Hypo Fuel Tube Immersion.
 (End View)



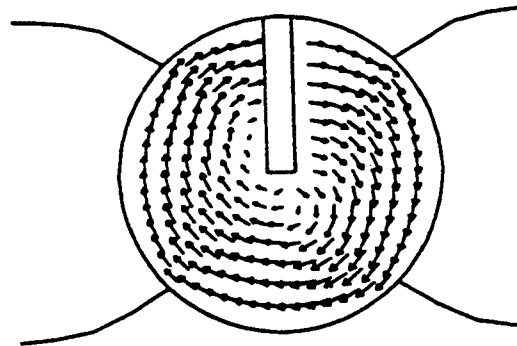
PDF-MEAN
 Configuration 4 - 4 Dome Cooling Dump Holes,
 Unequally Spaced, 20% Hypo Fuel Tube Immersion.
 (End View)

Figure 1.16 - CONCERT 3D results for IMFH tube. Plots of contours of constant vaporized fuel mass fraction are shown in the a radial-circumferential plane in the plane of 4 spent cooling air holes unequally spaced around the tube wall. Results are shown for 50% immersions of the fuel injector tube and 20% immersion. The injectors are centered at the top (not shown).

Comparison of the results for Cases 3 and 4 in Figures 1.15 through 1.16 reveals that the peak fuel mass fraction for Case 3 is 0.15, whereas the peak mass fraction for Case 4 is 0.21. The peak mass fraction findings for Case 4 support the conclusions drawn about the mixer tube exit fuel/air distribution regarding the single-cup test of Swirl-IMFH with 20% injector immersion in Section 3.3.1. The measured data for the 50% immersion case has lower NO_x emissions and better combustion efficiency, because the 50% injector immersion results in a more uniform mixture. The better mixing of the 50% injector immersion is consistent with the fuel being nearer the wall, as shown in Figures 1.1.4 through 1.16, where the mixture is subjected to more shear within the tube.

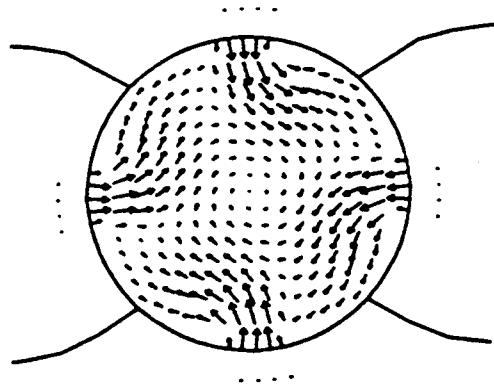
Both immersions yield a fuel rich streak near the tube centerline (although the beneficial effect of the mixing of the spent cooling air ejection is not included in these results). For a given level of non-uniformity at the exit of the tube, it is preferable for the richer gases to be nearer the centerline, because that mixture will not enter the mixing boundary layer till later (where they would be slowed down and ignited) and be unlikely to enter the recirculation zone. Thus once ignited, the hotter centerline gases will tend to have a much lower residence time to produce NO_x than the cooler regions. For a given a level of mixture non-uniformity at the exit of the tube, having the leaner gases near the wall is expected to be less detrimental to combustion efficiency. Entering the combustor near the tube wall, they will enter the mixing boundary layer first where they are ignited, slowed down, and also be more likely to recirculate. The leaner gases would therefore tend to have the longer residence time they need to burn efficiently. These arguments would indicate the emissions performance of the IMFH has some tolerance to fuel-air mixing non-uniformity of the type seen in Figure 1.16 (richer gases in the center).

In order to investigate the effect of swirl added at the inlet of the IMFH tube (swirl angle = 11.5°), CFD Cases 5A and 6 were run. Case 5A used the four equally spaced cooling dump holes with a 50% fuel injector tube immersion. Case 6 adds 11.5° swirl to the Case 4 parameters (unequal spacing of the spent cooling air dump holes and the 20% fuel injector tube immersion). Figure 1.17 shows the flow field vector plots of Case 5A in the radial-circumferential plane at the axial positions of the fuel injector and the spent cooling air injection holes. The swirling flow field of Case 5A and its interactions with the injector and the spent cooling air are readily evident.



→ 96.756

Plane of the fuel injector



→ 130.979

Plane of the 4 spent cooling air injection holes

Figure 1.17 - CONCERT 3D results for IMFH tube. 50% fuel injector tube immersion. Plots of velocity vectors are shown in the radial-circumferential plane in the plane of the fuel injector and the 4 spent cooling air holes equally spaced around the tube wall. The flow into the tube has an 11.5 degree swirl angle.

Figure 1.18 shows the fuel vapor mass fraction for Case 5A. It is seen that the Case 5A peak fuel mass fraction decreased to 0.09 from 0.12 in Case 2 when swirl was added to the mixer tube. This is lower than any of the previous cases. Figure 1.19 compares the fuel vapor mass fraction for Case 5A to Case 2. The cross-sectional area over which the fuel spreads is very similar, although the area in the swirling case appears slightly larger. Figure 1.20 shows the fuel droplet trajectories for Case 5A. Figure 1.21 compares the droplet trajectories for Cases 2 and 5A. The swirling flow pushed a significant amount of fuel to the mixer tube walls where it would be instantly vaporized (the model's boundary condition). This vaporization may have increased the peak fuel mass fraction for Case 5A over what it would have been without the vaporization at the wall boundary condition.

Figure 1.22 shows the flow field vector plot for Case 6 in the radial-circumferential plane at the axial positions of the fuel injector and the spent cooling air injection holes. Again the swirl and its interactions are clearly seen. Figure 1.23 shows the fuel droplet trajectories in the radial-circumferential plane and the radial axial plane. Figure 1.24 shows the fuel vapor mass fraction contours in the radial-axial plane. It can be seen that by reducing the fuel injector tube immersion to 20%, the fuel contacting the mixer tube wall has actually increased. This can be explained by considering the flow field relative to the tip of the fuel injector. In the 50% immersion case, the fuel is injected at the center of the swirling stream. Thus as the fuel travels away from the injector tip, the angular velocity of the air increases from zero, slowly increasing the radial acceleration. In the 20% immersion case, the local flow field is highly swirling at the injector tip. The radial acceleration the droplets see is high right from the time it is injected, so the fuel is centrifuged to the mixer tube wall. Based upon these results and their interpretation, it appears that for swirling flow within an IMFH tube, a 50% fuel injector immersion is optimum.

1.1.3 Combustor System CFD Modeling

CONCERT 3D CFD modeling was used to investigate design variations of the Multistage Radial Axial (MRA) combustor. A mechanical layout of the original MRA was never performed before the design evolved to a significantly different design (the "inverted MRA" still being

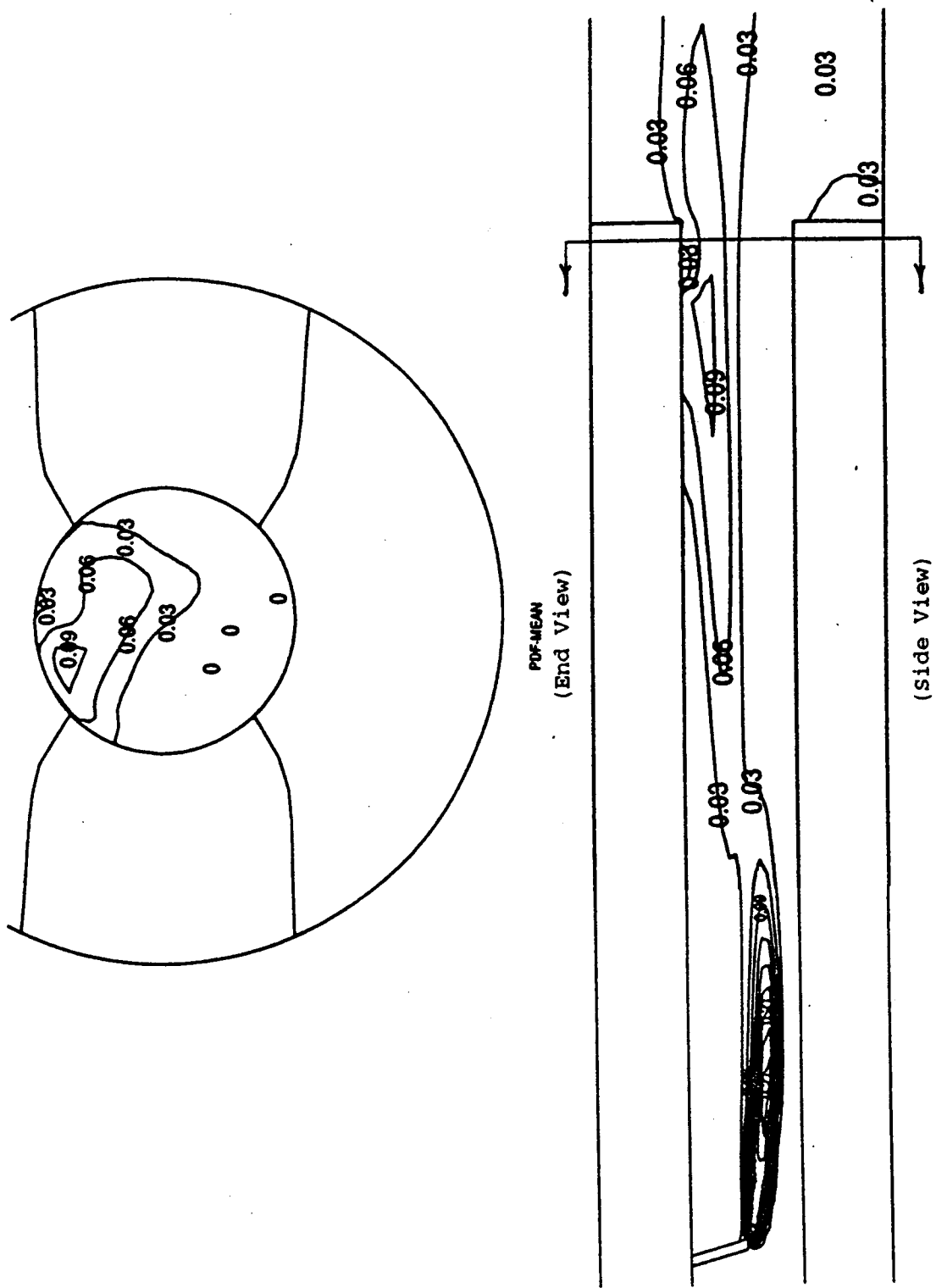
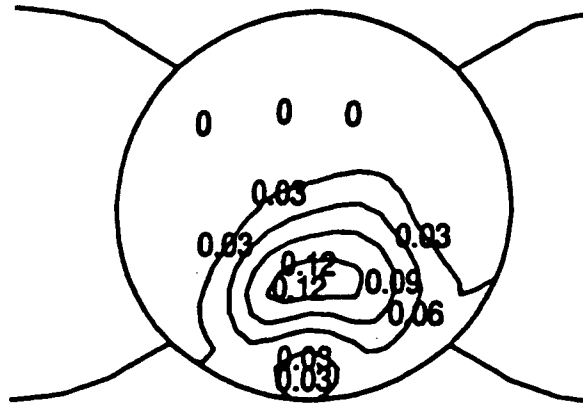
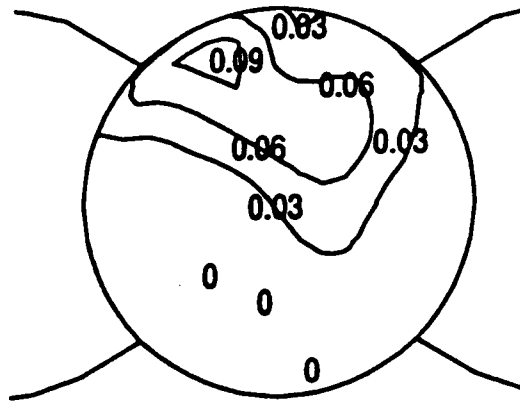


Figure 1.18 - CONCERT 3D results for IMFH tube. Plots of contours of constant vaporized fuel mass fraction are shown in the radial-circumferential plane and the radial-axial plane. The flow in the tube has an 11.5-degree swirl angle. There are 4 spent cooling air holes.



Configuration 2, Non-swirling



Configuration 5A, 11.5-degree swirl

Figure 1.19 - CONCERT 3D results for IMFH tube. Plots of contours of constant vaporized fuel mass fraction are shown in the a radial-circumferential plane in the plane of 4 spent cooling air holes equally spaced around the tube wall. 50% immersion of the fuel injector tube. Results with no swirl (Configuration 2) are compared with 11.5-degree swirl angle (Configuration 5A).

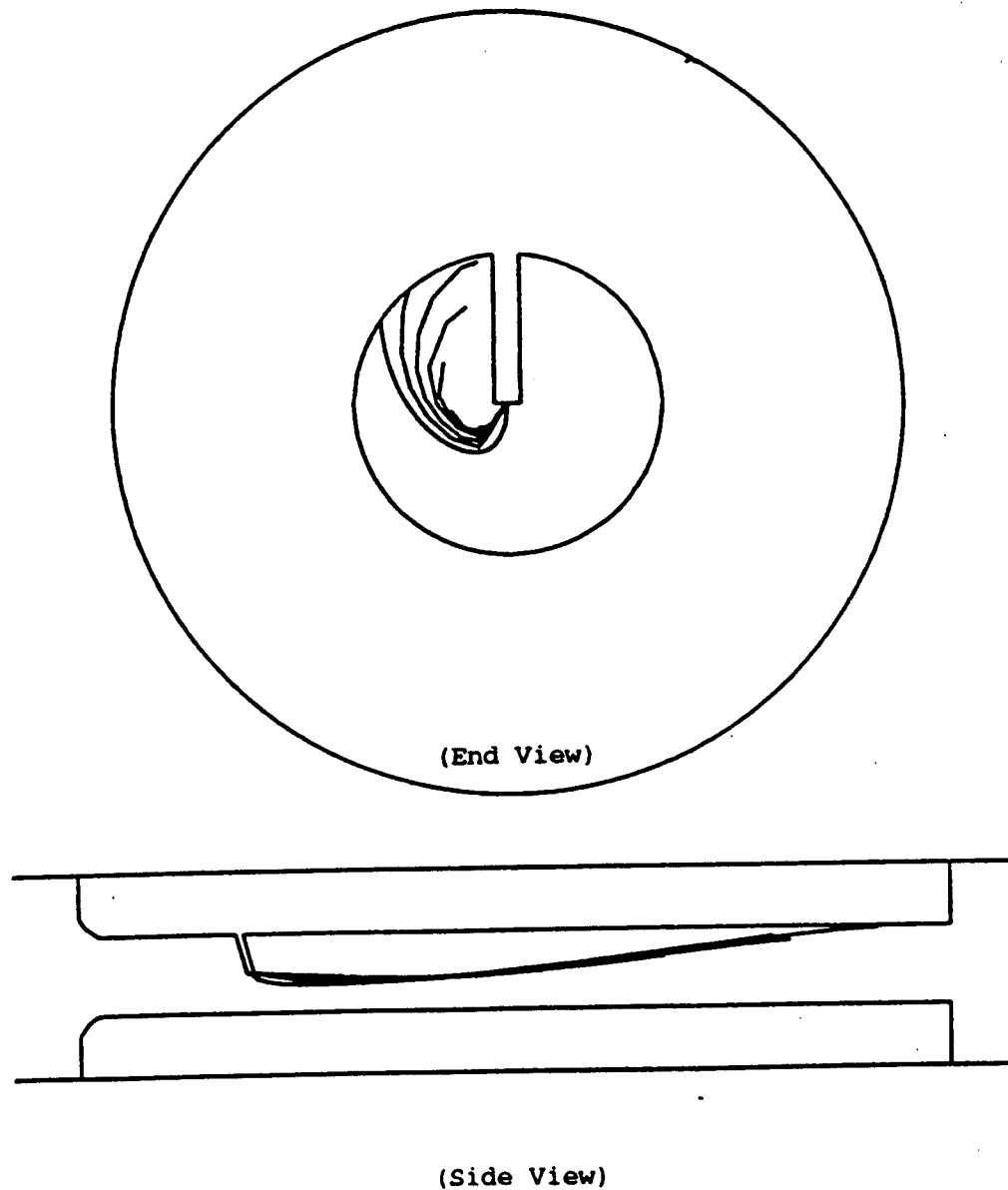
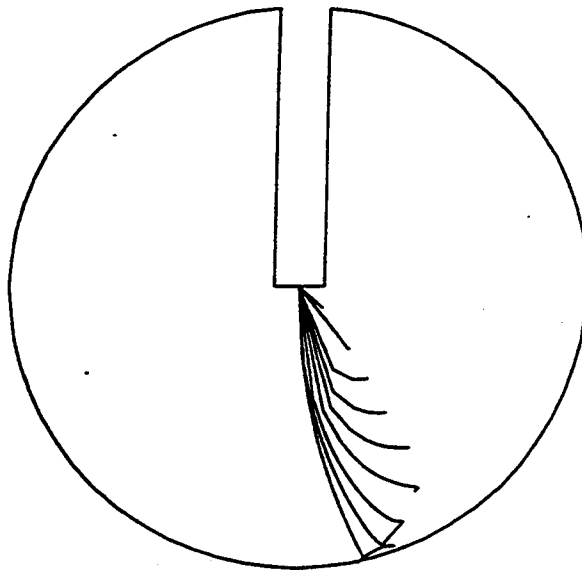
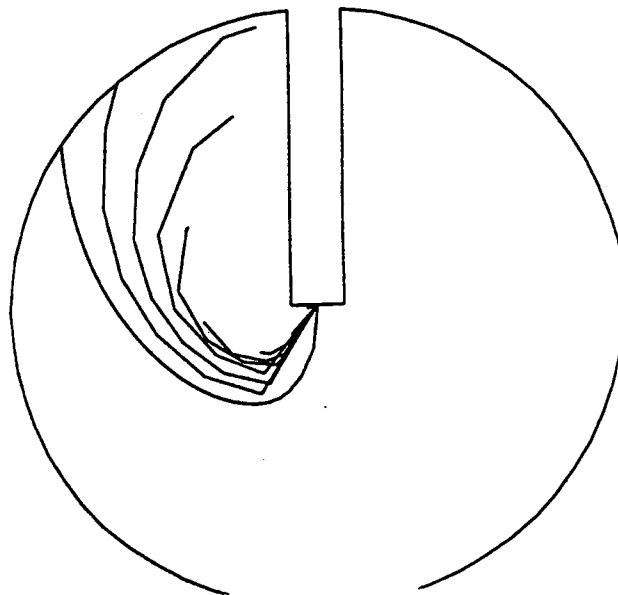


Figure 1.20 - CONCERT 3D results for IMFH tube. Plots of fuel droplet trajectories are shown in the radial-circumferential plane and the radial-axial plane. The 4 spent cooling air holes equally spaced around the tube wall. 50% immersion of the fuel injector tube. Results are with 11.5-degree swirl angle (Configuration 5A).

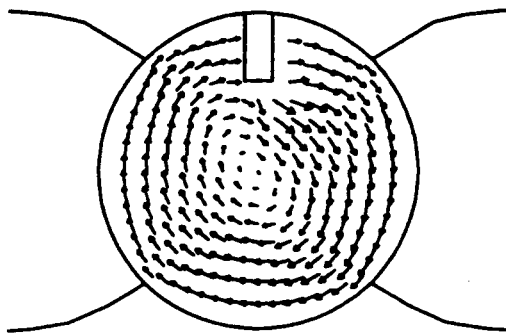


Configuration 2, no swirl



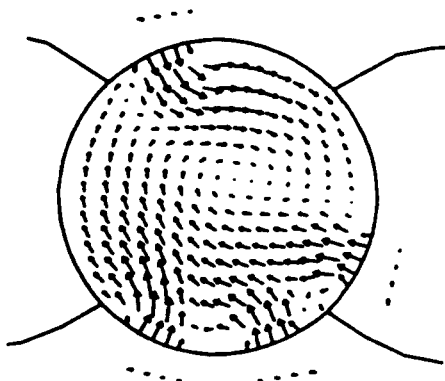
Configuration 5A, 11.5-degree swirl

Figure 1.21 - CONCERT 3D results for IMFH tube. Plots of fuel droplet trajectories are shown in the a radial-circumferential plane. The 4 spent cooling air holes equally spaced around the tube wall. 50% fuel injector immersion. The results for no swirl (Configuration 2) are compared to 11.5-degree swirl (Configuration 5A).



→ 124.828

Plane of the fuel injector



→ 128.948

Plane of the 4 spent cooling air injection holes

Figure 1.22 - CONCERT 3D results for IMFH tube. Configuration 6. Plots of velocity vectors are shown in the radial-circumferential plane in the plane of the fuel injector and in the plane of the 4 spent cooling air holes unequally spaced around the tube wall. The fuel injector immersion is 20%. The flow in the tube has an 11.5 degree swirl angle.

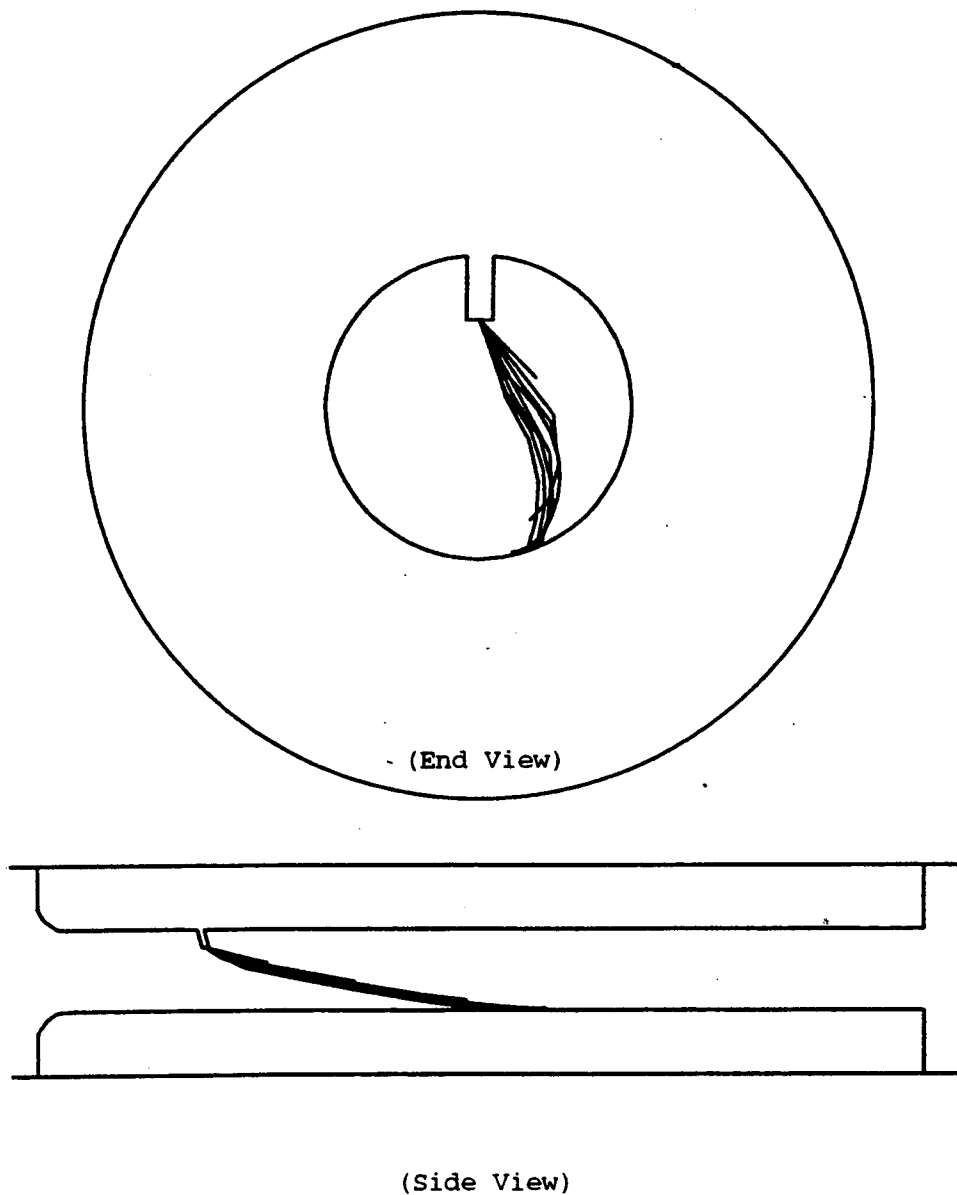
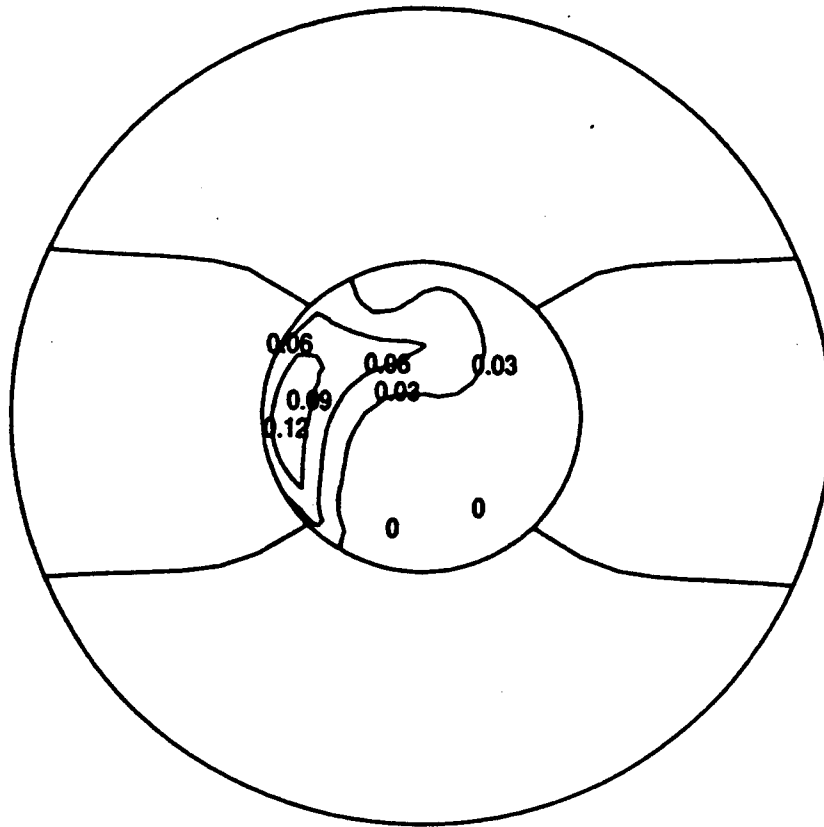
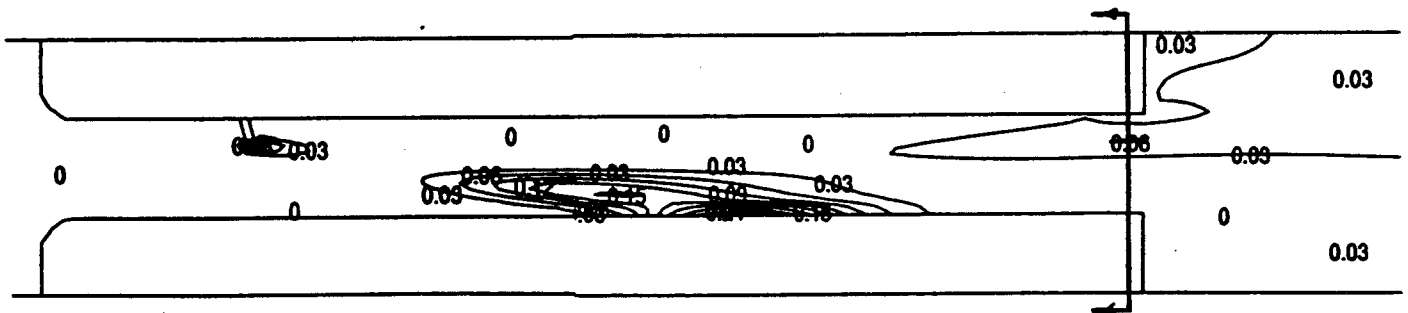


Figure 1.23 - CONCERT 3D results for IMFH tube. Plots of fuel droplet trajectories are shown in the radial-circumferential plane and the radial-axial plane. The flow in the tube has an 11.5-degree swirl angle. The fuel injector has a 20% immersion. The 4 spent dome cooling air holes are unequally spaced.



PDF-MEAN
(End View)



(Side View)

Figure 1.24 - CONCERT 3D results for IMFH tube. Plots of contours of constant fuel vapor mass fraction are shown in the radial-circumferential plane and the radial-axial plane. The flow in the tube has an 11.5-degree swirl angle. The fuel injector has a 20% immersion. The 4 spent dome cooling air holes are unequally spaced.

developed). An engineering flowpath sketch of the original MRA is shown in Figure 1.25. All the design variations of the original MRA combustor have in common a single-annular dome of Cyclone Swirler pilots (30 to 36 cups) with the IMFH mixer tube injection from the outer combustor liner (16 - 23 IMFH tubes per Cyclone Swirler). The IMFH mixer tube arrangement, jet deflection angle, and swirl angle orientation were investigated in the CFD modeling. Ground idle, subsonic cruise, and supersonic cruise conditions were simulated. At ground idle, all the Cyclone Swirlers were fueled and the IMFH mixers unfueled. At subsonic cruise, a small fraction (4 - 6 per cup) of the IMFH mixers were fueled at an equivalence ratio equal to the Cyclone Swirler pilots. At supersonic cruise, all IMFH mixers were fueled at the equivalence ratio of the pilot swirlers.

In the initial MRA design, idle and subsonic cruise conditions were characterized by peaked exhaust gas temperature profiles caused by poor mixing patterns of the unfueled IMFH jets. Figure 1.26 shows the grid for the MRA combustor model. Figure 1.27 shows some typical CFD model results of an early version of the MRA combustor at subsonic cruise conditions.

The modeling activities focused on trying to determine a design which yielded increased penetration of the unfueled IMFH tube exit jets so that the turbine inlet profile was acceptable during partial fuel staging. The critical cycle point chosen was subsonic cruise. The independent design parameters included were the IMFH mixer tube arrangement on the outer liner, the IMFH tube jet axial injection angle, and the IMFH circumferential (swirl) injection angle. The principle barrier to obtaining good exit temperature profiles was limited penetration of the unfueled IMFH jets. Three strategies for maximizing the penetration of the unfueled IMFH jets were investigated:

1. Placement of the IMFH jets in the wakes of the upstream IMFH jets.
2. Use of the jet angle to optimize the penetration of the IMFH jets.
3. Maximize the utilization of the vortex from the Cyclone Swirler pilots to augment the penetration by using alternating swirl directions in the pilots.

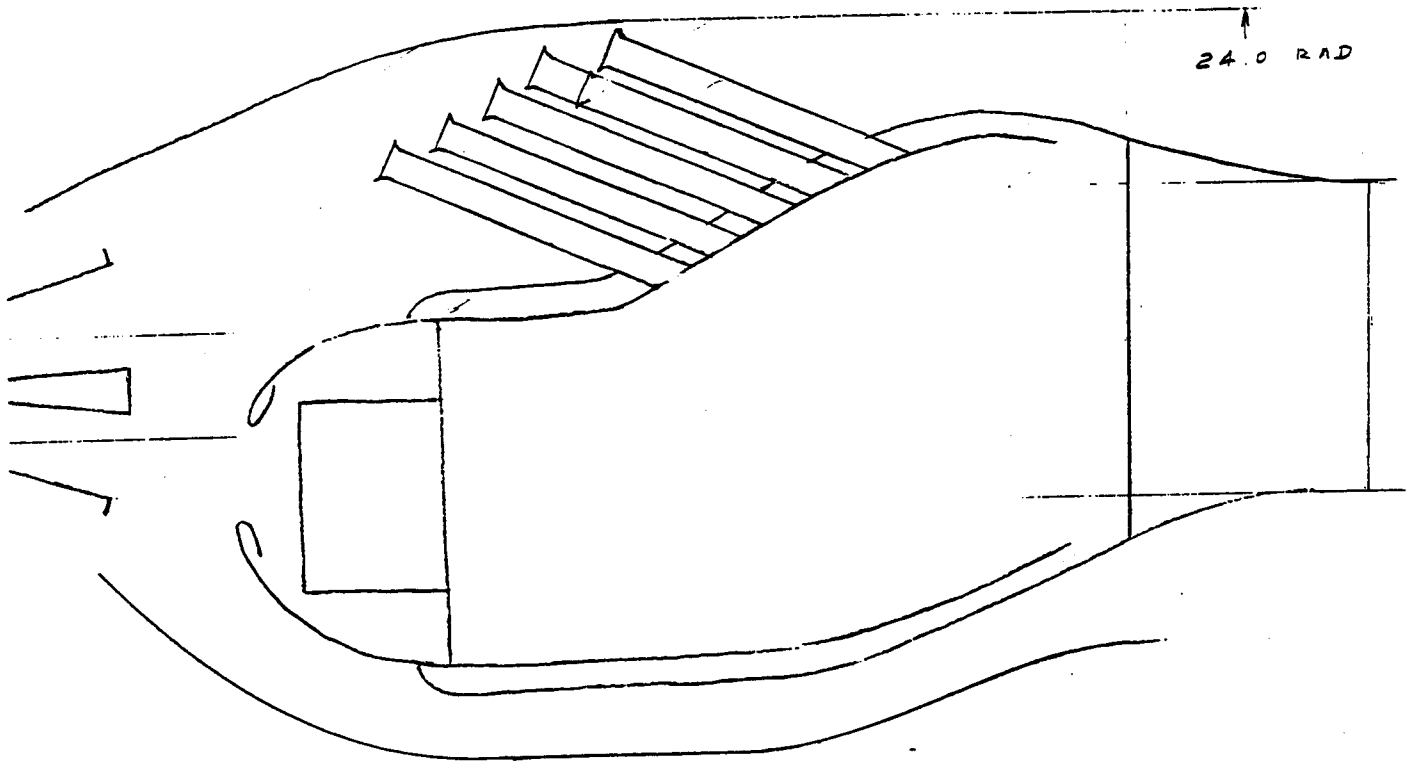


Figure 1.25 - Engineering flowpath sketch of an early Multi-Stage Radial-Axial (MRA) combustor system.

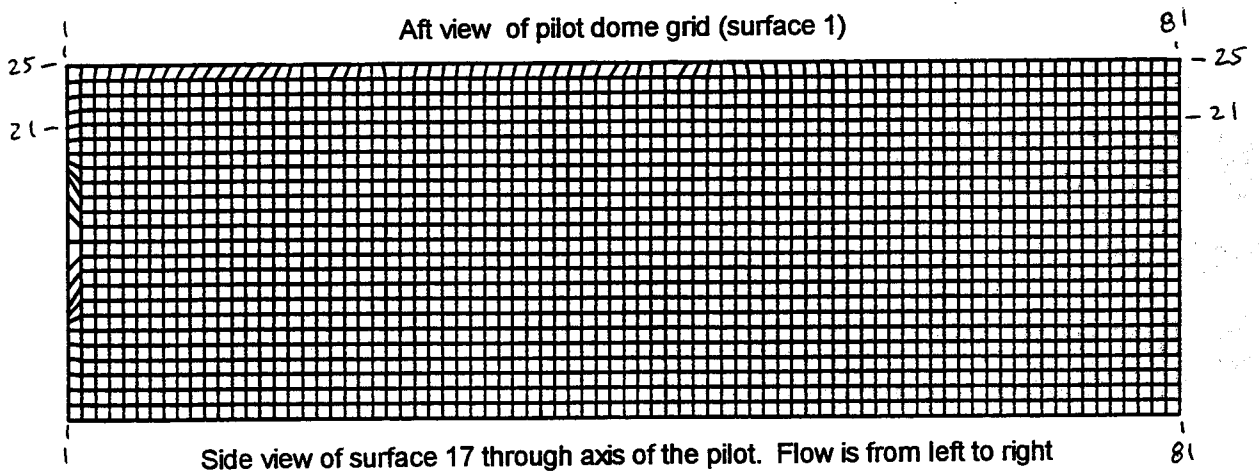
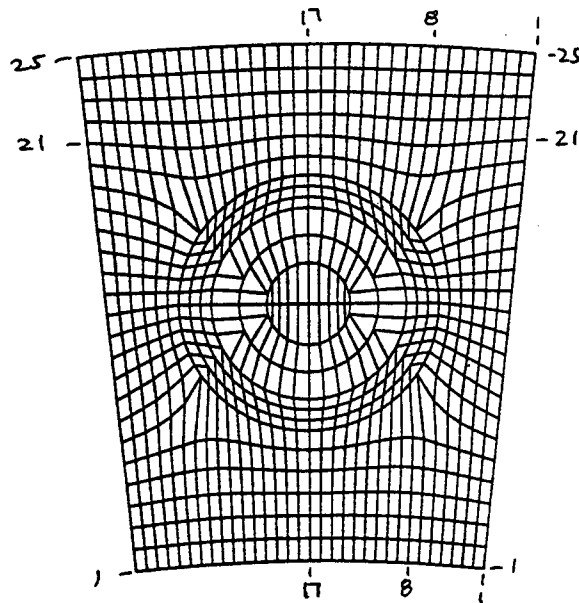
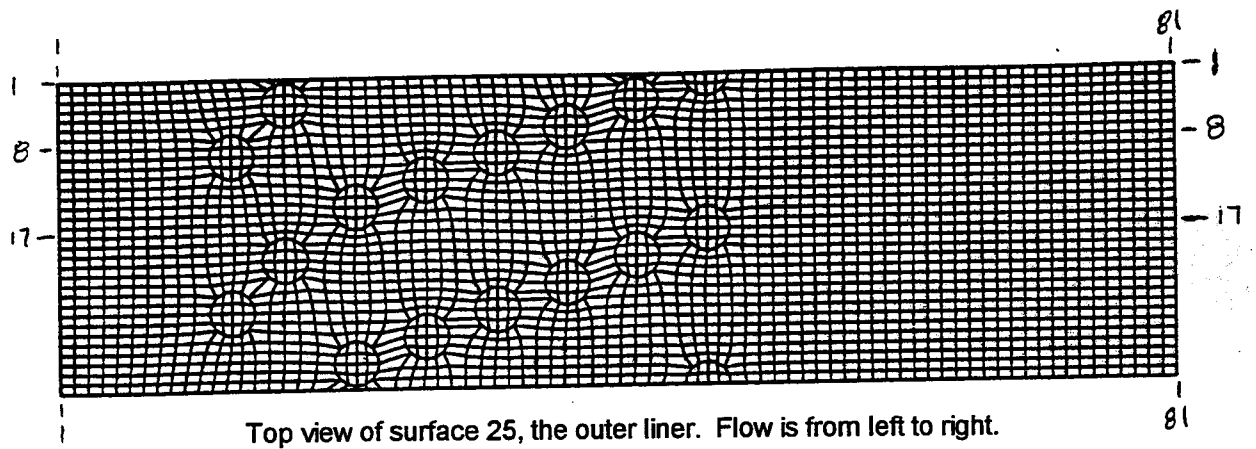
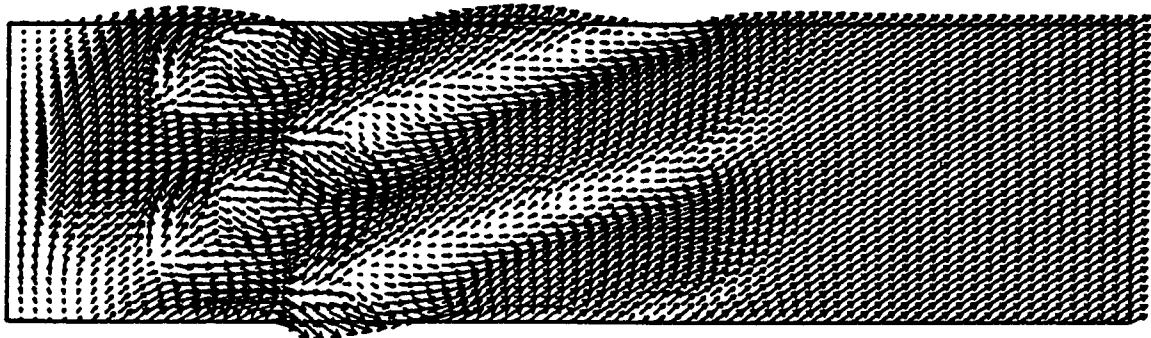
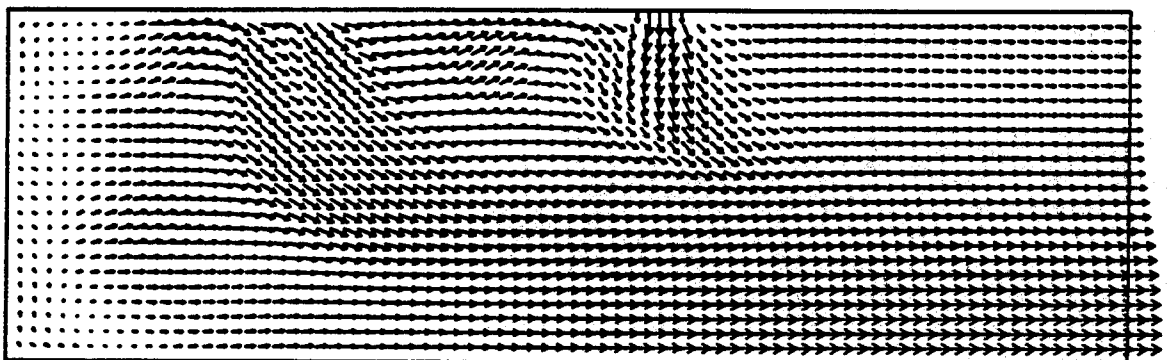


Figure 1.26 - Grid for the CONCERT 3D CFD model of a version of the Multi-Stage Radial-Axial (MRA) combustor. Shown are the top view of the grid, the pilot dome and the side view of the surface through the axis of the pilot. This version placed the jets from the IMFH tubes in the wakes of the upstream jets to maximize their penetration.



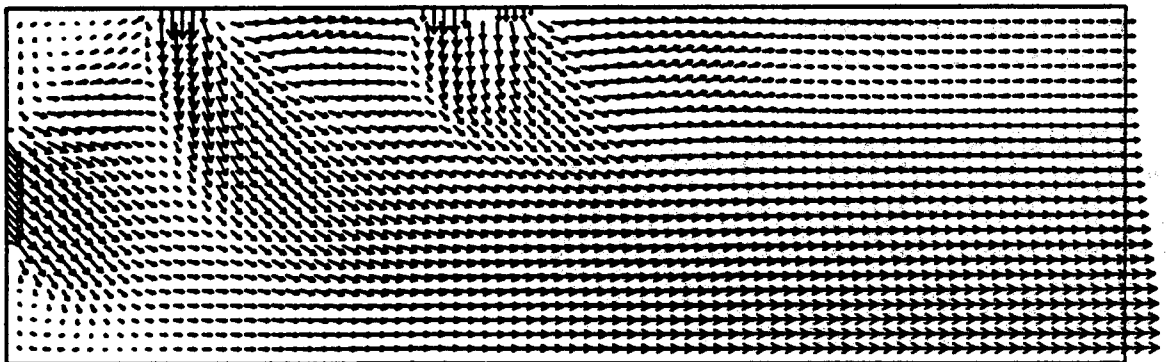
→ 239.146

Velocity vectors near outer liner. Surface 21. Flow is from left to right.



→ 449.978

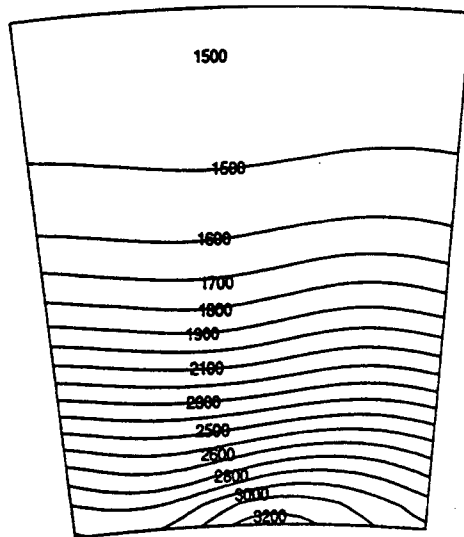
Velocity vectors in radial-axial plane. Surface 1 of grid. Flow is from left to right.



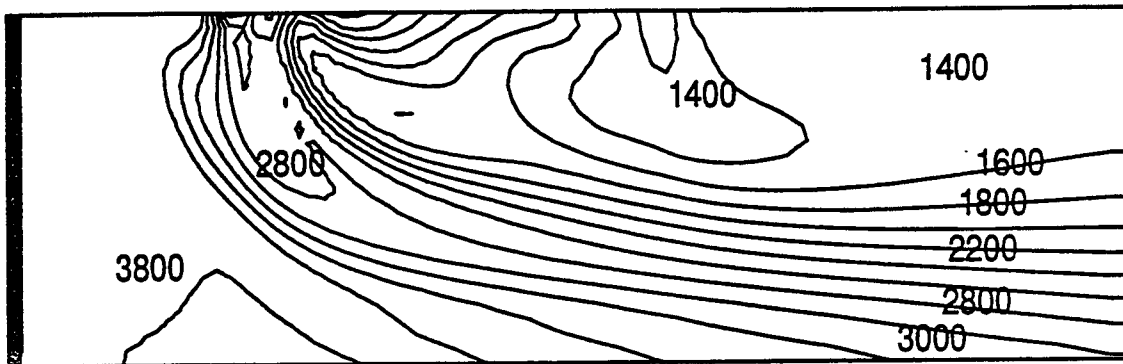
→ 458.633

Velocity vectors in radial-axial. Surface 8 of grid. Flow is from left to right.

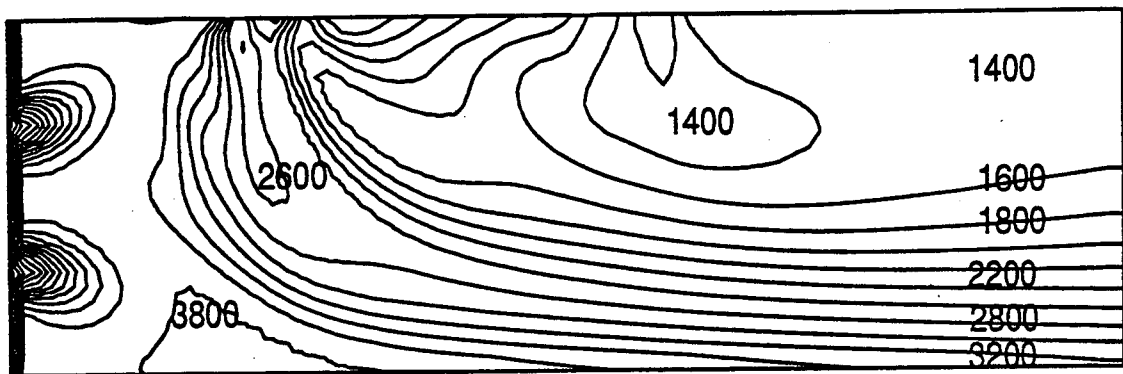
Figure 1.27a - CONCERT 3D CFD model velocity results for a version of the Multi-Stage Radial-Axial (MRA) combustor. This version placed the jets from the IMFH tubes in the wakes of the upstream jets to maximize their penetration. Subsonic cruise conditions are simulated. Shown are velocity vector fields on a surface near the outer liner and two surfaces in the radial-axial plane.



Temperature contours in degrees R at the exit plane.



Temperature contours in radial-axial plane. Surface 1 of grid. Flow is from left to right.



Temperature contours in radial-axial plane. Surface 17 of grid. Flow is from left to right.

Figure 1.27b - CONCERT 3D CFD model temperature results for a version of the Multi-Stage Radial-Axial (MRA) combustor. This version placed the jets from the IMFH tubes in the wakes of the upstream jets to maximize their penetration. Subsonic cruise conditions are simulated. Shown are the exit plane temperature contours and the temperature contours on two radial-axial planes. Temperatures are in degrees R.

The best profile/pattern factor predicted by the CFD after applying the first two strategies was 1.8/1.8 at subsonic cruise. These profiles were inboard peaked. These profile factors were calculated as $(T_M - T_3)/(T_A - T_3)$. The profile factor defines T_M as the maximum circumferentially-averaged radial temperature, while pattern factor defines T_M as the maximum local temperature. T_A is the average combustor exit temperature.

For the third strategy, pairs of the Cyclone Swirler pilot were arranged in alternating swirl directions. The alternating swirl directions augment the strength of the Cyclone Swirlers, resulting in stronger downward and upward flow fields for improved mixing. A two-cup sector was modeled which still allowed the use of the periodic boundary condition feature of CONCERT 3D. The grid is shown in Figure 1.28. Figures 1.29 and 1.30 characterize the inlet flow field for the MRA combustor and compare it to the inlet flow field of the Stepped-Dome combustor. IMFH mixer arrangement and jet angle were selected to enhance mixing in the MRA's flow field. In Figure 1.30, the circumferential velocity component of the flow leaving the IMFH tubes and entering the combustor is a result of the canted angle of the tubes. Table 1.3 compares the input parameters for the MRA and Stepped-Dome subsonic cruise CFD models.

Table 1.3 - Inlet Parameters for Subsonic Cruise CFD Models		
Parameter	MRA	Stepped-Dome
Sector	2-Cup	1-Cup
Inlet Temperature	1073 R	1073 R
Pressure (psia)	86.18	86.18
Local equivalence ratio	0.775	0.775
IMFH tubes/cup	18	10
Fired IMFH tubes/cup	4	2.5
Side wall boundary condition	Periodic	Wall
Inlet fuel vaporization	90%	100%

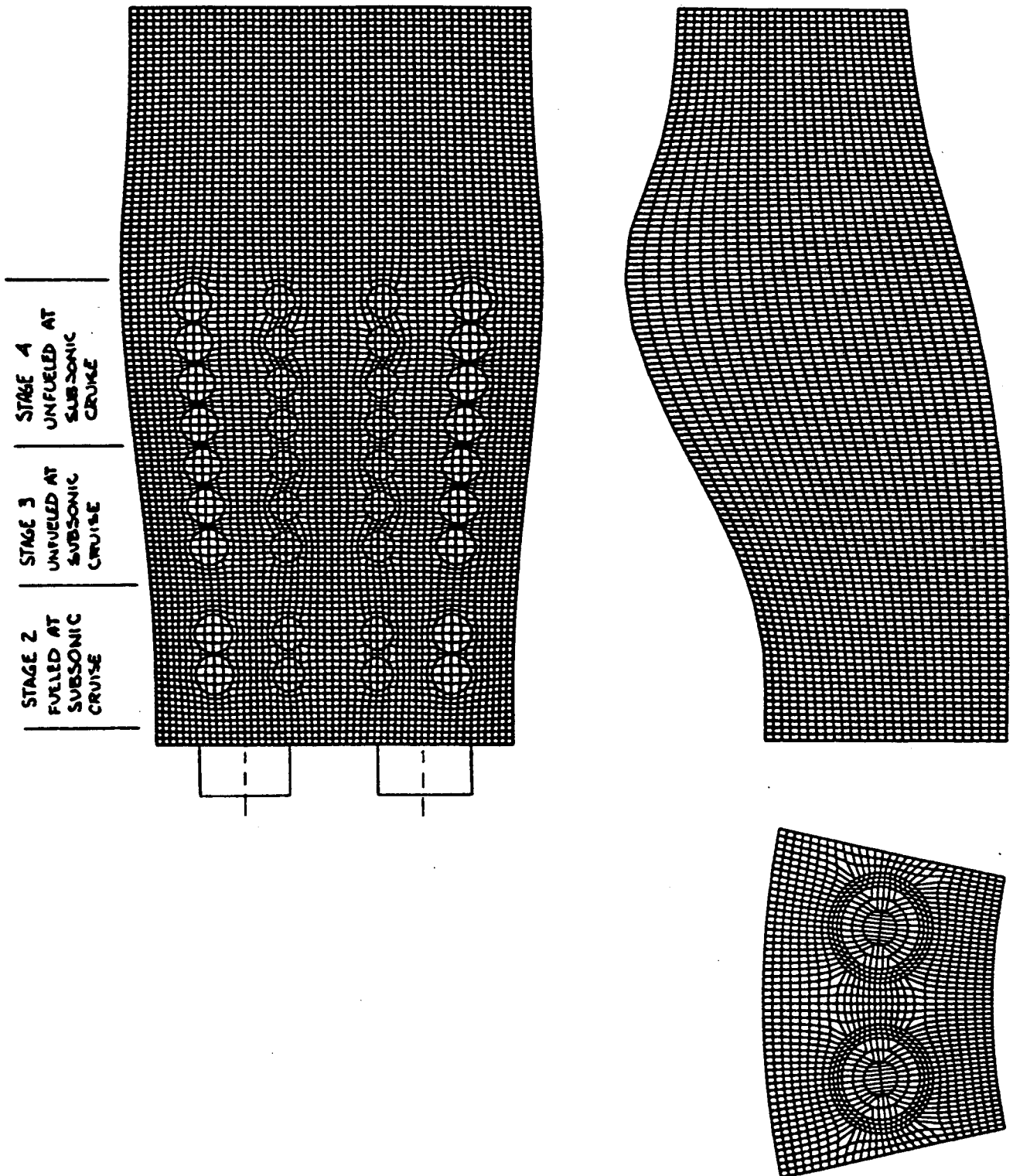
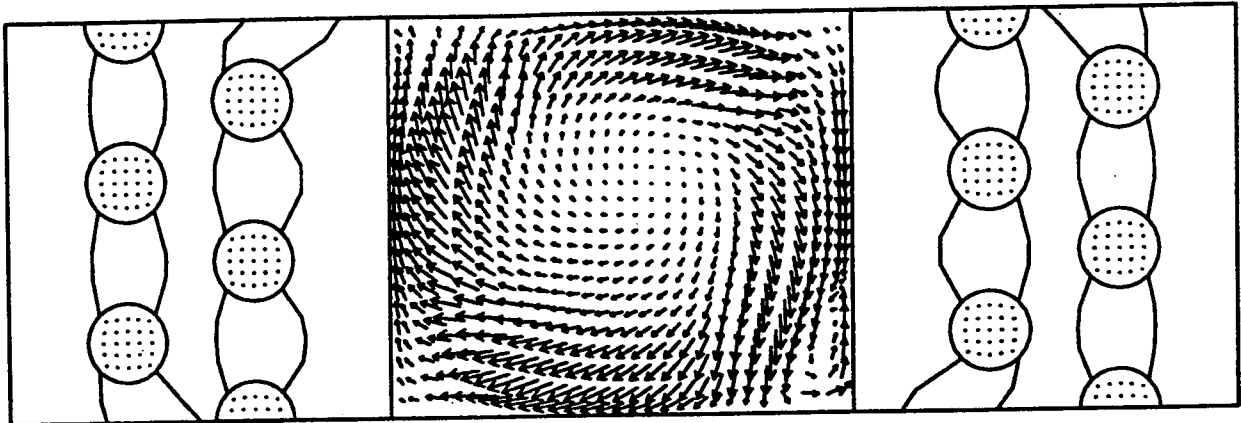
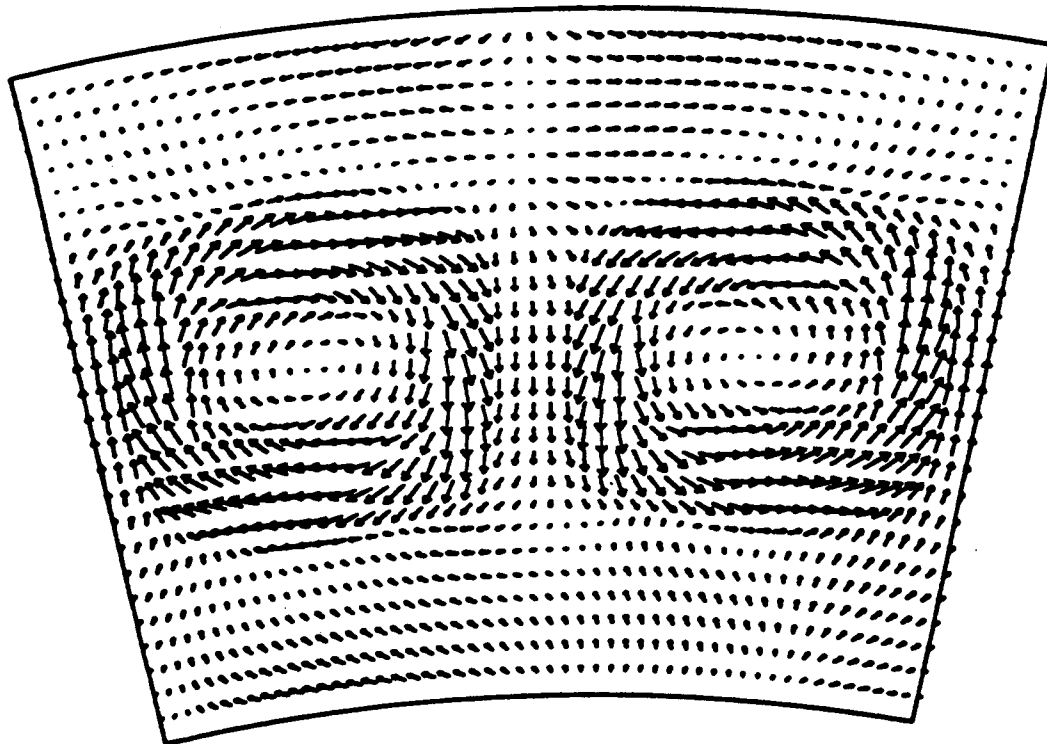


Figure 1.28 - Grid for the CONCERT 3D CFD model of a version of the Multi-Stage Radial-Axial (MRA). This version placed the IMFH tubes so the jets penetration was enhanced by the twin vortices initiated by the pilots. The pilot swirl direction alternated from cup-to-cup.



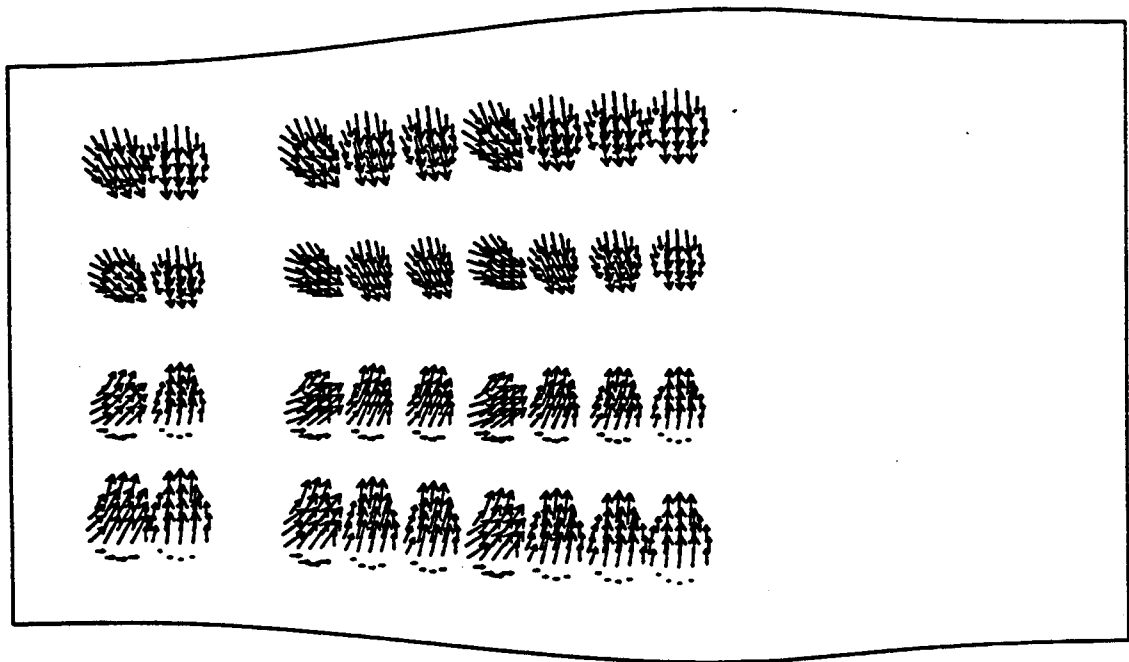
→ 262.595



→ 246.928

Figure 1.29 - Comparison of CONCERT 3D results for the velocity vectors at the dome of the Stepped-Dome Rectangular Sector (top) and the MRA combustor (bottom). The scales are different.

Top View Direction Surface Number 29



→ 424.21

Figure 1.30 - CONCERT 3D results for the velocity vectors at the IMFH tube exits at the outer liner of the MRA combustor.

Table 1.4 summarizes some of the results of the two models.

Table 1.4 - Results of Subsonic Cruise CFD Models		
Parameter	MRA	Stepped-Dome
CO EI (g/kg)	1.11	5.15
Combustion efficiency	99.9%	99.8%
Profile factor	1.26 @ 83% span	1.72 @ 75% span
Pattern factor	2.02 @ 41% span	2.01 @ 78% span

Further results of these subsonic cruise CFD models are compared in Figures 1.31 through 1.35 at subsonic cruise conditions. Figures 1.31 and 1.32 compare the internal velocity flowfields of the stepped-dome and the MRA in radial-axial planes. In the stepped-dome, the plane is through the axis of the Cyclone Swirler pilot. In the MRA, the plane is through the edge of the pilot and the exits of a row of IMFH tubes. The temperature contours for the two combustors are compared in the radial-axial plane in Figure 1.33 and the radial-circumferential plane at the exit in Figure 1.34. Performance attributes of the MRA combustor included a center-peaked exit gas temperature profile, with a cold spot at the inner liner between cups. Figure 1.35 shows the circumferentially-averaged combustor exit temperature profiles and the envelope of the peaks for the two combustors corresponding to the profile and pattern factors in Table 1.4.

Based upon these initial results for the alternating rotation of the pilots in the MRA, the positions of the IMFH tubes that were unfired during subsonic cruise were adjusted so that the tubes that were “aimed” at the hottest spots. This change improved the MRA’s exit temperature profile/pattern factor to 1.095/1.33 at the A5B subsonic cruise cycle condition, as shown in Figure 1.36. This was accomplished at the price of slightly irregular arrangement of the IMFH tubes. Figure 1.37 shows the inlet velocity field to the combustor resulting from the new tube arrangement. The location of the exits of the tubes and the velocity vectors at the exits shown in Figure 1.37 should give the reader a rough understanding of the tube arrangement. There is further discussion about this combustor in Section 6. A combustor layout of one attempt to fit the new tube arrangement into an engine flowpath is shown there in Figure 6.4.

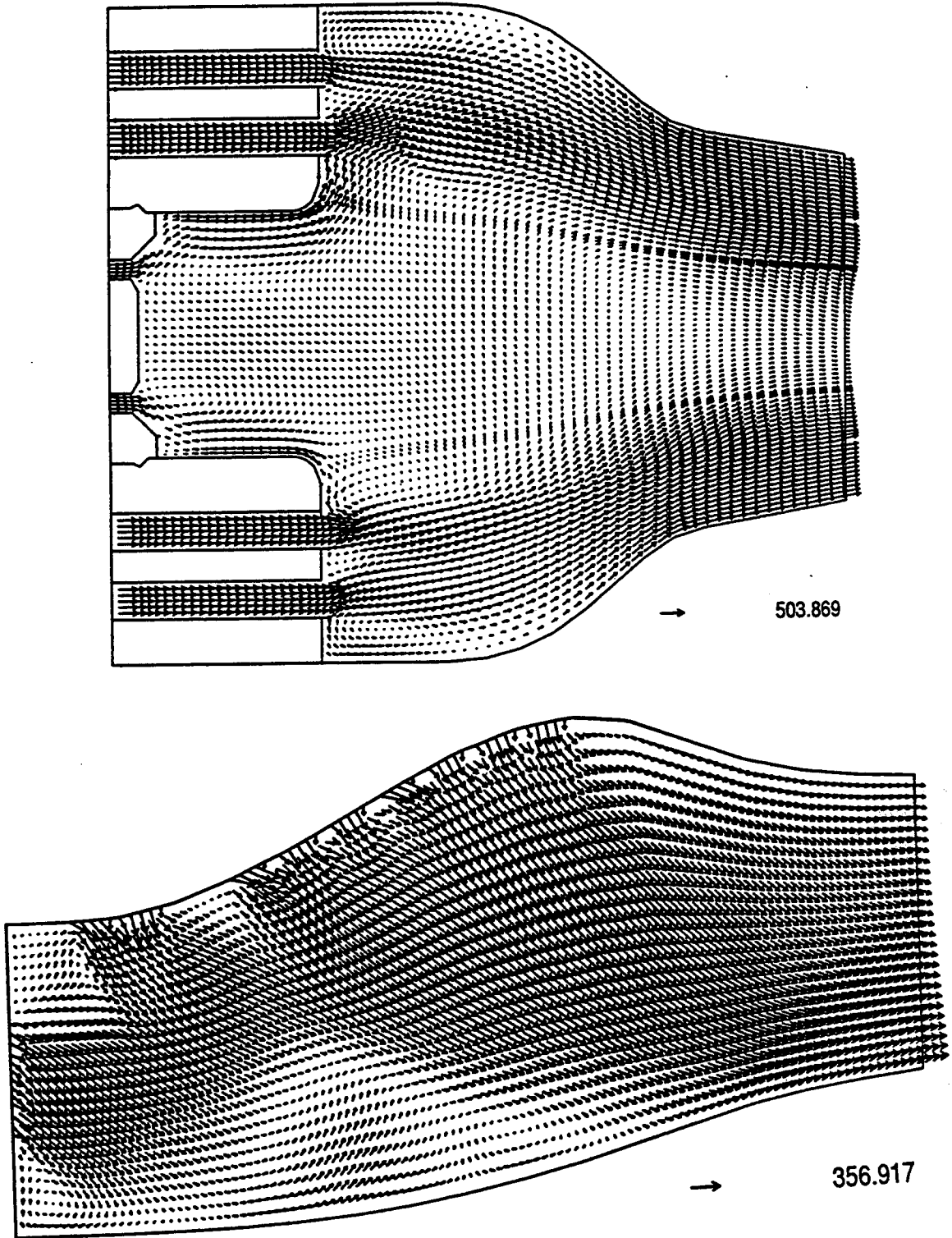
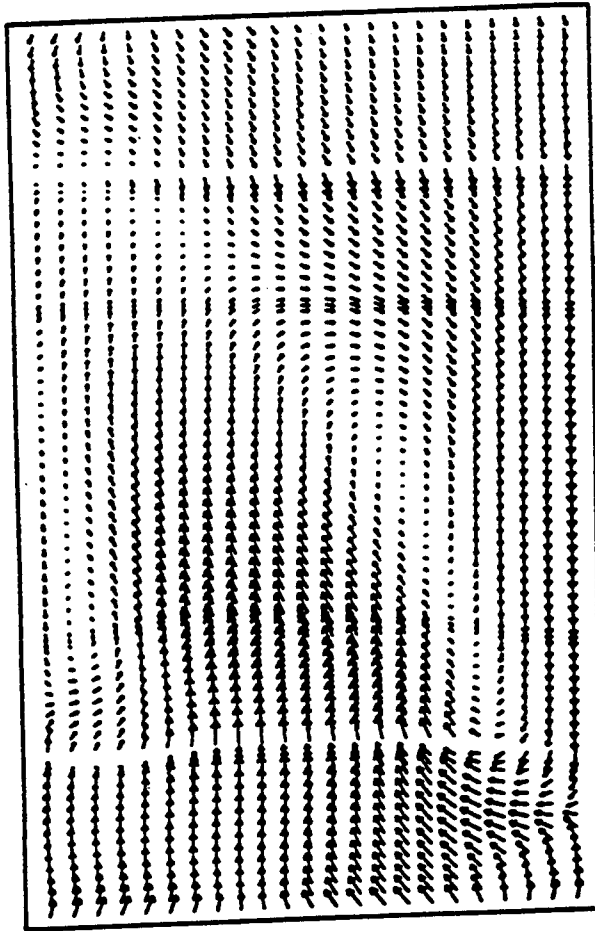
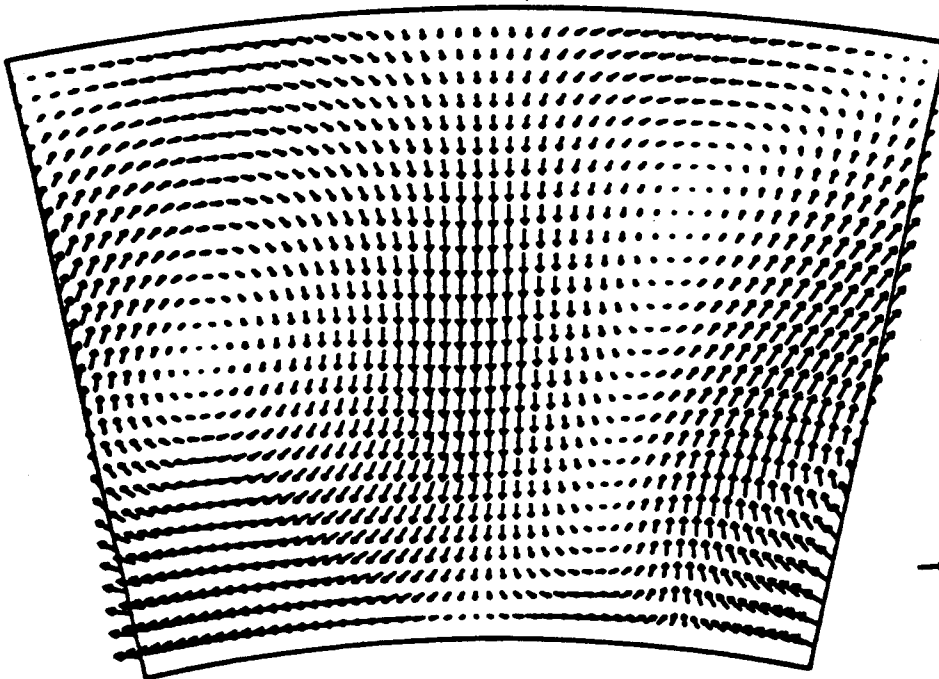


Figure 1.31 - Comparison of CONCERT 3D results for the velocity vectors in the radial-axial plane on a surface through the axis of the Cyclone Swirler pilot in the stepped-dome rectangular sector combustor (top) and a surface through the edge of the pilot and through a row of the IMFH tube exits in the MRA combustor (bottom). The scales for the results are different.



→ 113.178



→ 308.281

Figure 1.32 - Comparison of CONCERT 3D results for the velocity vectors at the exit planes of the stepped-dome rectangular sector combustor (top) and the MRA combustor (bottom).

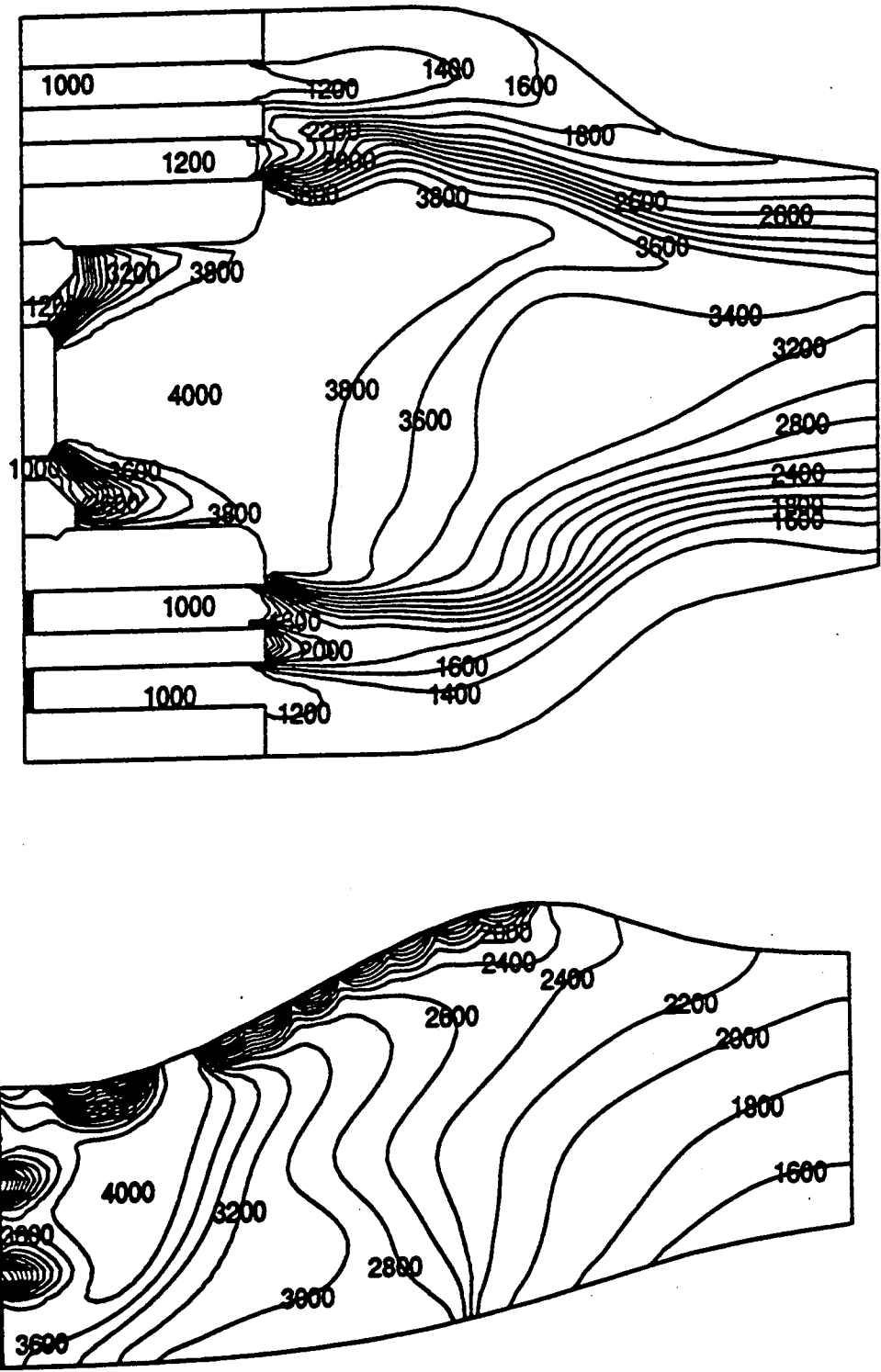


Figure 1.33 - Comparison of CONCERT 3D results for contours of constant temperature in degrees R on a surface through the axis of the Cyclone Swirler pilot of the stepped-dome rectangular sector combustor (top) and the MRA combustor (bottom).

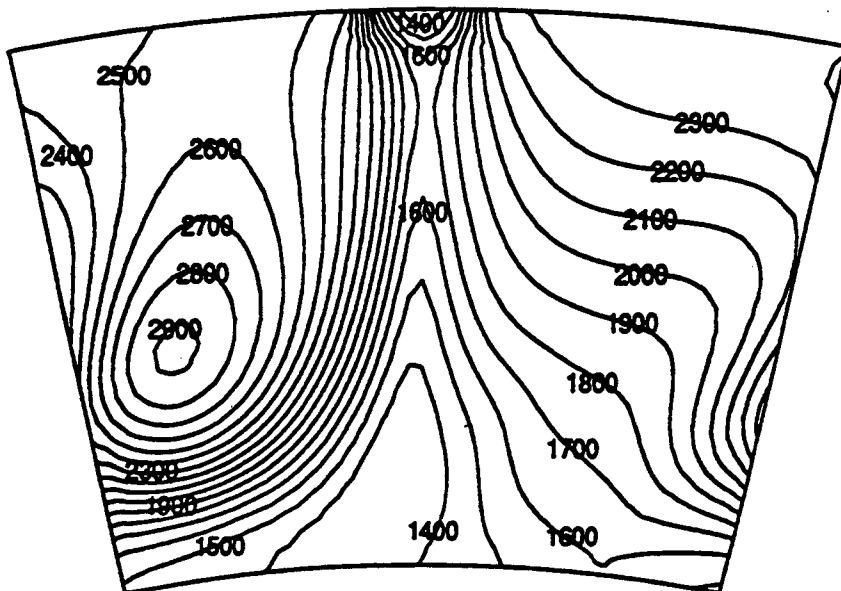
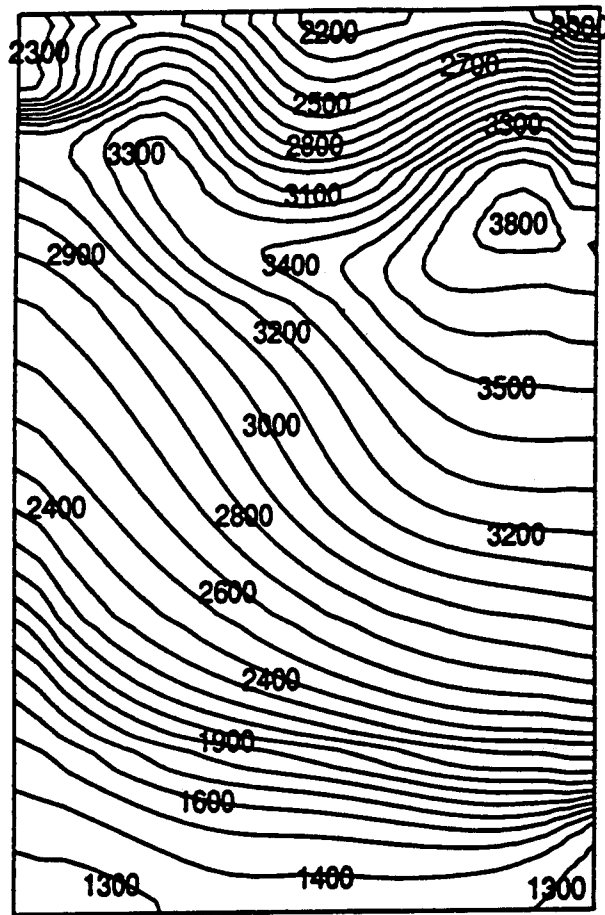
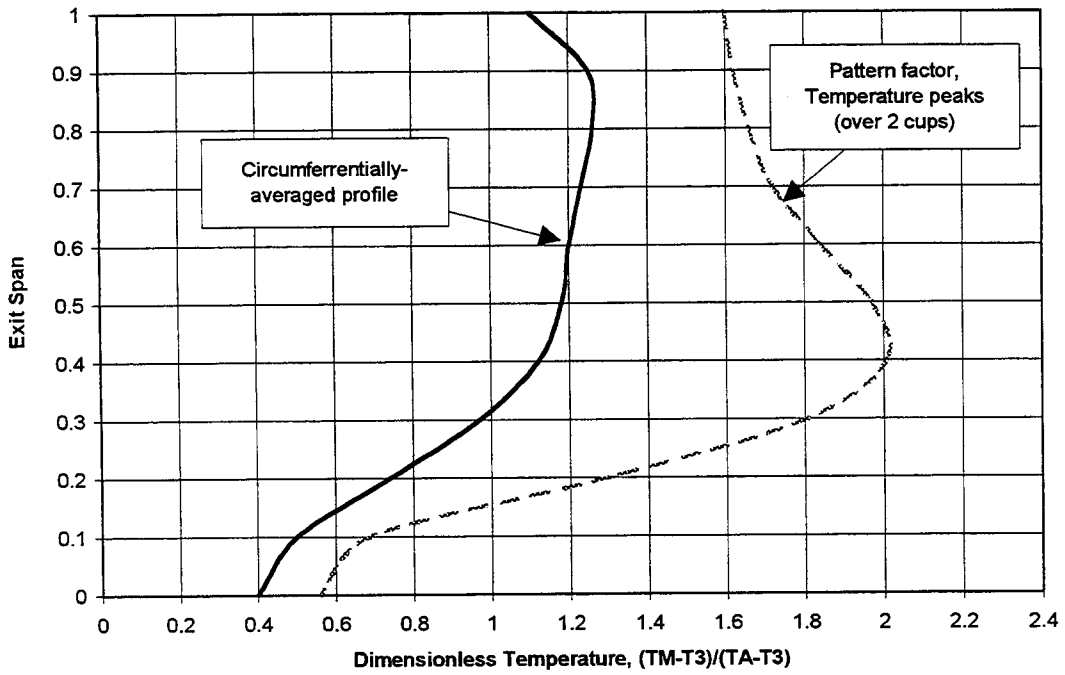


Figure 1.34 - Comparison of CONCERT 3D results for contours of constant temperature in degrees R at the exit planes of the stepped-dome rectangular sector combustor (top) and the MRA combustor (bottom).

MRA Combustor Before Final IMFH Tube Rearrangement at Subsonic Cruise



Stepped-dome Rectangular Sector at Subsonic Cruise

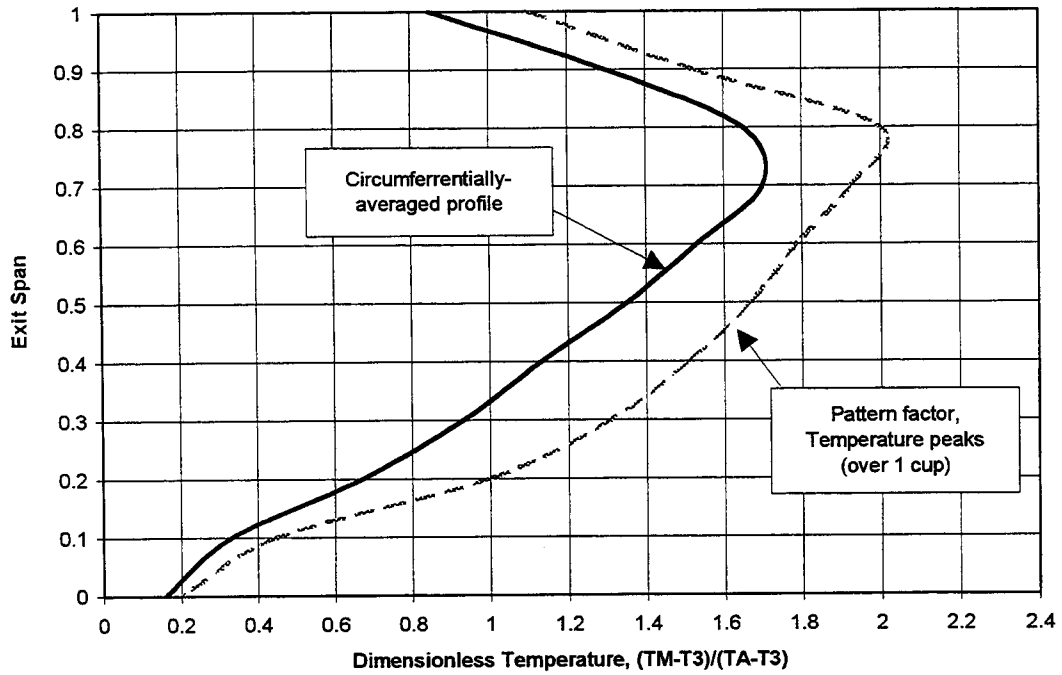


Figure 1.35 - Comparison of CONCERT 3D results for the Pattern and Profile Factors of the stepped-dome rectangular sector and the MRA combustors.

MRA Combustor With Final IMFH Tube Arrangement at Subsonic Cruise

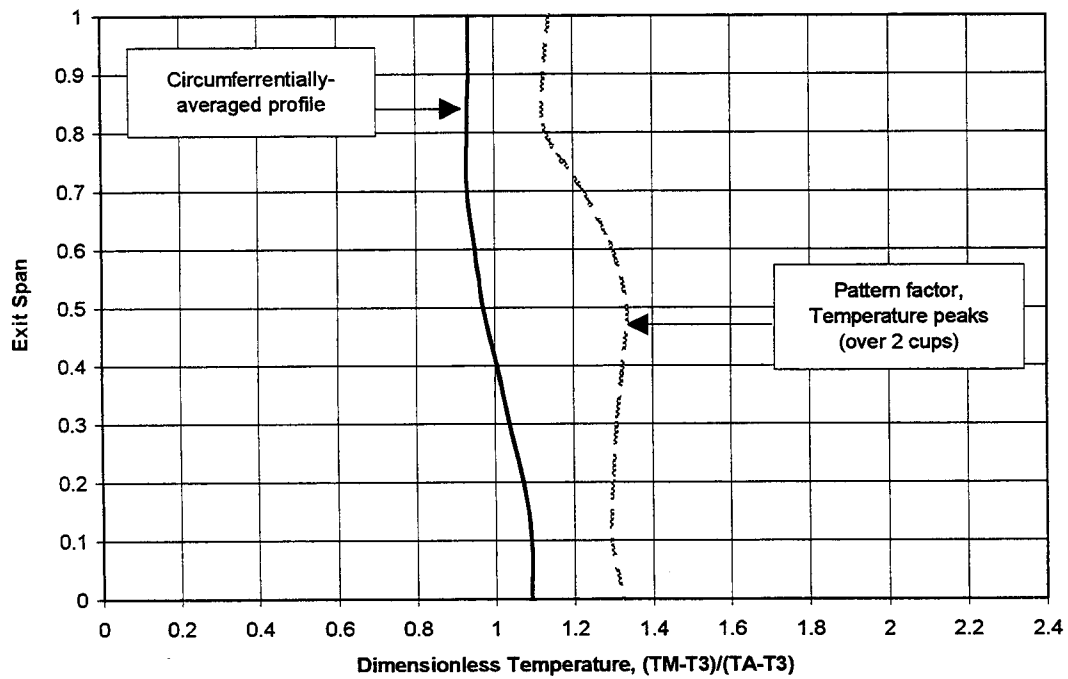
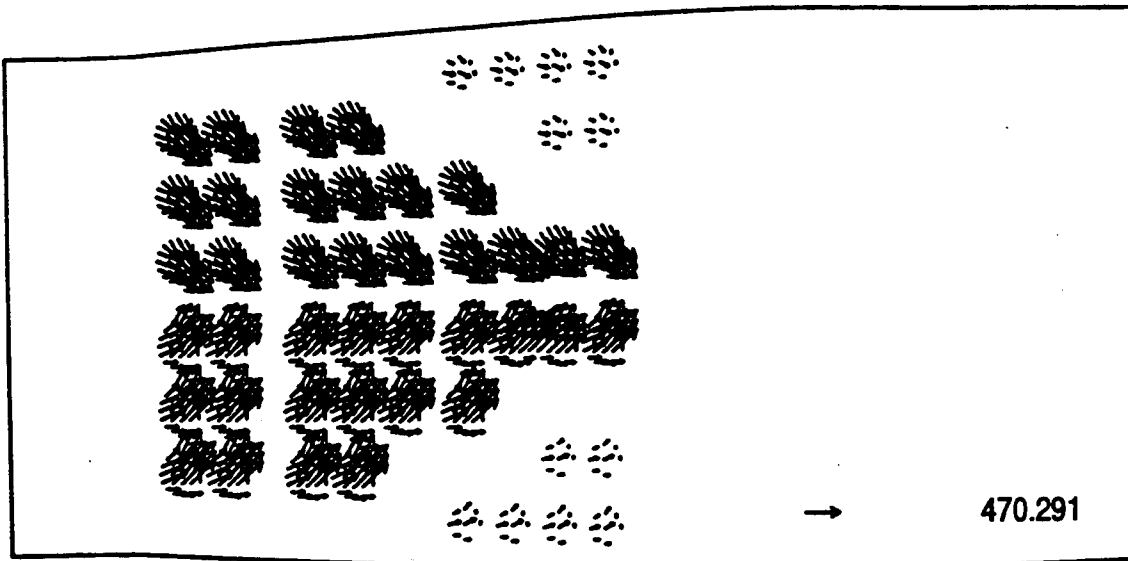
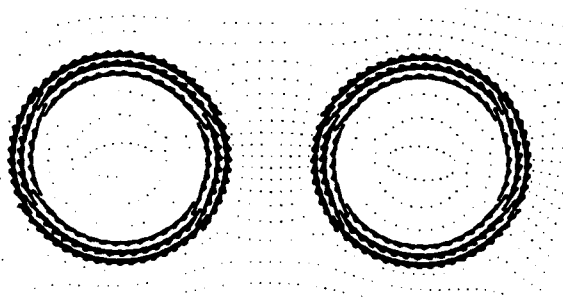


Figure 1.36 - CONCERT 3D results for the Pattern and Profile Factors of the MRA combustor with its IMFH tubes positioned to minimize hot streaks at the exit.

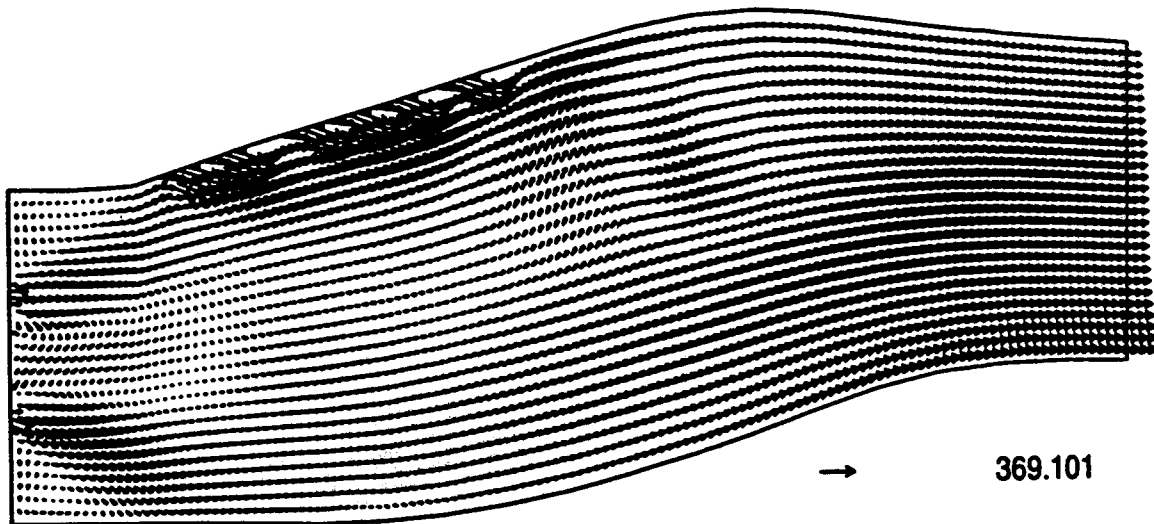
Figure 1.38 shows the velocity field and the temperature field at the exit plane using the new tube arrangement in the MRA. Note that the exit temperature field is asymmetrical, even though the model and all the boundary conditions are symmetrical with respect to the plane bisecting the model between the two cups. That this occurs physically, should not be surprising. The two vortices move to locations giving them more space. It is reassuring that CONCERT 3D predicts the asymmetry, despite the symmetry of the inputs to the model. These exit temperature profile results indicate that the MRA has the potential for a much flatter average circumferential temperature profile during partial fuel staging, making this MRA concept attractive in terms of turbine efficiency and turbine life.



Top View

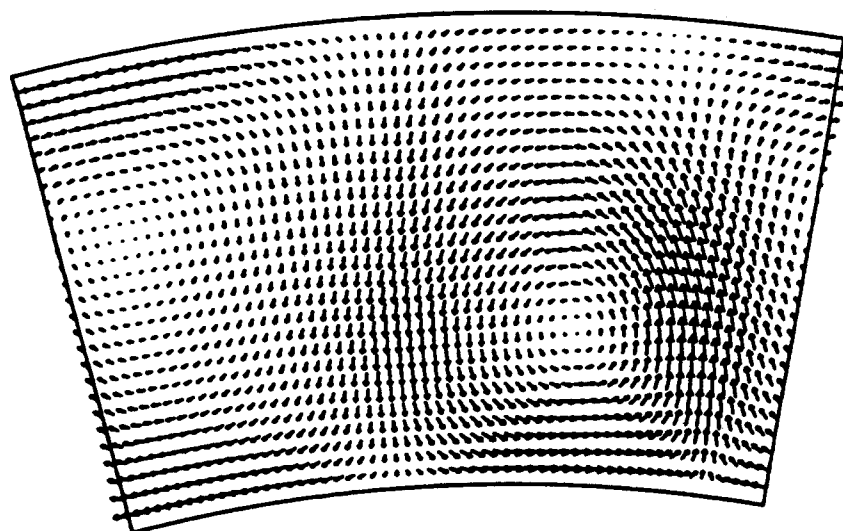


Front View (FLA)



Side View

Figure 1.37 - CONCERT 3D results for velocity vectors in the MRA combustor at the exit of the IMFH tubes at the outer liner, at the pilot dome, and on a radial-axial surface through the axis of the cyclone swirler pilot.



→ 154.836

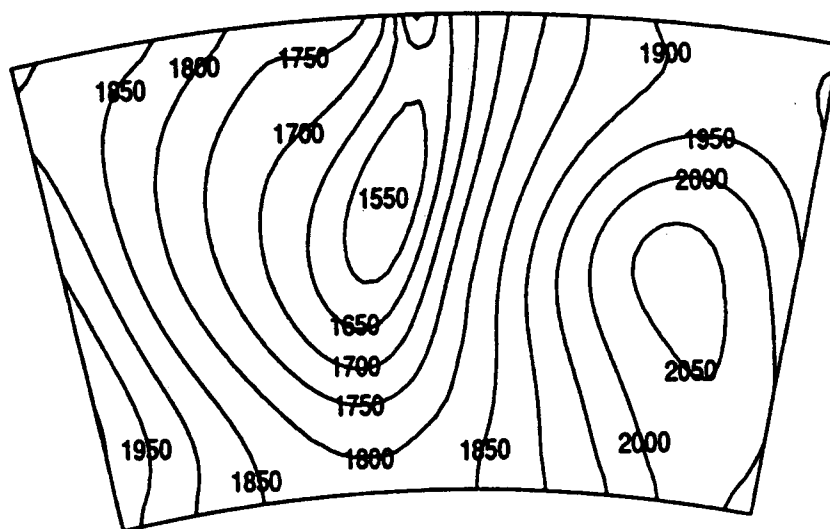


Figure 1.38 - CONCERT 3D results for the for the velocity vectors and contours of constant temperature at the exit plane of the MRA combustor with its IMFH tubes positioned to minimize hot streaks at the exit.

1.2 Spreadsheet Models of Combustor Systems

Spreadsheet models of the HSCT combustor systems were first generated in the conceptual design phase of APT Task 5. The models were motivated by the convenience of automating tedious calculations which had to be repeated each time a combustor system design changed.

1.2.1 General Description of Spreadsheet Combustor System Models

The spreadsheet combustor system models were generated in several different applications, including Excel (Microsoft, Inc.) and Matlab (MathWorks, Inc.). Most of the models were generated using Mathcad (Mathsoft, Inc.). The choice of application depends mainly on the engineer's preferences. A generic outline of the format of the spreadsheet model follows.

1. Steady-state engine cycle data is read as input. Generally, these data include altitude, Mach number, power code, thrust, fuel flow rate, air flow rates, cycle pressures, cycle temperatures, and mission time (for mission data). Early models used only about two dozen mission points. Later models used hundreds of cycle points covering the entire flight envelope, as well as specific mission profiles. Special cycle points such as those used to calculate the landing-takeoff (LTO) emissions parameters were included.
2. Specific combustor performance correlations are defined. A correlation for flame temperature calculations is always necessary, since flame temperature is the principle factor in determining the emissions performance of an LPP combustor. Since emissions performance is the primary metric of the HSCT combustor, emissions correlations were always provided. Optional correlations which might be supplied depending on the refinement of the model and which performance projections were desired, are: 1) stability (lean blow out); 2) diffuser

performance in terms of static pressure recovery; 3) fuel jet penetration; 4) heat transfer; and 5) combustor exit profile. These correlations come from text books, the open literature, proprietary design practices, or combustor data bases developed in the HSR Program.

3. The diffuser system design is defined and its performance in terms of static pressure recoveries is estimated using correlations. This step was omitted in early models and the pressure recoveries at the combustor's dome were estimated and given as input.
4. The number of fuel stages and their flow splits are defined and the geometry of the combustor system is determined interactively.
5. Basic parameters of the combustor are calculated; such as residence times and dome and passage velocities. These are compared to the standard design practices, when appropriate.
6. An automated control function for the fuel staging is defined. The control function is applied by the system model to determine the number of fuel stages used at each cycle point.
7. Emissions performance is determined at each cycle point using the correlations. LTO emissions parameters are calculated.
8. Other details of the combustor operation can be examined depending on the correlations provided. Often all that is desired are the minima and maxima of critical parameters over the entire flight envelope. These might include: 1) for a given fuel system design, the maximum fuel manifold pressure and the minimum injector pressure drop; 2) the maximum and minimum fuel jet penetration; 3) an estimate of maximum fuel temperature rise; 4) the cooling effectiveness required to maintain the liner temperature below a given limit; 5) an estimate of the combustor exit profile factor 6) an estimate required turbine vane cooling

effectiveness to maintain the vane material temperatures below a given limit; and 7) an estimate of the minimum margin on combustor stability.

9. The extensive input data for the CFD models can be generated.

The usefulness of these spreadsheet combustor system models was evident as soon as they were developed. The system models were refined in numerous ways in LET Task 10 and on into Phase II of the HSR program.

1.2.2 IMFH Fuel Jet Penetration Study

An IMFH Fuel Injector Penetration study was conducted in order to obtain experimental correlations relating to the penetration of liquid jets that are injected normal to an air stream. The results of this study were used to better determine the optimum radial location of the IMFH fuel injectors. The fuel jet penetration results complement the CFD studies of the same topic reported above in Section 1.1.2. The correlations from this study were ultimately used in the spreadsheet combustor system models. There, the correlations could be used to make a global assessment of fuel jet penetration everywhere in the flight envelope, not just the few cases that could be run with CFD. Also, the jet penetration correlations, although basically empirical, have the advantage of being based upon data, whereas the CFD models of two-phase flow require simplifying assumptions. This jet penetration study consisted of a review of open literature in order to obtain experimental correlations relating to the penetration of liquid jets that are injected normal into an air stream.

The IMFH mixer design studies have addressed fuel injection from the wall and from a fuel injector cantilevered out into the centerline of the air stream. The Pennsylvania State University (PSU) diagnostic studies, to be discussed in Section 2.1, indicated that fuel injected normal to the air stream from a fuel injector immersed to the premixer tube centerline penetrated to the opposite wall, whereas the fuel injected at the wall penetrated to the mixer tube centerline where it mixed well with the air. However, IMFH single-cup burning tests with wall injection were characterized by low combustion efficiencies relative to centerline injection. Trying to

understand this apparent contradiction was one of the driving forces for the attention given to the topic of fuel jet penetration.

From the literature search, five jet penetration correlations were identified. Their predictions are summarized for the case of a 0.02-inch inner diameter fuel injector in Figure 1.39. The predicted penetration is plotted versus injector pressure drop for 36 different HSCT mission points for the A5B cycle. The predictions by the different correlations are referred to by the last name of the first author of the publication; Chelko⁽¹⁻²⁾, Schetz⁽¹⁻³⁾, Adelberg⁽¹⁻⁴⁾, Yates⁽¹⁻⁵⁾, and Geery⁽¹⁻⁶⁾. The predictions of these correlations for the fuel penetration ranged from 0.1 to 0.4 inches and show trends similar to the results obtained in the PSU studies discussed in the next section of this report. The Adelberg correlation is based upon data taken with supersonic air velocities, so its predictions are expected to be the least reliable for IMFH conditions. The results from the Adelberg and the Schetz correlations suggests that when the IMFH fuel injectors are immersed to the premixer tube centerline, the fuel penetrates to the opposite wall at many cycle conditions. If this actually occurs, it is not desirable. However, the 50% immersion of a transverse fuel injector tube has yielded the lowest emissions in the fired tests of the 0.5-inch diameter IMFH tube.

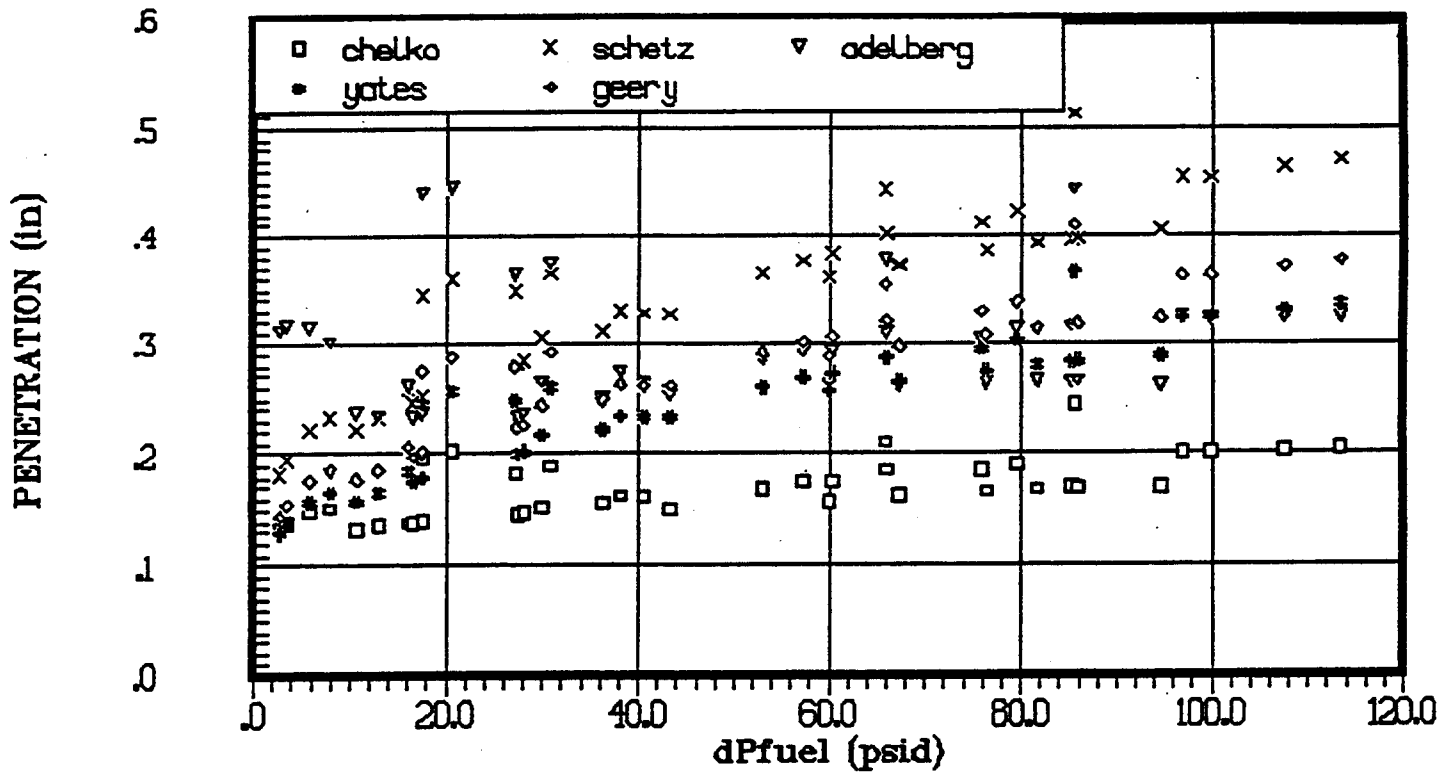


Figure 1.39 - Fuel jet penetration transverse to air flow in an IMFH tube plotted versus injector pressure drop. The predictions of five correlations from the open literature are compared. The points each correspond to an actual engine operating point on a mission. The cycle is the A5B MFTF.

Section 2

Premixer Laser Diagnostic Studies

Laser diagnostic studies of the premixers were performed at the Pennsylvania State University (PSU) and GE Corporate Research and Development (GE CR&D). These laser diagnostic studies were initiated under Task 5 of NASA Contract NAS3-25951, the Aero Propulsion Technology (APT) Program. Follow-on studies were continued under this Task of NASA Contract NAS3-26617, the Large Engine Technology (LET) Program.

The primary focus of the PSU program was to identify an injector geometry for an Integrated Mixer Flame Holder (IMFH) configuration that would enhance the fuel/air mixing and vaporization. A secondary objective was to improve the packaging of the injector/IMFH tube system into a more practical design for an engine. (During the program, the priorities of these two objectives were switched.) The study investigated three different variations of injector tube tips: two fan-shaped and one with a beveled tip. Based on the laser diagnostics, a Lee Company Spin Jet nozzle appeared to have a slight advantage over the best tube-type fuel injector. A complete copy of the final report for the PSU program is included in Appendix B of this report.

The primary purpose of the GE CR&D diagnostics program was to identify the cause of the transition to higher NO_x emissions as the severity of the inlet conditions increased. The laser diagnostic tools available at CR&D included a Raman system for the measuring temperature and species and a Phase Doppler Particle Analyzer (PDPDA) for measuring velocity flow fields and droplet size distributions.

2.1 Pennsylvania State University Combustor Diagnostics Program

The PSU HSCT Combustor Diagnostics Program was directed by Professor Dom Santavicca. The principle investigator was Richard Steinberger. The overall objective of

defining an IMFH fuel injector system with improved fuel/air mixing and vaporization for the IMFH configuration was to be accomplished in four steps:

1. Fuel injector modifications.
2. Mixer tube length reduction.
3. Mixer tube diameter modifications.
4. Air injection at the mixer tube exit.

Tasks 1 and 2 were completed as planned. The equipment for Tasks 3 and 4 was designed and fabricated. However, the decision was made at GEAE to shift the emphasis of the laser diagnostics from a study of the fundamental fuel-air mixing to the secondary goal of improving the packaging of the IMFH fuel injectors. The desire to have more information about a new and more practical injector geometry caused deferral of work for Tasks 3 and 4 and expansion of work in Tasks 1 and 2 to include new geometries. Results of the Task 1 and 2 testing will be summarized later in this section of the report. Details may be found in the body of the PSU Final Report to GEAE on Mixing and Vaporization Evaluation of IMFH Configurations contained in Appendix B of this report.

Table 2.1 summarizes the test conditions for all the PSU testing unless otherwise specified. The high temperature, high pressure continuous flow system used for these tests was capable of operation at inlet temperatures to about 1300° F (1760 R) and pressures to 10 atmospheres. The exciplex fluorescence measurements were carried out in an oxygen-free environment. Images were recorded using a Princeton Instruments image intensifying camera employing a 578 x 384 pixel CCD. The camera was always positioned to view the test section from the side. Images were recorded with the CCD camera, stored on disk, and later viewed and analyzed with the Princeton Instruments CCD Spectrometric Multichannel Analysis Software. Details on the design and structure of the test apparatus and test procedures are found in Appendix B.

Table 2.1 Experimental Conditions for LET Task 10 PSU Diagnostics Studies		
Parameter	Case A (High Inlet T)	Case B (Low Inlet T)
Air inlet temperature	950° F (510° C)	650° F (344° C)
Pressure	65 psia	65 psia
N2 flow rate	0.049 lb/sec	0.063 lb/sec
Mixer tube velocity	100 m/sec	100 m/sec
Major component of fuel	Tetradecane (84%)	Tetradecane (84%)
Fuel flow rate	4.84 to 7.26 lb/hr	9.22 to 12.3 lb/hr
Equivalence ratio	0.4 to 0.6	0.6 to 0.8

Task 1 involved testing the IMFH mixer with an coaxial injector tube, a transverse injector tube, and an axial Lee Company Spin Jet atomizer. The coaxial injector hardware incorporated a 0.042-inch outer diameter, 0.020-inch inner diameter injector tube situated on the centerline and supported by an aerodynamic strut. This tube projected 1.3 inches downstream from the rounded inlet to the IMFH tube. Refer to Figure 3 in the PSU final report (Appendix B) for a schematic of the injector. A completely vaporized uniform mixture was created for exciplex calibration purposes, which allowed the exciplex data to be calibrated before or after an actual injector test. At low inlet temperature, the liquid and vapor appeared to be confined to a core region near the centerline; the liquid especially showed very little spreading. At high inlet temperature, the liquid and vapor were still heavily concentrated in the central core region.

A coaxially-mounted, conical spray fuel injector (Lee Company Spin Jet) was tested in a 0.5-inch inner diameter IMFH mixer tube. The Spin Jet was chosen because of its small outer diameter (0.187 inches). At 950° F (1410 R) inlet temperature, the Spin Jet injector appeared to generate a less concentrated central fuel streak and to have improved vaporization at the mixer tube. A comparison of the test results of a coaxially-mounted, conical spray fuel injector with that of the baseline transverse (wall-mounted) injector tube revealed that the transverse injector tube dispersed the fuel liquid and vapor almost as well as the conical spray fuel injection by the

time the mixture reached the mixer tube exit. A comparison of the Spin Jet injector, the coaxially-mounted injector tubes, and some previous data from tests of a transversely mounted hypo injector indicated that the axial injector tube performed the worst in that it left much of the liquid unvaporized and produced a very non-uniform vapor field. Both the transverse injector tube and Spin Jet performed similarly, although there was less liquid fuel remaining unvaporized at the IMFH tube exit with the Spin Jet. Figures 2.1 and 2.2 showing false color representations of the liquid and vapor concentrations at the exit of the IMFH mixer tube (Figures 6 and 7 from PSU Final Report) support these observations. The results indicate only the slightest indication of any liquid only at the highest equivalence ratio tested (0.6). Refer to Figure 2 in the PSU Final Report for a schematic of the experimental setup and the measurement section. Based on these results, the Spin Jet was chosen for Task 2 testing described at the beginning of this section.

Based on the PSU diagnostic results, GEAE made the decision to modify the designs of the tips of the injector tubes so that they might perform as well as the Spin Jet. Three injector tips were sent to PSU for testing: two producing a fan-type spray (#2 and #5) and one syringe-type injector tip (#8). Figure 2.3 (Figure 15 from the PSU Final Report) show the tips and their positioning. Exciplex imaging experiments were run on these three tips at an inlet temperature of 650° F (1110 R) and an equivalence ratio of 0.6. The images for all three injectors showed that neither vapor nor liquid was significantly present in the bottom quarter of the mixing tube. The injector tube apparently created a wake region and the fuel never got into that region of the mixing tube. In general, the liquid and vapor were still confined to the middle region of the mixer tube. Fan tip #5 did a poorer job than either fan tip #2 or the syringe cut tip #8 in terms of spreading the fuel out vertically. It was concluded that no injector tube tip configuration performed much better than any other, at least with their tips positioned at the centerline. Fuel was not distributed well to the combustor, and the vapor and fuel tended to remain confined to a core, jet-like region near the centerline.

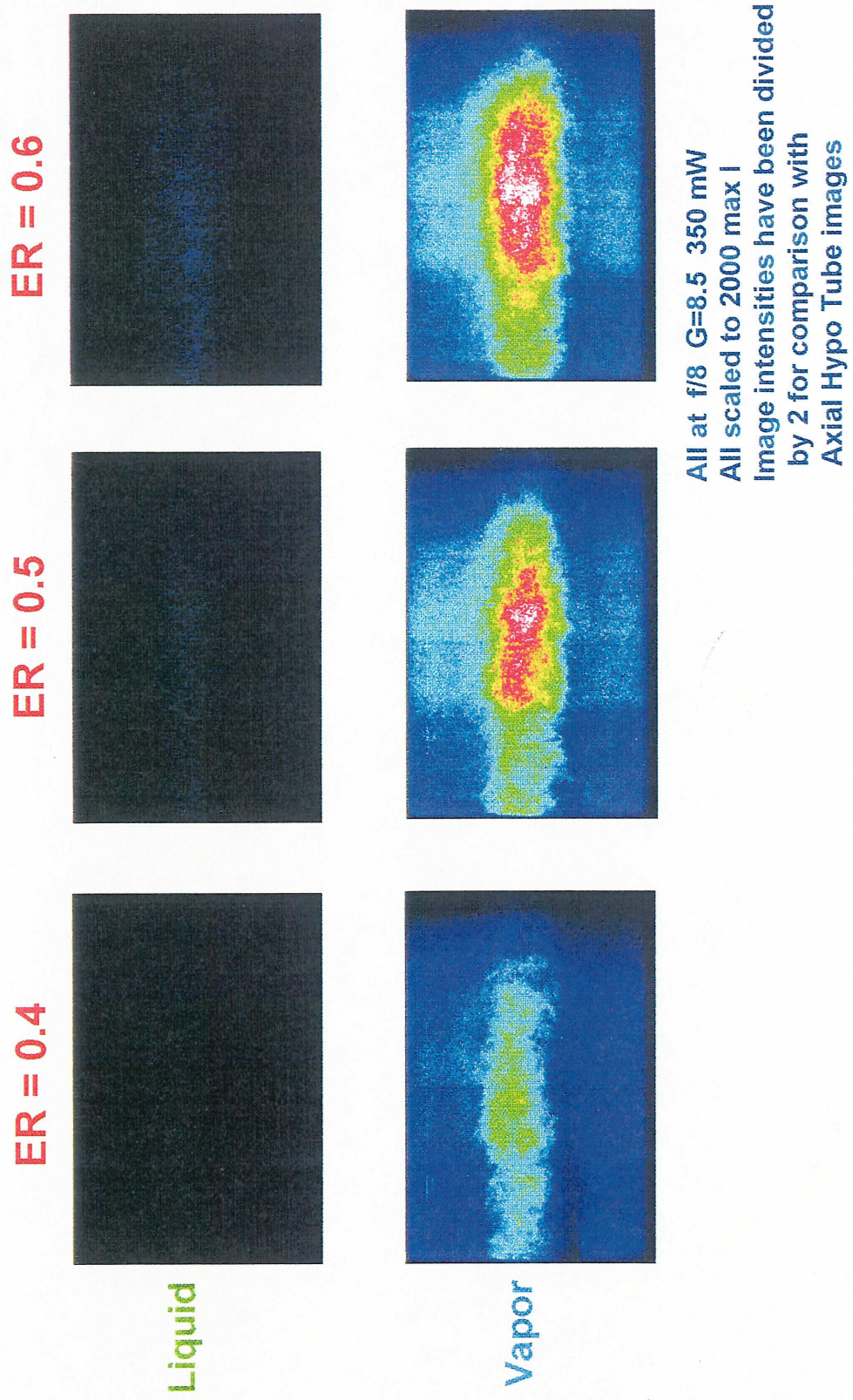
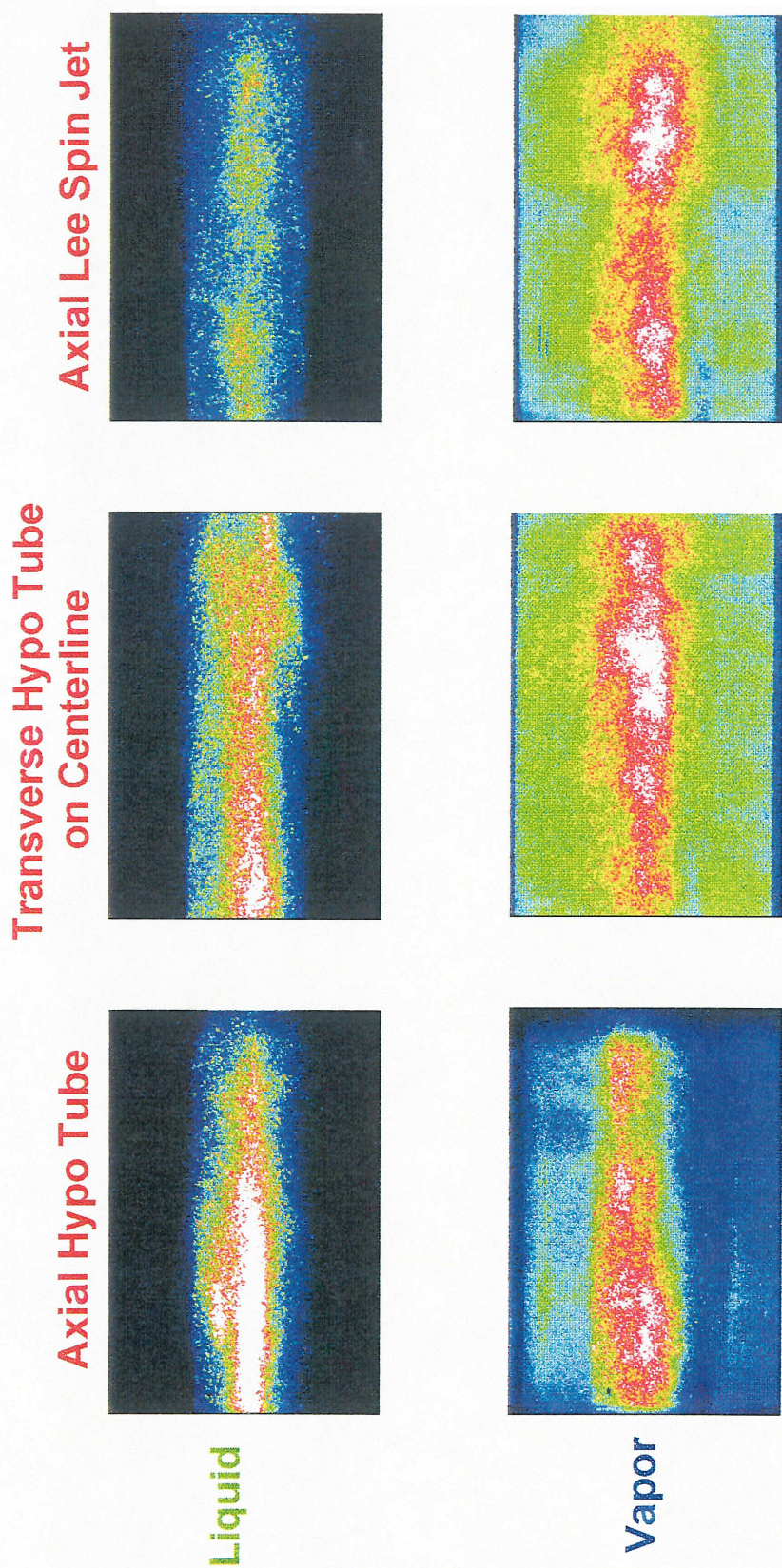
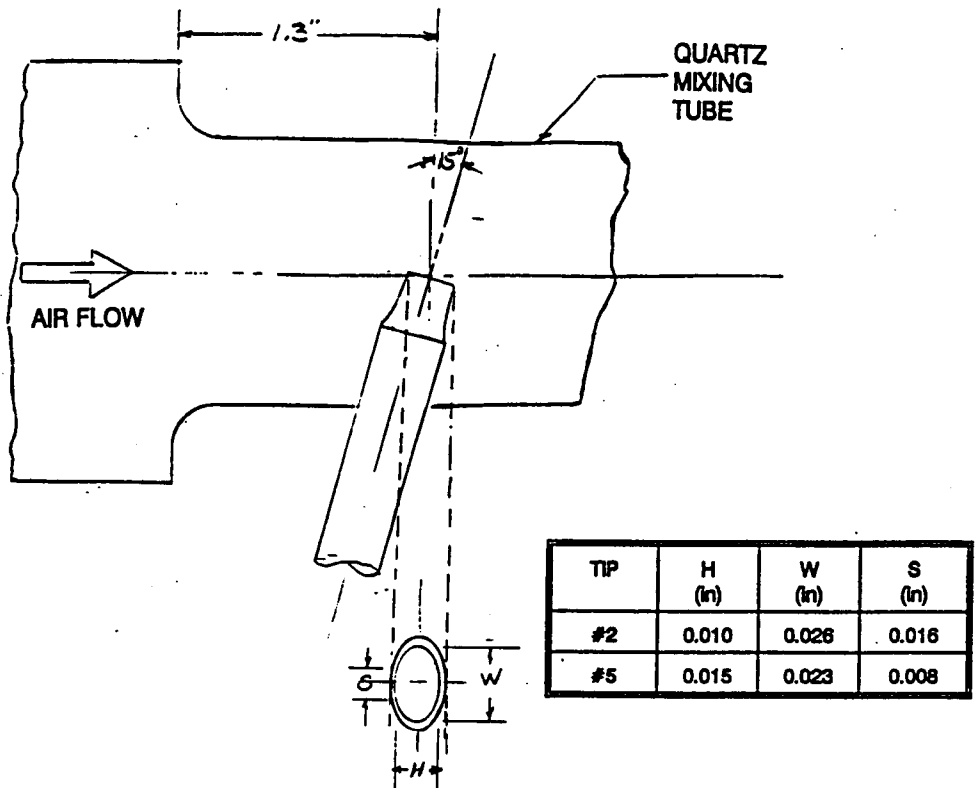


Figure 2.1 - False color representation of fuel liquid and vapor concentrations. Lee Company Spin Jet Atomizer used for fuel injection. Images show the concentration of fuel liquid and vapor at the IMFH tube exit at an inlet nitrogen temperature of 950 F and equivalence ratios of 0.4, 0.5 and 0.6.

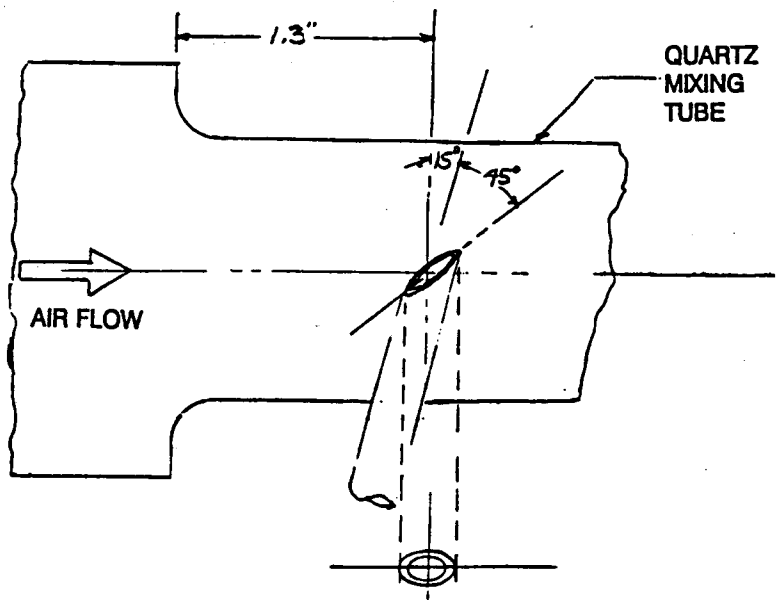


Images adjusted to correct for differing camera gains and lens settings for direct comparisons

Figure 2.2 - Effect of fuel injector type on the concentration of fuel liquid and vapor at the IMFH tube exit at an inlet nitrogen temperature of 650 F and an equivalence ratio of 0.6.



A) #2 & #5 OVALIZED FAN SPRAY TIPS



B) #8 SYRINGE CUT TIP

Figure 2.3 - Details of injector tube modifications. A) Injector tubes #2 and #5 with ovalized fan spray tips. B) Injector tubes #8 with syringe tip (beveled).

In Task 2, the Lee Spin Jet injector was used as the injector because it provided the best mixing performance in Task 1. Experiments were conducted that recorded exciplex images along the length of the mixer tube, both at low and high temperature conditions, at an equivalence ratio of 0.6. Figure 2.4 (Figures 12 and 13 from PSU Final Report) shows that when the Lee Spin Jet injector was used, the mixing tube length could not be reduced below its standard 4.5 inch length without reducing the amount of vaporization at the mixing tube exit well below the desired 98%.

Another conclusion from this study will affect future testing where highly turbulent flows are involved. It was concluded that for meaningful comparisons of imaging data with combustion performance test data, averaging over many images is required. The technique of employing on-chip accumulation of images for this averaging was tested and proved to be an excellent and practical method of obtaining average images of these flows.

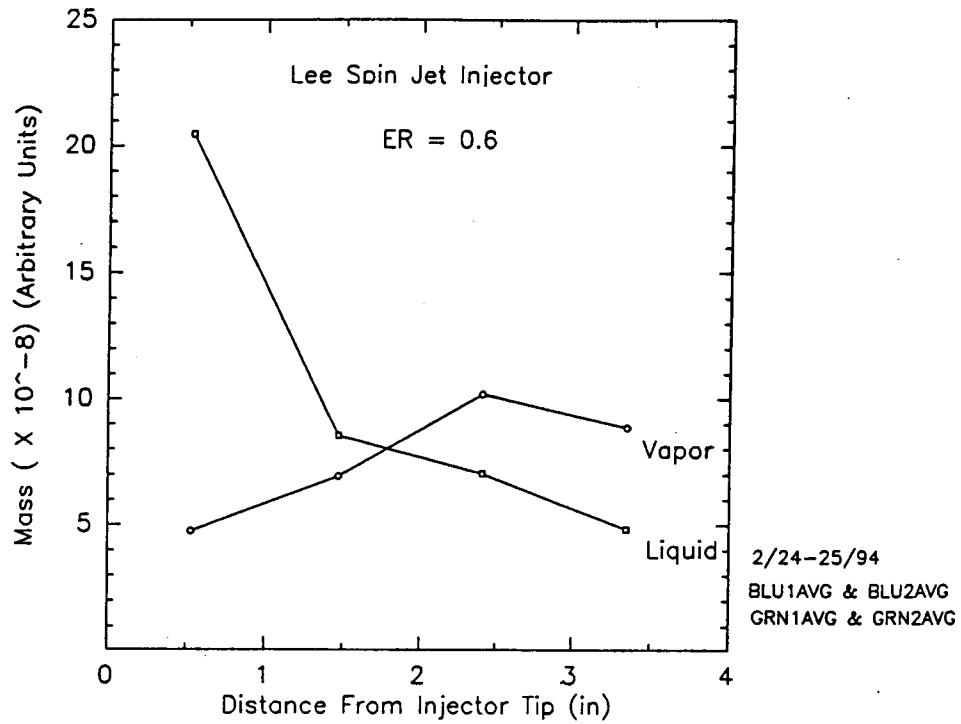


Figure 2.4a - Calculated mass parameter for fuel liquid and vapor versus axial position in IMFH tube using Lee Company Spin Jet atomizer. Inlet temperature = 650° F.

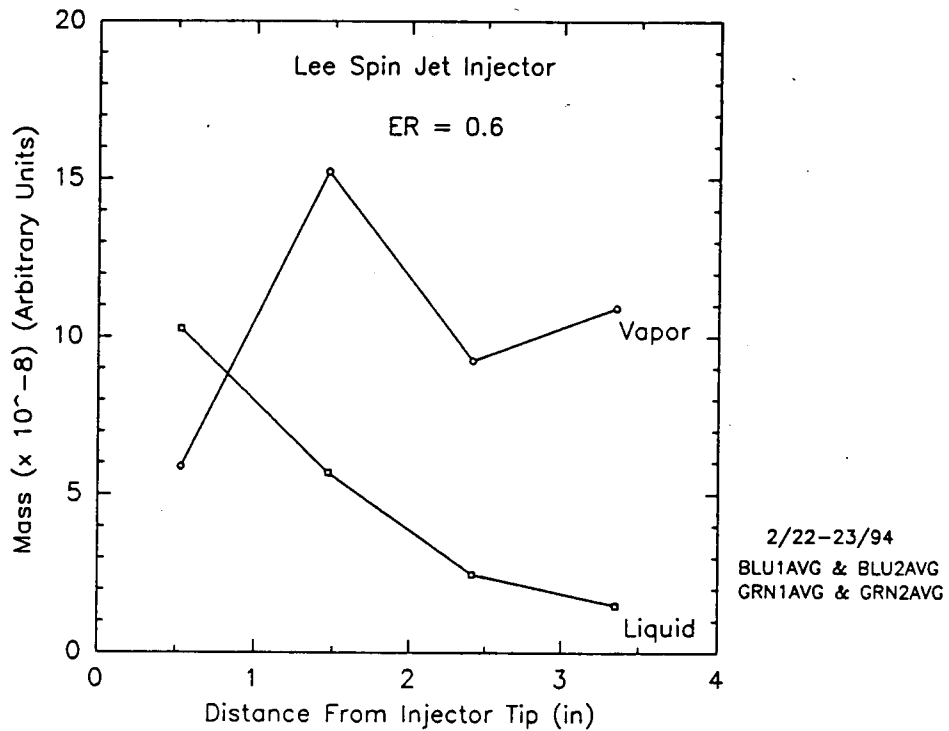


Figure 2.4b - Calculate mass parameter for fuel liquid and vapor versus axial position in IMFH tube using Lee Company Spin Jet atomizer. Inlet Temperature = 950° F.

2.2 GE Corporate R&D Diagnostics Studies

The GE CR&D combustor rig has a large space between the windows, making the rig especially suitable for larger fuel-air mixers with swirling, diverging flows. Therefore, the CR&D diagnostic program concentrated on the Cyclone Swirler pilot. The GE CR&D rig operates with inlet conditions up to 990° F (1450 R) and 15 atmospheres. The specific objectives of the GE CR&D diagnostics program were to:

1. Reduce the Cyclone Swirler's NO_x emissions at cruise conditions by studying and improving the uniformity of fuel/air mixture leaving the Cyclone Swirler.
2. Develop a better understanding of the droplet size distribution of the unvaporized fuel leaving the Cyclone Swirler at low inlet temperatures.
3. Develop a better understanding of the velocity flow field downstream of the Cyclone Swirler.
4. Make visual observations and recordings of combustor operation at pressure.

The Cyclone Swirler tests at GE CR&D were performed with Configuration 2. That configuration was the original HSCT design (Configuration 1) with the added spent dome cooling air injection holes. Configuration 2 is very close in design to Configuration 3 used in the rectangular sector combustor discussed in Section 4. A cross-section of the Configuration 3 single-cup version is shown in Figure 3.37 in Section 3.4. The primary differences between Configuration 2 and 3 is that the size and effective flow area was reduced from Configuration 2 to Configuration 3. Configuration 2 had an effective flow area of 0.74 in². Configuration 3 had an effective flow area of 0.57 in². The number of fuel injectors was reduced from eight in Configuration 2 to six in Configuration 3 (injectors per effective flow area was kept roughly constant). The Configuration 3 hardware was generally much more robust, mechanically, than the Configuration 2 design.

The laser diagnostic capabilities of GE CR&D included Raman measurements of temperature and major species, and Phase Doppler Particle Analyzer (PDPA) measurements of the velocity flow field and fuel droplet size distribution of the unvaporized fuel emitted from the

Cyclone Swirler. PDPA measurements were taken using ambient and preheated air at atmospheric pressure. Droplet size and distribution measurements were made at a number of axial planes with liquid fuel over a range of simulated low power conditions. The effect of fuel injector tube diameter and fuel jet velocity on droplet sizes and NOx emissions exiting the Cyclone Swirler was studied using fuel injector tubes with 0.020-inch and 0.012-inch inner diameters.

2.2.1 PDPA Measurements in an Unfired Cyclone Swirler Pilot

Test conditions for the initial studies of fuel atomization in the Cyclone Swirler Pilot are summarized in Table 2.2. Figures 2.5 and 2.6 present PDPA droplet diameter data taken at the Cyclone Swirler exit. D_{10} is the mean diameter which is calculated from the "number" mean, calculated from $\sum n_i d_i / \sum n_i$. D_{32} is the Sauter mean diameter which is calculated by dividing the volume of the droplets by the surface area. The Sauter mean diameter equals $\sum n_i d_i^3 / \sum n_i d_i^2$. Droplet exit profiles in this test ($D_{10} < 10 \mu\text{m}$ and $D_{32} < 15 \mu\text{m}$ most places) indicated that the degree of atomization of the kerosene droplets leaving the Cyclone Swirler was excellent. At low inlet temperatures (ambient) the small droplet sizes are attributed mainly to the effect of atomization rather than vaporization.

Inlet Air Temperature	80° F (27 C)
Pressure	Ambient
Swirler pressure drop	5%
Fuel	Kerosene
Fuel Injector I.D.	0.012 inches
Fuel flow rate	14.2 PPH

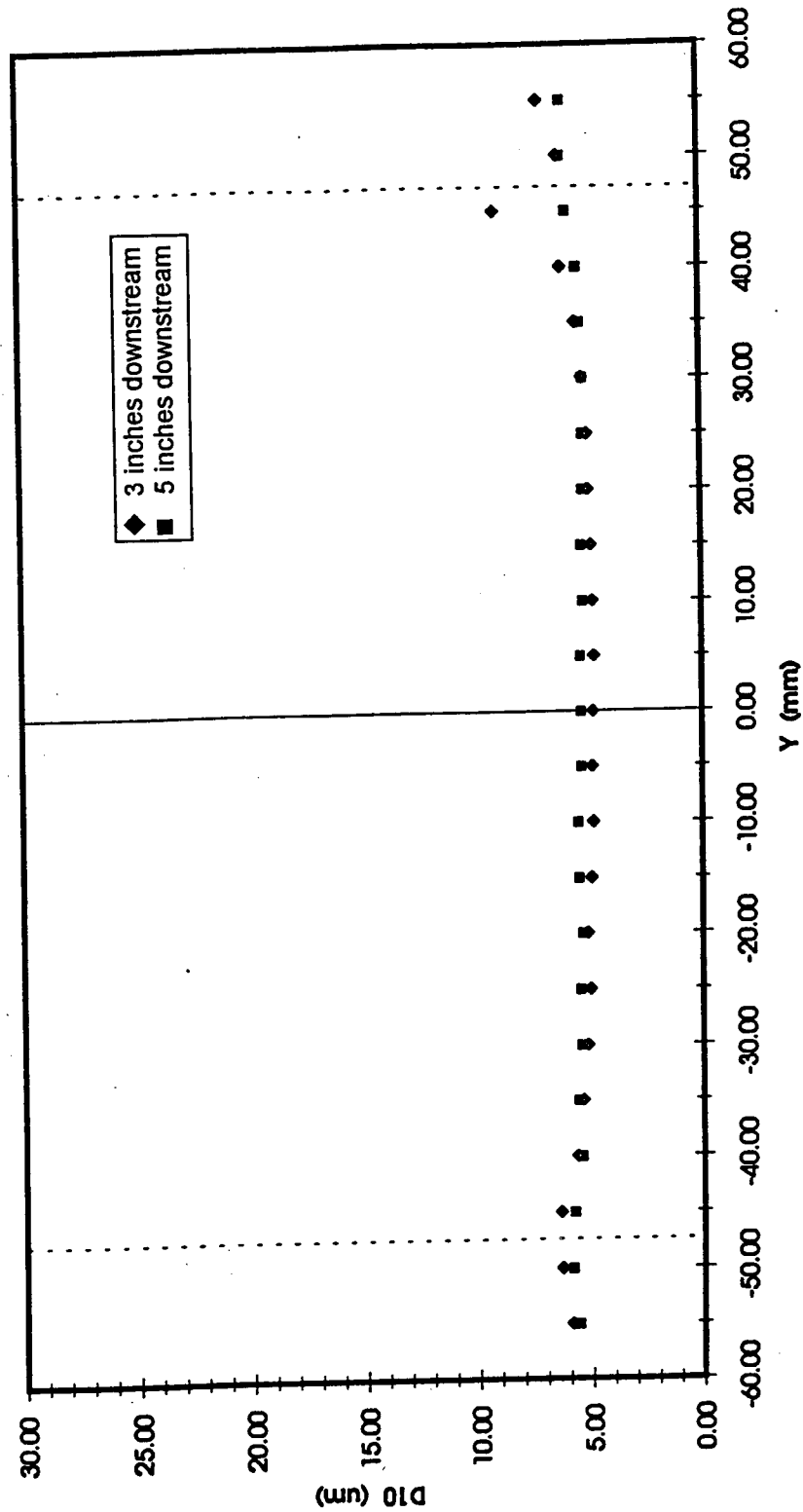


Figure 2.5 - Cyclone Swirler PDPA results for mean droplet diameter at 3 inches and 5 inches downstream from the exit plotted versus radial position. The inlet air temperature is 80° F.

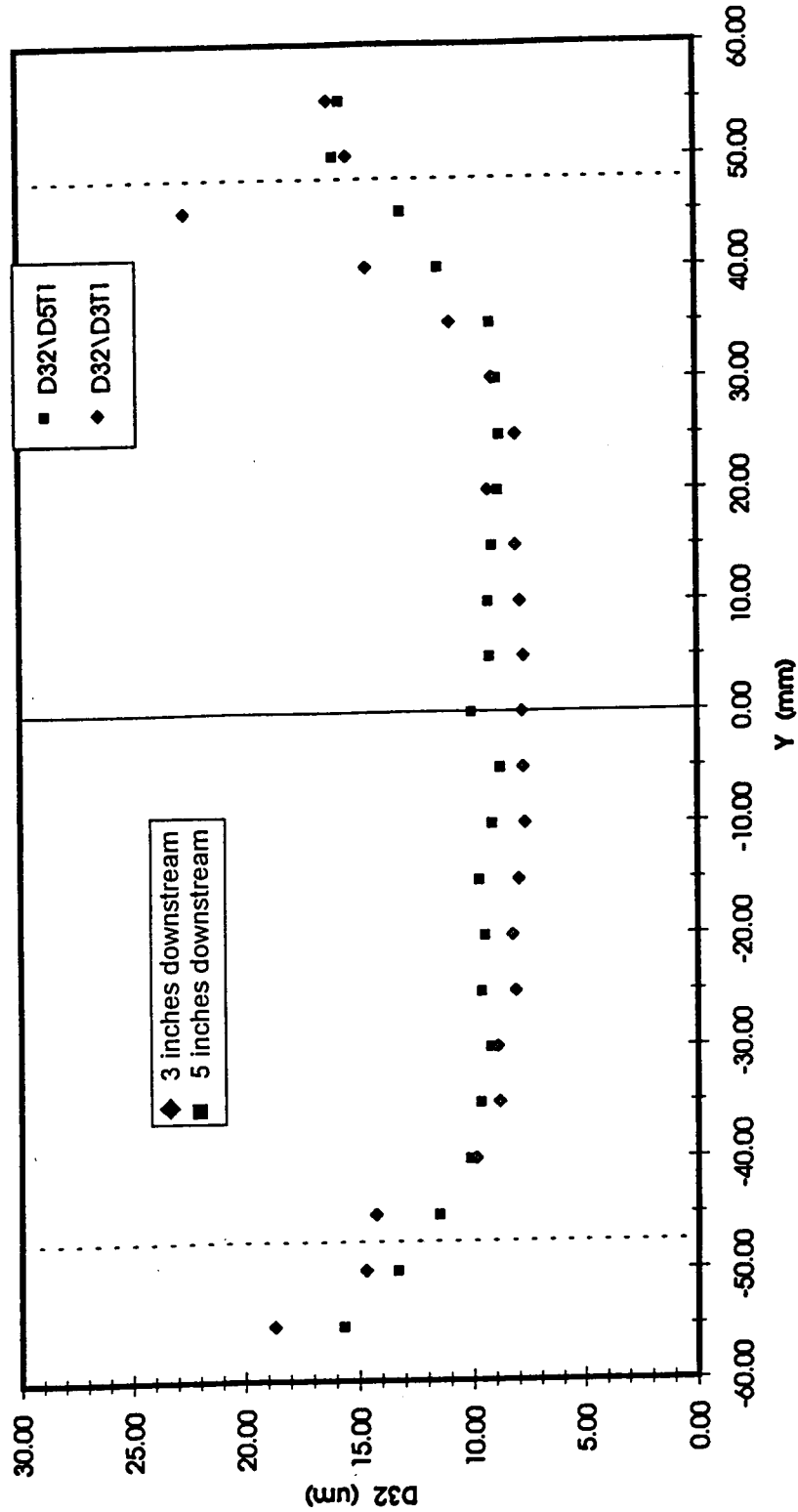


Figure 2.6 - Cyclone Swirler PDPA results for Sauter mean droplet diameter at 3 inches and 5 inches downstream from the exit plotted versus radial position. Inlet air temperature is 80° F.

The corresponding results for the axial component of the mean droplet velocity are shown in Figures 2.7. Figure 2.8 shows the velocity of the air. The air velocity is determined from the smallest droplets ($< 3 \mu\text{m}$), assuming that they track with the air. Because none of the droplets are much bigger than $3 \mu\text{m}$ and the axial component does not accelerate (relative to the tangential component), the difference between the velocities in Figures 2.7 and 2.8 are detectable only upon close examination.

To determine the relative effectiveness of fuel atomization by the Cyclone Swirler versus by the air blast fuel injector alone, PDPA measurements were made on one of the eight radial air blast fuel injectors while not installed in the Cyclone Swirler. All conditions in terms of air temperature, pressure drop, etc. were kept the same as those listed in Table 2.2. Figure 2.9 compares the mean droplet size of both tests three inches downstream from the exit of the Cyclone Swirler to three inches downstream from the fuel injector exit. Figure 2.10 makes the same comparison using the Sauter mean diameter. These data indicate that atomization of the air blast fuel injector alone was in a typical range for an airblast atomizer. The Cyclone Swirler significantly reduces the droplet size from the plain jet airblast atomizer. This could be due atomization and/or vaporization. The strong vortex in the Cyclone Swirler should enhance both atomization and vaporization. The vapor pressure of kerosene at room temperature is high enough that significant vaporization cannot be ruled out. Additional measurements would be required to determine the relative effects of atomization and vaporization. Figure 2.11 compares the droplet velocities from the Cyclone Swirler with the atomizer nozzle.

In the next series of tests, the inlet air temperature was increased and the measurements were repeated. In this case, the fuel/air ratio was also varied to determine their effects on droplet size distributions. Table 2.3 summarizes the test conditions during these measurements. Figures 2.12 and 2.13 compare the mean droplet sizes and Sauter mean droplet sizes at 400°F versus 80°F (860 R versus 540 R) versus radial position. The plots verify that higher inlet temperatures produce smaller droplets from the Cyclone Swirler (all other conditions being the same as the prior tests). The reduced droplet size should be primarily an effect of increase vaporization rate.

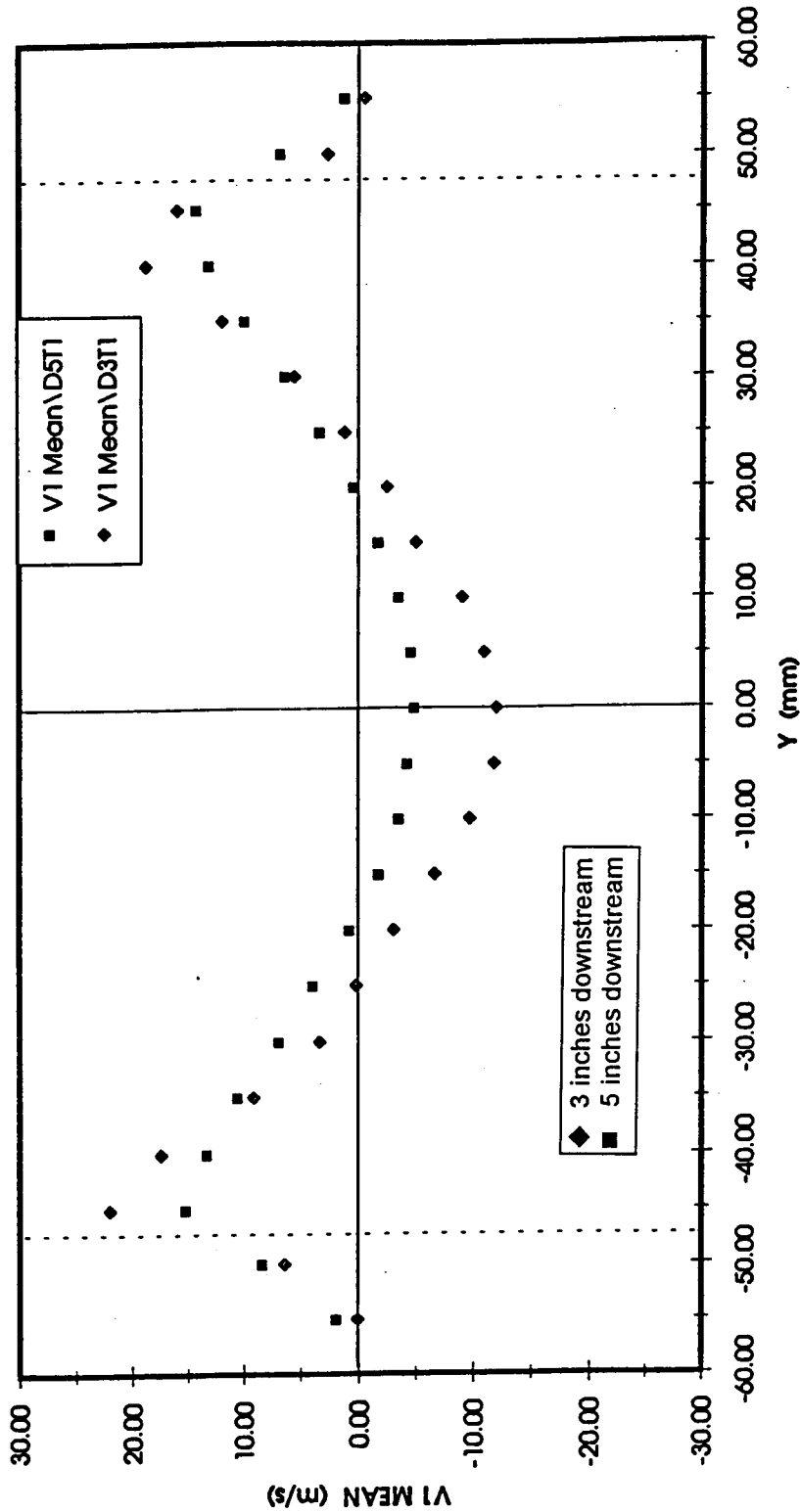


Figure 2.7 - Cyclone Swirler PDPA results for the mean droplet axial velocity component at 3 inches and 5 inches downstream from the exit plotted versus radial position. The inlet air temperature is 80° F. The fuel injector tube inner diameter is 0.012 inches. The fuel flow rate is 14.2 pounds per hour.

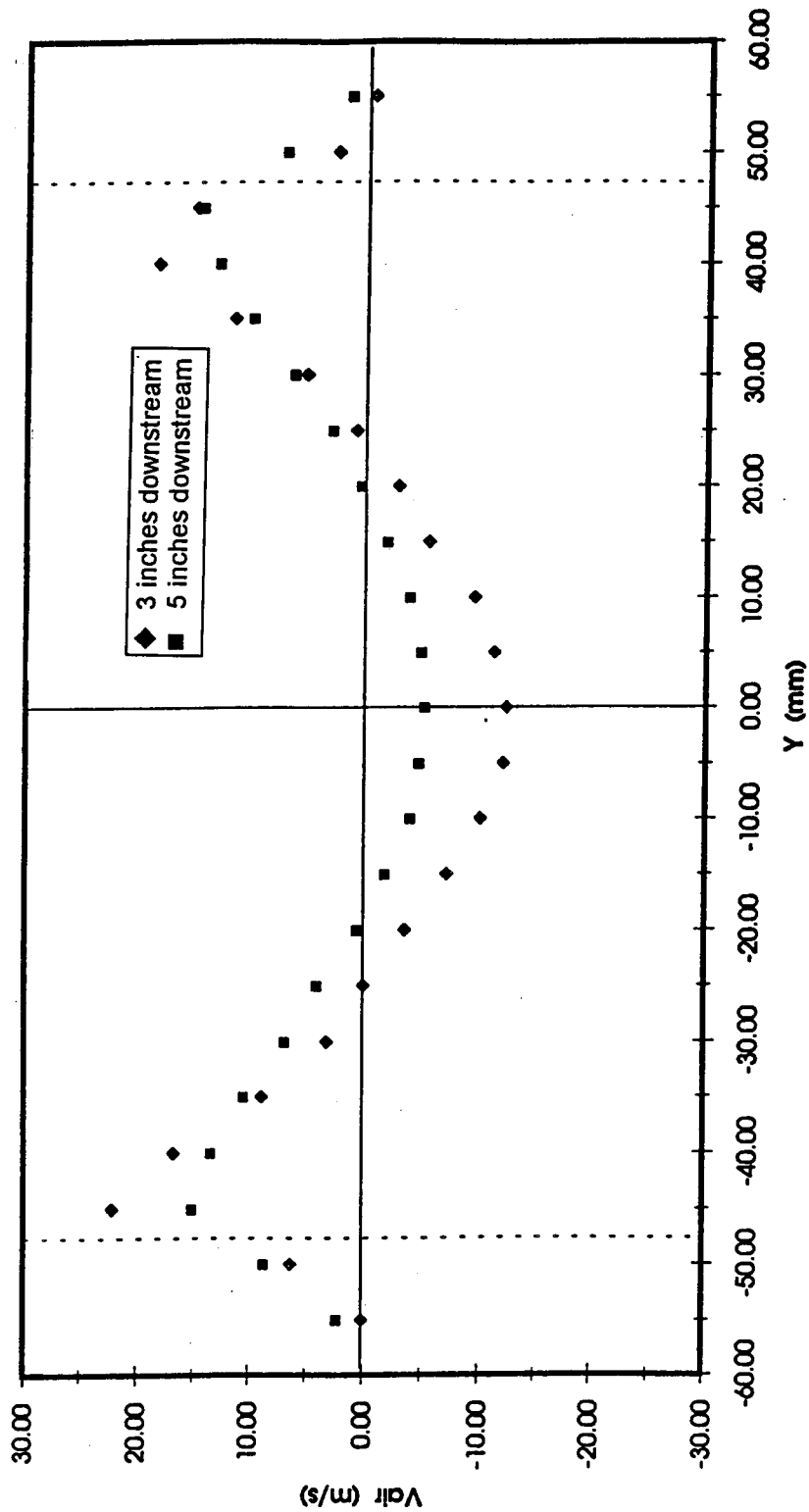


Figure 2.8 - Cyclone Swirler PDDA results for the mean axial velocity component of the air at 3 inches and 5 inches downstream from the exit plotted versus radial position. The inlet air temperature is 80° F. The fuel injector tube inner diameter is 0.012 inches. The fuel flow rate is 14.2 pounds per hour.

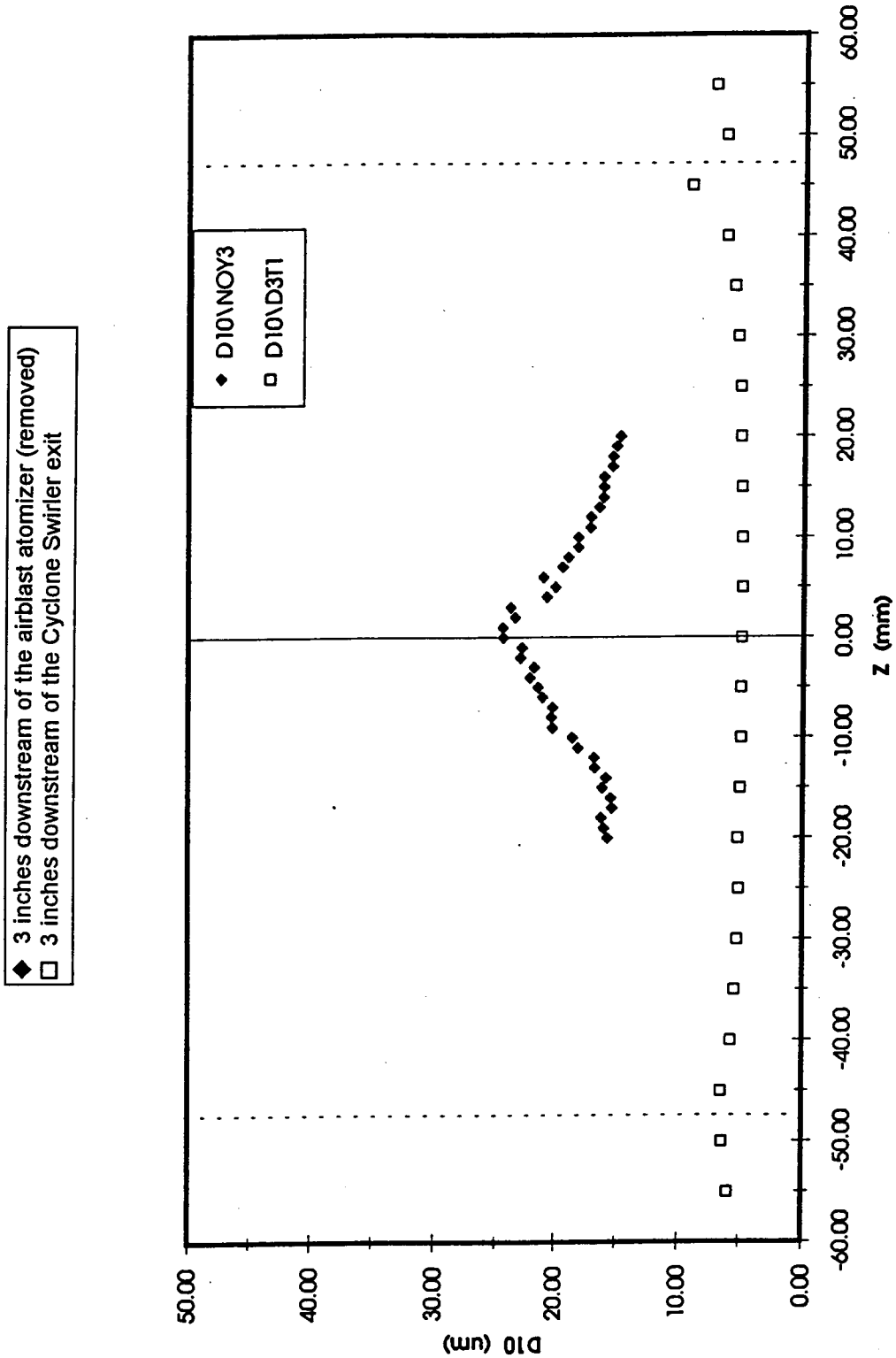


Figure 2.9 - PDPA results for mean droplet diameter at 3 inches downstream from the exit of the Cyclone Swirler compared with the same measurement 3 inches downstream of the airblast atomizer (uninstalled), both plotted versus radial position. Inlet air temperature is 80° F.

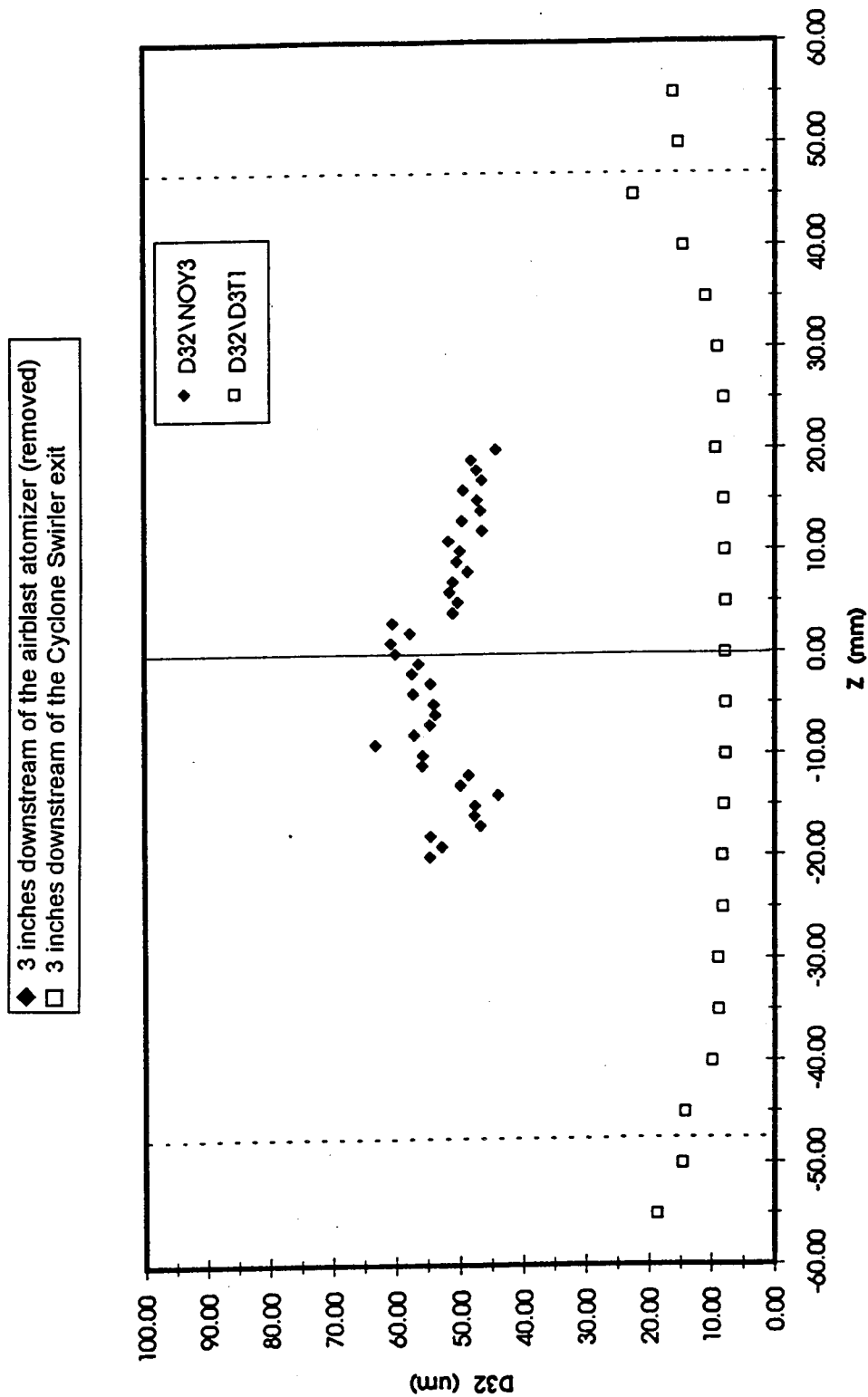


Figure 2.10 - PDPA results for Sauter mean droplet diameter at 3 inches downstream from the exit of the Cyclone Swirler compared with the same measurement 3 inches downstream of the airblast atomizer (uninstalled), both plotted versus radial position. Inlet air temperature is 80° F.

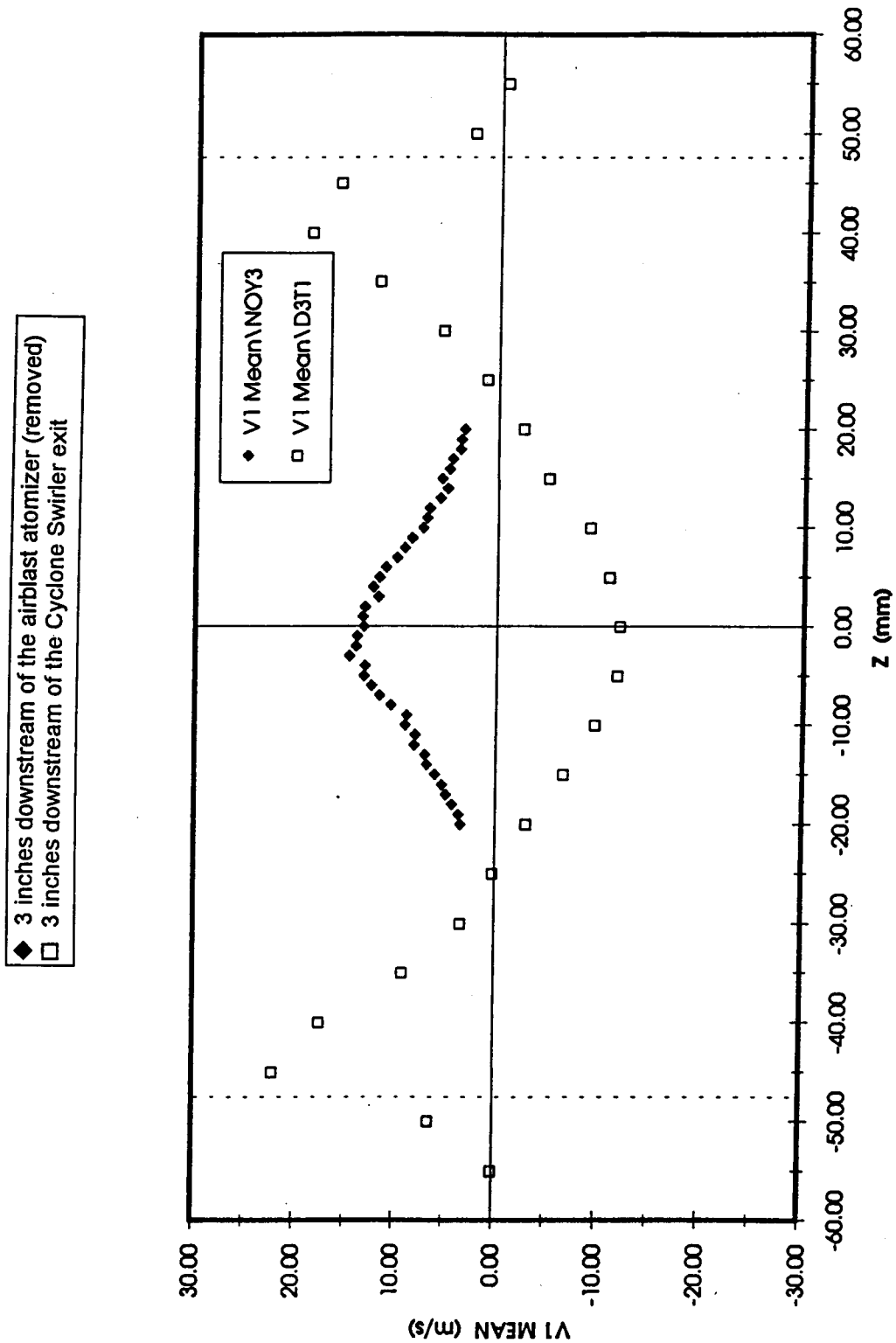


Figure 2.11 - PDPA results for the mean axial component of the droplet velocity at 3 inches downstream from the exit of Cyclone Swirler compared with the the same measurement 3 inches downstream of the plain-jet airblast atomizer (uninstalled), both plotted versus radial position. Inlet air temperature is 80°F.

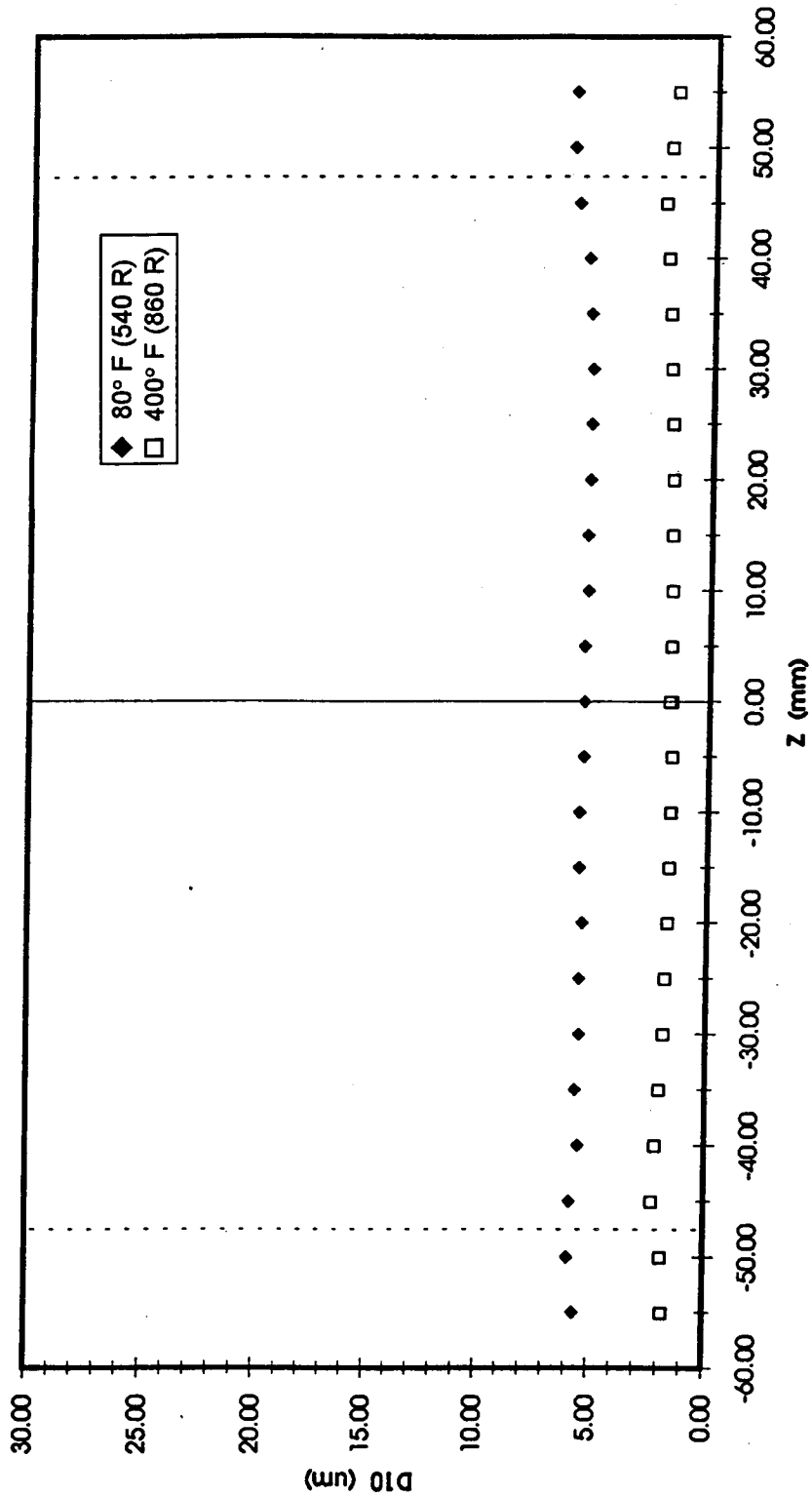


Figure 2.12 - PDPA results for the mean droplet diameter at 5 inches downstream from the exit of Cyclone Swirler plotted versus radial position. Results for an inlet air temperature of 80° F (540 R) compared with results for an inlet air temperature of 400° F (860 R).

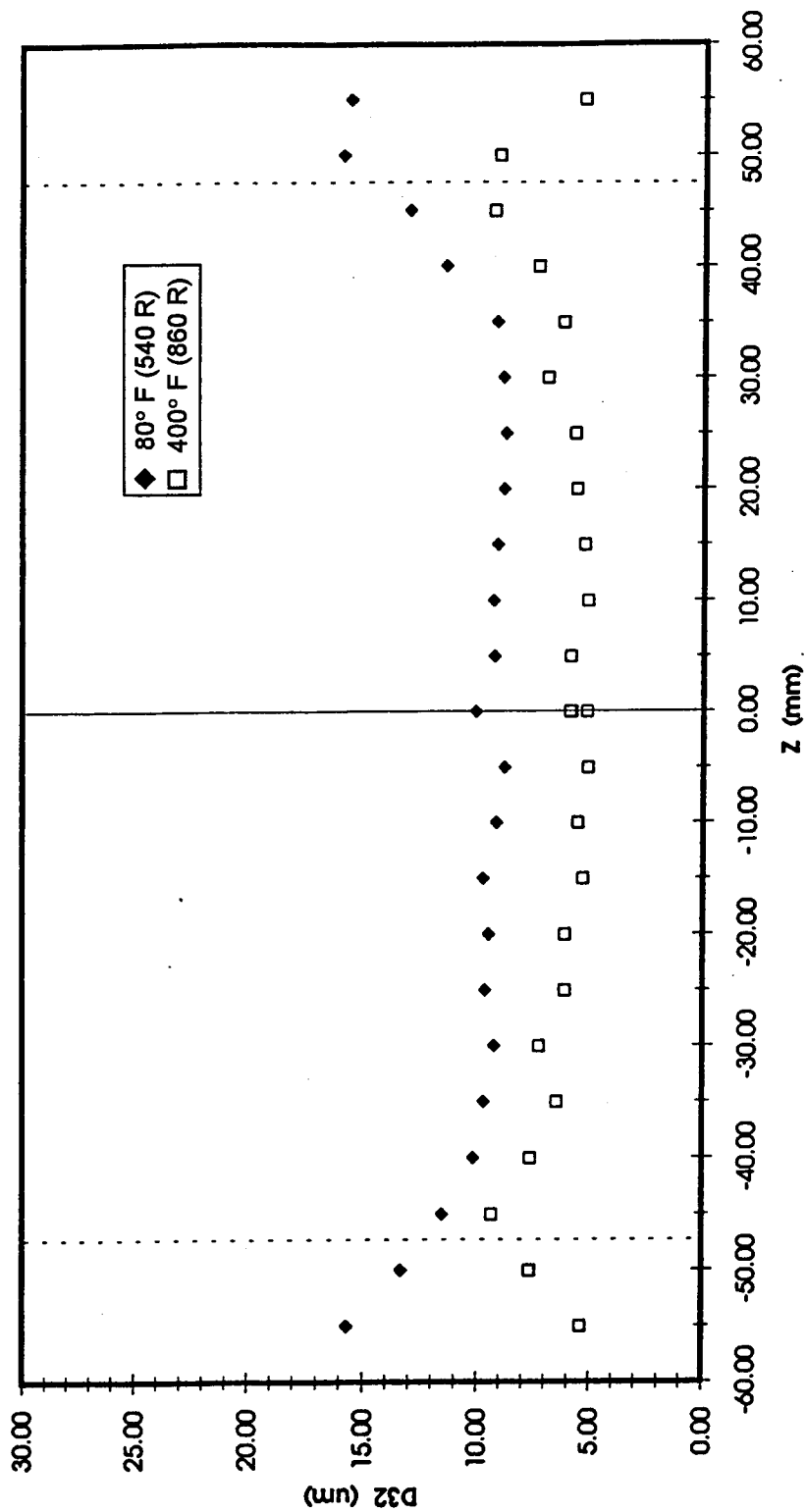


Figure 2.13 - PDPA results for the Sauter mean droplet diameter at 5 inches downstream from the exit of Cyclone Swirler plotted versus radial position. Results for an inlet air temperature of 80° F (540 R) compared with results for an inlet air temperature 400° F (860 R).

Varying fuel/air ratio did not produce any significant effect on the droplet sizes or their distribution, so these results are not shown.

Inlet Air Temperature	400° F (204 C)
Pressure	Ambient
Swirler pressure drop	5%
Fuel	Kerosene
Fuel flow rate	14.2 PPH

2.2.2 Mie Scattering Tests

A complete image of the flow field downstream of the Cyclone Swirler exit plane was constructed using an Argon-Ion laser sheet operating at 2W and placed normal to the flow direction. Mie scattering from liquid droplets in the plane of the light was collected using a standard video camera operating at shutter speeds between 1/60 and 1/4000 second. The observations and video were made at an inlet air temperature low enough to prevent fuel from fully vaporizing (so that Mie scattering was strong), but not so low in inlet air temperature that the fuel hit the observation windows. Observations based on the video images obtained from this simple system included:

1. There was significant unsteadiness in the flow field.
2. Fuel streaks from all eight injectors were clearly discernible at 0.5 inches downstream. Farther downstream these streaks appeared to have different lifetimes and the surviving streaks moved around. This could have been due to unsteady fuel flow rates from the individual injectors, or unsteady degree of atomization from the eight injectors, or variations

in lifetimes of parcels of fuel and air resulting from differing degrees of vaporization as they exited the Cyclone Swirler due to the unsteadiness of the flow field.

3. The fuel left the Cyclone Swirler in a hollow cone spray; this was expected given the large center-body and the characteristics of the vortex flow field.
4. The images showed increasing amounts of liquid fuel as the temperature of the inlet air was lowered.

An increased awareness of the unsteadiness of the flow field resulted from these observations. However, unsteadiness is known to be a dominant characteristic of all turbine combustor flow fields.

2.2.3 Fired Tests

The Cyclone Swirler was installed in the CR&D single-cup combustor diagnostics rig. The rig is an 8-inch diameter pressure vessel with a quartz liner with an inner diameter of 3.7 inches. The fuel injector tube inner diameter for these tests was 0.012 inches. The combustor was operated at a pressure up to 125 psig with the flame front recorded using standard video equipment. NO_x measurements were obtained simultaneously using conventional probe sampling. It was found that the combustor operated in two modes during this test:

1. At lean equivalence ratios (just above LBO), the flame was only anchored to the center-body. The flame increased in area and filled the liner as it did so.
2. At higher equivalence ratios the flame was anchored to the centerbody and in the corner of the recirculation zones. The mode was also characterized by an increase in NO_x emissions.

That the flame did not appear to be stabilized in the outside corners at the dome is inconsistent with GEAE experience, especially in the sector combustors. This difference is

thought to be due to leakage at the seal between the dome and the upstream end of the quartz liner in the CR&D rig.

Additional fired tests were then run at a pressure of 200 psia with the Cyclone Swirler in the single-cup 8-inch diameter rig at GE CR&D. The tests were also conducted with a 3.7 inch inner diameter ceramic liner. The fuel injector tube inner diameter for these tests was increased to 0.020 inches, consistent with Configuration 3. Inlet temperatures were varied from 600° F (1060 R) to a maximum of 900° F (1360 R). NO_x, CO and CO₂/O₂ emissions data with standard probe sampling were obtained at various steady state conditions at a number of pressures. The following observations were made:

1. When inlet temperature was increased beyond 800° F (1260 R), the combustion oscillations observed in the previous tests did not occur, while at lower inlet temperatures they did occur.
2. Most of the emissions data agreed with emissions data taken in tests at GEAE.
3. The sudden rise in NO_x with elevated pressures and temperatures that was observed in GEAE single cup testing did not occur in these tests up to the maximum conditions of 200 psia and 900° F (1360 R).

Figure 2.14 shows the CR&D NO_x emissions measurements for Cyclone Swirler Configuration 2. Figure 2.15 show that there was a increase in NO_x emissions with inlet temperature when the flame temperature was held at a constant value of 3500 R. These results indicated the presence of a break point where the NO_x emissions transition to a steeper dependence on inlet temperature.

The experiment was repeated. To improve the determination of the inlet temperature at which the slope change occurs, the measurements were made at smaller increments of inlet temperature. The pressure and the constant flame temperature were selected to be more relevant to supersonic cruise conditions. Flame temperature was held constant at 3550 R.

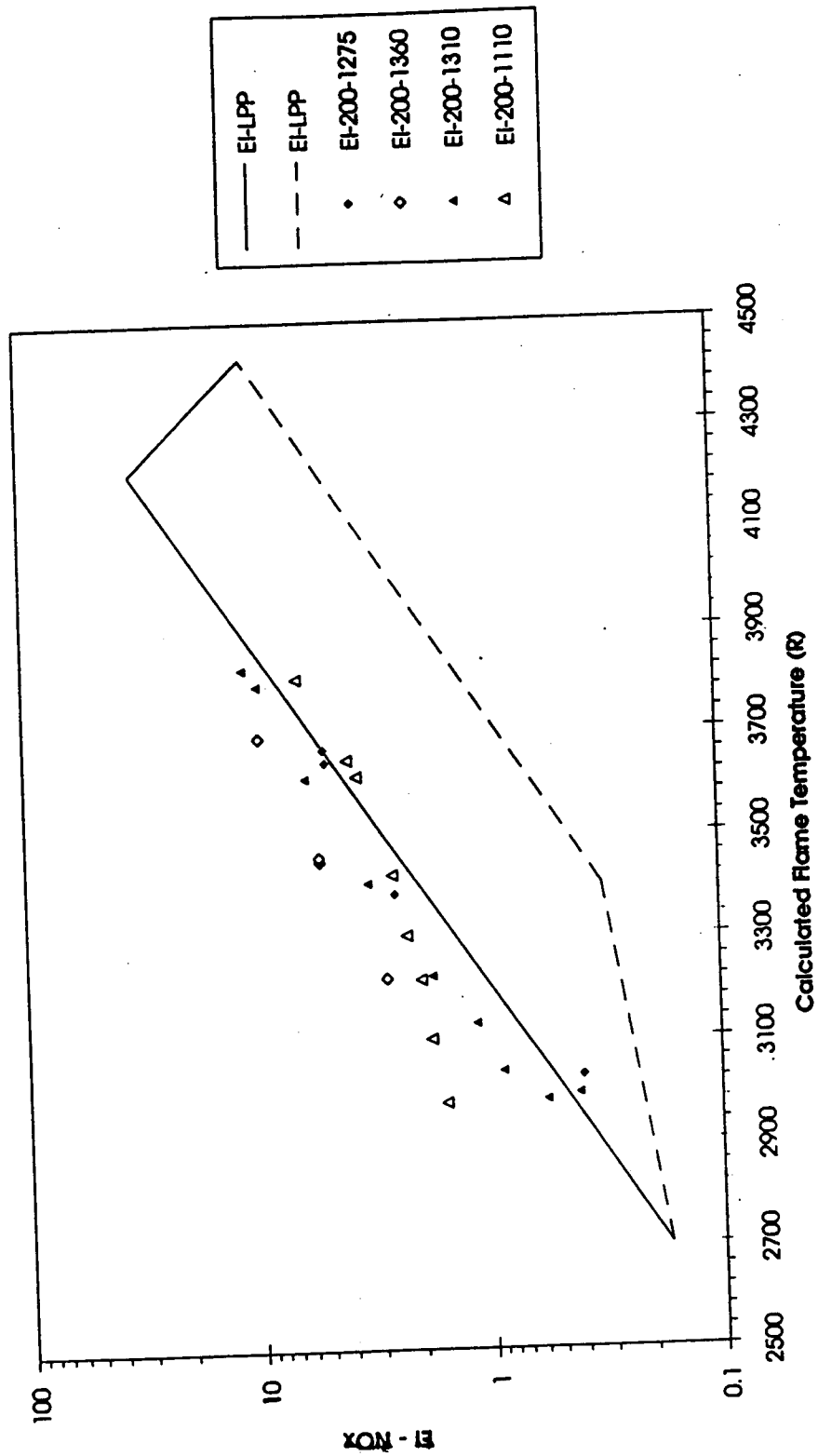


Figure 2.14 - NOx Emissions Index plotted versus flame temperature at inlet air temperatures ranging from 1110 R to 1360 R according to the legend. Pressure is 200 psia. These test conditions and the results are comparable to test results obtained at GEAE.

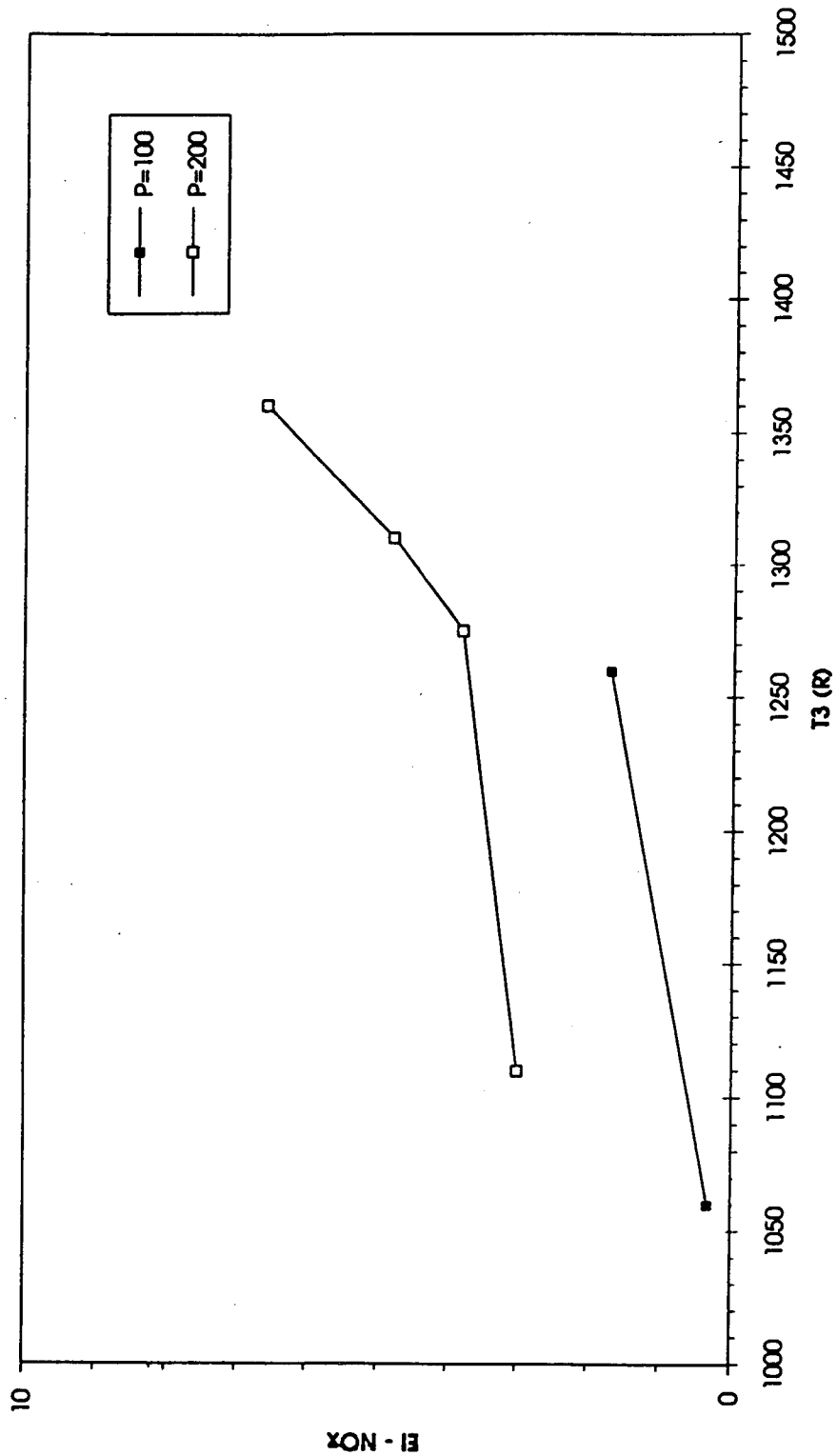


Figure 2.15 - NOx Emissions Index plotted versus inlet air temperature with flame temperature held constant at 3500 R. Inlet pressure is 100 psia and 200 psia as indicated by the legend.

Inlet pressure was held at 150 psia. Inlet temperature was varied from 590° F to 820° F (1050 R to 1280 R). The pressure drop across combustor was held at 5%. The NO_x emissions are plotted versus inlet temperature in Figure 2.16. Over the range of inlet temperatures studied, the NO_x emissions were observed to increase gradually. There were no sudden increase in the measured NO_x emissions, but the slope relative to inlet temperature did change at about 740° F (1200 R).

The purpose of these pressure tests of the Cyclone Swirler and the probe measurements of the NO_x emissions were supposed to be preliminary in preparation to making detailed Raman measurements of all the major species. The Raman measurements were to be done at supersonic cruise conditions, except that T_3 would be have to be lower, subject to the same facility limits as the above tests. The Raman measurements were to be done point-wise and were to map out the flame zone. A few preliminary Raman measurements were done at atmospheric pressure, but the Raman measurements were not completed before the budget was expended.

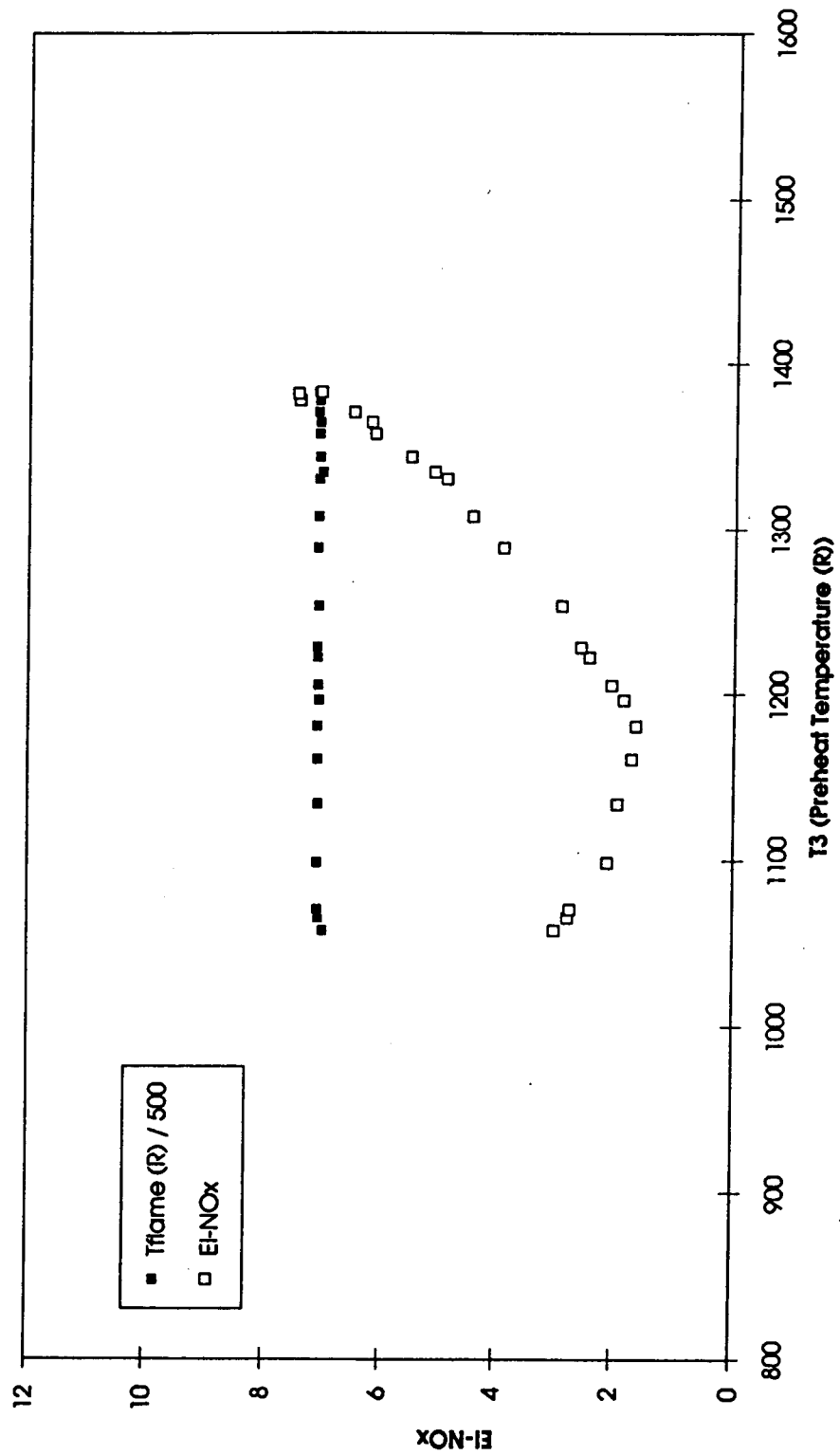


Figure 2.16 - Measured NOx Emissions Index plotted versus inlet air temperature with flame temperature maintained constant at 3550 R. Pressure drop is 5%. Inlet pressure is 150 psia.

Section 3

Subcomponent Evaluations

This section describes the development and testing of six fuel-air premixer concepts selected for development in LET Task 10. These six fuel-air premixer concept studies are continuations of studies of the same concepts (or very similar concepts) in NASA Contract NAS3-25951, Aero-Propulsion Technology, Task 5. The six fuel-air premixer concepts are:

1. Integrated Mixer Flame Holder (IMFH)
2. Curved Tube IMFH
3. Swirl-IMFH
4. Cyclone Swirler
5. Mini-Swirl IMFH
6. Swirl-Jet

The IMFH tube is the underlying concept for four of the above concepts. The IMFH is a straight tube with a fuel injector near the entrance. The tube exits through the combustor dome resulting in a perforated plate-type flame-holder. Hence the name. The Cyclone Swirler utilizes the high radial acceleration inside a radial swirler to maintain a relative velocity between the fuel and air, thereby enhancing fuel atomization and vaporization. The Swirl-Jet is another adaptation of a swirler for prevaporizing and premixing fuel in air. In the Swirl-Jet the premixing takes place in an axial flow after the swirler, rather than inside the swirler. The swirl is generally fairly weak to help prevent recirculation. The APT Task 5 Final Report ⁽³⁻¹⁾ should be referred to for more detail on the LPP premixer concepts and their early development history.

Throughout Section 3, IMFH Configurations 5A and 5B will be used as the baseline for comparison with the new designs for the main stage premixers. The designations A and B refer to the low pressure and the high pressure flame tube rigs, respectively. There are no design

differences between the A and B versions. The IMFH configuration was the same in both installations. However, there were differences in the combustion zone. The low pressure rig had a combustor diameter of 4.89 inches and a length to the sample probe of 7.42 inches. The high pressure rig had a combustor diameter of 4.5 inches and a length from the dome to the probe of 9.45 inches. Configuration 5 of the IMFH is the design used in the stepped-dome sector combustor.

3.1 Integrated Mixer Flame Holder (IMFH) Evaluations

The development program for the IMFH emphasized the evaluation of the performance of alternative fuel injector concepts and the effects of mixer tube length and diameter. Minor design variations such as the spent dome cooling air injection hole design were also studied. A third generation (Gen III) of the IMFH flametube hardware was designed and fabricated for these tests. The hardware was designed to be modular for maximum flexibility in the test configurations. The Gen III modules consisted of an inlet section, mixer tubes, impingement baffle, and flame holder. The modules were bolted together in a way that allowed for the convenient variation of the mixer tube lengths. The coaxial fuel injector supports were attached to the inlet section of the premixer. Some form of coaxial injector bodies would allow the fuel injector to be separated from the IMFH tube, possibly allowing a more conventional fuel injection system for the IMFH. A typical 7-tube configuration is shown in Figure 3.1.

Two configurations were tested using coaxially-mounted, 0.190 inch outer diameter, conical spray Lee Spin Jet fuel injectors. Configuration 7 located the Lee Spin Jet injector tips 1.0 inch downstream from the mixer tube inlets, which yields a fuel-air mixing length of 4.5 inches. Configuration 8 increased the mixing length to 5.25 inches by moving the injector tips forward 0.75 inches. The tests were generally run with a pressure drop of 4.4 to 5.0%. When pressure drop was varied from this nominal range, the values are noted in the legends of the plots. NO_x emissions for Configuration 7 were slightly higher than the IMFH Configurations 5A and 5B single-cup results as shown in Figure 3.2, at inlet temperatures ranging from 495° F to

Coaxial Fuel Injector
Mounting Hardware

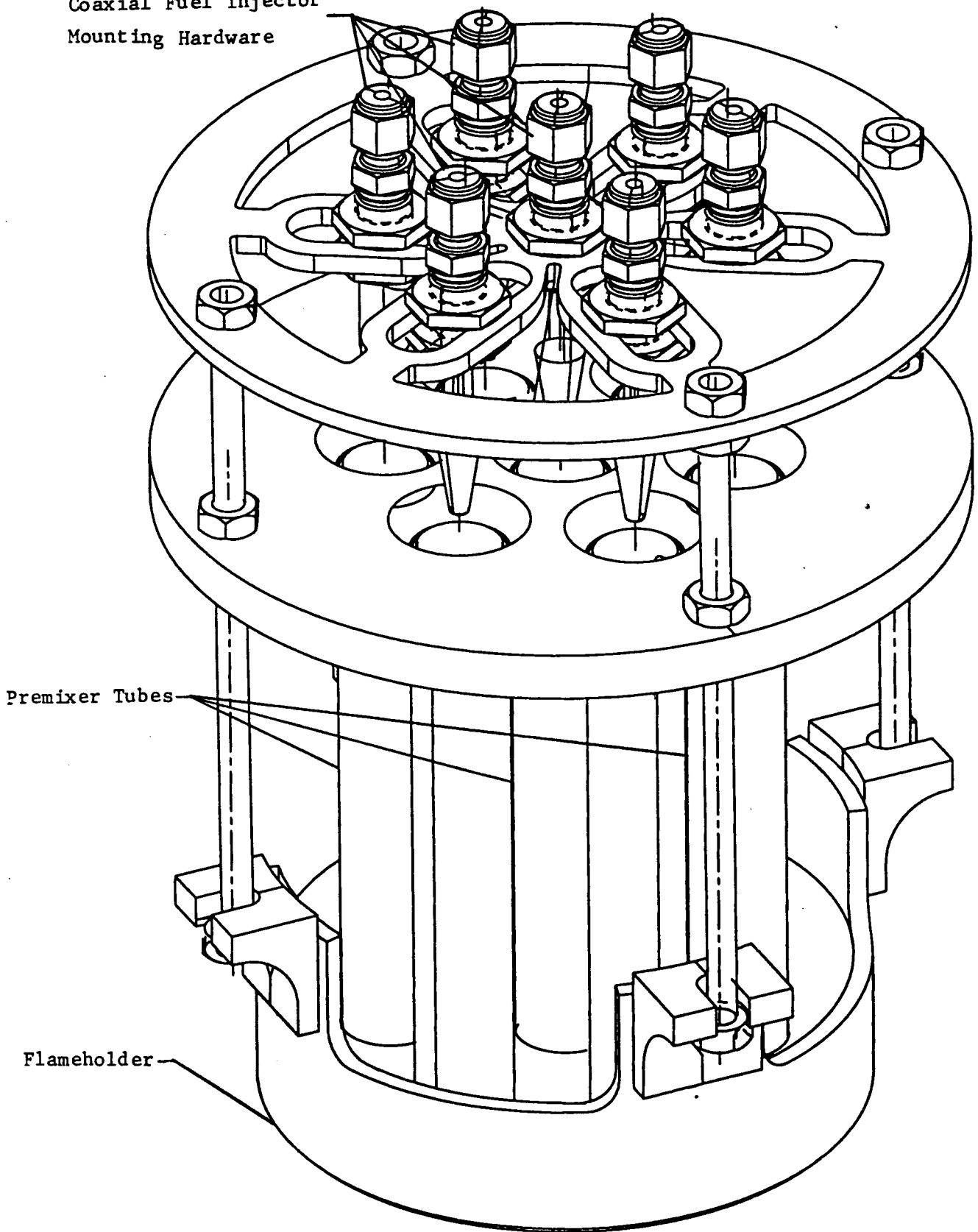


Figure 3.1 - IMFH Generation III premixer hardware. The Generation III hardware was modular in design to facilitate modifications.

950° F (955 to 1410 R) at 4 atmospheres inlet pressure. The dashed line in Figure 3.2 defines the envelope of the NO_x EI's from a number of laboratory studies of LPP combustion. As shown in Figure 3.3, CO emissions for Configurations 5 and 7 were comparable at an inlet temperature of 650° F (1110 R), while Configuration 7's CO emissions were higher than Configuration 5 at 950° F (1410 R). Increasing the mixing length in Configuration 8 had a minor impact on NO_x. In Figure 3.4, Configuration 8's NO_x emissions were slightly lower than Configuration 7's at an inlet temperature of 650° F (1110 R) and higher at inlet temperature of 950° F (1410 R) when flame temperatures were less than 3500 R. In Figure 3.5, the difference in CO emissions was slight.

Coaxially-mounted, conical spray, Textron fuel injectors were tested as Configuration 9 of the IMFH. Configuration 9 resulted in higher NO_x and CO emissions when compared to the baseline transverse mounted tube injector (Configurations 5A and 5B) or the Lee Spin Jet results. The emissions for Configuration 9 are compared to Configurations 7 and 8 in Figure 3.6 (NO_x emissions) and Figure 3.7 (NO emissions). These tests completed the coaxial spray injector evaluation testing.

The IMFH baseline fuel injector configuration was retested with the Gen III hardware to establish the IMFH data baseline for a seven mixer tube assembly (Configuration 11) and for comparison with the previous baseline results with the thirteen mixer tube IMFH assembly (Configuration 5). There was no other change in mixer or injector features between the two configurations. However, Configuration 11 had more combustor liner area per unit dome effective flow area. This was quantified as the ratio C/A_{EFF} (the flame tube liner inner circumference divided by the combustor dome effective flow area). This ratio was 6.8 for Configuration 5 and 8.1 for Configuration 11. Therefore, Configuration 11 heated nearly 20% more liner area for a given heat release than the mixers in Configuration 5. There was no discernible impact on NO_x emissions for data compared at similar inlet conditions (Figures 3.8 and 3.9). There was, however, a significant difference in combustion efficiency, as show in Figure 3.10. Based on this observation of the effect of C/A_{EFF} , a reassessment of IMFH mixers with NO_x emissions similar to or lower than IMFH Configuration 5, but with poorer combustion

HSCT IMFH CONFIG. 5 & 7 NO_x EMISSIONS

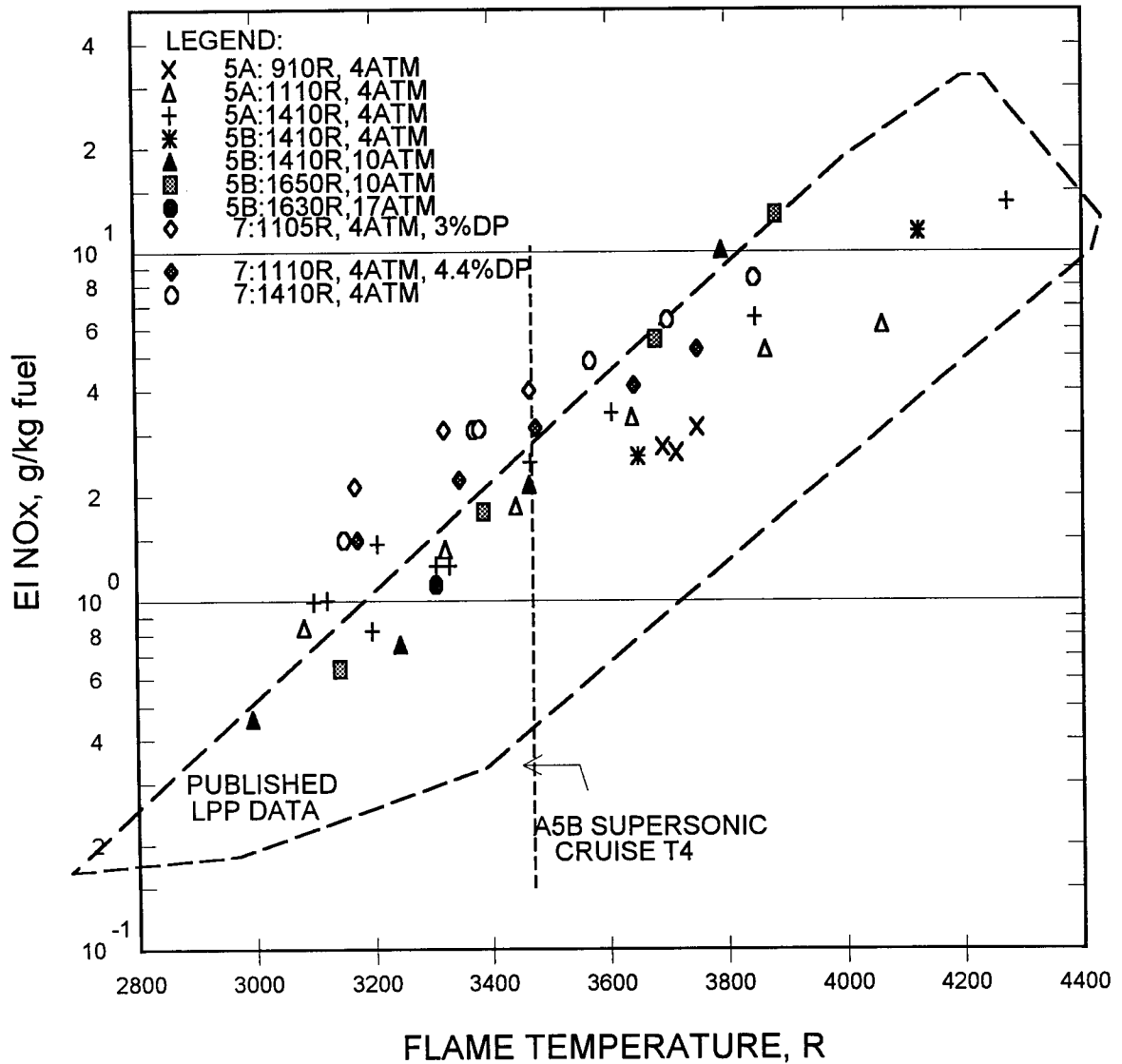


Figure 3.2 - NO_x Emissions Index plotted versus flame temperature for IMFH Configurations 5A, 5B and 7. Data obtained at several combinations of inlet temperature and pressure as indicated by the legend. The pressure drop was 4.4% unless indicated otherwise. The dashed boundary indicates the envelope of LPP NO_x emissions obtained in several laboratory flame tube studies published in the open literature.

HSCT IMFH CONFIG. 5 & 7 CO EMISSIONS

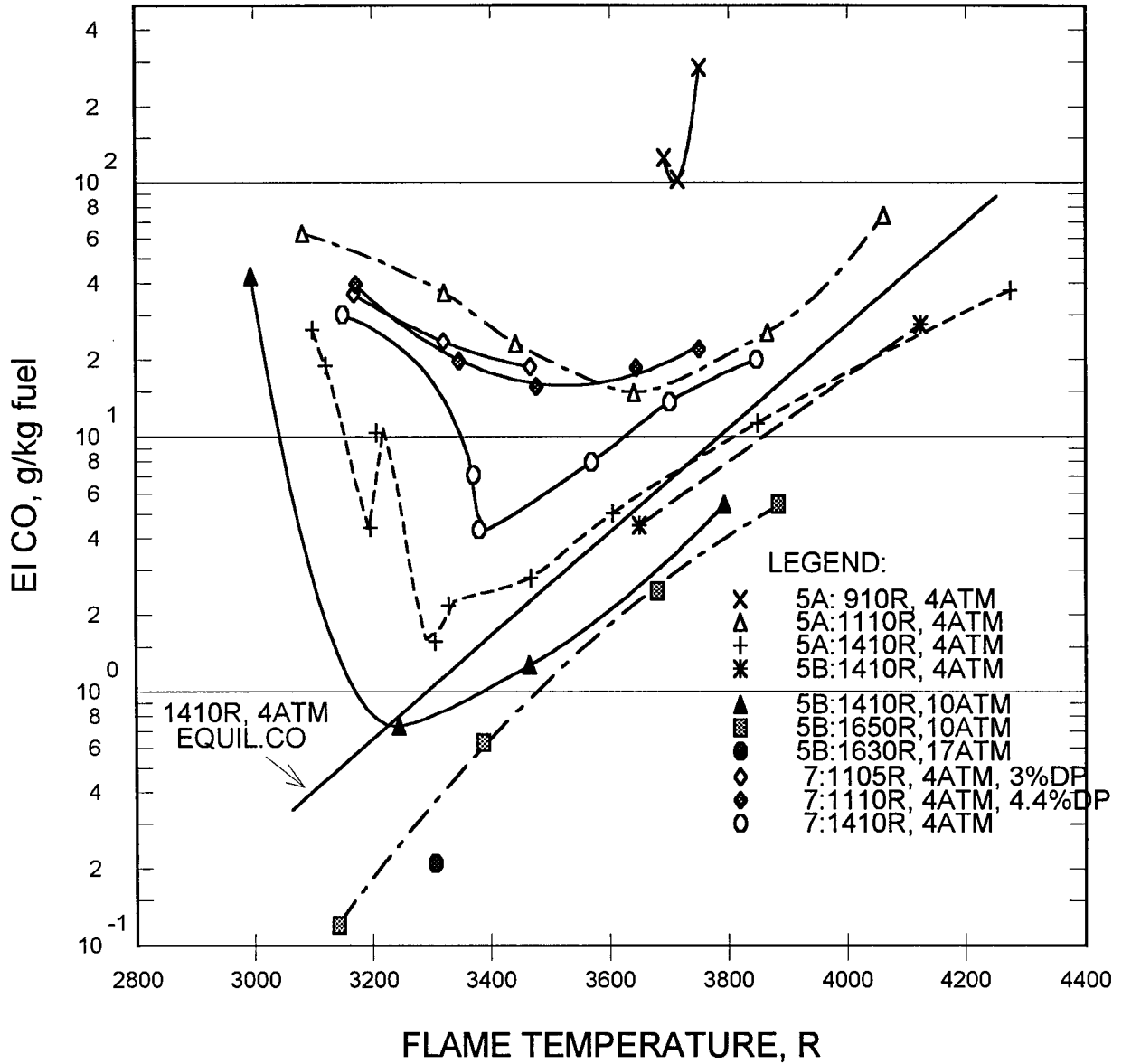


Figure 3.3 - CO Emissions Index plotted versus flame temperature for IMFH Configurations 5A, 5B and 7. Data obtained at several combinations of inlet temperature and pressure as indicated by the legend. The pressure drop was 4.4% unless indicated otherwise.

HSCT IMFH CONFIG. 7 & 8 NO_x EMISSIONS

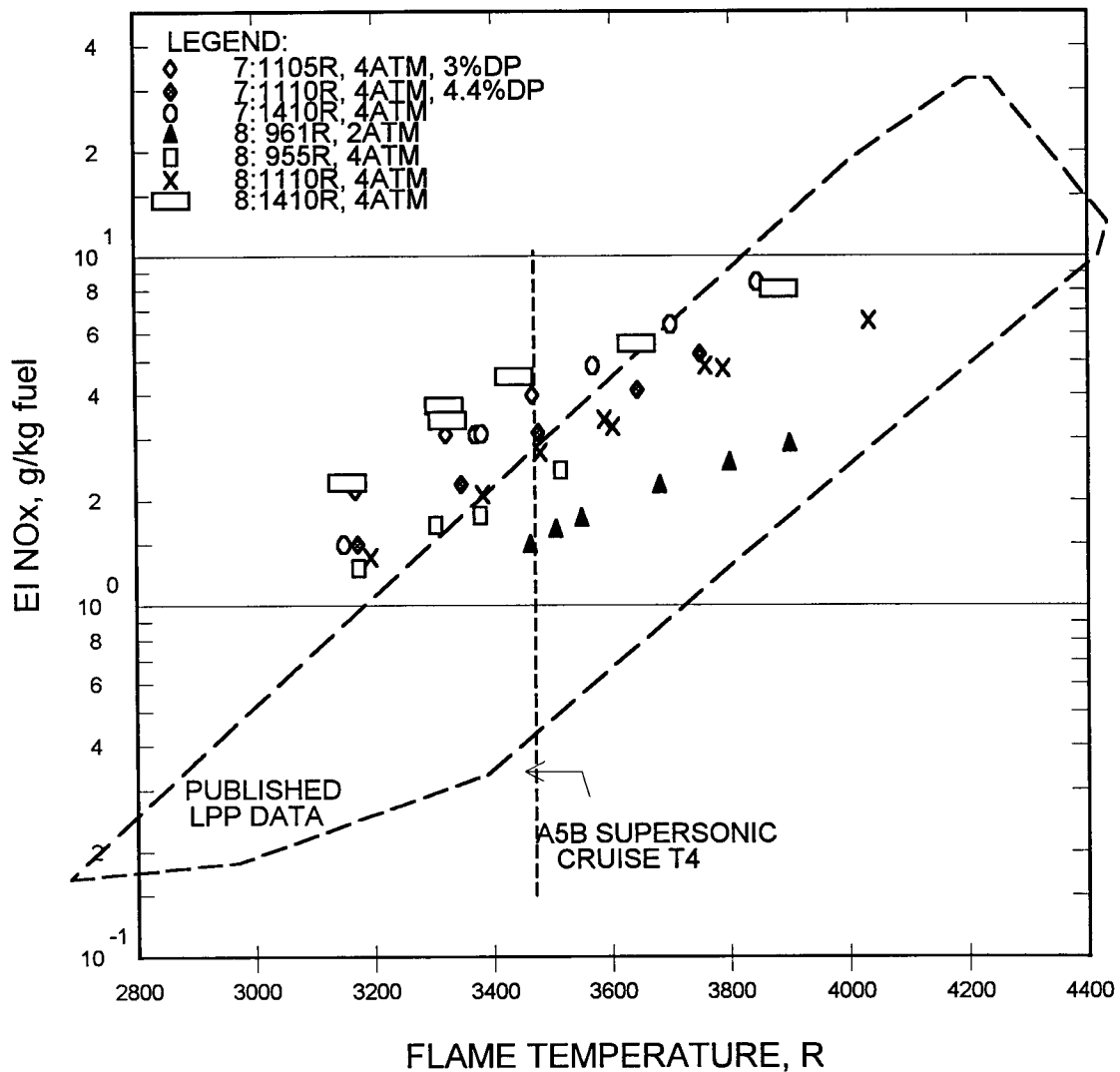


Figure 3.4 - NO_x Emissions Index plotted versus flame temperature for IMFH Configurations 7 and 8. Data obtained at several combinations of inlet temperature and pressure as indicated by the legend. The pressure drop was 4.4% unless indicated otherwise. The dashed boundary indicates the boundary of LPP NO_x emissions obtained in several laboratory flame tube studies.

HSCT IMFH CONFIG. 7 & 8 CO EMISSIONS

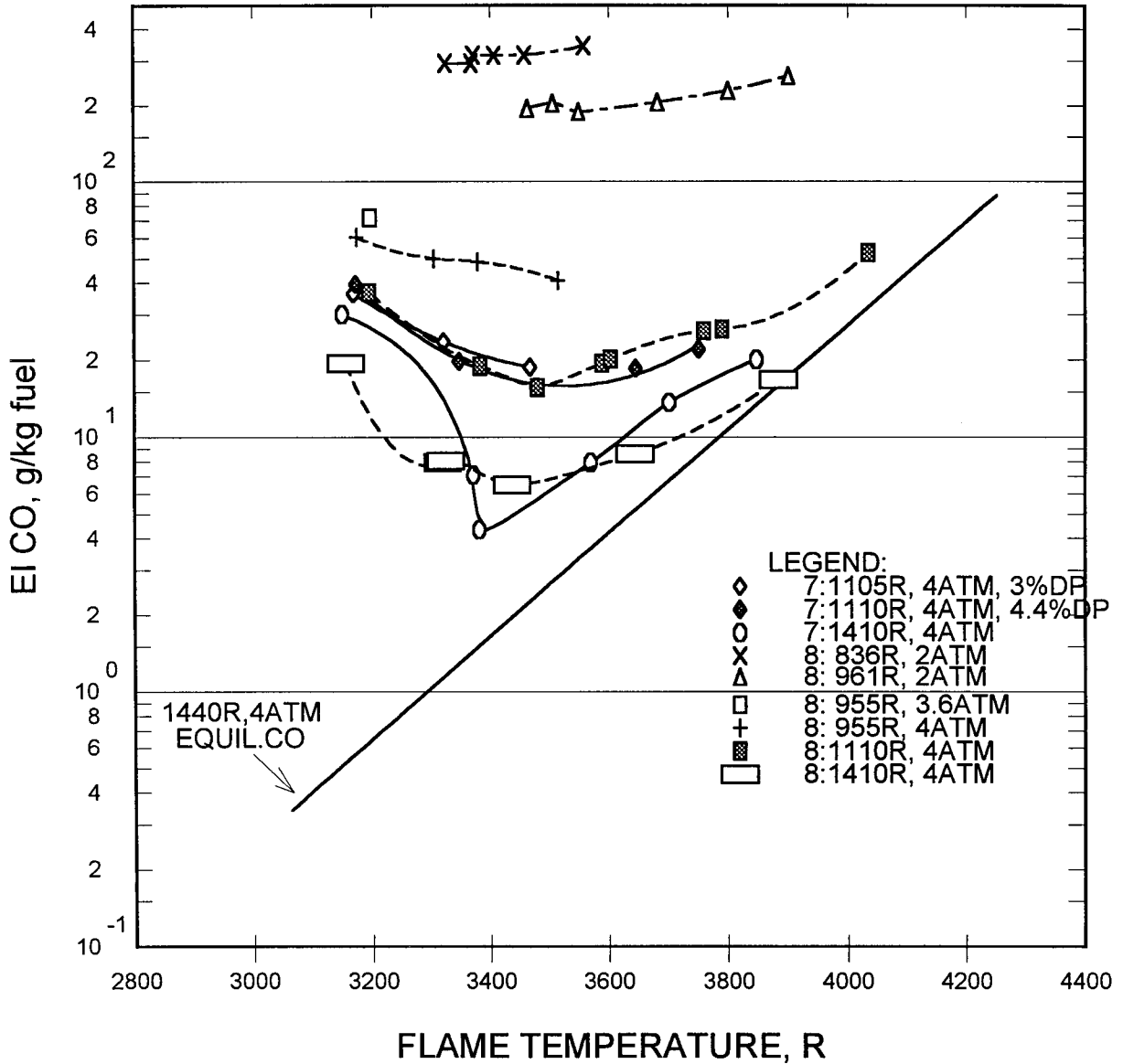


Figure 3.5 - CO Emissions Index plotted versus flame temperature for IMFH Configurations 7 and 8. Data obtained at several combinations of inlet temperature and pressure as indicated by the legend. The pressure drop was 4.4% unless indicated otherwise. The equilibrium line is for an inlet temperature of 1410 R and pressure of 4 atmospheres.

IMFH CONFIG. 7, 8 & 9 NOx EMISSIONS

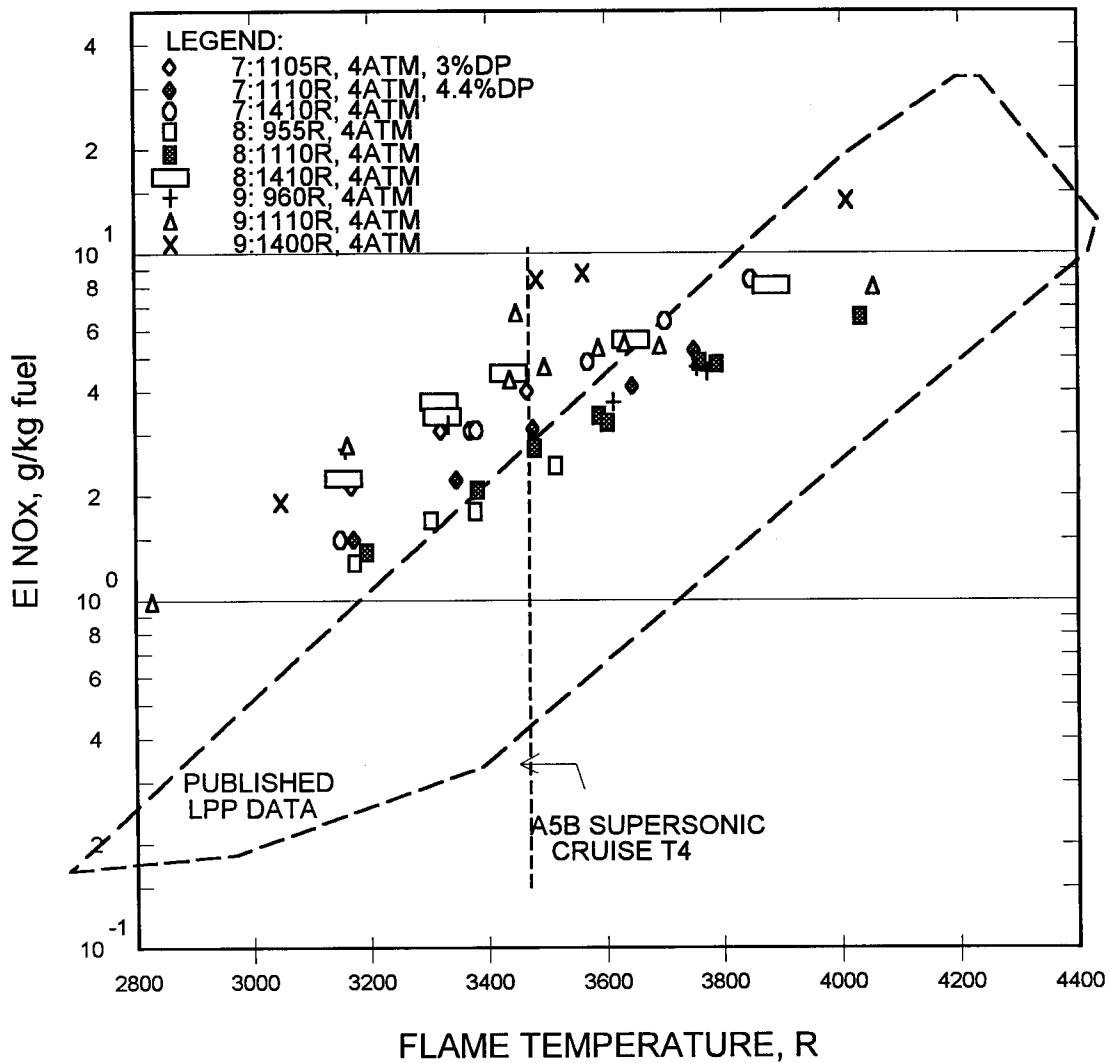


Figure 3.6 - NO_x Emissions Index plotted versus flame temperature for IMFH Configurations 7, 8 and 9. Data obtained at several combinations of inlet temperature and pressure as indicated by the legend. The pressure drop was 4.4% unless indicated otherwise. The dashed boundary indicates the boundary of LPP NO_x emissions obtained in several laboratory flame tube studies.

IMFH CONFIG. 7, 8 & 9 CO EMISSIONS

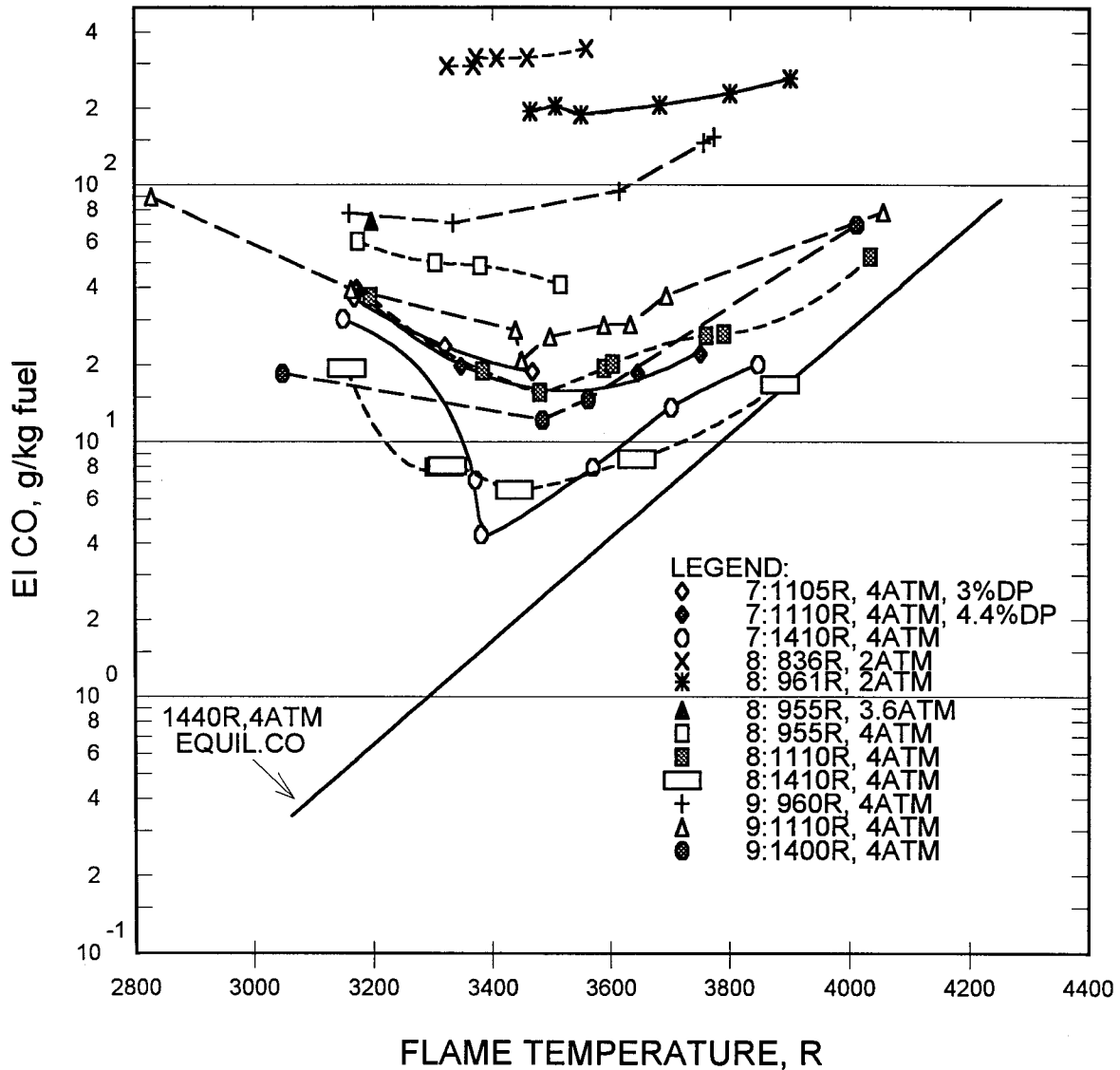
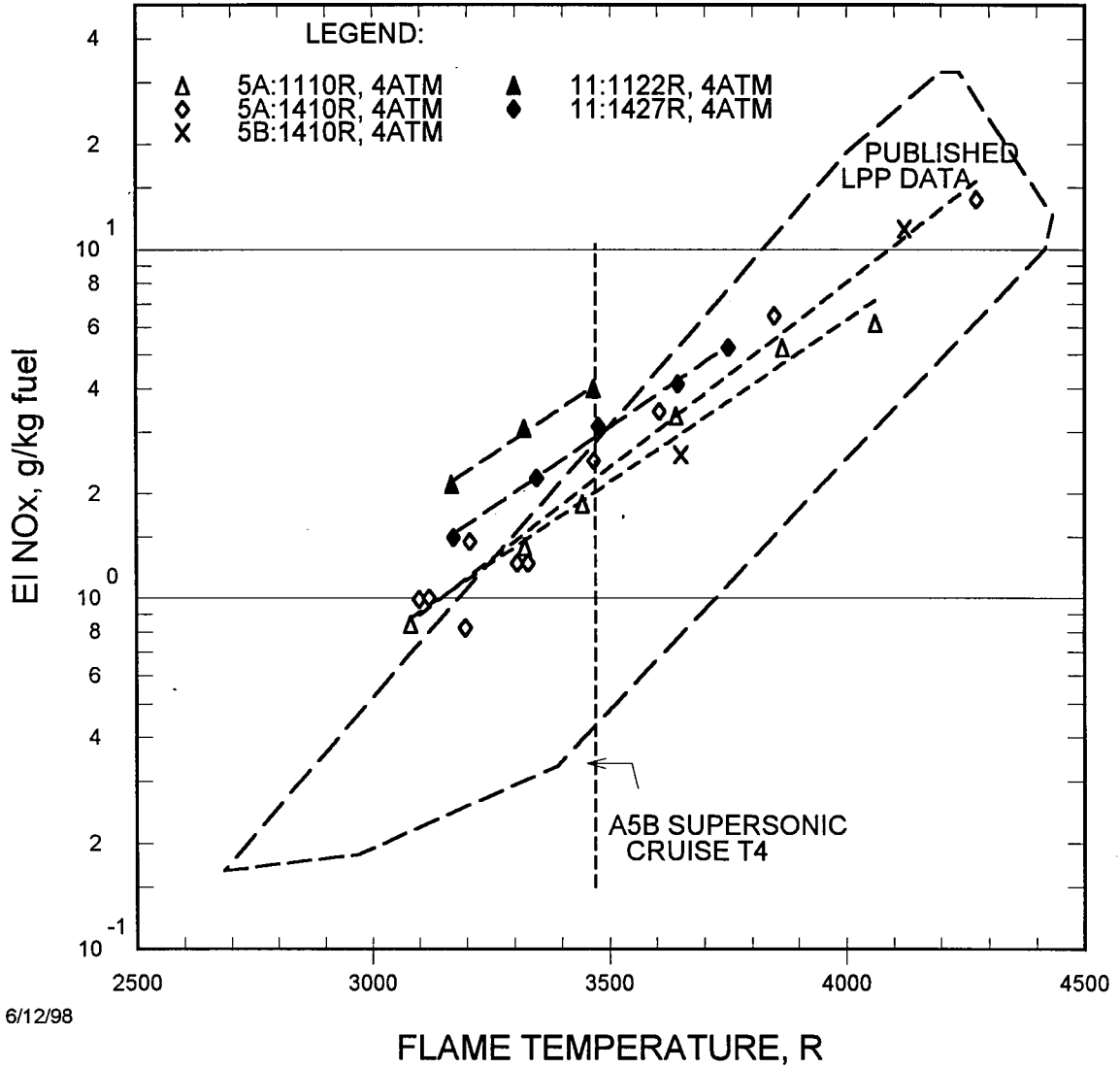


Figure 3.7 - CO Emissions Index plotted versus flame temperature for IMFH Configurations 7, 8 and 9. Data obtained at several combinations of inlet temperature and pressure as indicated by the legend. The pressure drop was 4.4% unless indicated otherwise. The equilibrium line is for an inlet temperature of 1410 R and pressure of 4 atmospheres.

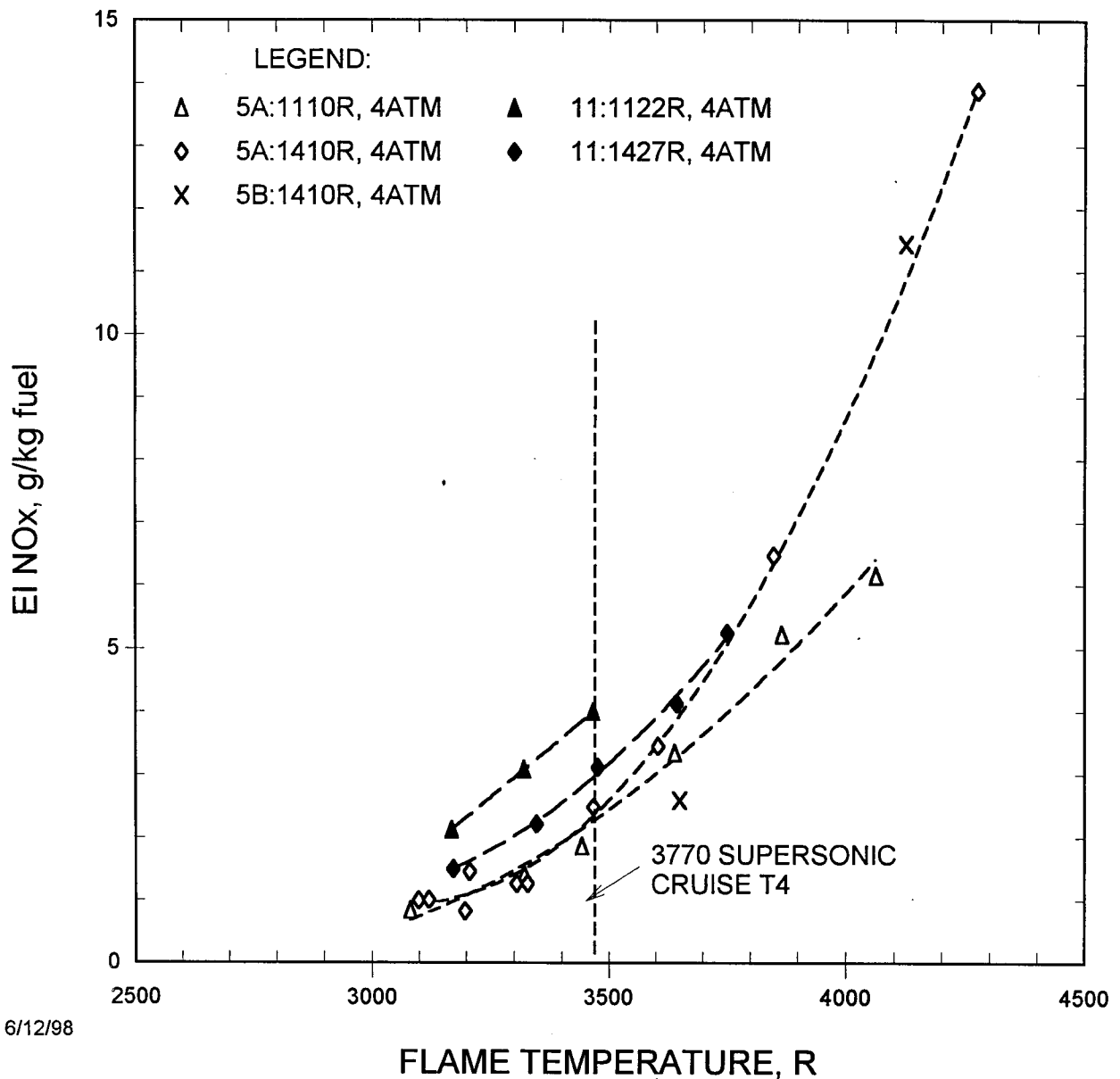
HSCT IMFH BASELINE NOx EMISSIONS



6/12/98

Figure 3.8 - NO_x Emissions Index plotted versus flame temperature for IMFH Configurations 5 and 11. NO_x EI on a log scale. Data obtained at several combinations of inlet temperature and pressure as indicated by the legend. The pressure drop was 4.4%. The dashed boundary indicates the boundary of LPP NO_x emissions obtained in several laboratory flame tube studies.

HSCT IMFH BASELINE NO_x EMISSIONS



6/12/98

Figure 3.9 - NO_x Emissions Index plotted versus flame temperature for IMFH Configurations 5 and 11. NO_x EI on a linear scale. Data obtained at several combinations of inlet temperature and pressure as indicated by the legend. The pressure drop was 4.4%. The dashed boundary indicates the boundary of LPP NO_x emissions obtained in several laboratory flame tube studies.

HSCT IMFH BASELINE COMBUSTION INEFFICIENCY

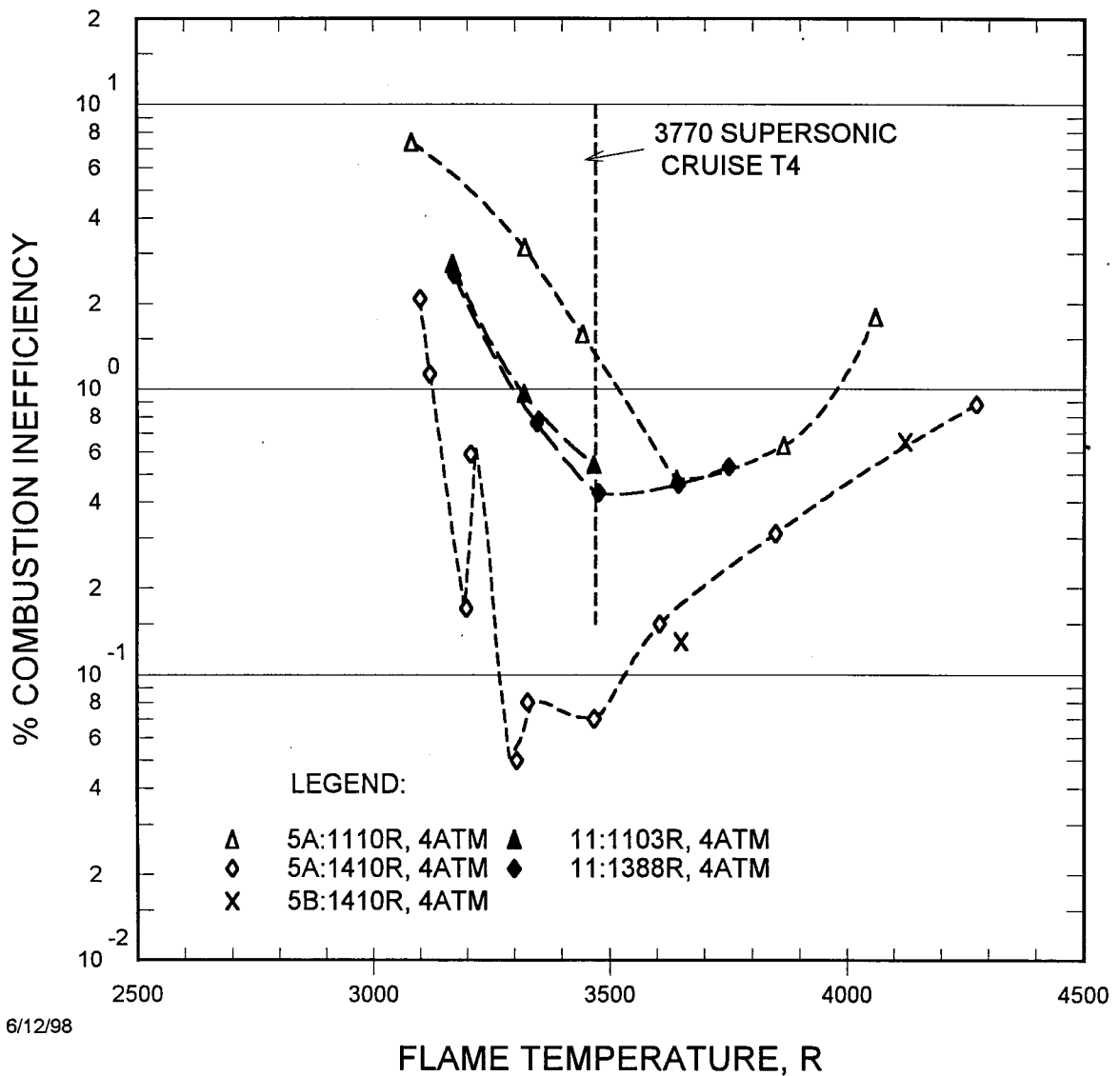


Figure 3.10 - CO Emissions Index plotted versus flame temperature for IMFH Configurations 5 and 11. Data obtained at several combinations of inlet temperature and pressure as indicated by the legend. The pressure drop was 4.4%.

inefficiency was needed. If the C/A_{EFF} of these mixers are closer to that of Configuration 11, then the comparison of combustion efficiency was made to Configuration 11. If the mixer's C/A_{EFF} was closer to that of Configuration 5, then the original comparison of combustion efficiency was used (with Configuration 5). Mixers with NO_x emissions worse than the Configuration 5 baseline were still considered poor performers. One interesting conclusion reached as a result of these baseline tests was that when the test results of the 0.652-inch diameter mixer tube in a 3.7 inch diameter flame tube (Performed in CPC Program, NASA contract NAS3-27235) were compared with the test results of the above configurations (0.495 inch diameter mixer tubes), the conclusion was that the 0.652-inch mixer tube had significantly poorer combustion efficiency than the 0.495-inch diameter mixer tube configurations.

Table 3.1 contains a list of the IMFH configurations tested as part of LET Task 10 of the NAS3-26617 contract. The table summarizes the design parameters and the test conditions.

TABLE 3.1 - Summary of IMFH Fuel-Air Mixer Development History

Boxed information indicates a change from previous configuration																			
Conf. #	Test Date	Mixer Tube Description	Mixer Tube #	Exit Diam. in.	Total Length in.	Mixing Length in.	Inlet Radius in.	Dome Cooling Air	Injector Type	Each Inj. Flow #	I.D. in.	O.D. in.	Axial Dist. from inlet in.	Immers. %	Combus. Liner Type	Diam. in.	Exit Se. P. in.	Test Type	
																			Large ID, transverse tube
Developed under NAS3-25652:																			
1	05-91	0.769" ID Straight mixer tube	7	0.769	5.100	4.500	20 deg flare	Bypass comb.	Large ID, transverse tube	1.5	1	0.069	0.125	0.600	50	Metal: H ₂ O Cooled	4.300	6.800	Atm. & Low P.
2	07-91	0.769" ID Straight mixer tube	7	0.769	5.100	4.500	20 deg flare	Bypass comb.	Transverse tube with 4 injection holes	1.4	4	0.008	0.125	0.600	30 & 70	Cast ceramic with air passages	4.300	6.400	Low pressure
3A1	09-91	0.560" ID Straight mixer tube	7	0.560	5.100	4.500	20 deg flare	Bypass comb.	Transverse tube with 2 injection holes	1.3	2	0.008	0.125	0.600	50	Cast ceramic with air passages	4.300	6.400	Low pressure
3A2	09-91	0.560" ID Straight mixer tube	7	0.560	5.100	4.500	20 deg flare	Bypass comb.	Transverse tube with 2 injection holes	1.3	2	0.008	0.125	0.600	50	Cast ceramic with air passages	4.300	6.400	Low pressure
3B	09-91	0.560" ID Straight mixer tube	7	0.560	5.100	4.500	20 deg flare	Bypass comb.	Transverse tube with 2 injection holes	1.3	2	0.008	0.125	0.600	50	Cast ceramic with air passages	4.300	6.400	Low pressure
4A	11-91	0.495" ID Straight mixer tube	13	0.495	5.500	4.500	0.188	Exst: 90 holes 0.085" diam at dome ring	Fine tube angled 15 deg.	1.2	1	0.020	0.040	1.000	50	Cast ceramic with air passages	4.300	6.800	Low pressure
Developed under NAS3-25951:																			
4B	01-92	0.495" ID Straight mixer tube	13	0.495	5.500	4.500	0.188	Bypass comb.	Fine tube angled 15 deg.	1.3	1	0.020	0.040	1.000	50	Cast Ceramic with air passages	4.888	7.423	Low pressure
5A	03-92	0.495" ID with dome cool air inj. into aft end of mixer tube	13	0.495	5.500	4.500	0.188	Inj. into mixers 6x 0.090" holes	Fine tube angled 15 deg.	1.3	1	0.020	0.040	1.000	50	Cast Ceramic with backside air cool.	4.888	7.423	Atm. & Low P.
5B	07-92	0.495" ID with dome cool air inj. into aft end of mixer tube	13	0.495	5.500	4.500	0.188	Inj. into mixers 6x 0.090" holes	Fine tube angled 15 deg.	1.3	1	0.020	0.040	1.000	50	Cast Ceramic	4.500	9.450	High pressure
6A	10-92	0.560" ID with dome cool air inj. thru dome near mixer exit	7	0.560	5.100	4.500	20 deg Flare	Through dome 6x 0.100" holes	Fine tube angled 15 deg.	1.3	1	0.020	0.040	1.000	50	Cast Ceramic	4.300	3.300	Low pressure
6B	01-93	0.560" ID with dome cool air inj. thru dome near mixer exit	7	0.560	5.100	4.500	20 deg Flare	Through dome 6x 0.100" holes	Fine tube angled 15 deg.	1.3	1	0.020	0.040	1.000	0	Cast Ceramic	4.300	3.300	Low pressure
Developed under NAS3-26617:																			
7	12-93	0.495" ID with dome cool air inj. into aft end of mixer tube	7	0.495	5.500	4.500	0.210	Inj. into mixers 6x 0.090" holes	Axial, blunt end, hollow conical spray injector	1.4	1	Spray Angle 70		1.000	50	Cast Ceramic	2.800	7.423	Low pressure
8	01-94	0.495" ID with dome cool air inj. into aft end of mixer tube	7	0.495	5.500	4.500	0.210	Inj. into mixers 6x 0.090" holes	Axial, blunt end, hollow conical spray injector	1.4	1	70	0.250	50	Cast Ceramic	2.800	7.423	Low pressure	
9	04-94	0.495" ID with dome cool air inj. into aft end of mixer tube	7	0.495	5.500	4.500	0.210	Inj. into mixers 6x 0.090" holes	Axial tapered end, hollow conical spray injector	1.6	1	54	0.050	50	Cast Ceramic	2.800	7.423	Low pressure	
10	03-94	0.495" ID with dome cool air inj. into red. length mixer tube	7	0.495	3.500	2.500	0.210	Inj. into mixers 6x 0.090" holes	Axial tapered end, hollow conical spray injector	1.6	1	54	0.050	50	Cast Ceramic	2.800	7.423	Low pressure	
11	11-94	0.495" ID with dome cool air inj. into aft end of mixer tube	7	0.495	5.500	4.500	0.210	Inj. into mixers 6x 0.090" holes	Fine tube angled 15 deg.	1.6	1	0.020	0.040	1.000	50	Cast Ceramic	2.800	7.423	Low pressure

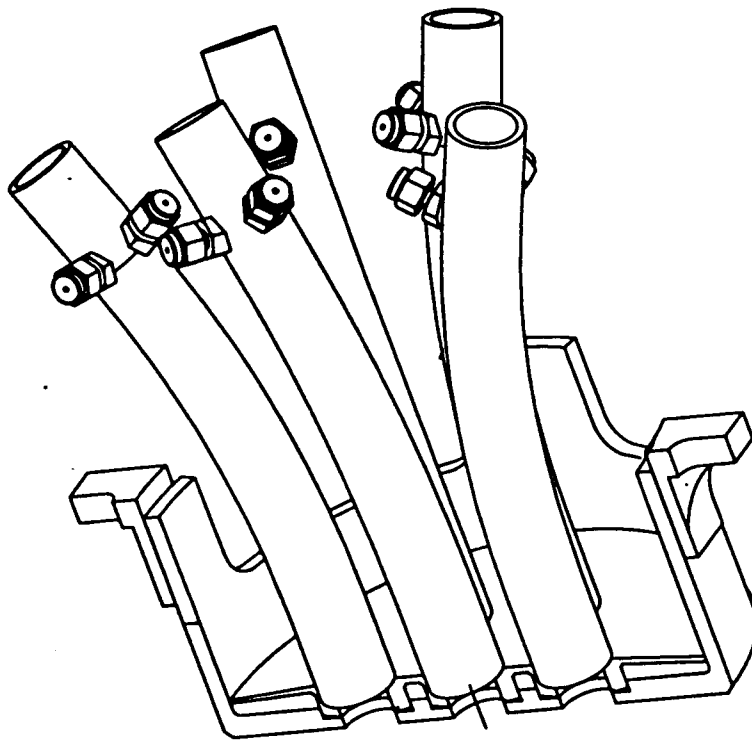
3.2 Curved Tube IMFH Evaluations

Single-cup IMFH configurations using curved IMFH premixer tubes were designed and tested. These were driven by engine envelope considerations for the original version of the Multistage Radial Axial (MRA) combustor shown in Figure 1.25. The evolution of the MRA combustor is discussed further in Section 6 of this report. Prior to the testing of the curved IMFH tube configurations, there were concerns about potential problems caused by curving the IMFH tubes. These were identified as:

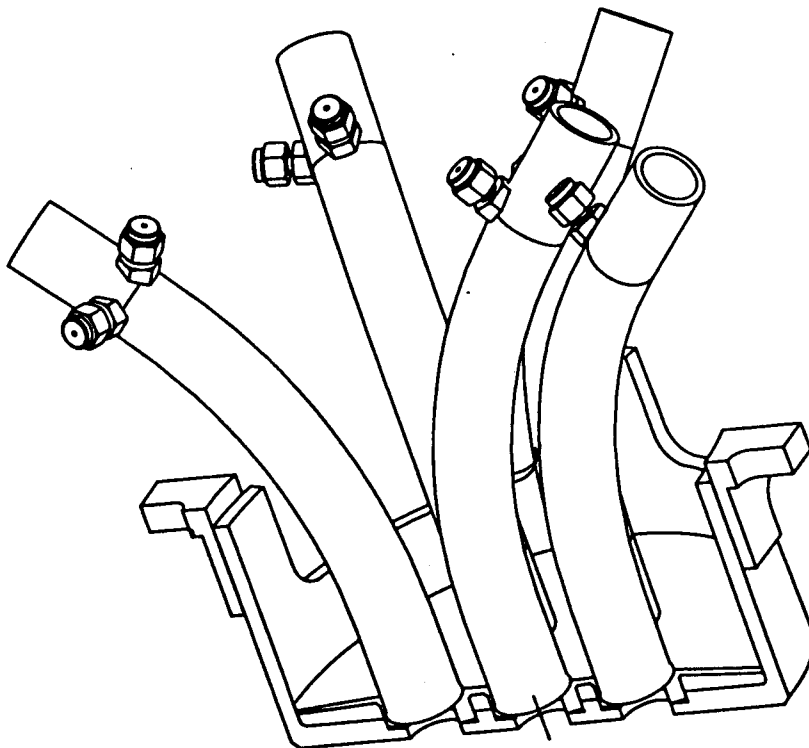
1. Flashback or autoignition caused by a large boundary layer building up along the inside radius of the curve, and
2. Poor fuel/air distribution at the exit of the premixer, possibly increasing NO_x emissions and decreasing combustion efficiency and stability limits.

Three mixer tube turning angles were selected for investigation: 22.5, 45, and 90 degrees. 90 degrees was the maximum turning angle that would be useful in the layouts of the MRA. Figure 3.11 illustrates two of the configurations considered. The mixer tubes themselves had a total centerline length of 5.5 inches, an outside diameter of 0.5 inches, and straight sections of 1.0 inch each at the inlet and exit of the tube. The transverse fuel injector tube was located 1.0 inch downstream of the inlet and was tested at various circumferential locations. The radii of curvature were: 90° - 2.23 inches, 45° - 4.46 inches, and 22.5° - 8.91 inches.

The 22.5 degree Curved Tube IMFH (CT-IMFH) configuration was tested at inlet temperatures ranging from 450 to 950° F (910 to 1410 R) and inlet pressures varying between 4.0 and 5.5 atmospheres. NO_x emissions were slightly higher and combustion efficiency was poorer than the IMFH Configurations 5A and 5B and lean stability was poor at all conditions tested. Post test inspection revealed a crescent shaped hole in the dome that resulted when a mixer tube/dome weld failed during the test. Therefore, the test was considered inconclusive with respect to NO_x, combustion efficiency, and lean stability. Plots of the data are not included here.



22.5° TUBE CONFIGURATION



45° TUBE CONFIGURATION

Figure 3.11 - Curved IMFH Tube subcomponent test hardware. 22.5-degree bend and 45-degree bend versions.

None of the evidence suggested that the hardware damage was due to flashback or autoignition within the mixer tubes themselves.

The MRA combustor would probably use tubes with bends in the range most closely approximated by the 45 degree tubes. Atmospheric testing of the 45 degree CT-IMFH with 75% fuel injector immersion showed a flame structure that appeared to be very similar to the straight tube IMFH configurations previously tested. No obvious fuel maldistribution was evident at the premixer tube exit. However, it would be expected that the radial acceleration of the flow field in the curved tubes would tend to separate the fuel towards the outside wall of the tube.

Three tests were conducted with the 45 degree CT-IMFH. They were performed at 4 atmospheres pressure at three immersions of the fuel injector tubes, 20%, 50% and 75%. Figures 3.12 through 3.14 compare NO_x emissions, combustion inefficiency, and CO emissions results for the 45 degree CT-IMFH for two immersions of the fuel injector tubes, 20% (short immersion) and 50% (center immersion). The two immersions had roughly comparable emissions performance, although the shorter immersion appears to yield lower NO_x emissions. Figure 3.15 shows that the NO_x emissions for the short injector immersion in CT-IMFH were very similar to Configuration 5A. However, Figures 3.16 and 3.17 show that combustion efficiency and CO emissions for the CT-IMFH with the short immersion injector was significantly worse than Configuration 5A at all except the lowest inlet temperature of 450° F (910 R). This may be due to poor fuel distribution. When compared to Configuration 5A, Figure 3.18 shows that the CT-IMFH with 75% immersion demonstrated good NO_x emissions performance. Apparently, the high immersion offset the radial acceleration effects, to some degree. However, the combustion efficiency, CO emissions, and stability were still poor relative to Configuration 5 (Figures 3.19 and 3.20).

Inspection of the hardware after the 75% immersion test revealed a small hole burned through the dome. The hole was apparently caused by the loss of the TBC coating, which appeared to result from over-heating of the dome face. Some sort of flashback or autoignition was suspected of causing the dome failures. Additional observation revealed evidence that fuel

HSCT 45DEG.CURVED TUBE IMFH NOx EMISSIONS

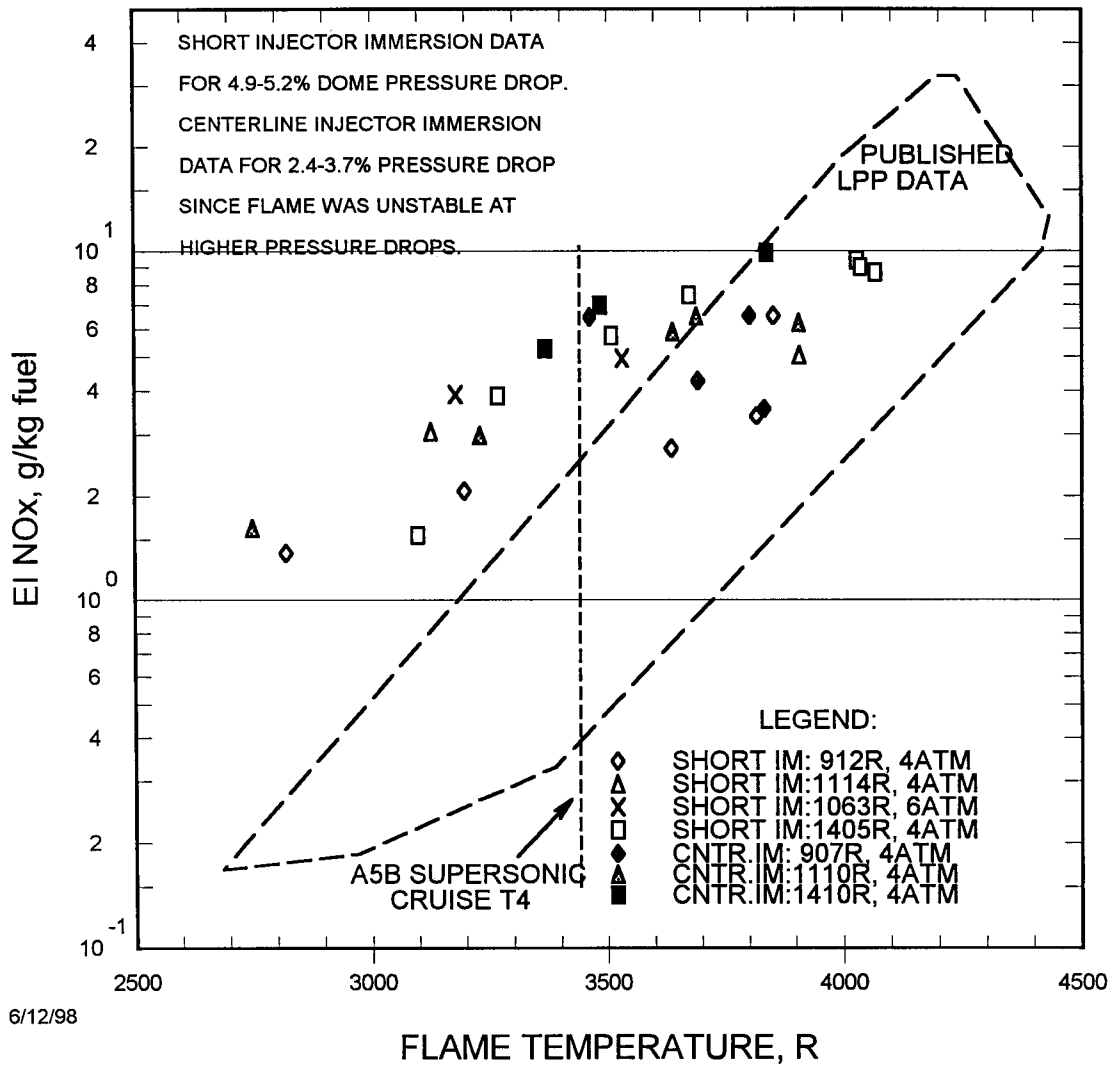


Figure 3.12 - NOx Emissions Index plotted versus flame temperature for 45-degree curved tube IMFH. Data shown for 20% immersion (short) and 50% immersion (center) of the fuel injector tube. The dashed boundary indicates the envelope of LPP NOx emissions obtained in several laboratory flame tube studies published in the open literature.

HSCT 45DEG.CURVED TUBE IMFH COMBUSTION INEFFICIENCY

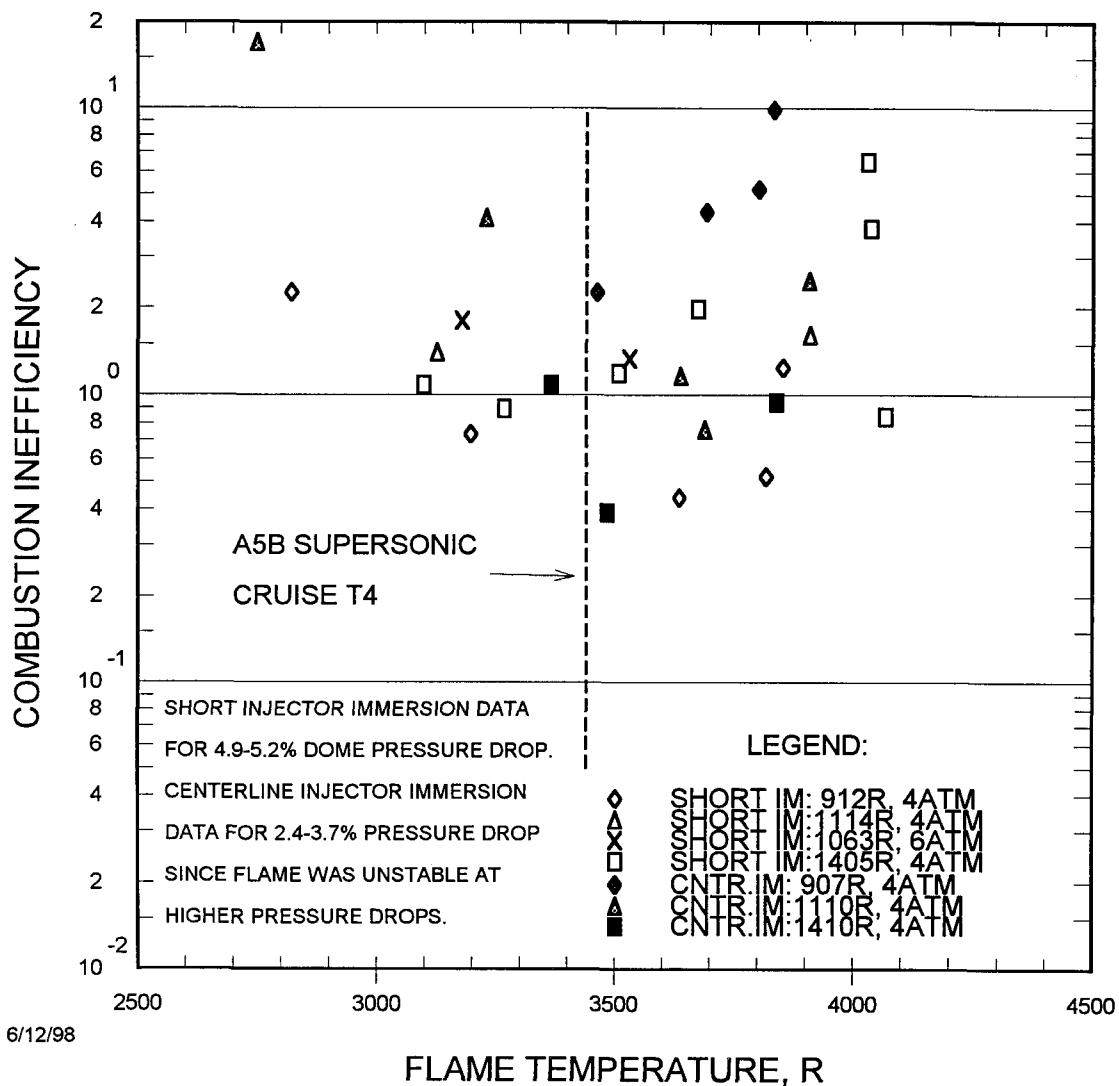


Figure 3.13 - Combustion Inefficiency plotted versus flame temperature for 45-degree curved tube IMFH. Data shown for 20% immersion (short) and 50% immersion (center) of the fuel injector tube.

HSCT 45DEG.CURVED TUBE IMFH CO EMISSIONS

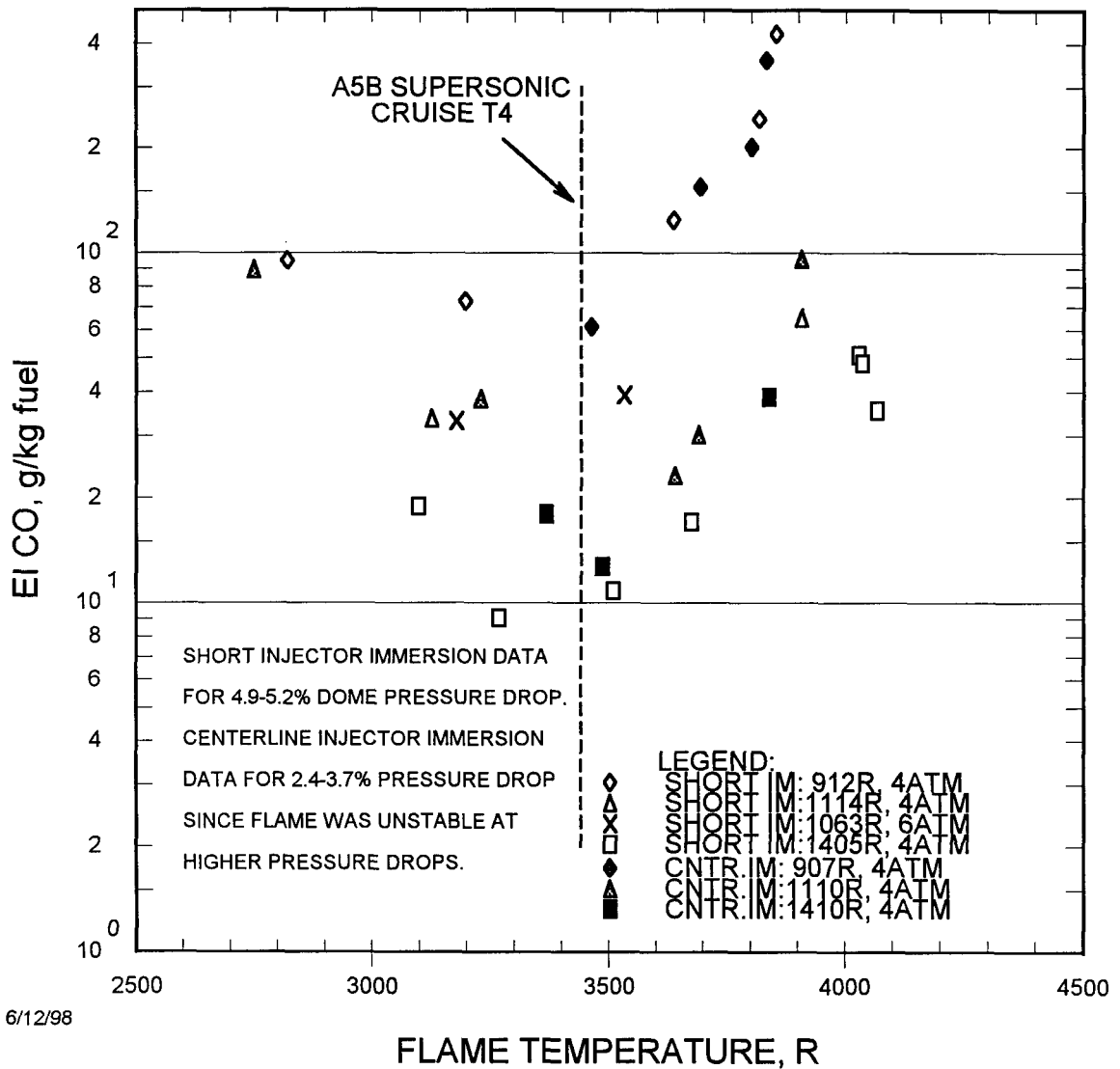


Figure 3.14 - CO Emissions Index plotted versus flame temperature for 45-degree curved tube IMFH. Data shown for 20% immersion (short) and 50% immersion (center) of the fuel injector tube.

HSCT 45DEG.CURVED TUBE & CONF.5 IMFH NOx EMISSIONS

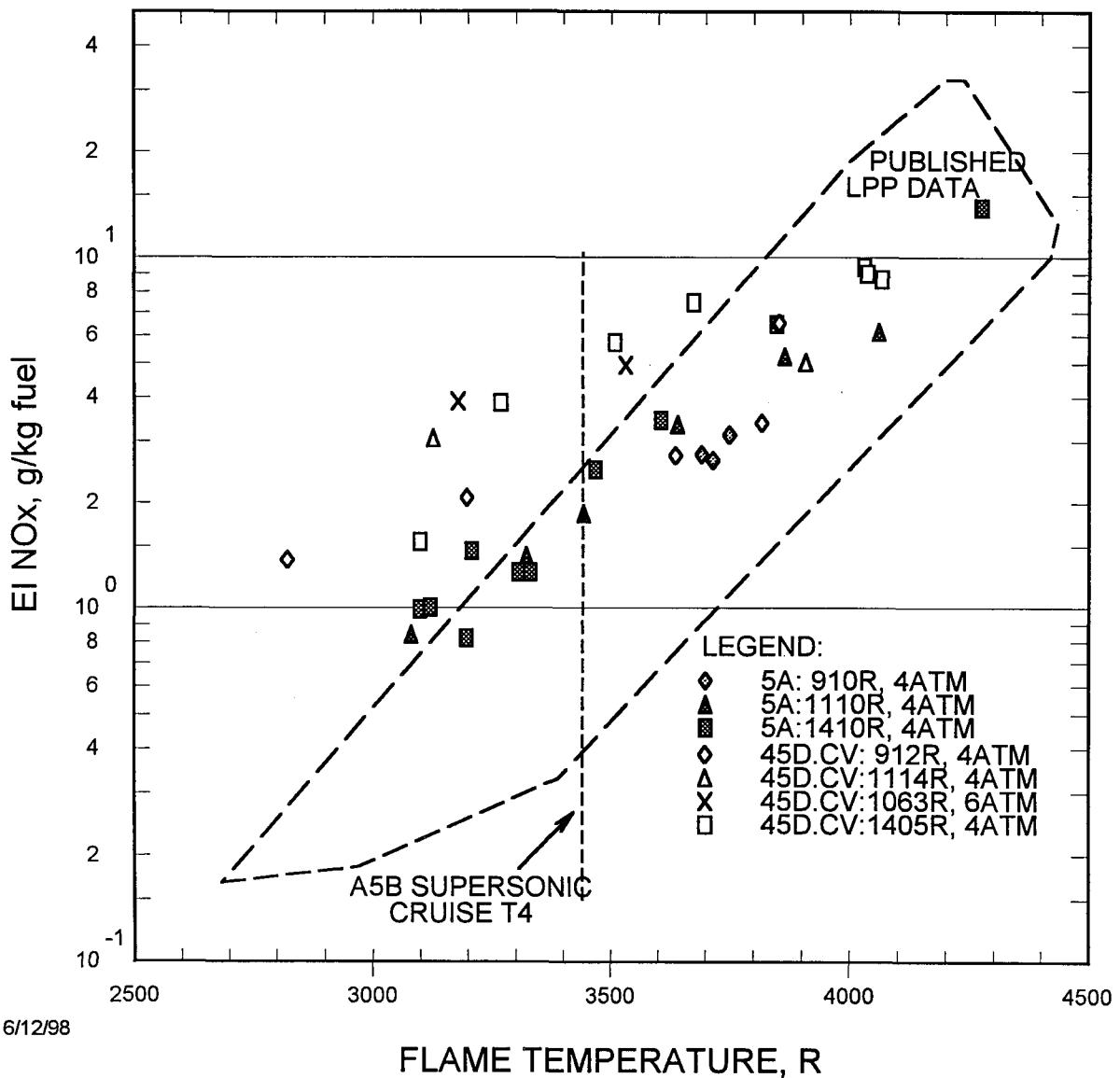


Figure 3.15 - NOx Emissions Index plotted versus flame temperature for 45-degree curved tube IMFH. Data for 20% immersion (short) of fuel injector tube is compared to the baseline straight IMFH tube which has a 50% immersion (Configuration 5). The dashed boundary indicates the boundary of LPP NOx emissions obtained in several laboratory flame tube studies published in the open literature.

45 DEG. CURVED TUBE & CONF 5 IMFH COMBUSTION INEFF

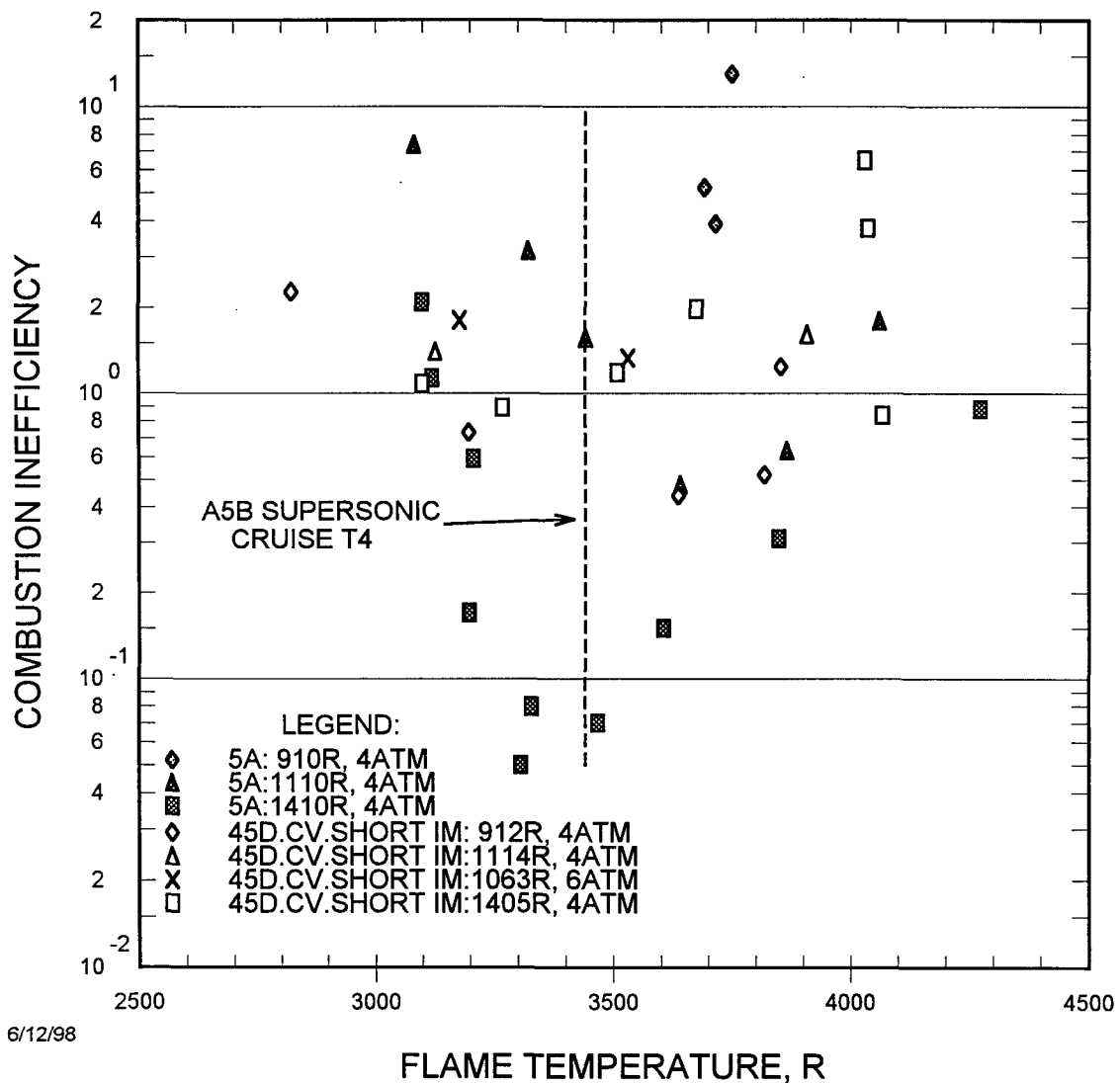


Figure 3.16 - Combustion inefficiency plotted versus flame temperature for 45-degree curved tube IMFH. Data for 20% immersion (short) of fuel injector tube is compared to the baseline straight IMFH tube which has a 50% immersion (Configuration 5).

45 DEG CURVED TUBE & CONF 5 IMFH CO EMISSIONS

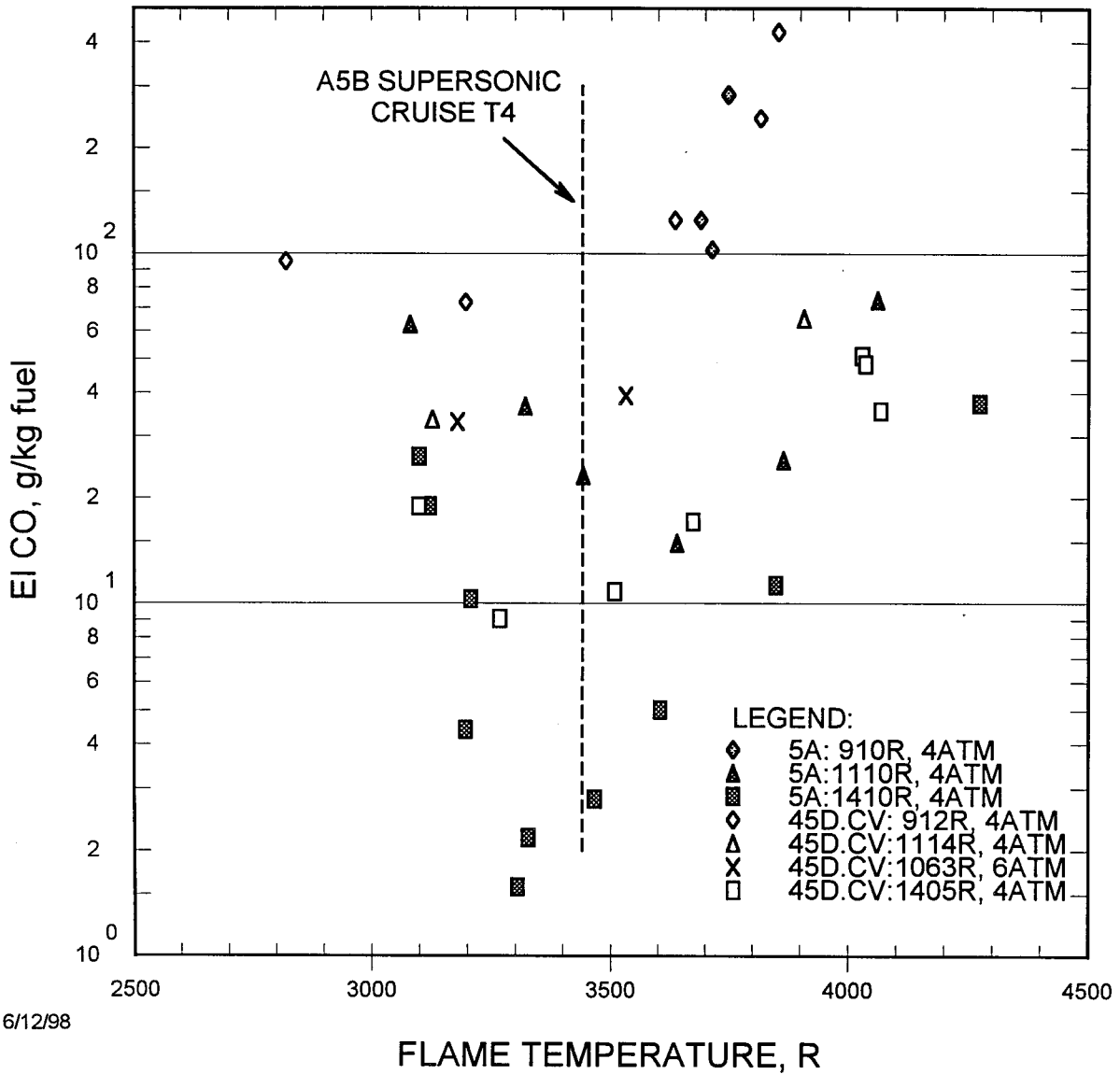


Figure 3.17 - CO Emissions Index plotted versus flame temperature for 45 degree curved tube IMFH. Data for 20% immersion (short) immersion of fuel injector tube is compared to the baseline straight IMFH tube which has a 50% immersion (Configuration 5).

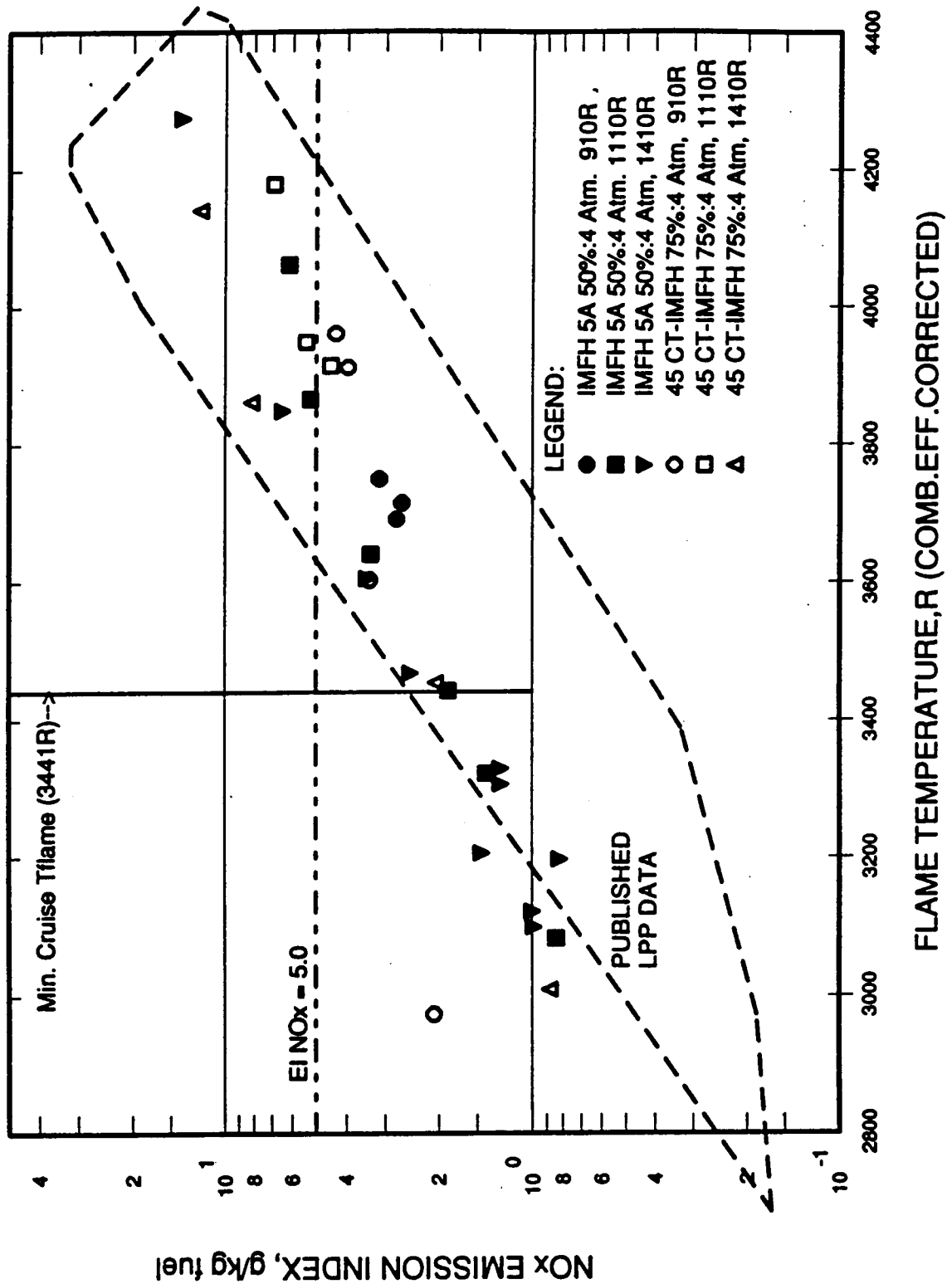


Figure 3.18 - NO_x Emissions Index plotted versus flame temperature for 45 degree curved tube IMFH. Data for 75% immersion of the fuel injector tube is compared to the baseline straight IMFH tube which has a 50% immersion (Configuration 5). The dashed boundary indicates the envelope of LPP NO_x emissions obtained in several laboratory flame tube studies published in the open literature.

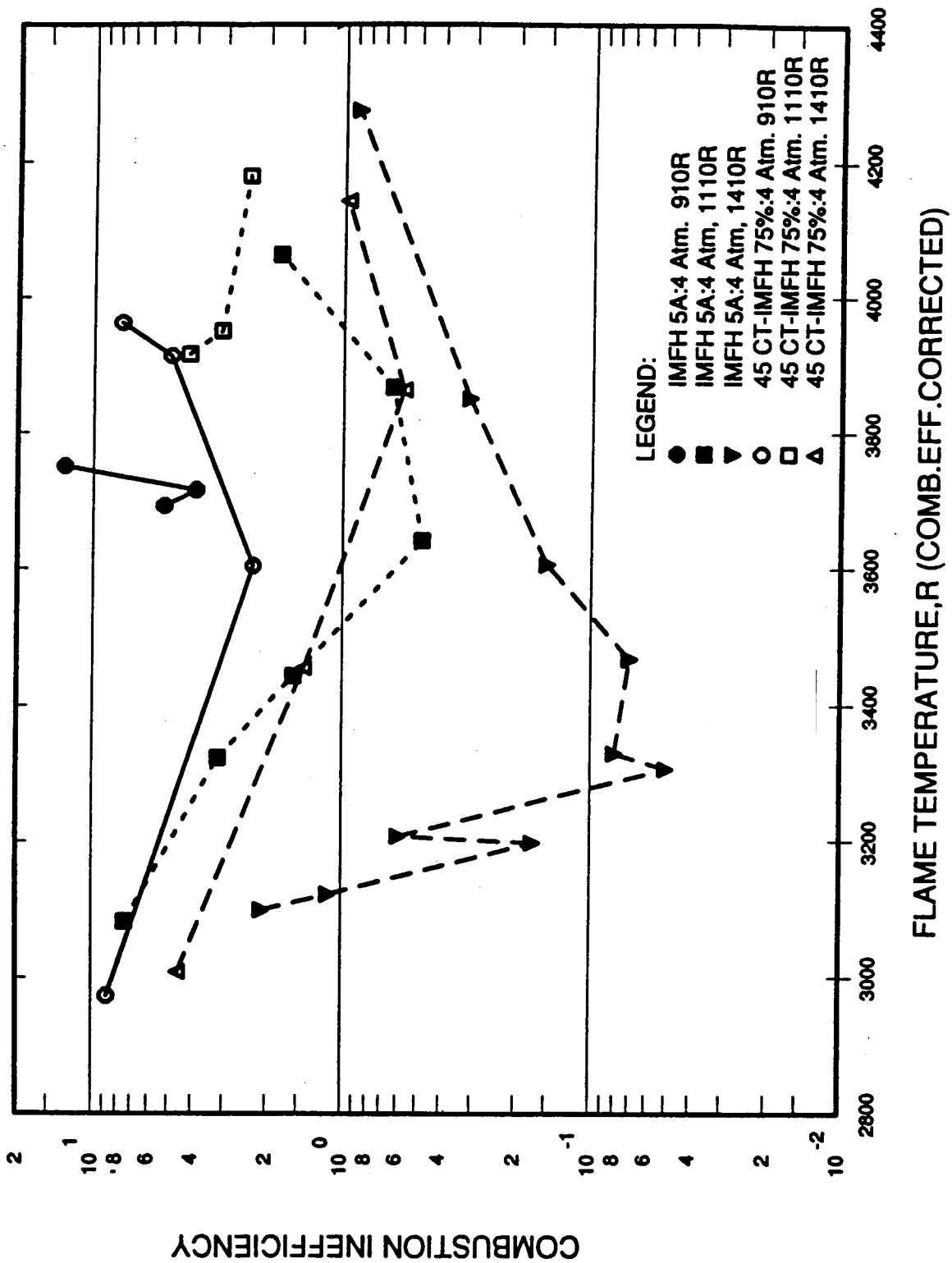


Figure 3.19 - Combustion inefficiency plotted versus flame temperature for 45 degree curved tube IMFH. Data for 75% immersion of the fuel injector tube is compared to the baseline straight IMFH tube which has a 50% immersion (Configuration 5).

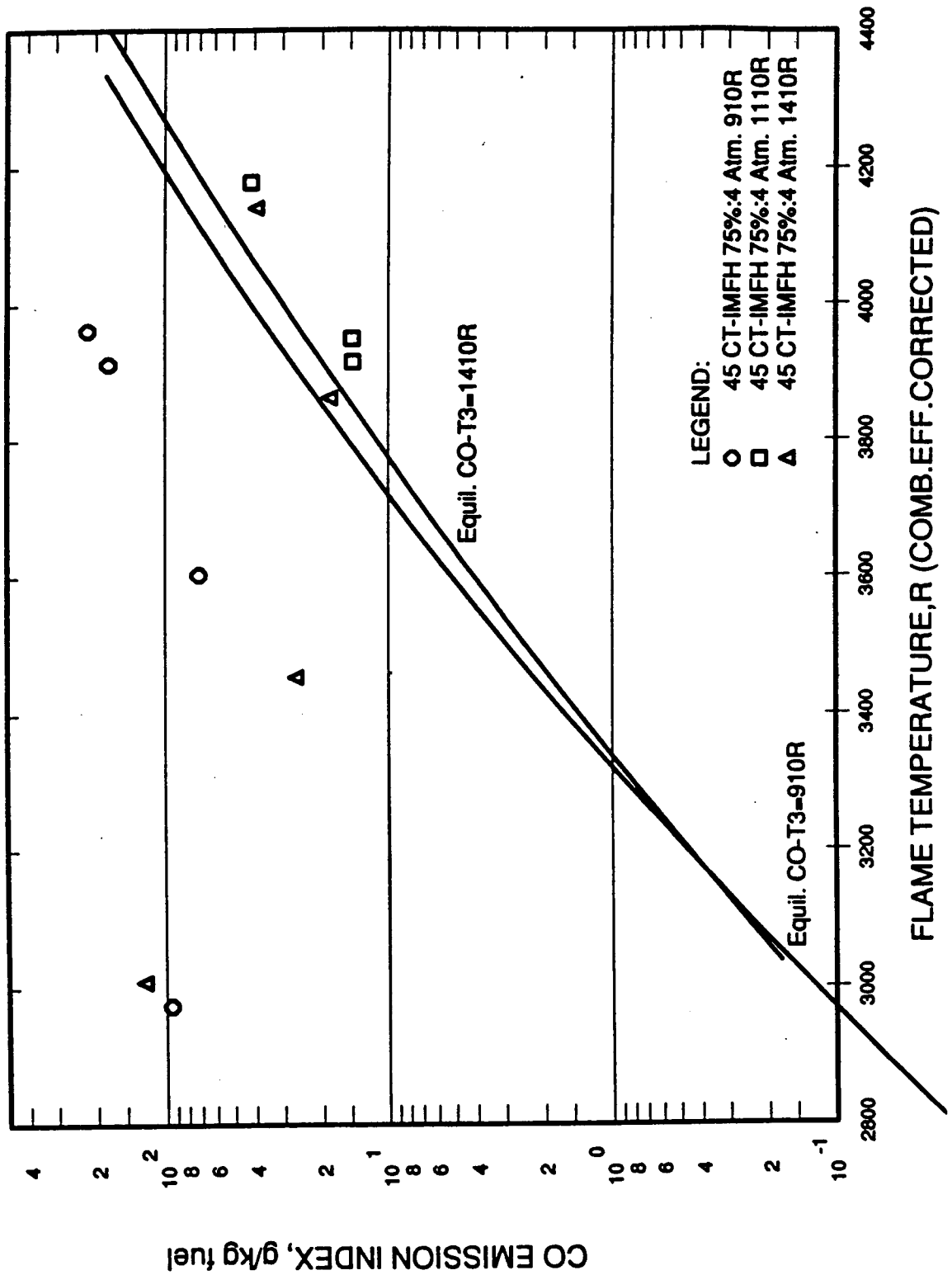


Figure 3.20 - CO Emissions Index plotted versus flame temperature for 45 degree curved tube IMFH. Data for 75% immersion of the fuel injector tube.

was impinging on the mixer tube wall just downstream of the fuel injector and was washed down the side of the tube by high velocity air. It was also observed that nearly all of the fuel evaporated off the mixer tube wall before exiting the premixer tube, indicating a very skewed fuel/air profile at the exit of the premixer tube.

In general, the curved tube configurations had poorer combustion efficiency, stability problems, and higher NO_x emissions than the IMFH 5B configuration. Also, there was evidence that the performance of the CT-IMFH has a high sensitivity to pressure drop (or velocity in the tube). These problems were probably due to poor fuel distribution caused by radial acceleration of the flow field in the curved tube. There was also an increased risk of flashback and autoignition within the curved tube configurations. By itself, the poor stability of the curved tube IMFH is not considered to be a disadvantage. The original MRA combustor design provides a forced flow of burnt gases from the pilot across the IMFH dome. This flow of burnt gases provides the stability of the combustor. The pilot gases would ignite and stabilize the fueled IMFH jets. However, the other disadvantages of the curved tube IMFH were considered unacceptable and it was eliminated from consideration for further development. Meanwhile, the MRA combustor evolved to a design not requiring curved IMFH tubes. This change in the MRA combustor's design was principally driven by the lack of a workable fuel injector design for the original MRA, although the poor performance of the curved IMFH tubes was also a consideration. The evolution of the MRA combustor design is discussed in more detail in Section 6.5.

3.3 Swirl-IMFH Evaluations

The Swirl-IMFH refers to the concept of combining a small number of IMFH tubes in a package with an integrated fuel injection system. The individual IMFH tubes did not have any swirl in the flow but the tubes were arranged to impart a net swirl to the flow exiting the package. The Swirl-IMFH concept was thought to offer the following advantages over previous IMFH configurations:

1. The introduction of swirl could improve mixing of the discrete jets exiting the fuel/air mixer and improve emissions and/or allow reduction of the IMFH tube length.
2. The swirl could increase recirculation in the combustion zone for improved combustion stability.
3. The circular arrangement of the mixer tubes was analogous to a conventional swirl cup package and lends itself to conventional fuel injector concepts which could simplify the combustor mechanical design.
4. The fuel system passages could be an integral part of the tube casting (in production). This would greatly reduce the complexity of the fuel system for the IMFH design. It also would allow for a single flow divider or staging valve to be used for all mixer tubes in a Swirl-IMFH group.
5. The centerline simplex pilot nozzle could potentially improve stability. This "concentric" staging concept could make the Swirl-IMFH acceptable as a pilot, thereby eliminating the need for a separate pilot stage in the combustor.

3.3.1 Swirl-IMFH (Standard Tube Dimensions) Evaluations

The Swirl-IMFH fuel/air mixer concept, shown in Figure 3.21, packaged the IMFH mixer tubes into a 2.5 inch diameter circular pattern with each tube angled to impart a small amount of swirl (13.5°) into the combustion zone. The IMFH tubes had a 0.50-inch inner diameter and were

5.5 inches long. The tube exit matrix formed a perforated plate flame holder. Fuel injector tubes had the standard 0.020-inch inner diameter.

Four configurations of fuel injector tubes were used: 1) coaxial into the mixer tube inlet terminating one inch from the tube entrance, 2) transverse injection one inch downstream from the tube entrance with the injector ending at the wall, 3) with 20% immersion, and 4) with 50% immersion. This provided 4.5 inches of mixing/vaporization length in all cases. The schematic in Figure 3.22 compares the coaxial configuration with the transverse configuration with 50% immersion. A simplex pressure atomizing fuel injector was located at the centerline of the Swirl-IMFH module to act as a pilot. This pilot burns in a diffusion flame and would be used only during low power conditions to improve combustion efficiency and stability.

An atmospheric pressure test of the Swirl-IMFH with the coaxial injector configuration consisting of main stage only (premixer only) operation was run at inlet temperatures ranging from ambient up to 650° F (1110 R). Stability appeared to be good. The lean blowout data are plotted versus inlet temperature in Figure 3.23. The flame was mostly blue, with a yellow flame near the center at some operating conditions. The flame exiting each premixer tube appeared to have a blue streak at the center.

Figures 3.24 through 3.26 compare the results of the 50% immersion wall injector (data points F and G) and coaxial injectors (data points H and I) in four-atmosphere tests. NO_x emissions were significantly higher for the coaxial injection case, while combustion inefficiencies were similar for both configurations. At elevated inlet temperatures, the wall injection configuration reached equilibrium CO levels and had a lower CO at the bucket than the coaxial configuration. It was concluded that the coaxial injectors had the more non-uniform of the fuel/air profiles at the exit of the premixer tubes. The observation of centerline streaks in the atmospheric test of the coaxial injector configuration is consistent with this conclusion.

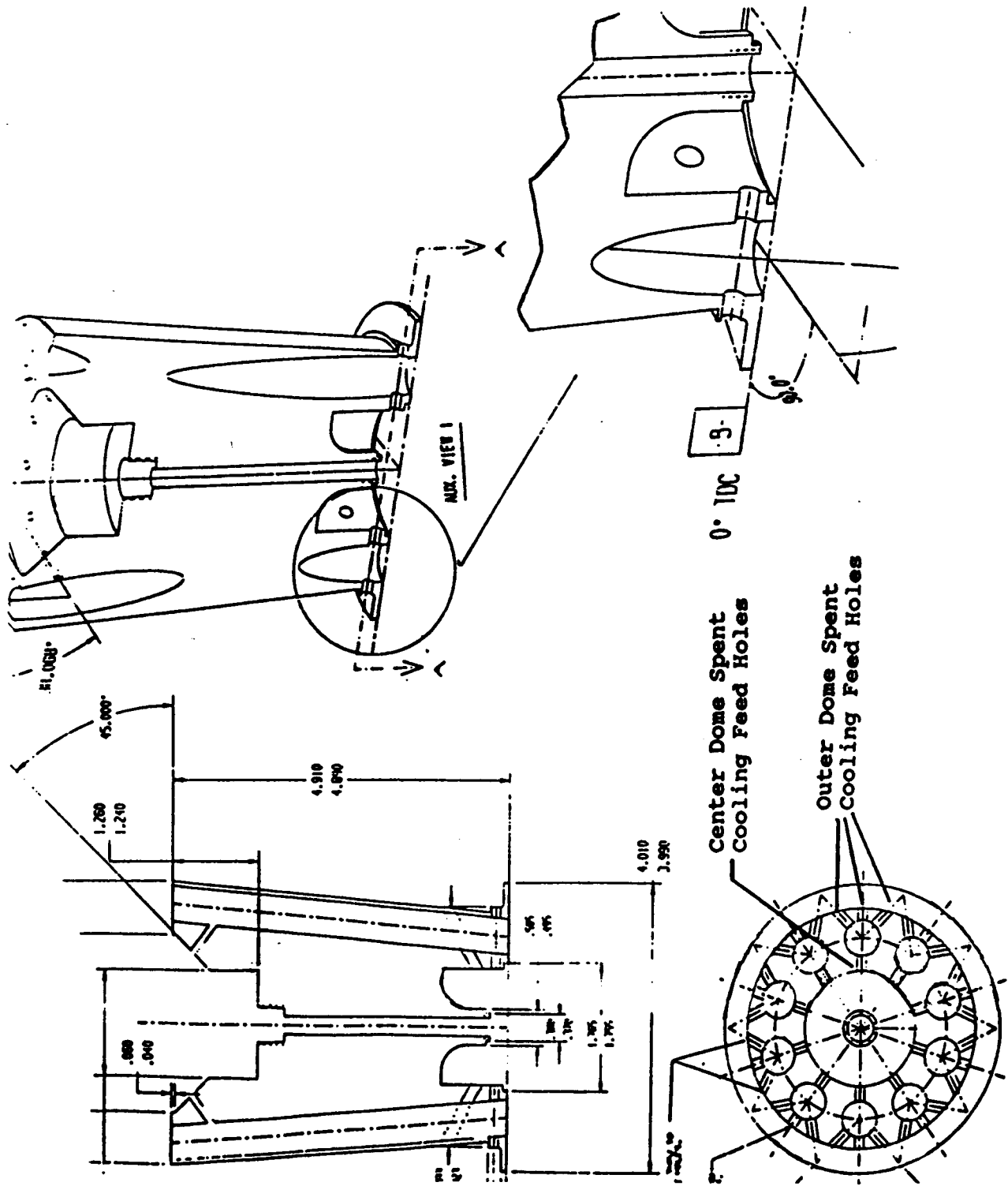
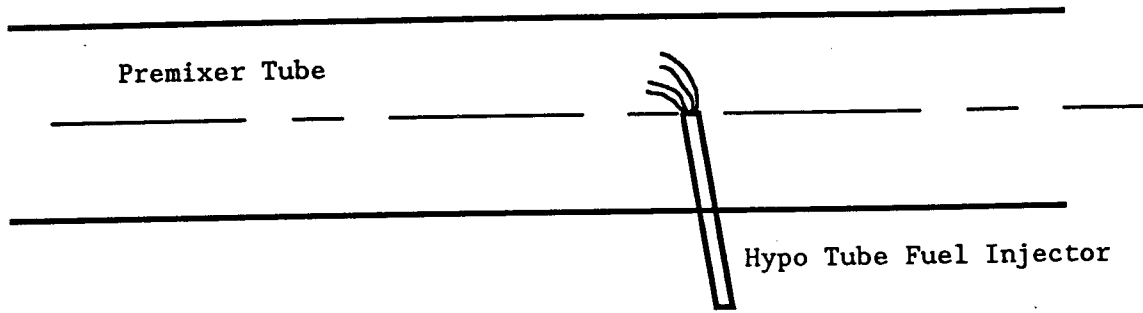
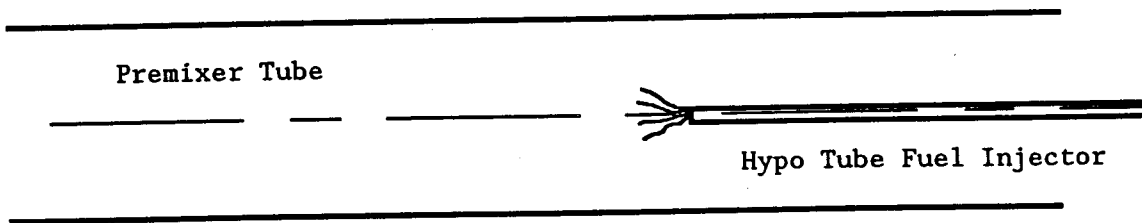


Figure 3.21 - Swirl-IMFH Fuel-Air Mixer subcomponent test hardware.



Wall Injection



Coaxial Injection

Figure 3.22 - Swirl-IMFH fuel injector configurations. The 50% immersion transverse injector and coaxial injector are standard injector configurations also tested in the baseline IMFH configuration. The air flow is right to left in this figure.

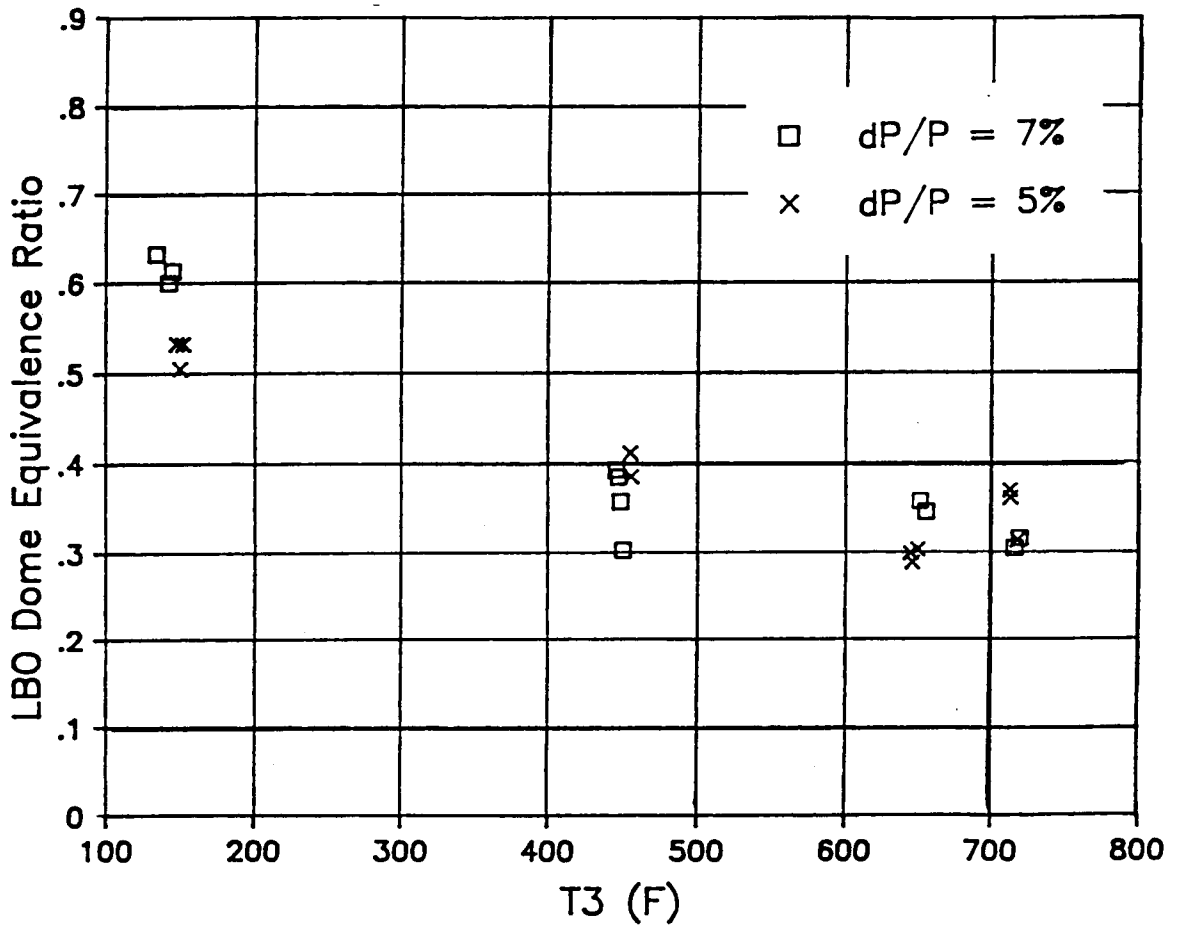


Figure 3.23 - Lean blow out Results for the Swirl-IMFH with the coaxial injector at 5% and 7% dome pressure drop. Lean blow out equivalence ratio is plotted versus T₃.

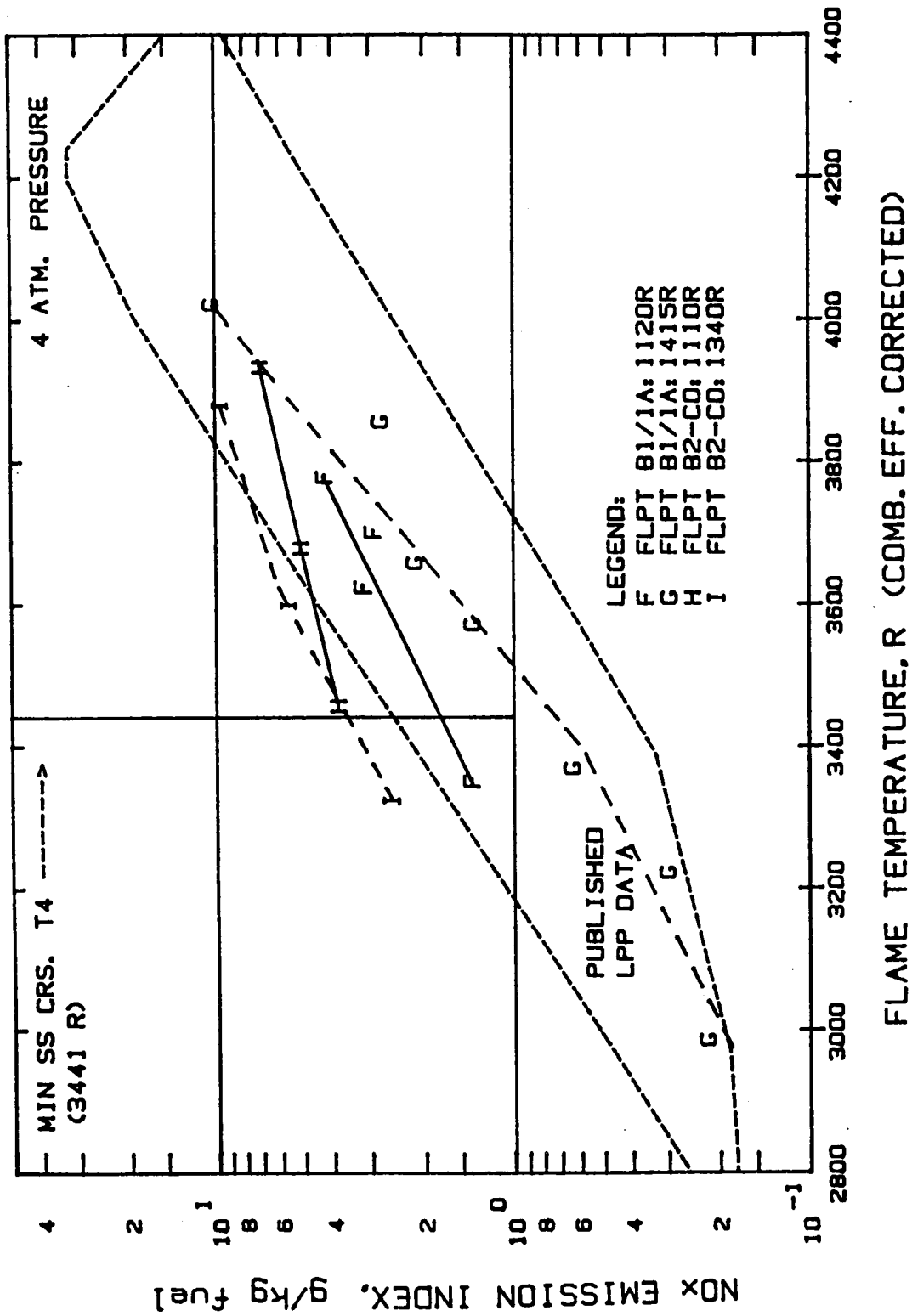


Figure 3.24 - NOx emissions index plotted versus flame temperature for the Swirl-IMFH with the 50% immersion transverse fuel injector (Build 1, points F and G) compared to the coaxial fuel injector configuration (Build 2, points H and I).

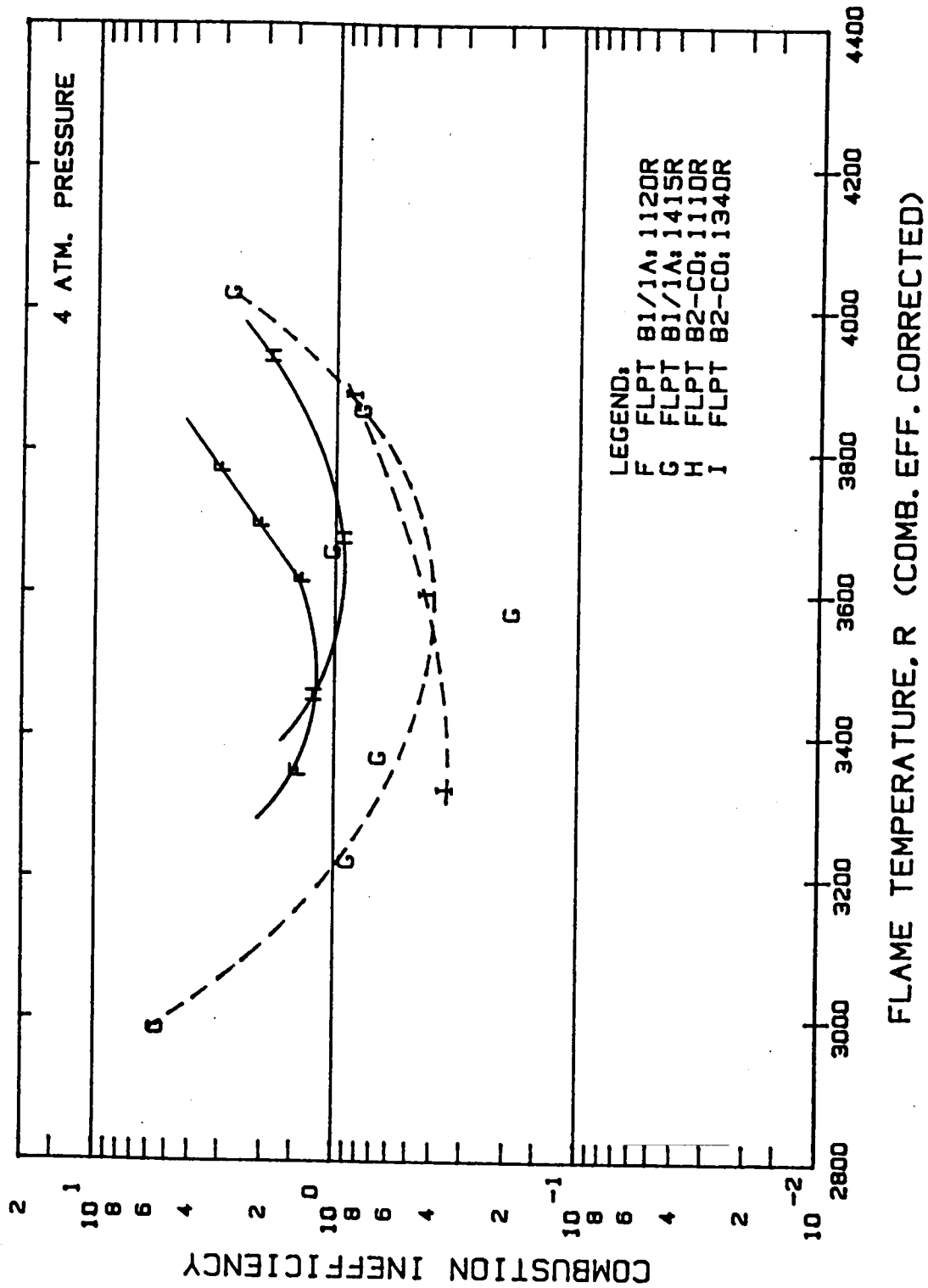


Figure 3.25 - Combustion inefficiency plotted versus flame temperature for the Swirl-IMFH with the 50% immersion transverse fuel injector (Build 1, points F and G) compared to the coaxial fuel injector configuration (Build 2, points H and I).

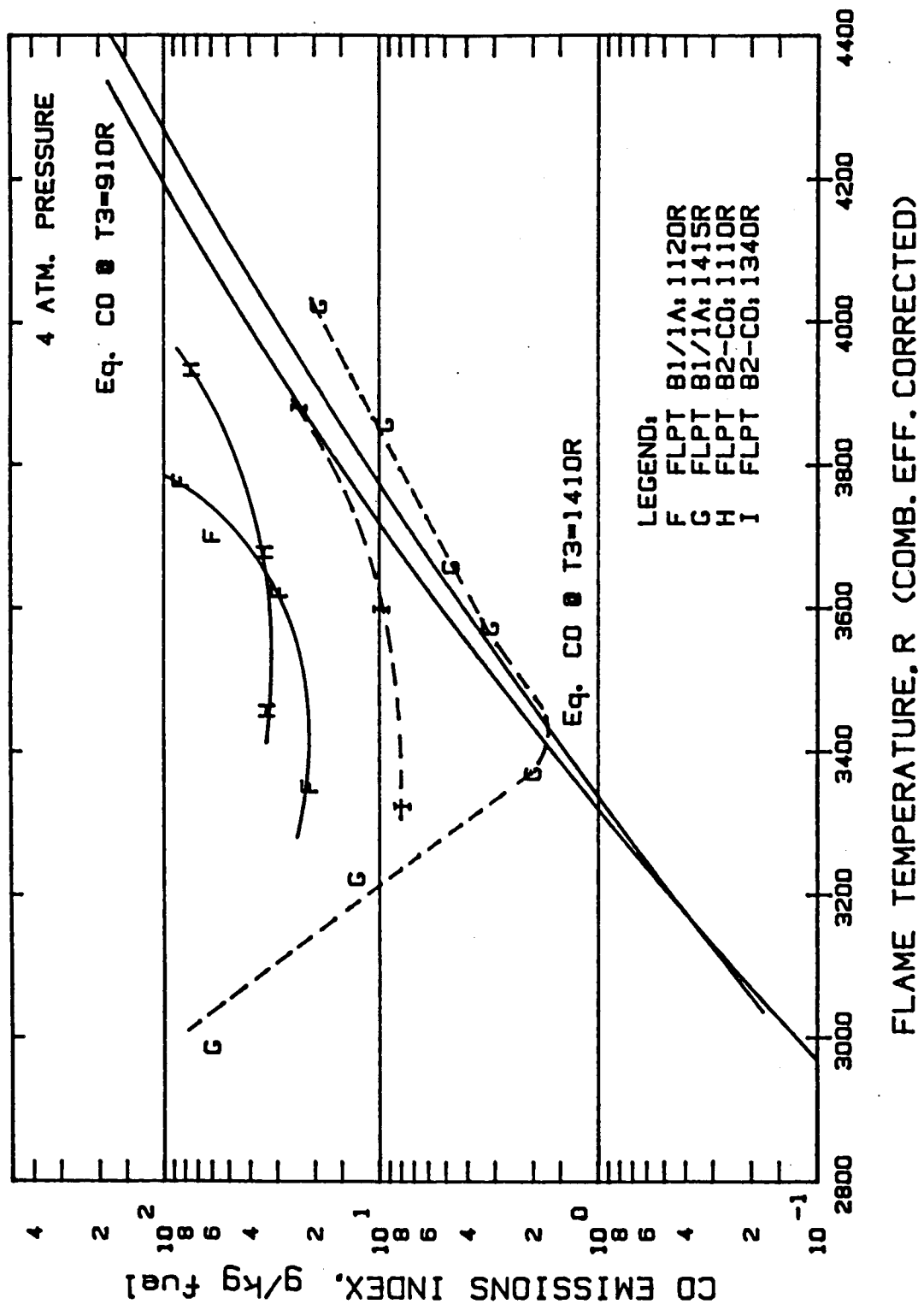


Figure 3.26 - CO emissions index plotted versus flame temperature for the Swirl-IMFH with the 50% immersion transverse fuel injector (Build 1, points F and G) compared to the coaxial fuel injector configuration (Build 2, points H and I)

Figures 3.27 through 3.29 compare NO_x emissions, combustion inefficiency, and CO emissions for the Swirl-IMFH for 20% and 50% fuel injector immersions. The 20% fuel injector tube immersion produced significantly higher NO_x emissions than either the 50% immersion or IMFH Configuration 5A at flame temperatures below 3900 R. At high inlet temperatures (1410 R), the combustion inefficiency for the 20% immersion Swirl-IMFH was similar to IMFH Configuration 5A and lower than the 50% immersion. The low NO_x emissions for the 50% immersion injector were offset by the poor combustion efficiency results relative to Configuration 5A shown in Figure 3.28. The flatness of the NO_x data versus calculated flame temperature for the 20% immersion Swirl-IMFH and the wide range of the combustion inefficiencies, suggests that the flame had some diffusion burning. It is also possible that at the higher inlet temperatures, the fuel was prevaporized, but not uniformly premixed. Post-test inspection of the 50% immersion configuration revealed significant carbon formation in the center of the dome after only 6 hours of testing, as well as a dime-sized hole burned through the dome.

3.3.2 Mini Swirl-IMFH Evaluations

A new set of hardware for the Swirl-IMFH with scaled-down dimensions was designed and fabricated. The intent was to investigate a Swirl-IMFH concept that could be substituted for the Cyclone Swirler pilot in the pilot dome of the rectangular sector combustor and to provide data on the minimum premixer tube length required for fuel vaporization. The inner diameter of the IMFH mixer tubes was reduced to 0.36 inches. The fuel injector retained the standard inner diameter (0.020 inches). The hardware was modular. Two mixing lengths for the IMFH tubes could be used, the standard 4.5 inches (to allow the effects of the other changes to be isolated) or 3.2 inches. Two domes were available with two diameters of the exit circle for the IMFH tubes; 0.900 inches and 1.163 inches. Both domes maintained the pilot simplex atomizer at the module centerline. Figure 3.30 shows a cross-section of the Mini Swirl-IMFH.

Only one configuration was tested and that test was a visual test at atmospheric pressure. The configuration used the 4.5 inch mixing length, a 50% immersion of transverse fuel

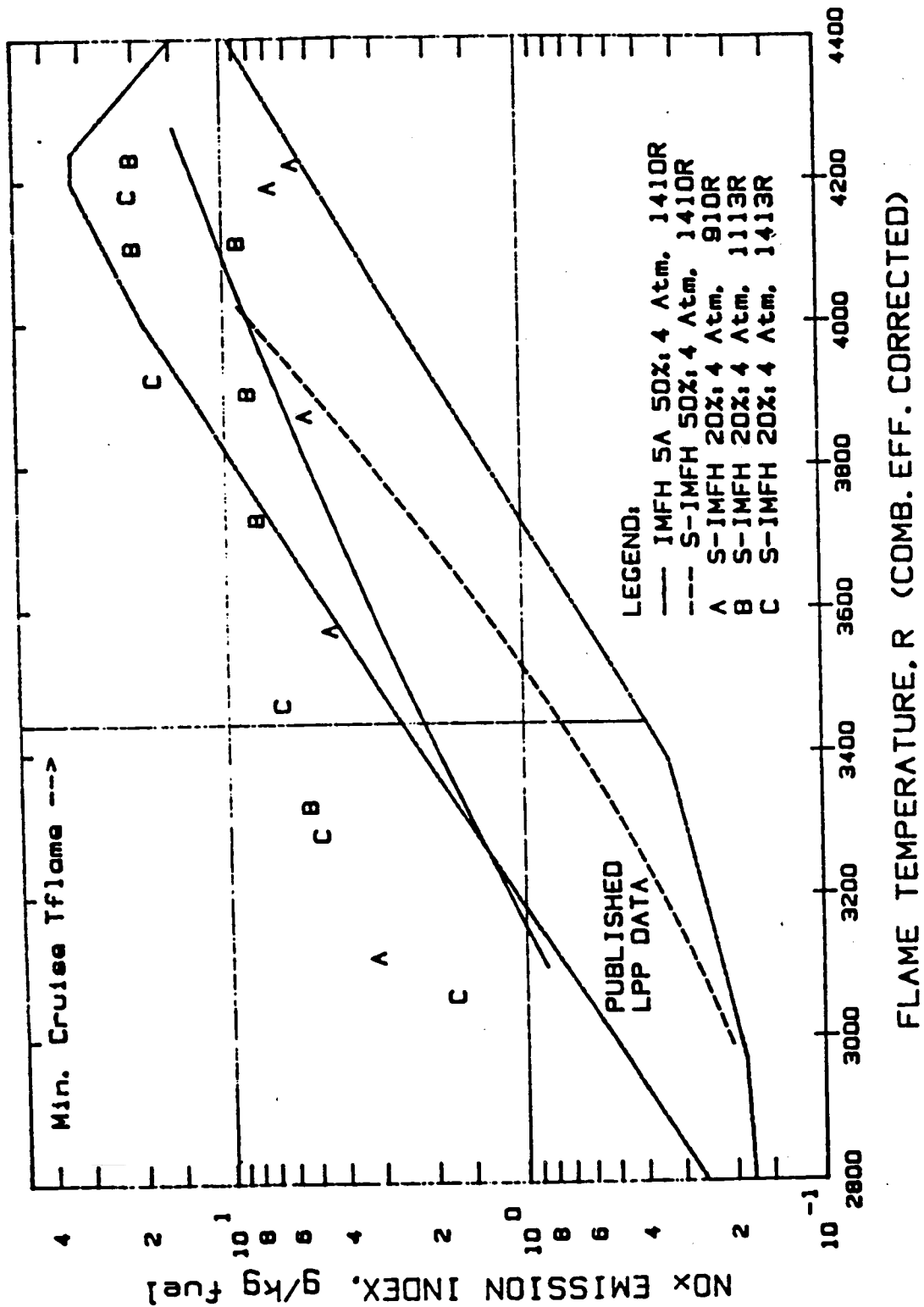


Figure 3.27 - NO_x emissions index plotted versus flame temperature for the Swirl-IMFH with the 20% immersion transverse fuel injector (points A, B and C) compared to fit lines of emissions data for the 50% immersion transverse injector in the Swirl-IMFH and 50% immersion injector in the baseline IMFH configuration (Configuration 5). The dot-dash boundary indicates the envelope of LPP NO_x emissions obtained in several laboratory flame tube studies published in the open literature.

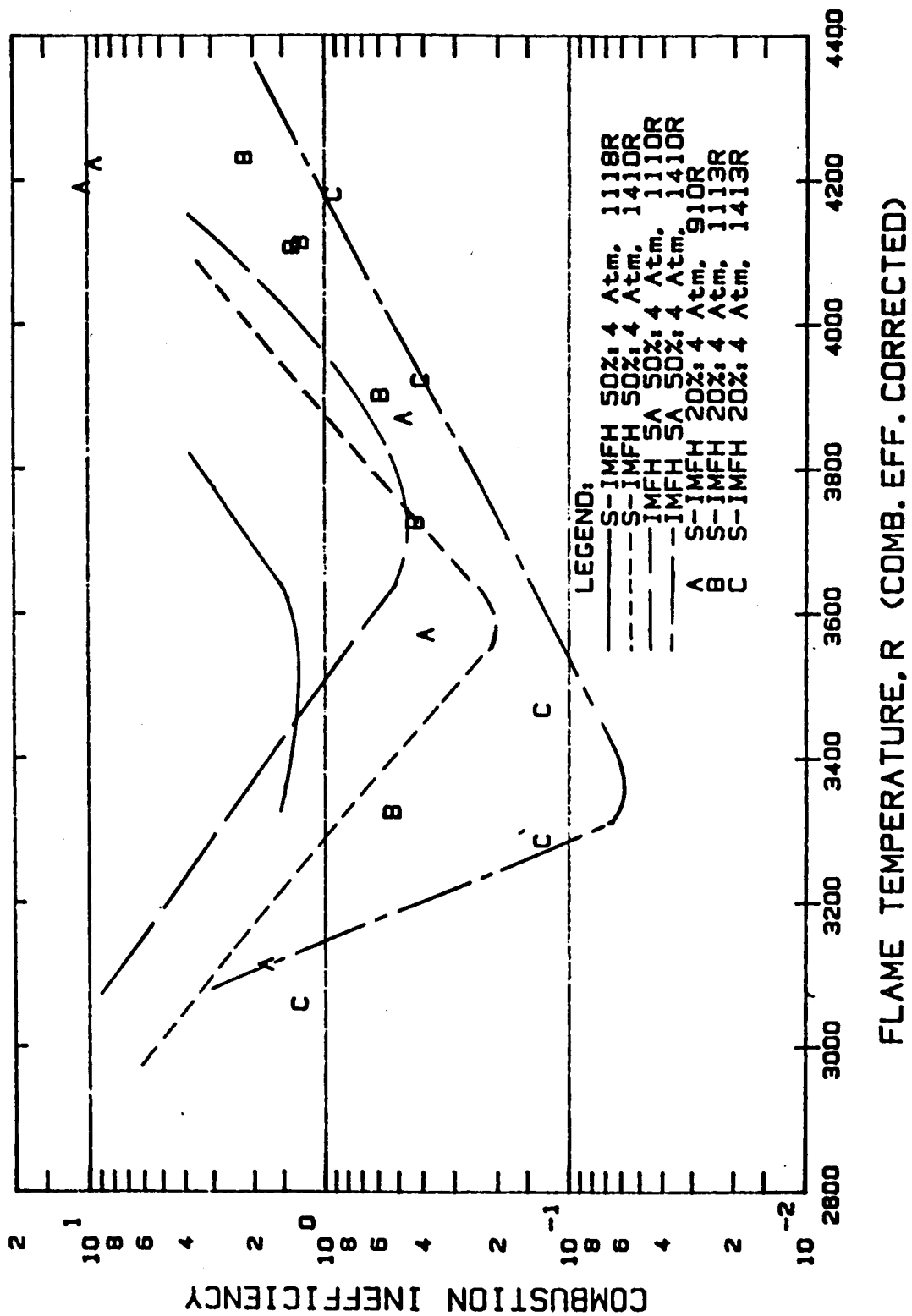


Figure 3.28 - Combustion inefficiency plotted versus flame temperature for the Swirl-IMFH with the 20% immersion transverse fuel injector (points A, B and C) compared to fit lines of emissions data for the 50% immersion transverse injector in the Swirl-IMFH and 50% immersion injector in the baseline IMFH configuration (Configuration 5).

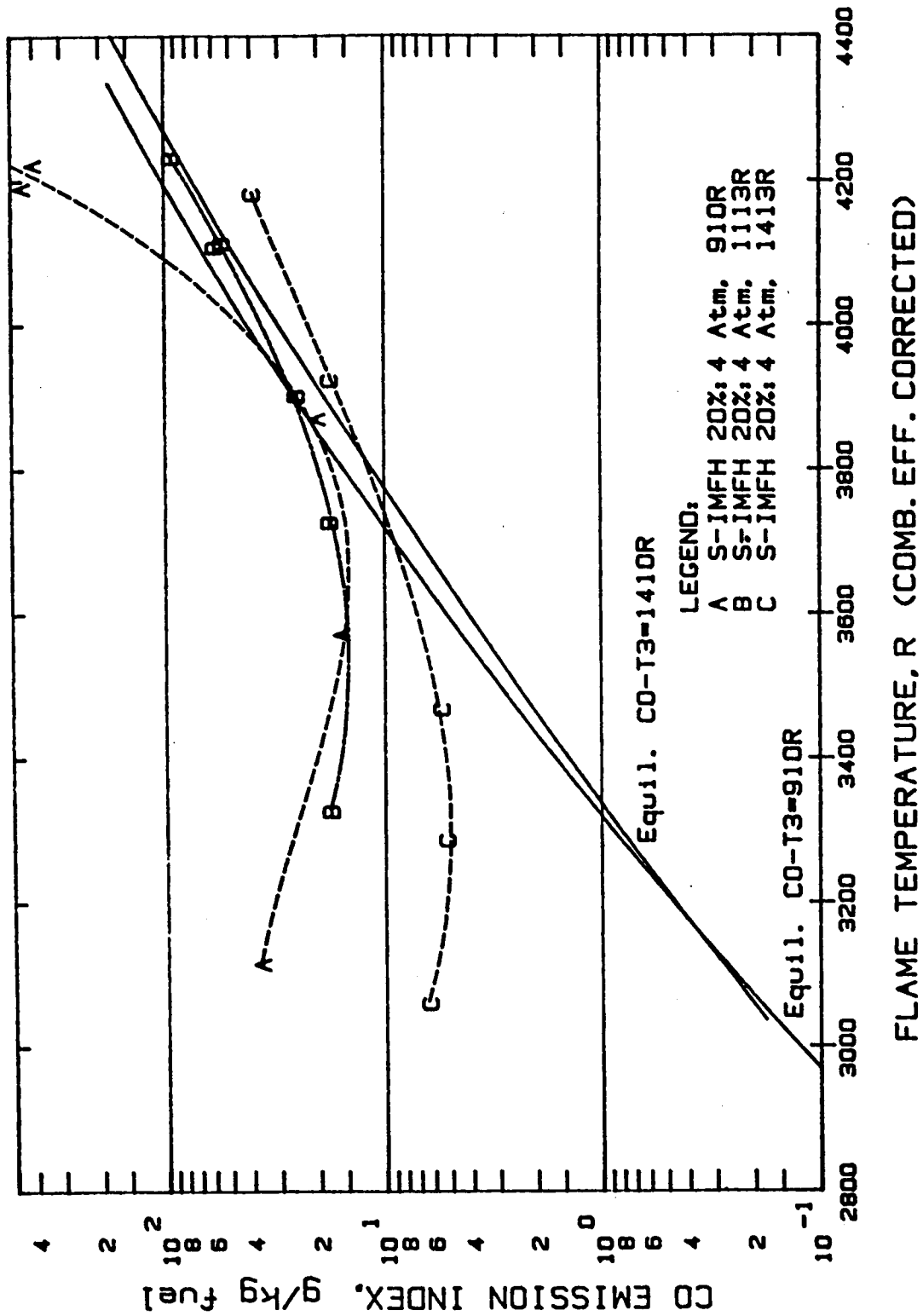


Figure 3.29 - CO emissions index plotted versus flame temperature for the Swirl-IMFH with the 20% immersion transverse fuel injector (points A, B and C) compared to fit lines of emissions data for the 50% immersion transverse injector in the Swirl-IMFH and 50% immersion injector in the baseline IMFH configuration (Configuration 5).

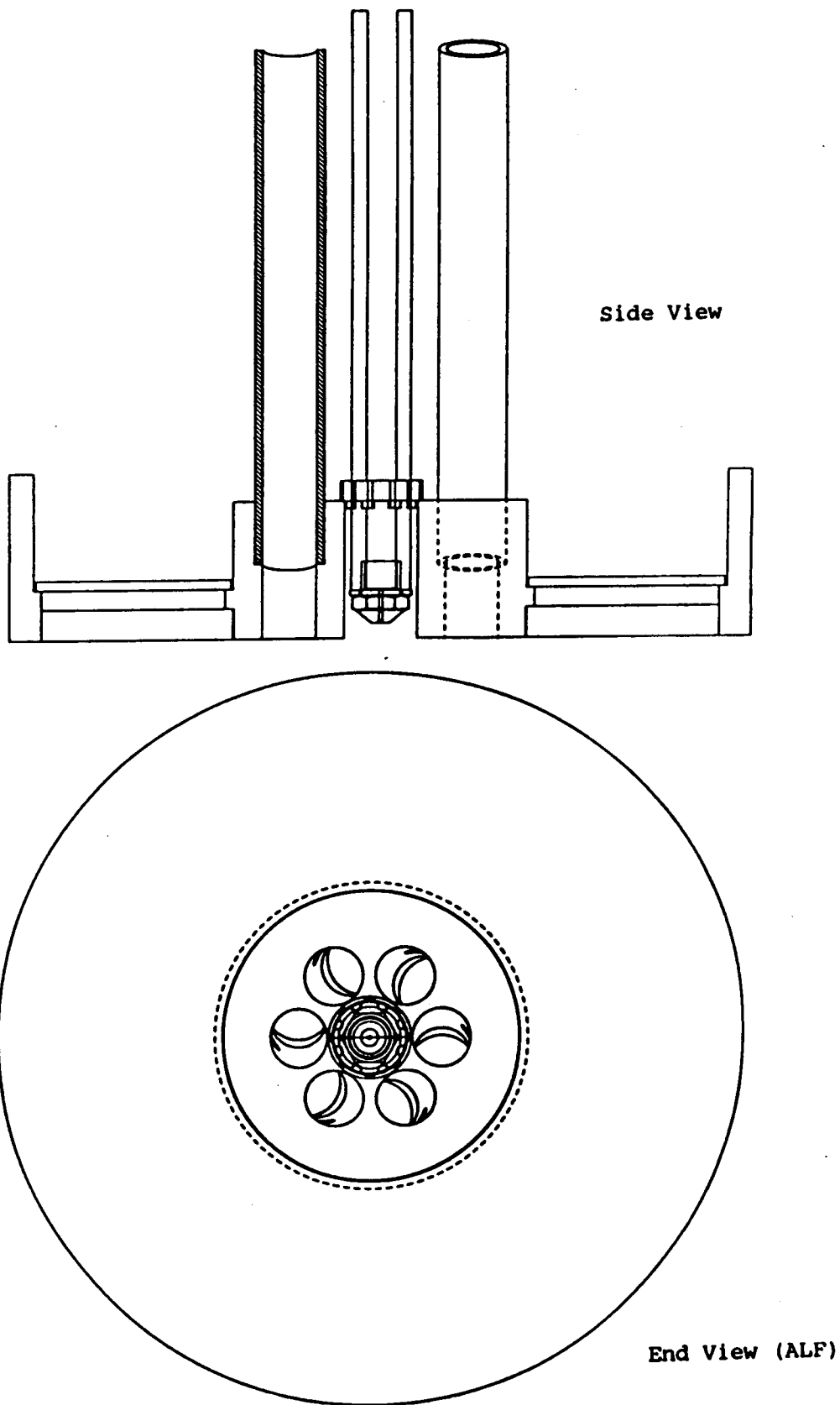


Figure 3.30 - Mini Swirl IMFH subcomponent test hardware

injector tubes, and the dome with the 0.900 inch diameter exit circle. The visual observations of the combustion indicated the flame was lifted off the dome at all conditions tested. The post-test inspection revealed that the dome and about 1 inch of the forward length of the liner was coated with carbon. As the internal configuration of the individual IMFH tubes was that of the baseline design, the conclusion was that the small exit circle and close proximity of the tube exits resulted in high local dome velocities. This prevented a sufficient recirculation zone from forming, hampering stability. No other configurations of the Mini Swirl-IMFH were tested.

3.3.3 Venturi Swirl-IMFH Evaluations

The potential advantages of the Venturi-IMFH are discussed in the APT Task 5 Final Report ⁽³⁻¹⁾. The primary benefit of a venturi is that it yields higher local velocities at the point of fuel injection, resulting in better fuel atomization. Disadvantages of the venturi include the requirement for added length if a constant residence time is maintained (not done in these designs), added cost, and the potential for separation in the conical diffuser (which may lead to flashback). An additional advantage is that the static temperature of the air is reduced in the throat, which calculations indicate adds significantly to the autoignition delay. This could be exploited by further increases in length. However, with a high Mach number in the throat, the friction losses became significant. Thus, the throat lengths need to be kept short to obtain the intended velocities. Calculations indicated that there should still be a net improvement in mixing performance. Carburetors used for premixing gasoline and air for internal-combustion engines generally use a venturi at the point of fuel injection.

In this development effort, the Venturi-IMFH and the Swirl-IMFH concepts were merged and called the Venturi Swirl-IMFH (VS-IMFH). Three designs for the venturi were investigated. Figure 3.31 is a schematic of Configurations 1 and 2. All three designs had 0.75-inch long converging sections, used wall fuel injectors immersed to the centerline and located 1.0 inch from the inlet, and injected the spent cooling air 0.2 inches upstream of the dome. The inlet had a diameter of 0.600 inches. The throat had a diameter of 0.475 inches. The exit diameter was

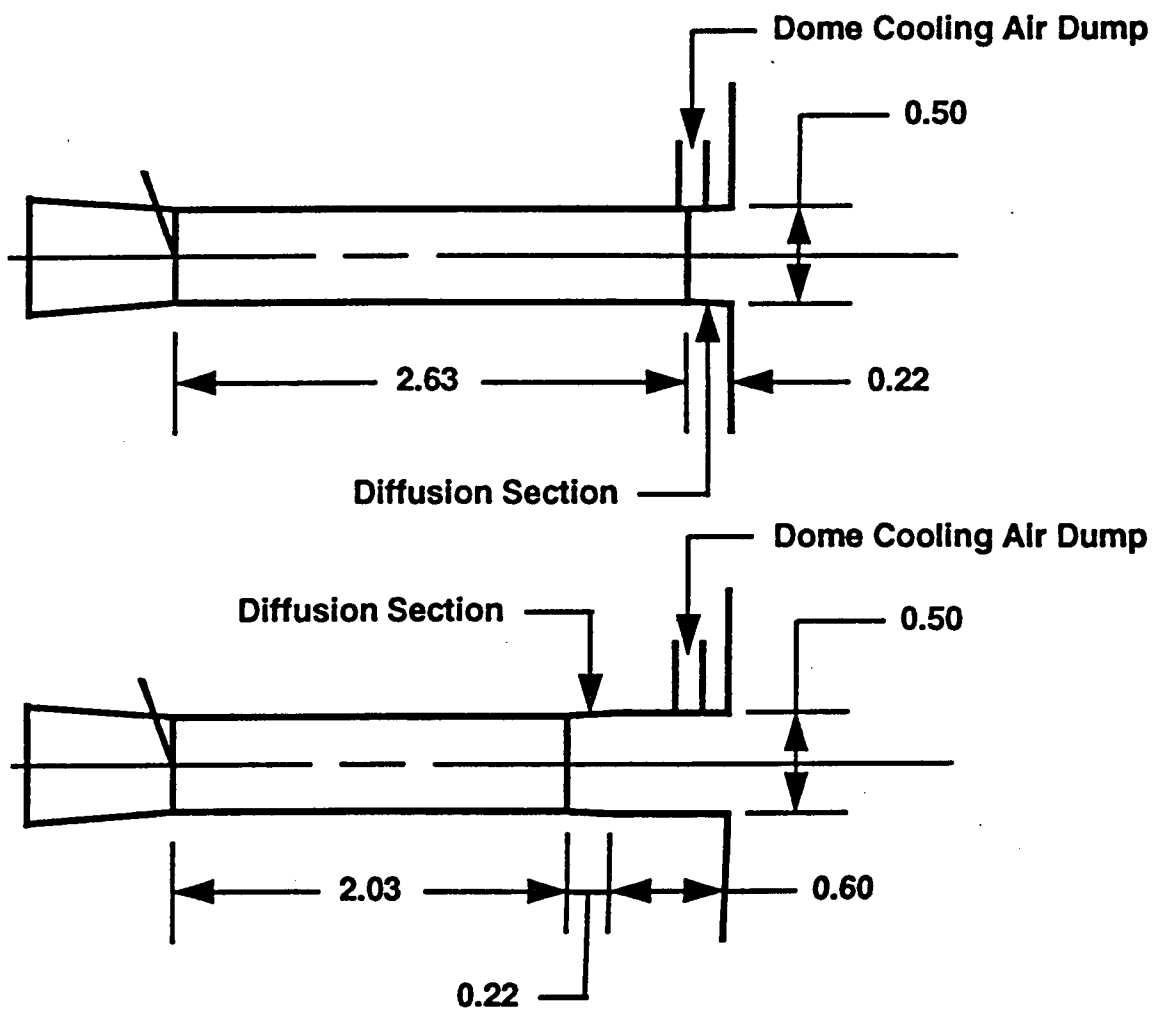


Figure 3.31 - Venturi Swirl IMFH configurations with the 2.63-inch (Configuration 1, shown at the top) and 2.03-inch (Configuration 2, shown at the bottom) long throats. The diameter of the throats is 0.475 inches.

0.500 inches. The half-angle of the diverging section of all the designs was 3.25 degrees. The area ratio of the conical diffuser was intentionally kept small to maintain a conservative design. Larger area ratios could always be investigated later, if a benefit was observed. Configuration 1 had the longest throat length (2.63 inches), with a conical diffuser section that was 0.22 inches long, ending at the dome. The overall length was 3.60 inches. Configuration 2 had a 2.03-inch long throat, a 0.22-inch long conical diffuser, and a 0.60-inch straight section. Configuration 3 had a 0.53-inch long throat, a 0.22-inch long conical diffuser, and a 2.10-inch straight section.

Configuration 1 was tested at 4 atmospheres and inlet temperatures of 450° F and 650° F (910 R and 1110 R). Although the emissions data were comparable to IMFH Configuration 5A, the effective flow area data indicated the diffuser was separated. The pressure drop characteristics of Configuration 1 acted like the dump from a 0.475-inch diameter tube, or the venturi's throat diameter. This indicated that the flow was separating in the diverging section, probably because of interaction with the spent cooling air jets.

A pre-test pressure flow check of Configuration 2 indicated there was no flow separation in the venturi's diffuser. This conclusion was based upon the observed pressure loss appearing to correspond to a dumping loss consistent with the calculated velocity at the exit of tube rather than the throat. Thus, the flow in the diffuser section of the venturi appeared to remain attached. Possibly, the flow separated and then re-attached (if so, the design would be prone to flashback/autoignition). However, observations during the test and the post-test inspection were consistent with the conclusion that no separation occurred within the premixer tubes. Configuration 2 emissions data were taken at 4 and 6 atmospheres inlet pressure and inlet temperatures ranging from 446° F and 674° F (906 R to 1134 R). Figure 3.32 shows the VS-IMFH NO_x emissions plotted versus flame temperature and compares these results to the IMFH Configuration 5A and straight tube Swirl-IMFH (S-IMFH) data at 4 atmospheres inlet pressure and 1410 R inlet temperature. The VS-IMFH NO_x emissions were similar to Configuration 5A, particularly at elevated inlet temperatures. The combustion inefficiency data and the CO

NO_x EI vs. FLAME TEMPERATURE VENTURI SWIRL IMFH w/2.03-INCH LONG THROAT

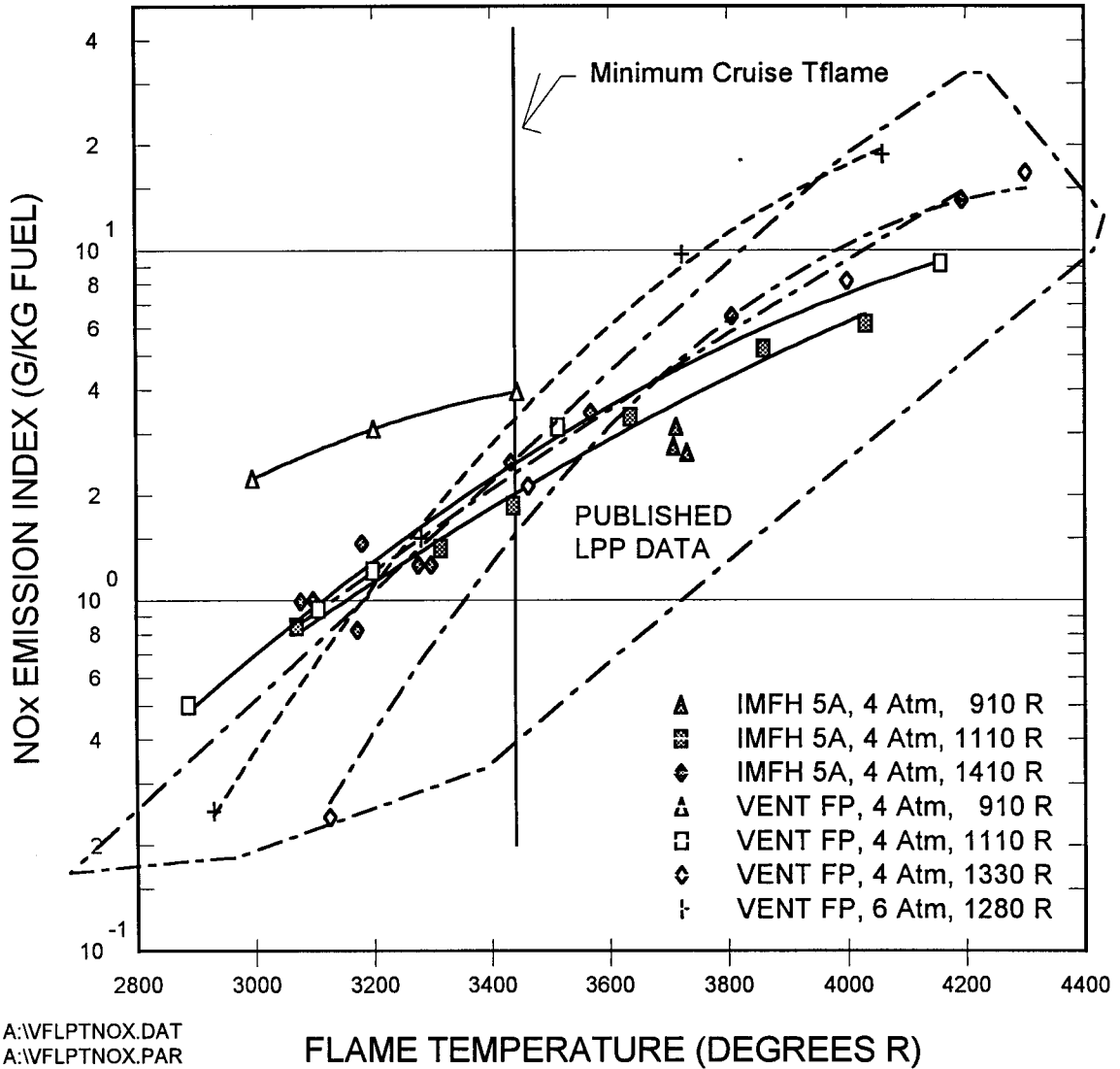


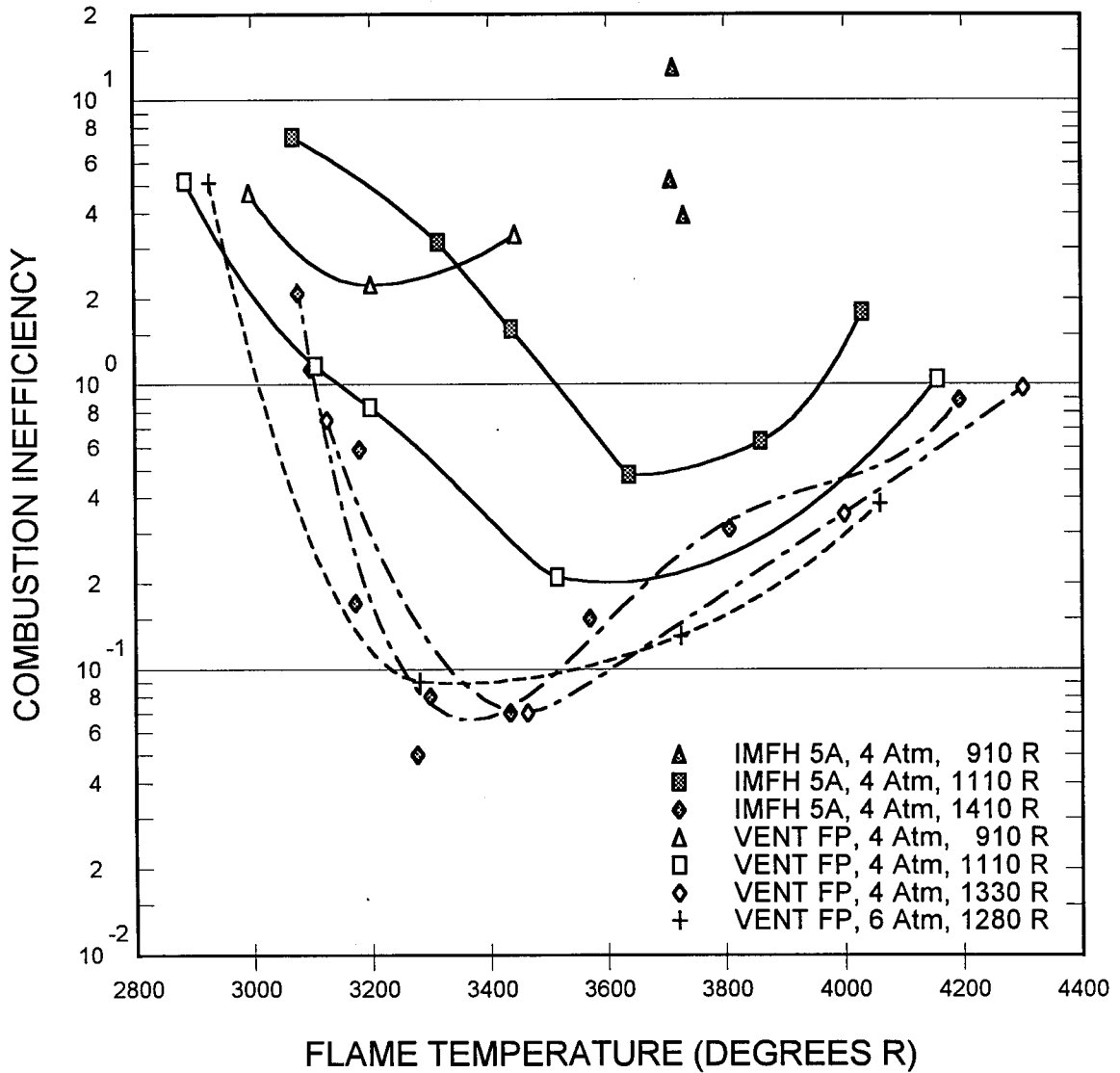
Figure 3.32 - NO_x emissions index plotted versus flame temperature for Configuration 2 of the Venturi Swirl-IMFH (2.03-inch long throat). Results are compared to the baseline configuration of the IMFH (Config 5) and the Swirl-IMFH with the 50% immersion fuel injector.

emissions data are plotted in Figures 3.33 and 3.34. The combustion inefficiency at intermediate inlet temperatures was lower for the VS-IMFH than for either the IMFH Configuration 5A or the S-IMFH.

An atmospheric test of the Venturi Swirl-IMFH with a 0.53-inch long throat (Configuration 3) showed a well mixed and circumferentially uniform flame structure attached to the dome. Initial emissions measurements at 4 atmospheres pressure were similar to earlier data. NO_x, CO, and UHC emissions measurements were taken at inlet temperatures ranging from 450° F to 950° F (910 to 1410 R). The NO_x and CO emissions data are presented in Figures 3.35 and 3.36. In general, NO_x emissions were higher than for Configuration 2 (with the 2.03-inch long throat) and the combustion efficiency was poorer. The increase in NO_x and combustion inefficiency was attributed to poorer fuel dispersion within the 0.5-inch length throat premixer tube, which in turn was due to a greater fraction of the fuel entering the diffusion section not being vaporized.

Based on these results, it was concluded that the longer venturi (approx. 2.0 inches) design (Configuration 2) might provide some benefit relative to the baseline Configuration 5 in improving combustion efficiency at the inlet temperatures of 650° F (1110 R) and above with the possibility of a small NO_x penalty. This improvement in performance at subsonic cruise combustor inlet conditions is especially attractive for the IMFH main stages operating at subsonic cruise. Based upon IMFH flametube emissions results, combustion efficiency has been a concern. NO_x emissions at subsonic cruise are not as critical as supersonic cruise.

COMBUSTION INEFFICIENCY vs. FLAME TEMPERATURE VENTURI SWIRL IMFH w/2.03-INCH LONG THROAT



6/12/98

Figure 3.33 - Combustion inefficiency plotted versus flame temperature for Configuration 2 of the Venturi Swirl-IMFH (2.03-inch long throat). Results are compared to the baseline configuration of the IMFH (Configuration 5) and the Swirl-IMFH with the 50% immersion fuel injector.

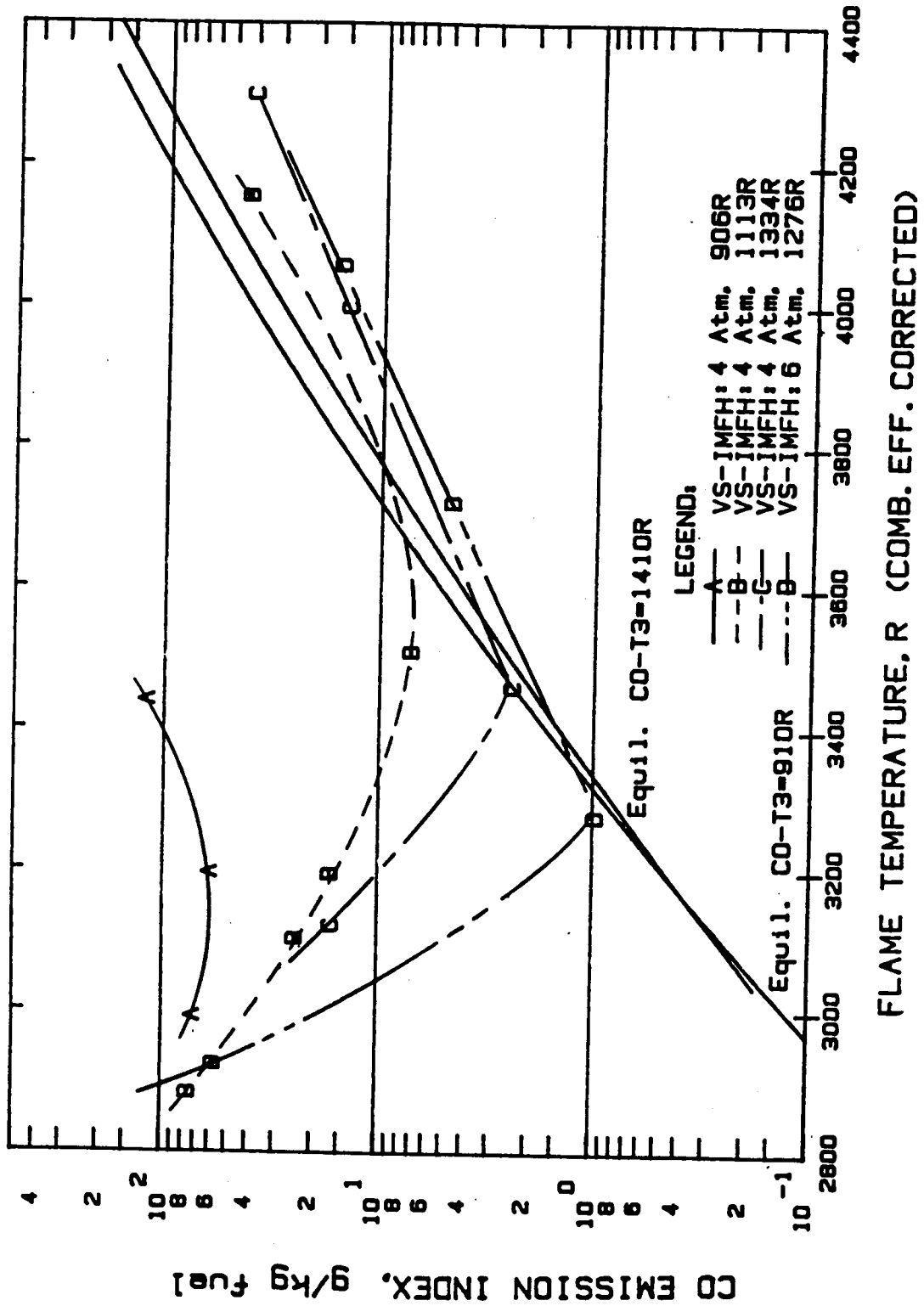


Figure 3.34 - CO emissions index plotted versus flame temperature for Configuration 2 of the Venturi Swirl-IMFH (2.03-inch long throat). Results are compared the calculated equilibrium line for CO for inlet temperatures of 910 R and 1410 R.

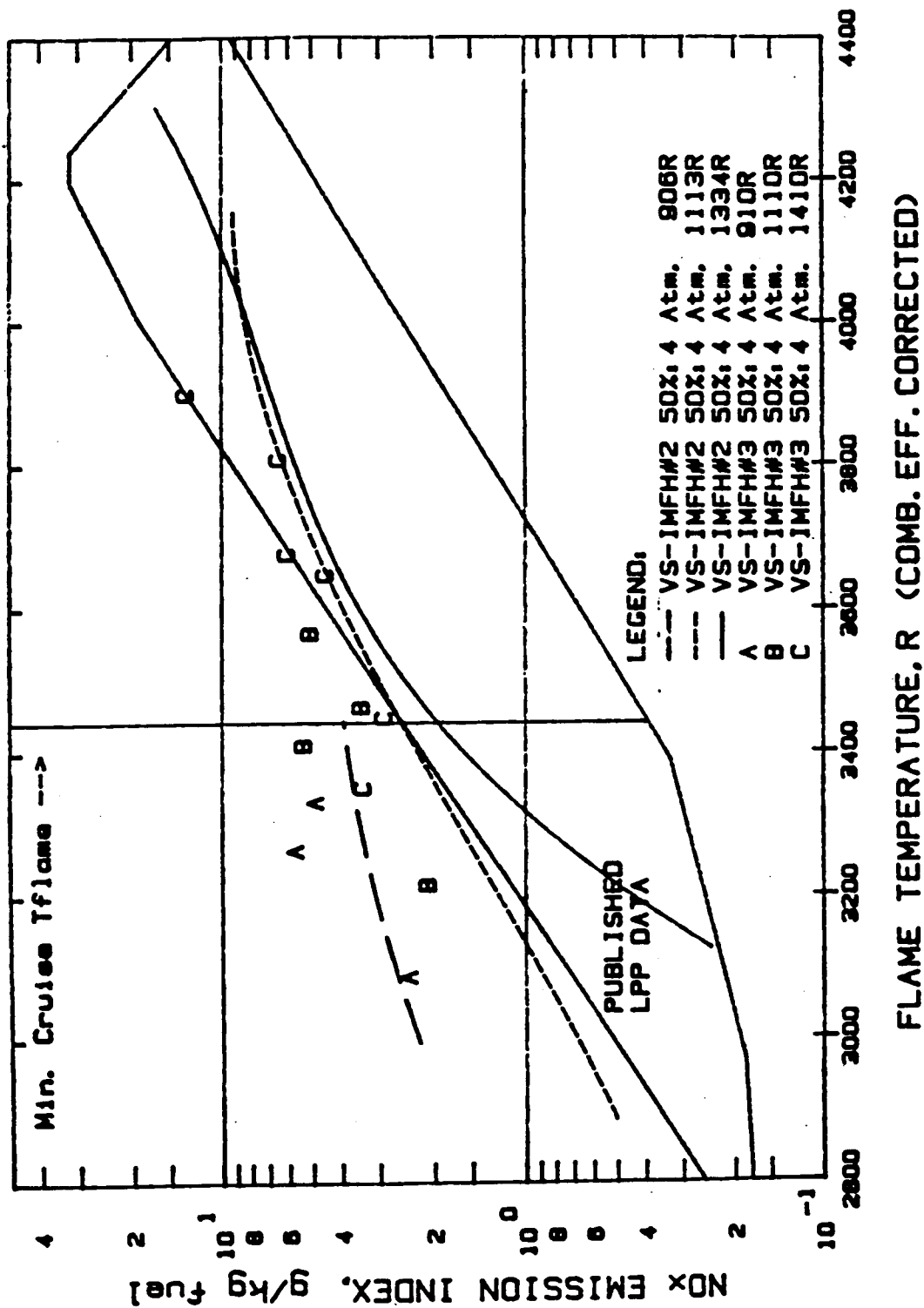


Figure 3.35 - NO_x emissions index plotted versus flame temperature for Configuration 2 (2.03-inch long throat) and Configuration 3 (0.53-inch long throat) of the Venturi Swirl-IMFH. The dot-dash boundary indicates the envelope of LPP NO_x emissions obtained in several laboratory flame tube studies published in the open literature.

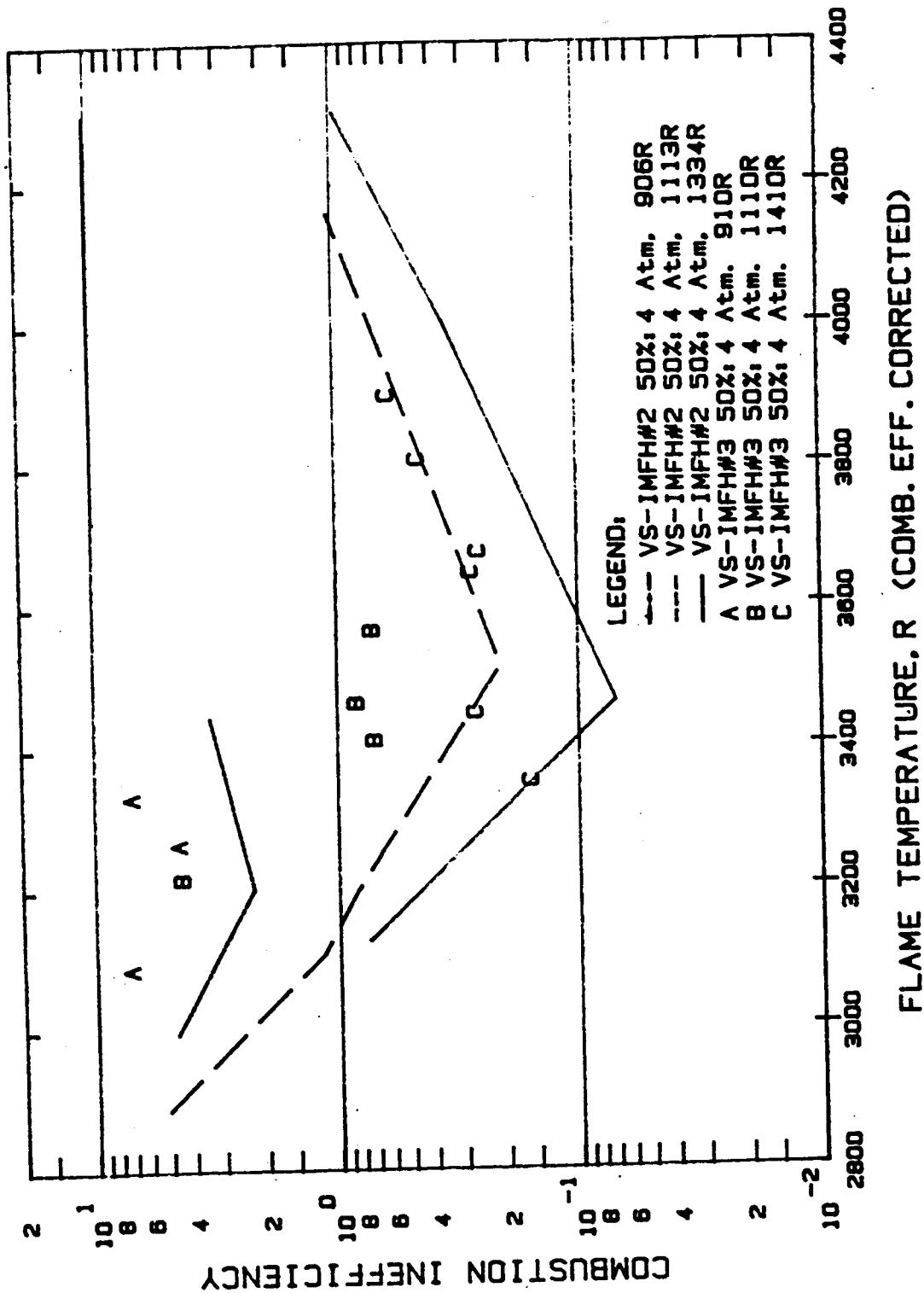


Figure 3.36 - Combustion inefficiency plotted versus flame temperature for Configuration 2 (2.03-inch long throat) and Configuration 3 (0.53-inch long throat) of the Venturi Swirl-IMFH.

3.4 Cyclone Swirler Evaluations

Configurations 3 and 4 of the Cyclone Swirler pilot were evaluated in single-cup tests in LET Task 10. Configuration 3 was a slightly scaled down version of Configuration 2 (in terms of size and effective flow area). The number of plain-jet air-blast fuel injectors mounted radially on the centerbody was reduced from eight injectors in Configuration 2 to six injectors in Configuration 3. The inner diameter of the fuel injector tubes was increased from 0.012 inches to 0.020 inches (Configuration 2 was eventually retrofitted with 0.020-inch injectors for the CR&D tests discussed in Section 2.2). Configuration 3 is the pilot used in the stepped dome sector combustor (discussed in Section 4 of this report) and the highly-mixed MRA sector combustor⁽³⁻²⁾. A cross-section of the Cyclone Swirler Configuration 3 single-cup hardware is shown in Figure 3.37. Configuration 4 is identical to Configuration 3, except the atomizing air passage was partially restricted. Configuration 5 was designed and fabricated in LET Task 10. It modified the centerbody/fuel nozzle design to incorporate a simplex fuel atomizing nozzle into the centerbody. The simplex fuel nozzle operated on a second fuel circuit, separate from the air-blast nozzles. The simplex fuel nozzle could be used to extend the operating range of the cyclone, if necessary. The Configuration 5 hardware was never tested. Table 3.2 summarizes the design parameters of Cyclone Swirler configurations 1 through 5.

Cyclone	Ae total	Calc.	Slot	Slot	#	Swirler	Slot	#	Comment
Config	Meas.	Swirl	Length	Width	of	Aphys	Angle	Fuel	
#	(in ²)	Number	(in)	(in)	Slots	(in ²)	(deg.)	Inj.	
0	-	0.94	0.60	0.030	60	1.08	70	8	
1	0.74	0.94	0.60	0.030	60	1.08	70	8	0 with fuel injector tubes added
2	0.74	0.94	0.60	0.030	60	1.08	70	8	1 with spent cooling air injection
3	0.57	1.04	0.50	0.025	60	0.75	70	6	2 scaled down
4	-	1.04	0.50	0.025	60	0.75	70	6	3 with reduced air-blast air flow
5	-	1.04	0.50	0.025	60	0.75	70	6	Simplex nozzle at centerbody end

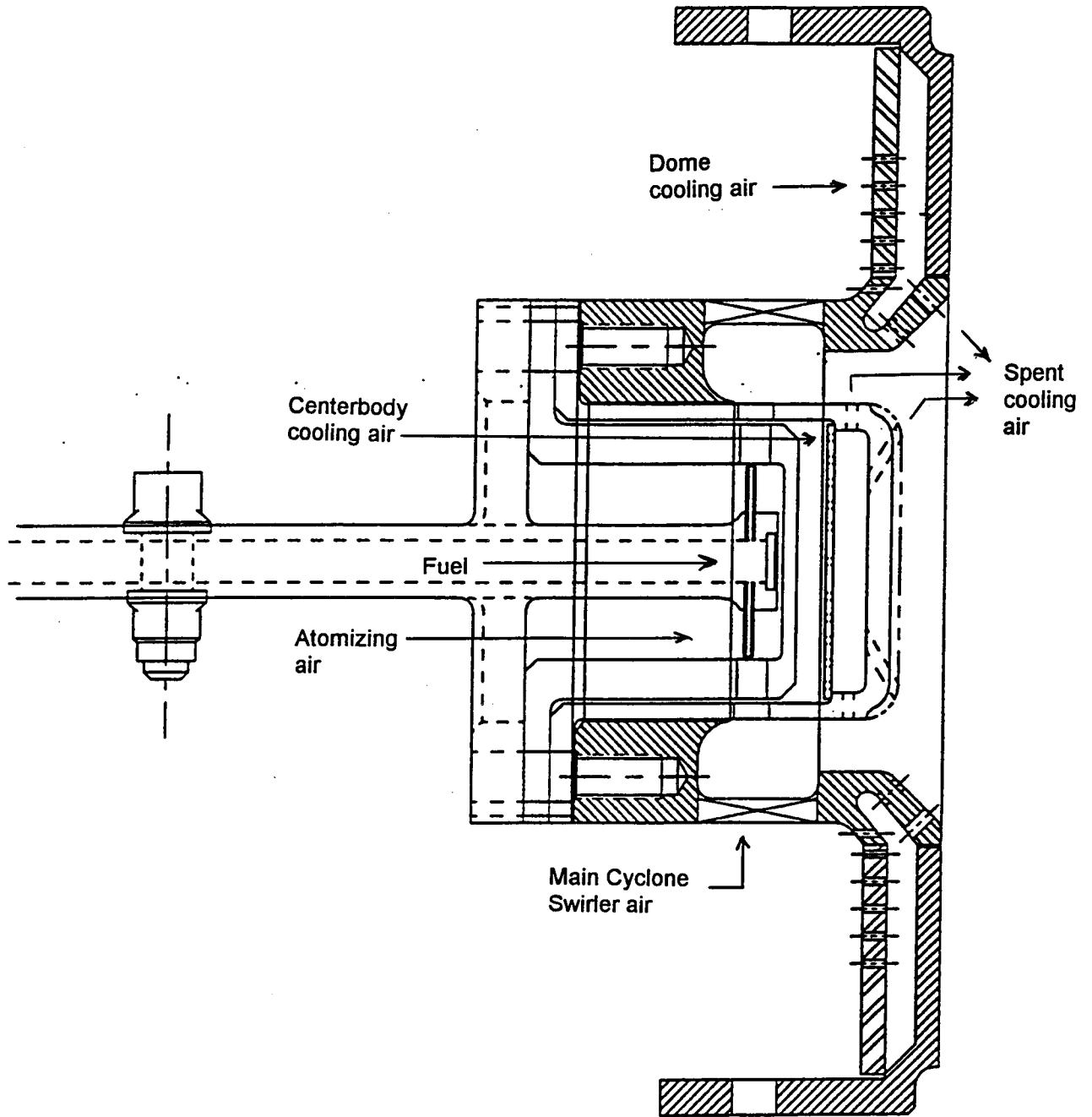
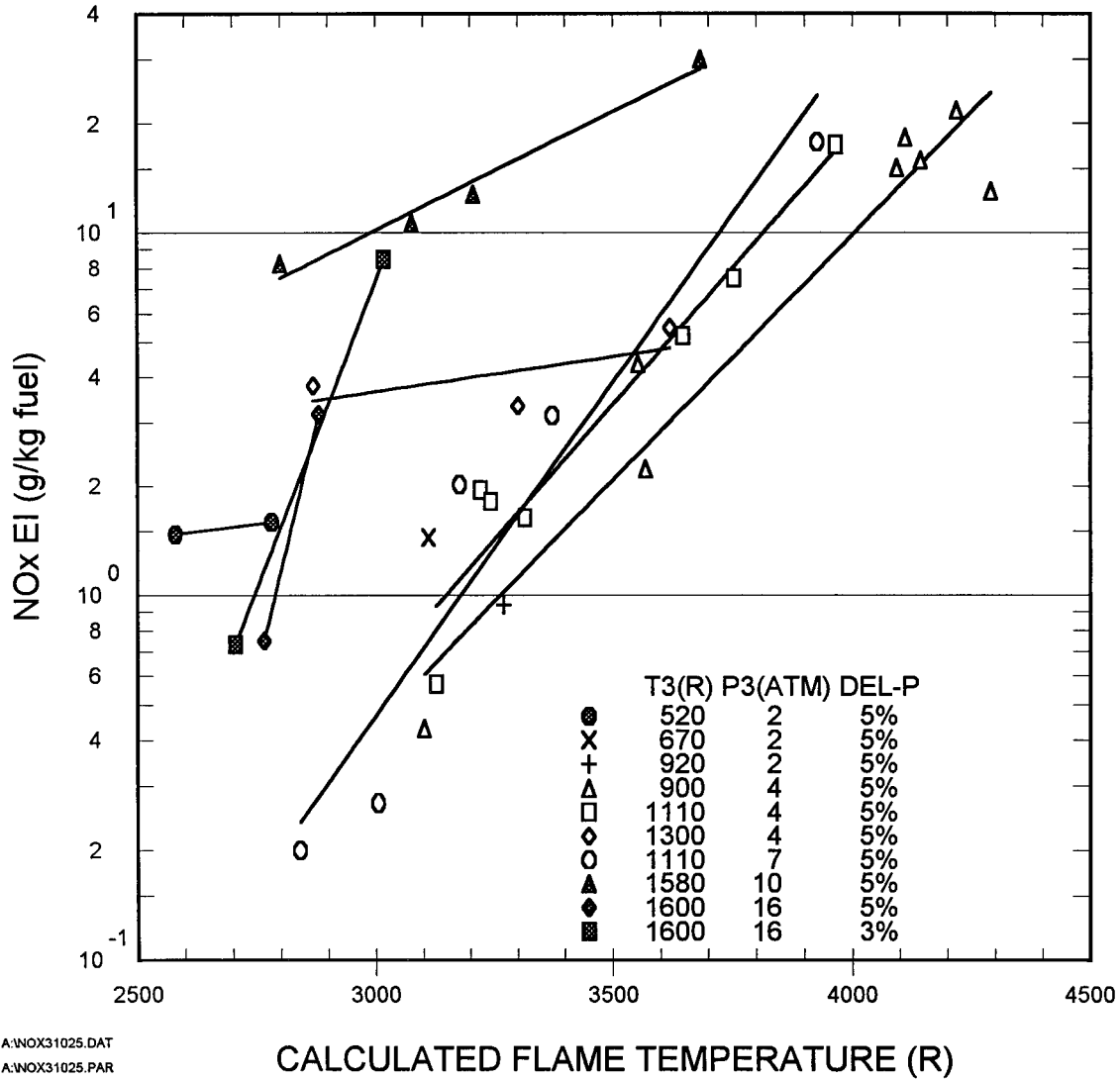


Figure 3.37 - Cyclone Swirler single-cup test hardware. Configuration 3 is shown. The same hardware was used for Configuration 4 by restricting the atomizing air inlet passage.

A four atmosphere test of Configuration 3 yielded excellent emissions performance. However, some combustion oscillations were audible. Configuration 3 was then tested in a high pressure rig in GEAE's Cell A5 to obtain data at full supersonic cruise conditions. In the Cell 5 test, the rig was instrumented with dynamic pressure transducers. During the Cell 5 test no combustion oscillations were audible, nor detected with the instrumentation. The occurrence of combustion oscillation is very dependent on the acoustic characteristics of the particular rig installation. The emissions data for the different tests of Configuration 3 are shown in Figures 3.38 and 3.39. The NO_x results indicated that combustion transitioned to a diffusion flame at higher pressures. This was similar to the observations of a previous Configuration 2 Cyclone Swirler test. This indicates that the performance of the Cyclone Swirler was not sensitive to the changes made from Configuration 2 to Configuration 3. This robust behavior of the Cyclone Swirler has continued through later versions. Its performance has remained relatively constant, despite the numerous changes in its design. The 3% and 5% combustor pressure drop NO_x and CO emissions data were in excellent agreement, consistent with past evaluations of the Cyclone Swirler. This suggests that simplified variable geometry schemes which would result in large changes in combustor pressure drop might be feasible. The high NO_x emissions at high pressures noted for Configuration 3 were hypothesized to be the result of rich streaks of partially vaporized fuel. These streaks were generated by smaller droplets of fuel prematurely exiting the swirler, and burn either in a diffusion type flame or in a premixed mode close to stoichiometric.

A test of Configuration 4, which reduced the air flow rate for the plain-jet air-blast fuel atomization nozzles from Configuration 3, was run at 4 atmospheres. The reduced airflow for the atomization nozzles was predicted to roughly double the Sauter mean diameter (SMD) from plain-jet air-blast fuel nozzles. The larger SMD could have a positive or negative impact on NO_x emissions in a Cyclone Swirler. The Cyclone Swirler depends on the radial acceleration to maintain relative velocity between unvaporized fuel and the air. The radial accelerations can easily exceed 10^4 g's. The effectiveness of the radial acceleration in generating high relative

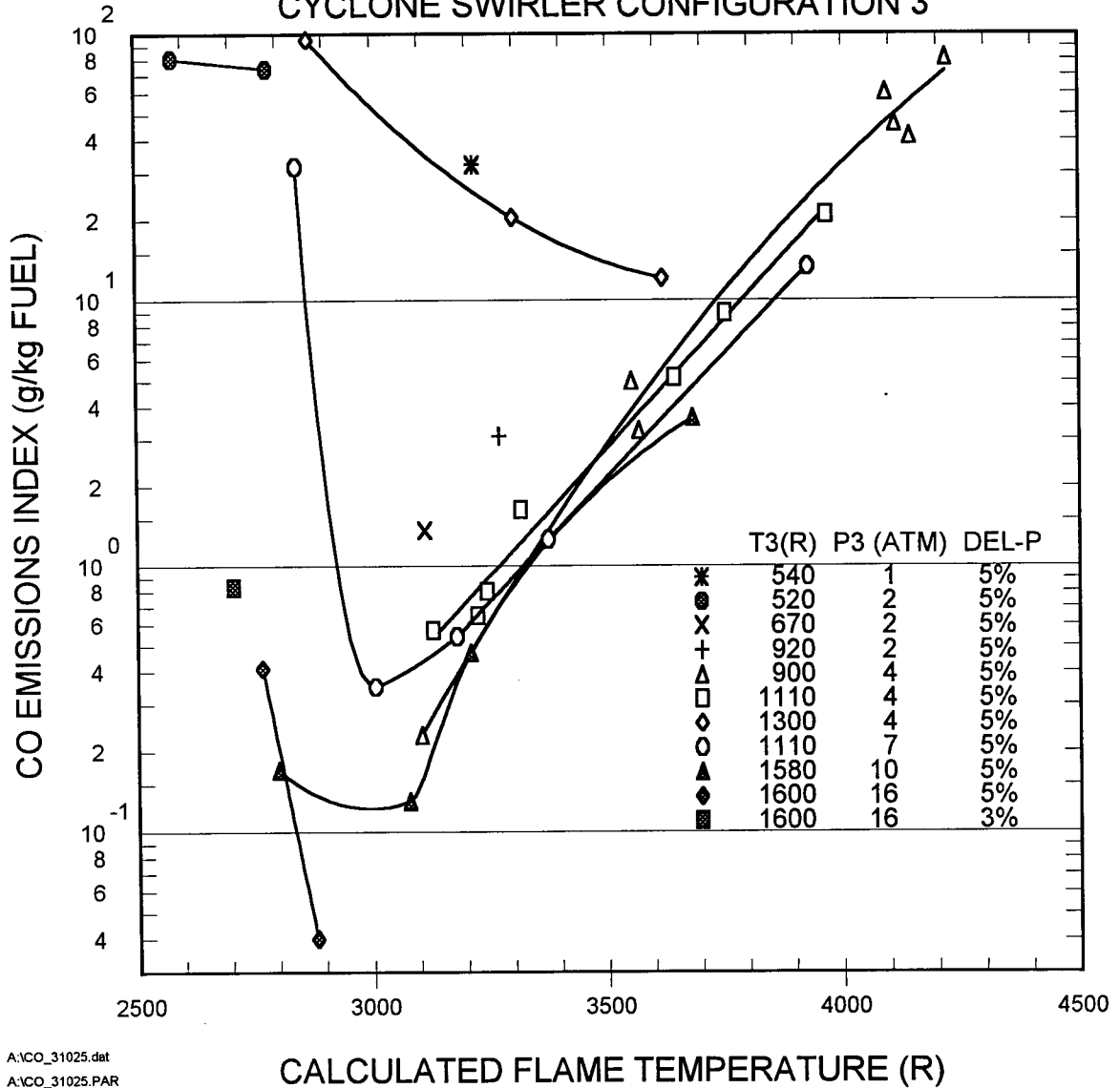
NOx EMISSIONS INDEX vs. FLAME TEMPERATURE CYCLONE SWIRLER CONFIGURATION 3



A:\NOX31025.DAT
A:\NOX31025.PAR
6/12/98

Figure 3.38 - NOx emissions index plotted versus flame temperature for Configuration 3 of the Cyclone Swirler.

CO EMISSIONS INDEX VS. FLAME TEMPERATURE CYCLONE SWIRLER CONFIGURATION 3



A:\CO_31025.dat
A:\CO_31025.PAR
6/12/88

Figure 3.39 - CO emissions index plotted versus flame temperature for Configuration 3 of the Cyclone Swirler.

velocities between the unvaporized fuel and the air improves with larger drop sizes. There are also a number of mechanisms by which the droplets can be further atomized in the cyclone. These mechanisms could blanket the effect of reducing the atomizing air flow rate to the nozzles.

Figure 3.40 shows that the NO_x emissions for a repeat of the baseline test of Configuration 3. This test was repeated in preparation for the test of Configuration 4, because test Configuration 4 test was to be performed in another test cell. The NO_x emissions in Figure 3.40 are in good agreement with the NO_x emissions in Figure 3.38, indicating there was no effect in switching test cells.

The NO_x emissions for Configuration 4 are plotted in Figure 3.41 and compared to the average of the two plots in Figure 3.40 (Figure 3.41 would be too cluttered if both curves in Figure 3.40 were shown). The similar emissions performance of Configurations 3 and 4 is evidence that the Cyclone Swirler itself atomizes the fuel. This is consistent with the drop size measurements made at GE CR&D for the Configuration 2 fuel nozzle, with and without the Cyclone Swirler. The CR&D results are reported in Section 2.

The follow-on efforts in the Cyclone Swirler pilot development were performed in LET Task 43. Those results are reported in the Final Report for LET Task 43⁽³⁻²⁾.

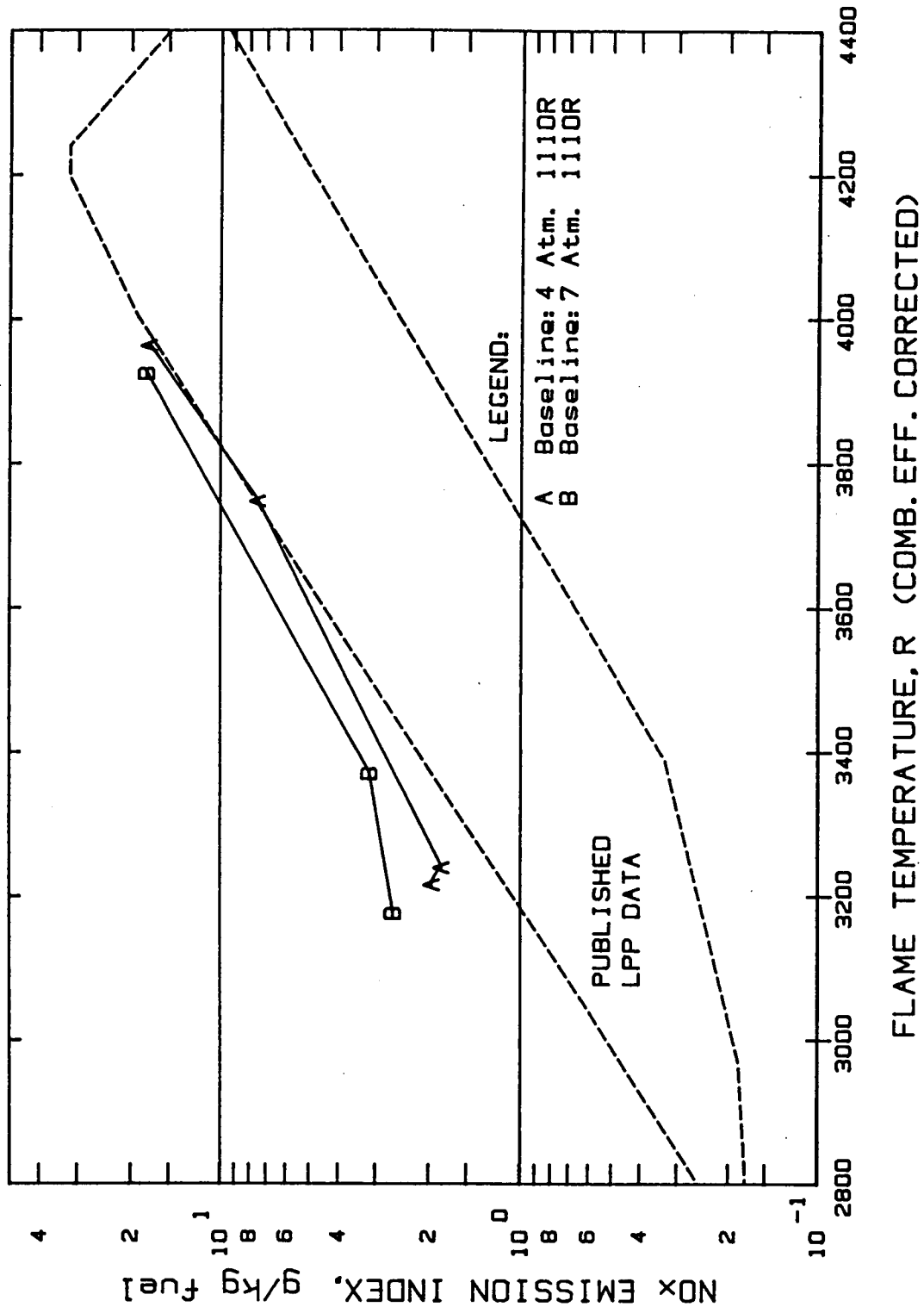


Figure 3.40 - NOx emissions index plotted versus flame temperature for Configuration 3 of the Cyclone Swirler. These were obtained in a different cell than those in Figure 3.38. The dashed boundary indicates the envelope of LPP NOx emissions obtained in several laboratory flame tube studies published in the open literature.

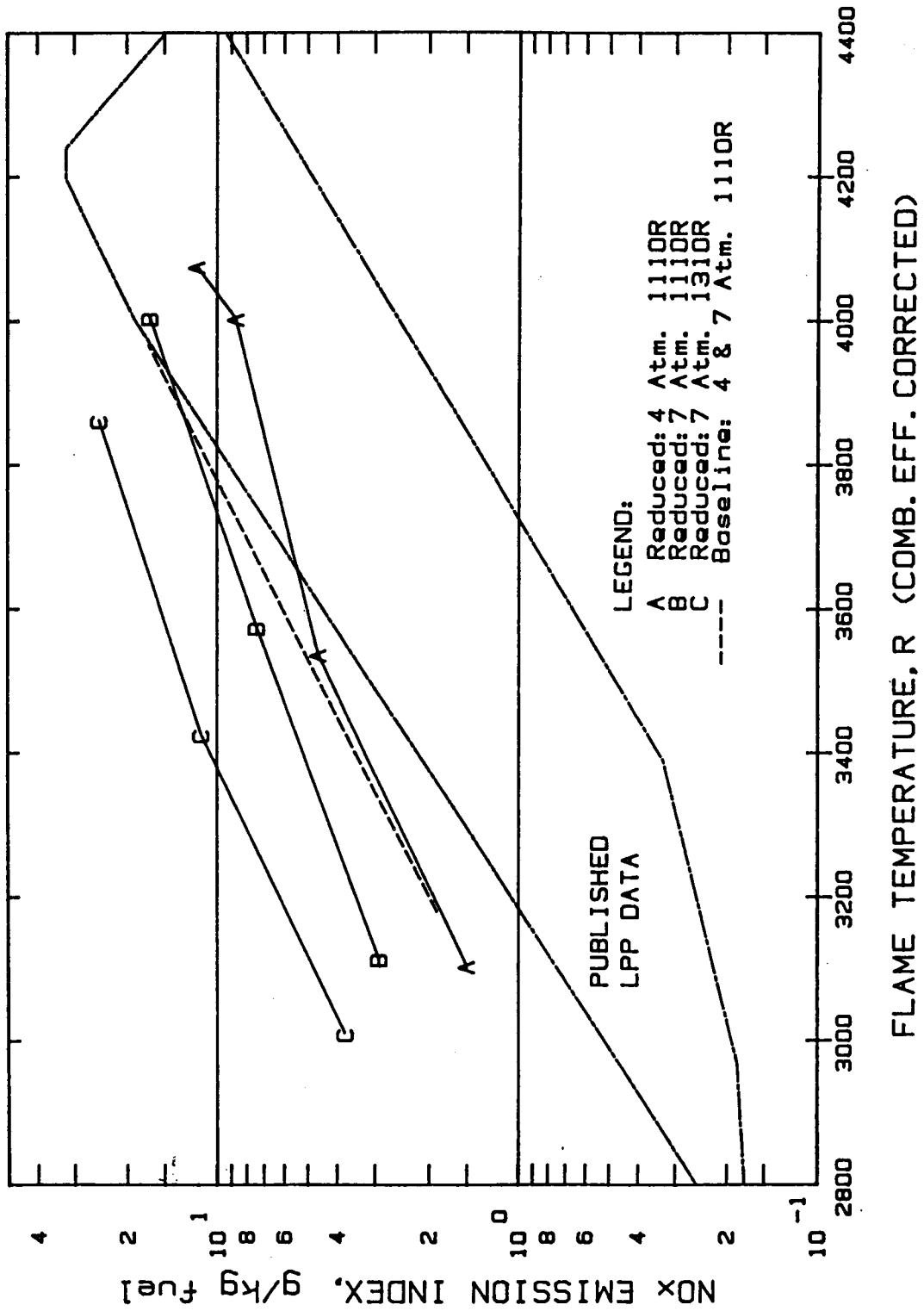


Figure 3.41 - NO_x emissions index plotted versus flame temperature for Configuration 4 of the Cyclone Swirler. The average of the Configuration 3 NO_x emissions results obtained at the two inlet conditions in Figure 3.40 are shown for reference. The dashed boundary indicates the envelope of LPP NO_x emissions obtained in several laboratory flame tube studies published in the open literature.

3.5 Swirl-Jet Premixer Evaluations

The Gen I Swirl-Jet premixer was designed and evaluated under Task 5 of the APT Program, NASA Contract NAS3-25951. The principle advantage of the design was that it had a very large effective flow area even when compared to swirlers for conventional diffusion flame combustors. Having a larger than normal swirler size is not unreasonable, since the HSCT combustor is several times as large as a conventional combustor in a large subsonic jet engine. With the large Swirl-Jet premixer, the number of premixers required for a full size HSCT combustor could be kept comparable to the number of swirlers in a conventional combustor. Because the Swirl-Jet was physically large, the tolerances for locating the fuel nozzles could also be larger. As will be discussed in Section 6 of this report, these factors allowed somewhat conventional fuel systems to be considered. However, the emissions performance of the Gen I Swirl-Jet was poor.

Because of the potential advantages of the Swirl-Jet concept, the decision was made to evaluate a second generation of Swirl-Jet designs in LET Task 10. Gen II would be smaller and simpler than Gen I. The Gen II design had some similarity to a large IMFH with a swirler at the inlet. The swirl was to be kept low, and like the Gen I Swirl-Jet, an axial jet, either swirled or non-swirled, would be used instead of a center-body to counteract the tendency for a recirculation zone to form within the premixer. Several configurations of the Gen II Swirl-Jet were planned. All of those configurations had an internal diameter of the tube of 1.25 inches. The design effective flow areas and the premixer length of all the designs yielded a bulk residence time of about 0.7 milliseconds (roughly equal to that of the IMFH).

Figure 3.42 shows a cross-section of Configuration 1 of the Gen II Swirl-Jet. It utilized an axial swirler and air-blast fuel atomizer. In Configuration 1, the center jet was swirled. The first test of Configuration 1 was at atmospheric pressure. The test focused on establishing lean blowout limits and visual examination of combustion flame quality. The lean blowout data are plotted versus inlet temperature in Figure 3.43 and compared to the required lean blowout for a combustor system design over a range of engine operating conditions. The results were

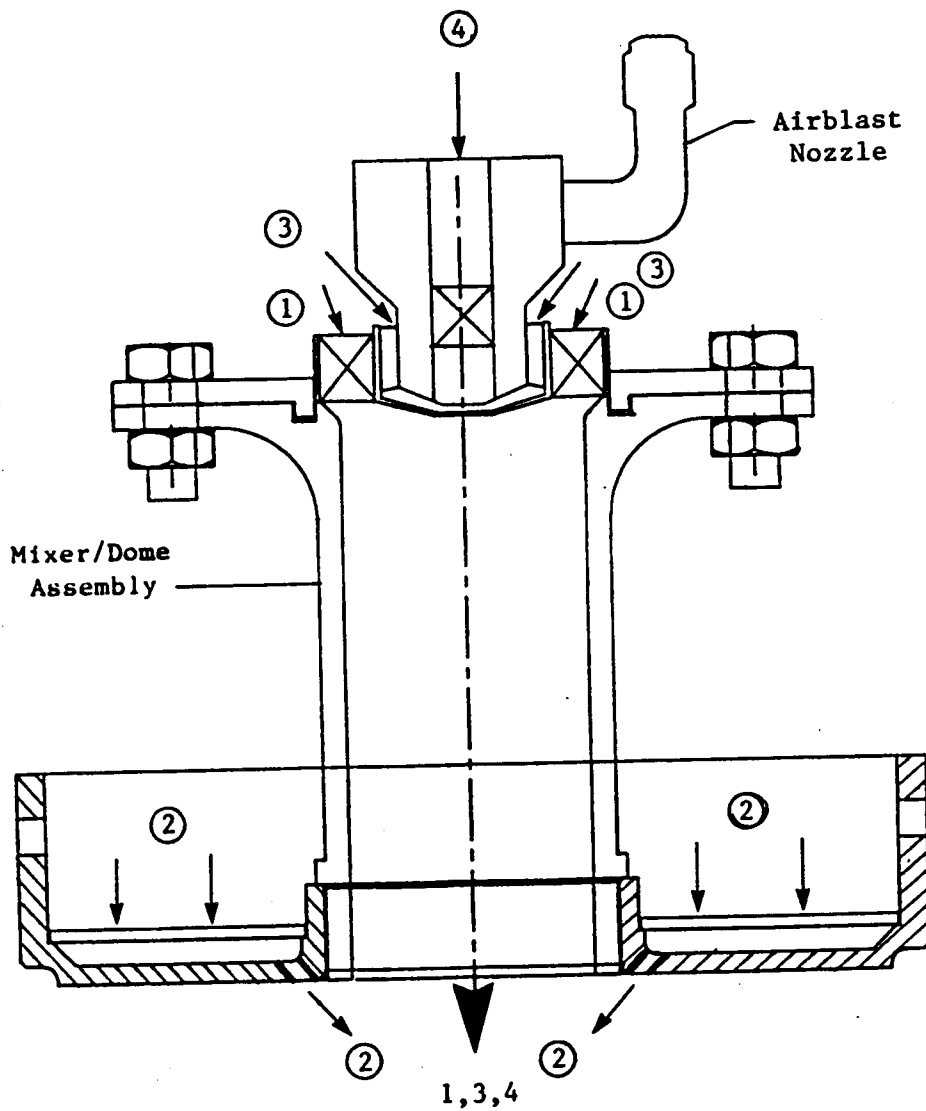


Figure 3.42 - Configuration 1 of Swirl-Jet Gen II fuel-air mixer subcomponent test hardware. The internal diameter of the tube is 1.25 inches. An axial swirler is used. The fuel is injected with an air-blast atomizer. The numbered passages are as follows: (1) the primary air swirler (axial), (2) the dome cooling air in (baffle) and out (spent cooling holes), (3) airblast nozzle air, and (4) center swirler of airblast nozzle.

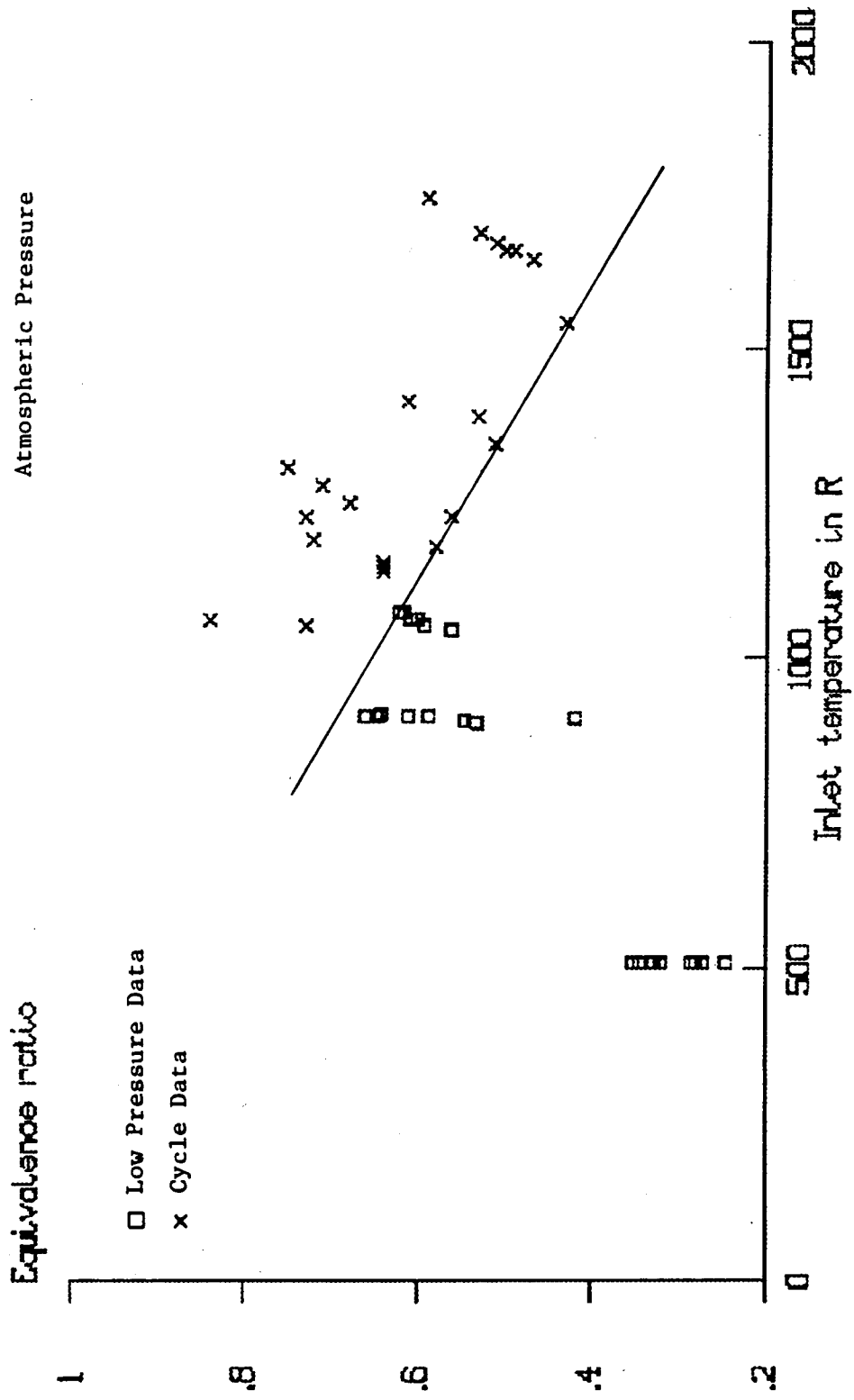


Figure 3.43 - Swirl-Jet Gen II lean blow out equivalence ratio's (squares) plotted versus inlet temperature for Configuration 1 of the Gen II Swirl-Jet. The X's denote where the Swirl-Jet would operate over a mission in an actual engine.

promising, especially considering the flame gases from the pilot stage might enhance the stability of the Swirl-Jet. A four-atmosphere test was then performed to obtain emissions data. The NO_x emissions results are summarized in Figures 3.44. The NO_x EI values at flame temperatures around 3600 R were at best, a little greater than 5 g/kg, which is about double the IMFH Configuration 5A. The higher NO_x values were attributed to inadequate prevaporization and premixing due to large droplet sizes from the air-blast atomizer. The Swirl-Jet Configuration 1 inefficiency results are compared to IMFH Configurations 5A and 5B inefficiency results in Figure 3.45. The Swirl-Jet combustion efficiencies were only fair, by comparison.

Configuration 2 of the Gen II Swirl-Jet used Configuration 1's air-blast fuel injector, but with the center axial swirler removed. An orifice plate was used to provide blockage similar to the center swirler that was removed from the air-blast nozzle. Figure 3.46 shows that the NO_x emissions are still roughly double the IMFH Configuration 5A. The CO emissions and inefficiency data are plotted in Figures 3.47 and 3.48. The efficiency results are similar to Configuration 1 of the Swirl-Jet and averaged over the flame temperature range about as good as the IMFH Configuration 5A. Figure 3.49 compares the lean blowout characteristics of Configuration 1 and Configuration 2. Operating conditions in a combustor system design for key mission conditions for the A5B MFTF cycle are also shown. These results show that Configuration 1 had better stability characteristics than Configuration 2. It was concluded that elimination of the center swirler did not have a significant impact on NO_x and only served to narrow the range of flame temperatures at which the device could operate efficiently.

Configuration 3 used a radial swirler at the inlet with a relatively low swirl instead of the axial swirler. A cross-section is shown in Figure 3.50. An axial jet was used to prevent recirculation. An atmospheric test was conducted. As shown in Figure 3.51, lean blowout equivalence ratio decreased as the inlet temperature increased. At low inlet temperatures, the air-blast fuel nozzle in Configurations 1 and 2 had a lower lean blowout limit; however at inlet temperatures above 800 R, the lean blowout limits were similar. Examination of the test video tape showed a yellow swirling flame that indicated the premixer was not vaporizing and mixing the fuel before combustion. This was probably due to the coaxial air jet around the fuel nozzle

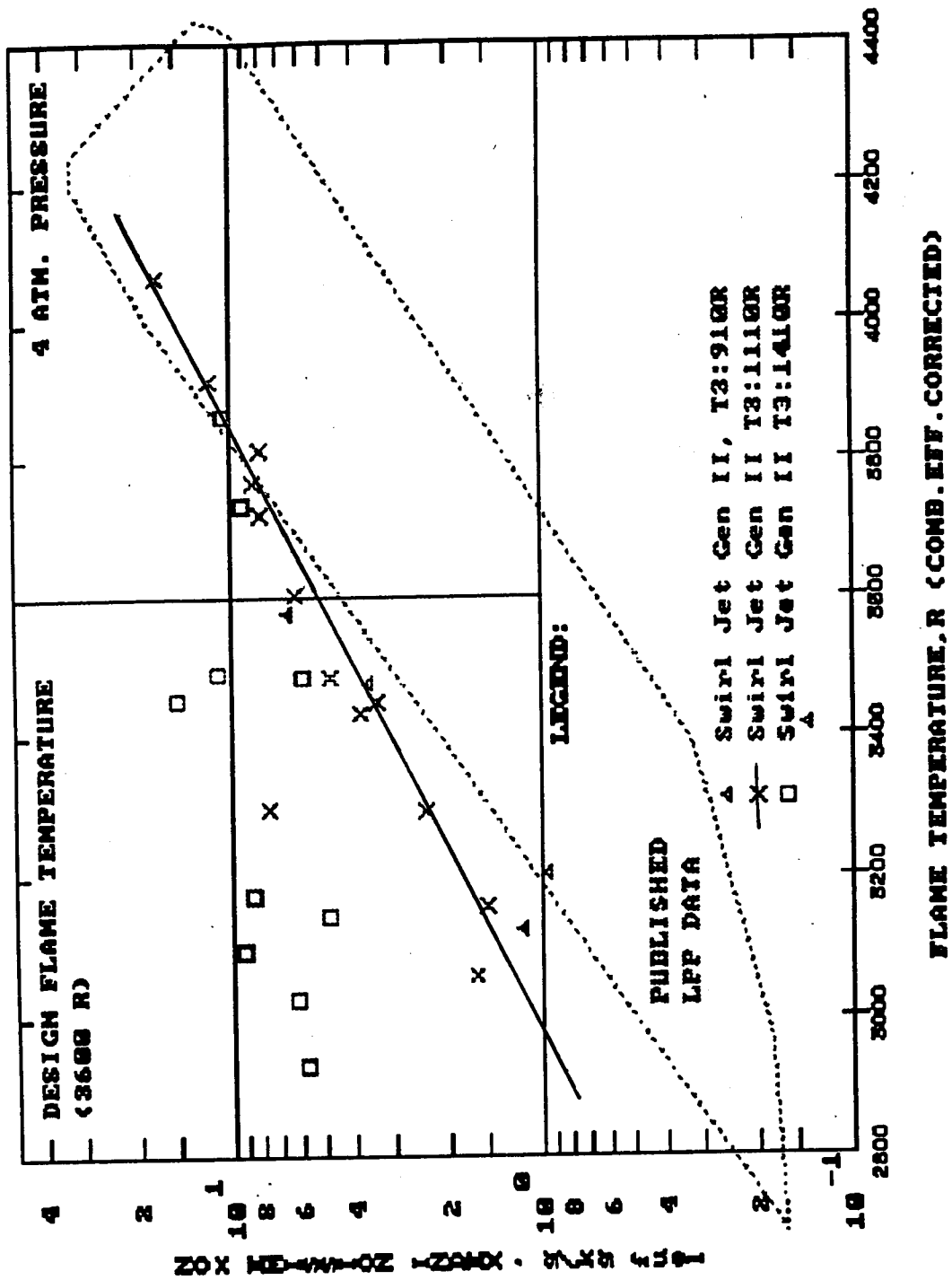


Figure 3.44 - NOx Emissions Index for Configuration 1 of the Swirl-Jet Gen II plotted versus flame temperature. The dotted line boundary indicates the envelope of LPP NOx emissions obtained in several laboratory flame tube studies published in the open literature.

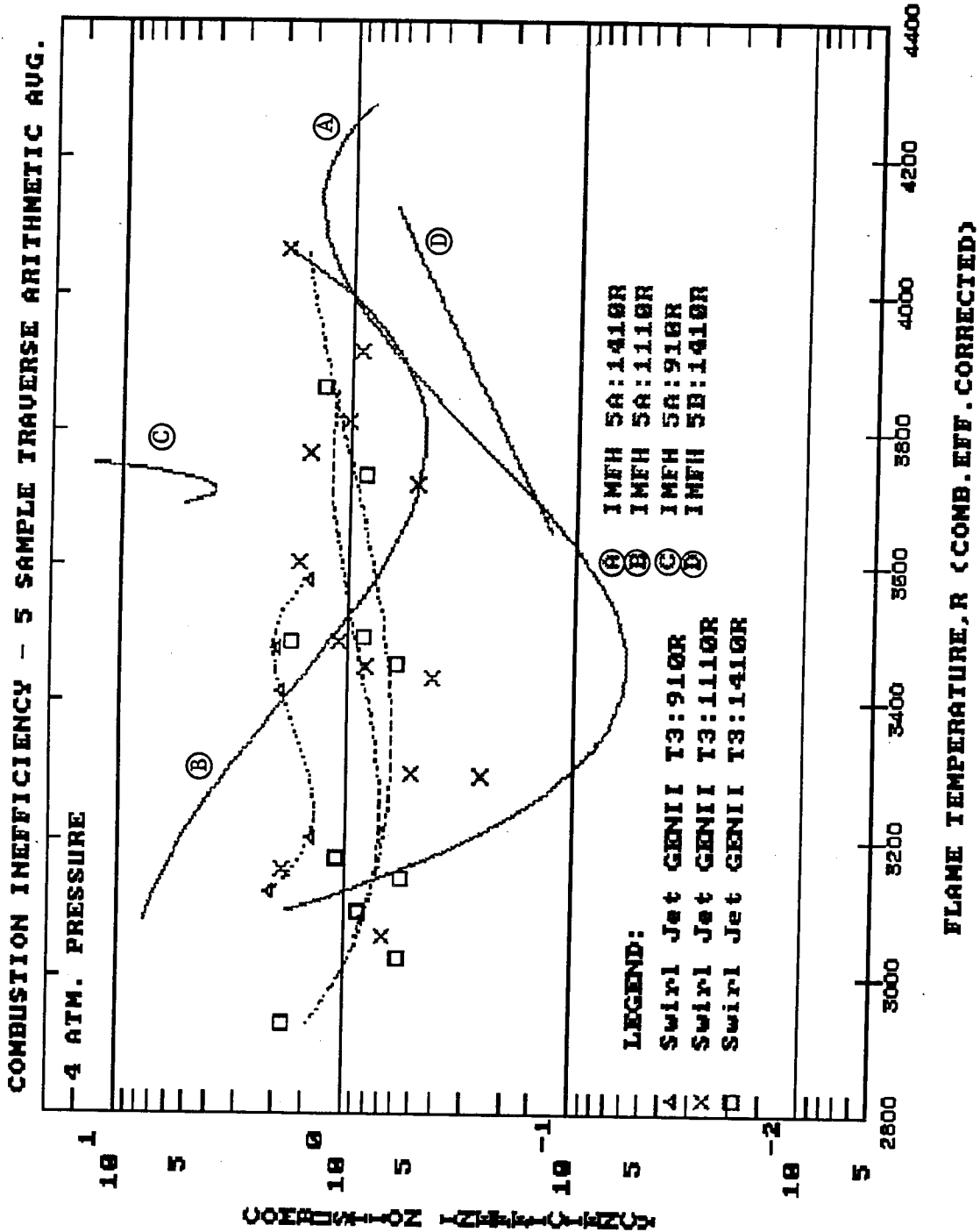


Figure 3.45 - CO Emissions Index for Configuration 1 of the Swirl-Jet Gen II plotted versus flame temperature.

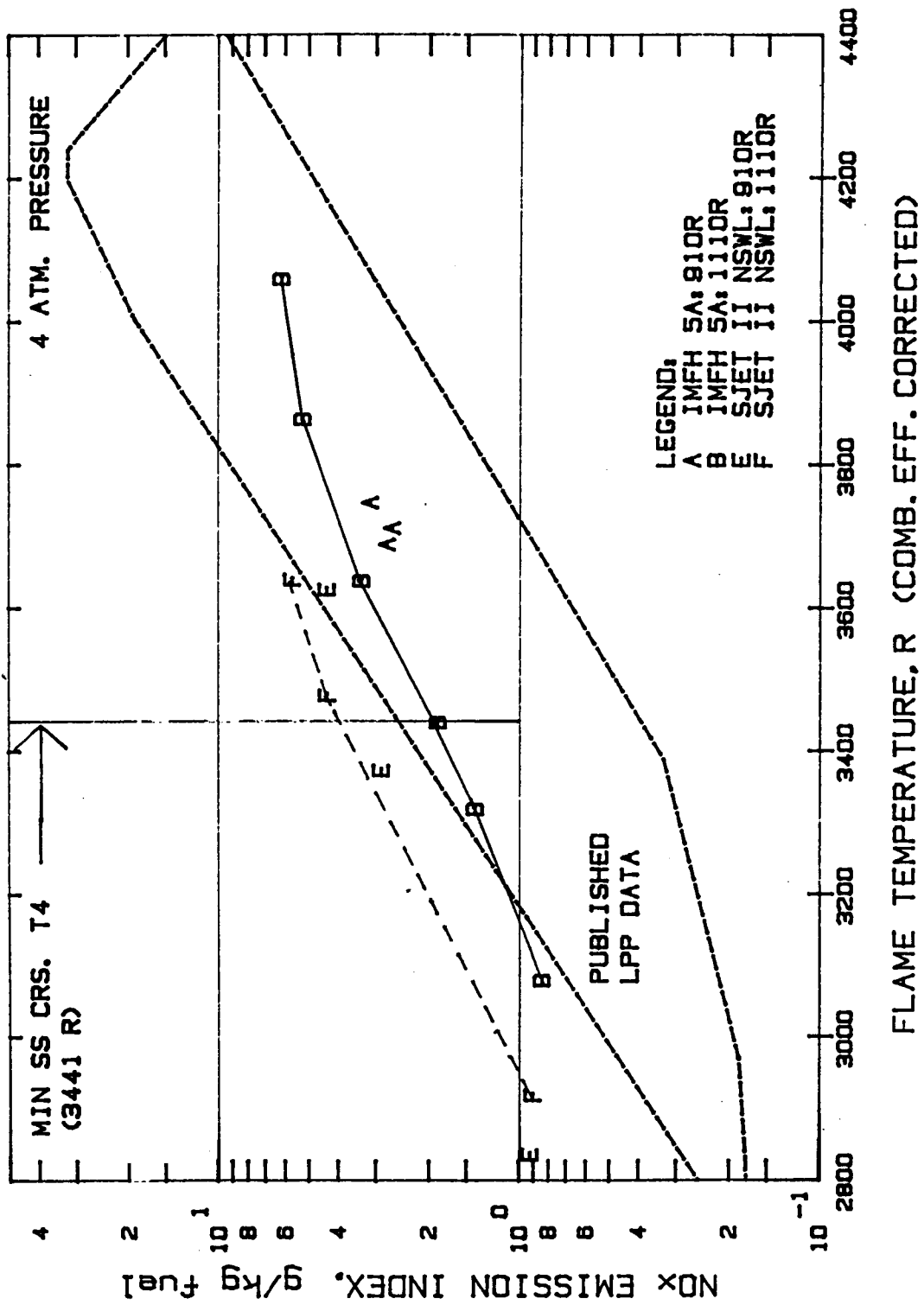


Figure 3.46 - NOx Emissions Index for Configuration 2 of the Swirl-Jet Gen II plotted versus flame temperature. The dotted line boundary indicates the envelope of LPP NOx emissions obtained in several laboratory flame tube studies published in the open literature.

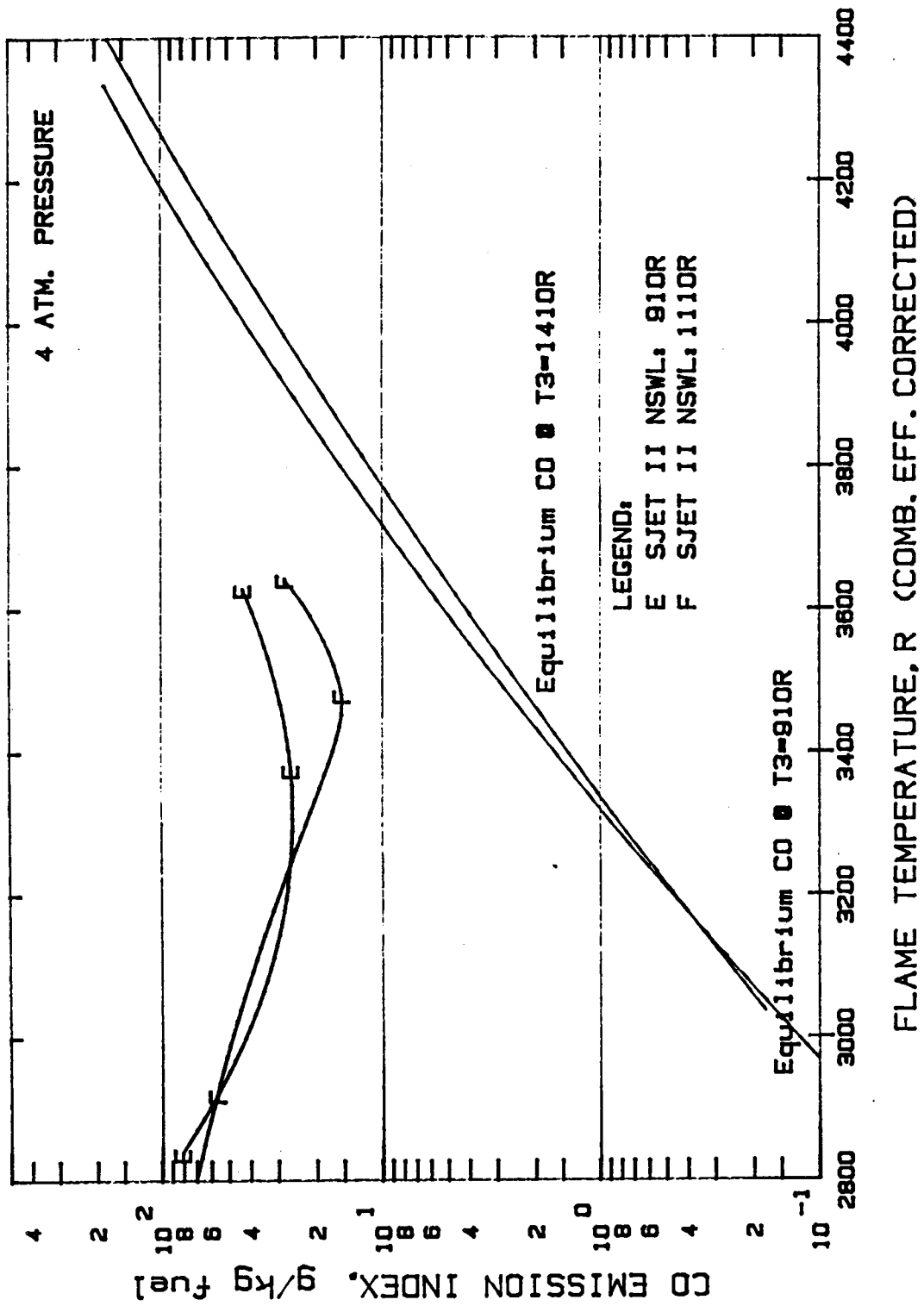


Figure 3.47 - CO Emissions Index for Configuration 2 of the Swirl-Jet Gen II plotted versus flame temperature. The calculated CO equilibrium line at 60 psia with 1410 R inlet temperature is shown for reference.

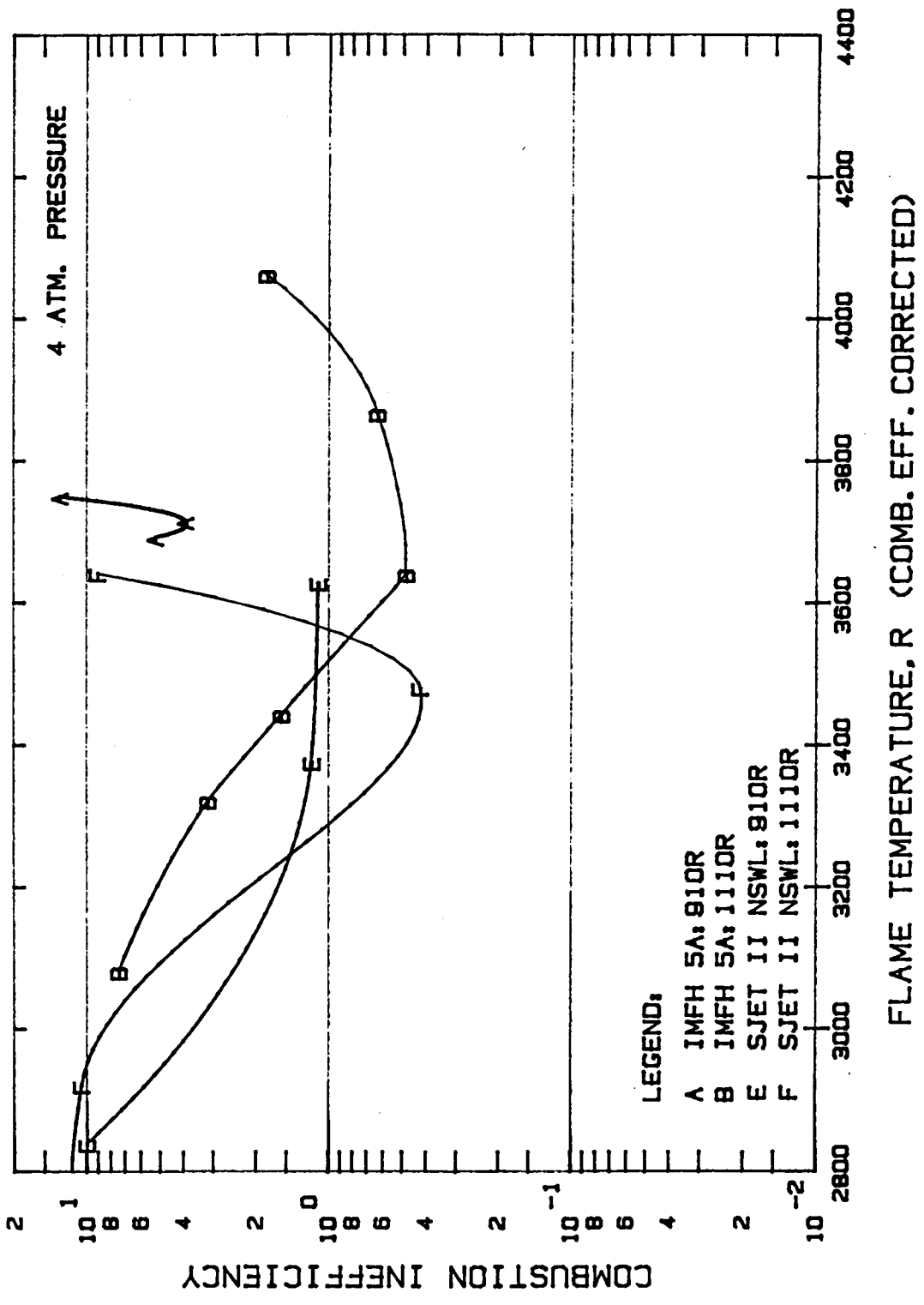


Figure 3.48 - Combustion inefficiency for Configuration 2 of the Swirl-Jet Gen II plotted versus flame temperature.

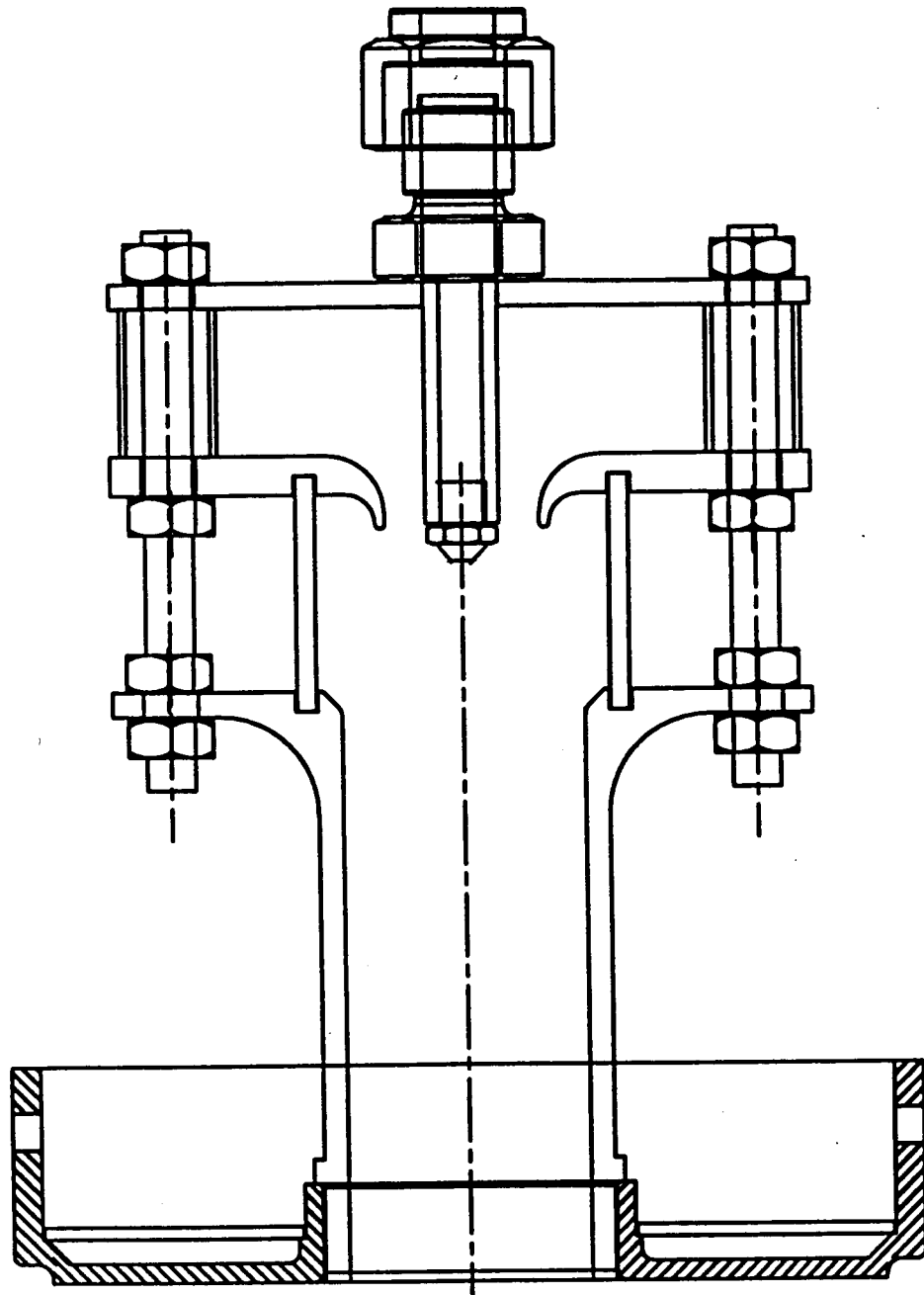


Figure 3.50 - Swirl-Jet Gen II, Configuration 3, single-cup test hardware. A radial swirler is used instead of an axial swirler. The fuel is injected with a simplex atomizer within a concentric air jet. The concentric air jet has a contoured inlet. The spent cooling air holes are not shown, but they are in the same location as are shown in Figure 3.42

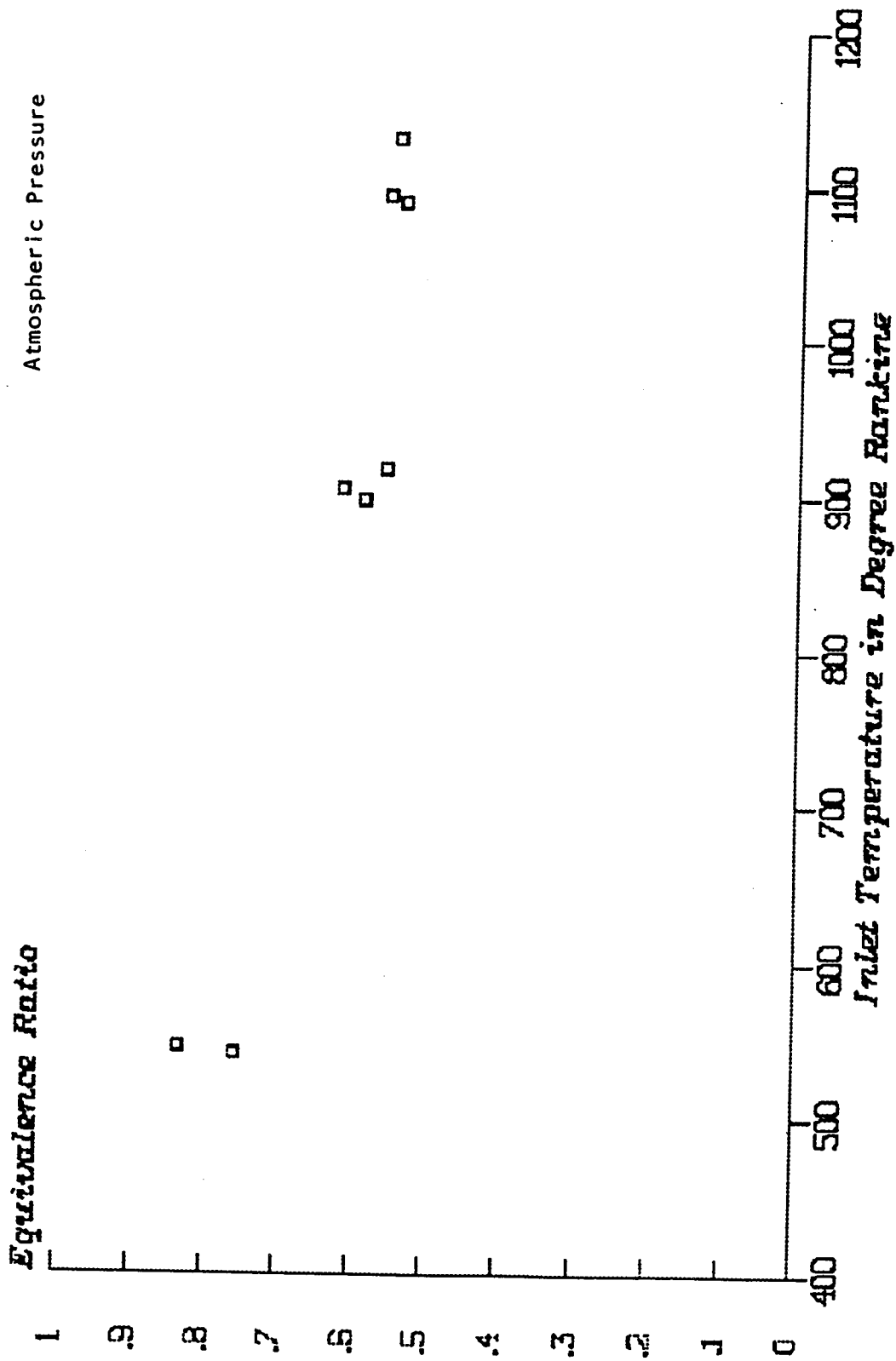


Figure 3.51 - Lean blow out equivalence ratio plotted versus inlet temperature of Configuration 3 of the Swirl-Jet Gen II.

carrying the fuel into the combustor before the droplets had time to vaporize. The initial results of these tests of Configurations 1, 2 and 3 of the Gen II Swirl-Jet were judged not very promising. The development of the Gen II Swirl-Jet was discontinued.

However, as the final part of this test series, a Configuration 4 was assembled using the available Gen II Swirl-Jet hardware. Configuration 4 used no swirler and was, in reality, a short IMFH with a concentric simplex fuel nozzle at the inlet of the tube. An atmospheric pressure test was run. The flame was about 2 feet long and was not firmly anchored to the dome. Based upon the observations in this test, the fuel almost certainly was not well mixed across the tube but was concentrated at the centerline.

3.6 Summary of Subcomponent Evaluations

Based on the results of the subcomponent testing in LET Task 10, the IMFH tube and Cyclone Swirler pilot mixer concepts were selected as the primary mixer concepts for future subscale sector combustor evaluations, confirming the conclusions of APT Task 5. The IMFH tube concept was selected for the main combustor stage. The Cyclone Swirler was selected for use in the pilot stage of the combustor. The other fuel-air mixer concepts (with the exception of the Multi-Venturi, an LDI concept [Lean-Direct-Injection] being tested at NASA-Lewis) were dropped from consideration for the subscale sector combustor tests because they did not meet the emissions performance requirements and/or stability requirements or, in the case of the curved tube IMFH, were inclined to flashback.

Section 4

Sector Combustor Design and Evaluation

Four tests of sector combustors were planned at GE Aircraft Engines in LET Task 10. The baseline hardware configuration was the sector combustor designed and fabricated in Task 5 of NASA Contract NAS3-25951. The sector combustor hardware is described in more detail in the final report for Task 5⁽³⁻¹⁾. A rectangular sector was chosen for the design rather than a sector of an annulus, in order to minimize costs and meet the schedule. The added design details (like the flowpath radii) of the curved sector would have been contrived, since the specific subscale demonstration engine had not been determined at the time the sector combustors basic layout had to be frozen.

The rectangular sector combustor's dome was divided into three sections; one central pilot dome, with five cyclone swirler pilots, and two main domes, each with 24 IMFH tubes. Each main dome had 4 separate fuel manifolds such that each manifold fueled six IMFH tubes. No isolation was provided between the four fueling regions on a main dome. This allowed evaluation of the effect of having no isolation between the fueled and unfueled IMFH stages. The length that the pilot dome was recessed relative to the main domes was adjustable, allowing evaluation of that design parameter. The liner and sidewalls were impingement and convectively cooled. No film cooling was used in the liners sidewalls in the baseline design. This was the conservative approach, since there was evidence in the open literature that LPP combustion suffered a significant penalty in combustion efficiency when film cooling is used. Not introducing film-cooling air into the combustor also simplified the interpretation of the emissions data, since all the air in the combustor flowed through one of the fuel-air premixers. Figure 4.1 shows the a sectional view of the rectangular sector combustor.

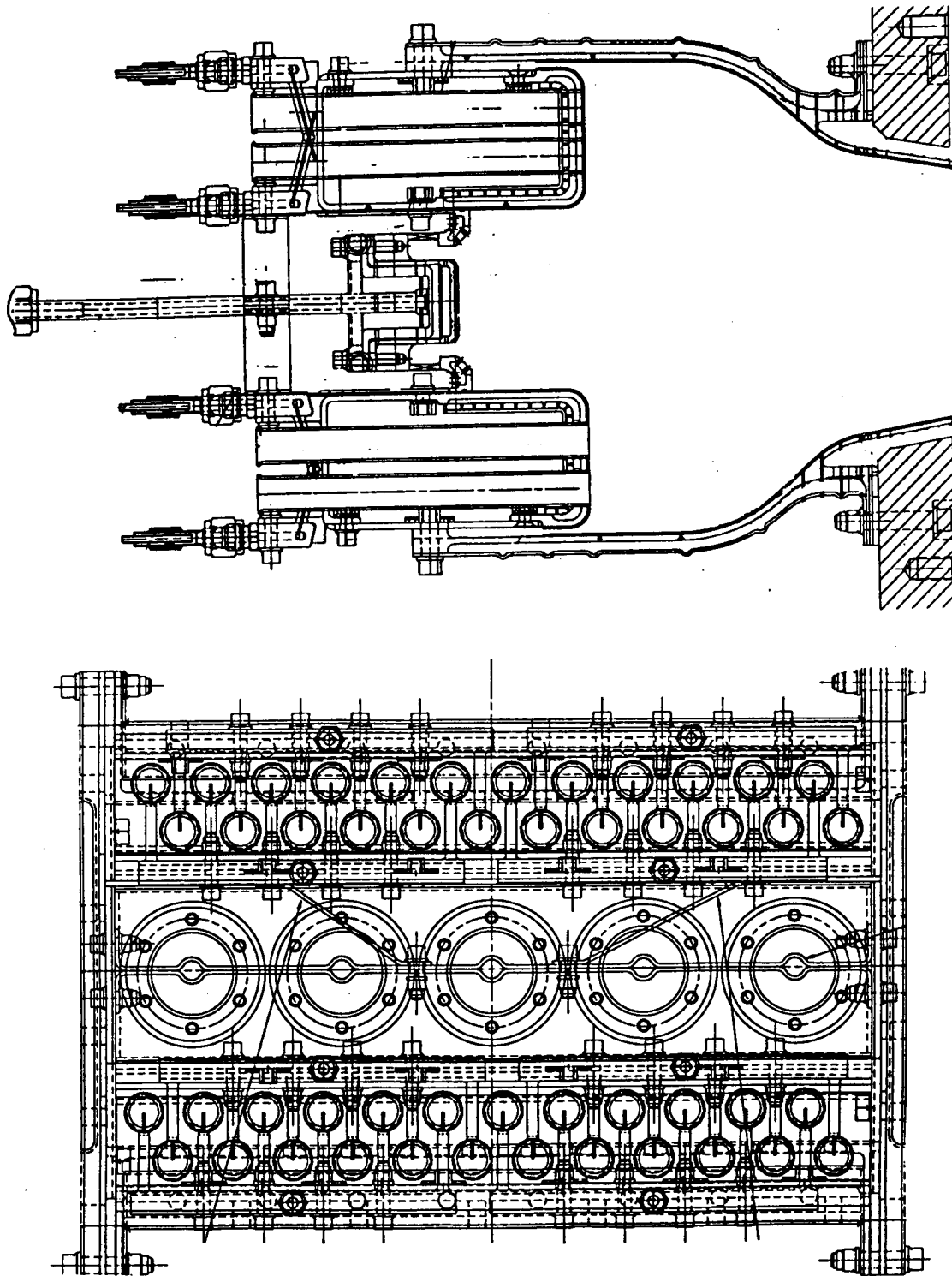


Figure 4.1 - Two views of the LPP rectangular sector combustor. The recessed center dome with the Cyclone Swirlers is the pilot stage. The two main domes with the IMFH tubes are the main stages. Each main dome has four separate fuel systems.

As a part of LET Task 10, a second rectangular sector combustor was designed and fabricated for testing at NASA-Lewis. The dome was essentially identical to the 5-cup sector above, except that it had three Cyclone Swirler pilots on the central pilot dome and 14 IMFH tubes on each of the two main domes. The dome and the fuel injectors were supplied to NASA by GEAE. Instead of using convectively-cooled liners and sidewalls, the combustion zone walls were castable ceramic, similar to those used for single-cup tests at NASA-Lewis and GEAE. The 3-cup sector combustor would be used primarily for diagnostic studies.

At the time the planning was being done for the first tests of the HSCT 5-cup sector, there was no aero performance data on how the Cyclone Swirler pilot and the IMFH would operate together as a system. There were also a number of mechanical design and cooling design features in the sector combustor which were new and required evaluation. The preliminary list of requirements for the HSCT low emissions combustor (to be discussed in Section 6 of this report) led to a long list of test objectives. The highest priority test objectives were considered to be (in rough order of priority):

1. Establish that the combustor would operate.
2. Evaluation of emissions at inlet conditions comparable to the single-cup emissions data base for the Cyclone Swirler pilot and the IMFH. This would allow back-to-back comparisons of the effect of the installation of premixers in the combustor system.
3. Evaluation of emissions at Supersonic Cruise conditions. This is the primary metric for the HSCT low emissions combustor development program.
4. With maximum pilot stage isolation (maximum pilot recess), evaluation of CO emissions with one and both main domes turned off. This would establish with the largest recess, whether CO emissions would be acceptable during part staging.
5. With minimum pilot stage isolation (minimum pilot recess), evaluation of CO emissions and pilot stability with one and both main domes turned off

This would establish if the combustor can perform without isolation between the pilot and main stages. The isolation was believed to be mandatory for low CO emissions, but also is costly in terms added combustor complexity, weight, overall length, cooling air requirements, and fuel-system complexity.

6. Evaluation of main stage stability and CO emissions with adjacent rows of fired and unfired IMFH tubes. Isolation of IMFH main stages from each other raises the same issue of CO emissions performance versus design complexity as the pilot/main stage isolation.
7. Evaluation of the material temperatures and durability of the convectively cooled liners. At the time, there was very little experience with convectively-cooled liners at GEAE.
8. Evaluation of the effect of film-cooled liners (Lamilloy[®] liners supplied by Allison) on CO emissions.

The first objective may seem unwarranted, since the Cyclone Swirler pilot and IMFH had already been run in single-cup tests. However, some considered those tests inconclusive since the stability of the Cyclone Swirler and IMFH in the single-cup tests could have benefited from the hot castable ceramic walls used in the single-cup rigs. Also, there was a concern about stability during part-stage operation. Other possible objectives for the testing were also identified, but were considered to have a lower priority.

Emissions data from the sector combustor evaluations continue to be plotted versus fired dome flame temperature, as they were with the sub-component flametube results. Local flame temperature is the single most important parameter determining emissions from LPP combustors. The emissions data, thus presented, can easily be interpreted for new engine cycles as they evolve using the corresponding combustor system design to calculate the local fuel-air ratios and flame temperatures.

4.1 Sector Test 1 - Pressure Test of Baseline Sector Combustor

The first sector combustor test began on October 29, 1993 and was completed on November 4. The goals of the test were to demonstrate stable operation of the combustor system and obtain emissions data at conditions the data could be compared to single-cup data. A secondary goal was to reach supersonic cruise conditions, if the test went well. Stable operation of the IMFH/Cyclone Swirler dome system was demonstrated for inlet temperatures up to 1405 R (945° F), inlet pressures up to 8 atmospheres, and pressure drops ranging from 2.9% to 4.0%. Stable operation of the combustor was demonstrated with the pilot only operating at combustor conditions roughly corresponding to engine idle, an inlet temperature of 872 R (412° F) and inlet pressure of 47 psia. The test was terminated when inspection showed 13 of the 48 fuel injector tips had been clipped off by interference with the IMFH tube walls. The differential thermal expansion of the dome parts was greater than could be accommodated by the clearance hole in the walls of the IMFH tubes. The fuel from the clipped off fuel injectors apparently still went into the IMFH tubes or catastrophic damage would have occurred. The simple solution was to enlarge the clearance holes in the IMFH tube walls. Post-test hardware inspection indicated that the dome cooling design appeared to perform as intended. Minor TBC spalling occurred on the sector side walls near the pilot and at the ends of the main domes. The aft end of the liners warped. However these problems were not unexpected. In the interest of cost and simplicity, the sector combustor design had not entirely eliminated all the potential locations for thermal fight. This design simplicity, combined with the flat panels and simple curvature of the hot structures in this rectangular design, were expected to lead to some degree of warping and cracking.

A summary of the nominal combustor inlet conditions at which the combustor was operated in this first sector test is given in Table 4.1. The measurements for the NO_x emissions index in the first sector test are plotted in Figure 4.2. The highest measured NO_x emissions at the highest inlet temperature (1405 R or 945° F) was 4.3 EI NO_x at a flame temperature of 3490 R. This would extrapolate to a NO_x EI of about 5 to 6 g/kg at a flame temperature of 3530 R, the supersonic cruise design point flame temperature at that time. Combustion efficiencies were

99.9% or higher when all the fuel stages were on at the highest inlet temperature of 945° F (1405 R). The sector combustor's NOx data were slightly higher than the IMFH single cup test data, but followed the same trend.

Non-uniform temperature profiles were investigated. Reduction in the pilot dome flame temperature by 180° F relative to the main dome flame temperature reduced the NOx emissions by about 20% from the trendline flame temperature data (point 31, Appendix A), which confirmed predictions that the Cyclone Swirler pilot stage contributed proportionally more NOx than the IMFH stages. Increasing the outer main dome flame temperature by 130 and 190° F relative to the inner main dome, raised NOx emissions slightly from the trendline (points 32 and 33, Appendix A). The non-uniform points are shown as the shaded diamonds and solid circles, respectively, in Figure 4.2.

The pre-test flow check of the hardware indicated that the pilot dome flow split of rectangular stepped-dome sector combustor was significantly higher (27%) than the HSCT combustor system designs at that time (which had about a 20% pilot flow split). All else equal, the HSCT combustor (or the subscale demo engine combustor) with the correct pilot stage flow split would have lower emissions than measured in the 5-cup rectangular sector combustor. Adjusting the NOx emissions data for the correct pilot stage flow split indicated the program goal of a NOx EI of 5 g/kg would be met.

Table 4.1			
Sector Test 1 Combustor Inlet Conditions, Nominal			
T3 [R]	P _{INLET} [psia]	ΔP/P	Fuel Stages
1130	74	3.5%	All
872	47	2.9%	Pilot
1070	78	3.5%	All
1228	86	3.4%	All
1410	120	3.8%	All

NO_x EMISSIONS vs. FLAME TEMPERATURE FIRST SECTOR TEST

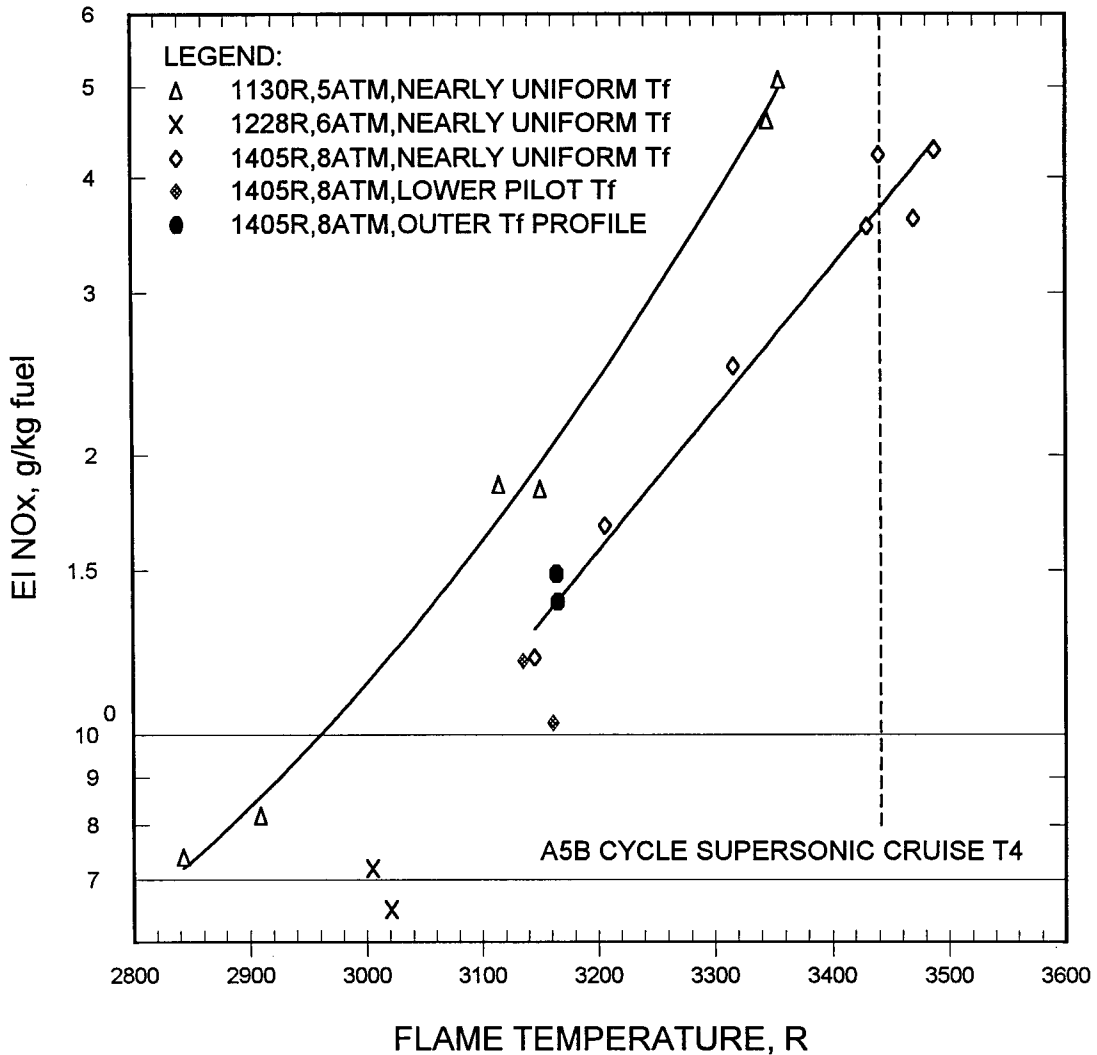


Figure 4.2 - NO_x emissions index plotted versus flame temperature for the first rectangular sector test. All the fuel stages are fired. Flame temperature and combustor exit temperature are equivalent. Data from the first rectangular sector combustor test. The pilot flame temperatures reductions were 86° F and 183° F relative to the IMFH main stage (solid diamonds).

4.2 Sector Test 2 - Atmospheric Pressure Test of Baseline Sector

The second rectangular sector combustor test was performed at atmospheric pressure in the Advanced Combustor Laboratory at GEAE. The test began on April 6, 1994 and ended on April 8. The first day of the atmospheric pressure tests were run with the gas sampling rakes in place. The primary objectives were to obtain exit temperature profile factor results with the pilot stage only operating and to make visual observations of the combustion zone. The profiles were determined by gas sample analysis. The gas sampling rakes were then removed and LBO data obtained and visual observations made of the flame with different staging configurations.

The exit temperature profile factor is plotted in Figure 4.3. The profile factor is center-peaked, which is desirable. However, the peak value is higher than normal for a conventional turbine combustor, even if fuel-staged. The gas analyses used to obtain the sample fuel-air ratios also yielded emissions data. NO_x and CO emissions at one atmosphere are not relevant to engine conditions so the data are not reproduced here.

The pilot stage lean blow out data is plotted in Figures 4.4. In Figure 4.5 the pilot stage lean blow out data is replotted along with single-cup Cyclone Swirler configuration 2 lean blow out data. Both sets of lean blow out data are very consistent over the inlet temperature range of 250° F to 600° F (710 R - 1060 R).

IMFH light-off and lean blow out equivalence ratios are plotted versus pilot equivalence ratios in Figure 4.6. The light-off data are labeled LO and the lean blow out data are labeled LBO. Light-off and lean blow out data were obtained for the inner (bottom) main dome when the outer (upper) main dome was fired and for the outer dome when the inner dome was not fired. There was little difference between the two sets of data. However, the pilot dome equivalence ratio is seen to have a significant effect. Both the IMFH light-off and lean blow out equivalence ratios dropped with increased pilot dome equivalence ratio.

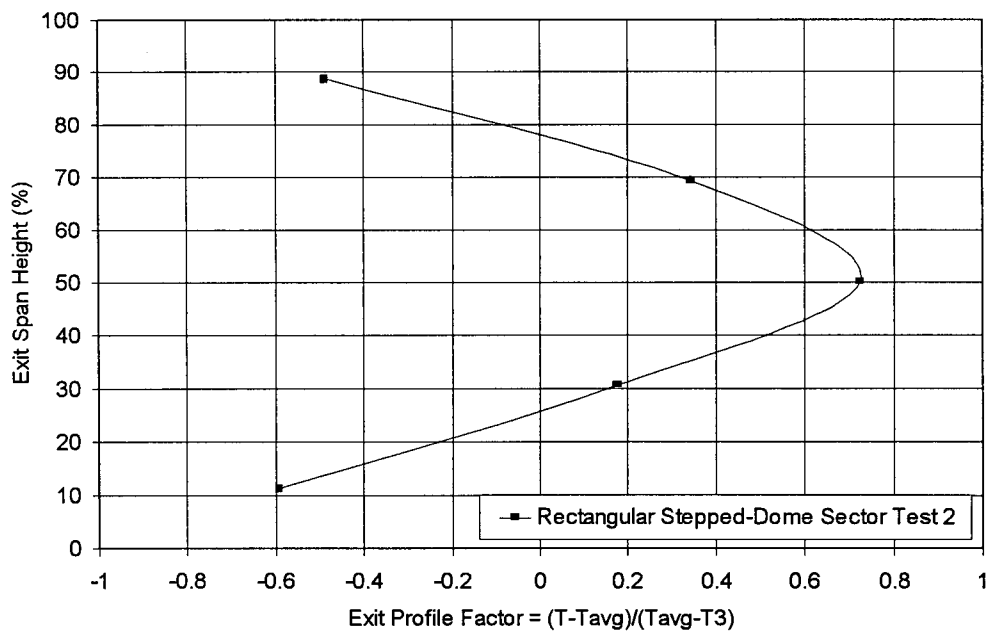


Figure 4.3 - Rectangular sector exit temperature profile factor with pilot stage only operating. Temperatures are calculated from analysis of gas samples. Atmospheric pressure. Inlet temperature was 861 R (402° F). Data from the second rectangular sector combustor test.

IMFH/CYCLONE SECTOR TEST 2
PILOT LBO vs. INLET TEMPERATURE

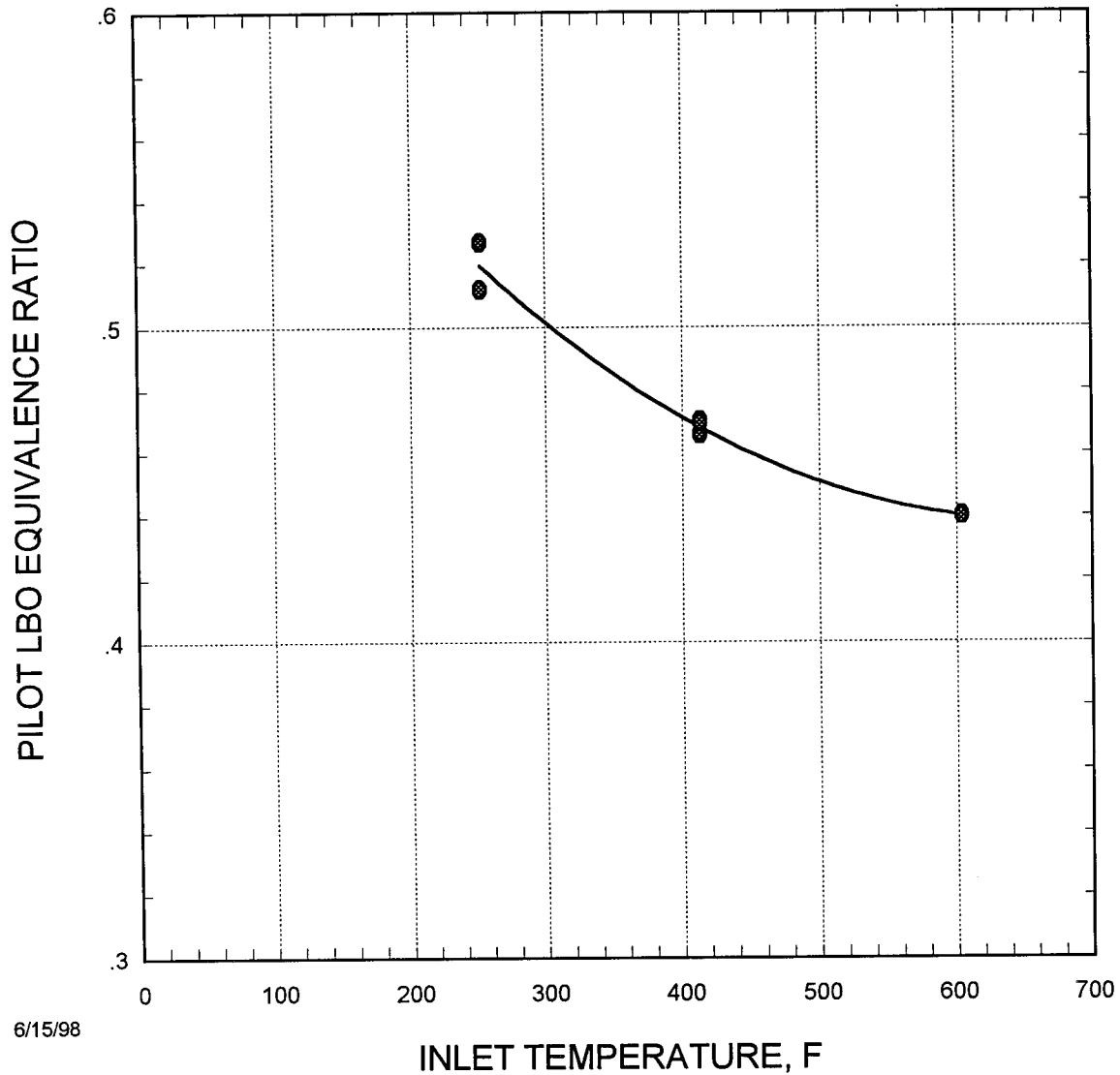


Figure 4.4 - Pilot lean blow out equivalence ratio plotted versus inlet temperature. Data from the second rectangular sector combustor test performed at atmospheric pressure.

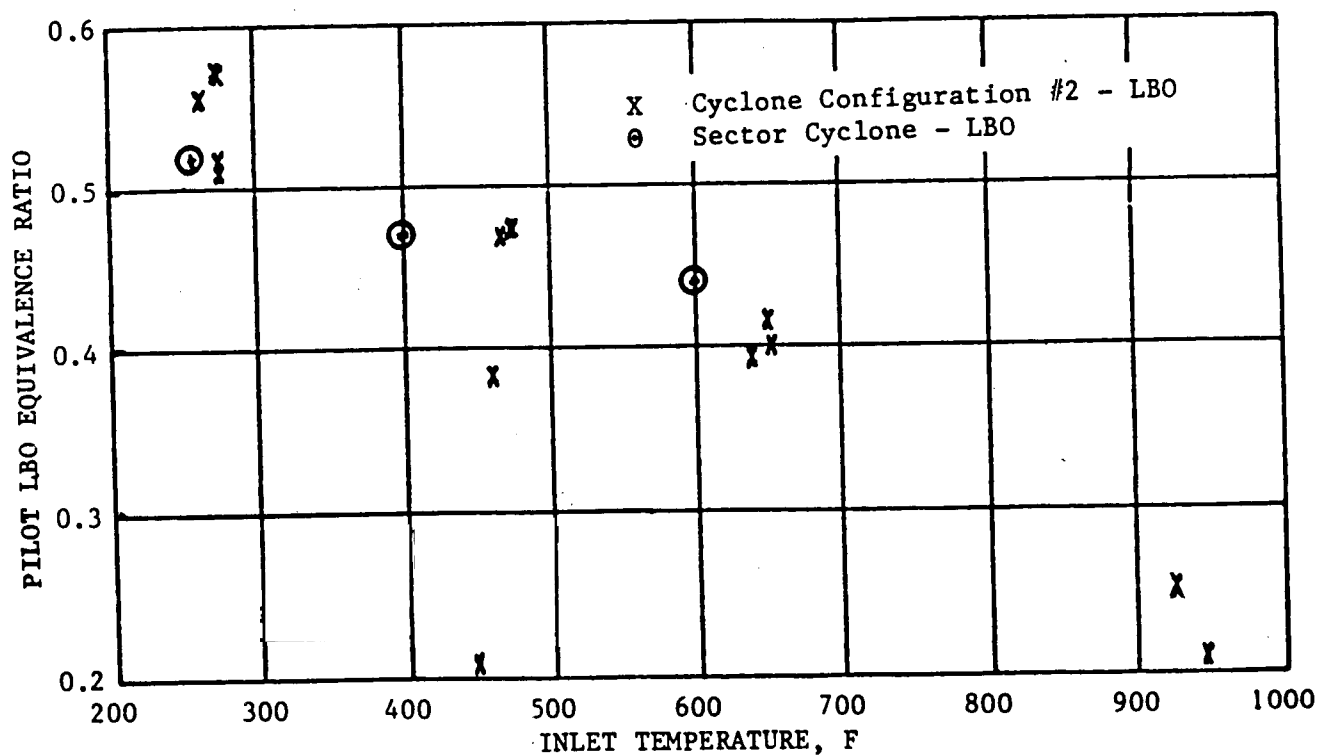
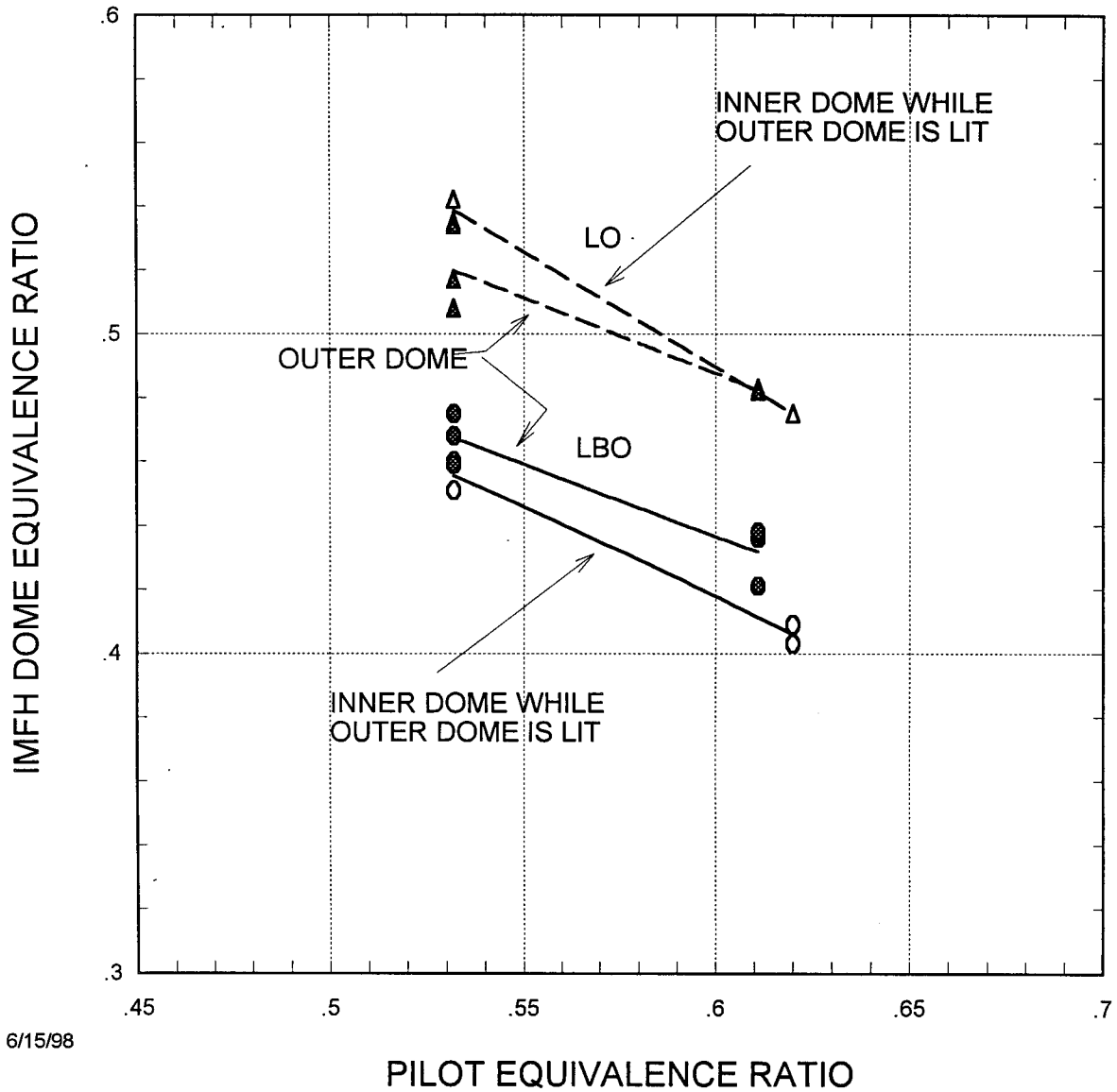


Figure 4.5 - Pilot lean blow out equivalence ratio plotted versus inlet temperature. Data from the second rectangular sector combustor test compared to single-cup data for Cyclone Swirler Configuration 2 obtained in APT Task 5⁽³⁻¹⁾.

IMFH/CYCLONE SECTOR TEST 2 IMFH DOME LO & LBO
413-422 F INLET TEMPERATURE



6/15/98

Figure 4.6 - IMFH light-off (labeled LO) and lean blow out (labeled LBO) equivalence ratio plotted versus pilot stage equivalence ratio. Data from the second rectangular sector combustor test performed at atmospheric pressure.

4.3 Sector Test 3 - Second Pressure Test of Baseline Sector Combustor

The third sector combustor test was run in GEAE's Cell A5 in June, 1994. The emphasis of the test was part-stage operation. With part stage operation, the sector combustor's NOx emissions are dominated by the Cyclone Swirler pilot stage, because the pilot is burning a greater proportion of the fuel. The NOx emissions during different staging configurations over a wide range of inlet conditions are shown in Figures 4.7 (with the pilot and outer dome fired), Figure 4.8 (with the pilot and the closest IMFH row in the outer dome fueled), and Figure 4.9 (with the pilot dome only fueled). The lowest NOx emissions are obtained with the pilot stage only fired. This is attributed to dilution of the pilot flame gases by the air from the unfired main stages. NOx emissions increase when one IMFH row is fired in addition to the pilot dome. This is attributed to the pilot being partially blanketed by the single row of fired IMFH tubes, so that the inherently higher NOx emissions of the Cyclone Swirler were not reduced by air entrainment or by large fractions of the fuel being burned by the IMFH. With the one IMFH row closest to pilot fired, the NOx emissions were the highest observed in the test. With that staging configuration, the NOx emissions increased with increasing inlet temperature. The trends with inlet temperature are consistent with the Cyclone Swirler single-cup test results in Section 3.

The same data are re-plotted in Figures 4.10 and 4.11 to clarify the effect of changes in staging configuration on NOx emissions at constant inlet conditions. In Figure 4.10, with an inlet temperature of 1410 R and a pressure of 8 atmospheres, turning on the last IMFH stages is shown to yield lower NOx emissions than with partial staging of the IMFH main domes. This is a result of the better NOx emissions characteristics of the IMFH relative to the Cyclone Swirler at the high inlet temperature. Figure 4.11 shows that at inlet temperatures near 1100 R, NOx emissions increase when more IMFH stages are turned on. At this lower inlet temperature, the Cyclone Swirler NOx emissions are nearly as low as the IMFH and the blanketing effect dominates. In general, NOx emissions were sensitive to the staging configuration, but the effect of changes in dome staging configurations on NOx depends on the combustor inlet conditions.

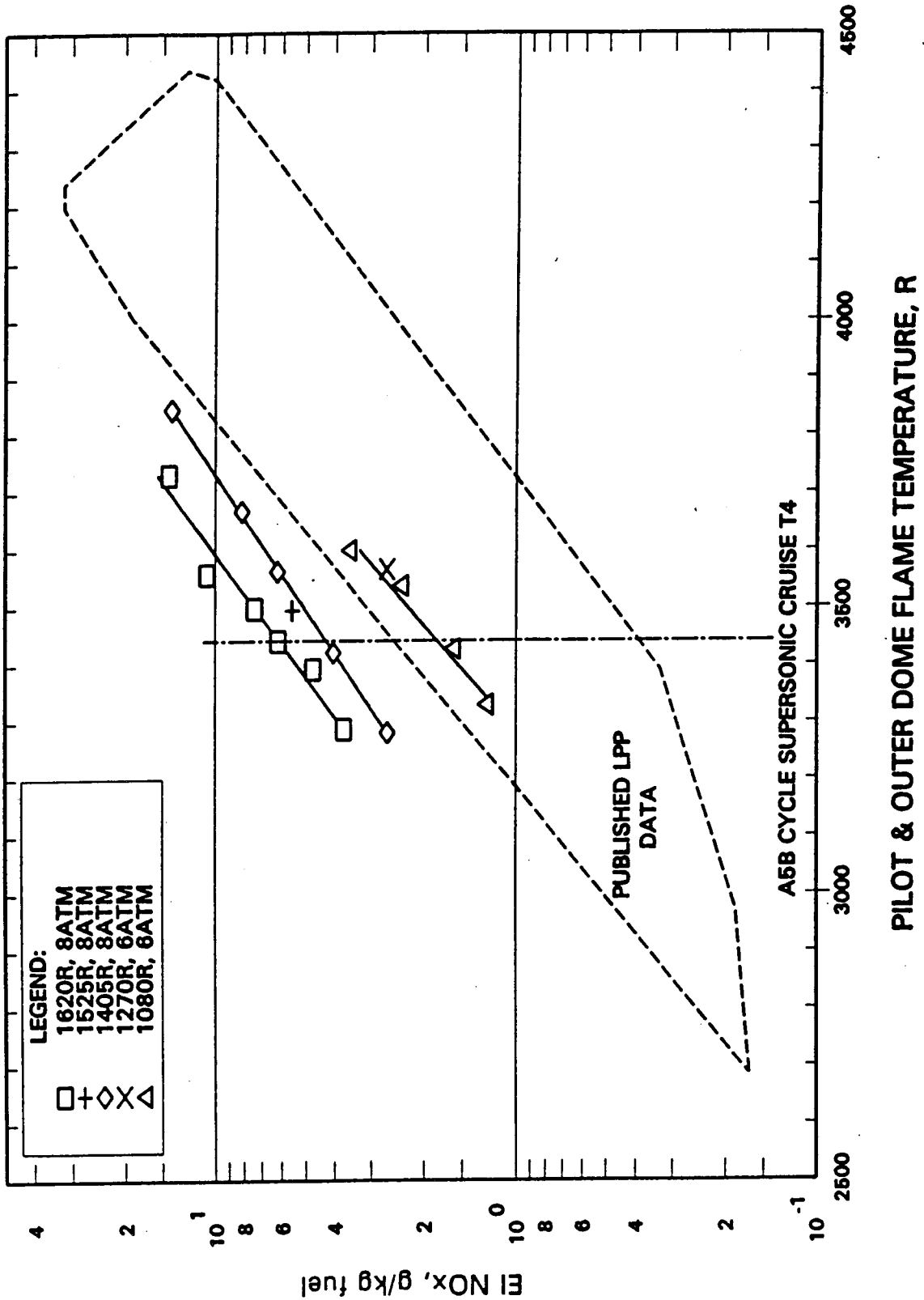


Figure 4.7 - NOx emissions index plotted versus flame temperature with the pilot and outer main dome fired. Data from the third rectangular sector combustor test.

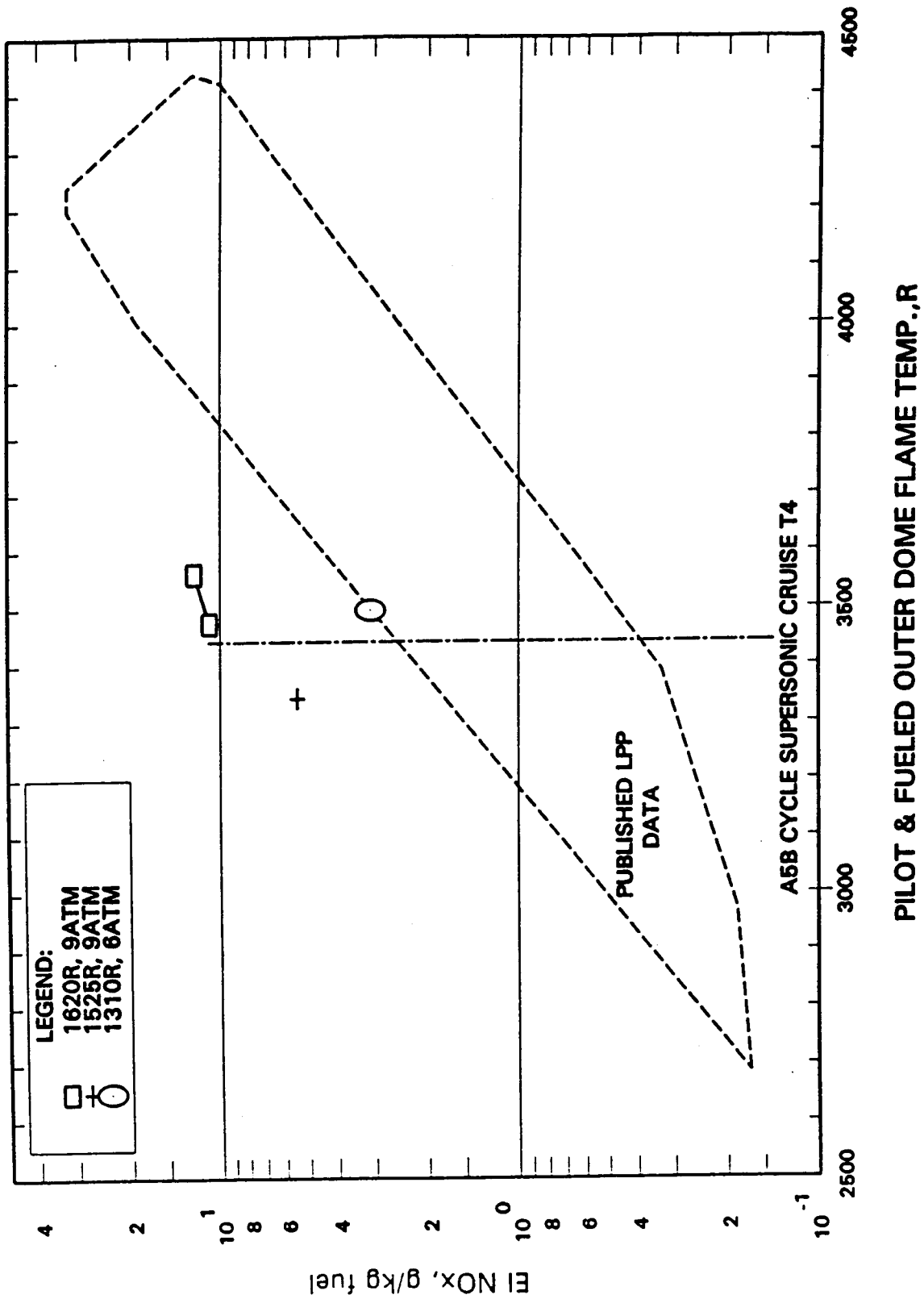


Figure 4.8 - NOx emissions index plotted versus flame temperature with the pilot and inner row of IMFH tubes on outer main dome fired. Data from the third rectangular sector combustor test.

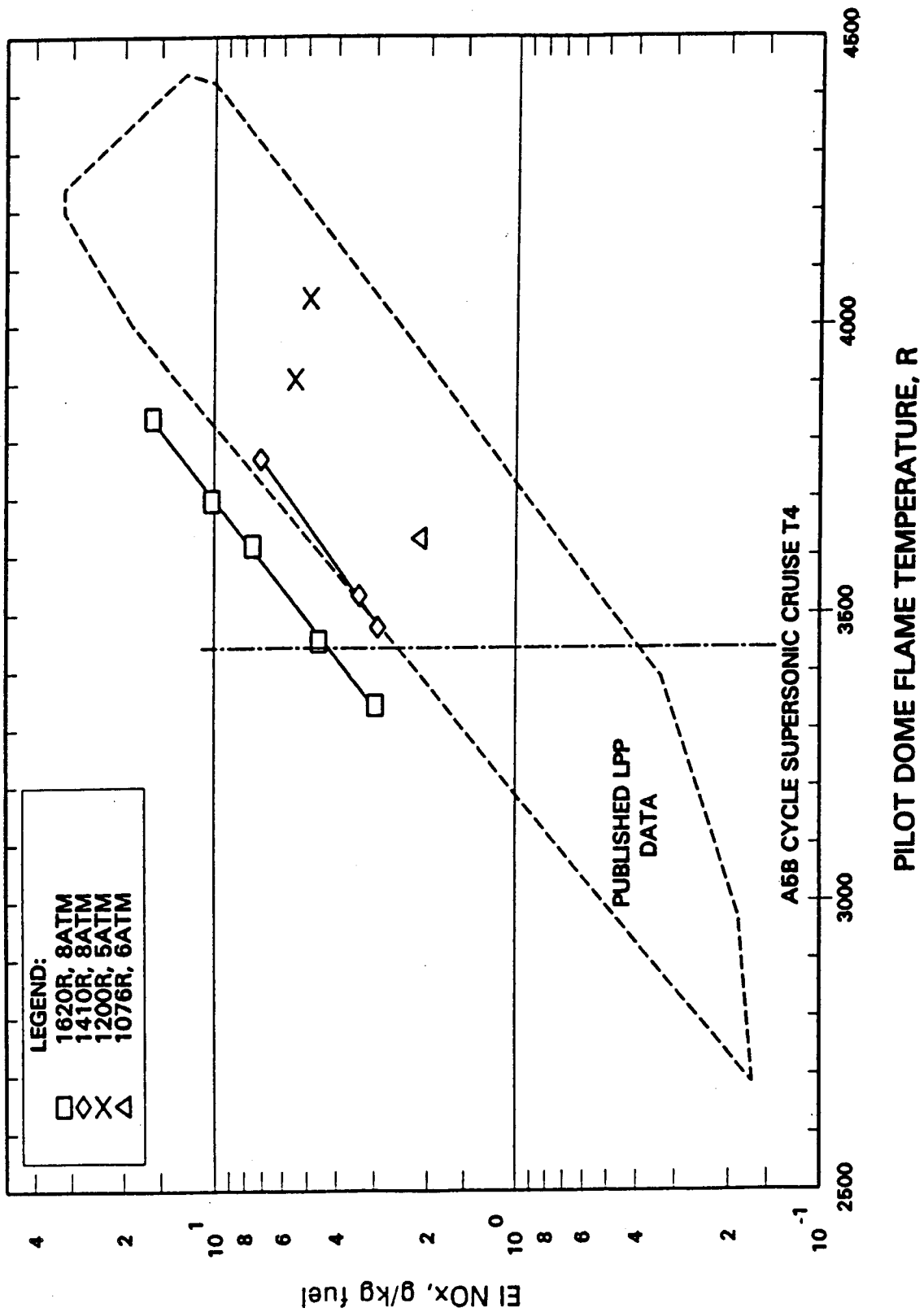


Figure 4.9 - NOx emissions index plotted versus flame temperature with the pilot stage only fired. Data from the third rectangular sector combustor test.

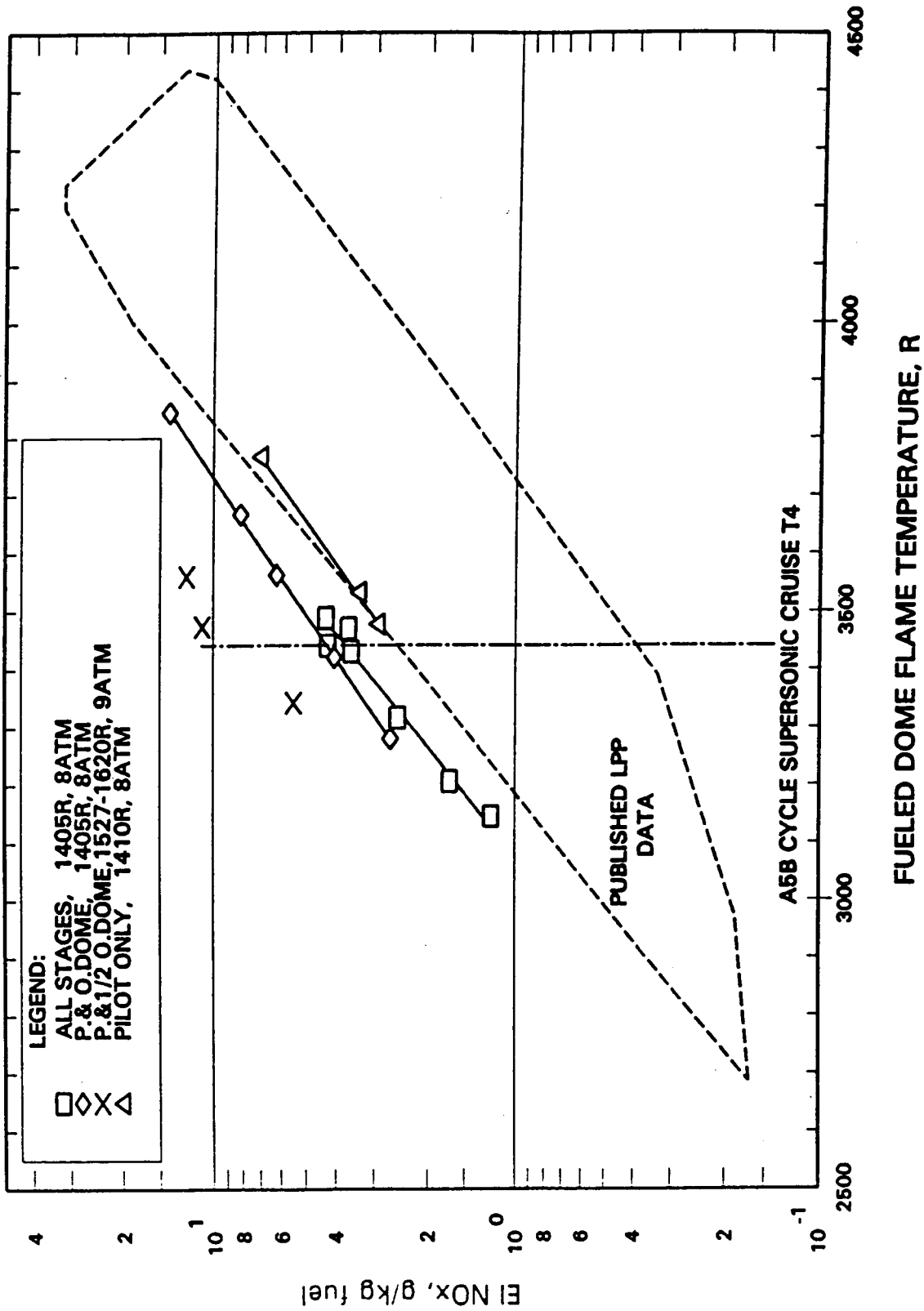


Figure 4.10 - NOx emissions index plotted versus flame temperature with various staging configurations compared. Combustor inlet temperature of approximately 1400 R and a pressure of 8 or 9 atmospheres. Data from the third rectangular sector combustor test.

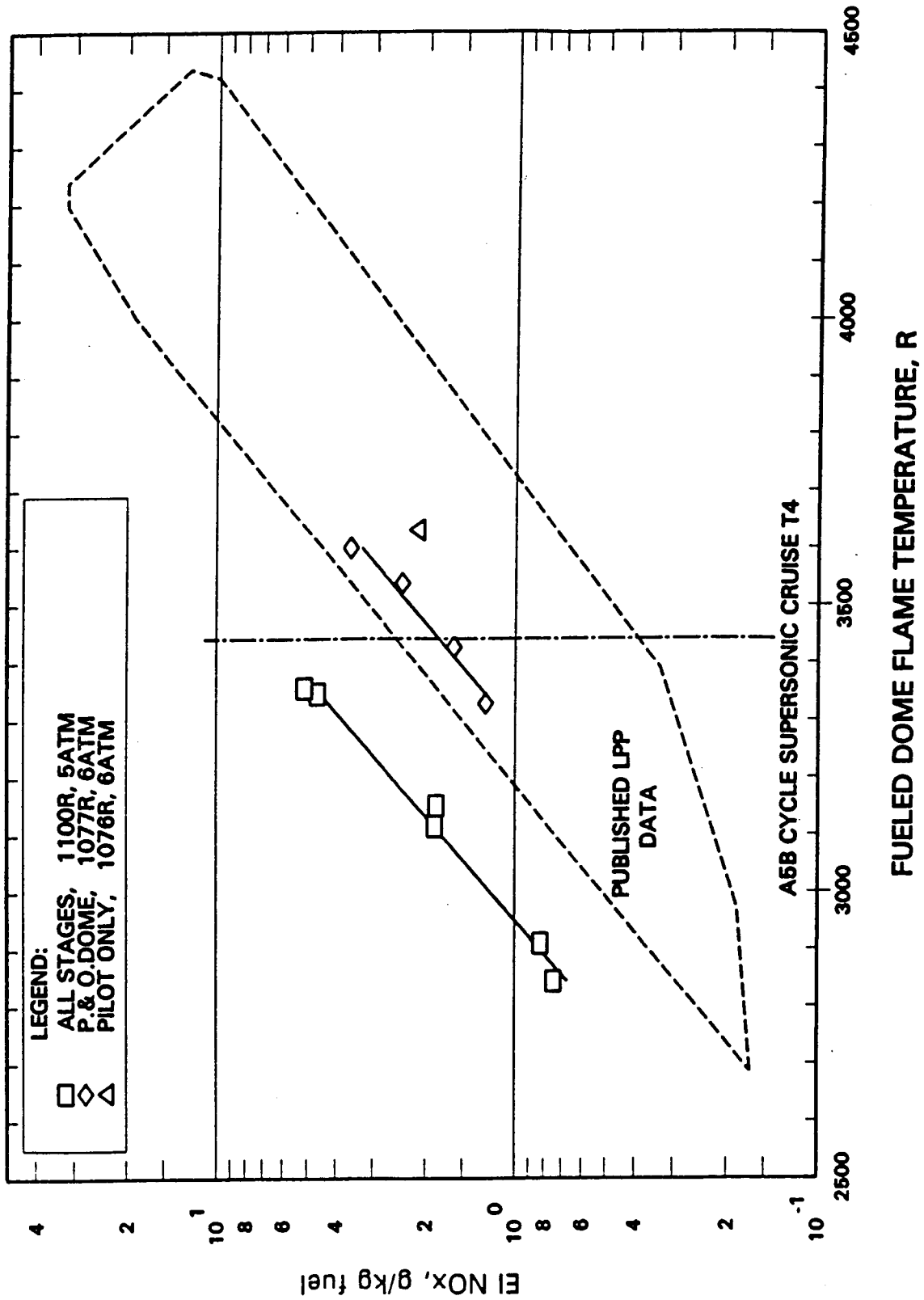


Figure 4.11 - NO_x emissions index plotted versus flame temperature with various staging configurations compared. Combustor inlet temperature of approximately 1090 R and pressure of 5 or 6 atmospheres. Data from the third rectangular sector combustor test.

In Figures 4.10 and 4.11, with all the fuel stages fired, the sector combustor's emissions were dominated by the IMFH's emissions characteristics, because most of the fuel is burned by the main stages. Over the range of Inlet temperatures run in the test, the NO_x emissions decreased with increasing inlet temperature, due to the more complete fuel evaporation and mixing in the IMFH. This is consistent with the IMFH single-cup data.

Before the third sector combustor test, there was a concern that partial fuel staging would result in low combustion efficiency due to the quenching of the CO combustion. However, the combustion efficiencies observed in this test during partial fuel staging, were very promising. Combustion inefficiency data for these tests is presented in Figures 4.12 through 4.14. All the inefficiency data are presented as a function of the fueled dome (local) flame temperature. At low inlet temperatures, combustion inefficiency was lowest for pilot-only operation, higher for pilot and one IMFH dome operation, and higher still for all domes fired. As inlet temperatures rose, the difference diminished between pilot-only and all domes fired combustion inefficiency. It was also evident that a small change in fueled dome flame temperature could result in a large increase in combustion efficiency for the pilot and one IMFH row operation. Overall, combustion efficiencies were greater than 99% for most of the test conditions. The fully fired points with higher combustion inefficiencies in Figures 4.12 and 4.13 are not a major concern. The points were run as part of the parametric test plan, but an actual combustor would not be run fully-staged at such low power inlet conditions.

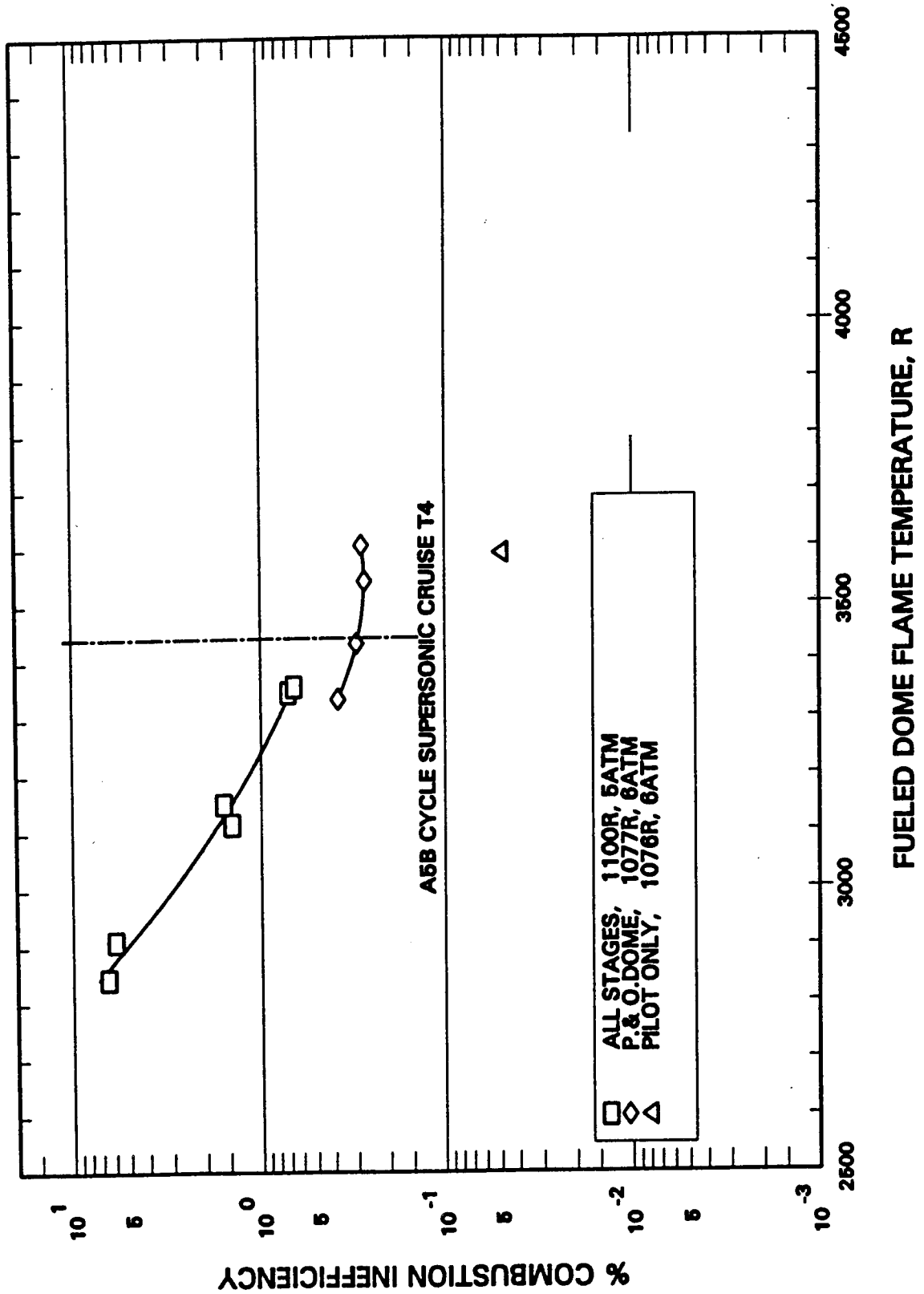


Figure 4.12 - Combustion inefficiency plotted versus flame temperature with various staging configurations compared. Combustor inlet temperature of approximately 1090 R and a pressure of 5 or 6 atmospheres. Data from the third rectangular sector combustor test.

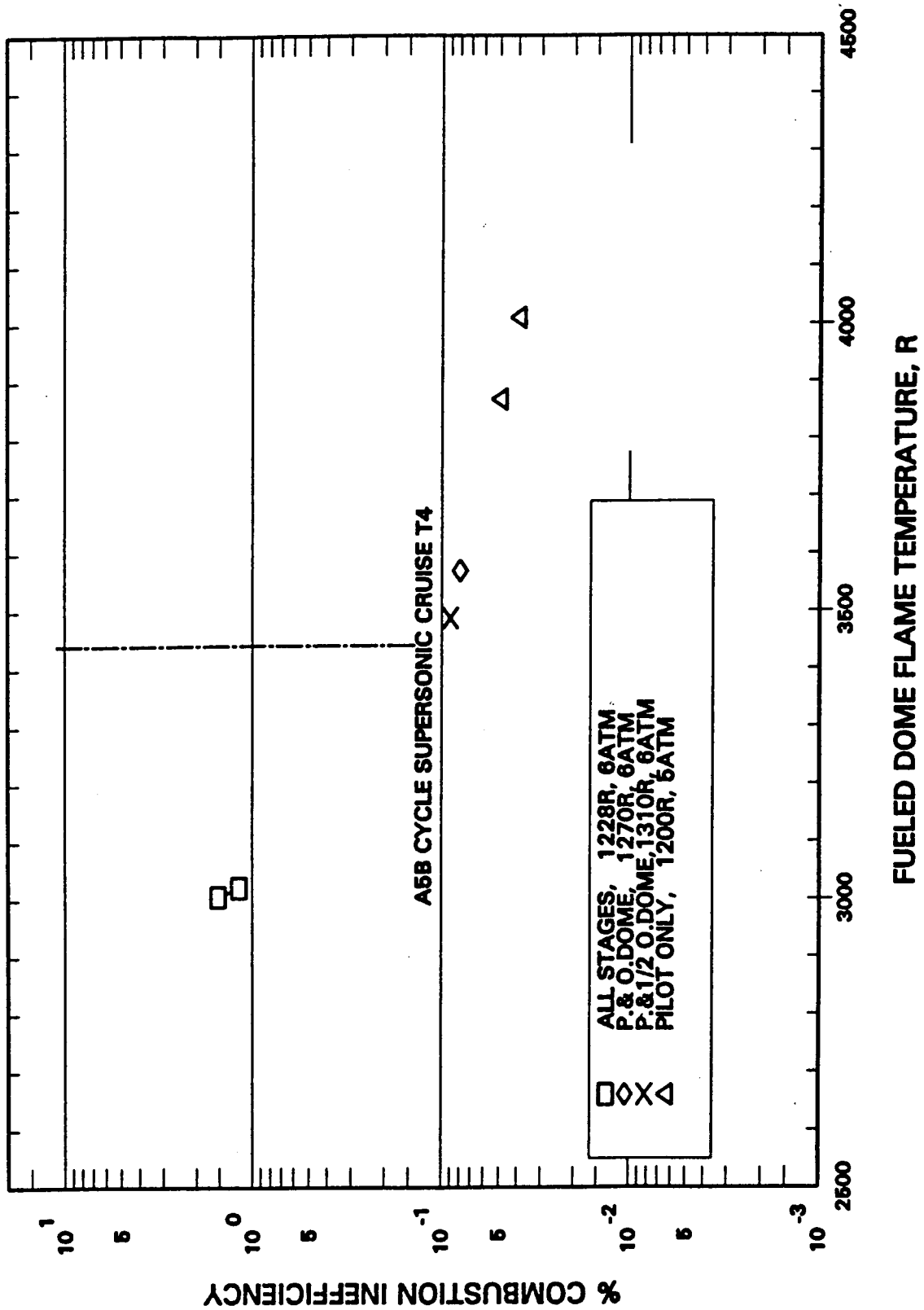


Figure 4.13 - Combustion inefficiency plotted versus flame temperature with various staging configurations compared. Combustor inlet temperature of 1200 R to 1310 R and a pressure of 5 or 6 atmospheres. Data from the third rectangular sector combustor test.

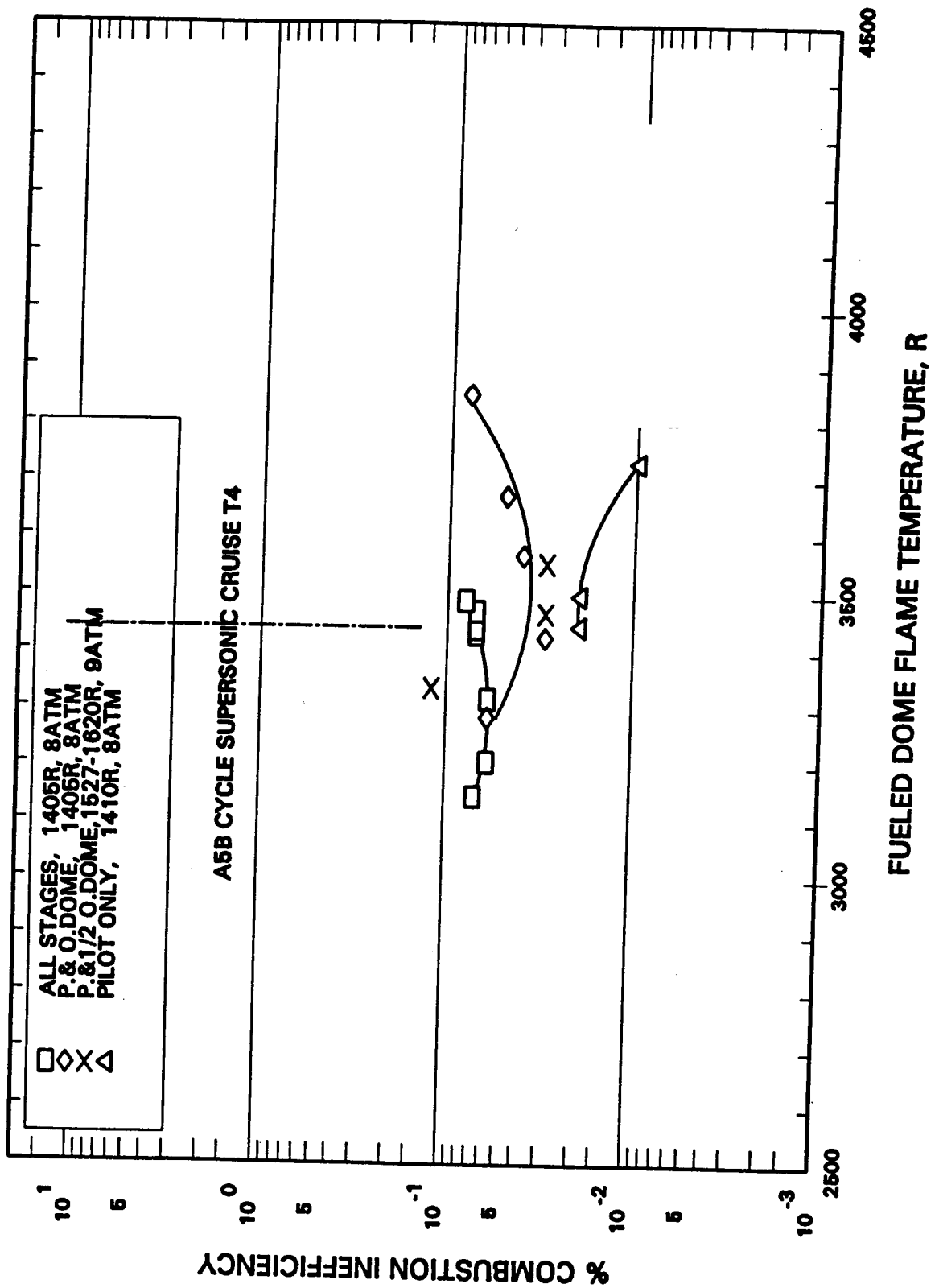


Figure 4.14 - Combustion inefficiency plotted versus flame temperature with various staging configurations compared. Combustor inlet temperature of 1410 R and a pressure of 8 atmospheres or inlet temperature of 1527 R to 1620 R and a pressure of 9 atmospheres. Data from the third rectangular sector combustor test.

4.4 Sector Test 4 - Lamilloy[®] Liner Sector Combustor Test

The fourth sector test used Lamilloy[®] liners designed and fabricated by Allison Gas Turbine specifically for the GEAE rectangular sector combustor. The rest of the sector combustor hardware (fuel system, pilot and main domes, side walls, and the rig hardware) was the same as used in the other LET Task 10 sector tests. The Lamilloy[®] sector test was funded by the EPM Program, so the results of the test are only summarized in this report. A complete set of the data is included in Appendix D.

The test was run in Evendale's Cell A5 in October, 1994. Over 60 data points were obtained. Emissions were measured at inlet temperatures from 1420 R to 1620 R and over a range of inlet pressures up to 132 psia. The test points very nearly encompassed the supersonic cruise conditions of the 3770 MFTF engine cycle. A recent Cell A5 enhancement, a servo-controlled sampling valve system, allowed single-point emissions sampling for the first time. This was timely because it allowed better understanding of the source of the CO emissions resulting from the film-cooling air.

The NO_x emissions with all the domes fired at a uniform flame temperature are plotted versus the dome flame temperature in Figure 4.15. The NO_x emissions obtained at an inlet temperature of 1620 R were the first obtained in the HSCT LPP combustor at close to supersonic cruise conditions. Those results were the first to clearly indicate that the LPP combustor is capable of meeting the HSR Program goal of a supersonic cruise NO_x EI of 5 g NO_x/kg of fuel: The usual qualification for the rectangular sector applies, that the pilot dome air split is high so that the pilot NO_x is too heavily weighted. The NO_x emissions at 1410 R inlet temperature are a little lower than the NO_x emissions with the impingement cooled liner. This is interpreted as an effect of the flame temperature being reduced by the film-cooling air.

Of more significance, the film-cooling air from the Lamilloy[®] liners increased CO emissions relative to the impingement liners results. This quenching effect was not unexpected and was the reason the original rectangular sector design utilized impingement cooled liners.

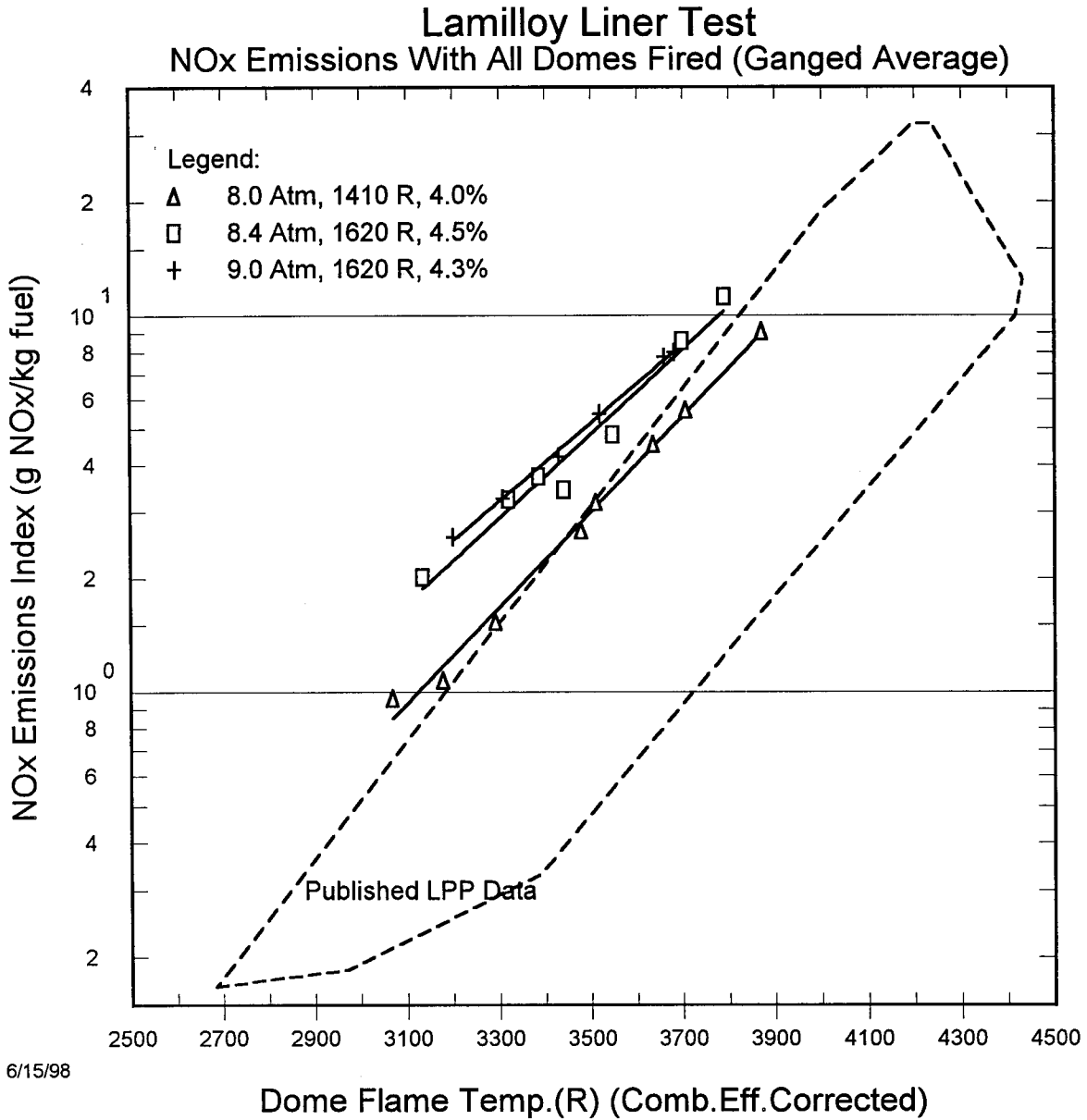


Figure 4.15 - NOx Emissions plotted versus dome flame temperature. Combustor inlet conditions as indicated in the legend. Data from the fourth rectangular sector combustor test using Lamilloy[®] liners.

At an inlet pressure of 8 atmospheres, an inlet temperature of 1410 R, a dome pressure drop of 4%, a flame temperature of 3160 R, and with the impingement-cooled liners; the combustion efficiency was 99.94% using ganged sample rakes (Point 31 of Sector Test 1). With the Lamilloy[®] liners at the same conditions, except the flame temperature was 3180 R (or slightly more favorable for low CO emissions), the combustion efficiency was 95.83% (Point 14 of Sector Test 4). These results are shown plotted versus flame temperature in Figure 4.16. The CO emissions for the same points are plotted versus flame temperature in Figure 4.17. At a flame temperature of 3200 R, the CO emissions using the Lamilloy[®] liners are more than 15 times higher than with the impingement cooled liners.

At conditions roughly corresponding to subsonic cruise combustor inlet conditions, for the two liner types, combustion inefficiencies are plotted in Figure 4.18 and CO emissions are plotted in Figure 4.19. Less of a difference is seen at these conditions. At a flame temperature of about 3100 R, the CO emissions using the Lamilloy[®] liners are about 2.5 times higher than with the impingement cooled liners.

These results confirmed the supposition that film-cooling air quenches the CO burnout reactions in an LPP combustor. This effect could be offset by maintaining higher flame temperatures, but this would narrow the operating range of the combustor requiring more fuel stages and would result in higher NO_x emissions.

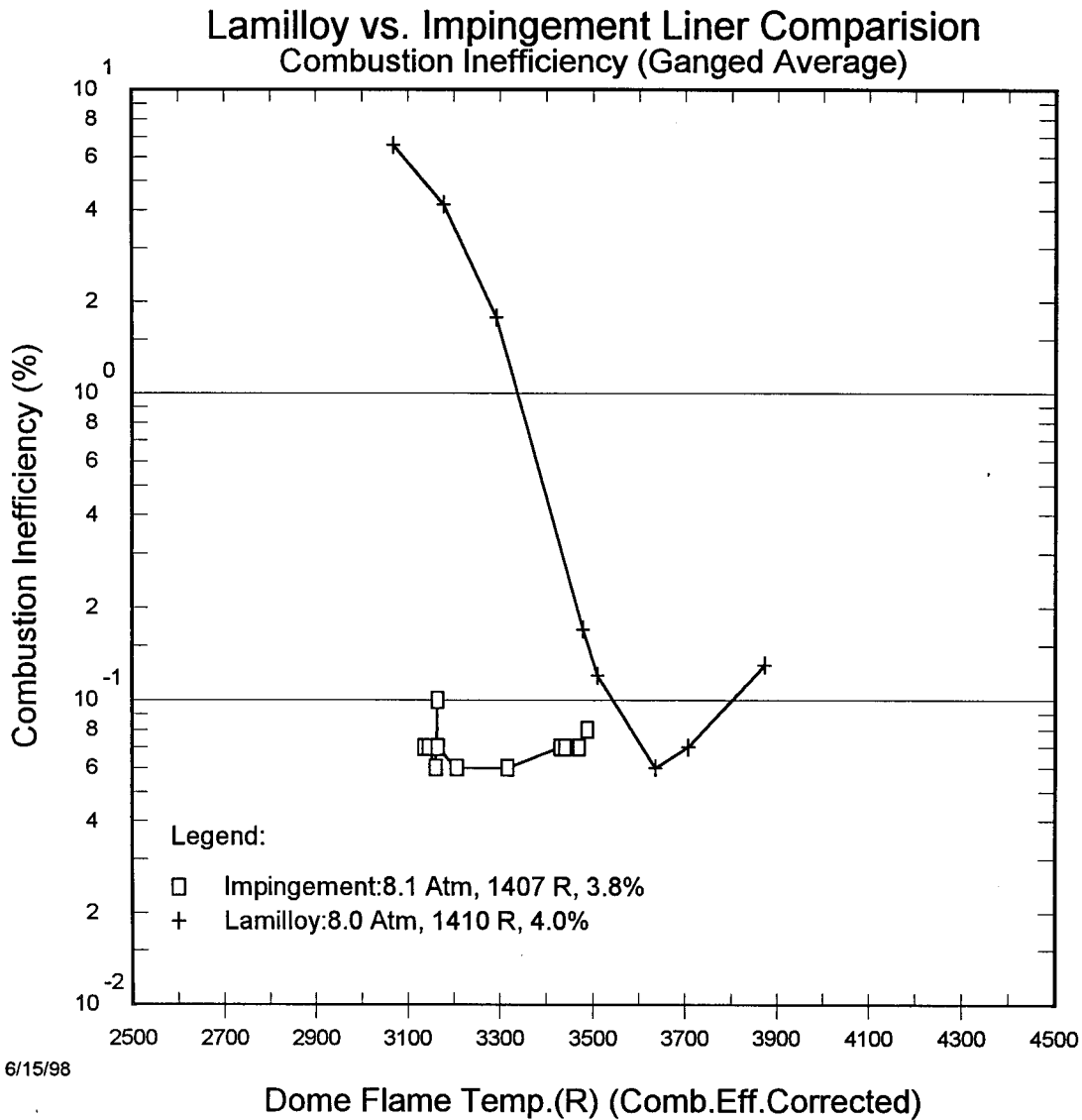


Figure 4.16 - Combustion inefficiency plotted versus flame temperature with Lamilloy[®] liners compared to impingement cooled liners. Combustor inlet temperature of 1410 R and a pressure of 8 atmospheres. Data from the fourth rectangular sector combustor test.

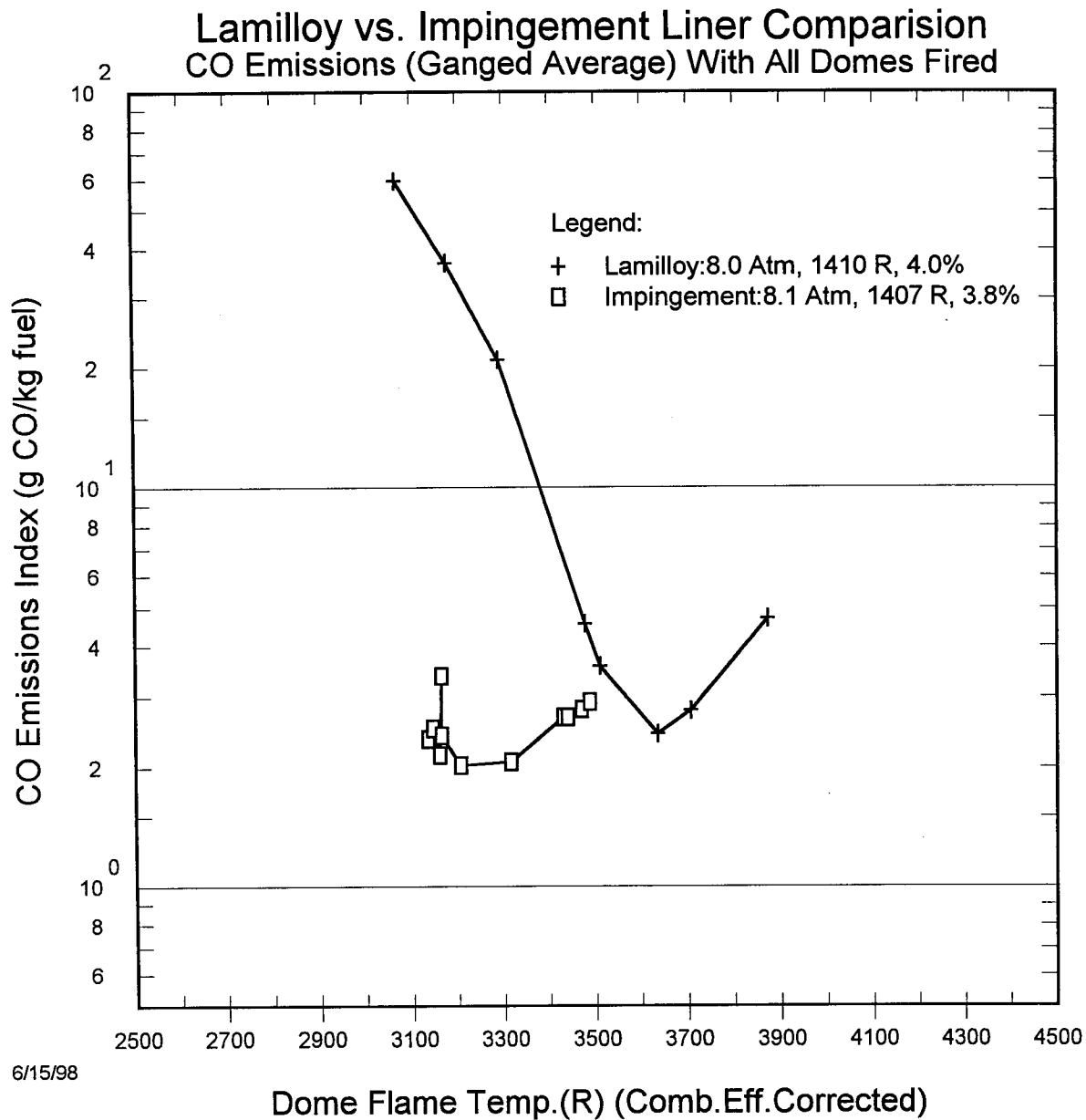


Figure 4.17 - CO emissions index plotted versus flame temperature with Lamilloy[®] liners compared to impingement cooled liners. Combustor inlet temperature of 1410 R and a pressure of 8 atmospheres. Data from the fourth rectangular sector combustor test.

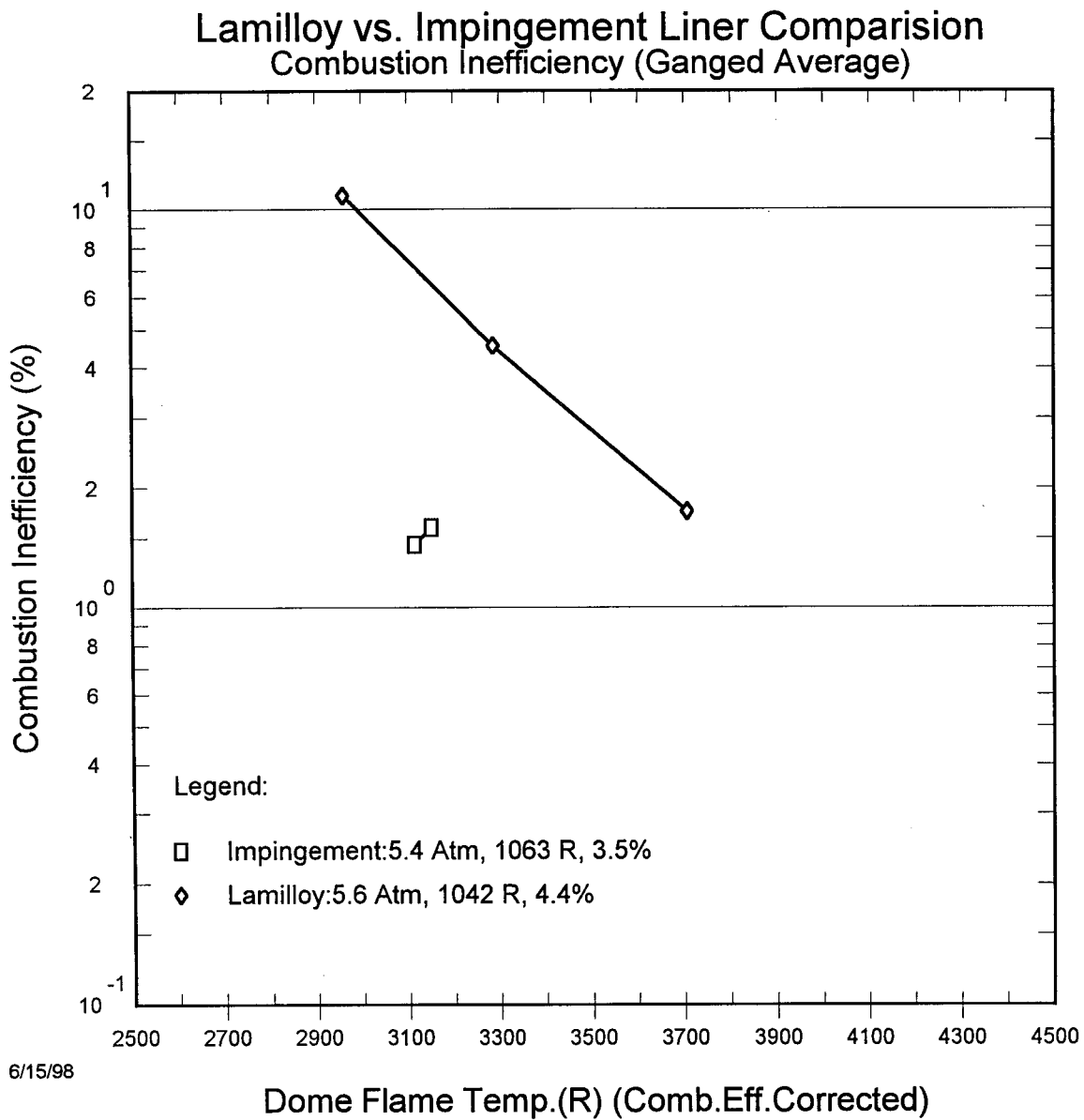


Figure 4.18 - Combustion inefficiency plotted versus flame temperature with Lamilloy[®] liners compared to impingement cooled liners at combustor inlet conditions roughly corresponding to subsonic cruise. Data from the fourth rectangular sector combustor test.

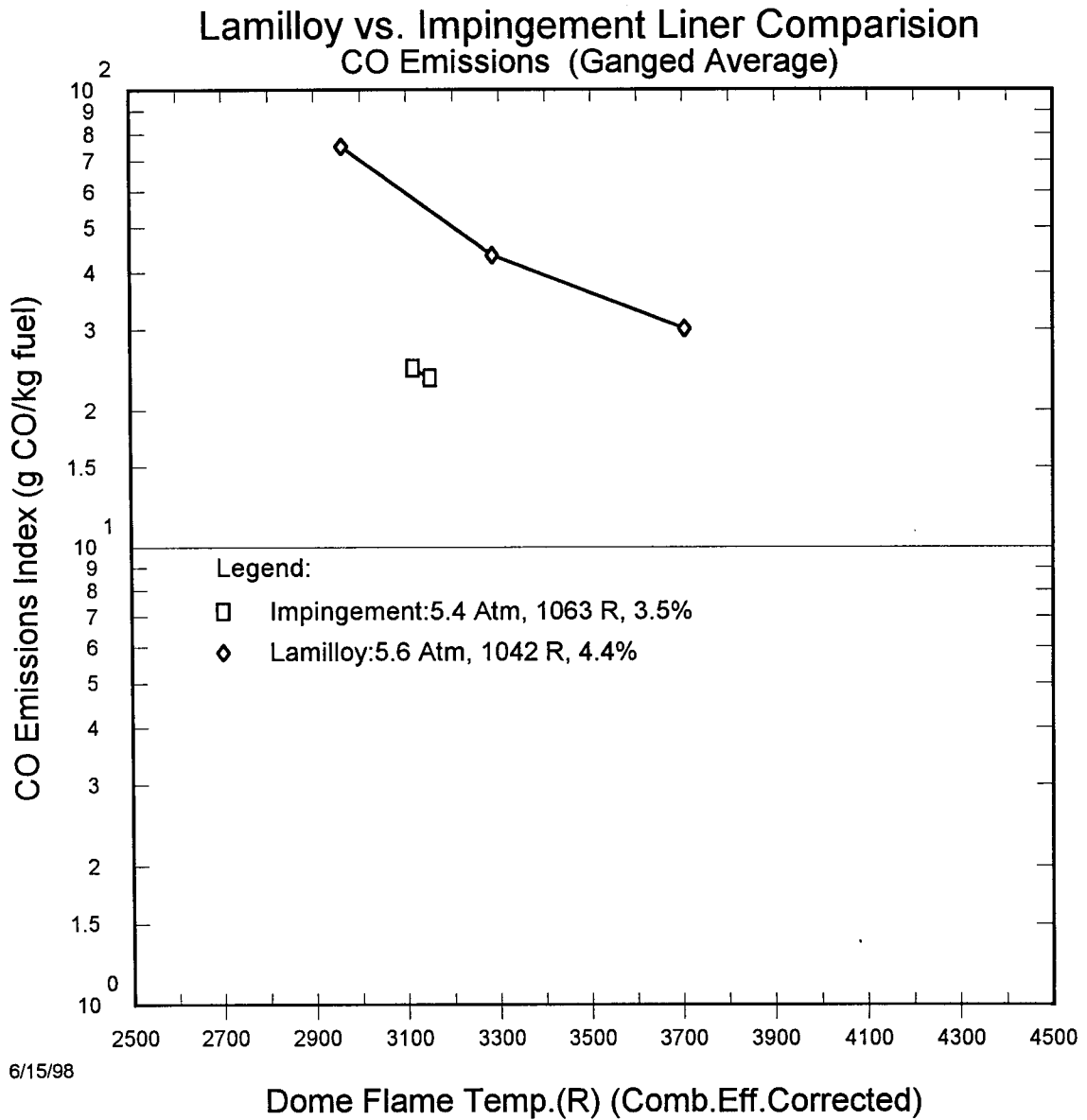


Figure 4.19 - CO emissions index plotted versus flame temperature with Lamilloy[®] liners compared to impingement cooled liners at combustor inlet conditions roughly corresponding to subsonic cruise. All the domes are fired. Data from the fourth rectangular sector combustor test.

4.5 Sector Test 5 - Pilot Aft and Heat Transfer Sector Test

The objective of this sector test was to obtain emissions data with the pilot dome adjusted to its full aft position (minimum isolation). Also, the impingement liners were heavily instrumented to obtain fundamental heat transfer data. The test was run in Test Cell A5. It began and ended on April 24, 1995. The test was shut down because of high indicated temperatures upstream of the dome. Inspection verified that extensive damage occurred when a fuel line broke that supplied the upper left bank of 6 IMFH injectors on the lower main dome (aft looking forward). The fuel line broke at a support bracket. The support bracket (and several of the others) were found to have a small ridge that put a crease around the fuel tube. The ridge was caused by a machining operation to place a chamfer at the ends of the clamping surfaces. The chamfer was included in the design of the clamp specifically to minimize stressing the fuel tube. The break occurred at the only location where the fuel line was single-wall (to accommodate a fitting). A factor that may have contributed to the failure was that the fuel line already had about 40 hours of test time prior to this test and may have been fatigued. Even with the fuel line failure, damage should have been minimal except that two safety systems were not working properly; the system for automatically calculating the fuel system flow numbers and an automatic trip on the safety thermocouples. No data was obtained in the fifth sector combustor test. However, the lessons learned were applied to the subsequent tests.

4.6 NASA 3-Cup Sector Design and Fabrication

The NASA 3-cup sector combustor is illustrated in Figures 4.20 through 4.22. The three domes and fuel injectors were designed and procured by GEAE. The Cyclone Swirler pilot and IMFH mixer tubes, as well as their respective fuel injectors, were of the same design as in the 5-cup sector combustor. The domes were very similar in design as the 5-cup sector, including the provisions for an adjustable pilot recess. Differences in the respective designs were that the NASA pilot dome had three Cyclone Swirler pilots instead of five and the main domes each had 14 IMFH tubes instead of 24. The rig's pressure vessel was designed and fabricated by NASA and their subcontractors. Its liners and sidewall were made of the same castable ceramic NASA-Lewis used in their flametube tests. There were four optical access windows installed in the rig to allow optical access to the combustion zone at different locations, depending how the rig parts were assembled.

Subsequently, two modified versions of the sector were design and procured. A new center dome was designed which used IMFH tubes. The purpose of the this dome was not to evaluate the effectiveness of the IMFH as a pilot, but rather to evaluate the effect of different step heights (length of the recess) isolating fired and unfired IMFH stages, on the emissions (primarily CO). The second design modification was to replace the two IMFH main domes with two new main domes with the multiple-venturi LDI (lean direct injection) fuel-air mixers.

All the tests of the 3-cup sector were done at NASA-Lewis. A GEAE engineer was in attendance for the earliest tests. The results of the laser diagnostics studies of the two versions of the sector combustor with IMFH tubes are documented in a NASA technical memorandum ⁽³⁻³⁾.

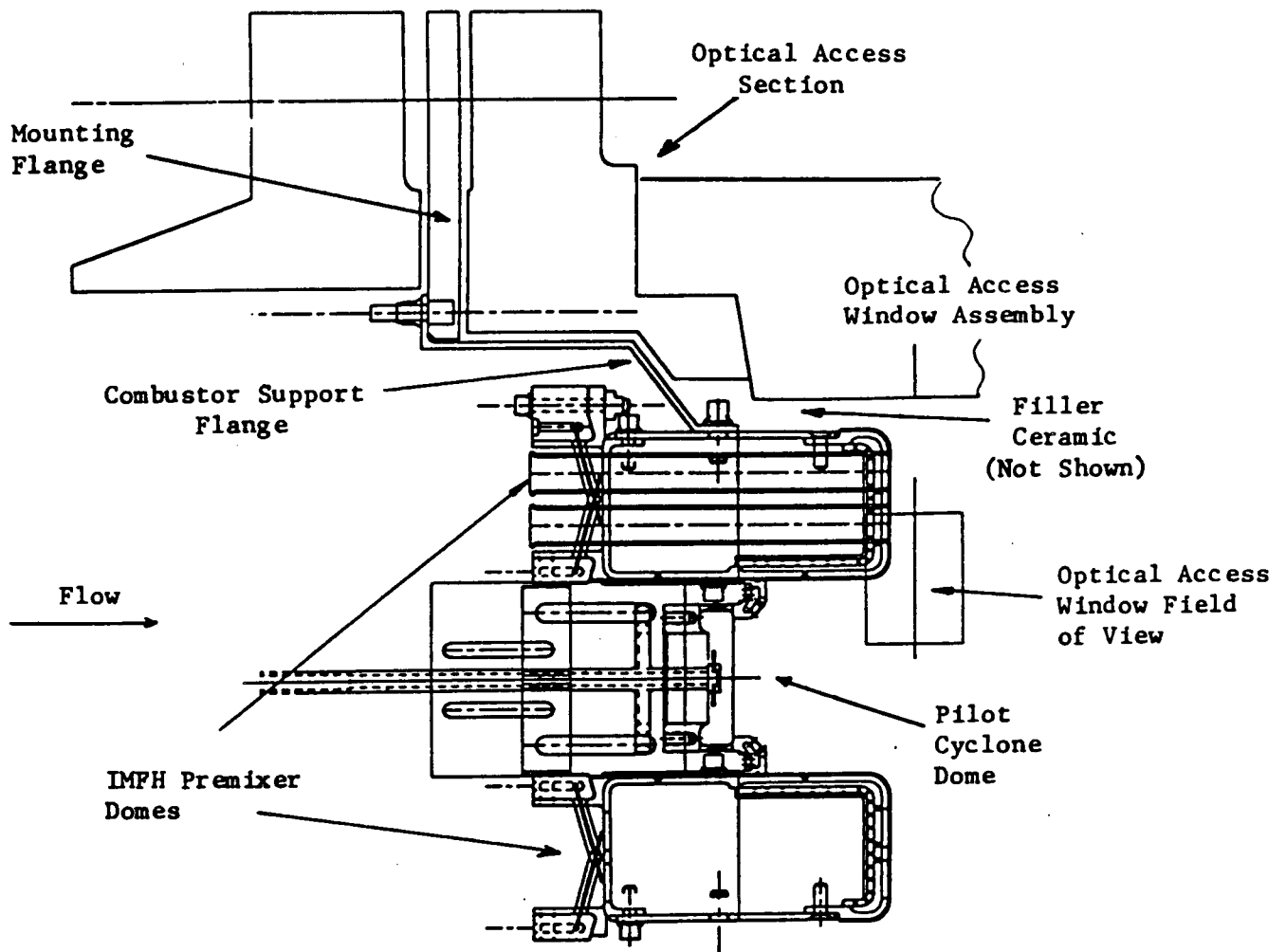


Figure 4.20 - Side view of the IMFH/Cyclone Swirler 3-cup sector combustor shown with a partial section of the NASA diagnostics rig to show the mounting interface.

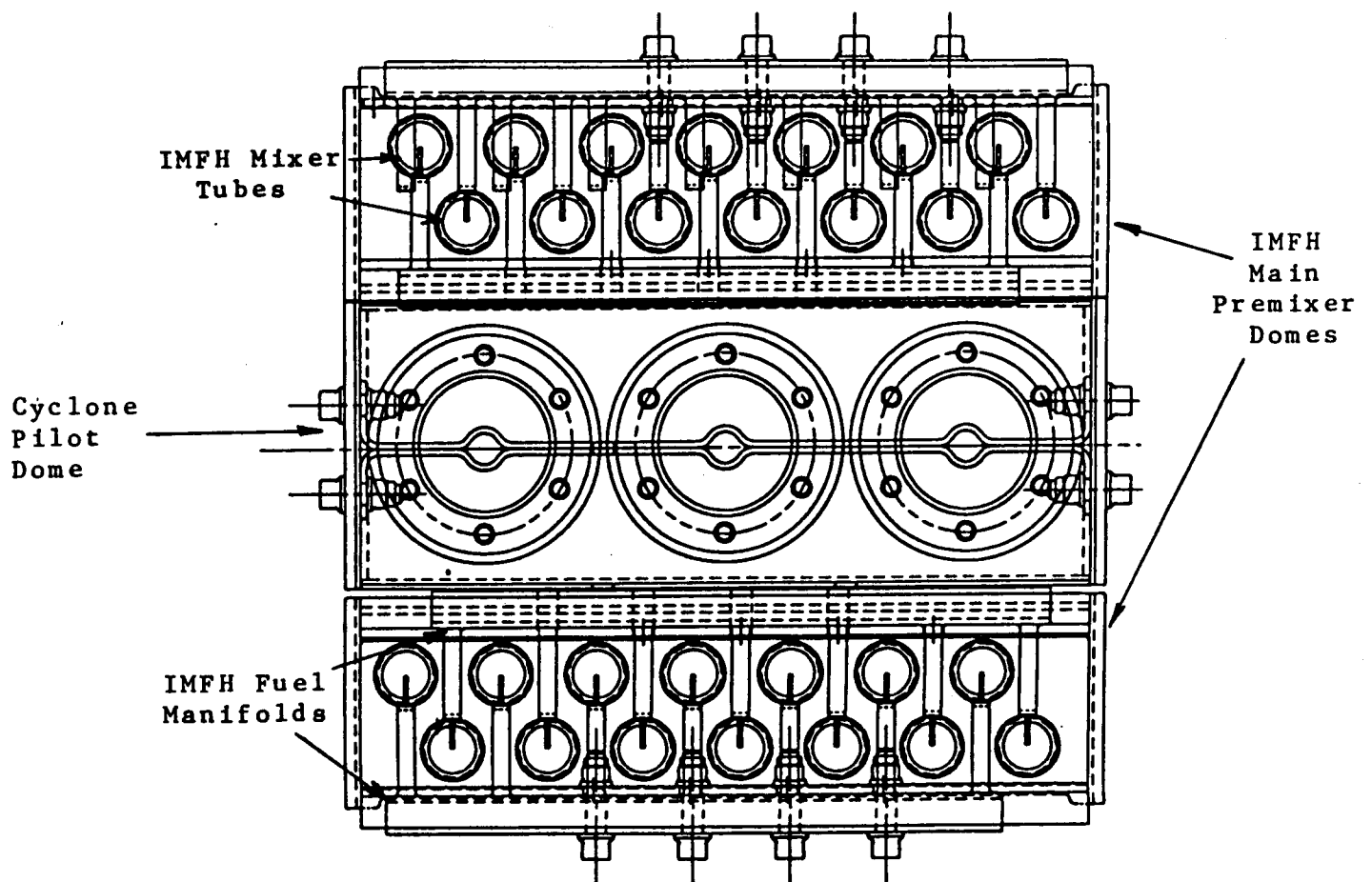


Figure 4.21 - View of the IMFH/Cyclone Swirler 3-cup sector combustor dome (aft looking forward).

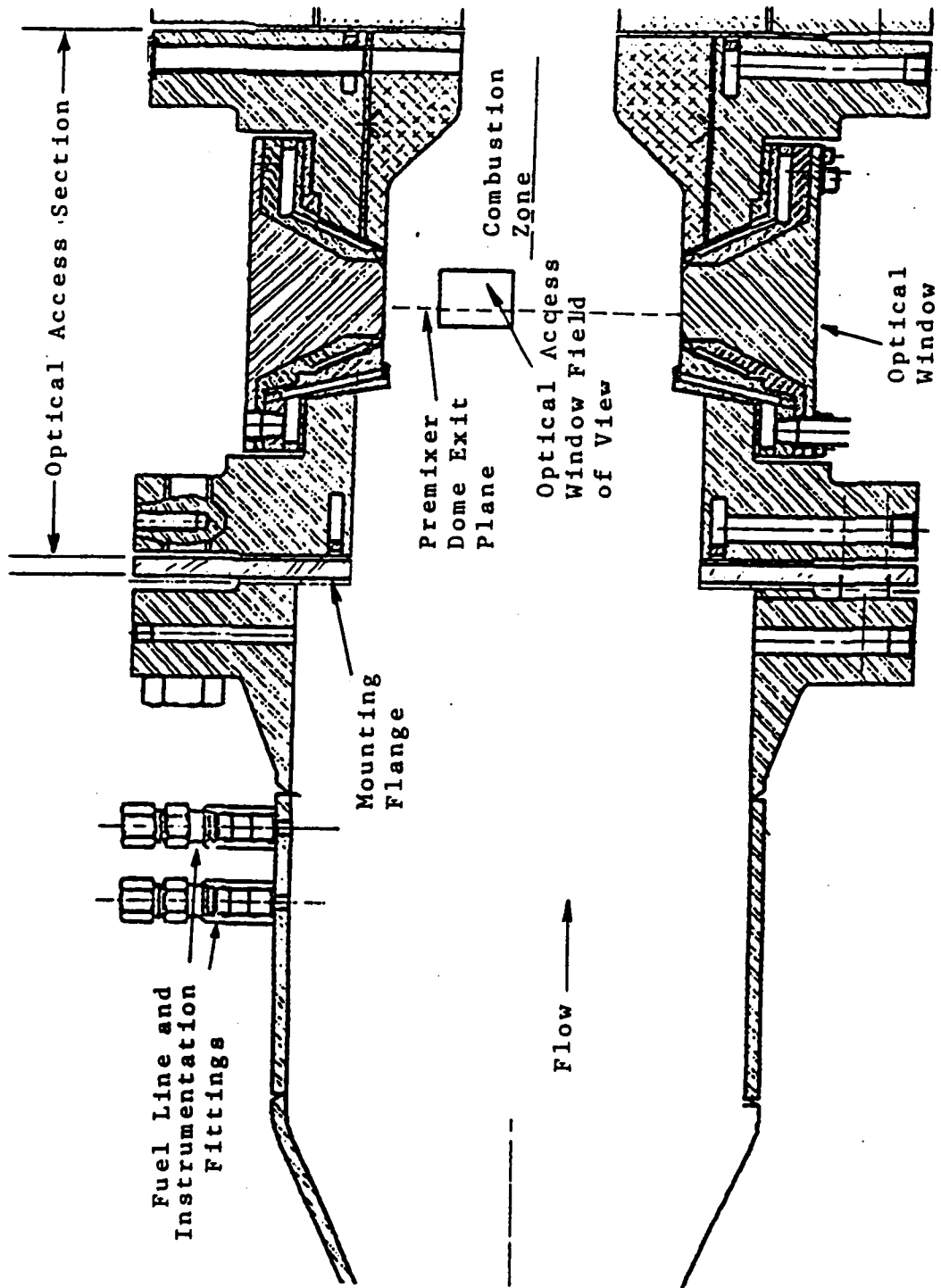


Figure 4.22 - Schematic of the NASA 3-cup sector combustor diagnostics rig.

4.7 Summary and Conclusions, LPP Sector Combustor Tests

The IMFH/Cyclone combustor sector tests successfully demonstrated the basic operation of the baseline IMFH/Cyclone Swirler combustor system under a wide range of conditions. Significant interactions between the stages were clearly evident, even in this parallel-staged configuration. These interactions affected both the NO_x and CO emissions. The most significant result of the first five sector tests was that the combustion efficiency of the IMFH at mid-power inlet conditions was determined to be significantly better than indicated by the single-cup tests of the IMFH. Based on the single-cup IMFH test results, alone, there had been a concern that the IMFH operation would not meet efficiency requirements at subsonic cruise conditions. The high efficiencies while partially fuel staged observed in these tests indicated that it might be possible to reduce the isolation (the recess) of the pilot from the main stage, thereby reducing the cost and complexity of the combustor system. Another significant result was that the NO_x emissions of the Cyclone Swirler were significantly reduced when some or all of the IMFH fuel stages were turned off. However, at high power, the sector test results demonstrated the need to improve the Cyclone Swirler pilot stage performance for high power NO_x emissions.

The Lamilloy[®] liner test showed that combustion efficiency is compromised at lower flame temperatures when the liner cooling utilized film-cooling air. The conclusion from this test is that film-cooling air requires the use of higher flame temperatures. The higher flame temperatures will result in increased NO_x emissions.

The fuel system failure which occurred in the fifth sector test indicates the need for careful review of all aspects of the fuel system. Although great care was taken in the design of the fuel system for the sector combustor, one mistake (the failure to detect the small ridge on the fuel clamps) caused an expensive failure.

A lesson-learned in the design of combustors was to keep the module size as small as possible. In this sector design there were 48 IMFH tubes per 5 pilots. Similarly the NASA 3-cup sector had 28 IMFH tubes per 3 pilots. The combustors could not be divided into a smaller module

with an integer number of tubes per pilot. This required compromises when comparing results of the 5-cup sector test, the 3-cup sector test and the 1-cup sector CFD model. Although only a minor problem, it was an unnecessary one. There was no reason not to have an integer number of IMFH tubes per pilot in the sector combustors. There are already an abundance of unavoidable difficulties in interpreting and comparing measured combustion data and CFD results. This particular difficulty was unnecessary.

Section 5

Variable Geometry Lean-Burn Fuel-Air Mixer

Control of the flame temperature within narrow limits is crucial to the emissions performance of Lean Premixed, Prevaporized (LPP) and Lean Direct Injection (LDI) gas turbine combustors. The systems used for controlling the flame temperature in LPP or LDI turbine combustors are fuel staging, air-scheduling, or a combination of the two methods.

Fuel staging involves turning on additional fuel injectors as the overall combustor fuel-air ratio increases. Each fuel injector has its own air supply, so that the additional fuel is mixed with an increasingly larger fraction of the combustor's total airflow. Modern diffusion flame turbine combustors, which because of their intense mixing, have some of the characteristics of a lean direct injection combustor, often rely upon fuel staging as a means to reduce emissions by maintaining the fuel-air ratio of the combustion zone between narrower limits than would otherwise be allowed by the engine cycle. Most production GEAE turbine combustors use some form of fuel staging. GEAE's LM6000 and LM2500 DLE premixed combustors use fuel staging to maintain the flame temperature between very narrow limits. This experience base with production fuel-staging systems led to the natural choice of fuel-staging as the baseline system for controlling flame temperature in the HSCT LPP and LDI low emissions combustors.

Air-scheduling involves redistributing the air to locations where the fuel is already being injected as the overall combustor fuel-air ratio increases. Fluidic devices aside, air-scheduling requires some form of variable geometry or moving parts within the combustor air flow. Placing moving parts in this environment has been the principle deterrent to the application of air-scheduling in production turbine combustors.

5.1 Fuel Staging Compared to Air-scheduling

As a method of controlling combustor fuel-air ratio, fuel staging has several advantages. The moving parts (the fuel valves) are immersed in the fuel which is generally kept under 300° F (760 R). In a fuel-staged combustor system, the moving parts are very small relative to air-scheduling valves because of the smaller volume flow of the fuel relative to the air (due to the fuel's smaller mass flow and its higher density than the air). An incidental advantage of a fuel staging system is that it automatically supplies turndown capability to the fuel injector system. Otherwise separate staging valves often have to be provided at the fuel injector tips to maintain the fuel injector pressure drop within a practical range.

The fundamental type of control system and valving required for fuel-staging is on-off. Air-scheduling systems generally involve continuous control. Continuous control is more complicated to implement, adjust and regulate. On-off control, while an advantage of fuel staging (because of its simplicity), is also responsible for one of the principle challenges of fuel-staging. Turning fuel systems off in a high temperature environment requires special design provisions to accommodate the resulting stagnant fuel in the manifolds and injectors and the loss of the cooling effect of the flowing fuel.

Controlling the fuel-air ratio and flame temperature by managing the air distribution instead of the fuel distribution also has advantages. A primary incentive for developing a variable-geometry lean-burn fuel/air mixer is to limit the use of fuel staging to low power conditions where it would be easier to manage the thermal effects of turning off the fuel flow in fuel passages. A second advantage, potentially, would be that combustor exit temperature profiles could be improved at low power, since fuel injectors would not be turned off. A third potential advantage of variable geometry would introduce a new continuous control mechanism into the combustor operation that could be used to meet specific performance requirements. This last advantage is a catch-all for the benefits are likely to be discovered as experience is gained with variable geometry.

The challenges of designing the variable-geometry system were recognized from the onset of the effort. As mentioned above, variable geometry requires moving parts that have to operate in the severe combustor environment. For the HSCT application, this would require materials, including bearings and lubricants, that would be reliable at temperatures up to at least 1200° F (1660 R). A second challenge is to integrate the variable geometry into the premixer design itself rather than add a separate valve placed in series upstream of the premixer. With the air valve integrated into the premixer, the premixer will have higher velocities in at least some locations. With a valve in series, the air velocities and pressure drop through the premixer would become very low at low power, reducing the fuel-air mixing. There might also be an increased risk of autoignition and/or flashback because of the lower air velocities.

5.2 Variable Geometry Premixer Design

The starting point for the conceptual designs for variable geometry premixers were the fixed geometry fuel-air mixer designs developed in NASA contracts NAS3-25552 and NAS3-25951. The Cyclone Swirler was quickly chosen as the baseline premixer for development of the variable geometry due to its acceptable emissions and operability performance at both high and low power. (The selection of the Cyclone Swirler presumed that its performance would be improved during the ongoing subcomponent development program.) Another reason for using the Cyclone Swirler was that its test results generally indicated that its performance is relatively insensitive to pressure drop variations. Depending on the specifics of the combustor system design, the effective flow area of the combustor and its pressure drop might change over its operating range.

An additional requirement imposed on the variable geometry Cyclone Swirler limited the types of variable geometry that would be considered. This requirement was that the swirl angle would be maintained constant as the effective area changed. That requirement was a consequence of a relationship that exists between the optimum diameter of the centerbody (that diameter can not easily be varied by variable geometry) and the swirl number. Another

requirement was that the premixer residence time would not exceed about 0.5 milliseconds when in the high power configuration.

The conceptual effort first concentrated on designs which incorporated a coarse screw thread into the radial swirler. In these designs, relatively large control movements would be required for small changes in the premixer's effective flow area. This would allow precise metering of the air irrespective of any sloppiness in the control linkage. The screw actuated designs ended up being very complicated. The effort was then redirected to designs involving a simple sliding mechanism. Figure 5.1 shows an axial section of the final design which resulted from this effort. Although this design was considered promising, a detailed mechanical design was never initiated due to considerations of the combustor system for the variable geometry premixer.

5.3 Conceptual Design of Combustor System

In parallel with the design of the variable geometry premixer, conceptual designs of the combustor system to use the variable geometry premixer were studied. The most promising system design was simulated with a spreadsheet analyses like those discussed in Section 1.2. Subcomponents were sized and the operation of the combustor system studied at key engine cycle points. The conceptual design effort resulted in a greater appreciation for one of the design challenges; moving a major fraction of the dome flow area from one location to another. Keeping the amount of air diverted within reasonable limits led to the chosen system design being a hybrid of variable geometry and fuel staging. This design allowed combustor operation with all burners fired down to engine cycle points corresponding to subsonic cruise. Fuel circuits were not turned off at combustor inlet temperatures above about 540° F (1000 R).

With the hybrid design and it's use of both methods of flame temperature control, came a realization that variable geometry designs would greatly add to the length of the list of combustor technologies needing development, not just change the technologies on the list. Meanwhile, the schedule for the HSR combustor development (at that time) called for a

definition of a workable concept for a lean low emissions combustor system in 1994. This combustor development schedule dictated that efforts be focused on the least risky design approaches. The variable geometry did not appear to meet this requirement. In April 1994, a Technical Redirection was agreed upon by GEAE and NASA. This Technical Redirection terminated the LPP variable geometry design effort. The subtask in Task 10 was replaced with a new subtask which provided funding for an engineer to be present at NASA during the tests at NASA-Lewis of the 3-cup sector combustor discussed in Section 4.6.

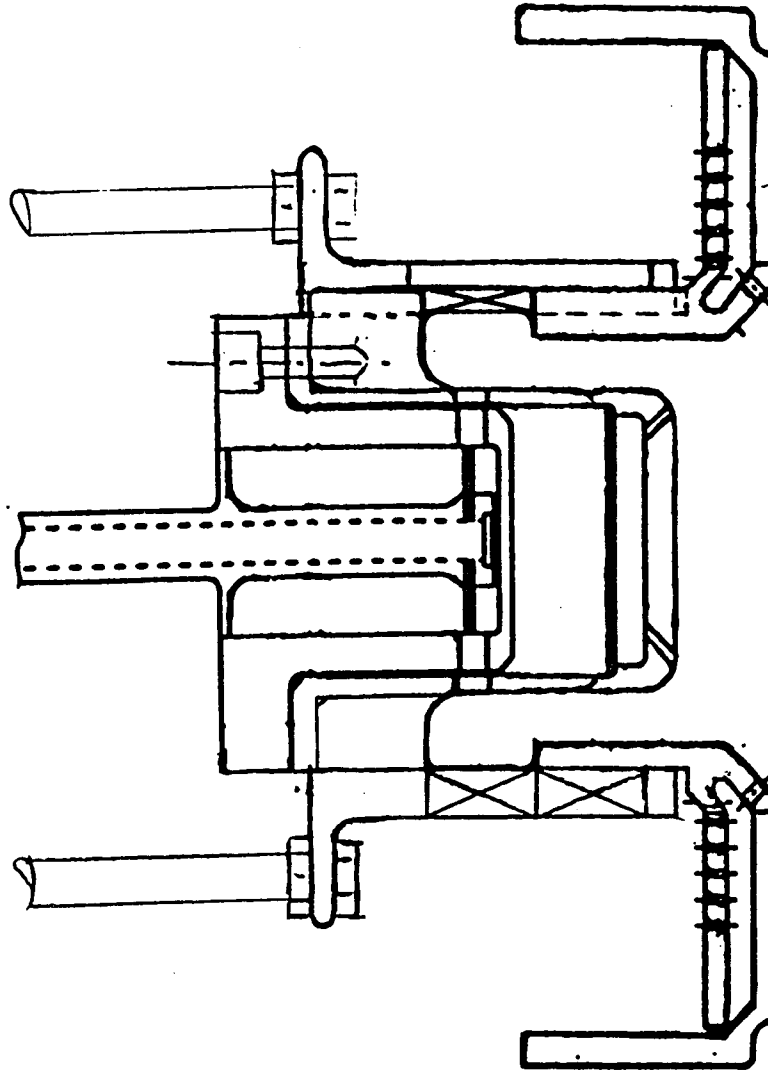


Figure 5.1 - Axial section of variable geometry Cyclone Swirler shown in an engineering sketch of rig hardware. In the actual combustor, the vanes would slide relative the position of the centerbody and the dome. Although the length of open vanes would be constant, the open area of the vanes per unit length would vary.

Section 6

Demonstration Engine Combustor Preliminary Design

In preparation for the HSR Phase II CPC Program, conceptual designs of annular combustor systems for the subscale HSCT demonstration engine were studied and several preliminary designs were generated. These preliminary designs consisted of the aero-thermal definition of the combustion system, including sizing of the premixers. For some of the designs, mechanical layouts were generated with basic flowpath dimensions. Some of these layouts were initially done for a full size engine so the features of the actual product design could be evaluated.

6.1 Design Requirements

An initial step in any design process is to define the requirements for the component or system being designed. The requirements for the HSCT low emissions combustor for the subscale engine demonstration originate from at least four sources: 1) general requirements for any combustor which operates in a gas turbine, 2) requirements specific to LPP/LDI gas turbine combustors, 3) requirements of the HSR program, and 4) interface requirements specific to the existing design of the demonstration engine for which the combustor was being designed.

A preliminary list of the HSCT combustor requirements from the first three sources had been compiled early in Phase I. They are discussed in the final report for Task 5 of NASA contract NAS3-25951. The requirement list for the HSCT low emissions combustor continued to be refined through Phase I and Phase II of the HSR program.

The only HSR program requirement for the HSCT combustor at the start of LET Task 10 was that the NO_x EI at supersonic cruise would be less than 5 g/kg fuel. A second, unofficial, program requirement was that the liner cooling air budget for the lean combustors would be 5%

of the combustor air (W36) or less, including leakage. The premixers and the combustion zone would therefore be designed for 95% of the combustor air. The combustor system designs of LET Task 10 have the potential to meet the NO_x EI of 5 g/kg as best can be determined with the existing data base. These data come from subcomponent tests in flametubes and tests of the rectangular sector performed in Task 10. The rectangular sector combustor data base did not include supersonic cruise conditions until the fourth sector combustor test performed in October, 1994. When first proposed, the 5% liner cooling goal was viewed as realistic only if the EPM Program developed a viable CMC liner material. Later, the 5% liner cooling budget became accepted as an attainable goal even for metallic liners. Until viable liners with a 5% cooling air budget were available, additional liner cooling air for the HSCT LPP combustors would be "borrowed" from the turbine cooling air budget. This allowed the size of the combustor premixers to remain constant as the liner cooling designs evolved. By the time the lean annular rig was to be run, the plan was to limit the liner cooling air budget to 10% of W36. Again, half of the 10% liner cooling would be borrowed, so that a 95% dome design was maintained. The demonstration engine combustor would, of course, not be allowed to borrow turbine cooling air and the liners (whether metallic or CMC) would have to be designed either to the 5% cooling air budget or the 95% dome air goal would have to be compromised.

The general gas turbine combustor requirements consist of the normal operability requirements for a combustor to operate in a gas turbine and the accepted design practices to meet those requirements. Some of these practices (which evolved for diffusion flame combustors) would be modified because of the special performance characteristics of LPP/LDI combustors. Examples of the latter would be main stage dome velocities, the combustor passage velocities and design practices relating the spacing of fuel-air mixers and dome heights to the combustor length.

The system requirements specific to LPP combustors refer primarily to the need to control the flame temperature within a narrow range. The narrow range of flame temperatures is bounded on the low side by the requirement to maintain acceptably low CO and unburned hydrocarbon emissions and, ultimately, maintain a margin on lean blowout. The flame

temperature range is bounded on the high side primarily by the NO_x emissions, but it can also be bounded by material temperatures and the peak in the combustor exit temperature profiles. Together with the design of the fuel-air mixers themselves, the need to control fuel-air ratio or flame temperature within a narrow range are the two most significant features that differentiate LPP and LDI combustors from conventional diffusion flame combustors. This flame temperature control is a system attribute and generally requires the use of fuel staging and/or variable geometry for air scheduling.

A major milestone in the planning of the HSR low emissions combustor development program was the subscale engine demonstration test of the downselected lean or RQL combustor late in HSR Phase II. The decision was made to use a P&W engine for the engine demonstration test during the course of LET Task 10. The exact combustor interface requirements dictated by the choice of the demonstration engine were not made available to GE prior to completion of LET Task 10. These include the definition of the combustor envelope, the compressor exit velocity profile, the specific requirements for the combustor exit profile, and the engine cycle or operating lines over which the combustor would be required to operate. The normal procedures for designing a gas turbine combustor require this basic interface information. Instead, a few key parameters for the demonstration engine supplied by P&W allowed the HSCT A5B cycle conditions to be used for the combustor design with appropriate scaling factors. The parameters supplied by P&W were W₃, T₃ and P₃ at the design point conditions (nominal supersonic cruise for the HSCT). These allowed the determination of the Mach number at the inlet to the diffuser at nominal supersonic cruise and the combustor flow function. For these preliminary designs, a realistic combustor envelope was defined by using the combustor envelope for a similar GE engine.

Since the detailed interface requirements for the demonstration engine were not available at the time the Task 10 preliminary design work was being done, GEAE followed the reverse procedure of supplying to P&W the layouts and the predictions of the LPP combustor operating parameters (e.g.; fuel-air ratio, T₄, etc.) at approximately 50 key operating points over a mission and the flight envelope. These predictions were generated using the scaled A5B

Mixed Flow Turbofan (MFTF) cycle and a spreadsheet model of the LPP combustor system. These early projections of the LPP combustor operating parameters were reviewed by the P&W owners of the demonstration engine. The first review of these results by P&W quickly led to a joint meeting and further exchanges, until the apparent inconsistencies were resolved. The inconsistencies were determined, not unexpectedly, to be due to differences in the flight envelopes, the mission and the cycles of the two engines. This early communication was invaluable and led to a discussion and a better understanding of how the demonstration core engine would need to be operated in the test cell during the combustor's engine test (in HSR Phase II) to simulate the HSCT conditions.

6.2 Previous HSCT LPP/LDI Combustor System Designs

The preliminary designs of this subtask evolved from the conceptual designs developed in Task 5 of NASA Contract NAS3-25951, Aero Propulsion Technology (APT). A wide variety of conceptual designs were considered in APT Task 5. Those designs were documented in sketches, some of which are presented in the final report for Task 5. The more promising conceptual designs were brought to the next level of design. The combustor's subcomponents were sized and preliminary analyses of how the combustor system would operate over key engine cycle points were performed.

In APT Task 5, four conceptual designs were brought to the level of preliminary mechanical layouts. Two of those designs used the Swirl-Jet for the main stages. The Swirl-Jet was used because its large size required the fewest fuel injectors, allowing a relatively conventional fuel system design. A third mechanical layout utilized Jet-Mix LDI fuel-air mixers for the main stage. However, in subcomponent tests, the IMFH proved to have the best emissions performance of the fuel-air mixer designs tested. Therefore, in Task 5, the fourth mechanical layout was a stepped-dome combustor utilizing inner and outer IMFH main stages and a cyclone swirler pilot center-stage. The dome design was similar to the LPP rectangular sector combustor, however the fuel system in the stepped-dome combustor was not designed in APT Task 5.

6.3 Stepped Dome with Internal Fuel Manifolds

The challenges in designing a conventional fuel injection system for the IMFH main stages led to consideration of designs with internal fuel manifolds. Figure 6.1 shows a design with an internal fuel manifold for the IMFH main stages drawn for the full scale 3770 MFTF engine. This IMFH fuel system design was chosen for a more detailed design and thermal analysis in LET Task 42⁽⁶⁻¹⁾. The combustor system design with internal fuel manifolds was considered viable. However, a combustor with internal fuel manifolds was not developed further because of a perception at GEAE of customer resistance to internally manifolded combustors in civil aircraft. Thus, the subscale LPP combustor design using internal manifolds only reached the conceptual stage and a layout for the demonstration engine was never made. A ground rule requiring removable fuel injectors for the HSCT LPP and LDI combustors was adopted by GEAE for future designs, even though the installation of the engine in the HSCT would almost certainly preclude the removal of most of the fuel injectors while the engine is on the wing.

6.4 Stepped Dome with Removable Main Injectors

A mechanical design of a stepped dome with removable fuel injectors never evolved because of the challenge of accommodating the multiple fuel injection points. Figure 6.2 shows a very preliminary layout for a stepped-dome combustor in which the fuel injectors are not shown. The challenge of designing the fuel injection system for this combustor dome is apparent. This design placed the pilot outboard. This accomplished two goals. With the pilot near the outer casing, the design of the ignitor is simplified. Because the position of the dome changes gradually in one direction, it is possible to imagine a removable fuel injector design could be made to work. However, the design of the fuel injector for this dome was never accomplished. This design would probably have very poor combustor exit temperature profiles at low power.

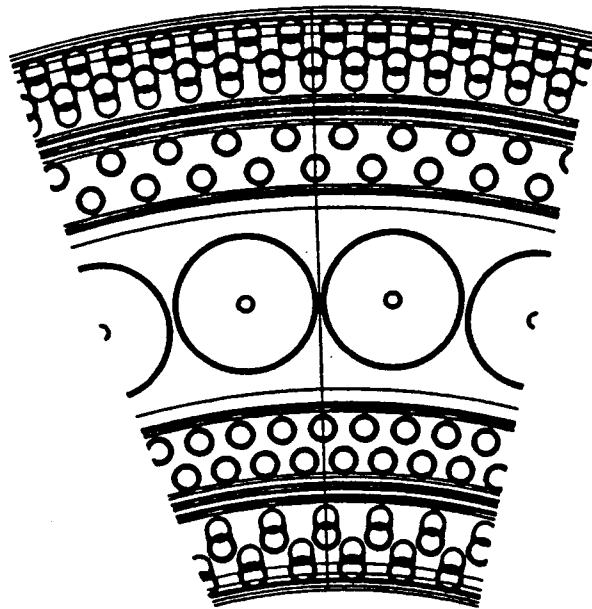
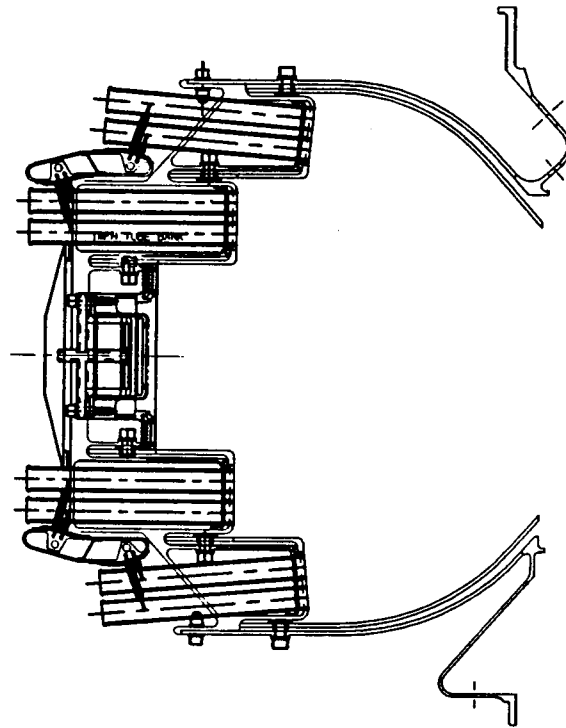


Figure 6.1 - Cyclone Swirler - IMFH combustor with stepped domes and internal fuel manifolds for the IMFH main stages. This layout is for a full size engine. The system design is a direct extension of the LPP rectangular sector layout. Side view shown on top. View of dome (aft looking forward) on the bottom.

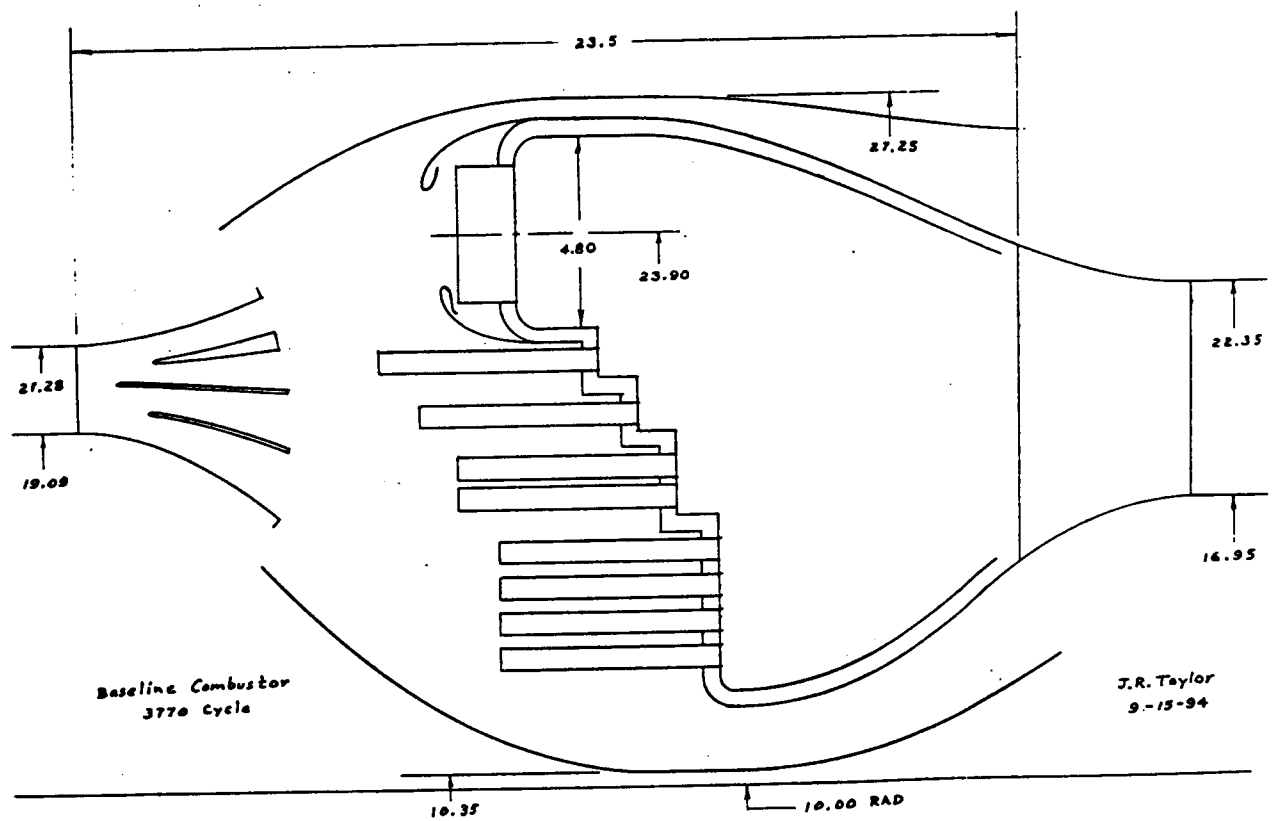


Figure 6.2 - Cyclone Swirler - IMFH combustor with stepped domes. The fuel injector design is not defined. This layout is for a full size engine.

6.5 Multistage Radial Axial System Design (Original MRA)

The original MRA combustor concept was first proposed in early 1994. It arranged the IMFH tubes in a pattern along the outer liner and placed the pilot in the front of the combustor in-line with the diffuser. An early engineering sketch of this conceptual design is shown in Figure 6.3. This design intent of the MRA was to promote better mixing between the fired fuel stages and the unfired IMFH fuel stages. This mixing of the fired and unfired stages would improve the exit temperature profiles when fuel stages were turned off. CONCERT CFD models verified the potential for nearly ideal exit profiles during subsonic cruise, despite the fact that roughly half the fuel injectors were off. This CFD modeling of the MRA combustor is discussed in Section 1.1.3 of this report.

A second goal of the MRA was to eliminate the use of steps to isolate the stages. This would simplify construction, reduce the cost, and reduce the cooling requirements. Instead, the isolation of the fuel stages would be attained by the forced convection of the burned gases from the fired stages towards the unfired stages.

The original MRA was thought to have advantages for the fuel injector design for the IMFH tubes, since the inlets to the IMFH tubes would all be very close to the outer casing. Thus, there was the potential for developing externally manifolded, removable injector designs. The MRA, as originally conceived, had straight IMFH tubes, but early mechanical layouts led to the conclusion that curved IMFH tubes were desirable to fit the combustor within the required engine envelope. A mechanical layout for the combustor showing the curved tubes is shown in Figure 6.4. Meanwhile, single-cup tests of curved IMFH tubes indicated, not unexpectedly, that they performed poorly and were prone to flashback or autoignite (discussed in Section 3). Further efforts on a straight tube design could have resolved the envelope issue (and the main injector design issue), but a new MRA concept evolved. Efforts to solve the main injectors design challenges for the original MRA were terminated and instead, development efforts were focused on the new MRA concept.

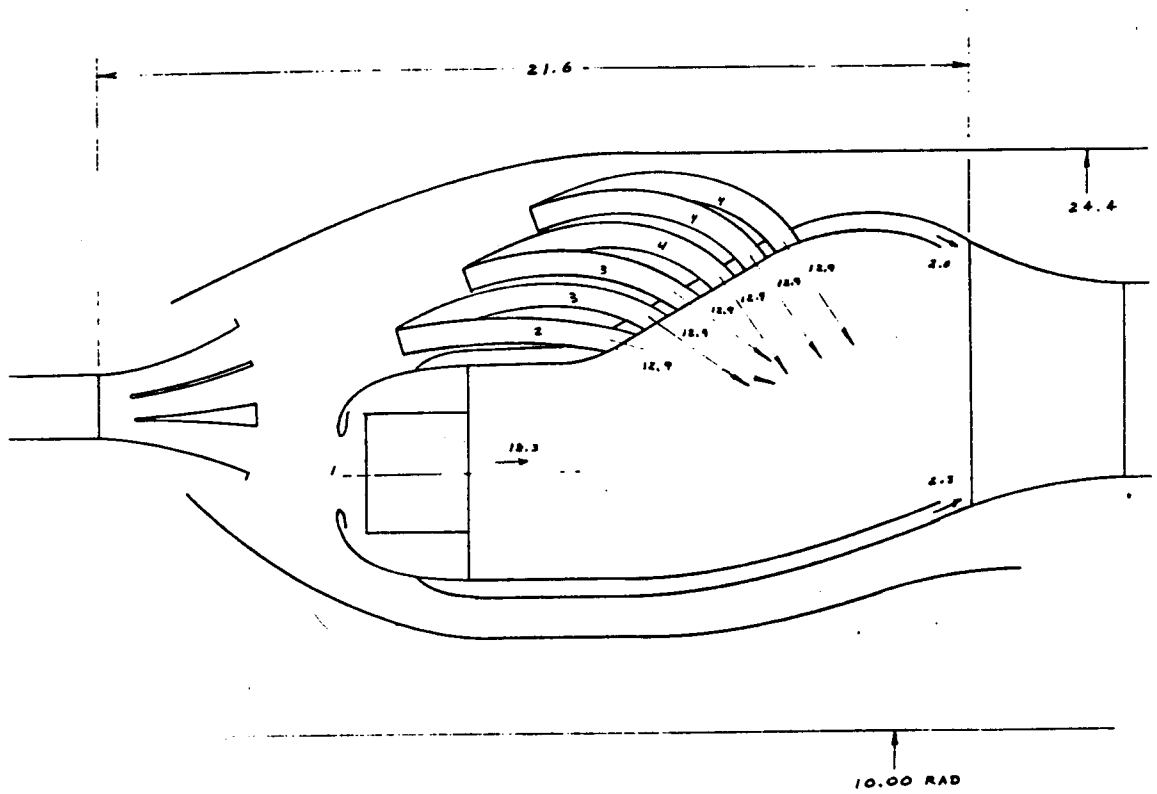


Figure 6.3 - Sketch of flowpath of the MRA (Multi-stage, radial, axial) combustor with curved tubes. Otherwise this design is equivalent to the design shown in Figure 1.25.

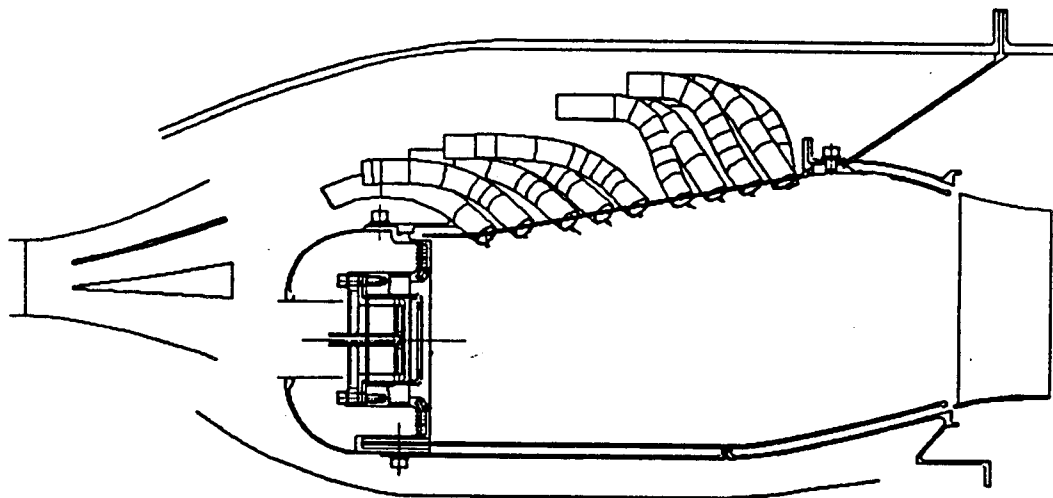


Figure 6.4 - Mechanical layout of the MRA combustor with curved tubes. The details of a practical fuel injector design for the IMFH tubes were never defined.

6.6 MRA Version II

In August, 1994, the concept of “flipping over” the MRA evolved. The new design concept placed straight IMFH tubes on the front dome and the pilot on the outside panel. This put the IMFH tubes inline with the diffuser, resulting in a very direct path for the passage of the main stage air (the largest fraction) through the combustor. An additional advantage of the new MRA concept over the stepped dome (with the normal pilot placement somewhere in the center of the dome) was better placement of the ignitor. The earliest layouts of this concept had the main dome at a 45 degree angle. One of those layouts is shown in Figure 6.5. The 45 degree design was expected to best retain the original feature of promoting mixing between fired and unfired stages, by forcing the burnt gases from the fired stages to flow towards the unfired stages, and also gave the large dome structure high rigidity. During the short time the 45 degree dome was being considered, the preliminary design of the first MRA sector design (which was rectangular) had to be frozen (to meet schedules). The detailed mechanical design and procurement of the rectangular MRA sector combustor (with the 45 degree main dome) proceeded under LET Task 43. The MRA sector combustor design is documented in the LET Task 43 final report.

The 45-degree main dome design quickly evolved to a main dome with a 75 degree angle to the engine centerline. This shortened the combustor and appeared to offer the potential of a relatively simple main fuel injector designs. The 75 degree dome retained the inherent rigidity of a dome which was a conical section, but raised concerns that the mixing characteristics of the original MRA (confirmed by CFD modeling) would be compromised. Cost, length, weight and complexity considerations resulted in vertical dome MRA (90 degrees to the engine centerline) layouts being considered by the end of August, 1994. Figure 6.6 shows an October, 1994 layout of a vertical dome MRA for the subscale demonstrator engine.

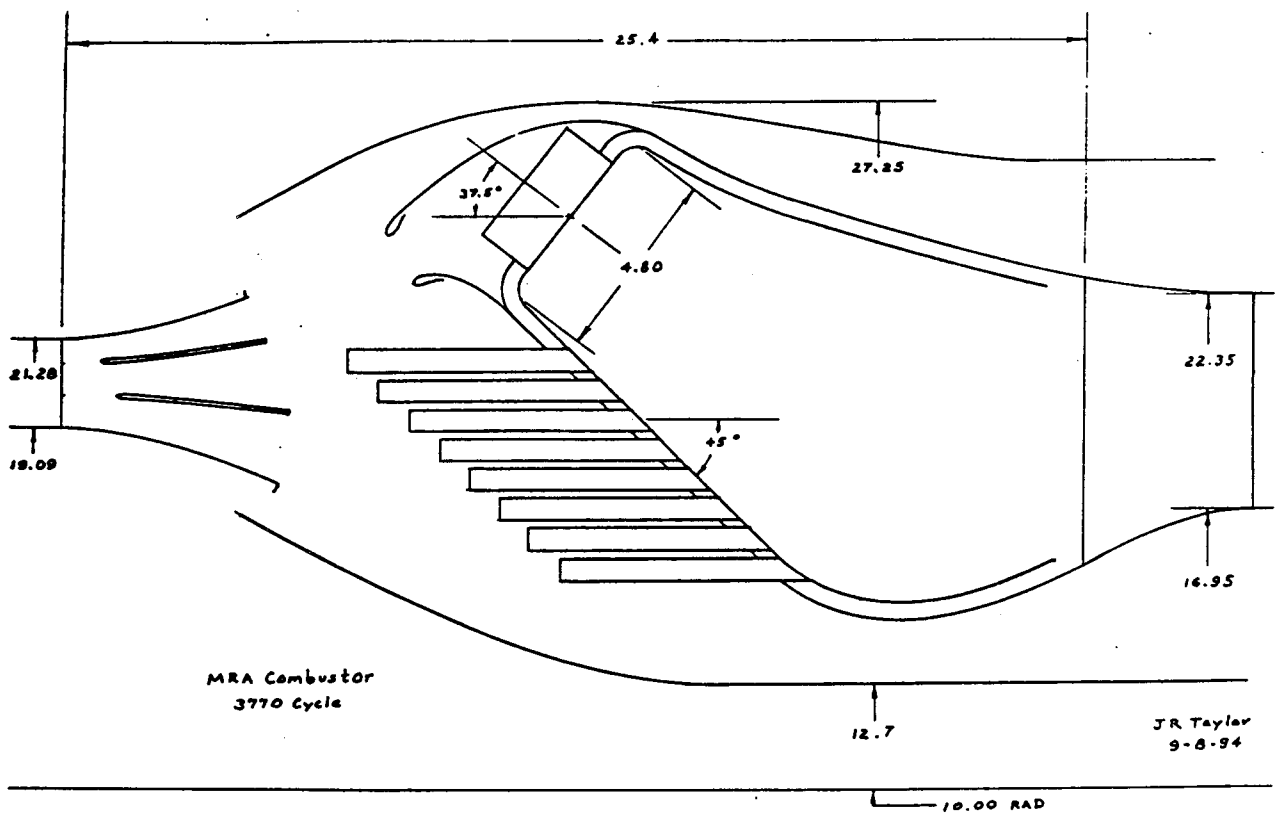


Figure 6.5 - MRA combustor after it was flipped over placing the IMFH tubes in-line with the diffuser. The main dome quickly evolved from 45 degrees to the radius (shown) to 75 degrees, and finally to vertical dome.

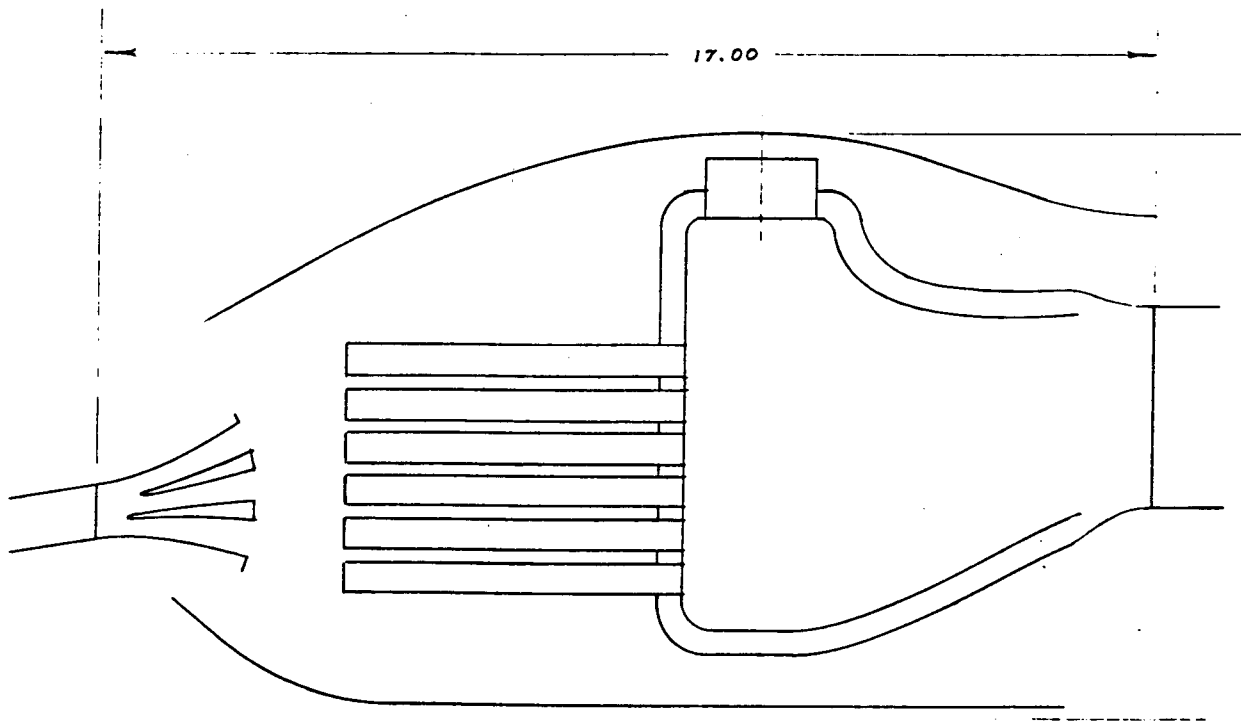


Figure 6.6 - Early layout of the MRA combustor with a vertical dome. This layout is sized for the subscale demonstrator engine.

6.7 Conclusion of Preliminary Combustor Designs

By mid-1995, the vertical dome MRA combustor design had been chosen for the LPP annular rig test in the Phase II CPC program (the LPP subscale annular rig test would later be changed to curved flowpath sector combustor test). The MRA design was chosen because a dome without steps would be inherently more durable than the stepped-dome designs. Also, the design of practical removable fuel injectors for the MRA appeared to be feasible. However, the design of those fuel injectors was to be very challenging. The preliminary design of the fuel injectors for the subscale MRA was not completed until September, 1996, under the Phase II CPC program. By that time, the rectangular MRA sector had been successfully tested (July and August of 1996). The results of that test indicated the MRA was capable of meeting its emissions and operability requirements.

Section 7

Summary and Conclusions

LET Task 10 efforts in the design, analysis, diagnostics, and subcomponent tests of combustor premixers continued similar efforts in APT Task 5. The Task 10 work supported the APT Task 5 conclusions that the Cyclone Swirler yielded the best overall performance in terms of operability and emissions for the pilot stage of the HSCT LPP low emissions combustor. Similarly, the IMFH yielded the best high power performance and was the best available choice for the main stage premixer. Tests of the stepped-dome rectangular LPP sector combustor using these premixers in this Task first confirmed their acceptable performance when integrated into a combustor system. However, significant interactions between the fuel stages were observed during low and mid-power operation. In the stepped-dome design, unfired IMFH stages appeared to degrade the stability of the adjacent fired IMFH stages. Other stage interactions were favorable, resulting in lower NO_x and CO emissions. The flame temperature of fired stages are reduced by dilution by the air from unfired stages, in turn reducing the NO_x emissions. CO emissions are reduced by further combustion of CO by the air from the unfired stages. During high power operation, with all the stages fired, the sector combustor emissions results are slightly lower than would be expected from the subcomponent test results.

Efforts to translate the stepped-dome LPP rig combustor into a practical subscale engine combustor met with significant challenges. Durability of the stepped dome and the development of a removable fuel injection system were the major barriers. During an eight-month period in 1994, the MRA (Multi-staged, Radial, Axial) combustor system design was conceived and evolved through several iterations to the vertical dome MRA design. The MRA was eventually chosen for the Phase II LPP subscale combustor testing. The advantages of the MRA in dome durability and removable fuel injectors were evident during the preliminary design of the combustor. However, the MRA combustor's satisfactory emissions and **operability performance**

were not confirmed until sector tests were performed in the HSR Phase II CPC Program in 1996 and 1997.

References

1-1) J.A. Kastl, P.V. Heberling, J.M. Matulaitis; Low NOx Combustor Development, Final Report for Task 5 of NASA Contract NAS3-25951, NASA Technical Memorandum HSR053 (August, 1997).

1-2) L.J. Chelko, Penetration of Liquid Jets Into a High Velocity Air Steam, NASA Technical Memoranda RME5SJ08 (February, 1954).

1-3) J.A. Schetz, A. Padhye, Penetration and Breakup of Liquid Jets in Subsonic Airstreams, AIAA Journal, Vol. 15, No. 10 (October, 1977).

1-4) M. Adelberg, Breakup Rate and Penetration of a Liquid Jet in a Gas Stream, AIAA Journal, p. 1408 (August, 1967)

1-5) C.L. Yates, Liquid Injection Into a Supersonic Airstream, Air Force Aero Propulsion Laboratory Report No. AFAPL-TR-71-97, Vol. 1 (March, 1972).

1-6) E.L. Geery, M.J. Margetts; Penetration of a High Velocity Gas Stream by a Water Jet, AIAA Paper No. 68-604 (June 10, 1968).

3-1) J.A. Kastl, P.V. Heberling, J.M. Matulaitis; Low NOx Combustor Development, Final Report for Task 5 of NASA Contract NAS3-25951, NASA Technical Memorandum HSR053 (August, 1997).

3-2) S.C. Greenfield, P.V. Heberling and G.E. Moertle; HSCT Sector Combustor Hardware Modifications for Improved Combustor Design; Final Report For Task 43 of NASA Contract NAS3-26617 (January, 1996).

3-3) Y.R. Hicks, R.C. Anderson and R.J.Locke; Laser-Based Flowfield Imaging in a Lean Premixed Prevaporized Sector Combustor; NASA Technical Memorandum HSR051 (February, 1997).

6-1) J.E. Barrett, T.J. Candy, J.J. Charneski, S.C. Greenfield, P.V. Heberling, and D.J. Rundell; HSR Combustor Heat Transfer, Final Report for Task 42 of NASA Contract NAS3-25951, NASA Technical Memorandum HSR036 (July, 1996).

Appendix A

5-Cup Rectangular Sector Combustor Test Data

Test 1

FIRST COMBUSTOR SECTOR, CELL 5 GAS SAMPLE PRESSURE TEST DATA		INPUTS FROM CELL 5 DATA ACQUISITION SYSTEM PRINTOUT												INPUTS FROM FRONT PAGE												INPUTS FROM GAS SAMPLE SHEET:								
Test: 10/29 & 11/04/93		INLET FUEL FLOW				OUTLET FUEL FLOW				INNER IMFH DOME FUEL FLOW				Pilot				Outer IMFH				Inner IMFH				Sample Fuel-Air Ratio		Combust. Efficiency %						
Rdg	Test Points	Main Airflow Meter'd pps	Pilot Main pph	Pilot Verif. pph	Avg. pph	Calc	Pilot pph	Avg. pph	Calc	Main pph	Avg. pph	Calc	Pilot pph	Avg. pph	Calc	Pin, pph	Tin, pph	Pstch (P4) pph	Pbaro pph	Manif. Pres. psia	Pilot Manif. Pres. psia	Outer IMFH Manif. Pres. psia	Inner IMFH Manif. Pres. psia	CO	HC	NOx	El	El	El	El				
Day 1	10/29/93																																	
16	500 All lit - ganged rakes	5.85	156.3	157.4	157.4	159.2	160.5	159.9	171.4	173.4	172.4	171.08	664	664	664	68.56	14.38	86.0	76.06	76.9	65.57	57.06	0.74	0.03032	93.50%									
16	500 All lit - ganged rakes	5.85	156.3	157.4	157.4	159.2	160.5	159.9	171.4	173.4	172.4	171.08	664	664	664	68.56	14.38	86.0	76.06	76.9	60.28	52.04	0.82	0.03146	94.06%									
17	500 All lit - ganged rakes	5.93	188.3	189.4	189.4	196.4	197.5	196.9	222.7	224.3	223.5	74.37	670	670	670	72.11	14.38	95.4	82.42	84.3	13.93	4.39	4.61	0.03807	99.29%									
17	500 All lit - ganged rakes	5.93	188.3	189.4	189.4	196.4	197.5	196.9	222.7	224.3	223.5	74.37	670	670	670	72.11	14.38	95.4	82.42	84.3	14.26	3.78	5.09	0.03826	99.34%									
Day 2	11/4/93																																	
19	201 Pilot only - no sample	4.58	157.6	159.3	158	0.0	0.0	0.0	0.0	0.0	0.0	46.81	412	412	412	45.47	14.39	62.6																
20	403 All lit - no sample	6.71	185.2	187.0	186	224.2	224.9	224.6	228.6	230.1	229.3	78.64	615	615	615	75.92	14.36	98.5	86.63	88.6														
21	403 All lit - ganged rakes	6.72	185.5	187.3	186	226.1	226.9	226.5	228.8	230.4	229.6	78.76	603	603	603	76.02	14.36	98.9	86.86	88.8	24.71	9.92	1.86	0.03466	98.56%									
21	403 All lit - ganged rakes	6.72	185.5	187.3	186	226.1	226.9	226.5	228.8	230.4	229.6	78.76	603	603	603	76.02	14.36	98.9	86.86	88.8	23.56	10.92	1.84	0.03545	98.41%									
22	502 All lit - ganged rakes	7.05	190.8	192.6	192	237.6	238.1	237.8	235.7	237.1	236.4	85.56	768	768	768	82.65	14.35	106.6	94.48	96.1	26.69	10.34	0.72	0.03012	98.47%									
22	502 All lit - ganged rakes	7.05	190.8	192.6	192	237.6	238.1	237.8	235.7	237.1	236.4	85.56	768	768	768	82.65	14.35	106.6	94.48	96.1	23.99	7.09	0.65	0.03030	98.82%									
23	70 All lit - ganged rakes	9.74	255.6	257.7	257	339.1	338.5	338.8	340.3	341.2	340.7	121.18	946	946	946	116.70	14.34	158.2	140.83	142.9	2.66	0.11	4.23	0.03560	99.93%									
	All lit rake A - ganged																																	
	All lit rake B - ganged																																	
	All lit rake C - ganged																																	
	All lit rake D - ganged																																	
24	53 All lit - ganged rakes	9.61	268.6	270.3	269	343.2	342.7	342.9	344.2	345.0	344.6	120.79	944	944	944	116.47	14.33	161.5	140.93	142.9	2.91	0.09	4.28	0.03661	99.92%									
25	52 All lit - ganged rakes	9.58	264.2	266.1	265	337.8	337.3	337.5	338.6	339.4	339.0	121.68	945	945	945	117.22	14.33	161.1	141.02	143.2	2.66	0.09	3.54	0.03540	99.93%									
	All lit rake A - ganged																																	
	All lit rake B - ganged																																	
26	51 All lit - ganged rakes	9.57	257.9	259.9	259	330.0	329.7	329.8	330.8	331.6	331.2	121.21	947	947	947	116.73	14.33	158.9	139.60	141.7	2.79	0.07	3.61	0.03620	99.93%									
27	51 All lit - ganged rakes	9.61	241.9	244.0	243	316.8	316.5	316.6	317.2	318.2	317.7	119.07	947	947	947	114.66	14.33	152.5	135.83	137.9	2.06	0.10	2.50	0.03307	99.94%									
28	99 All lit - ganged rakes	9.59	226.9	229.0	228	297.1	296.9	297.0	296.8	298.0	297.4	117.30	947	947	947	112.88	14.33	146.9	131.59	133.6	2.02	0.16	1.68	0.03086	99.94%									
29	98 All lit - ganged rakes	9.62	217.1	219.2	218	282.0	281.9	281.9	284.1	285.3	284.7	116.07	948	948	948	111.44	14.33	143.0	128.35	128.4	2.50	0.18	1.21	0.02962	99.93%									
30	97 All lit - ganged rakes	9.62	211.2	213.2	212	285.0	284.8	284.9	286.1	287.3	286.7	116.99	947	947	947	112.18	14.33	142.4	129.50	131.7	2.35	0.19	1.20	0.02944	99.93%									
	All lit rake A - ganged																																	
	All lit rake B - ganged																																	
	All lit rake C - ganged																																	
	All lit rake D - ganged																																	
31	96 All lit - ganged rakes	9.74	201.8	203.8	203	292.1	291.9	292.0	291.0	292.2	291.6	117.46	949	949	949	112.80	14.33	141.0	131.07	133.0	2.14	0.16	1.03	0.02992	99.94%									
32	75 All lit - ganged rakes	9.62	220.1	222.0	221	298.8	298.6	298.7	273.3	274.6	274.0	117.40	951	951	951	112.53	14.33	144.8	131.22	130.4	2.40	0.17	1.39	0.02997	99.93%									
33	76 All lit - ganged rakes	9.59	220.2	222.1	221	313.4	313.3	313.4	258.3	259.5	258.9	117.18	949	949	949	112.71	14.33	145.2	133.26	129.0	3.38	0.26	1.49	0.02999	99.90%									

FIRST COMBUSTOR SECTOR, CELL 5 GAS SAMPLE PRESSURE TEST DATA																		
Test: 10/29 & 11/04/93																		
Dimensions:																		
Width = 12.750																		
IMFH Dome Height = 2.300																		
IMFH Exit Aphys/Dome = 4.619																		
Pilot Dome Height = 3.000																		
Out.IMFH Dome Aeff = 3.602																		
IMFH Dome Aphys = 29.325																		
Pilot Dome Aeff = 2.834																		
Pilot Dome Aphys = 38.250																		
Inn.IMFH Dome Aeff = 3.607																		
AIR FLOWS																		
TOTAL DOME			PILOT DOME			OUTER DOME			INNER DOME									
Rdgt	Test Points	Wa_pps	Pilot Airflow_pps	Outer Dome Airflow_pps	Inner Dome Airflow_pps	V total dome (cold) ft/s	V total dome (hot) ft/s	V pilot (cold) ft/s	V pilot (hot) ft/s	V outer dome (cold) ft/s	V mixer exit o.dome (bulk) ft/s	V mixer @ inl. o.dome (hot) ft/s	V outer dome (hot) ft/s	V inner dome (cold) ft/s	V mixer exit i.dome (bulk) ft/s	V mixer @ inl. i.dome (hot) ft/s		
																	V mixer exit o.dome (bulk) ft/s	V mixer @ inl. o.dome (hot) ft/s
16	500 All lit - ganged rakes	4.40	1.24	1.58	1.58	39.7	100.4	28.4	383	76.8	299	340	113.5	47.1	383	299	340	118.0
16	500 All lit - ganged rakes	4.40	1.24	1.58	1.58	39.7	102.7	28.4	383	78.6	299	340	116.1	47.1	383	299	340	120.8
17	500 All lit - ganged rakes	4.25	1.20	1.53	1.53	36.7	108.5	26.2	354	81.7	276	314	121.4	43.5	354	276	314	130.3
17	500 All lit - ganged rakes	4.25	1.20	1.53	1.53	36.7	108.8	26.2	354	82.0	276	314	121.8	43.5	354	276	314	130.7
19	201 Pilot only - no sample	2.96	0.83	1.06	1.06	31.2	-	22.3	301	-	37.0	268	-	37.0	301	235	268	-
20	403 All lit - no sample	4.92	1.39	1.76	1.77	38.3	-	27.4	370	-	45.4	288	-	45.5	370	289	329	-
21	403 All lit - ganged rakes	4.97	1.40	1.78	1.78	38.2	111.9	27.3	369	81.3	369	288	131.4	45.4	369	288	328	132.5
21	403 All lit - ganged rakes	4.97	1.40	1.78	1.78	38.2	113.2	27.3	369	82.2	369	288	132.9	45.4	369	288	328	134.0
22	502 All lit - ganged rakes	4.96	1.40	1.78	1.78	40.6	99.3	29.0	392	71.7	48.1	392	117.4	48.2	392	306	348	117.1
22	502 All lit - ganged rakes	4.96	1.40	1.78	1.78	40.6	99.8	29.0	392	72.1	48.1	392	118.0	48.2	392	306	348	117.7
23	70 All lit - ganged rakes	6.85	1.93	2.46	2.46	45.4	111.1	32.5	438	78.3	438	342	132.3	53.9	438	342	389	132.7
	All lit rake A - ganged																	
	All lit rake B - ganged																	
	All lit rake C - ganged																	
	All lit rake D - ganged																	
24	53 All lit - ganged rakes	6.72	1.90	2.41	2.41	44.6	110.7	31.9	430	79.1	430	335	131.1	52.9	430	336	382	131.6
25	52 All lit - ganged rakes	6.85	1.93	2.46	2.46	45.2	110.3	32.3	436	78.8	436	340	130.7	53.6	436	340	388	131.0
	All lit rake A - ganged																	
	All lit rake B - ganged																	
26	51 All lit - ganged rakes	6.85	1.93	2.46	2.46	45.4	112.0	32.5	438	80.0	438	342	132.7	53.9	438	342	390	133.1
27	51 All lit - ganged rakes	6.74	1.90	2.42	2.42	45.5	107.2	32.5	439	75.9	439	342	127.4	54.0	439	343	390	127.7
28	99 All lit - ganged rakes	6.69	1.89	2.40	2.40	45.9	104.6	32.8	443	74.1	443	345	124.4	54.5	443	346	394	124.5
29	98 All lit - ganged rakes	6.81	1.92	2.44	2.45	47.3	105.7	33.8	457	75.1	457	356	125.4	56.2	457	357	406	126.1
30	97 All lit - ganged rakes	6.97	1.97	2.50	2.50	48.1	107.1	34.4	464	75.1	464	362	127.8	57.1	464	362	413	128.3
	All lit rake A - ganged																	
	All lit rake B - ganged																	
	All lit rake C - ganged																	
	All lit rake D - ganged																	
31	96 All lit - ganged rakes	6.87	1.94	2.47	2.47	47.2	105.9	33.7	456	72.6	456	355	127.7	56.0	456	356	405	127.7
32	75 All lit - ganged rakes	7.02	1.98	2.52	2.52	48.4	108.6	34.6	467	77.1	467	364	131.7	57.5	467	365	415	126.5
33	76 All lit - ganged rakes	6.72	1.90	2.41	2.41	46.2	103.8	33.0	446	73.8	446	348	128.9	54.9	446	348	397	117.8

Appendix B

5-Cup Rectangular Sector Combustor Test Data

Test 2

Atmospheric Pressure Sector Test

SECOND COMBUSTOR SECTOR STABILITY TEST RESULTS

BUILDING 306 ATMOSPHERIC DISCHARGE TEST

4/25/94

Sect.Tot.Aeff = 14.136 sq.in.
 Out.IMFH Dome Aeff= 3.674 sq.in.
 Pilot Dome Aeff = 2.834 sq.in.
 Inn.IMFH Dome Aeff= 3.679 sq.in.
 Tot.Dome Aeff = 10.187 sq.in.
 Dome/Sect.Tot. Air flow 72.06%
 Left/Right.Out.&Inn.Dome 3.677
 (or inner/outer IMFH rows)

JP5 stoichiometric f/a = 0.06815
 At: 25 psid 100 psid
 Out.Dome Flow # 71.0 72.9
 Pilot Dome Flow # 40.2 43.0
 Inn.Dome Flow # 70.6 72.9

Test Points	Pin, psia	% Pres. Drop	P4 psia	Pbaro		Pres. Drop, psid	H ₂ O		Tin F	Tin R	Sector Airflow			Flow Function: Wsqrt(T) P	Dome Fuel Flow, pph	% Fuel to Pilot	Pilot Fuel Flow, pph	Est. Pilot Injector Del.P psid	Total IMFH Domes Fuel Flow pph	% IMFH Fuel to Outer Dome	Outer IMFH Dome Fuel Flow, pph	Est. Outer IMFH Dome Injector Del.P psid	Inner IMFH Dome Fuel Flow pph
				"Hg	psia		"H ₂ O	F			R	pps	pps										
1 Checkout reading	15.26	5.90%	14.36	29.49	14.48	0.90	24.94	42	502	2.57	2.55	1.85	3.77	0.0	0.00%	0.0	0.0	0.0	0.0	0.00%	0.0	0.0	0.0
2 Pilot only with white smoke	15.31	3.46%	14.78	29.49	14.48	0.53	14.69	43	503	2.22	2.15	1.60	3.70	95.7	100.00%	95.7	5.7	0.0	0.00%	0.0	0.0	0.0	0.0
3 Checkout reading	15.29	5.89%	14.39	29.51	14.49	0.90	24.94	214	674	2.22	2.15	1.60	3.77	0.0	0.00%	0.0	0.0	0.0	0.00%	0.0	0.0	0.0	0.0
4 Pilot only	15.33	5.61%	14.47	29.51	14.49	0.86	23.83	218	678	2.16	2.15	1.56	3.68	61.7	100.00%	61.7	2.4	0.0	0.00%	0.0	0.0	0.0	0.0
5 Pilot only	15.36	5.73%	14.48	29.51	14.49	0.88	24.38	220	680	2.19	2.16	1.58	3.72	73.9	100.00%	73.9	3.4	0.0	0.00%	0.0	0.0	0.0	0.0
6 Pilot only	15.41	6.04%	14.48	29.52	14.49	0.93	25.77	354	814	2.06	2.10	1.48	3.81	64.6	100.00%	64.6	2.6	0.0	0.00%	0.0	0.0	0.0	0.0
7 All stages lit	15.52	6.12%	14.57	29.53	14.50	0.95	26.32	363	823	2.08	2.07	1.50	3.84	225.5	30.55%	68.9	2.9	156.6	49.23%	77.1	1.2	79.5	
8 All stages lit	15.48	5.81%	14.58	29.53	14.50	0.90	24.94	302	762	2.10	2.06	1.51	3.74	226.1	29.77%	67.3	2.8	158.8	49.75%	79.0	1.2	79.8	
9 Pilot: only 3 cups fueled	15.34	5.35%	14.52	29.55	14.51	0.82	22.72	289	749	2.01	2.05	1.45	3.59	69.1	100.00%	69.1	8.2	0.0	0.00%	0.0	0.0	0.0	0.0
10 Pilot only	15.46	6.02%	14.53	29.57	14.52	0.93	25.77	252	712	2.21	2.18	1.59	3.81	83.2	100.00%	83.2	4.3	0.0	0.00%	0.0	0.0	0.0	0.0
10 Pilot only LBO	15.46	6.02%	14.53	29.57	14.52	0.93	25.77	252	712	2.21	2.18	1.59	3.81	57.2	100.00%	57.2	2.0	0.0	0.00%	0.0	0.0	0.0	0.0
10 Pilot only LBO	15.46	6.02%	14.53	29.57	14.52	0.93	25.77	252	712	2.21	2.18	1.59	3.81	55.5	100.00%	55.5	1.9	0.0	0.00%	0.0	0.0	0.0	0.0
11 Pilot only	15.42	5.97%	14.50	29.57	14.52	0.92	25.49	413	873	1.98	2.01	1.43	3.79	54.5	100.00%	54.5	1.8	0.0	0.00%	0.0	0.0	0.0	0.0
11 Pilot only LBO	15.42	5.97%	14.50	29.57	14.52	0.92	25.49	413	873	1.98	2.01	1.43	3.79	45.4	100.00%	45.4	1.3	0.0	0.00%	0.0	0.0	0.0	0.0
11 Pilot only LBO	15.42	5.97%	14.50	29.57	14.52	0.92	25.49	413	873	1.98	2.01	1.43	3.79	45.7	100.00%	45.7	1.3	0.0	0.00%	0.0	0.0	0.0	0.0
11 Pilot on, o.main LO	15.42	5.97%	14.50	29.57	14.52	0.92	25.49	413	873	1.98	2.01	1.43	3.79	117.1	44.24%	51.8	1.7	65.3	100.00%	65.3	0.8	0.0	
11 Pilot on, o.main LO	15.42	5.97%	14.50	29.57	14.52	0.92	25.49	413	873	1.98	2.01	1.43	3.79	119.2	43.46%	51.8	1.7	67.4	100.00%	67.4	0.9	0.0	
11 Pilot on, o.main LO	15.42	5.97%	14.50	29.57	14.52	0.92	25.49	413	873	1.98	2.01	1.43	3.79	115.9	44.69%	51.8	1.7	64.1	100.00%	64.1	0.8	0.0	
11 Pilot on, o.main LBO	15.42	5.97%	14.50	29.57	14.52	0.92	25.49	413	873	1.98	2.01	1.43	3.79	109.7	47.22%	51.8	1.7	57.9	100.00%	57.9	0.7	0.0	
11 Pilot on, o.main LBO	15.42	5.97%	14.50	29.57	14.52	0.92	25.49	413	873	1.98	2.01	1.43	3.79	111.7	46.37%	51.8	1.7	59.9	100.00%	59.9	0.7	0.0	
11 Pilot on, o.main LBO	15.42	5.97%	14.50	29.57	14.52	0.92	25.49	413	873	1.98	2.01	1.43	3.79	110.9	46.71%	51.8	1.7	59.1	100.00%	59.1	0.7	0.0	
11 Pilot & o.main on, i.main LO	15.42	5.97%	14.50	29.57	14.52	0.92	25.49	413	873	1.98	2.01	1.43	3.79	187.5	27.63%	51.8	1.7	135.7	49.52%	67.2	0.9	68.5	
11 Pilot & o.main on, i.main LO	15.42	5.97%	14.50	29.57	14.52	0.92	25.49	413	873	1.98	2.01	1.43	3.79	186.6	27.76%	51.8	1.7	134.8	49.85%	67.2	0.9	67.6	
11 Pilot & o.main on, i.main LB	15.42	5.97%	14.50	29.57	14.52	0.92	25.49	413	873	1.98	2.01	1.43	3.79	177.1	29.25%	51.8	1.7	125.3	53.63%	67.2	0.9	58.1	
11 Pilot & o.main on, i.main LB	15.42	5.97%	14.50	29.57	14.52	0.92	25.49	413	873	1.98	2.01	1.43	3.79	176.0	29.43%	51.8	1.7	124.2	54.11%	67.2	0.9	57.0	
12 Pilot only	15.43	5.96%	14.51	29.56	14.51	0.92	25.49	422	882	1.97	2.03	1.42	3.79	59.2	100.00%	59.2	2.2	0.0	0.00%	0.0	0.0	0.0	0.0
12 Pilot on, o.main LO	15.43	5.96%	14.51	29.56	14.51	0.92	25.49	422	882	1.97	2.03	1.42	3.79	119.8	49.42%	59.2	2.2	60.6	100.00%	60.6	0.7	0.0	
12 Pilot on, o.main LO	15.43	5.96%	14.51	29.56	14.51	0.92	25.49	422	882	1.97	2.03	1.42	3.79	128.1	46.21%	59.2	2.2	68.9	100.00%	68.9	0.9	0.0	
12 Pilot on, o.main LO	15.43	5.96%	14.51	29.56	14.51	0.92	25.49	422	882	1.97	2.03	1.42	3.79	119.7	49.46%	59.2	2.2	60.5	100.00%	60.5	0.7	0.0	
12 Pilot on, o.main LBO	15.43	5.96%	14.51	29.56	14.51	0.92	25.49	422	882	1.97	2.03	1.42	3.79	112.0	52.86%	59.2	2.2	52.8	100.00%	52.8	0.6	0.0	
12 Pilot on, o.main LBO	15.43	5.96%	14.51	29.56	14.51	0.92	25.49	422	882	1.97	2.03	1.42	3.79	114.0	51.93%	59.2	2.2	54.8	100.00%	54.8	0.6	0.0	
12 Pilot on, o.main LBO	15.43	5.96%	14.51	29.56	14.51	0.92	25.49	422	882	1.97	2.03	1.42	3.79	114.2	51.84%	59.2	2.2	55.0	100.00%	55.0	0.6	0.0	
13 Pilot & o.main on	15.46	5.89%	14.55	29.56	14.51	0.91	25.22	419	879	1.96	2.02	1.41	3.77	131.4	45.59%	59.9	2.2	71.5	100.00%	71.5	1.0	0.0	
13 Pilot & o.main on, i.main LO	15.46	5.89%	14.55	29.56	14.51	0.91	25.22	419	879	1.96	2.02	1.41	3.77	182.5	32.82%	59.9	2.2	122.6	58.32%	71.5	1.0	51.1	
13 Pilot & o.main on, i.main LO	15.46	5.89%	14.55	29.56	14.51	0.91	25.22	419	879	1.96	2.02	1.41	3.77	191.0	31.36%	59.9	2.2	131.1	54.54%	71.5	1.0	59.6	
13 Pilot & o.main on, i.main LB	15.46	5.89%	14.55	29.56	14.51	0.91	25.22	419	879	1.96	2.02	1.41	3.77	182.7	32.79%	59.9	2.2	122.8	58.22%	71.5	1.0	51.3	
13 Pilot & o.main on, i.main LB	15.46	5.89%	14.55	29.56	14.51	0.91	25.22	419	879	1.96	2.02	1.41	3.77	181.9	32.93%	59.9	2.2	122.0	58.61%	71.5	1.0	50.5	
14 All stages lit	15.54	6.18%	14.58	29.56	14.51	0.96	26.60	496	956	1.94	1.95	1.40	3.86	198.7	30.45%	60.5	2.3	138.2	51.74%	71.5	1.0	66.7	
15 Pilot only LBO	15.42	5.97%	14.50	29.56	14.51	0.92	25.49	604	1064	1.79	1.82	1.29	3.79	38.8	100.00%	38.8	0.9	0.0	0.00%	0.0	0.0	0.0	0.0
15 Pilot only LBO	15.42	5.97%	14.50	29.56	14.51	0.92	25.49	604	1064	1.79	1.82	1.29	3.79	38.8	100.00%	38.8	0.9	0.0	0.00%	0.0	0.0	0.0	0.0
16 Pilot only	15.44	6.15%	14.49	29.56	14.51	0.95	26.32	619	1079	1.81	1.85	1.30	3.85	44.5	100.00%	44.5	1.2	0.0	0.00%	0.0	0.0	0.0	0.0
4/6/94: 28 Inner main only LBO	15.29	6.28%	14.33	29.15	14.31	0.96	26.60	607	1067	1.82	1.80	1.31	3.89	53.6	0.00%	0.0	0.0	53.6	0.00%	0.0	0.0	53.6	

SECOND COMBUSTOR SECTOR, 306 GAS SAMPLE TEST DATA AT ATMOSPHERIC DISCHARGE																														
Day	Test Points	Sect Tot Airf = Out IMFH Dome Airf = Inn IMFH Dome Airf = Tot Dome Airf = Dome/Sec Tot Air flow Let/Right Out & Inn Dome (or inner/outer IMFH rows)	14.136 3.674 3.679 10.187 3.677	sq.in. sq.in. sq.in. sq.in.	JP5 stoichiometric f/a = 0.06815	Test Date: Print Date:	4/6/94 6/1/94	Total IMFH Domes Flow pph	% IMFH Fuel to Dome	Outer IMFH Flow pph	Inner IMFH Flow pph	Est. Outer Dome psid	Est. Inner Dome psid	Total IMFH Domes Fuel to Dome pph	% IMFH Fuel to Dome	Outer IMFH Flow pph	Inner IMFH Flow pph	Est. Outer Dome psid	Est. Inner Dome psid	Sample Equiv. Ratio	Sample Equiv. Ratio									
																						Flow Function Wsgt(J) P	Pilot Fuel Flow pph	% Fuel to Pilot	Pilot Fuel Flow pph	Est. Pilot Injector Del.P psid	Est. Pilot Injector Del.P psid	Sample Equiv. Ratio	Sample Equiv. Ratio	
18	22	Pilot only - individual rake avg. Pilot only rake A - ganged Pilot only rake B - ganged Pilot only rake C - ganged Pilot only rake D - ganged P only - elem avg rake B&D P only - elem avg rake B P only - elem avg rake D Pilot only rake B - element 1 Pilot only rake B - element 2 Pilot only rake B - element 3 Pilot only rake B - element 4 Pilot only rake B - element 5 Pilot only rake B - element 6 Pilot only rake D - element 7 Pilot only rake D - element 8 Pilot only rake D - element 9 Pilot only rake D - element 10	15.23	6.04%	14.31	29.16	14.32	0.92	25.49	401	861	1.98	2.00	1.43	3.81	62.1	100.0%	62.1	0.00%	0.0	0.0	0.0	0.0	0.0	0.177	0.01493	0.219	-	0.648	
19	23	Pilot only - individual rake avg. Pilot only rake A - ganged Pilot only rake B - ganged Pilot only rake C - ganged Pilot only rake D - ganged Uniform Profiles	15.24	6.20%	14.29	29.15	14.31	0.95	26.19	413	873	1.99	2.01	1.44	3.87	56.5	100.0%	56.5	0.00%	0.0	0.0	0.0	0.0	0.0	0.160	0.01271	0.187	-	1.163	
20	30	All stages lit - indiv. rake avg. All stages lit rake A - ganged All stages lit rake B - ganged All stages lit rake C - ganged All stages lit rake D - ganged All lit - elem avg rake B All lit - elem avg rake D All lit rake B - element 1 All lit rake B - element 2 All lit rake B - element 3 All lit rake B - element 4 All lit rake B - element 5 All lit rake D - element 6 All lit rake D - element 7 All lit rake D - element 8 All lit rake D - element 9 All lit rake D - element 10	15.32	6.01%	14.40	29.13	14.30	0.92	25.49	403	863	1.98	2.01	1.43	3.80	222.9	28.2%	62.9	2.4	160.0	49.75%	79.6	1.3	80.4	1.3	0.636	0.03687	0.541	-	0.851
21	30	All lit - elem avg rake B All lit - elem avg rake D All lit rake B - element 1 All lit rake B - element 2 All lit rake B - element 3 All lit rake B - element 4 All lit rake B - element 5 All lit rake D - element 6 All lit rake D - element 7 All lit rake D - element 8 All lit rake D - element 9 All lit rake D - element 10	15.30	6.01%	14.38	29.13	14.30	0.92	25.49	399	859	1.99	2.02	1.43	3.81	222.6	27.9%	62.1	2.4	160.5	50.16%	80.5	1.3	80.0	1.3	0.634	0.03870	0.578	-	0.896

SECOND COMBUSTOR SECTOR, 306 GAS SAMPLE TEST DATA AT ATMOSPHERIC DISCHARGE																																				
Rd	Test Points	Sampling G-ganged I-individual G & I-both	Pin, psia	Pres. Drop %	P4 psia	Pbaro psia	Pres. Drop psid	H2O %	Tin F	Tin R	Tin E	Sector Airflow Total pps	Sector Airflow Meter pps	Dome Vla pps	Dome Vbr pps	Flow Function Wsgt(L) P	Dome Fuel Flow pph	% Fuel to Pilot	Pilot Fuel Flow pph	Est. Pilot Del.P psid	Est. Pilot Flow pph	Total IMFH Domes Fuel Flow pph	% IMFH Fuel to Dome	Est.			Est.			All Rate Sample Eq.R.I Sample Eq.R. Equiv. Ratio avg						
																								Outer IMFH Fuel Flow pph	Inner IMFH Fuel Flow pph	Outer IMFH Fuel Flow pph	Inner IMFH Fuel Flow pph	Outer IMFH Fuel Flow pph	Inner IMFH Fuel Flow pph		Outer IMFH Fuel Flow pph	Inner IMFH Fuel Flow pph				
28	99	I&O Main only lit-rake A avg	15.29	6.28%	14.33	29.15	14.31	0.96	26.60	607	1067	1.82	1.80	1.31	3.89	150.3	0.0%	0.0	0.0	0.0	150.3	49.83%	74.9	1.1	75.4	1.1	0.467	0.03068	0.450	0.964						
		I&O Main only lit-rake B gang																																		
		I&O Main only lit-rake C gang																																		
		I&O Main only lit-rake D gang																																		
Day 2																																				
32	50	All stages lit - indiv. rake avg.	15.58	5.97%	14.65	29.68	14.57	0.93	25.77	504	964	1.90	1.91	1.37	3.79	183.9	27.5%	50.6	1.6	133.3	49.98%	66.6	0.9	66.7	0.9	0.547	0.03489	0.512	0.936							
		All stages lit rake A - ganged																																		
		All stages lit rake B - ganged																																		
		All stages lit rake C - ganged																																		
		All stages lit rake D - ganged																																		
34	69	All stages lit - indiv. rake avg.	15.58	5.97%	14.65	29.69	14.58	0.93	25.77	600	1060	1.81	1.83	1.31	3.79	186.5	27.4%	51.1	1.6	135.4	49.93%	67.6	0.9	67.8	0.9	0.581	0.03763	0.552	0.950							
		All stages lit rake A - ganged																																		
		All stages lit rake B - ganged																																		
		All stages lit rake C - ganged																																		
		All stages lit rake D - ganged																																		
34	69	All stages lit - ganged rakes	15.58	5.97%	14.65	29.69	14.58	0.93	25.77	600	1060	1.81	1.83	1.31	3.79	186.5	27.4%	51.1	1.6	135.4	49.93%	67.6	0.9	67.8	0.9	0.581	0.03626	0.532	0.915							
		All lit-elem. avg rake B&D	15.58	5.97%	14.65	29.69	14.58	0.93	25.77	600	1060	1.81	1.83	1.31	3.79	186.5	27.4%	51.1	1.6	135.4	49.93%	67.6	0.9	67.8	0.9	0.581	0.04022	0.590	1.015							
		All lit-elem. avg rake B																																		
		All lit-elem. avg rake D																																		
		All lit rake B - element 1																																		
		All lit rake B - element 2																																		
		All lit rake B - element 3																																		
		All lit rake B - element 4																																		
		All lit rake B - element 5																																		
		All lit rake B - element 6																																		
		All lit rake D - element 7																																		
		All lit rake D - element 8																																		
		All lit rake D - element 9																																		
		All lit rake D - element 10																																		
35	62	Pilot only - individual rake avg.	15.55	6.43%	14.55	29.70	14.58	1.00	27.71	601	1061	1.88	1.84	1.35	3.94	49.9	100.0%	49.9	1.5	0.0	0.00%	0.0	0.0	0.0	0.0	0.150	0.01337	0.196	1.306							
		Pilot only rake A - ganged																																		
		Pilot only rake B - ganged																																		
		Pilot only rake C - ganged																																		
		Pilot only rake D - ganged																																		
35	62	Pilot only - ganged rakes	15.55	6.43%	14.55	29.70	14.58	1.00	27.71	601	1061	1.88	1.84	1.35	3.94	49.9	100.0%	49.9	1.5	0.0	0.00%	0.0	0.0	0.0	0.0	0.150	0.01238	0.182	1.209							
		P only-elem. avg rake B&D	15.55	6.43%	14.55	29.70	14.58	1.00	27.71	601	1061	1.88	1.84	1.35	3.94	49.9	100.0%	49.9	1.5	0.0	0.00%	0.0	0.0	0.0	0.0	0.150	0.01494	0.219	1.459							
		P only-elem. avg rake B																																		
		P only-elem. avg rake D																																		
		Pilot only rake B - element 1																																		
		Pilot only rake B - element 2																																		
		Pilot only rake B - element 3																																		
		Pilot only rake B - element 4																																		
		Pilot only rake B - element 5																																		
		Pilot only rake B - element 6																																		
		Pilot only rake D - element 7																																		
		Pilot only rake D - element 8																																		
		Pilot only rake D - element 9																																		
		Pilot only rake D - element 10																																		

Appendix C

5-Cup Rectangular Sector Combustor Test Data

Test 3

**THIRD COMBUSTOR SECTOR, CELL 5
GAS SAMPLE PRESSURE TEST DATA**

est: 6/8 & 13/1994
Print: 6/16/98

Rd	Test Points	AIRFLOW CORRECTED CALCULATED EQUIV. RATIOS						AIRFLOW UNCORRECTED, CALCULATED ADIABATIC FLAME TEMPERATURES						AIRFLOW CORRECTED ADIABATIC FLAME TEMPERATURES					
		Dome		Pilot		Total		Dome		Pilot		Total		Dome		Pilot		Total	
		Equiv. Ratio	Equiv. Ratio	Equiv. Ratio	Equiv. Ratio	IMFH	Inner IMFH	Temp., R	Temp., R	Temp., R	Temp., R	Temp., R	Temp., R	emp.,	emp.,	emp.,	emp.,	emp.,	emp.,
Day 1	Pilot only																		
8	3 Pilot only - no sample (JP8)	0.247	0.857	0.000	0.000	0.000	0.000	2256	4234	1068	1068	2191	4136	1068	1068				
9	4 All lit - howl	0.608	0.620	0.603	0.593	0.612	0.612	3438	3477	3454	3454	3485	3523	3469	3438				
10	5 All lit - individual rake avg. All lit rake A - ganged All lit rake B - ganged All lit rake C - ganged All lit rake D - ganged	0.514	0.684	0.445	0.438	0.452	0.452	3401	3967	3110	3167	3187	3737	2947	2922				
11	5 All lit	0.473	0.631	0.409	0.400	0.418	0.418	3243	3795	3000	3034	3088	3615	2864	2833				
17	100 Pilot only - no sample	0.161	0.560	0.000	0.000	0.000	0.000	1926	3452	1124	1124	1891	3363	1124	1124				
18	100 Pilot - individual rake avg. Pilot only A - ganged Pilot only B - ganged Pilot only C - ganged Pilot only D - ganged	0.184	0.639	0.000	0.000	0.000	0.000	2092	3759	1198	1198	2055	3665	1198	1198				
19	5 P&O.M. - individual rake avg. P.&O.M. lit rake A - ganged P.&O.M. lit rake B - ganged P.&O.M. lit rake C - ganged P.&O.M. lit rake D - ganged	0.369	0.537	0.301	0.598	0.000	0.000	2919	3536	2660	3743	2811	3389	2570	3588				
20	602 Pilot & O.Main lit - no sample	0.308	0.456	0.248	0.491	0.000	0.000	2843	3383	2616	3509	2764	3270	2550	3388				
21	602 P&O.M. - individual rake avg. P.&O.M. lit rake A - ganged P.&O.M. lit rake B - ganged P.&O.M. lit rake C - ganged P.&O.M. lit rake D - ganged	0.322	0.477	0.260	0.516	0.000	0.000	2929	3482	2898	3616	2855	3377	2636	3504				
22	8 P&O.M. - individual rake avg. P.&O.M. lit rake A - ganged P.&O.M. lit rake B - ganged P.&O.M. lit rake C - ganged P.&O.M. lit rake D - ganged	0.333	0.499	0.265	0.526	0.000	0.000	3013	3595	2770	3686	2950	3505	2718	3592				

**THIRD COMBUSTOR SECTOR, CELL 5
GAS SAMPLE PRESSURE TEST DATA**

Test: 6/8 & 13/1994
Print: 6/16/98

Rake emiss.norm.by all rake avg. for rakes
Element emiss.norm.by that rake avg.

MEASURED EMISSIONS

Rd	Test Points	Uncorr. Sample (Dome)		Uncorr. Sample (Pilot)		Uncorr. Sample (O.Dome)		Combust. Efficiency %	Corr. Sample (Dome)		Corr. Sample (Pilot)		Corr. Sample (O.Dome)		EI		EI		EI		EI		
		Flame Temp.,R	Temp.,R	Flame Temp.,R	Temp.,R	Flame Temp.,R	Temp.,R		Flame Temp.,R	Temp.,R	Flame Temp.,R	Temp.,R	Flame Temp.,R	Temp.,R	CO avg	NOx avg	HC avg	BCD	NOx avg	CO avg	HC avg	BCD	NOx avg
Day 1	Pilot only.																						
8	3 Pilot only - no sample(JP8)																						
9	4 All lit - howl																						
10	5 All lit - individual rake avg.	3001	3518	2759	3106	2865	3345	2641	2963	2641	3345	2641	2963	2641	3345	96.62	56.33	1.62	65.63				
	All lit rake A - ganged	3094	3629	2840	3204	2850	3320	2627	2947	2627	3320	2627	2947	2627	3320	108.57	111.83	1.88					
	All lit rake B - ganged	3171	3719	2908	3285	3127	3663	2869	3239	2869	3663	2869	3239	2869	3663	40.94	13.58	0.23	1.15				0.62
	All lit rake C - ganged	3153	3698	2891	3266	3008	3514	2765	3113	2765	3514	2765	3113	2765	3514	73.49	61.47	1.03	1.19				1.12
	All lit rake D - ganged	3017	3537	2773	3123	2895	3382	2667	2994	2667	3382	2667	2994	2667	3382	82.45	1.08	51.21	0.66				1.26
11	5 All lit																						
17	100 Pilot only - no sample																						
18	100 Pilot - individual rake avg.	2137	3869	1198	2558	2137	3868	1198	2557	1198	3868	1198	2557	1198	3868	1.48	0.18	4.29	1.40				1.35
	Pilot only A - ganged	2090	3753	1198	2493	2089	3752	1198	2492	1198	3752	1198	2492	1198	3752	1.36	0.22	4.94	1.35				
	Pilot only B - ganged	2132	3856	1198	2551	2131	3855	1198	2550	1198	3855	1198	2550	1198	3855	1.46	0.15	1.07	1.00				1.08
	Pilot only C - ganged	2098	3774	1198	2505	2098	3773	1198	2504	1198	3773	1198	2504	1198	3773	1.37	0.11	0.79	1.01				1.02
	Pilot only D - ganged	2247	4114	1198	2713	2247	4113	1198	2712	1198	4113	1198	2712	1198	4113	1.21	0.90	0.08	0.99				0.90
19	5 P.&O.M. - individual rake avg.	2862	3458	3661	3572	2860	3456	3659	3570	3659	3456	3659	3570	3659	3456	2.88	0.15	3.03	2.83				
	P.&O.M. lit rake A - ganged	2899	3508	3714	3624	2897	3505	3712	3621	3505	3712	3621	3505	3712	3621	3.96	1.27	0.24	1.92				
	P.&O.M. lit rake B - ganged	2798	3370	3568	3481	2796	3368	3566	3479	3368	3566	3479	3368	3566	3479	3.12	1.00	0.12	0.96				1.10
	P.&O.M. lit rake C - ganged	2676	3200	3385	3304	2675	3199	3384	3302	3199	3384	3302	3199	3384	3302	2.51	0.81	0.06	0.48				0.89
	P.&O.M. lit rake D - ganged	2931	3552	3761	3670	2930	3551	3759	3668	3551	3759	3668	3551	3759	3668	2.86	0.92	0.08	1.01				1.01
20	602 Pilot & O Main lit - no sample																						
21	602 P.&O.M. - individual rake avg.	2889	3426	3556	3498	2889	3425	3555	3498	3555	3425	3555	3498	3555	3425	0.90	0.08	5.02	1.08				
	P.&O.M. lit rake A - ganged	2931	3485	3619	3560	2930	3484	3618	3559	3484	3618	3559	3484	3618	3559	1.23	1.14	0.11	1.91				1.02
	P.&O.M. lit rake B - ganged	2797	3294	3416	3362	2797	3294	3415	3361	3294	3415	3361	3294	3415	3361	0.85	0.83	0.04	0.70				0.87
	P.&O.M. lit rake C - ganged	2783	3274	3394	3341	2782	3273	3393	3340	3273	3393	3340	3273	3393	3340	1.17	1.04	0.04	0.70				1.09
	P.&O.M. lit rake D - ganged	2946	3507	3642	3583	2946	3507	3642	3582	3507	3642	3582	3507	3642	3582	1.26	1.06	0.99	1.15				1.04
22	8 P.&O.M. - individual rake avg.	2964	3525	3613	3574	2964	3524	3612	3573	3612	3524	3612	3573	3612	3524	1.58	0.05	9.41	1.39				
	P.&O.M. lit rake A - ganged	3115	3741	3837	3795	3114	3740	3835	3793	3740	3835	3793	3740	3835	3793	1.14	1.67	0.10	1.90				
	P.&O.M. lit rake B - ganged	2888	3415	3498	3462	2888	3415	3498	3461	3498	3415	3498	3461	3498	3415	0.89	1.29	0.04	0.76				0.93
	P.&O.M. lit rake C - ganged	2858	3371	3452	3416	2857	3370	3451	3415	3370	3451	3415	3370	3451	3415	0.98	1.46	0.04	1.03				1.05
	P.&O.M. lit rake D - ganged	3038	3631	3723	3683	3037	3631	3722	3682	3631	3722	3682	3631	3722	3682	0.99	1.41	0.79	1.03				1.02

3RD COMBUSTOR SECTOR, CELL 5 GAS SAMPLE PRES. TEST DATA		INPUTS FROM CELL 5 DATA ACQUISITION SYSTEM PRINTOUT												INPUTS FROM FRONT PAGE						INPUT FROM GAS SAMPLE SHEET					
		INPUTS FROM PAGE #3: CALCULATIONS						INPUTS FROM PAGE #3: CALCULATIONS						Outer			Inner			Ei			Ei		
Rd	t, Points	Main Airflow East Meter'd pps	Pilot Main pph	Pilot Verif. pph	Avg. pph	Out. IMFH Dome Fuel Flow	Inn. IMFH Dome Fuel Flow	Avg. pph	Pin, pph	Tim F	Pstrch (P4) pph	Pilot Manif. pph	Outer IMFH Manif. Pres. pph	Inner IMFH Manif. Pres. pph	Ei CO	Ei HC	Ei NOX	Sample Fuel-Air Ratio	Combust. Efficiency %						
23	7	9.85	250.0	232.0	241	332.0	332.0	332.0	122.75	1151	116.89	14.38	152.7	139.55	0.93	0.04	6.16	0.02111	99.97%						
															1.87	0.09	6.73	0.02395	99.95%						
															0.71	0.02	4.72	0.01974	99.98%						
															0.68	0.02	4.93	0.01875	99.98%						
															1.02	0.04	7.39	0.02184	99.97%						
															1.97	0.07	7.72	0.02442	99.95%						
															0.82	0.02	6.77	0.01998	99.98%						
															0.80	0.02	6.61	0.02246	99.98%						
															0.64	0.02	4.71	0.02040	99.98%						
															1.19	0.05	5.52	0.02273	99.97%						
															0.55	0.01	4.06	0.01861	99.99%						
															0.46	0.02	3.92	0.02068	99.99%						
															0.83	0.05	4.85	0.02162	99.98%						
															0.62	0.02	2.19	0.01742	99.98%						
															0.34	0.02	2.64	0.01984	99.99%						
															2.12	0.02	14.34	0.02504	99.95%						
															3.80	0.04	15.88	0.02768	99.91%						
															2.08	0.02	9.14	0.02274	99.95%						
															2.11	0.02	10.97	0.02568	99.95%						
															0.45	0.07	15.98	0.01155	99.98%						
															0.47	0.08	13.30	0.01070	99.98%						
															0.40	0.04	14.28	0.01122	99.99%						
															0.34	0.03	17.26	0.01395	99.99%						
															0.32	0.05	7.47	0.01020	99.99%						
															0.16	0.09	5.13	0.00902	99.99%						
															0.16	0.04	5.07	0.01004	99.99%						
															0.18	0.04	8.08	0.01166	99.99%						
															0.26	0.04	10.17	0.01068	99.99%						
															0.23	0.09	6.28	0.00951	99.99%						
															0.19	0.04	7.64	0.01035	99.99%						
															0.19	0.04	10.29	0.01255	99.99%						
															0.29	0.04	4.55	0.00923	99.99%						
															0.23	0.05	3.42	0.00834	99.99%						
															0.10	0.01	3.79	0.00941	100.00%						
															0.09	0.00	4.64	0.01043	100.00%						
															0.22	0.11	2.97	0.00859	99.99%						
															0.22	0.19	1.96	0.00750	99.98%						
															0.12	0.05	1.92	0.00869	99.99%						
															0.28	0.04	2.66	0.00941	99.99%						

3RD COMBUSTOR SECTOR, CELL 5 GAS SAMPLE PRES. TEST DATA		PRESSURES				TEMP'S				AIR FLOWS				FUEL FLOWS & PRESSURES								
		Rd	Test Points	Pin psia	P4 psia	Pres Drop psid	% Pres. Drop	Tin F	Tin R	Total Meter pps	Sector Airflow Meter pps	Dome Wa, pp	Flow Function: Wsgt(L) P	Dome Flow, pph	Dome Fuel Flow, pph	Outer IMFH Dome Fuel Flow, pph	Inner IMFH Dome Fuel Flow, pph	% IMFH Fuel to Outer Dome	Pilot Manif. Pres.	Outer IMFH Manif. Pres.	Inner IMFH Manif. Pres.	
																						Outer IMFH Dome Fuel Flow, pph
23	7	Pilot only: P&O.M. - individual rake avg. P&O.M. lit rake A - ganged P&O.M. lit rake B - ganged P&O.M. lit rake C - ganged P&O.M. lit rake D - ganged	122.75	116.89	5.86	4.77%	1151	1611	9.31	9.85	7.22	3.05	573.0	241.0	332.0	332.0	0.0	42.1%	100.0%	152.70	139.55	-
24	7	P&O.M. - individual rake avg. P&O.M. lit rake A - ganged P&O.M. lit rake B - ganged P&O.M. lit rake D - ganged	122.65	116.81	5.84	4.76%	1156	1616	9.28	9.68	7.19	3.04	583.6	252.8	330.8	330.8	0.0	43.3%	100.0%	155.66	139.33	-
25	9	P&O.M. - individual rake avg. P&O.M. lit rake A - ganged P&O.M. lit rake B - ganged P&O.M. lit rake D - ganged	121.48	115.52	5.96	4.91%	1157	1617	9.33	9.88	7.23	3.09	542.1	234.6	307.5	307.5	0.0	43.3%	100.0%	149.79	135.30	-
26	10	P&O.M. - individual rake avg. P&O.M. lit rake A - ganged P&O.M. lit rake B - ganged P&O.M. lit rake D - ganged	121.32	115.15	6.17	5.09%	1154	1614	9.49	9.95	7.36	3.14	508.2	219.5	288.7	288.7	0.0	43.2%	100.0%	146.06	132.93	-
27	13	P&O.M. - individual rake avg. P&O.M. lit rake A - ganged P&O.M. lit rake B - ganged P&O.M. lit rake D - ganged	124.18	118.71	5.47	4.40%	1157	1617	9.03	9.44	7.00	2.93	655.2	280.9	374.3	374.3	0.0	42.9%	100.0%	165.21	147.26	-
28	213	Pilot - individual rake avg. Pilot only A - ganged Pilot only B - ganged Pilot only D - ganged	123.34	117.63	5.71	4.63%	1161	1621	9.19	9.66	7.12	3.00	281.1	281.1	0.0	0.0	100.0%	0.0%	164.32	-	-	
29	207	Pilot - individual rake avg. Pilot only A - ganged Pilot only B - ganged Pilot only D - ganged	122.07	116.29	5.78	4.73%	1160	1620	9.20	9.66	7.13	3.03	250.8	250.8	0.0	0.0	100.0%	0.0%	154.58	-	-	
30	208	Pilot - individual rake avg. Pilot only A - ganged Pilot only B - ganged Pilot only D - ganged	123.03	117.27	5.76	4.68%	1158	1618	9.23	9.64	7.15	3.02	263.5	263.5	0.0	0.0	100.0%	0.0%	156.92	-	-	
31	209	Pilot - individual rake avg. Pilot only A - ganged Pilot only B - ganged Pilot only D - ganged	121.73	115.90	5.83	4.79%	1158	1618	9.23	9.73	7.15	3.05	231.7	231.7	0.0	0.0	100.0%	0.0%	149.39	-	-	
32	210	Pilot - individual rake avg. Pilot only A - ganged Pilot only B - ganged Pilot only D - ganged	121.44	115.54	5.90	4.86%	1159	1619	9.27	9.81	7.19	3.07	215.9	215.9	0.0	0.0	100.0%	0.0%	145.34	-	-	

3RD COMBUSTOR SECTOR, CELL 5		MEASURED FUEL-AIR RATIOS/ EQUIVALENCE RATIOS												UNCORRECTED CALCULATED EQUIV. RATIOS															
GAS SAMPLE PRES. TEST DATA		FUEL FLOW NUMBERS						All Rakes (A,B,C,D)						Sample															
Rd	Test Points	Pilot Injector Flow		Outer IMFH Manif. Flow		Inner IMFH Manif. Flow		Pilot Test Flow		Outer IMFH Test Flow		Inner IMFH Test Flow		Sample Eq.R. Sample Eq.R.		Sample Dome Equiv. Ratio		Sample Airflow Corr. Dome Equiv. Ratio		Calc. Sample (Pilot& (O Dome) Equiv. Ratio		Dome Equiv. Ratio		Pilot Equiv. Ratio		Outer IMFH Dome Equiv. Ratio		Inner IMFH Dome Equiv. Ratio	
		Number	Flow	Number	Flow	Number	Flow	Number	Flow	Number	Flow	Number	Flow	Number	Flow	Ratio	Eq.R.	Ratio	Eq.R.	Ratio	Eq.R.	Ratio	Eq.R.	Ratio	Eq.R.	Ratio	Eq.R.	Ratio	Eq.R.
23	Pilot only. P.&O.M. -individual rake avg. P.&O.M. lit rake A - ganged P.&O.M. lit rake B - ganged P.&O.M. lit rake C - ganged P.&O.M. lit rake D - ganged	40.27		69.74		NA		1.00	0.98	NA		NA		0.310	1.135	0.957	1.013	0.452	0.513	0.500	0.543	0.324	0.473	0.263	0.522	0.000	0.000		
24	P.&O.M. -individual rake avg. P.&O.M. lit rake A - ganged P.&O.M. lit rake B - ganged P.&O.M. lit rake D - ganged	40.56		69.71		NA		1.01	0.98	NA		NA		0.320	1.041	0.969	1.011	0.482	0.506	0.506	0.495	0.331	0.497	0.263	0.522	0.000	0.000		
25	P.&O.M. -individual rake avg. P.&O.M. lit rake A - ganged P.&O.M. lit rake B - ganged P.&O.M. lit rake D - ganged	40.07		69.14		NA		1.00	0.97	NA		NA		0.299	1.028	0.979	1.038	0.450	0.473	0.463	0.463	0.306	0.459	0.243	0.483	0.000	0.000		
26	P.&O.M. -individual rake avg. P.&O.M. lit rake A - ganged P.&O.M. lit rake B - ganged P.&O.M. lit rake D - ganged	39.47		68.47		NA		0.98	0.96	NA		NA		0.279	1.014	0.992	1.039	0.419	0.442	0.431	0.431	0.281	0.422	0.225	0.445	0.000	0.000		
27	P.&O.M. -individual rake avg. P.&O.M. lit rake A - ganged P.&O.M. lit rake B - ganged P.&O.M. lit rake D - ganged	41.19		70.05		NA		1.02	0.99	NA		NA		0.367	1.043	0.964	1.007	0.547	0.585	0.568	0.568	0.381	0.568	0.306	0.607	0.000	0.000		
28	Pilot -individual rake avg. Pilot only A - ganged Pilot only B - ganged Pilot only D - ganged	41.13		NA		NA		1.02	NA	NA		NA		0.169	1.026	1.053	1.108	0.589	0.600	0.262	0.262	0.161	0.559	0.000	0.000	0.000	0.000		
29	Pilot -individual rake avg. Pilot only A - ganged Pilot only B - ganged Pilot only D - ganged	40.53		NA		NA		1.01	NA	NA		NA		0.150	1.208	1.044	1.096	0.520	0.520	0.231	0.231	0.143	0.498	0.000	0.000	0.000	0.000		
30	Pilot -individual rake avg. Pilot only A - ganged Pilot only B - ganged Pilot only D - ganged	40.82		NA		NA		1.02	NA	NA		NA		0.157	1.143	1.044	1.091	0.544	0.544	0.242	0.242	0.150	0.521	0.000	0.000	0.000	0.000		
31	Pilot -individual rake avg. Pilot only A - ganged Pilot only B - ganged Pilot only D - ganged	40.04		NA		NA		1.00	NA	NA		NA		0.135	1.175	1.026	1.082	0.470	0.470	0.209	0.209	0.132	0.458	0.000	0.000	0.000	0.000		
32	Pilot -individual rake avg. Pilot only A - ganged Pilot only B - ganged Pilot only D - ganged	39.54		NA		NA		0.98	NA	NA		NA		0.126	1.130	1.030	1.089	0.438	0.438	0.195	0.195	0.122	0.425	0.000	0.000	0.000	0.000		
														0.1095	1.095	0.00941	0.138	0.443	0.443	0.000	0.000	0.000	0.000	0.000	0.000	0.000	0.000	0.000	0.000

3RD COMBUSTOR SECTOR, CELL 5 GAS SAMPLE PRES. TEST DATA		INPUTS FROM CELL 5 DATA ACQUISITION SYSTEM PRINTOUT														INPUTS FROM GAS SAMPLE SHEET:						
		INPUTS FROM PAGE #3: CALCULATIONS														INPUTS FROM FRONT PAGE						
Rd	t Points	Main Airflow East Meterd pps	Pilot Main pph	Pilot Verif. pph	Avg. pph	Out IMFH Dome Fuel Flow pph	Avg. pph	Inn IMFH Dome Fuel Flow pph	Avg. pph	Pin. pph	Tin F	Psirch (P4) psia	Pbarto psia	Pilot Manif. Pres. psia	Outer IMFH Manif. Pres. psia	Inner IMFH Manif. Pres. psia	El CO	El HC	El NOx	El Fuel-Air Ratio	Sample Combust. Efficiency %	
Day 2 (6/13/94)																						
33	252	10.22	272.9	254.3	264	0.0	0.0	0.0	0.0	123.16	949	117.61	14.39	158.9	-	-	0.35	0.09	2.92	0.01025	99.98%	
																	0.38	0.14	1.83	0.00900	99.98%	
																	0.15	0.04	2.15	0.01004	99.99%	
																	0.25	0.04	2.14	0.01166	99.99%	
34	254	10.34	283.8	265.0	274	0.0	0.0	0.0	0.0	124.28	949	118.73	14.40	163.1	-	-	0.33	0.11	3.36	0.01057	99.98%	
																	0.36	0.09	1.95	0.00931	99.98%	
																	0.23	0.07	2.35	0.01030	99.99%	
																	0.22	0.03	2.62	0.01244	99.99%	
35	254	10.11	309.0	290.1	300	0.0	0.0	0.0	0.0	124.12	949	118.74	14.40	170.7	-	-	0.27	0.03	7.04	0.01199	99.99%	
																	0.34	0.08	5.51	0.01078	99.99%	
																	0.31	0.03	6.31	0.01418	99.99%	
																	2.05	0.02	8.14	0.02617	99.95%	
36	154	10.27	308.0	289.1	299	395.6	395.6	0.0	0.0	123.27	945	117.80	14.41	169.6	153.35	-	3.75	0.03	10.35	0.02871	99.91%	
																	2.31	0.02	4.93	0.02442	99.94%	
																	1.76	0.02	4.68	0.02621	99.96%	
37	153	10.31	292.1	273.4	283	377.6	377.6	0.0	0.0	122.68	947	117.02	14.41	164.1	149.35	-	1.54	0.03	6.19	0.02472	99.96%	
																	2.92	0.04	7.00	0.02734	99.93%	
																	1.70	0.02	3.51	0.02288	99.96%	
																	1.24	0.02	3.03	0.02488	99.97%	
38	152	10.34	272.6	254.2	263	344.4	344.4	0.0	0.0	119.98	948	114.21	14.41	155.8	141.34	-	1.24	0.05	4.02	0.02280	99.97%	
																	1.74	0.05	5.22	0.02481	99.96%	
																	1.55	0.04	2.46	0.02130	99.96%	
																	0.88	0.02	2.18	0.02348	99.98%	
39	151	10.25	245.9	228.2	237	323.1	323.1	0.0	0.0	117.39	946	111.53	14.41	146.3	135.74	-	2.28	0.12	2.64	0.02099	99.94%	
																	1.39	0.04	3.64	0.02269	99.96%	
																	3.66	0.19	1.33	0.01960	99.90%	
																	3.51	0.31	1.10	0.02129	99.89%	
40	155	9.75	326.6	307.1	317	414.8	414.8	0.0	0.0	124.98	946	120.13	14.41	177.4	158.88	-	3.19	0.04	13.99	0.02870	99.92%	
																	5.09	0.04	14.65	0.03031	99.88%	
																	3.90	0.02	9.05	0.02668	99.91%	
																	2.95	0.03	9.31	0.02822	99.93%	

**THIRD COMBUSTOR SECTOR, CELL 5
GAS SAMPLE PRESSURE TEST DATA**

Test: 6/27/94
Print: 6/16/98

Using Posttest flow check data

Rdg	Test Points	Day 3	6/27/94	INPUTS FROM CELL 5 DATA ACQUISITION SYSTEM PRINTOUT												INPUTS FROM FRONT PAGE						INPUTS FROM GAS SAMPLE SHEET					
				INPUTS FROM PAGE #3: CALCULATIONS						INPUTS FROM FRONT PAGE						INPUTS FROM GAS SAMPLE SHEET											
				Main Airflow Meter'd	Pilot Main	Pilot Verif.	Pilot Fuel Flow	Out.IMFH Row Fuel Flow	Inn.IMFH Row Fuel Flow	Pstcrh (P4)	Pbaro	Pstia	Pstia	Manif. Pres.	Manif. Pres.	Outer IMFH Row	Inner IMFH Row	CO	HC	NOX	El	El	El	Sample Fuel-Air Ratio	Combust. Efficiency %		
49	100 Pilot only-ganged rake sample			7.10	271.4	252.2	262	0.0	0.0	0.0	0.0	75.54	747	14.37	111.6	-	-	-	1.37	0.11	4.88	0.01490	99.96%				
59	225 Pilot only-ganged			8.38	284.0	281.1	283	0.0	0.0	0.0	0.0	91.08	616	87.10	14.36	136.4	120.96	132.5	1.46	0.23	2.15	0.01255	99.95%				
	Pilot only rake A																										
	Pilot only rake B																										
	Pilot only rake C																										
	Pilot only rake D																										
50	5 Pilot&Inn. Row/O. Dome ganged			6.96	211.1	194.4	203	0.0	0.0	0.0	150.2	153.4	151.8	87.76	850	105.8	-	105.8	3.15	0.19	3.09	0.01782	99.91%				
	Pilot&Inn. Row/O. Dome Rake A																										
	Pilot&Inn. Row/O. Dome Rake B																										
	Pilot&Inn. Row/O. Dome Rake C																										
	Pilot&Inn. Row/O. Dome Rake D																										
51	602 Pilot&Inn. Row/O. Dome ganged			10.07	272.8	253.0	263	0.0	0.0	0.0	174.4	177.7	176.0	1067	127.09	14.38	169.0	155.2	4.47	0.14	5.44	0.01480	99.88%				
	Pilot&Inn. Row/O. Dome Rake A																										
	Pilot&Inn. Row/O. Dome Rake B																										
	Pilot&Inn. Row/O. Dome Rake C																										
	Pilot&Inn. Row/O. Dome Rake D																										
52	13 Pilot&Inn. Row/O. Dome ganged			9.52	287.2	267.1	277	0.0	0.0	0.0	185.2	188.5	186.9	131.75	1159	126.48	14.37	172.4	158.6	0.76	0.08	12.24	0.01625	99.97%			
	Pilot&Inn. Row/O. Dome Rake A																										
	Pilot&Inn. Row/O. Dome Rake B																										
	Pilot&Inn. Row/O. Dome Rake C																										
	Pilot&Inn. Row/O. Dome Rake D																										
53	8 Pilot&Inn. Row/O. Dome ganged			9.67	278.3	258.7	269	0.0	0.0	0.0	175.3	178.7	177.0	130.74	1162	125.49	14.37	168.9	154.5	1.02	0.05	10.86	0.01538	99.97%			
	Pilot&Inn. Row/O. Dome Rake A																										
	Pilot&Inn. Row/O. Dome Rake B																										
	Pilot&Inn. Row/O. Dome Rake C																										
	Pilot&Inn. Row/O. Dome Rake D																										

THIRD COMBUSTOR SECTOR, CELL 5 GAS SAMPLE PRESSURE TEST DATA														
Sect.Tot.Aeff =		12.694	Mixer Tube Inlet Areas:		JP5 stoichiometric f/a =					0.06815				
Out.IMFH Dome Aeff=		3.533	O.D. Inlet =		3.152		25 psid							
Pilot Dome Aeff =		2.834	I.D. Inlet =		2.985		At:							
Inn.IMFH Dome Aeff=		3.473					Out.Dome Flow #		71.0					
Tot.Dome Aeff =		9.840					Pilot Dome Flow #		43.0					
Dome/Sect. Tot. Air flow		77.52%					Inn. Dome Flow #		72.9					
Left/Right. Out.&Inn.Dome		3.503												
(or inner/outer IMFH rows)														
Print: 6/16/98														
Sampling														
G=ganged														
I=individual														
G & I=both														
Rd	Test Points	Pin, psia	P4, psia	Pres Drop, %	F, R	Tin, R	Calc. Total Meter, pps	Sector Airflow Calc. Total Meter, pps	Flow Function: Wsqrt(T) P	Dome Fuel Flow, pph	Pilot Fuel Flow, pph	Total IMFH O.Dome Fuel Flow, pph	Outer IMFH Row Flow, pph	Inner IMFH Row Flow, pph
49	100 Pilot only-ganged rake sample	75.54	71.57	3.97	5.26%	747	1207	6.95	7.10	0.98	5.39	3.20	261.8	261.8
59	225 Pilot only ganged	91.08	87.10	3.98	4.37%	616	1076	8.09	8.38	0.97	6.27	2.91	282.6	282.6
	Pilot only rake A													
	Pilot only rake B													
	Pilot only rake C													
	Pilot only rake D													
50	5 Pilot&Inn. Row/O Dome ganged	87.76	84.42	3.34	3.81%	850	1310	6.59	6.96	0.95	5.11	2.72	354.5	202.7
	Pilot&Inn. Row/O Dome Rake A													
	Pilot&Inn. Row/O Dome Rake B													
	Pilot&Inn. Row/O Dome Rake C													
	Pilot&Inn. Row/O Dome Rake D													
51	602 Pilot&Inn. Row/O Dome ganged	132.47	127.09	5.38	4.06%	1067	1527	9.52	10.07	0.95	7.38	2.81	439.0	262.9
	Pilot&Inn. Row/O Dome Rake A													
	Pilot&Inn. Row/O Dome Rake B													
	Pilot&Inn. Row/O Dome Rake C													
	Pilot&Inn. Row/O Dome Rake D													
52	13 Pilot&Inn. Row/O Dome ganged	131.75	126.48	5.27	4.00%	1159	1619	9.13	9.52	0.96	7.08	2.79	464.0	277.1
	Pilot&Inn. Row/O Dome Rake A													
	Pilot&Inn. Row/O Dome Rake B													
	Pilot&Inn. Row/O Dome Rake C													
	Pilot&Inn. Row/O Dome Rake D													
53	8 Pilot&Inn. Row/O Dome ganged	130.74	125.49	5.25	4.02%	1162	1622	9.07	9.67	0.94	7.03	2.79	445.5	268.5
	Pilot&Inn. Row/O Dome Rake A													
	Pilot&Inn. Row/O Dome Rake B													
	Pilot&Inn. Row/O Dome Rake C													
	Pilot&Inn. Row/O Dome Rake D													

THIRD COMBUSTOR SECTOR, CELL 5 GAS SAMPLE PRESSURE TEST DATA

Test: 6/27/94
 Print: 6/16/98
 Using Posttest flow check data

Rd	Test Points	FUEL FLOW NUMBERS												MEASURED FUEL-AIR RATIOS/ EQUIVALENCE RATIOS												UNCORRECTED CALCULATED EQUIV. RATIOS					
		Pilot Injector Flow		Outer IMFH Manif. Flow		Inner IMFH Test Flow		Pilot Test Flow		Outer IMFH Cal. Flow		Inner IMFH Test Flow		Sample Airflow		All Rakes (A,B,C,D)		Sample Eq.R. avg		Sample I. Row O. Dome Equiv. Ratio		Sample Pilot & O. Dome Equiv. Ratio		Sample Calc. Pilot & O. Dome Equiv. Ratio		Total IMFH Dome Equiv. Ratio		Outer IMFH Row Equiv. Ratio		Inner IMFH Row Equiv. Ratio	
		Number	Number	Number	Number	Number	Number	Number	Number	Number	Number	Number	Number	Number	Number	Number	Number	Number	Number	Number	Number	Number	Number	Number	Number	Number	Number	Number	Number	Number	Number
49	100	41.39	NA	NA	NA	1.03	NA	NA	NA	NA	NA	1.103	1.128	0.01490	0.219	-	1.002	0.759	0.000	0.468	0.000	0.338	0.198	0.688	0.000	0.000	0.000	0.000	0.000	0.000	
59	225	40.25	NA	NA	NA	1.00	NA	NA	NA	NA	1.002	1.039	0.01255	0.184	-	1.000	0.639	0.000	0.394	0.000	0.285	0.184	0.638	0.000	0.000	0.000	0.000	0.000	0.000	0.000	
														0.01255	0.184	1.000		0.639	0.000	0.394	0.000	0.285									
														0.01099	0.161	0.876		0.560	0.000	0.345	0.000	0.249									
														0.01385	0.203	1.104		0.706	0.000	0.435	0.000	0.314									
50	5	40.62	NA	32.85	NA	1.01	NA	0.93	NA	0.93	0.925	0.976	0.01782	0.261	-	0.976	0.519	0.624	0.559	0.312	0.404	0.283	0.561	0.337	0.000	0.000	0.000	0.000	0.674		
														0.01740	0.255	0.976		0.507	0.609	0.546	0.304	0.395									
														0.01636	0.240	0.918		0.477	0.573	0.513	0.286	0.371									
														0.01666	0.244	0.935		0.485	0.583	0.523	0.292	0.378									
														0.02018	0.296	1.132		0.588	0.706	0.633	0.353	0.458									
51	602	40.64	NA	33.20	NA	1.01	NA	0.94	NA	0.94	0.896	0.947	0.01480	0.217	-	0.896	0.452	0.485	0.465	0.243	0.336	0.242	0.504	0.271	0.000	0.000	0.000	0.541			
														0.01478	0.217	0.999		0.451	0.484	0.464	0.242	0.335									
														0.01369	0.201	0.925		0.418	0.449	0.430	0.224	0.310									
														0.01430	0.210	0.966		0.436	0.469	0.449	0.234	0.324									
														0.01585	0.233	1.071		0.484	0.520	0.497	0.260	0.359									
52	13	40.90	NA	32.96	NA	1.02	NA	0.93	NA	0.93	0.892	0.930	0.01625	0.238	-	0.892	0.495	0.535	0.510	0.267	0.369	0.267	0.554	0.300	0.000	0.000	0.600				
														0.01625	0.238	1.000		0.495	0.535	0.510	0.267	0.369									
														0.01514	0.222	0.932		0.461	0.498	0.475	0.249	0.343									
														0.01587	0.233	0.977		0.483	0.522	0.498	0.261	0.360									
														0.01779	0.261	1.095		0.541	0.586	0.558	0.293	0.403									
53	8	40.75	NA	32.86	NA	1.01	NA	0.93	NA	0.93	0.874	0.932	0.01538	0.226	-	0.874	0.472	0.499	0.483	0.250	0.349	0.258	0.541	0.286	0.000	0.000	0.572				
														0.01538	0.226	1.000		0.472	0.499	0.483	0.250	0.349									
														0.01431	0.210	0.930		0.439	0.465	0.449	0.232	0.325									
														0.01489	0.218	0.968		0.457	0.483	0.467	0.242	0.338									
														0.01688	0.248	1.098		0.518	0.548	0.530	0.274	0.383									

THIRD COMBUSTOR SECTOR, CELL 5 GAS SAMPLE PRESSURE TEST DATA																			
Test: 6/27/94 Print: 6/16/98 Using Posttest flow check data																			
Rd	Test Points	AIRFLOW CORRECTED CALCULATED EQUIV RATIOS						AIRFLOW UNCORRECTED, CALCULATED ADIABATIC FLAME TEMPERATURES						AIRFLOW CORRECTED ADIABATIC FLAME TEMPERATURES					
		Dome Equiv. Ratio	Pilot Equiv. Ratio	Total IMFH Equiv. Ratio	Outer IMFH Equiv. Ratio	Inner IMFH Equiv. Ratio	Dome Equiv. Ratio	Dome Flame Temp., R	Pilot Flame Temp., R	Total IMFH Flame Temp., R	Outer IMFH Flame Temp., R	Inner IMFH Flame Temp., R	Dome Flame Temp., R	Pilot Flame Temp., R	Total IMFH Flame Temp., R	Outer IMFH Flame Temp., R	Inner IMFH Flame Temp., R		
49	100 Pilot only-ganged rake sample	0.194	0.673	0.000	0.000	0.000	0.000	2121	3818	1207	1207	1207	3775	1207	1207	1207			
59	225 Pilot only ganged Pilot only rake A Pilot only rake B Pilot only rake C Pilot only rake D	0.177	0.616	0.000	0.000	0.000	0.000	1946	3587	1076	1076	1076	3516	1076	1076	1076			
50	5 Pilot&Inn,Row/O,Dome ganged Pilot&Inn,Row/O,Dome Rake A Pilot&Inn,Row/O,Dome Rake B Pilot&Inn,Row/O,Dome Rake C Pilot&Inn,Row/O,Dome Rake D	0.268	0.532	0.319	0.000	0.639	2534	3497	2729	1310	3848	2479	3399	2666	1310	3742			
51	602 Pilot&Inn,Row/O,Dome ganged Pilot&Inn,Row/O,Dome Rake A Pilot&Inn,Row/O,Dome Rake B Pilot&Inn,Row/O,Dome Rake C Pilot&Inn,Row/O,Dome Rake D	0.229	0.477	0.256	0.000	0.512	2574	3469	2676	1527	3591	2525	3378	2623	1527	3495			
52	13 Pilot&Inn,Row/O,Dome ganged Pilot&Inn,Row/O,Dome Rake A Pilot&Inn,Row/O,Dome Rake B Pilot&Inn,Row/O,Dome Rake C Pilot&Inn,Row/O,Dome Rake D	0.256	0.532	0.287	0.000	0.575	2741	3697	2853	1619	3838	2702	3623	2811	1619	3761			
53	8 Pilot&Inn,Row/O,Dome ganged Pilot&Inn,Row/O,Dome Rake A Pilot&Inn,Row/O,Dome Rake B Pilot&Inn,Row/O,Dome Rake C Pilot&Inn,Row/O,Dome Rake D	0.242	0.507	0.268	0.000	0.536	2712	3655	2808	1622	3753	2654	3546	2746	1622	3640			

THIRD COMBUSTOR SECTOR, CELL 5 GAS SAMPLE PRESSURE TEST DATA																			
Test: 6/27/94 Print: 6/16/98 Using Posttest flow check data		Dimensions: Width = 12.750 IMFH Dome Height = 2.300 Pilot Dome Height = 3.000 IMFH Dome Aphys = 29.325 Pilot Dome Aphys = 38.250		IMFH Diam. = 0.495 IMFH Exit Aphys/Dome = 4.619 Out. IMFH Dome Aeff = 3.533 Pilot Dome Aeff = 2.834 Inn. IMFH Dome Aeff = 3.473															
Rd	Test Points	AIRFLOWS				AIR VELOCITIES													
		TOTAL DOME		PILOT DOME		OUTER DOME				INNER DOME									
		Calc. Dome	Wa_pps	Pilot Airflow	Outer Dome Airflow	Inn Dome Airflow	V total dome (cold) ft/s	V total dome (hot) ft/s	V pilot (cold) ft/s	V mixer exit pilot ft/s	V pilot (hot) ft/s	V outer dome (cold) ft/s	V mixer exit o.dome (bulk) ft/s	V mixer @ inj. o.dome ft/s	V outer dome (hot) ft/s	V inner dome (cold) ft/s	V mixer exit i.dome (bulk) ft/s	V mixer @ inj. i.dome ft/s	
49	100 Pilot only-ganged rake sample	5.39	1.55	1.81	1.93	1.90	50.0	91.2	36.4	492	121.1	59.3	492	376	439	59.3	58.3	492	370
59	225 Pilot only-ganged Pilot only rake A Pilot only rake B Pilot only rake C Pilot only rake D	6.27	1.81	1.81	2.25	2.21	42.6	77.1	31.1	420	103.7	50.6	420	321	375	50.6	49.7	420	316
50	5 Pilot&Inn. Row/O. Dome ganged Pilot&Inn. Row/O. Dome Rake A Pilot&Inn. Row/O. Dome Rake B Pilot&Inn. Row/O. Dome Rake C Pilot&Inn. Row/O. Dome Rake D	5.11	1.47	1.84	1.84	1.80	43.6	81.8	31.8	430	81.5	51.8	430	329	383	104.2	50.9	430	323
51	602 Pilot&Inn. Row/O. Dome ganged Pilot&Inn. Row/O. Dome Rake A Pilot&Inn. Row/O. Dome Rake B Pilot&Inn. Row/O. Dome Rake C Pilot&Inn. Row/O. Dome Rake D	7.38	2.13	2.65	2.61	2.61	48.8	79.2	35.6	480	76.7	57.9	480	368	429	97.5	56.9	480	361
52	13 Pilot&Inn. Row/O. Dome ganged Pilot&Inn. Row/O. Dome Rake A Pilot&Inn. Row/O. Dome Rake B Pilot&Inn. Row/O. Dome Rake C Pilot&Inn. Row/O. Dome Rake D	7.08	2.04	2.54	2.50	2.50	49.8	81.2	36.3	491	78.6	59.1	491	375	438	100.1	58.1	491	369
53	8 Pilot&Inn. Row/O. Dome ganged Pilot&Inn. Row/O. Dome Rake A Pilot&Inn. Row/O. Dome Rake B Pilot&Inn. Row/O. Dome Rake C Pilot&Inn. Row/O. Dome Rake D	7.03	2.02	2.52	2.48	2.48	50.0	79.9	36.5	492	77.1	59.3	492	377	439	98.0	58.3	492	370

3RD COMBUSTOR SECTOR, CELL 5 GAS SAMPLE PRE-TEST DATA		AIRFLOW CORRECTED CALCULATED EQUIV. RATIOS						AIRFLOW UNCORRECTED, CALCULATED ADIABATIC FLAME TEMPERATURES						AIRFLOW CORRECTED ADIABATIC FLAME TEMPERATURES					
		Dome Equiv. Ratio	Pilot Equiv. Ratio	Total IMFH Domes Equiv. Ratio	Outer IMFH Dome Equiv. Ratio	Inner IMFH Dome Equiv. Ratio		Dome Flame Temp., R	Pilot Flame Temp., R	Total IMFH Domes Flame Temp., R	Outer IMFH Dome Flame Temp., R	Inner IMFH Dome Flame Temp., R		Dome Flame emp.,	Pilot Flame emp.,	Total IMFH Domes Flame emp.,	Outer IMFH Dome Flame emp.,	Inner IMFH Dome Flame Temp., R	
Rd	Test: 6/27/94 Print: 6/16/98 Using Posttest flow check data																		
54	200 Pilot&O.Dome ganged	0.422	0.642	0.660	0.661	0.659	3003	3760	3814	3818	3810	2951	3691	3745	3748	3741			
55	217 Pilot&O.Dome ganged	0.429	0.642	0.681	0.677	0.686	2939	3681	3802	3790	3814	2877	3601	3722	3710	3734			
	Pilot&O.Dome rake A																		
	Pilot&O.Dome rake B																		
	Pilot&O.Dome rake C																		
	Pilot&O.Dome rake D																		
56	218 Pilot&O.Dome ganged	0.405	0.601	0.645	0.638	0.652	2846	3548	3690	3667	3713	2788	3470	3610	3588	3633			
	Pilot&O.Dome rake A																		
	Pilot&O.Dome rake B																		
	Pilot&O.Dome rake C																		
	Pilot&O.Dome rake D																		
57	219 Pilot&O.Dome ganged	0.383	0.569	0.609	0.603	0.615	2773	3453	3587	3567	3607	2707	3363	3494	3475	3514			
	Pilot&O.Dome rake A																		
	Pilot&O.Dome rake B																		
	Pilot&O.Dome rake C																		
	Pilot&O.Dome rake D																		
58	220 Pilot&O.Dome ganged	0.363	0.541	0.578	0.573	0.583	2693	3346	3473	3456	3491	2636	3267	3390	3373	3407			
	Pilot&O.Dome rake A																		
	Pilot&O.Dome rake B																		
	Pilot&O.Dome rake C																		
	Pilot&O.Dome rake D																		

3RD COMBUSTOR SECTOR, CELL 5 GAS SAMPLE PRE-TEST DATA		AIR FLOWS				AIR VELOCITIES												
		TOTAL DOME		PILOT DOME		OUTER DOME				INNER DOME								
Rd	Test Points	Calc. Dome Wt, pps	Pilot Airflow pps	Outer Dome Airflow pps	Inner Dome Airflow pps	V total dome (cold) ft/s	V total dome (hot) ft/s	V pilot (cold) ft/s	V pilot (hot) ft/s	V outer dome (cold) ft/s	V mixer exit o.dome ft/s	V mixer exit i.dome (bulk) ft/s	V outer dome (cold) ft/s	V mixer exit o.dome ft/s	V mixer exit i.dome (bulk) ft/s	V inner dome (cold) ft/s	V mixer exit i.dome (bulk) ft/s	V mixer @ inj. i.dome ft/s
54	200 Pilot&O Dome ganged	6.43	1.85	2.31	2.27	42.3	-	30.8	416	50.1	416	318	371	49.3	416	313	358	
55	217 Pilot&O Dome ganged	6.34	1.83	2.28	2.24	41.5	108.9	30.3	409	49.3	409	313	365	48.4	409	307	351	
56	218 Pilot&O Dome ganged	6.40	1.84	2.30	2.26	42.7	110.3	31.1	420	50.7	420	322	375	49.8	420	316	361	
57	219 Pilot&O Dome ganged	6.38	1.84	2.29	2.25	43.0	107.9	31.3	423	51.0	423	324	378	50.1	423	318	364	
58	220 Pilot&O Dome ganged	6.41	1.85	2.30	2.26	43.8	107.3	31.9	431	51.9	431	330	385	51.1	431	324	371	

Appendix D

5-Cup Rectangular Sector Combustor Test Data

Test 4

Lamilloy Liner Sector Test

FOURTH COMBUSTOR SECTOR, CELL 5 GAS SAMPLE PRESSURE DATA										Test:	10/18/94	Print:	6/8/98
Flow check data:										Dimensions:			
Sacrl.Tot.Aeff =	13.174	sq.in.								Width =	12.750	IMFH Diam. =	0.495
Out.IMFH Dome Aeff =	3.533	sq.in.								IMFH Dome Height =	2.300	IMFH Extl Aphys/Dome =	4.618612
Pilot Dome Aeff =	2.801	sq.in.								Pilot Dome Height =	3.000	Out.IMFH Dome Aeff =	3.533
Inn.IMFH Dome Aeff =	3.473	sq.in.								IMFH Dome Aphys =	29.325	Pilot Dome Aeff =	2.801
Tot.Dome Aeff =	9.807	sq.in.								Pilot Dome Aphys =	38.250	Inn.IMFH Dome Aeff =	3.473
Dome/Sacrl.Tot. Air flow	74.4%												
Left/Right.Out.&Inn.Dome	3.503	sq.in.								JPS stoichiometric f/a =	0.06815		
(or inner/outer IMFH rows)										At: At:	25 100	psid	
O.Liner Aeff =	0.605	sq.in.								Out.Dome Flow #	71.0	72.9	
I.Liner Aeff =	0.621	sq.in.								Pilot Dome Flow #	40.2	43.0	
										Inn.Dome Flow #	70.6	72.9	

FOURTH COMBUSTOR SECTOR, CELL 5 GAS SAMPLE PRESSURE DATA										Test:	10/18/94	Print:	6/8/98
--	--	--	--	--	--	--	--	--	--	-------	----------	--------	--------

LIMITED EXCLUSIVE RIGHT NOTICE		INPUTS FROM CELL 5 DATA ACQUISITION SYSTEM PRINTOUT																						
THESE DATA ARE SUBJECT TO		INPUTS FROM PAGE #3: CALCULATIONS										INPUTS FROM FRONT PAGE					INPUTS FROM GAS SAMPLE SHEET:							
LIMITED EXCLUSIVE RIGHTS UNDER		Main		Out.IMFH Dome				Inn.IMFH Dome				Patch		Pilot			Inner							
GOVERNMENT CONTRACT NUMBER		Airflow		Fuel Flow				Fuel Flow				(P4)		Manif.			Manif.			EI		EI		
NAS3-26617 OR NAS3-27235		East		Avg.				Avg.				Pin		Pres.			Pres.			CO		HC		
Rdg Test Points		Main		pph				pph				psi		psi			psi			%		%		
Day 1		pph		CALC				CALC				F		psi			psi			Ratio		Efficiency		
10/18/94		pph		pph				pph				psi		psi			psi			Ratio		Efficiency		
1	1	All IM - all rakes ganged	5.95	226.0	219.6	223	176.5	179.0	177.8	179.8	181.4	180.5	60.75	646	58.12	14.41	88.2	63.62	65.5	96.62	56.33	1.36	0.03135	92.83%
		All IM rake A - ganged																		108.57	111.83	1.31	0.03316	87.73%
		All IM rake B - ganged																		40.94	13.58	1.87	0.03468	97.86%
		All IM rake C - ganged																		73.49	61.47	1.92	0.03431	92.93%
		All IM rake D - ganged																		82.45	51.21	1.07	0.03166	93.61%
		All IM - Individual rake avg.																		76.36	59.52	1.54	0.03345	93.03%
1	1	All IM rake A element 1																		96.62	56.33	1.36	0.03135	92.83%
		All IM rake A element 2																		108.57	111.83	1.31	0.03316	87.73%
		All IM rake A element 3																		40.94	13.58	1.87	0.03468	97.86%
		All IM rake A element 4																		73.49	61.47	1.92	0.03431	92.93%
		All IM rake A element 5																		82.45	51.21	1.07	0.03166	93.61%
1	1	All IM rake B element 6																		96.62	56.33	1.36	0.03135	92.83%
		All IM rake B element 7																		108.57	111.83	1.31	0.03316	87.73%
		All IM rake B element 8																		40.94	13.58	1.87	0.03468	97.86%
		All IM rake B element 9																		73.49	61.47	1.92	0.03431	92.93%
		All IM rake B element 10																		82.45	51.21	1.07	0.03166	93.61%
1	1	All IM rake C element 11																		96.62	56.33	1.36	0.03135	92.83%
		All IM rake C element 12																		108.57	111.83	1.31	0.03316	87.73%
		All IM rake C element 13																		40.94	13.58	1.87	0.03468	97.86%
		All IM rake C element 14																		73.49	61.47	1.92	0.03431	92.93%
		All IM rake C element 15																		82.45	51.21	1.07	0.03166	93.61%
1	1	All IM rake D element 16																		96.62	56.33	1.36	0.03135	92.83%
		All IM rake D element 17																		108.57	111.83	1.31	0.03316	87.73%
		All IM rake D element 18																		40.94	13.58	1.87	0.03468	97.86%
		All IM rake D element 19																		73.49	61.47	1.92	0.03431	92.93%
		All IM rake D element 20																		82.45	51.21	1.07	0.03166	93.61%

FOURTH COMBUSTOR SECTOR, CELL 5 GAS SAMPLE PRESSURE DATA																		Test:	10/18/94	Print:	6/8/98
FUEL FLOW NUMBERS									SAMPLE BASED EQUIVALENCE RATIOS									DEL. P BASED EQUIV. RATIOS			
LIMITED EXCLUSIVE RIGHT NOTICE																					
THESE DATA ARE SUBJECT TO																					
LIMITED EXCLUSIVE RIGHTS UNDER																					
GOVERNMENT CONTRACT NUMBER																					
NAS3-26617 OR NAS3-27235																					
Rdn	Test Points	Injector	Outer	Inner	Pilot	Outer	Inner	Sample	Sample	Eq. B.I	Sample	Calc.	Calc.	Calc.	Dome	Pilot	Domes	Dome			
		Flow	Manif.	Manif.	Flow	Flow	Flow												Flow	Fuel-Air	Eq. R.
		Number	Number	Number	Number	Number	Number	Ratio	Ratio	Ratio	Ratio	Ratio	Ratio	Ratio	Ratio	Ratio	Ratio	Ratio			
1	1	All Ilt -all rakes ganged	40.65	75.79	66.67	1.01	1.07	0.94	0.03135	0.460	0.937	0.618	0.391	0.404	0.579	0.777	0.499	0.491	0.508		
		All Ilt rake A - ganged							0.03316	0.487	0.991	0.653	0.413	0.427							
		All Ilt rake B - ganged							0.03468	0.509	1.037	0.683	0.432	0.446							
		All Ilt rake C - ganged							0.03431	0.503	1.026	0.676	0.427	0.442							
		All Ilt rake D - ganged							0.03166	0.465	0.946	0.624	0.394	0.407							
		All Ilt -Individual rake avg.							0.03345	0.491	-	0.559	0.417	0.431							
1	1	All Ilt rake A element 1							0.03135	0.460	0.949	0.618	0.391	0.404							
		All Ilt rake A element 2							0.03316	0.487	1.004	0.653	0.413	0.427							
		All Ilt rake A element 3							0.03468	0.509	1.050	0.683	0.432	0.446							
		All Ilt rake A element 4							0.03431	0.503	1.039	0.676	0.427	0.442							
		All Ilt rake A element 5							0.03166	0.465	0.958	0.624	0.394	0.407							
1	1	All Ilt rake B element 6							0.03135	0.460	0.949	0.618	0.391	0.404							
		All Ilt rake B element 7							0.03316	0.487	1.004	0.653	0.413	0.427							
		All Ilt rake B element 8							0.03468	0.509	1.050	0.683	0.432	0.446							
		All Ilt rake B element 9							0.03431	0.503	1.039	0.676	0.427	0.442							
		All Ilt rake B element 10							0.03166	0.465	0.958	0.624	0.394	0.407							
1	1	All Ilt rake C element 11							0.03135	0.460	0.949	0.618	0.391	0.404							
		All Ilt rake C element 12							0.03316	0.487	1.004	0.653	0.413	0.427							
		All Ilt rake C element 13							0.03468	0.509	1.050	0.683	0.432	0.446							
		All Ilt rake C element 14							0.03431	0.503	1.039	0.676	0.427	0.442							
		All Ilt rake C element 15							0.03166	0.465	0.958	0.624	0.394	0.407							
1	1	All Ilt rake D element 16							0.03135	0.460	0.949	0.618	0.391	0.404							
		All Ilt rake D element 17							0.03316	0.487	1.004	0.653	0.413	0.427							
		All Ilt rake D element 18							0.03468	0.509	1.050	0.683	0.432	0.446							
		All Ilt rake D element 19							0.03431	0.503	1.039	0.676	0.427	0.442							
		All Ilt rake D element 20							0.03166	0.465	0.958	0.624	0.394	0.407							

FOURTH COMBUSTOR SECTOR, CELL 5 GAS SAMPLE PRESSURE DATA															Test:	10/18/94	Print:	6/8/98
LIMITED EXCLUSIVE RIGHT NOTICE THESE DATA ARE SUBJECT TO LIMITED EXCLUSIVE RIGHTS UNDER GOVERNMENT CONTRACT NUMBER NAS3-26517 OR NAS3-27235		MAIN AIRFLOW BASED CALCULATED EQUIV RATIOS					DEL P BASED, CALC. ADIABATIC FLAME TEMPERATURES					MAIN AIRFLOW BASED ADIABATIC FLAME TEMPERATURES						
		Dome Equiv. Ratio	Pilot Equiv. Ratio	Domes Equiv. Ratio	Dome Equiv. Ratio	Inner Equiv. Ratio	Dome Flame Temp_R	Pilot Flame Temp_R	Domes Flame Temp_R	Dome Flame Temp_R	Dome Flame Temp_R	Pilot Flame Temp_R	Domes Flame Temp_R	Dome Flame Temp_R	Inner Flame Temp_R			
Rdg	Test Points																	
1	1 All III -all rakes ganged	0.535	0.718	0.461	0.454	0.469	3407	3989	3138	3110	3167	3260	3835	3006	2980	3033		
	All III rake A - ganged																	
	All III rake B - ganged																	
	All III rake C - ganged																	
	All III rake D - ganged																	
	All III -individual rake avg.																	
1	1 All III rake A element 1																	
	All III rake A element 2																	
	All III rake A element 3																	
	All III rake A element 4																	
	All III rake A element 5																	
1	1 All III rake B element 6																	
	All III rake B element 7																	
	All III rake B element 8																	
	All III rake B element 9																	
	All III rake B element 10																	
1	1 All III rake C element 11																	
	All III rake C element 12																	
	All III rake C element 13																	
	All III rake C element 14																	
	All III rake C element 15																	
1	1 All III rake D element 16																	
	All III rake D element 17																	
	All III rake D element 18																	
	All III rake D element 19																	
	All III rake D element 20																	

FOURTH COMBUSTOR SECTOR, CELL 5 GAS SAMPLE PRESSURE DATA											Test: 10/18/94		Print: 6/8/98								
Normalized rake emissions = rake i emission/average (rake A-D)																					
Normalized element emissions = element i emission/average (elements a,b,c,d,e of a selected rake)																					
LIMITED EXCLUSIVE RIGHT NOTICE																					
THESE DATA ARE SUBJECT TO																					
LIMITED EXCLUSIVE RIGHTS UNDER																					
GOVERNMENT CONTRACT NUMBER																					
NAS3-26617 OR NAS3-27235																					
											MEASURED EMISSIONS										
											Uncorr.	Uncorr.	Uncorr.	Uncorr.	Corr.	Corr.	Corr.	Corr.	EI	EI	EI
											Sample	Sample	Sample	Sample	Sample	Sample	Sample	Sample	NOx	CO	HC
											Flame	Flame	Flame	Flame	Flame	Flame	Flame	Flame	avg	avg	avg
											Temp_R	Temp_R	Temp_R	Temp_R	Temp_R	Temp_R	Temp_R	Temp_R	NOx	CO	HC
											Temp_R	Temp_R	Temp_R	Temp_R	Temp_R	Temp_R	Temp_R	Temp_R	avg	avg	avg
Rdg	Test	Points	Temp_R	Temp_R	Temp_R	Temp_R	Efficiency	Temp_R	Temp_R	Temp_R	Temp_R	Temp_R	Temp_R	Temp_R	Temp_R	Temp_R	Temp_R	Temp_R	Temp_R	Temp_R	Temp_R
1	1	All III -all rakes ganged	3001	3534	2755	2801	92.83%	2865	3360	2636	2679	1.36	0.88	96.62	1.27	56.33	0.95				
		All III rake A - ganged	3094	3646	2835	2884	87.73%	2850	3334	2623	2666	1.31	0.85	108.57	1.42	111.83	1.88				
		All III rake B - ganged	3171	3736	2902	2953	97.86%	3127	3680	2864	2913	1.87	1.24	40.94	0.54	13.58	0.23				
		All III rake C - ganged	3153	3714	2886	2936	92.93%	3008	3530	2760	2807	1.92	1.24	73.49	0.96	61.47	1.03				
		All III rake D - ganged	3017	3554	2768	2815	93.61%	2895	3397	2662	2706	1.07	0.69	82.45	1.08	51.21	0.86				
		All III -individual rake avg.	3109	3662	2848	2897	93.03%	2970	3485	2727	2773	1.54	-	76.36	-	59.52	-				
1	1	All III rake A element 1	3001	3534	2755	2801	92.83%	2865	3360	2636	2679	1.36	0.90	96.62	1.20	56.33	0.96				
		All III rake A element 2	3094	3646	2835	2884	87.73%	2850	3334	2623	2666	1.31	0.87	108.57	1.35	111.83	1.90				
		All III rake A element 3	3171	3736	2902	2953	97.86%	3127	3680	2864	2913	1.87	1.24	40.94	0.51	13.58	0.23				
		All III rake A element 4	3153	3714	2886	2936	92.93%	3008	3530	2760	2807	1.92	1.27	73.49	0.91	61.47	1.04				
		All III rake A element 5	3017	3554	2768	2815	93.61%	2895	3397	2662	2706	1.07	0.71	82.45	1.03	51.21	0.87				
1	1	All III rake B element 6	3001	3534	2755	2801	92.83%	2865	3360	2636	2679	1.36	0.90	96.62	1.20	56.33	0.96				
		All III rake B element 7	3094	3646	2835	2884	87.73%	2850	3334	2623	2666	1.31	0.87	108.57	1.35	111.83	1.90				
		All III rake B element 8	3171	3736	2902	2953	97.86%	3127	3680	2864	2913	1.87	1.24	40.94	0.51	13.58	0.23				
		All III rake B element 9	3153	3714	2886	2936	92.93%	3008	3530	2760	2807	1.92	1.27	73.49	0.91	61.47	1.04				
		All III rake B element 10	3017	3554	2768	2815	93.61%	2895	3397	2662	2706	1.07	0.71	82.45	1.03	51.21	0.87				
1	1	All III rake C element 11	3001	3534	2755	2801	92.83%	2865	3360	2636	2679	1.36	0.90	96.62	1.20	56.33	0.96				
		All III rake C element 12	3094	3646	2835	2884	87.73%	2850	3334	2623	2666	1.31	0.87	108.57	1.35	111.83	1.90				
		All III rake C element 13	3171	3736	2902	2953	97.86%	3127	3680	2864	2913	1.87	1.24	40.94	0.51	13.58	0.45				
		All III rake C element 14	3153	3714	2886	2936	92.93%	3008	3530	2760	2807	1.92	1.27	73.49	0.91	61.47	1.04				
		All III rake C element 15	3017	3554	2768	2815	93.61%	2895	3397	2662	2706	1.07	0.71	82.45	1.03	51.21	0.87				
1	1	All III rake D element 16	3001	3534	2755	2801	92.83%	2865	3360	2636	2679	1.36	0.90	96.62	1.20	56.33	0.96				
		All III rake D element 17	3094	3646	2835	2884	87.73%	2850	3334	2623	2666	1.31	0.87	108.57	1.35	111.83	1.90				
		All III rake D element 18	3171	3736	2902	2953	97.86%	3127	3680	2864	2913	1.87	1.24	40.94	0.51	13.58	0.23				
		All III rake D element 19	3153	3714	2886	2936	92.93%	3008	3530	2760	2807	1.92	1.27	73.49	0.91	61.47	1.04				
		All III rake D element 20	3017	3554	2768	2815	93.61%	2895	3397	2662	2706	1.07	0.71	82.45	1.03	51.21	0.87				

LIMITED EXCLUSIVE RIGHT NOTICE		AIR FLOWS				AIR VELOCITIES														
THESE DATA ARE SUBJECT TO		TOTAL DOME				PILOT DOME				OUTER DOME				INNER DOME						
LIMITED EXCLUSIVE RIGHTS UNDER		Outer	Inner	V total	V total	V pilot	V pilot	V pilot	V pilot	V outer	V outer	V outer	V outer	V inner	V inner	V inner	V inner			
GOVERNMENT CONTRACT NUMBER		Calc.	Pilot	Dome	Dome	(cold)	(hot)	(cold)	(hot)	(cold)	(hot)	(cold)	(hot)	(cold)	(hot)	(cold)	(hot)			
NAS3-26617 OR NAS3-27235		Dome	Airflow	Airflow	Airflow	(cold)	(hot)	(cold)	(hot)	(cold)	(hot)	(cold)	(hot)	(cold)	(hot)	(cold)	(hot)			
Rdg	Test Points	Wts. pps	pps	pps	pps	ft/s	ft/s	ft/s	ft/s	ft/s	ft/s	ft/s	ft/s	ft/s	ft/s	ft/s	ft/s			
1	1 All lit -all rakes ganged	4.09	1.17	1.47	1.45	42.8	111.0	31.0	423	94.2	51.0	423	324	378	121.6	50.1	423	318	364	121.5

4TH COMBUSTOR SECTOR, CELL 5		PRESSURES		TEMPS		AIRFLOWS				FUEL FLOWS & PRESSURES													
GAS SAMPLE PRES. TEST DATA																							
Using Posttest flow check data																							
Test: 10/18/94																							
Print: 6/8/98																							
Rdg	Test Points	Sampling G=ganged I=Individual G & I=both	Pin. psia	P4 psia	Pres Drop psid	% Drop	Tin F	Tin R	Sector Airflow		Flow Function: Wspn(CT) F	Dome Fuel Flow pph	Pilot Fuel Flow pph	Total IMFH		Outer IMFH pph	Inner IMFH pph	% IMFH Fuel to Outer Dome	Pilot Pres. psia	Outer IMFH Manf. psia	Inner IMFH Manf. psia		
									Total ppm	Total ppm				Dome Wt. ppm	Dome Fuel Flow pph							Dome Fuel Flow pph	Dome Fuel Flow pph
1	All III -all rakes ganged	all ganged	60.75	58.12	2.63	4.33%	646	1106	5.50	5.95	0.92	4.09	3.01	581.1	222.8	358.3	177.8	180.5	38.3%	49.62%	88.16	63.62	65.5
	All III rake A - ganged	G rake																					
	All III rake B - ganged	G rake																					
	All III rake C - ganged	G rake																					
	All III rake D - ganged	G rake																					
	All III -Individual rake avg.	G rake avg.																					
1	All III rake A element 1	Indiv.																					
	All III rake A element 2	Indiv.																					
	All III rake A element 3	Indiv.																					
	All III rake A element 4	Indiv.																					
	All III rake A element 5	Indiv.																					
1	All III rake B element 6	Indiv.																					
	All III rake B element 7	Indiv.																					
	All III rake B element 8	Indiv.																					
	All III rake B element 9	Indiv.																					
	All III rake B element 10	Indiv.																					
1	All III rake C element 11	Indiv.																					
	All III rake C element 12	Indiv.																					
	All III rake C element 13	Indiv.																					
	All III rake C element 14	Indiv.																					
	All III rake C element 15	Indiv.																					
1	All III rake D element 16	Indiv.																					
	All III rake D element 17	Indiv.																					
	All III rake D element 18	Indiv.																					
	All III rake D element 19	Indiv.																					
	All III rake D element 20	Indiv.																					
2	All III -all rakes ganged	all ganged	60.75	58.12	2.63	4.33%	646	1106	5.50	5.95	0.92	4.09	3.01	581.1	222.8	358.3	177.8	180.5	38.3%	49.62%	88.16	63.62	65.5
	All III rake A - ganged	G rake																					
	All III rake B - ganged	G rake																					
	All III rake C - ganged	G rake																					
	All III rake D - ganged	G rake																					
	All III -Individual rake avg.	G rake avg.																					
2	All III rake A element 1	Indiv.																					
	All III rake A element 2	Indiv.																					
	All III rake A element 3	Indiv.																					
	All III rake A element 4	Indiv.																					
	All III rake A element 5	Indiv.																					
2	All III rake B element 6	Indiv.																					
	All III rake B element 7	Indiv.																					
	All III rake B element 8	Indiv.																					
	All III rake B element 9	Indiv.																					
	All III rake B element 10	Indiv.																					
2	All III rake C element 11	Indiv.																					
	All III rake C element 12	Indiv.																					
	All III rake C element 13	Indiv.																					
	All III rake C element 14	Indiv.																					
	All III rake C element 15	Indiv.																					
2	All III rake D element 16	Indiv.																					
	All III rake D element 17	Indiv.																					
	All III rake D element 18	Indiv.																					
	All III rake D element 19	Indiv.																					
	All III rake D element 20	Indiv.																					
1	All III -all rakes ganged	all ganged	60.75	58.12	2.63	4.33%	646	1106	5.50	5.95	0.92	4.09	3.01	581.1	222.8	358.3	177.8	180.5	38.3%	49.62%	88.16	63.62	65.5
	All III rake A - ganged	G rake																					
	All III rake B - ganged	G rake																					
	All III rake C - ganged	G rake																					
	All III rake D - ganged	G rake																					
	All III -Individual rake avg.	G rake avg.																					
1	All III rake A element 1	Indiv.																					
	All III rake A element 2	Indiv.																					
	All III rake A element 3	Indiv.																					
	All III rake A element 4	Indiv.																					
	All III rake A element 5	Indiv.																					
1	All III rake B element 6	Indiv.																					
	All III rake B element 7	Indiv.																					
	All III rake B element 8	Indiv.																					
	All III rake B element 9	Indiv.																					
	All III rake B element 10	Indiv.																					
1	All III rake C element 11	Indiv.																					
	All III rake C element 12	Indiv.																					
	All III rake C element 13	Indiv.																					
	All III rake C element 14	Indiv.																					
	All III rake C element 15	Indiv.																					
1	All III rake D element 16	Indiv.																					
	All III rake D element 17	Indiv.																					
	All III rake D element 18	Indiv.																					
	All III rake D element 19	Indiv.																					
	All III rake D element 20	Indiv.																					

4TH COMBUSTOR SECTOR, CELL 5		FUEL FLOW NUMBERS						MEASURED FUEL-AIR RATIOS/ EQUIVALENCE RATIOS						UNCORRECTED CALCULATED EQUIV RATIOS								
GAS SAMPLE PRES. TEST DATA		Outer		Inner		Outer		Inner		All Rakes (A,B,C,D)		Sample		Calc.		Sample		Calc.				
Test:	Using Posttest flow check data	Injector	Manif.	Manif.	Test	Cal.	Cal.	Test	Cal.	Sample (Dome)	Eq.R. (Pilot)	Eq.R. (O.Dome)	Eq.R. (Pilot)	Eq.R. (O.Dome)	Eq.R. (Pilot)	Eq.R. (O.Dome)	Dome	Pilot	Domes	Dome	Inner	
Print:	6/8/98	Flow Number	Flow Number	Flow Number	Flow Number	Flow Number	Flow Number	Flow Number	Flow Number	Fuel-Air Ratio	Eq.R. Ratio	Eq.R. Ratio	Eq.R. Ratio	Eq.R. Ratio	Eq.R. Ratio	Eq.R. Ratio	Eq.R. Ratio	Eq.R. Ratio	Eq.R. Ratio	Eq.R. Ratio	Eq.R. Ratio	
Rdg	Test Points	Number	Number	Number	Number	Number	Number	Number	Number													
1	1	All III -all rakes ganged	40.65	75.79	66.67	1.01	1.07	0.94	0.03135	0.460	0.937	0.618	0.391	0.404	0.579	0.777	0.499	0.491	0.508			
		All III rake A - ganged							0.03316	0.487	0.991	0.653	0.413	0.427								
		All III rake B - ganged							0.03468	0.509	1.037	0.683	0.432	0.446								
		All III rake C - ganged							0.03431	0.503	1.026	0.676	0.427	0.442								
		All III rake D - ganged							0.03166	0.465	0.946	0.624	0.394	0.407								
		All III -individual rake avg.							0.03345	0.491	-	0.659	0.417	0.431								
		All III rake A element 1							0.03135	0.460	0.949	0.618	0.391	0.404								
		All III rake A element 2							0.03316	0.487	1.004	0.653	0.413	0.427								
		All III rake A element 3							0.03468	0.509	1.050	0.683	0.432	0.446								
		All III rake A element 4							0.03431	0.503	1.039	0.676	0.427	0.442								
		All III rake A element 5							0.03166	0.465	0.958	0.624	0.394	0.407								
		All III rake B element 6							0.03135	0.460	0.949	0.618	0.391	0.404								
		All III rake B element 7							0.03316	0.487	1.004	0.653	0.413	0.427								
		All III rake B element 8							0.03468	0.509	1.050	0.683	0.432	0.446								
		All III rake B element 9							0.03431	0.503	1.039	0.676	0.427	0.442								
		All III rake B element 10							0.03166	0.465	0.958	0.624	0.394	0.407								
		All III rake C element 11							0.03135	0.460	0.949	0.618	0.391	0.404								
		All III rake C element 12							0.03316	0.487	1.004	0.653	0.413	0.427								
		All III rake C element 13							0.03468	0.509	1.050	0.683	0.432	0.446								
		All III rake C element 14							0.03431	0.503	1.039	0.676	0.427	0.442								
		All III rake C element 15							0.03166	0.465	0.958	0.624	0.394	0.407								
		All III rake D element 16							0.03135	0.460	0.949	0.618	0.391	0.404								
		All III rake D element 17							0.03316	0.487	1.004	0.653	0.413	0.427								
		All III rake D element 18							0.03468	0.509	1.050	0.683	0.432	0.446								
		All III rake D element 19							0.03431	0.503	1.039	0.676	0.427	0.442								
		All III rake D element 20							0.03166	0.465	0.958	0.624	0.394	0.407								
2	1	All III -all rakes ganged	40.65	75.79	66.67	1.01	1.07	0.94	0.03135	0.460	0.937	0.618	0.391	0.404	0.579	0.777	0.499	0.491	0.508			
		All III rake A - ganged							0.03316	0.487	0.991	0.653	0.413	0.427								
		All III rake B - ganged							0.03468	0.509	1.037	0.683	0.432	0.446								
		All III rake C - ganged							0.03431	0.503	1.026	0.676	0.427	0.442								
		All III rake D - ganged							0.03166	0.465	0.946	0.624	0.394	0.407								
		All III -individual rake avg.							0.03345	0.491	-	0.659	0.417	0.431								
		All III rake A element 1							0.03135	0.460	0.949	0.618	0.391	0.404								
		All III rake A element 2							0.03316	0.487	1.004	0.653	0.413	0.427								
		All III rake A element 3							0.03468	0.509	1.050	0.683	0.432	0.446								
		All III rake A element 4							0.03431	0.503	1.039	0.676	0.427	0.442								
		All III rake A element 5							0.03166	0.465	0.958	0.624	0.394	0.407								
		All III rake B element 6							0.03135	0.460	0.949	0.618	0.391	0.404								
		All III rake B element 7							0.03316	0.487	1.004	0.653	0.413	0.427								
		All III rake B element 8							0.03468	0.509	1.050	0.683	0.432	0.446								
		All III rake B element 9							0.03431	0.503	1.039	0.676	0.427	0.442								
		All III rake B element 10							0.03166	0.465	0.958	0.624	0.394	0.407								
		All III rake C element 11							0.03135	0.460	0.949	0.618	0.391	0.404								
		All III rake C element 12							0.03316	0.487	1.004	0.653	0.413	0.427								
		All III rake C element 13							0.03468	0.509	1.050	0.683	0.432	0.446								
		All III rake C element 14							0.03431	0.503	1.039	0.676	0.427	0.442								
		All III rake C element 15							0.03166	0.465	0.958	0.624	0.394	0.407								
		All III rake D element 16							0.03135	0.460	0.949	0.618	0.391	0.404								
		All III rake D element 17							0.03316	0.487	1.004	0.653	0.413	0.427								
		All III rake D element 18							0.03468	0.509	1.050	0.683	0.432	0.446								
		All III rake D element 19							0.03431	0.503	1.039	0.676	0.427	0.442								
		All III rake D element 20							0.03166	0.465	0.958	0.624	0.394	0.407								
1	1	All III -all rakes ganged	40.65	75.79	66.67	1.01	1.07	0.94	0.03135	0.460	0.937	0.618	0.391	0.404	0.579	0.777	0.499	0.491	0.508			
		All III rake A - ganged							0.03316	0.487	0.991	0.653	0.413	0.427								
		All III rake B - ganged							0.03468	0.509	1.037	0.683	0.432	0.446								
		All III rake C - ganged							0.03431	0.503	1.026	0.676	0.427	0.442								
		All III rake D - ganged							0.03166	0.465	0.946	0.624	0.394	0.407								
		All III -individual rake avg.							0.03345	0.491	-	0.659	0.417	0.431								
		All III rake A element 1							0.03135	0.460	0.949	0.618	0.391	0.404								
		All III rake A element 2							0.03316	0.487	1.004	0.653	0.413	0.427								
		All III rake A element 3							0.03468	0.509	1.050	0.683	0.432	0.446								
		All III rake A element 4							0.03431	0.503	1.039	0.676	0.427	0.442								
		All III rake A element 5							0.03166	0.465	0.958	0.624	0.394	0.407								
		All III rake B element 6							0.03135	0.460	0.949	0.618	0.391	0.404								
		All III rake B element 7							0.03316	0.487	1.004	0.653	0.413	0.427								
		All III rake B element 8							0.03468	0.509	1.050	0.683	0.432	0.446								
		All III rake B element 9							0.03431	0.503	1.039	0.676	0.427	0.442								
		All III rake B element 10							0.03166	0.465	0.958	0.624	0.394	0.407								

4TH COMBUSTOR SECTOR, CELL 5		AIRFLOW CORRECTED					AIRFLOW UNCORRECTED, CALCULATED					AIRFLOW CORRECTED				
GAS SAMPLE PRES. TEST DATA		CALCULATED EQUIV RATIOS					ADIABATIC FLAME TEMPERATURES					ADIABATIC FLAME TEMPERATURES				
Using Posttest flow check data				Total	Outer	Inner			Total	Outer	Inner			Total	Outer	Inner
Test: 10/18/94		Dome	Pilot	IMFH	IMFH	IMFH	Dome	Pilot	IMFH	IMFH	IMFH	Dome	Pilot	IMFH	IMFH	IMFH
Print: 6/8/98		Eqv.	Eqv.	Dome	Dome	Dome	Dome	Dome	Dome	Dome	Dome	Dome	Pilot	Dome	Dome	Dome
		Ratio	Ratio	Ratio	Ratio	Ratio	Temp_R	Temp_R	Temp_R	Temp_R	Temp_R	Temp_R	Temp_R	Temp_R	Temp_R	Temp_R
Rdn	Test Points															
1	1 All III - all rakes ganged	0.535	0.718	0.461	0.454	0.469	3407	3989	3138	3110	3167	3260	3835	3006	2980	3033
	All III rake A - ganged															
	All III rake B - ganged															
	All III rake C - ganged															
	All III rake D - ganged															
	All III - individual rake avg.															
1	1 All III rake A element 1															
	All III rake A element 2															
	All III rake A element 3															
	All III rake A element 4															
	All III rake A element 5															
1	1 All III rake B element 6															
	All III rake B element 7															
	All III rake B element 8															
	All III rake B element 9															
	All III rake B element 10															
1	1 All III rake C element 11															
	All III rake C element 12															
	All III rake C element 13															
	All III rake C element 14															
	All III rake C element 15															
1	1 All III rake D element 16															
	All III rake D element 17															
	All III rake D element 18															
	All III rake D element 19															
	All III rake D element 20															
2	1 All III - all rakes ganged	0.535	0.718	0.461	0.454	0.469	3407	3989	3138	3110	3167	3260	3835	3006	2980	3033
	All III rake A - ganged															
	All III rake B - ganged															
	All III rake C - ganged															
	All III rake D - ganged															
	All III - individual rake avg.															
2	1 All III rake A element 1															
	All III rake A element 2															
	All III rake A element 3															
	All III rake A element 4															
	All III rake A element 5															
2	1 All III rake B element 6															
	All III rake B element 7															
	All III rake B element 8															
	All III rake B element 9															
	All III rake B element 10															
2	1 All III rake C element 11															
	All III rake C element 12															
	All III rake C element 13															
	All III rake C element 14															
	All III rake C element 15															
2	1 All III rake D element 16															
	All III rake D element 17															
	All III rake D element 18															
	All III rake D element 19															
	All III rake D element 20															
1	1 All III - all rakes ganged	0.535	0.718	0.461	0.454	0.469	3407	3989	3138	3110	3167	3260	3835	3006	2980	3033
	All III rake A - ganged															
	All III rake B - ganged															
	All III rake C - ganged															
	All III rake D - ganged															
	All III - individual rake avg.															
1	1 All III rake A element 1															
	All III rake A element 2															
	All III rake A element 3															
	All III rake A element 4															
	All III rake A element 5															
1	1 All III rake B element 6															
	All III rake B element 7															
	All III rake B element 8															
	All III rake B element 9															
	All III rake B element 10															
1	1 All III rake C element 11															
	All III rake C element 12															
	All III rake C element 13															
	All III rake C element 14															
	All III rake C element 15															
1	1 All III rake D element 16															
	All III rake D element 17															
	All III rake D element 18															
	All III rake D element 19															
	All III rake D element 20															
1	1 All III - all rakes ganged	0.535	0.718	0.461	0.454	0.469	3407	3989	3138	3110	3167	3260	3835	3006	2980	3033
	All III rake A - ganged															
	All III rake B - ganged															
	All III rake C - ganged															
	All III rake D - ganged															
	All III - individual rake avg.															
1	1 All III rake A element 1															
	All III rake A element 2															
	All III rake A element 3															
	All III rake A element 4															
	All III rake A element 5															
1	1 All III rake B element 6															
	All III rake B element 7															
	All III rake B element 8															
	All III rake B element 9															
	All III rake B element 10															
1	1 All III rake C element 11															
	All III rake C element 12															
	All III rake C element 13															
	All III rake C element 14															
	All III rake C element 15															
1	1 All III rake D element 16															
	All III rake D element 17															
	All III rake D element 18															
	All III rake D element 19															
	All III rake D element 20															

4TH COMBUSTOR SECTOR, CELL 5		MEASURED EMISSIONS																		
GAS SAMPLE PRES. TEST DATA																				
Using Posttest flow check data																				
Test: 10/18/94																				
Print: 6/8/98																				
Rdg	Test Points	Uncorr. Sample	Uncorr. Sample	Uncorr. Sample	Uncorr. Sample	Combust. Efficiency	Corr. Sample	Corr. Sample	Corr. Sample	Corr. Sample	EI	NOx	EI	CO	EI	HC	EI			
		(Dome)	(Pilot)	(O.Dome)	(O.Dome)		(Dome)	(Pilot)	(O.Dome)	(O.Dome)								(O.Dome)	(O.Dome)	NOx
		Temp_R	Temp_R	Temp_R	Temp_R	%	Temp_R	Temp_R	Temp_R	Temp_R										
1	All IR -all rakes ganged	3001	3534	2755	2801	92.83%	2965	3360	2636	2679	1.36	0.88	96.62	1.27	56.33	0.95				
	All IR rake A - ganged	3094	3646	2835	2884	87.73%	2950	3334	2623	2666	1.31	0.85	108.57	1.42	111.83	1.88				
	All IR rake B - ganged	3171	3736	2902	2953	97.86%	3127	3680	2864	2913	1.87	1.24	40.94	0.54	13.58	0.23				
	All IR rake C - ganged	3153	3714	2886	2936	92.93%	3008	3530	2760	2807	1.92	1.24	73.49	0.96	61.47	1.03				
	All IR rake D - ganged	3017	3554	2768	2815	93.61%	2895	3397	2662	2706	1.07	0.69	82.45	1.08	51.21	0.86				
	All IR -individual rake avg.	3109	3662	2848	2897	93.03%	2970	3485	2727	2773	1.54	-	76.36	-	59.52	-				
1	All IR rake A element 1	3001	3534	2755	2801	92.83%	2865	3360	2636	2679	1.36	0.90	96.62	1.20	56.33	0.96				
	All IR rake A element 2	3094	3646	2835	2884	87.73%	2850	3334	2623	2666	1.31	0.87	108.57	1.35	111.83	1.90				
	All IR rake A element 3	3171	3736	2902	2953	97.86%	3127	3680	2864	2913	1.87	1.24	40.94	0.51	13.58	0.23				
	All IR rake A element 4	3153	3714	2886	2936	92.93%	3008	3530	2760	2807	1.92	1.27	73.49	0.91	61.47	1.04				
	All IR rake A element 5	3017	3554	2768	2815	93.61%	2895	3397	2662	2706	1.07	0.71	82.45	1.03	51.21	0.87				
1	All IR rake B element 6	3001	3534	2755	2801	92.83%	2865	3360	2636	2679	1.36	0.90	96.62	1.20	56.33	0.96				
	All IR rake B element 7	3094	3646	2835	2884	87.73%	2850	3334	2623	2666	1.31	0.87	108.57	1.35	111.83	1.90				
	All IR rake B element 8	3171	3736	2902	2953	97.86%	3127	3680	2864	2913	1.87	1.24	40.94	0.51	13.58	0.23				
	All IR rake B element 9	3153	3714	2886	2936	92.93%	3008	3530	2760	2807	1.92	1.27	73.49	0.91	61.47	1.04				
	All IR rake B element 10	3017	3554	2768	2815	93.61%	2895	3397	2662	2706	1.07	0.71	82.45	1.03	51.21	0.87				
1	All IR rake C element 11	3001	3534	2755	2801	92.83%	2865	3360	2636	2679	1.36	0.90	96.62	1.20	56.33	0.96				
	All IR rake C element 12	3094	3646	2835	2884	87.73%	2850	3334	2623	2666	1.31	0.87	108.57	1.35	111.83	1.90				
	All IR rake C element 13	3171	3736	2902	2953	97.86%	3127	3680	2864	2913	1.87	1.24	40.94	0.51	13.58	0.23				
	All IR rake C element 14	3153	3714	2886	2936	92.93%	3008	3530	2760	2807	1.92	1.27	73.49	0.91	61.47	1.04				
	All IR rake C element 15	3017	3554	2768	2815	93.61%	2895	3397	2662	2706	1.07	0.71	82.45	1.03	51.21	0.87				
1	All IR rake D element 16	3001	3534	2755	2801	92.83%	2865	3360	2636	2679	1.36	0.90	96.62	1.20	56.33	0.96				
	All IR rake D element 17	3094	3646	2835	2884	87.73%	2850	3334	2623	2666	1.31	0.87	108.57	1.35	111.83	1.90				
	All IR rake D element 18	3171	3736	2902	2953	97.86%	3127	3680	2864	2913	1.87	1.24	40.94	0.51	13.58	0.23				
	All IR rake D element 19	3153	3714	2886	2936	92.93%	3008	3530	2760	2807	1.92	1.27	73.49	0.91	61.47	1.04				
	All IR rake D element 20	3017	3554	2768	2815	93.61%	2895	3397	2662	2706	1.07	0.71	82.45	1.03	51.21	0.87				
2	All IR -all rakes ganged	3001	3534	2755	2801	92.83%	2865	3360	2636	2679	1.36	0.88	96.62	1.27	56.33	0.95				
	All IR rake A - ganged	3094	3646	2835	2884	87.73%	2850	3334	2623	2666	1.31	0.85	108.57	1.42	111.83	1.88				
	All IR rake B - ganged	3171	3736	2902	2953	97.86%	3127	3680	2864	2913	1.87	1.24	40.94	0.54	13.58	0.23				
	All IR rake C - ganged	3153	3714	2886	2936	92.93%	3008	3530	2760	2807	1.92	1.24	73.49	0.96	61.47	1.03				
	All IR rake D - ganged	3017	3554	2768	2815	93.61%	2895	3397	2662	2706	1.07	0.69	82.45	1.08	51.21	0.86				
	All IR -individual rake avg.	3109	3662	2848	2897	93.03%	2970	3485	2727	2773	1.54	-	76.36	-	59.52	-				
2	All IR rake A element 1	3001	3534	2755	2801	92.83%	2865	3360	2636	2679	1.36	0.90	96.62	1.20	56.33	0.96				
	All IR rake A element 2	3094	3646	2835	2884	87.73%	2850	3334	2623	2666	1.31	0.87	108.57	1.35	111.83	1.90				
	All IR rake A element 3	3171	3736	2902	2953	97.86%	3127	3680	2864	2913	1.87	1.24	40.94	0.51	13.58	0.23				
	All IR rake A element 4	3153	3714	2886	2936	92.93%	3008	3530	2760	2807	1.92	1.27	73.49	0.91	61.47	1.04				
	All IR rake A element 5	3017	3554	2768	2815	93.61%	2895	3397	2662	2706	1.07	0.71	82.45	1.03	51.21	0.87				
2	All IR rake B element 6	3001	3534	2755	2801	92.83%	2865	3360	2636	2679	1.36	0.90	96.62	1.20	56.33	0.96				
	All IR rake B element 7	3094	3646	2835	2884	87.73%	2850	3334	2623	2666	1.31	0.87	108.57	1.35	111.83	1.90				
	All IR rake B element 8	3171	3736	2902	2953	97.86%	3127	3680	2864	2913	1.87	1.24	40.94	0.51	13.58	0.23				
	All IR rake B element 9	3153	3714	2886	2936	92.93%	3008	3530	2760	2807	1.92	1.27	73.49	0.91	61.47	1.04				
	All IR rake B element 10	3017	3554	2768	2815	93.61%	2895	3397	2662	2706	1.07	0.71	82.45	1.03	51.21	0.87				
2	All IR rake C element 11	3001	3534	2755	2801	92.83%	2865	3360	2636	2679	1.36	0.90	96.62	1.20	56.33	0.96				
	All IR rake C element 12	3094	3646	2835	2884	87.73%	2850	3334	2623	2666	1.31	0.87	108.57	1.35	111.83	1.90				
	All IR rake C element 13	3171	3736	2902	2953	97.86%	3127	3680	2864	2913	1.87	1.24	40.94	0.51	13.58	0.23				
	All IR rake C element 14	3153	3714	2886	2936	92.93%	3008	3530	2760	2807	1.92	1.27	73.49	0.91	61.47	1.04				
	All IR rake C element 15	3017	3554	2768	2815	93.61%	2895	3397	2662	2706	1.07	0.71	82.45	1.03	51.21	0.87				
2	All IR rake D element 16	3001	3534	2755	2801	92.83%	2865	3360	2636	2679	1.36	0.90	96.62	1.20	56.33	0.96				
	All IR rake D element 17	3094	3646	2835	2884	87.73%	2850	3334	2623	2666	1.31	0.87	108.57	1.35	111.83	1.90				
	All IR rake D element 18	3171	3736	2902	2953	97.86%	3127	3680	2864	2913	1.87	1.24	40.94	0.51	13.58	0.23				
	All IR rake D element 19	3153	3714	2886	2936	92.93%	3008	3530	2760	2807	1.92	1.27	73.49	0.91	61.47	1.04				
	All IR rake D element 20	3017	3554	2768	2815	93.61%	2895	3397	2662	2706	1.07	0.71	82.45	1.03	51.21	0.87				
2	All IR rake A element 1	3001	3534	2755	2801	92.83%	2865	3360	2636	2679	1.36	0.88	96.62	1.27	56.33	0.95				
	All IR rake B - ganged	3094	3646	2835	2884	87.73%	2850	3334	2623	2666	1.31	0.85	108.57	1.42	111.83	1.88				
	All IR rake C - ganged	3171	3736	2902	2953	97.86%	3127	3680	2864	2913	1.87	1.24	40.94	0.54	13.58	0.23				
	All IR rake D - ganged	3153	3714	2886	2936	92.93%	3008	3530	2760	2807	1.92	1.24	73.49	0.96	61.47	1.03				
	All IR -individual rake avg.	3109	3662	2848	2897	93.03%	2970	3485	2727	2773	1.54	-	76.36	-	59.52	-				
1	All IR rake A element 1	3001	3534	2755	2801	92.83%	2865	3360	2636	2679	1.36	0.90	96.62	1.20	56.33	0.96				
	All IR rake A element 2	3094	3646	2835	2884	87.73%	2850	3334	2623	2666	1.31	0.87	108.57	1.35	111.83	1.90				
	All IR rake A element 3	3171	3736	2902	2953	97.86%	3127	3680	2864	2913	1.87	1.24	40.94	0.51	13.58	0.23				
	All IR rake A element 4	3153	3714	2886	2936	92.93%	3008	3530	2760	2807	1.92	1.27	73.49	0.91	61.47	1.04				
	All IR rake B element 5	3017	3554	2768	2815	93.61%	2895	3397	2662	2706	1.07	0.71	82.45	1.03	51.21	0.87				
1	All IR rake B element 6	3001	3534	2755	2801	92.83%	2865	3360	2636	2679	1.36	0.90	96.62	1.20	56.33	0.96				
	All IR rake B element 7	3094	3646	2835	2884	87.73%	2850	3334	2623											

1	1	All III -all rakes ganged	4.09	1.17	1.47	1.45	42.8	111.0	31.0	423	94.2	51.0	423	324	378	121.6	50.1	423	318	364	121.5
1	1	All III -all rakes ganged	4.09	1.17	1.47	1.45	42.8	111.0	31.0	423	94.2	51.0	423	324	378	121.6	50.1	423	318	364	121.5
1	1	All III -all rakes ganged	4.09	1.17	1.47	1.45	42.8	111.0	31.0	423	94.2	51.0	423	324	378	121.6	50.1	423	318	364	121.5
1	1	All III -all rakes ganged	4.09	1.17	1.47	1.45	42.8	111.0	31.0	423	94.2	51.0	423	324	378	121.6	50.1	423	318	364	121.5

Appendix E

Pennsylvania State University Laser Diagnostics Study

Final Report

**Mixing and Vaporization Evaluation of Integrated Injector
Mixer Flame Holder (IMFH) Configurations**

by

**D.A. Santavicca and R.L. Steinberger
The Pennsylvania State University
Department of Mechanical Engineering
University Park, Pennsylvania 16802**

September, 1994

I. INTRODUCTION

This report documents experimental work done at Penn State intended to define an injector geometry for optimized fuel-air mixing and vaporization for the integrated injector mixer flame holder (IMFH) configuration. The experiments were carried out in the high pressure, high temperature flow apparatus described in the previous final report (dated September, 1993). A schematic diagram of the overall facility is shown in Figure 1. All the experiments employed 2-D laser-induced exciplex fluorescence which allows instantaneous and separate visualization of the liquid and vapor distributions in an operating liquid fuel-injected high speed flow.

The main objective of these tests was to determine a fuel injector type and geometry and length of mixing section for optimized fuel vaporization and fuel-air mixing at the mixing section outlet.

This overall goal was divided into four tasks, each of which will be described in detail:

Task 1: Fuel Injector Modifications

Task 2: Mixer Tube Length Reduction

Task 3: Mixer Tube Diameter Modifications

Task 4: Air Injection at the Mixer Tube Exit

Tasks 1 and 2 were completed as posed. The equipment was designed and built for Tasks 3 and 4. However, because of changed priorities and the desire to have more information about new injector geometries, experimental work in tasks 3 and 4 was deferred, and Tasks 1 and 2 were expanded to include these new geometries.

II. APPARATUS AND PROCEDURE

The Penn State high temperature high pressure continuous flow system described in a previous report is capable of operation at inlet temperatures to about 1300°F and pressures to 10 atm. As shown in Figure 1, the heated air flows into a stainless steel entrance section about 5" long, proceeds through a rounded inlet section, and flows through a smaller diameter (13 mm

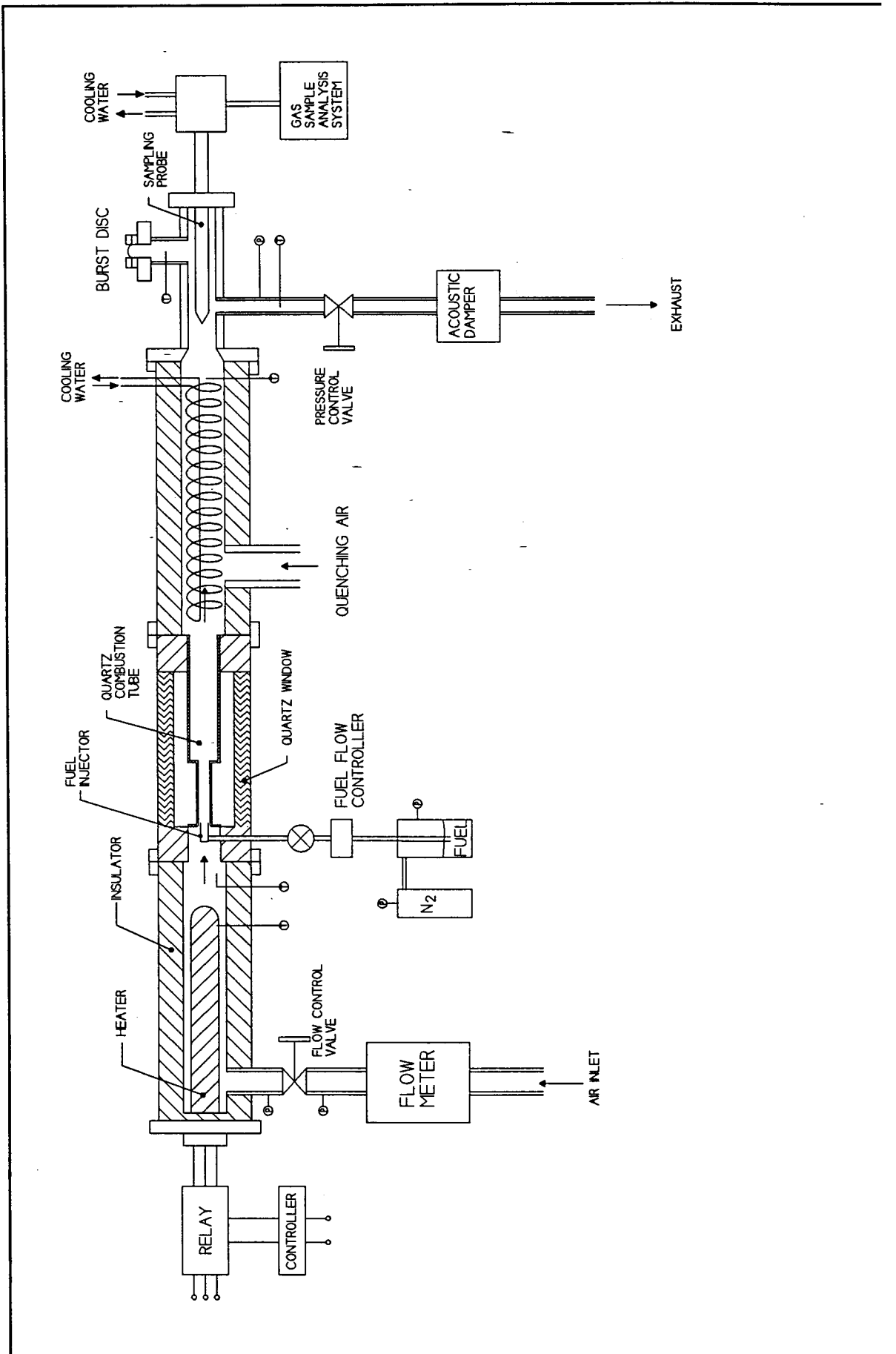


Figure 1 High Pressure / High Temperature Combustion Test Facility

(0.52") i.d. in this case) quartz mixing tube. A short, specially designed stainless steel adapter joins the mixing section to the larger diameter [28 mm i.d. (1.10")] quartz flame tube. The two quartz sections are sealed with loose ceramic fiber insulation and a compression-type fitting. The flow then exits through a longer section of stainless steel tube into the exhaust region. The system is designed to accommodate a variety of fuel injector types and locations.

Fuel was supplied from a nitrogen pressurized steel tank. In all of the visualization tests reported here, the fuel simulant was a mixture of 84% Tetradecane (from Humphrey Chemical Co.), 15% 1-Methylnaphthalene and 1% N N N'-N' Tetramethyl p-phenylenediamine (TMPD) (From Spectrum Chemical Co.) by mass. The chemicals were used and mixed as received. All controls and instrumentation were the same as those reported previously.

The fuel was usually prepared in a 1-2 liter batch. Because oxygen rapidly degrades the TMPD, the fuel tank was always purged with nitrogen prior to filling. Nitrogen was also bubbled through the mixture for 15-30 minutes prior to use.

Since the exciplex fluorescence process is very susceptible to oxygen quenching, it must be carried out in an oxygen-free environment. During any given test, steady state inlet conditions were achieved using air flow. Then, the air flow was stopped and nitrogen flow commenced. The entire system was then purged of air by flowing nitrogen for 2-3 minutes before recording any data.

The fluorescence images were recorded using a Princeton Instruments image intensifying camera employing a 578 x 384 pixel CCD. Exciplex fluorescence was stimulated by 355 nm light pulses from an Nd:YAG laser with a frequency tripling crystal, operating at 10 Hz with a pulse duration of ~8 ns. Light pulses from the laser were passed through an iris to try to eliminate as much of the stray, second harmonic green (532 nm) light as possible, then through a 610 mm focal length quartz spherical lens and a 65 mm focal length quartz cylindrical lens to spread the beam into a sheet and to focus it down to < 0.5 mm width in the test section.

For these experiments, the camera was always positioned to view the test section from the side. The camera and laser sheet were always at right angles. A Nikon 60 mm f/2.8 lens was used to image the test section on the camera CCD. A schematic of this setup is shown in Figure 2.

The vapor and liquid fluorescence signals were separated using a Corion P1-500-R-1952, 500 nm center/10 nm FWHM band pass filter for the green (liquid) signal and a Corion S25-400-R-0008, 400 nm center/25 nm FWHM band pass filter for the blue (vapor) signal. The procedure in a typical exciplex experiment was as follows:

1. Set up the directory structure for storing images on the computer.
2. Set the air flow to the desired value and adjust the inlet temperature set point.
3. Allow air to flow while the system heats up and reaches equilibrium.
4. View images with the CCD camera in real-time in order to focus and adjust its position.
5. Once the system is at equilibrium, position the green filter on the camera lens, and switch to nitrogen flow.
6. Having purged air from the system, begin spraying exciplex liquid.
7. Record a set of liquid images.
8. Switch the filter on the camera and record a set of vapor images.

Included in each set of liquid and vapor images was an image under the same conditions but with no liquid flow, which provided background data. All exciplex images were recorded with the room lights off.

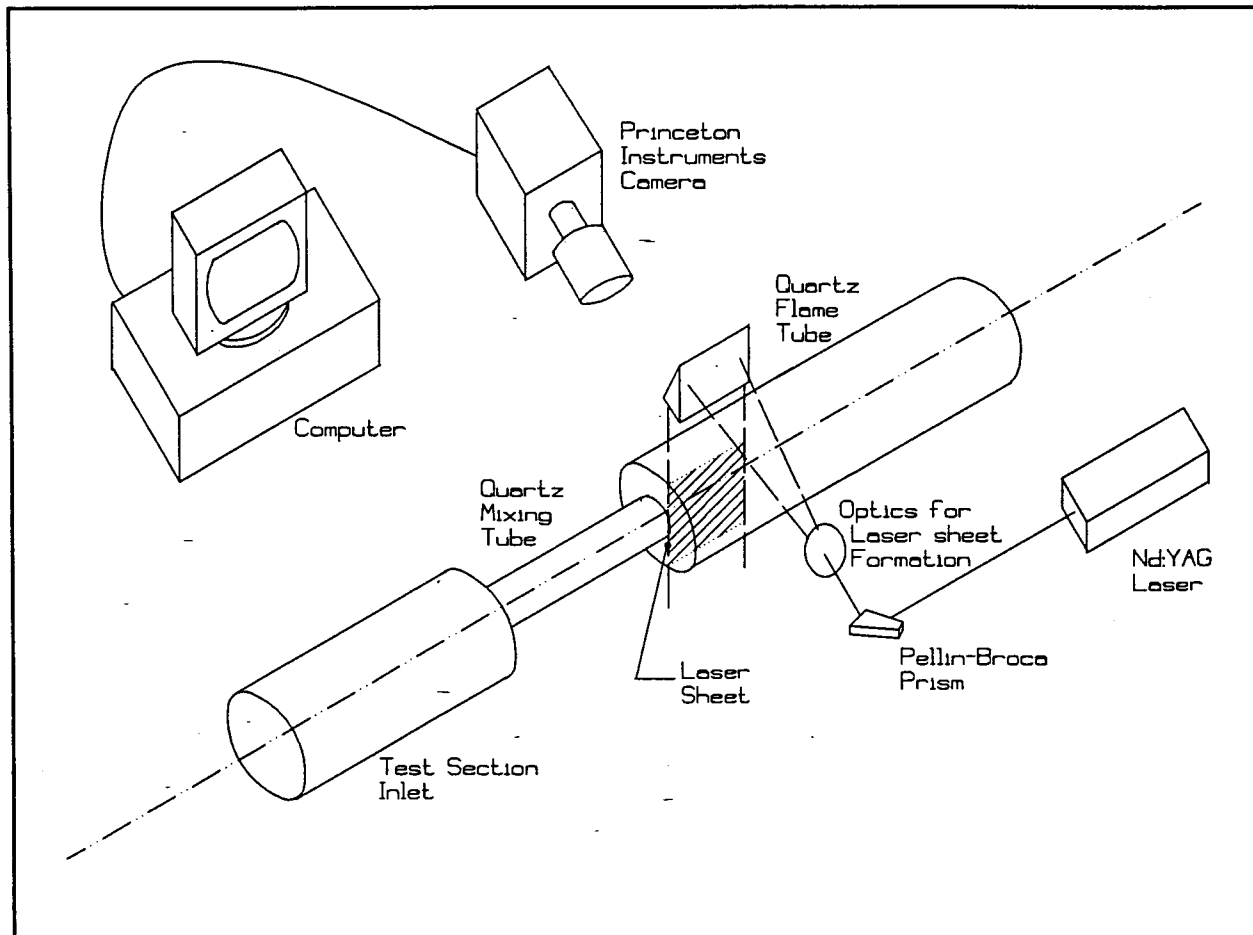


Figure 2 Experimental Setup

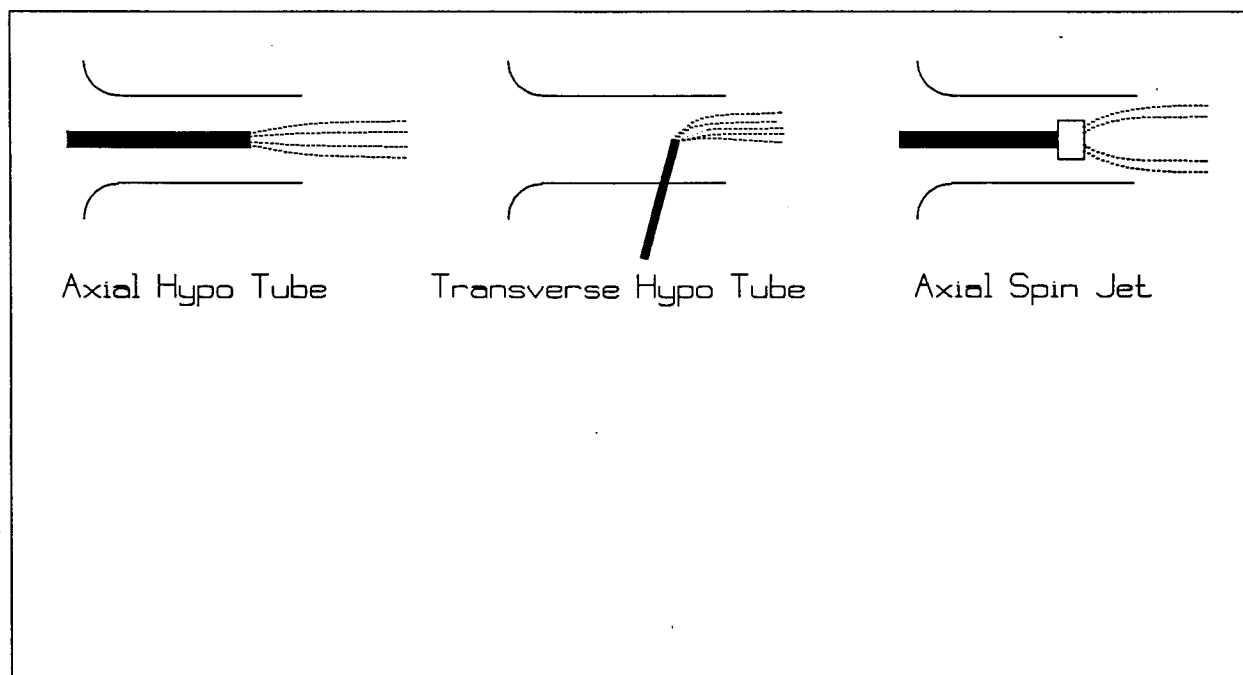


Figure 3 Fuel Injector Configurations

TABLE 1: Test Conditions

Case	Inlet Temp (°F)	System Pressure (psia)	Air(N ₂) Flow Rate (lb/s)	Mixing Tube Air Speed (m/s)	Liquid Flow Rate (lb/hr) for Equivalence Ratios of:				
					0.4	0.5	0.6	0.7	0.8
A (High Inlet Temp)	950	64-66	0.049	100	4.84	605	7.26	\	\
B (Low Inlet Temp)	650	64-66	0.063	100	\	\	9.22	10.8	12.3

The above table summarizes test conditions for all experiments reported herein. Images recorded with the CCD camera are stored on disk and are later viewed and analyzed with the Princeton Instruments CCD Spectrometric Multichannel Analysis Software. Generally, a set of five liquid or vapor images was averaged. The background image was then subtracted to produce a final image. The software can assign colors to the various intensity levels in the image and display a false color image on the video screen. Eventually, a 35 mm color print of this image was made and a set of these prints was given to GE for most of the cases discussed in this report. A recently acquired color printer now enables direct production of a hard copy of the computer image; for most cases, such prints are included with this report.

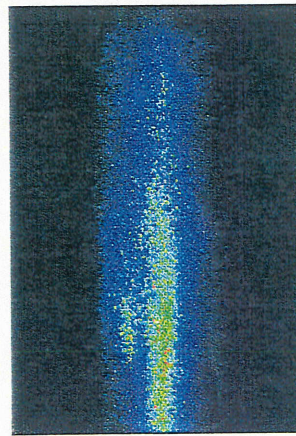
III. TASK 1 - FUEL INJECTOR MODIFICATIONS

Using the 0.5" i.d. mixing tube and an axially positioned hypo tube injector, as shown in Figure 3, a series of liquid and vapor images were recorded in the flame tube at the exit of the mixing tube. The injector tube had a 0.040" o.d. and a 0.020" i.d. Images were recorded at both the high and low temperature conditions of Table 1. Results are shown in Figures 4 and 5. All the images in Figure 4 were recorded at the same camera and lens settings and at the same laser power. The images in Figure 5 were also all recorded at the same settings but those

EFFECT OF EQUIVALENCE RATIO

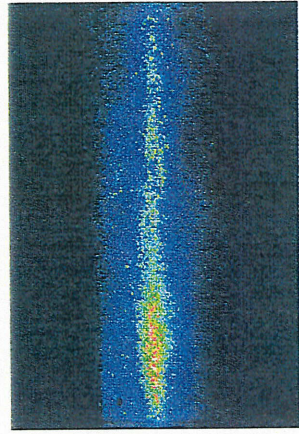
- T = 650 F
- Axial Hypo Tube
- Combustor at Mixing Tube Exit

ER = 0.6

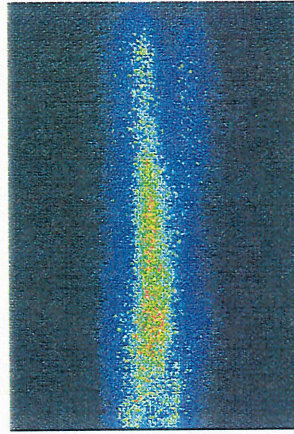


Liquid

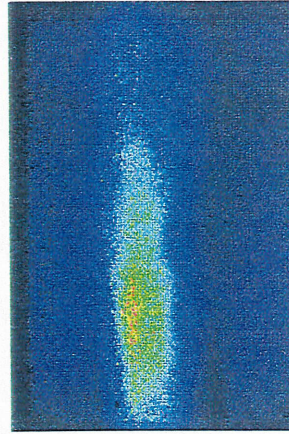
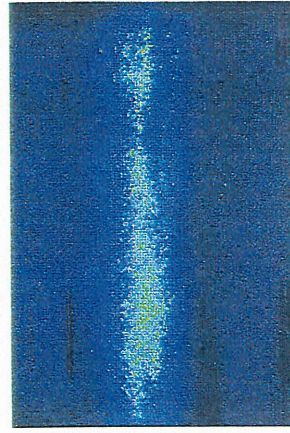
ER = 0.7



ER = 0.8



Vapor



All at f/11 G=7.5 380 mW
All scaled to 2000 max I
Data from 9/3, 9/7, 9/15/93

Figure 4 Axial Hypo Tube Images in the Flame Tube at the Mixing Tube Exit for 650 F Inlet and Three Equivalence Ratios

EFFECT OF EQUIVALENCE RATIO

- $T = 950\text{ F}$
- Axial Hypo Tube
- Combustor at Mixing Tube Exit

ER = 0.4

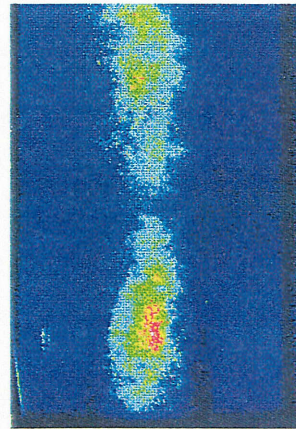
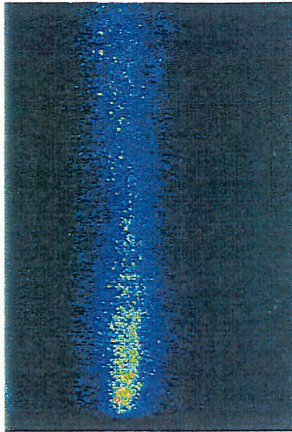


Liquid

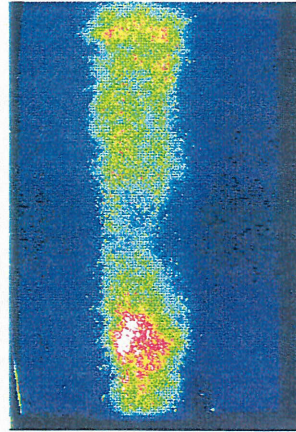
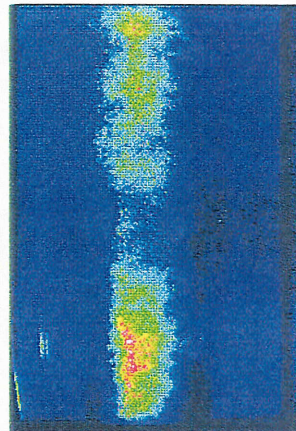
ER = 0.5



ER = 0.6



Vapor



All at $f/11$ $G=8.5$ 390 mW
All scaled to 2000 max I
Data from 11/23-24/93

Figure 5 Axial Hypo Tube Images in the Flame Tube at the Mixing Tube Exit for 950 F Inlet and Three Equivalence Ratios

settings differed slightly from those used in Figure 4. In particular the camera gain used in Figure 5 is higher than that in Figure 4. Thus, no attempt to make quantitative comparisons between Figure 4 and 5 should be made.

With the axial hypo tube injector at the low inlet temperature (Figure 4), the liquid and vapor appear to be confined to a core region near the centerline. The liquid especially shows very little spreading, retaining a jet-like appearance after emerging from the mixing tube. At the high inlet temperature (Figure 5), the liquid and vapor are still heavily concentrated in a central core region, but the vapor shows some spreading to all portions of the flame tube.

In consultations with Paul Heberling and John Matulaitis at GE, it was decided to test an injector employing a Lee Spin Jet tip. This tip was fabricated onto a strut which adapted to the injector ring in the same way as did the axial hypo-tube. Liquid and vapor images were recorded at the mixing tube exit using this injector for the high temperature condition only, and the results are shown in Figure 6. In this case, because of differences in camera and lens settings, the original intensity values have been modified for direct comparison with Figure 5. With the spin jet injector under high inlet temperature conditions (Figure 6), there is more obvious spreading of vapor in the flame tube. Also, with the spin jet, there is much less liquid present, and, there is much more vapor present than there was in the hypo-tube injector case. The spin jet injector does a better job of producing a well-mixed, heavily vaporized region at the exit of the mixing tube.

A direct comparison of three injectors is shown in Figure 7 in which previously recorded images for a transversely mounted hypo tube injector are included. All images have been adjusted and scaled so quantitative comparisons are possible. From this comparison, clearly the axial hypo tube performs worst, leaving much of the liquid unvaporized, and producing a very non-uniform vapor field. While the transverse hypo tube and the spin jet perform somewhat similarly, from the liquid images there is clearly less liquid remaining in the spin jet case. Non-uniformities in the spin jet vapor image were felt to be due more to laser sheet intensity

EFFECT OF EQUIVALENCE RATIO

- T = 950 F
- Lee Spin Jet
- Combustor at Mixing Tube Exit

ER = 0.4

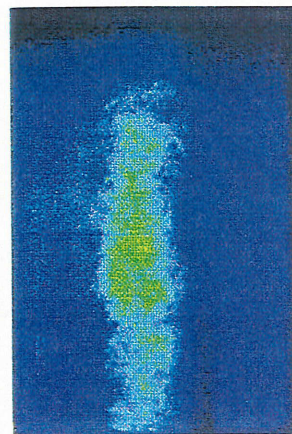


Liquid

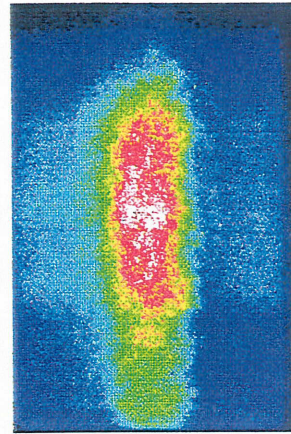
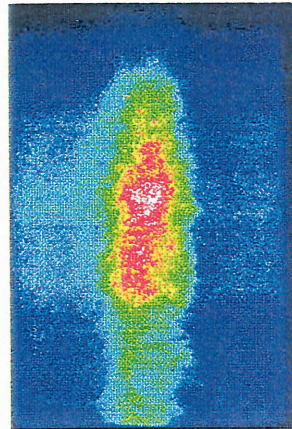
ER = 0.5



ER = 0.6



Vapor



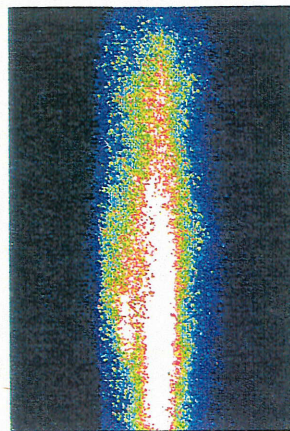
All at f/8 G=8.5 350 mW
All scaled to 2000 max I
Image intensities have been divided
by 2 for comparison with
Axial Hyvo Tube images

Figure 6 Lee Spin Jet Images in the Flame Tube
at the Mixing Tube Exit for 950 F and
Three Equivalence Ratios

FUEL INJECTOR COMPARISON

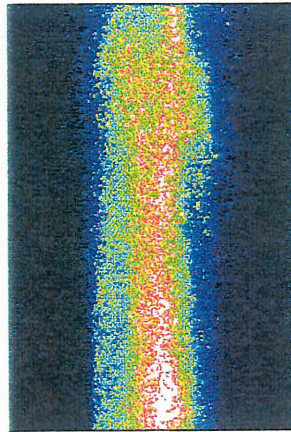
- $T = 650\text{ F}$
- $ER = 0.6$
- Combustor at Mixing Tube Exit

Axial Hypo Tube

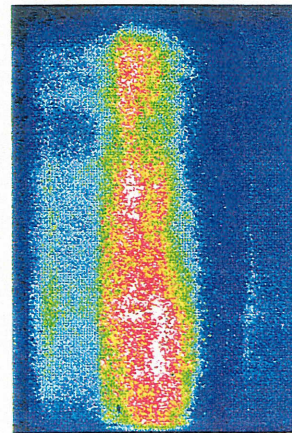
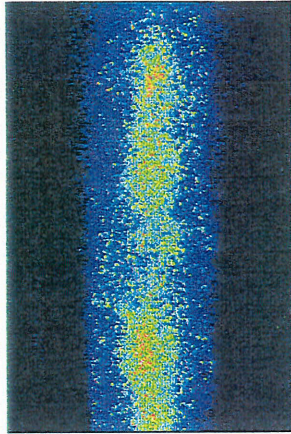


Liquid

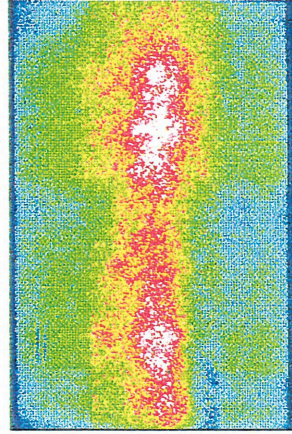
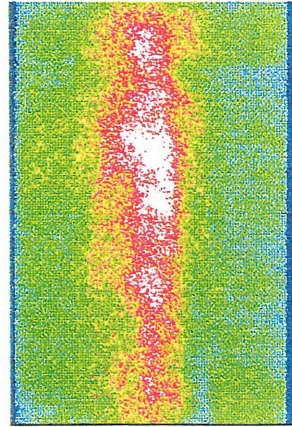
Transverse Hypo Tube
on Centerline



Axial Lee Spin Jet



Vapor



Images adjusted to correct for differing camera gains and lens settings for direct comparisons

Figure 7 Injector Comparison Images in the Flame Tube at the Mixing Tube Exit for a 650 F Inlet and an Equivalence Ratio of 0.6

variations than to actual vapor non-uniformities. The spin jet was thus chosen for use in the mixing tube study of Task 2.

IV. TASK 2 - MIXER TUBE LENGTH REDUCTION

Having selected the Lee Spin Jet injector as providing the best mixing performance, experiments were conducted to record exciplex images along the length of the mixer tube, from the injector tip to approximately 0.5" upstream of the mixer tube exit. A schematic drawing of the image recording areas is shown in Figure 8. Liquid and vapor images were recorded for Positions A, B, C and D, each of which is about 24.5 mm (0.96") in extent. The laser sheet was set to extend over two of these regions at a time, thus minimizing the number of times the laser and optics would have to be moved. However, this introduced the problem that the laser sheet intensity variation is not the same over Region A as it is over Region B, and likewise for Regions C and D. The images though, with the exception of one or two cases, do not show large deficiencies due to this problem.

In a given test, the camera would be set to record images over Position A, with the laser sheet covering A and B. A set of liquid and vapor images would then be recorded for A, and with the system still operating (fuel flow off), the camera moved to record at Position B. Once the liquid and vapor images were recorded at Position B, the system would be shut down and allowed to cool, since positioning the laser sheet requires opening the test section. Then, the laser and optics would be moved and aligned to cover Positions C and D, and the camera moved on a traverse to Position C. Finally, the system would be re-started, brought to operating temperature as previously described, and liquid and vapor images recorded for Positions C and D.

Mixing tube images were recorded using the Lee Spin Jet injector at both the low and high temperature conditions, at the single equivalence ratio of 0.6, which is common to both inlet temperature conditions. These spin jet images, which were recorded under identical camera, lens and laser conditions, are shown in Figures 9 and 10. Also, mixing tube images

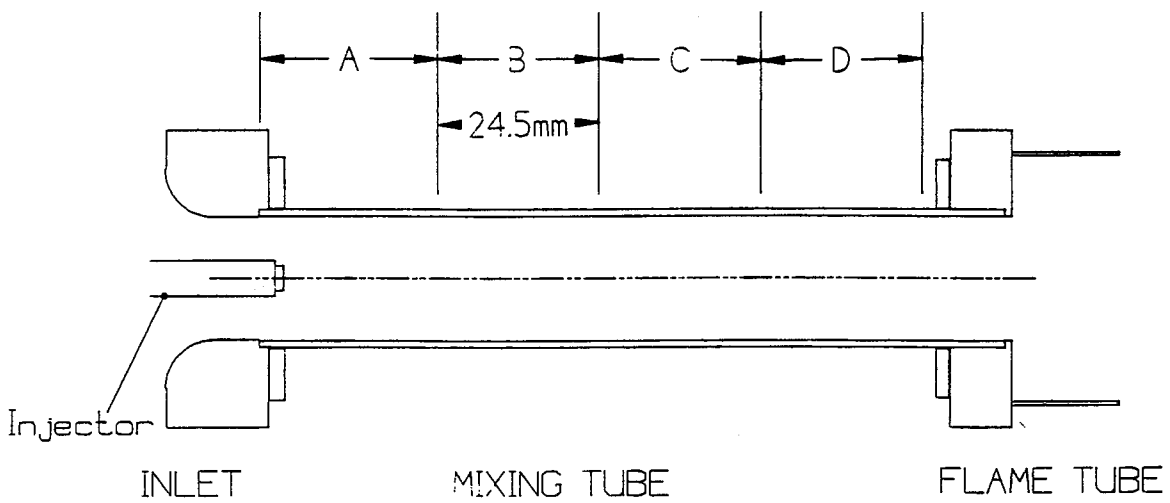


Figure 8 View Locations and Extent for Mixing Tube Images

MIXING TUBE IMAGES LEE SPIN JET INJECTOR

- Tube dia = 0.5 in.
- Air Speed = 100 m/s
- ER = 0.6
- T = 650 F

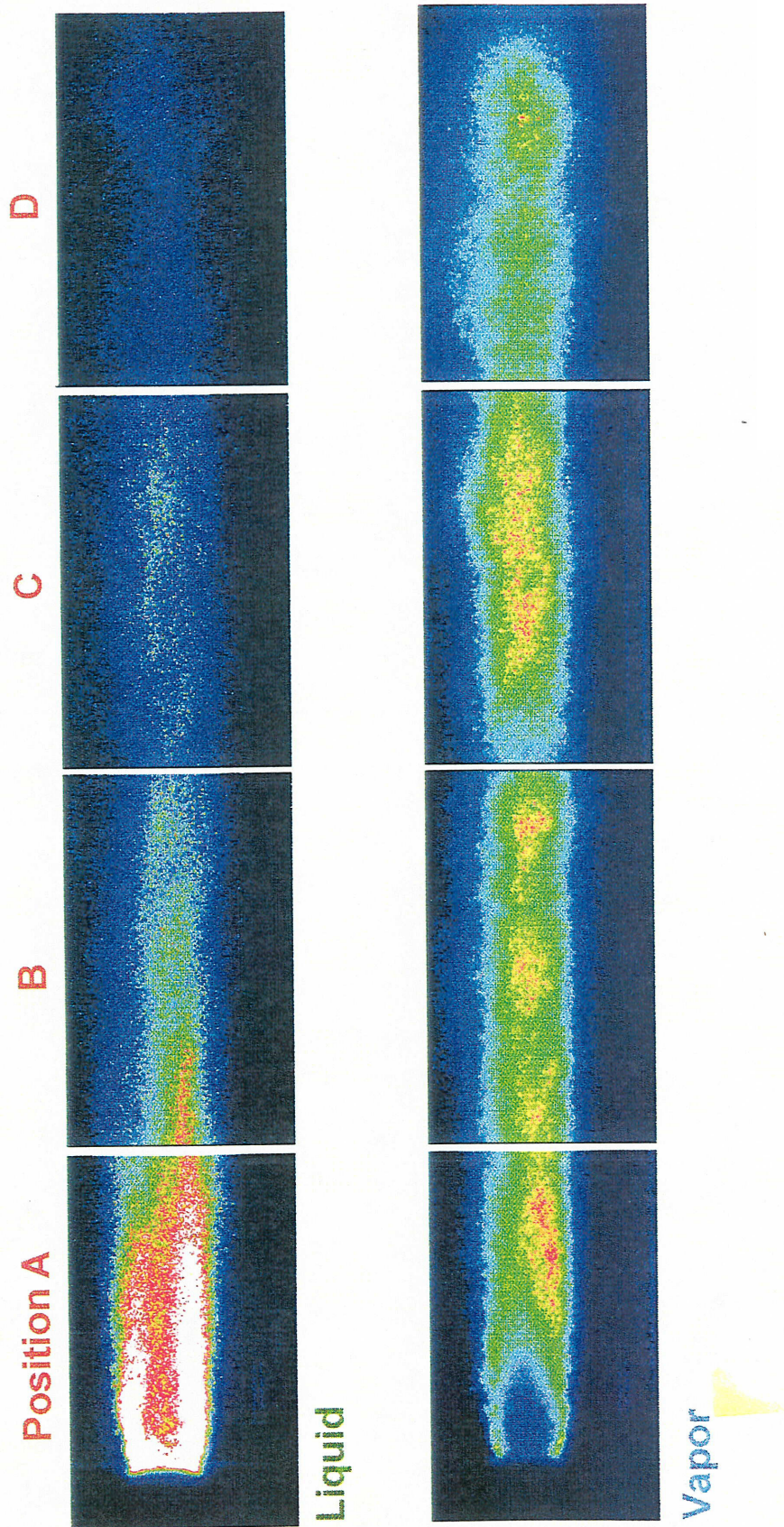


Figure 9 Mixing Tube Images with the Lee Spin Jet Injector for 650 F Inlet and an Equivalence Ratio of 0.6

MIXING TUBE IMAGES LEE SPIN JET INJECTOR

- Tube dia = 0.5 in. • Air Speed = 100 m/s
- ER = 0.6 • T = 950 F

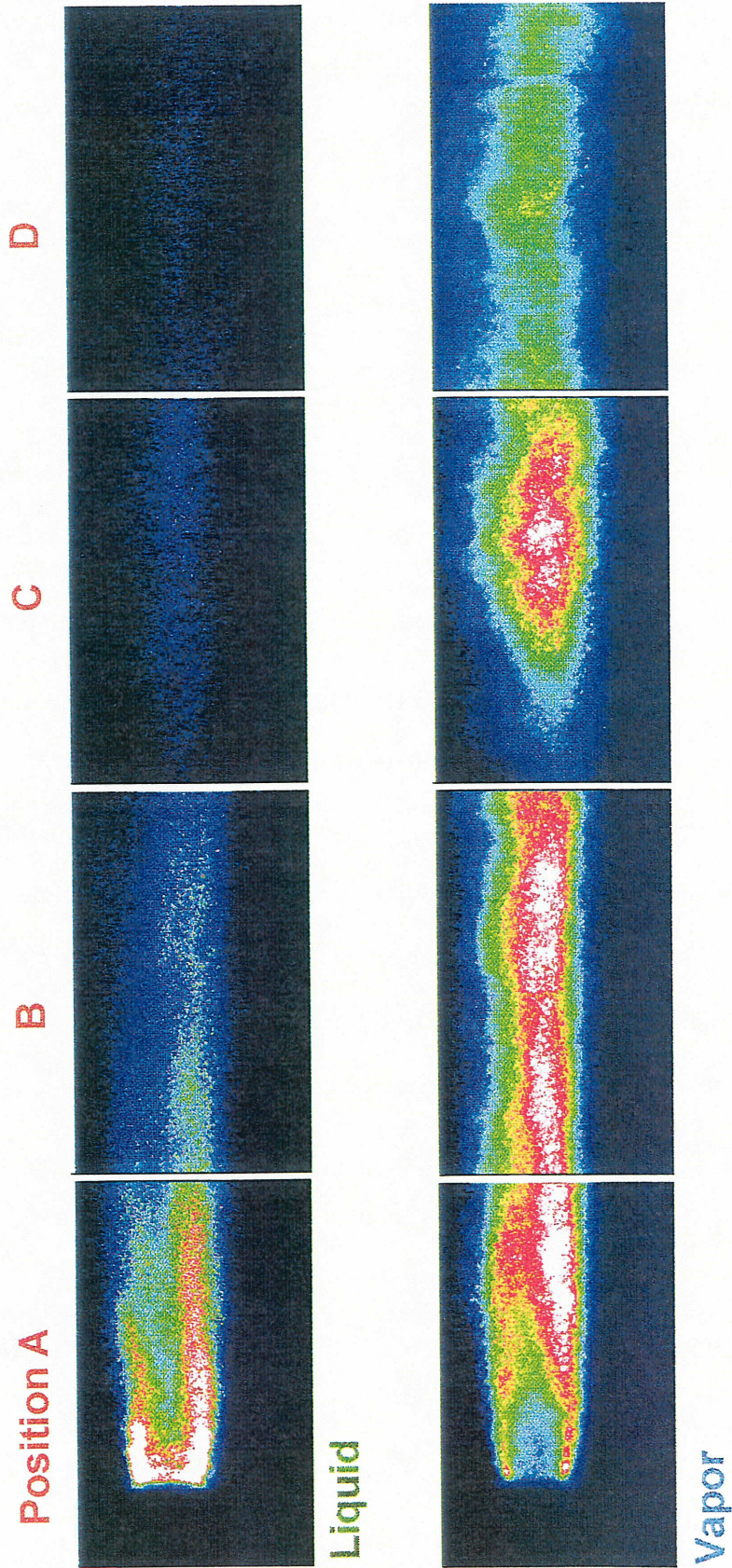


Figure 10 Mixing Tube Images with the Lee Spin Jet Injector for 950 F Inlet and an Equivalence Ratio of 0.6

were recorded for the transversely mounted hypo tube injector positioned with its tip on the flow centerline for the low temperature case, as shown in Figure 11, for comparison purposes.

Comparing Figures 9 and 10, one can see that there is more vapor present at each location at the higher temperature inlet condition than at the lower, as would be expected. There is also some indication of vapor hitting the upper wall of the mixer tube (Figure 9, Positions C and D), but this may have been due to a slight asymmetry in the construction of the nozzle support strut itself. It can be seen that very little liquid remains at the end of the mixing tube in the high temperature case. Note that there is a clear discontinuity in the vapor sequence of Figure 10 at Position C. While great care is exercised in aligning the laser sheet with the field of view of the camera, apparently in this case, there was poor alignment; the low intensity region at the upstream end of Figure 10C (vapor) was due to the alignment of the field of view with the edge of the laser sheet, rather than with the more uniform central portion of the sheet.

In an attempt to better quantify these results, a parameter proportional to the mass of liquid or vapor was calculated for each image and plotted against location in the mixing tube for the Spin Jet injector. For these calculations, it was assumed that the flow was axisymmetric about an axial line defined by the radial coordinate of the "center of mass" of the entire image. The results of these calculations are shown in Figures 12 and 13, where the disappearance of liquid along the length of the mixing tube is clearly shown. However, the trend of the vapor data is not so easily interpretable, for example, the vapor signal has a temperature dependence which we are presently investigating. The graphs along with the images do show that 98% vaporization cannot be achieved in the present mixing tube length, especially at the lower inlet temperature. In the high temperature case, there clearly appears to be greater vaporization but not enough to insure that only 2% or less of the liquid remains. Thus, it was concluded that there is no reason to shorten the mixing tube.

MIXING TUBE IMAGES TRANSVERSE HYPO TUBE ON CENTERLINE

- Tube dia = 0.5 in.
- Air Speed = 100 m/s
- ER = 0.6
- T = 650 F

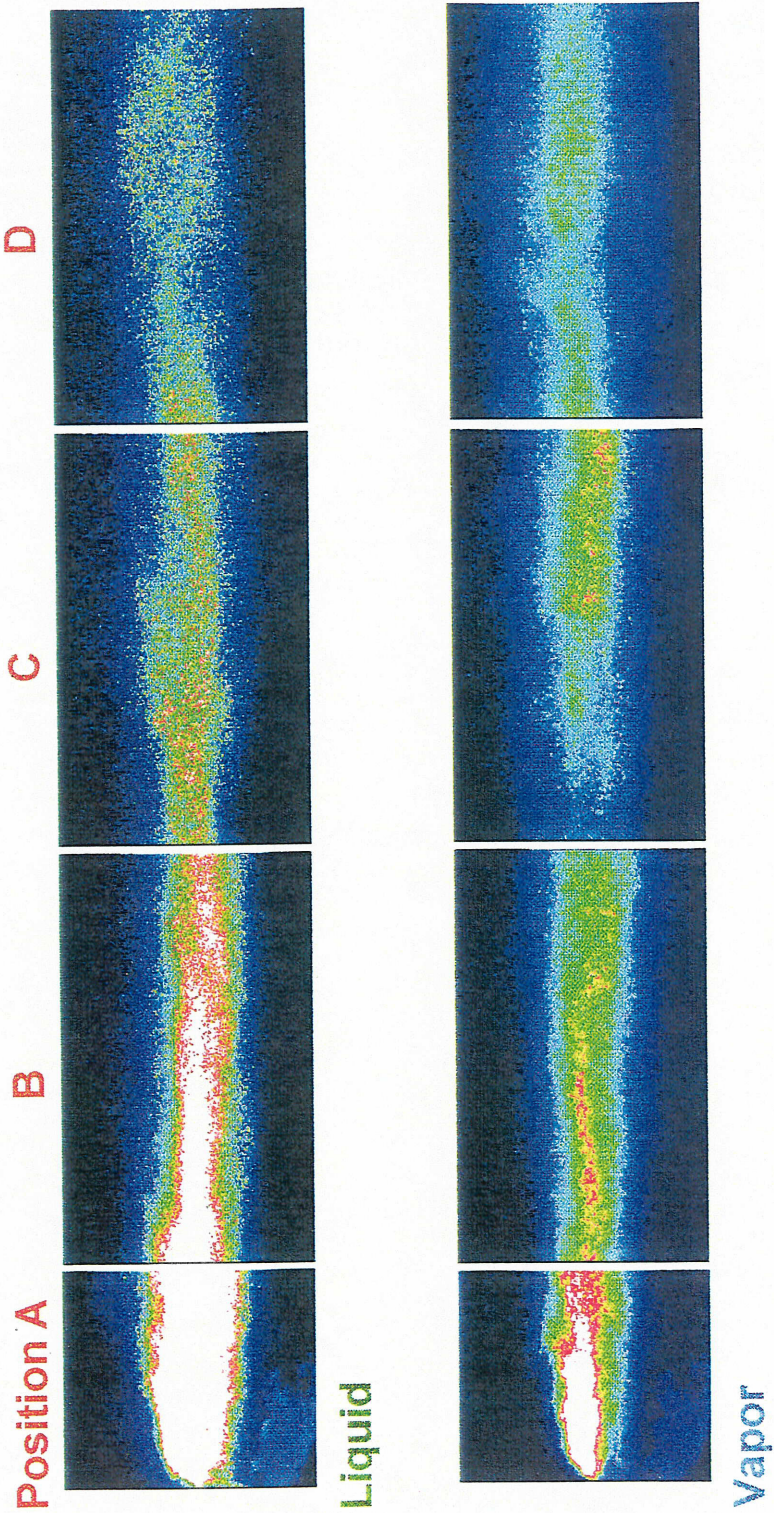


Figure 11 Mixing Tube Images with the Transverse Hypo Tube Injector on the Centerline for 650 Inlet and an Equivalence Ratio of 0.6

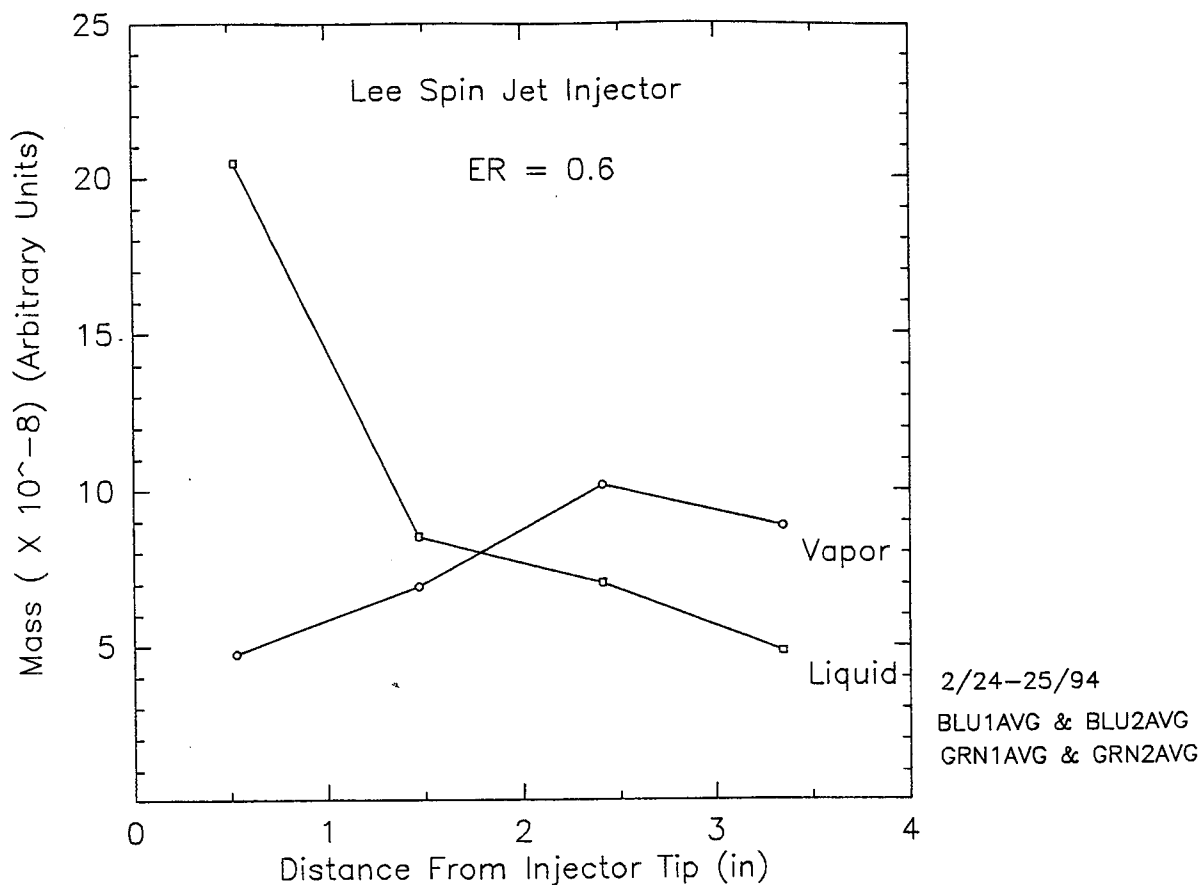


Figure 12 Calculated Mass Parameter Along the Mixing Tube with 650 F Inlet

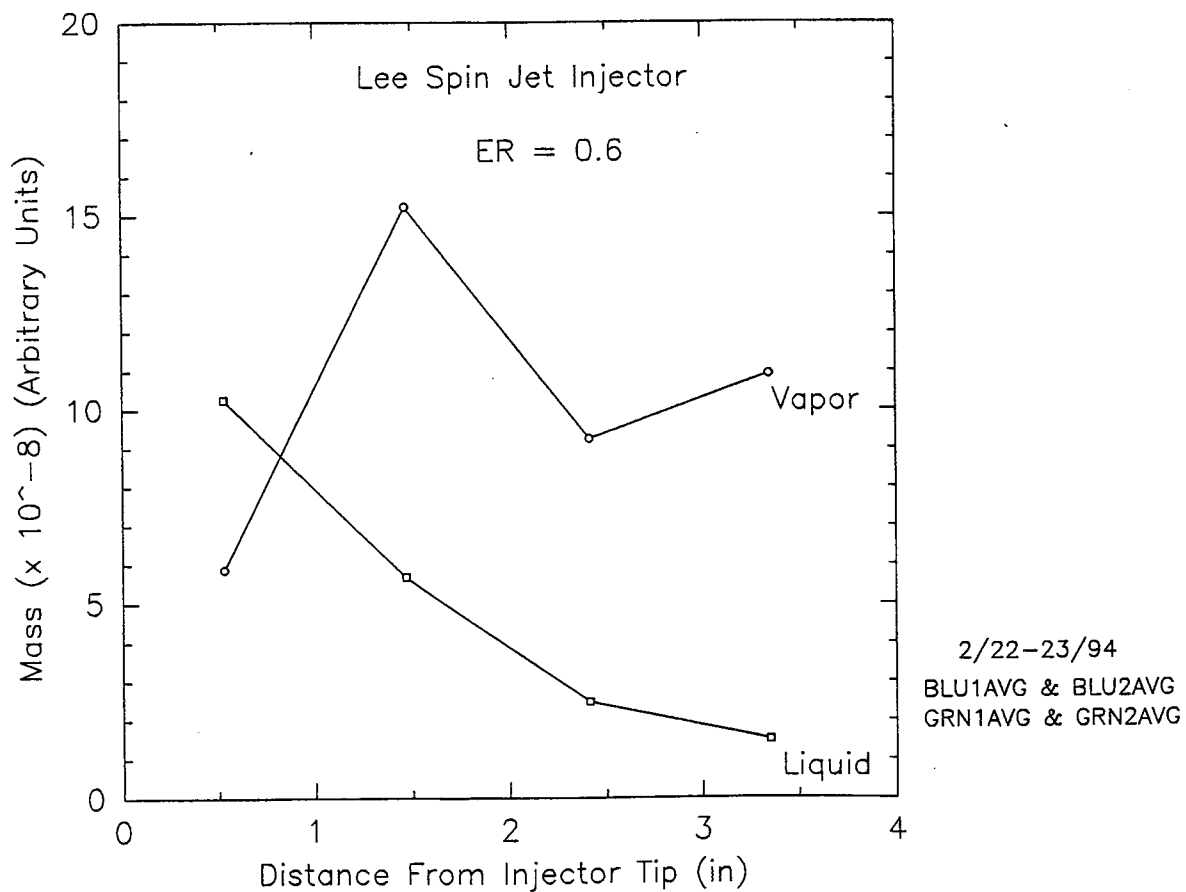


Figure 13 Calculated Mass Parameter Along the Mixing Tube with 950 F Inlet

V. TASK 3 - MIXER TUBE DIAMETER MODIFICATIONS AND TASK 4 - AIR INJECTION AT THE MIXER TUBE EXIT

The objective of Task 3 is to evaluate the effect of increased mixer tube diameter (while maintaining the area ratio for the flame tube diameter) on the degree of vaporization using the previously chosen injector and mixer tube length. In Task 4, this larger diameter system is to be used to evaluate the effect of air injection at the mixer tube exit on fuel mixing and vaporization.

To meet these objectives, a new system was designed and built which employs a 0.67" (17 mm) i.d. quartz mixing tube and a 1.46" (37 mm) i.d. quartz flame tube. The two tubes are held together by a stainless steel joiner, shown in Figure 14. This joiner incorporates internal passages which allow air injection to the mixer tube just upstream of its exit at the flame tube. The interchangeable ring shown in Figure 14 permits use of the system without air injection simply by using a ring with no holes through its wall. The new system is set up so that a portion of the main air flow can be bled off and separately controlled, metered, and pre-heated before it is injected.

In consultation with Paul Heberling and John Matulaitis at GE, however, it was decided to postpone running experiments using this larger diameter system in favor of further testing of three new injector tip geometries in the original, 0.5" diameter mixing tube.

VI. CONTINUED FUEL INJECTOR MODIFICATIONS

Discussions with Paul Heberling and John Matulaitis conveyed that there was keen interest in trying to develop a style of hypo tube injector tip which would perform as well as the Spin Jet tip. Various tip designs were discussed and GE fabricated and sent to us three for testing. These tips and their positioning are shown in Figure 15.

Exciplex imaging experiments were run with these three tips at an inlet temperature of 650°F and an equivalence ratio of 0.6. In the same manner as previously reported in Section IV,

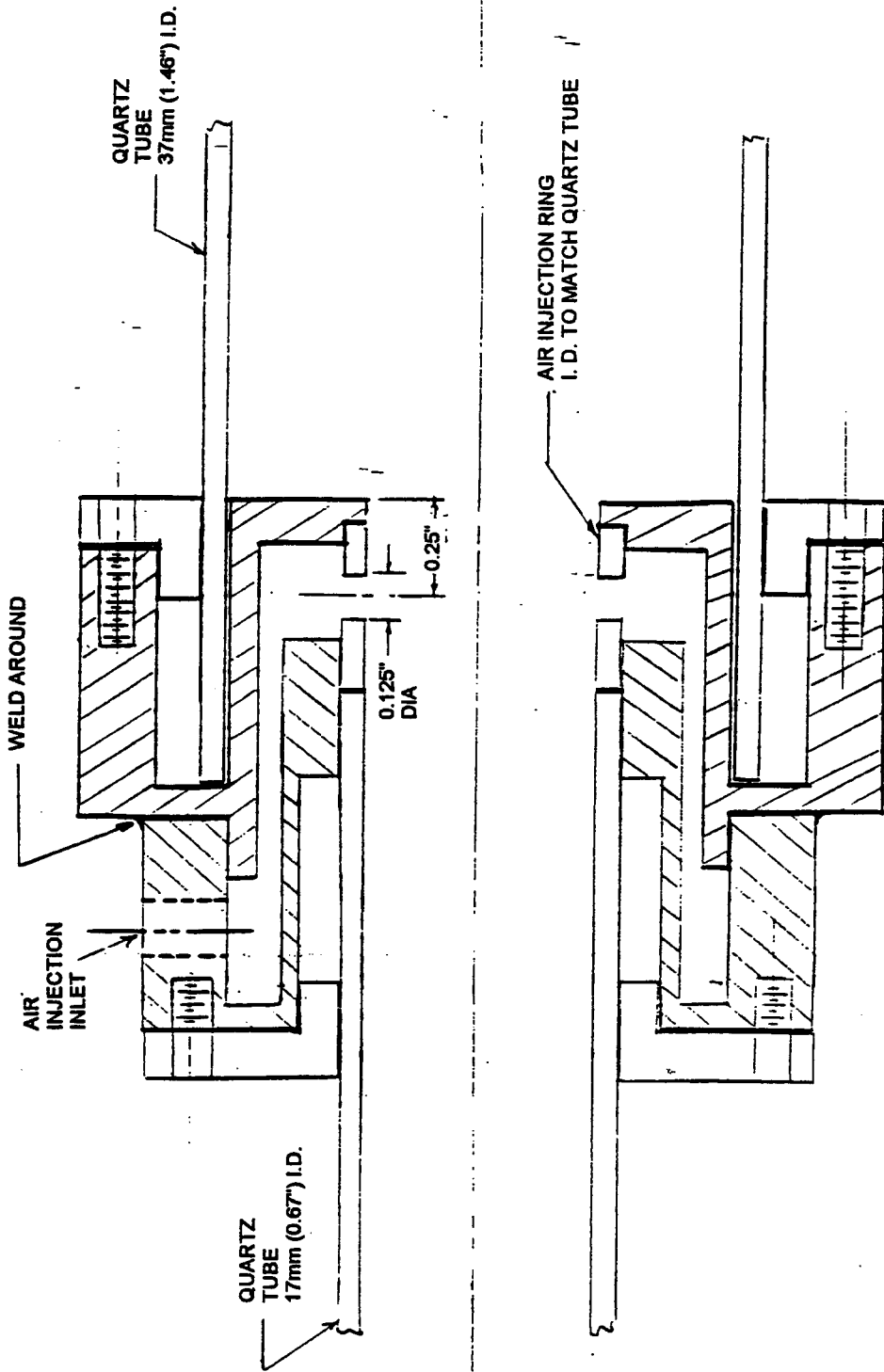
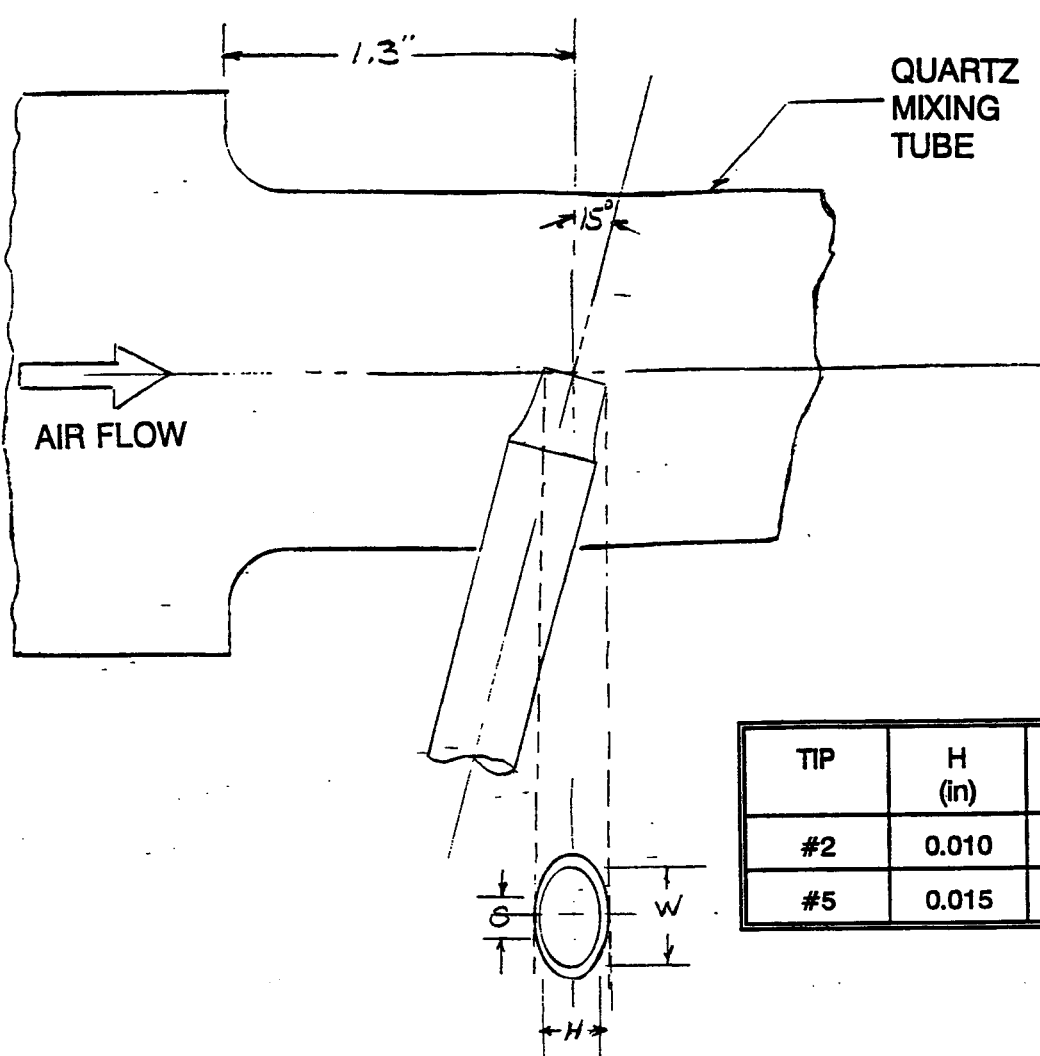
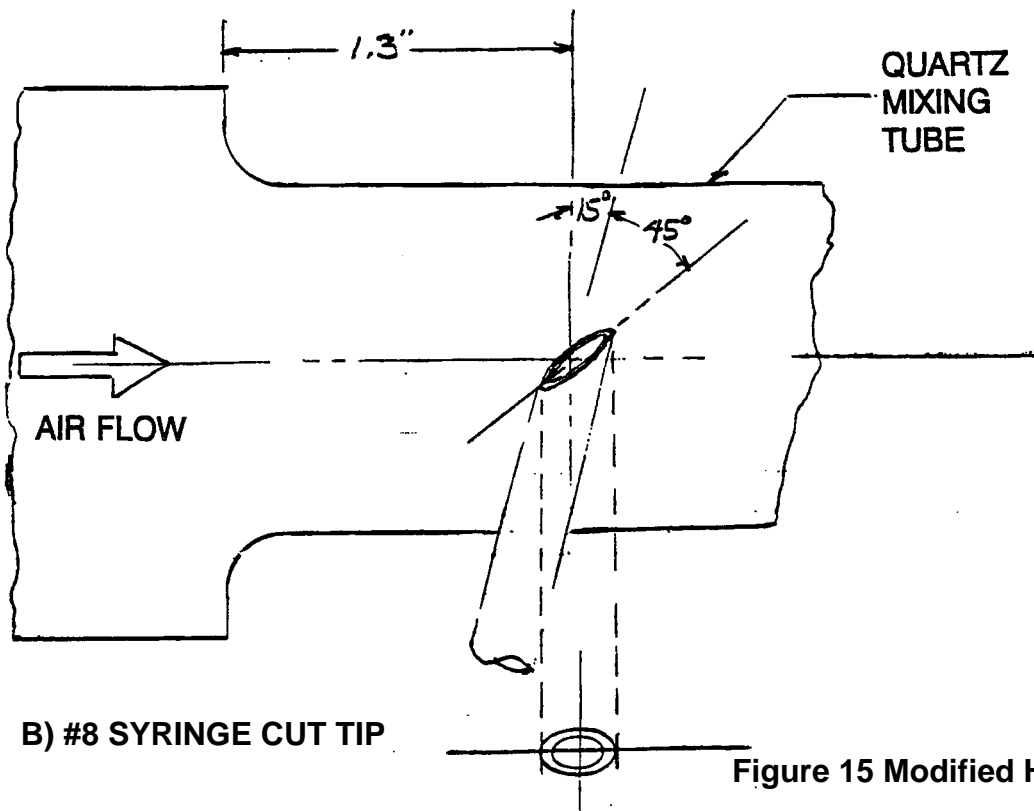


Figure 14 Transition Piece with Air Injection for Larger Diameter Mixing Tube



A) #2 & #5 OVALIZED FAN SPRAY TIPS



B) #8 SYRINGE CUT TIP

Figure 15 Modified Hypo Tube Injector Tips

liquid and vapor images were recorded along the mixing tube at positions A, B, C and D (Figures 16-18), as well as at the mixing tube exit in the flame tube (Figures 19-21) for each nozzle tip.

In these tests, the images are not the result of averaging a group of five laser shots, as in all previously shown images, but are individual records of a single laser shot. This was done because we came to realize that the result of averaging five images does not represent a true average in this highly turbulent flow.

In the mixing tube images, Figures 16-18, the field of view in the streamwise direction is about 24.5 mm (0.96") for positions B, C and D, and about 19.0 mm (0.75") for Position A. All the images were recorded under the same laser, camera and lens conditions. The intensity false-color scaling is the same in all the liquid images, and in all the vapor images (but not the same from liquid to vapor).

In the flame tube images (Figures 19-21), the streamwise field of view is about 42.7 mm (1.68"). The intensity false color scaling is the same in all flame tube images, and the same for liquid and vapor pictures, but is not the same as that in the mixing tube images. Note that the oddly shaped, glowing region around the base of the injector in the mixing tube images (Position A) is an image of the cement used to hold the injector in place. It either fluoresces itself when struck by the UV laser light, or is reflecting fluorescence from the brightly fluorescing fuel.

From reviewing the images, perhaps one of the most noticeable things about them is how similarly the three injectors seem to behave. In the mixing tube images, with the injector tip on the centerline, the images for all three injectors show that neither vapor nor liquid is significantly present in the bottom say quarter of the mixing tube. The hypo tube creates a wake region, and the fuel just never gets into that region, at least in the mixing tube. In general, the liquid and vapor are still confined to the middle region of the tube, though perhaps the #2 fan tip and the #8 syringe cut tip seem to spread the fuel out vertically a little better than does the #5 fan tip. It should be noted that we cannot tell from these images what the fuel distribution is like in the third dimension; however, perhaps we can conclude that the

MIXING TUBE IMAGES TRANSVERSE HYPO TUBE #2 FAN TIP ON CENTERLINE

- Tube dia = 0.5 in.
- Air Speed = 100 m/s
- ER = 0.6
- T = 650 F

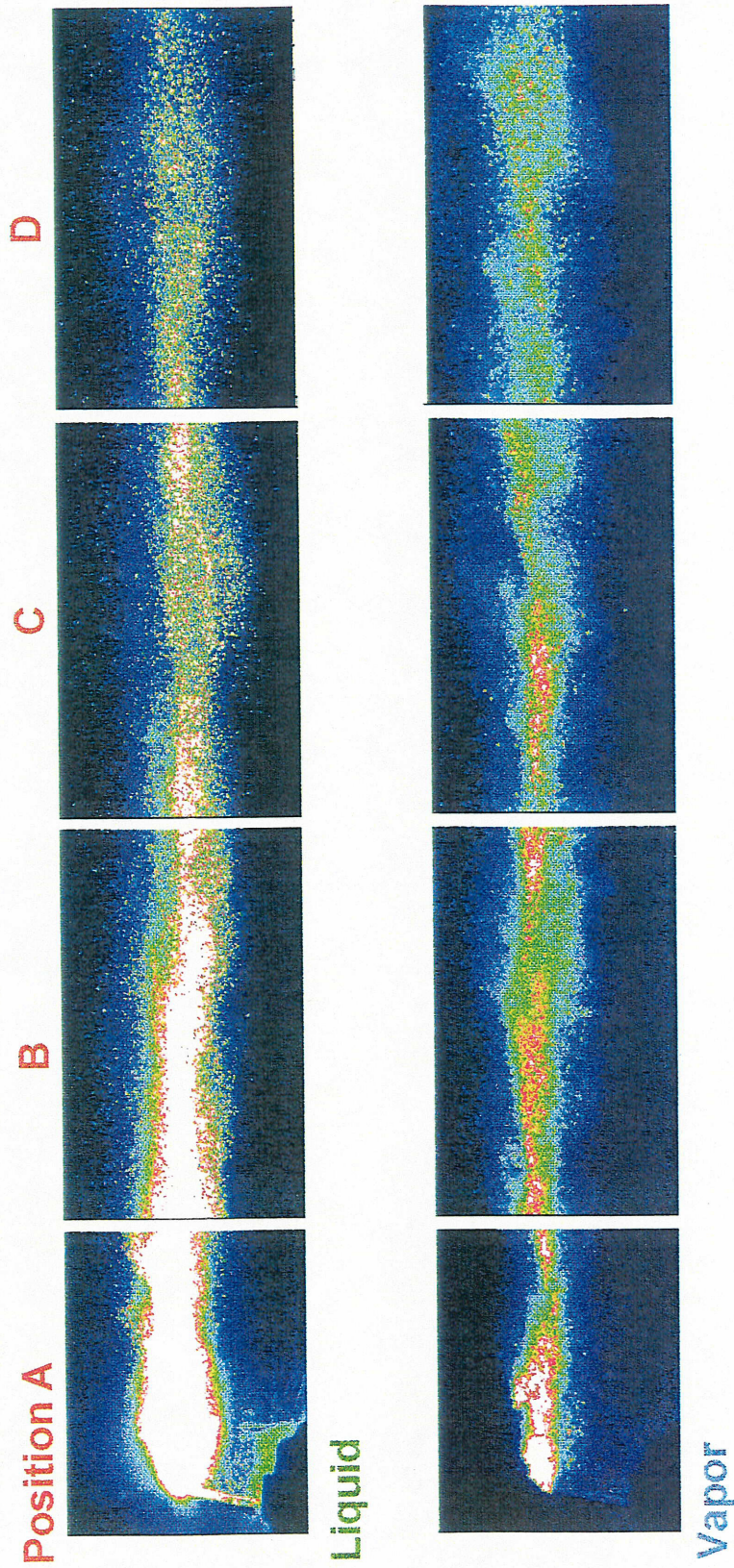


Figure 16 Mixing Tube Images with the #2 Fan Tip Hypo Tube Injector on the Centerline for 650 F Inlet and an Equivalence Ratio of 0.6

**MIXING TUBE IMAGES
 TRANSVERSE HYPO TUBE
 #8 SYRINGE CUT TIP ON CENTERLINE**

- Tube dia = 0.5 in.
- ER = 0.6
- Air Speed = 100 m/s
- T = 650 F

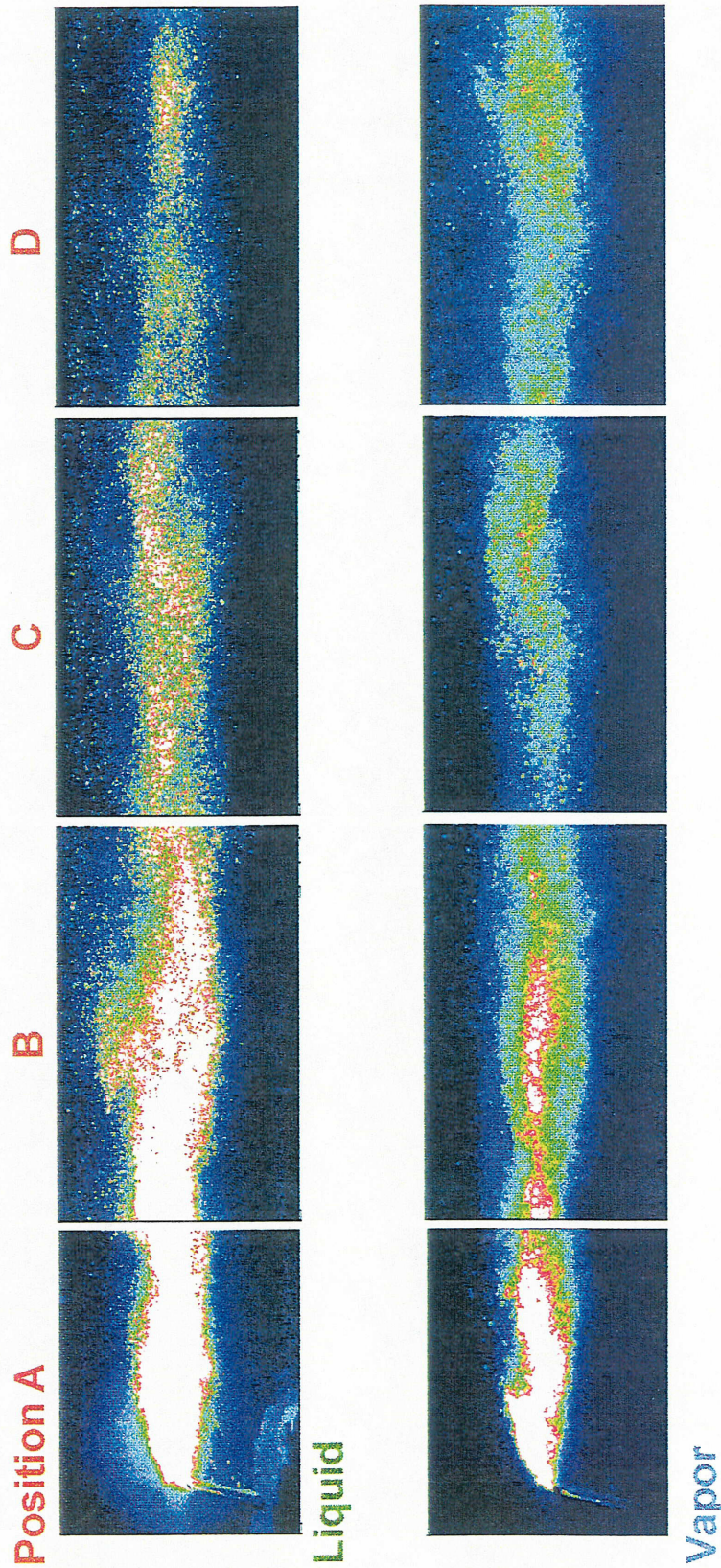


Figure 17 Mixing Tube Images with the #8 Syringe Cut Tip Hypo Tube Injector on the Centerline for 650 F Inlet and an Equivalence Ratio of 0.6

MIXING TUBE IMAGES TRANSVERSE HYPO TUBE #5 FAN TIP ON CENTERLINE

- Tube dia = 0.5 in.
- ER = 0.6
- Air Speed = 100 m/s
- T = 650 F

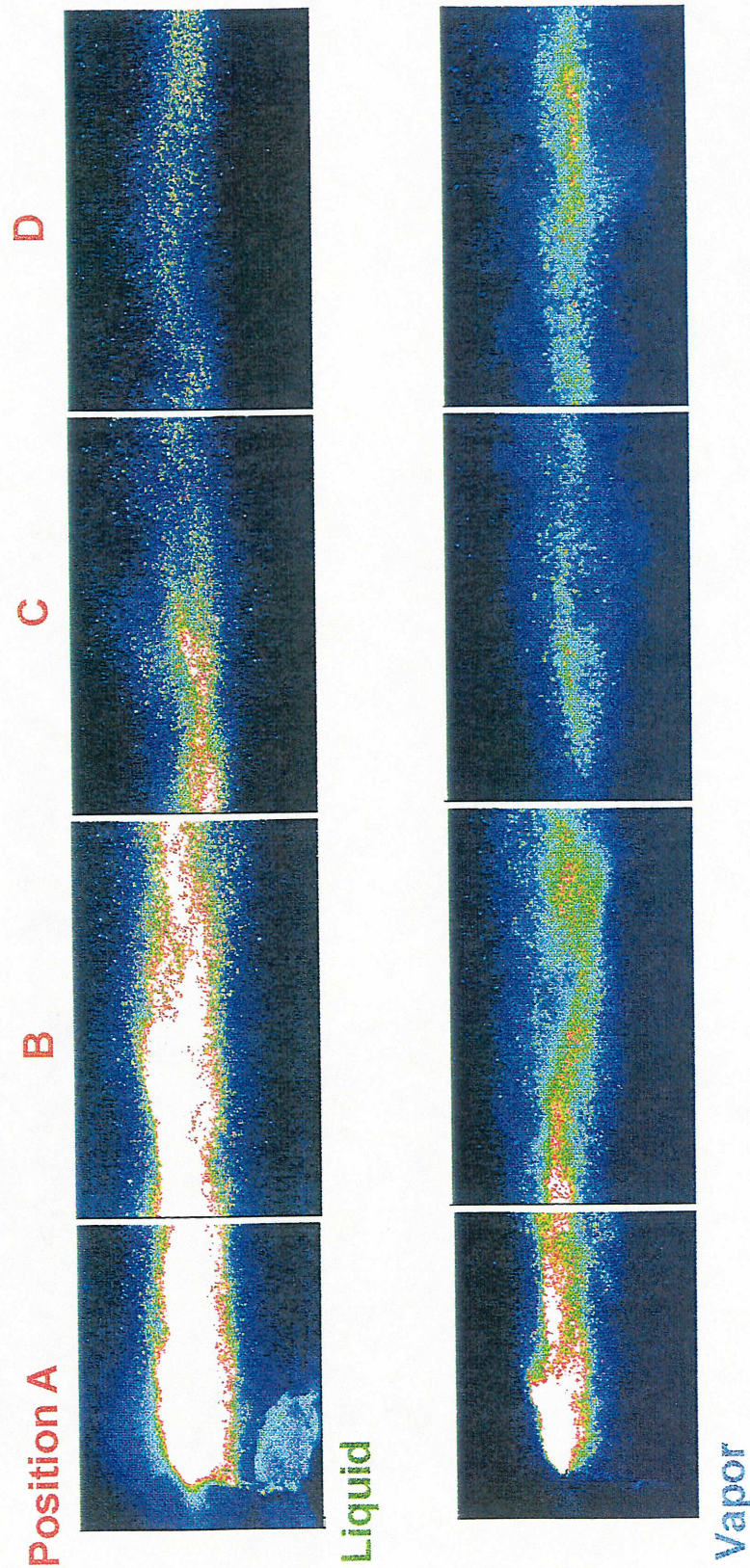
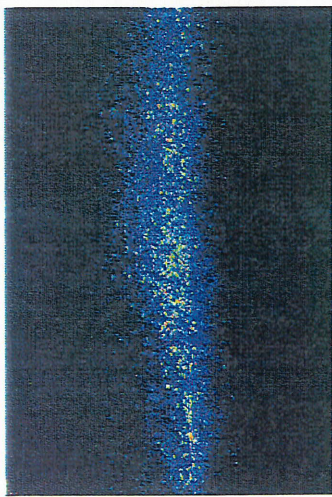


Figure 18 Mixing Tube Images with the #5 Fan Tip Hypo Tube Injector on the Centerline for 650 F Inlet and an Equivalence Ratio of 0.6

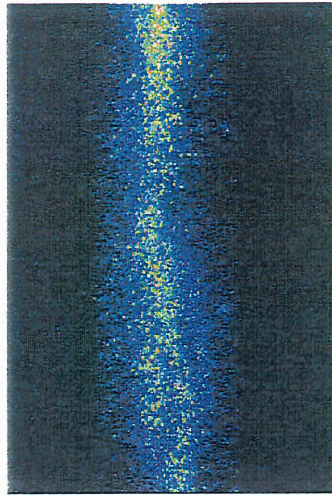
5/26/94 #2 Fan Tip Hypo Tube on Centerline



g2.2

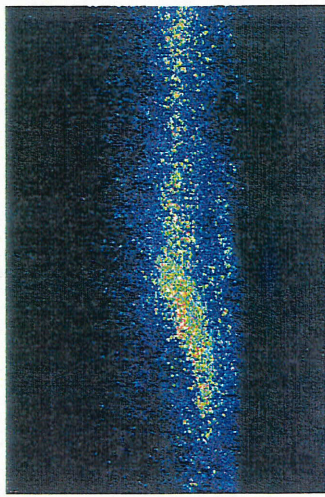


g2.3

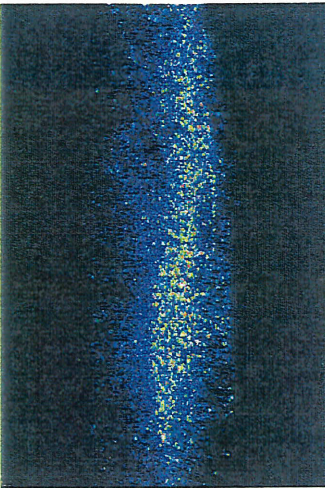


g2.4

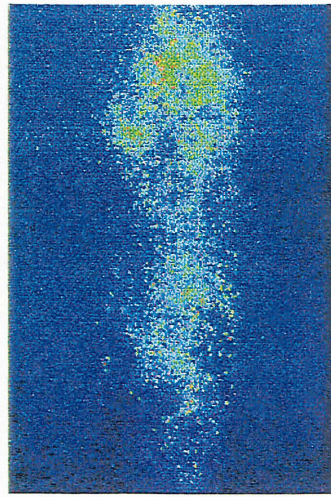
Liquid



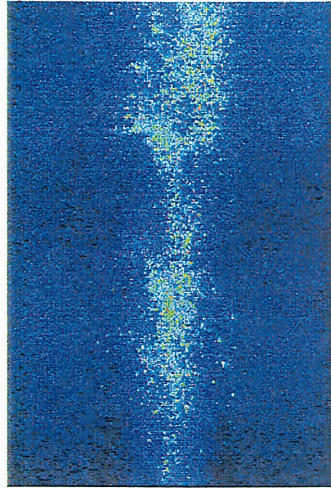
g2.5



g2.6



b2.2



b2.3

Vapor

All scaled to 2000 max
f/16 G=8.5 350 mW
Scale: 40% in PwrPt

Figure 19 Flame Tube Images at the Mixing Tube Exit with the #2 Fan Tip Injector on the Centerline for 650 F Inlet and an Equivalence Ratio of 0.6

6/3/94 #8 Syringe Cut Tip Hypo Tube on Centerline

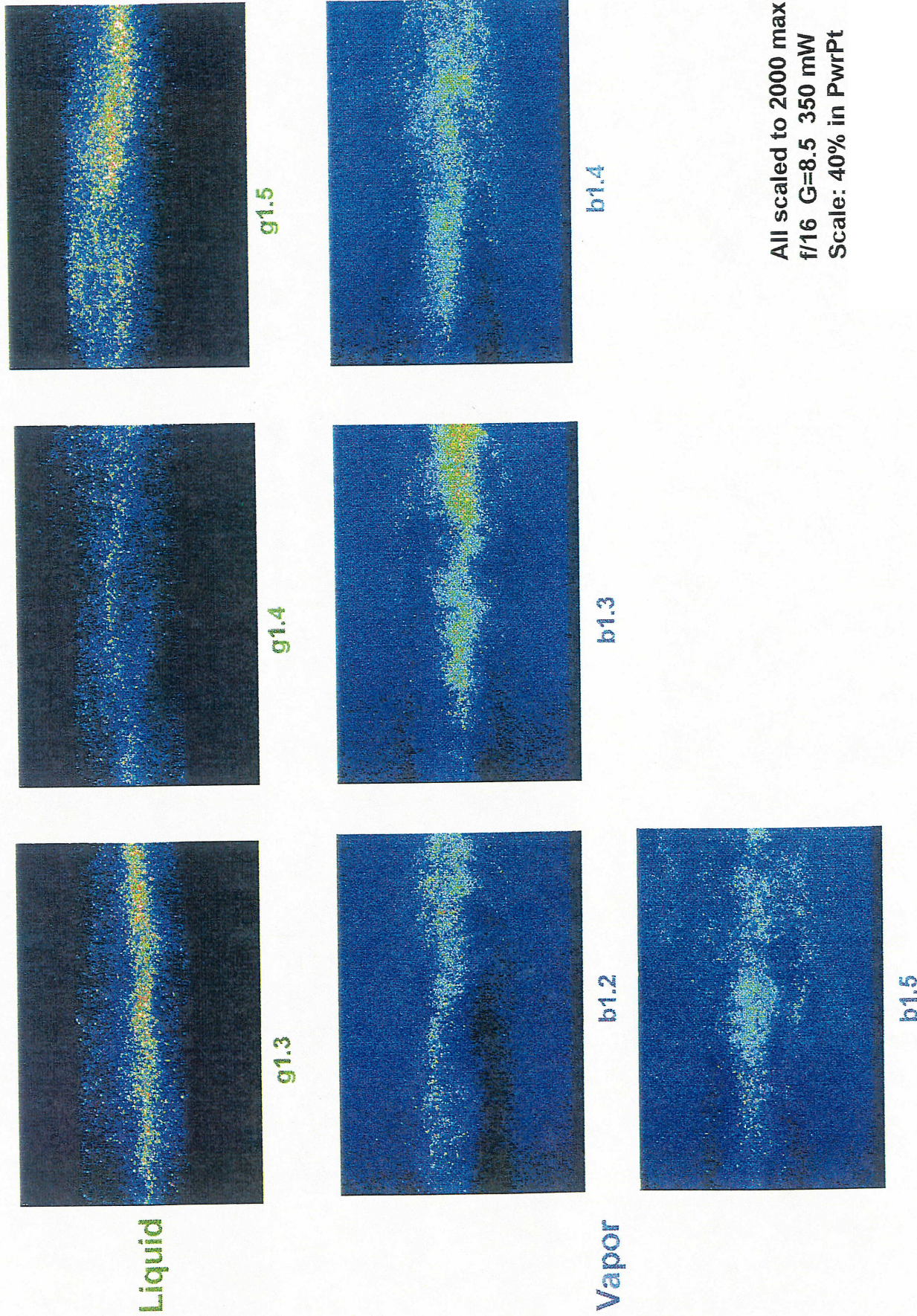
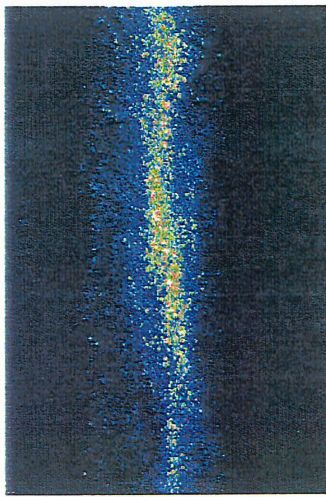


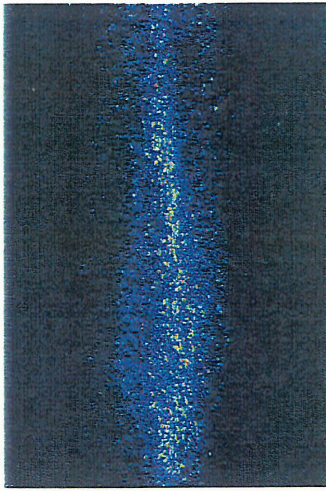
Figure 20 Flame Tube Images at the Mixing Tube Exit with the #8 Syringe Cut Tip Injector on the Centerline for 650 F Inlet and an Equivalence Ratio of 0.6

6/9/94 #5 Fan Tip Hypo Tube on Centerline

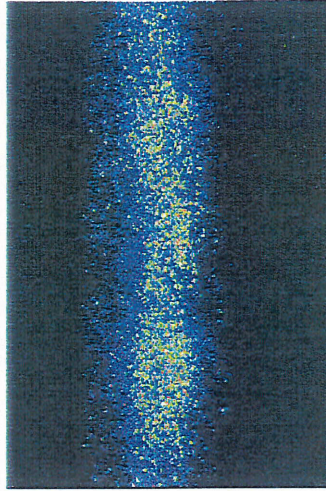


Liquid

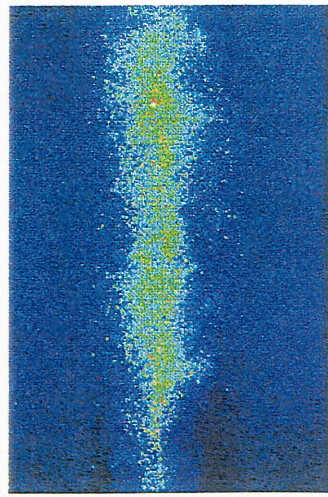
g1.2



g1.3

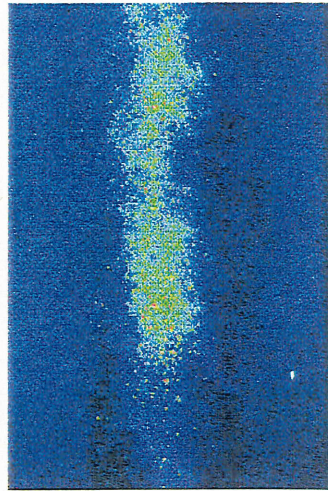


g1.4

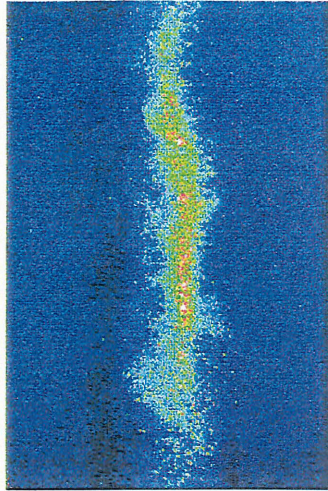


b1.2

Vapor



b1.3



b1.4

All scaled to 2000 max
f/16 G=8.5 350 mW
Scale: 40% in PwrPt

Figure 21 Flame Tube Images at the Mixing Tube Exit with the #5 Fan Tip Injector on the Centerline for 650 F Inlet and an Equivalence Ratio of 0.6

that direction than does the syringe-cut tip, simply by virtue of their shape. The combustor images (at the mixing tube exit) also appear strikingly similar. In all cases, the remaining liquid is clearly confined to a central core region. The vapor does spread to most regions of the field of view, but is still noticeably more concentrated near the centerline.

From visual observation of the injection process in the mixing tube with the laser firing, it was seen that the fuel stream generally dances around wildly but does seem to favor the top half of the tube, as shown in the images. Also, it seemed that some fuel always hit the upper wall of the mixing tube before reaching its exit. Confirmation of this can be seen in the last vapor images of Figures 16 and 17.

The main conclusions from this portion of the study are that no one hypo tube injector tip configuration performs much better than any other. Perhaps averaging over many images would reveal some clear distinction; development of an averaging method will be discussed in the next section. Also, at least with the tips positioned as they were, on the centerline, the fuel is not distributed well in the combustor. Instead, the liquid, and to a lesser extent, the vapor and fuel tend to remain confined to a core, jet-like region near the centerline.

VII. AVERAGING OF IMAGES

Because of the highly turbulent nature of this flow, individual images recorded with a single laser shot can vary considerably. Thus, average images are more useful and meaningful for comparisons with predictions and actual combustor performance. However, having observed many images which were the result of averaging five individual images, it was concluded that the result of averaging only five images was quite inadequate to yield a true average. Indeed, by investigating the standard deviation and average intensity from regions of these images, it was concluded that the number of images required to give a reasonable average representation would make the image acquisition and processing procedure impractical. For example, consider the images of Figure 9D. A small (10 pixels x 10 pixels) square region near the center of each of the

five images which were averaged to produce the liquid and vapor images shown here was extracted and analyzed. Assuming variations in intensity of these large "pixels" are normally distributed about the true average from laser shot to laser shot, these samples were then used to determine the number of sample images required to say with a 95% confidence interval that the calculated average intensity lies within 10% of the true average. In the case of the vapor image, at least 10 images are required. And in the case of the liquid image, at least 50 images are required. Other such investigations showed that it is not unusual to find that 50 to 100 images are required.

Even with a computer running at 33 MHz, given the present capabilities of the camera and the CSMA software, the time required to acquire and store 50 images at a single test condition is prohibitive (approximately 15-20 minutes) since the present nitrogen supply capabilities, with 12 bottles, allow for run times on this order. Additionally, the time required to average and otherwise process such a large number of images would be very large.

While it is understood that only acquisition and saving of individual images enables the calculation of standard deviations, these time limitations presently seem insurmountable.

Recently, some work has been done utilizing features of the Princeton Instruments camera and associated hardware which enable "on-chip" (meaning on the CCD chip) accumulation of images. The camera allows separate control of gating (which turns the intensifier on and off) and shuttering (which opens the camera to light). In recent tests, the camera has been gated for a few microseconds around each laser pulse, and shuttered for between 5 and 30 seconds. With the laser operating at 10 Hz, this allows the accumulation of 50 to 300 laser shot records on the chip. Once the shuttering time expires, the hardware stores the resulting image on disk. The problem which arises in using this method is that of properly choosing the number of accumulations, the camera gain, and lens aperture setting to insure a meaningful average and to be sure that an image is recorded with a good signal-to-noise ratio, while also being sure that the pixels are not saturated. This is particularly difficult to achieve with a single group of settings in

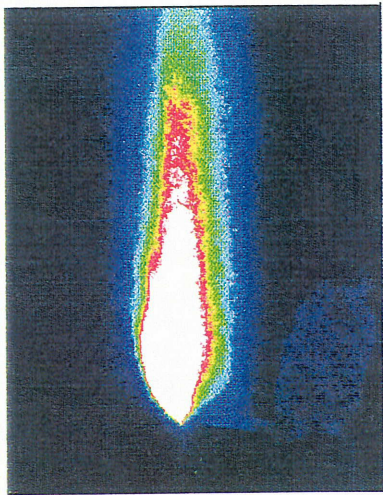
a flow with greatly varying liquid and vapor concentrations, as occurs in the mixing tube.

The on-chip accumulation technique for creating an average image has been used to record images at two locations in the mixing tube, at the low inlet temperature condition, at an equivalence ratio of 0.6. Figure 22 shows both liquid and vapor images recorded at the mixing tube Position A under the same conditions of laser power, and camera and lens settings. Figures 22A and C are images resulting from exposure to 50 laser shots, while Figure 22B and D are the result of exposure to 100 laser shots. The intensity values in A & C have been multiplied by 2 so that when the intensities are scaled for the color scheme, A & C can be compared with B & D. One of the more noticeable features of these images is that the edges of the liquid or vapor envelope are now smooth, unlike those in the images of Figure 18 where the unsteadiness and turbulence of the flow are recorded as fluctuations and eddy-like structures on the boundaries. Comparing images A & B, it can be seen that the distributions of liquid depicted in the images are remarkably similar visually. The similarities are even more striking in the vapor images C & D. At this point, no analysis has been done to more quantitatively determine the strength of the similarities. But it does appear that, at least for these flow conditions at Position A, accumulating 100 laser shots is adequate to record an accurate average image.

Figure 23 shows liquid images and Figure 24 vapor images, recorded at the mixing tube Position D under the same conditions of laser power, and camera and lens settings. In both figures, images A, B, & C correspond to accumulating 100, 200 and 300 laser shots, respectively. Again, in order to be able to compare the three images after false-color scaling, the intensities in image A were multiplied by 3, and those in image B by 1.5. Visual inspection of the liquid images shows that the liquid boundary in image 23B is noticeably smoother than that in image 23A; the change is not as noticeable from B to C. The core of the liquid region looks similar in images A and B, but there appear to be many more pixels with intensities greater than 100 in image C than in either A or B. Similar comments can be made about the vapor images of

6/29/94 Mixing Tube Images @ Position A #5 Fan Tip Hypo Tube Injector on Centerline

Liquid Images

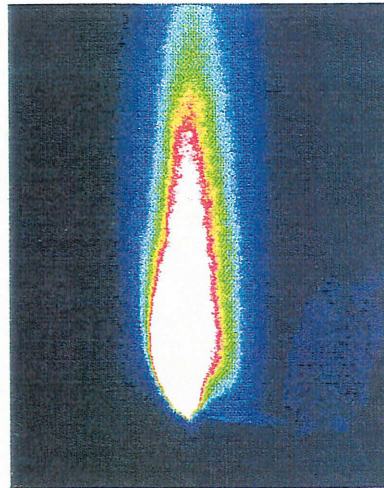


A

Background subtracted
Clipped at zero intensity
Images cut to O. D. of tube
Flow from left to right
Liquid scaled to 2500 max I
Vapor scaled to 1000 max I
Laser Power = 100 mW
+10/-0 mW
WinView Zoom Factor: 1.065
PwrPnt Scale: 50%

g3

50 shots f/32 G=2.00 100mW Imax=14560
(multiplied by 2)



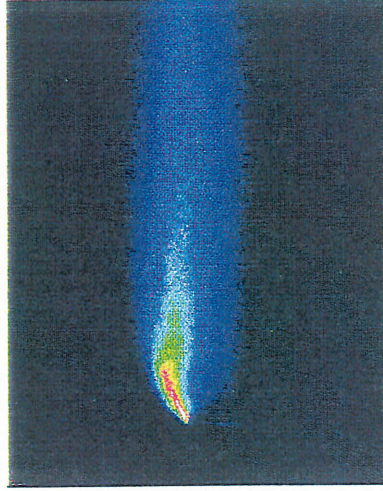
B

g4

100 shots f/32 G=2.00 100mW Imax=16320

On Chip Accumulation of Images

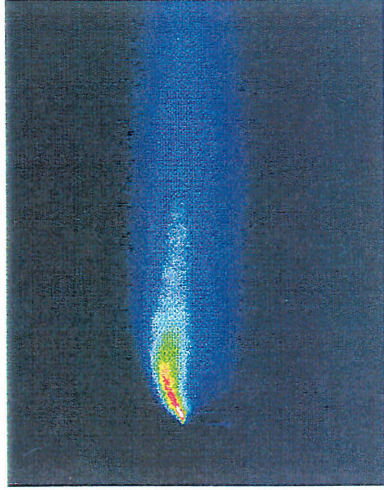
Vapor Images



C

b3

50 shots f/32 G=2.00 100mW Imax=645
(multiplied by 2)



D

b4

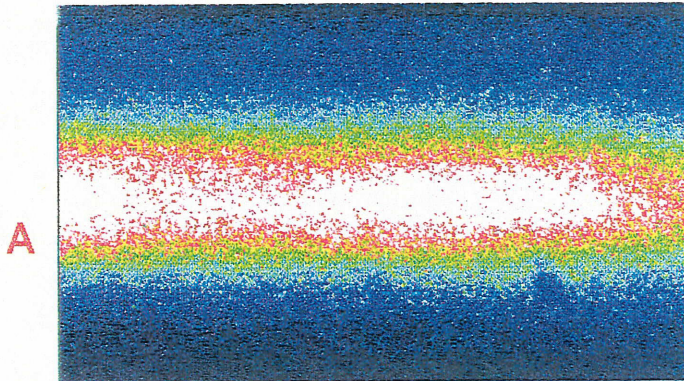
100 shots f/32 G=2.00 100mW Imax=1195

Figure 22 Mixing Tube Images @ Position A with the #5 Fan Tip Injector Using On-Chip Accumulation for Averaging

6/30/94

Mixing Tube Images @ Position D #5 Fan Tip Injector on Centerline On Chip Accumulation of Images

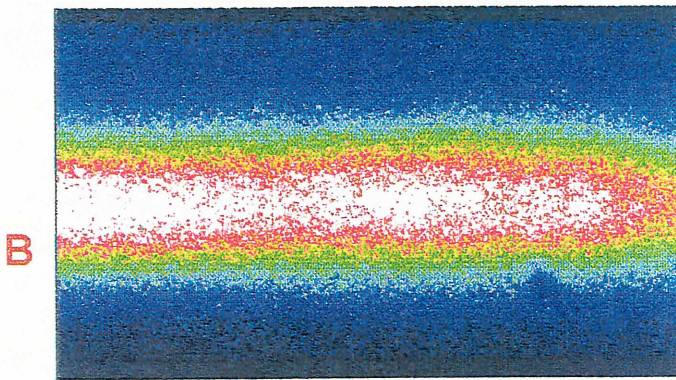
Liquid Images



A

g1

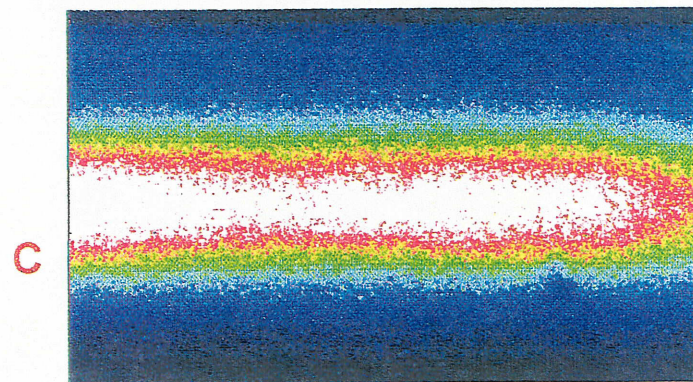
100 shots f/32 G=2.00 100mW I_{max}=73
(multiplied by 3)



B

g2

200 shots f/32 G=2.00 100mW I_{max}=121
(multiplied by 1.5)



C

g3

300 shots f/32 G=2.00 100mW I_{max}=167

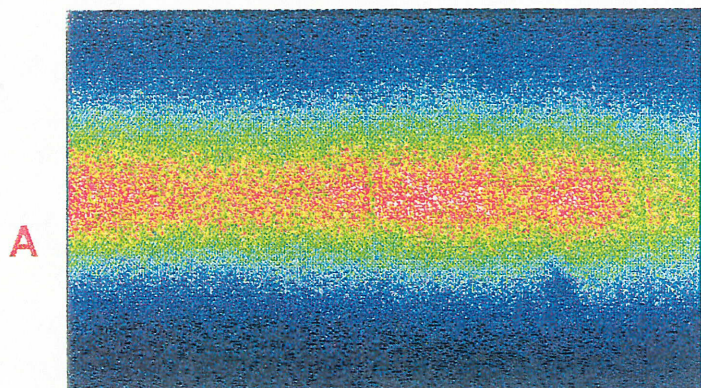
Background subtracted
Clipped at zero intensity
Images cut to O. D. of tube
Flow from left to right
Liquid scaled to 100 max I
Laser Power = 100 mW +10/-0 mW
WinView Zoom Factor: unchanged
PwrPnt Scale: 50%

Figure 23 Mixing Tube Liquid Images @ Position D with the #5 Fan Tip Injector
Using On-Chip Accumulation for Averaging

6/30/94

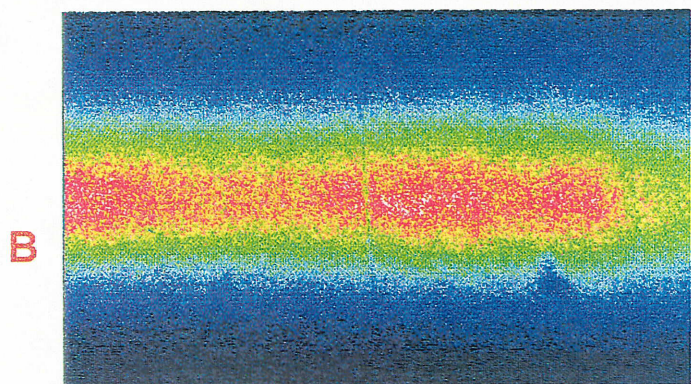
Mixing Tube Images @ Position D #5 Fan Tip Injector on Centerline On Chip Accumulation Of Images

Vapor Images



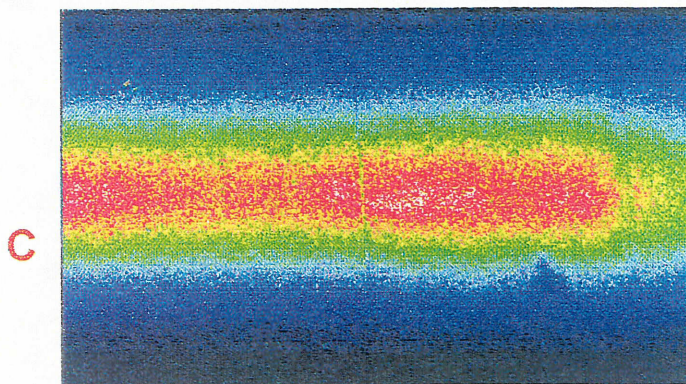
b1

100 shots f/32 G=2.00 100mW I_{max}=31
(multiplied by 3)



b2

200 shots f/32 G=2.00 100mW I_{max}=70
(multiplied by 1.5)



b3

300 shots f/32 G=2.00 100mW I_{max}=113

Background subtracted
Clipped at zero intensity
Images cut to O. D. of tube
Flow from left to right
Vapor scaled to 75 max I
Laser Power = 100 mW +10/-0 mW
WinView Zoom Factor: unchanged
PwrPnt Scale: 50%

Figure 24 Mixing Tube Vapor Images @ Position D with the #5 Fan Tip Injector
Using On-Chip Accumulation for Averaging

Figure 24. It may be that a larger number of accumulations, perhaps 200-300, are necessary to obtain an accurate average image at the downstream end of the mixing tube. Further studies are needed to clarify this question. It will also be necessary to investigate this point for image recording in the combustor at the mixing tube exit.

While we realize that standard deviation information is lost when using this averaging technique, it does appear to yield accurate average information and is a very practical method. It is currently planned that all future images will be acquired using this method.

VIII. CONCLUSIONS

Laser-induced exciplex fluorescence imaging has been used to study the vaporization and mixing characteristics of various IMFH configurations. Initial tests found that an axial hypo tube injector left most of the liquid and vapor confined to a central core region of the flame tube at both high and low inlet temperatures. A Lee spin jet injector was found to produce a better mixed, more vaporized fuel-air region at the exit of the mixing tube.

Using the spin jet injector, it was found that the mixing tube length could not be reduced from its present 4.5" length without reducing the amount of vaporization at the mixing tube exit well below the desired 98%.

During this contract period, a transparent, larger diameter mixing tube/flame holder configuration, which provides for air injection, was designed and built. Its use, however, was delayed in favor of further testing of other injector configurations.

In an effort to design an injector tip which would produce mixing and vaporization characteristics similar to those of the spin jet, but which would be simpler to produce and implement, the sprays generated by three new hypo tube injector tips were studied. Two were ovalized tips designed to produce a fan spray and one was a syringe cut tip. All were mounted transverse to the flow with the tip on the flow centerline. The main conclusion, however, is that no one of these hypo tube-style tips performs very much better than any other. In general they

all do a rather poor job of spreading the fuel to create a uniform field, especially at the low inlet temperature condition. The fuel mixture tends to remain confined to a central core region.

Finally, it was concluded that for meaningful comparisons of imaging data with combustor performance test data, averaging over many images is required. A technique employing on-chip accumulation of images for averaging has been tried and appears to be an excellent, practical method of obtaining average images in these highly turbulent flows.

REPORT DOCUMENTATION PAGE

Form Approved
OMB No. 0704-0188

Public reporting burden for this collection of information is estimated to average 1 hour per response, including the time for reviewing instructions, searching existing data sources, gathering and maintaining the data needed, and completing and reviewing the collection of information. Send comments regarding this burden estimate or any other aspect of this collection of information, including suggestions for reducing this burden, to Washington Headquarters Services, Directorate for Information Operations and Reports, 1215 Jefferson Davis Highway, Suite 1204, Arlington, VA 22202-4302, and to the Office of Management and Budget, Paperwork Reduction Project (0704-0188), Washington, DC 20503.

1. AGENCY USE ONLY <i>(Leave blank)</i>	2. REPORT DATE October 2004	3. REPORT TYPE AND DATES COVERED Final Contractor Report	
4. TITLE AND SUBTITLE HSCT Sector Combustor Evaluations for Demonstration Engine		5. FUNDING NUMBERS WBS-22-714-09-46 NAS3-26617	
6. AUTHOR(S) Stuart Greenfield, Paul Heberling, John Kastl, John Matulaitis, and Cynthia Huff			
7. PERFORMING ORGANIZATION NAME(S) AND ADDRESS(ES) General Electric Aircraft Engines Advanced Engineering Programs Department 1 Neumann Way Cincinnati, Ohio 45215-6301		8. PERFORMING ORGANIZATION REPORT NUMBER E-14637	
9. SPONSORING/MONITORING AGENCY NAME(S) AND ADDRESS(ES) National Aeronautics and Space Administration Washington, DC 20546-0001		10. SPONSORING/MONITORING AGENCY REPORT NUMBER NASA CR-2004-213132	
11. SUPPLEMENTARY NOTES This research was originally published internally as HSR063 in June 1998. Responsible person, Diane Chapman, Ultra-Efficient Engine Technology Program Office, NASA Glenn Research Center, organization code 2100, 216-433-2309.			
12a. DISTRIBUTION/AVAILABILITY STATEMENT Unclassified - Unlimited Subject Categories: 01 and 07 Available electronically at http://gltrs.grc.nasa.gov This publication is available from the NASA Center for AeroSpace Information, 301-621-0390.		12b. DISTRIBUTION CODE	
13. ABSTRACT <i>(Maximum 200 words)</i> In LET Task 10, critical development issues of the HSCT lean-burn low emissions combustor were addressed with a range of engineering tools. Laser diagnostics and CFD analysis were applied to develop a clearer understanding of the fuel-air premixing process and premixed combustion. Subcomponent tests evaluated the emissions and operability performance of the fuel-air premixers. Sector combustor tests evaluated the performance of the integrated combustor system. A 3-cup sector was designed and procured for laser diagnostics studies at NASA Glenn. The results of these efforts supported the earlier selection of the Cyclone Swirler as the pilot stage premixer and the IMFH (Integrated Mixer Flame Holder) tube as the main stage premixer of the LPP combustor. In the combustor system preliminary design subtask, initial efforts to transform the sector combustor design into a practical subscale engine combustor met with significant challenges. Concerns about the durability of a stepped combustor dome and the need for a removable fuel injection system resulted in the invention and refinement of the MRA (Multistage Radial Axial) combustor system in 1994. The MRA combustor was selected for the HSR Phase II LPP subscale combustor testing in the CPC Program.			
14. SUBJECT TERMS Emissions; Combustors; Premixers; Lean-burn		15. NUMBER OF PAGES 322	
		16. PRICE CODE	
17. SECURITY CLASSIFICATION OF REPORT Unclassified	18. SECURITY CLASSIFICATION OF THIS PAGE Unclassified	19. SECURITY CLASSIFICATION OF ABSTRACT Unclassified	20. LIMITATION OF ABSTRACT

